iRHOM2 in skin disease and oesophageal cancer

Sarah Louise Etheridge

A Thesis presented for the degree of

Doctor of Philosophy

2015

Supervisor: Professor David Kelsell

Centre for Cutaneous research
The Blizard Institute
Barts and the London School of Medicine and dentistry
Queen Mary, University of London

Abstract

Mutations in *RHBDF2,* the gene encoding inactive rhomboid protein iRHOM2, result in the dominantly inherited condition Tylosis with oesophageal cancer (TOC). TOC causes plamoplantar keratoderma, oral precursor lesions and up to a 95 % life-time risk of oesophageal squamous cell carcinoma (SCC). The role of iRHOM2 in the epidermis is not well characterised, although we previously showed dysregulated epidermal growth factor receptor (EGFR) signalling and accelerated migration in TOC keratinocytes, and a role for iRHOM2 was shown in trafficking the metalloproteinase ADAM17. Substrates of ADAM17 include EGFR ligands and adhesion molecules.

iRHOM2 localisation and function were investigated in frozen sections and keratinocyte cell lines from control and TOC epidermis. Although iRHOM2 was predicted to be an ER-membrane protein, it showed cell-surface expression in control epidermis, with variable localisation in TOC. Increased processing and activation of ADAM17 was seen in TOC keratinocytes compared with control cells, suggesting that increased ADAM17-mediated processing of EGFR ligands may cause the changes in EGFR signalling. Downstream of iRHOM2-ADAM17, Eph/Ephrin and NOTCH signalling also appeared affected. Additionally, desmosomes in TOC epidermis lacked the electron-dense midline of the mature desmosomes seen in normal skin; this was accompanied by increased processing of desmoglein 2, a substrate of ADAM17. Expression and localisation of iRHOM2 was also investigated in TOC and sporadic SCC. iRHOM2 expression varied between SCC cell lines, and appeared to correlate with ADAM17 and NOTCH1 expression in oesophageal SCC and head and neck SCC cells.

In summary, iRHOM2 mutations in TOC appear to be gain-of-function in nature, resulting in increased ADAM17 processing and enhanced EGFR signalling. Questions remaining include the reason why iRHOM2 is found at the plasma membrane. Future study of the iRHOM2-ADAM17 pathway may provide additional insight into the mechanism of epidermal wound healing and the pathogenesis of oesophageal SCC.

Table of Contents

Figures and Tables

List of Figures

Appendix figures

List of Tables

Statement of Originality

I, Sarah Louise Etheridge, confirm that the research included within this thesis is my own work or that where it has been carried out in collaboration with, or supported by others, that this is duly acknowledged below and my contribution indicated. Previously published material is also acknowledged below.

I attest that I have exercised reasonable care to ensure that the work is original, and does not to the best of my knowledge break any UK law, infringe any third party's copyright or other Intellectual Property Right, or contain any confidential material.

I accept that the College has the right to use plagiarism detection software to check the electronic version of the thesis.

I confirm that this thesis has not been previously submitted for the award of a degree by this or any other university.

Signature:

Date:

Collaborations and publications

Collaborations

Epidermal skin equivalent 3D models and the associated western blots and staining presented in chapters 3 and 4 were performed by Dr Spiro Getsios and Dr Nihal Kaplan, Northwestern University, Chicago, USA. Electron microscopy shown in chapter 3 was performed by Dr Akemi Ishida-Yamamoto, Asahikawa Medical Centre, Asahikawa, Japan, with original observations made by Mr Graham McPhail, BICMS core pathology facility, QMUL. DAB staining of the paraffin-embedded oesophageal biopsies shown in Chapter 5 was performed by the BICMS Core Pathology Facility, and in collaboration with Dr Laura Gay and Professor David Kelsell, Blizard Institute, QMUL. Flow cytometry was performed with Dr Luke Gammon, Blizard Institute, QMUL. Any work presented in this thesis that was carried out by, or in collaboration with, another researcher from the group has been acknowledged in the text and/or figure associated with that work. However, I would like to acknowledge at this point Dr Diana Blaydon and Dr Matthew Brooke, with whom I have worked closely on some of the experiments in this thesis.

Primary publications

Brooke MA, **Etheridge SL**, Kaplan N, Simpson C, O'Toole EA, Ishida-Yamamoto A, Marches O, Getsios S, Kelsell DP. iRHOM2-dependent regulation of ADAM17 in cutaneous disease and epidermal barrier function. *Hum Mol Genet.* 2014; 23(15):4064-4076

Blaydon DC, **Etheridge SL**, Risk JM, Hennies HC, Gay LJ, Carroll R, Plagnol V, McRonald FE, Stevens HP, Spurr NK, Bishop DT, Ellis A, Jankowski J, Field JK, Leigh IM, South AP, Kelsell DP. RHBDF2 mutations are associated with tylosis, a familial esophageal cancer syndrome. *Am J Hum Genet.* 2012 Feb 10;90(2):340-346

Review articles

Nitoiu D, **Etheridge SL**, Kelsell DP. Insights into desmosome biology from inherited human skin disease and cardiocutaneous syndromes. *Cell Commun Adhes*. 2014; 21(3):129-140.

Etheridge SL, Brooke MA, Kelsell DP, Blaydon DC. Rhomboid proteins: a role in keratinocyte proliferation and cancer. *Cell Tissue Res.* 2013; 351(2):301-307

Oral Presentations

Etheridge SL, Brooke MA, Blaydon DC, South AP, Kelsell DP. EGF and Ephrin signalling is dysregulated in Tylosis with Oesophageal Cancer; UK-Singapore Translational Skin Biology Symposium, Singapore, December 2012

Etheridge SL, Blaydon DC, Brooke MA, Risk J, South AP, Kelsell DP. iRHOM2 mutations affect EGF signalling in Tylosis with Oesophageal Cancer; British Society for Investigative Dermatology (BSID), Exeter, April 2012

Etheridge SL, Blaydon DC, Risk JM, Stevens HP, John Field, A. Ellis, Hennies H-C, Leigh IM, South AP, Kelsell DP. *RHBDF2* mutations in Tylosis with Oesophageal Cancer cause dysregulation of downstream EGF and Ephrin B3 signalling; William Harvey Day, Barts and the London School of Medicine and Dentistry, QMUL, October 2011

Etheridge SL, Blaydon DC, Risk JM, Stevens HP, Field J, Ellis A, Hennies H-C, Leigh IM, South AP, Kelsell DP. *RHBDF2* mutations in Tylosis with Oesophageal Cancer. European society for Dermatological Research, Barcelona, September 2011

Poster Presentations

Brooke MA, **Etheridge SL**, Balydon DC, Getsios S, Kelsell, DP. Dysregulated iRHOM2/ADAM17 in Tylosis with Oesophageal Cancer affects Ephrin- and EGF-family-mediated keratinocyte adhesion and migration. International Investigative Dermatology, Edinburgh, May 2013

Etheridge SL, Blaydon DC, Getsios S, South AP, Kelsell DP. Eph/Ephrin signalling in Tylosis with Oesophageal Cancer; William Harvey Day, Barts and the London School of Medicine and Dentistry, October 2012

Acknowledgements

Firstly, I would like to thank my supervisor, Professor David Kelsell, for his support and guidance throughout the project, and the opportunities during the three years. I am also grateful to the British Skin Foundation for funding this project.

I would like to thank those that I have worked with in the lab during this project, and those that have kindly provided materials for the experimental research. Thank you to Dr Diana Blaydon with whom I collaborated on the phospho-tyrosine kinase arrays and early stages of the iRHOM2 project, and also for providing the GFP-tagged iRHOM2 constructs and primers for reverse-transcriptase PCR. Thank you to Dr Matthew Brooke, for collaborating on cell culture and the iRHOM2-ADAM17 signalling section of this thesis, and for providing primers, materials and guidance for qPCR and ELISA experiments. Also, a big thank you to Dr Luke Gammon, centre for cutaneous research (CCR), QMUL, for his assistance with performing the flow cytometry experiments shown in chapter 3. Thanks to Dr Spiro Getsios, Northwestern University, Chicago, for feedback on Eph/Ephrin signalling data and for providing the antibodies used for staining and western blotting. I would also like to thank both Dr Spiro Getsios and Dr Nihal Kaplan, Northwestern, for sharing the data relating to 3D epidermal equivalents.

Many thanks to Dr Akemi Ishida-Yamamoto of Asahikawa Medical University, Asahikawa, Japan and Graham McPhail, core pathology facility, Blizard Institute, who processed samples for electron microscopy, and to Dr Akemi Ishida-Yamamoto for performing the electron microscopy shown in chapter 3. Thank you to Dr My Mahoney, Thomas Jefferson University, Philadelphia, for the DSG2 antibodies, and to Dr Helena Emich, CCR, for the HNSCC cell lines and Dr Karin Purdie, CCR for the frozen cutaneous SCC sections. I would also like to thank Dr Laura Gay, Centre for Digestive Diseases, QMUL, for collaboration on the OSCC staining in chapter 5 and for providing the anti-CD68 antibody. I would also like to say a big thank you to the Core Pathology Facility, particularly Rebecca Carroll, Pauline Levy, Mark Childs and Chris Evagora for cutting of frozen skin sections, and to Rebecca Carroll for performing immunohistochemistry on paraffin-embedded OSCC sections.

I am grateful to everyone involved with the smooth running of the lab and core facilities. The Blizard laboratory management team: Chris Pelling, Jeff Maskell, Bob Pritchard, Kifaia Rashid; Dr Ann Wheeler, Katie, Ishma Ali, Amanda Price of the BALM facility; and Dr Gary Warnes of the Blizard flow cytometry facility. Also, thanks to Dr Ros Hannan, Dr Cleo Bishop, Zoe Drymoussi, Dr Jamie Upton and Dr Matthew Brooke for the running of the tissue culture facilities. Also thank you to the graduate studies administration team,

Dr Paul Allen, Brenda Bell, Susanne Bell and Jacqui Frith, and also to my second supervisor Professor Edel O'Toole for feedback in the PhD progression reports. I am also very grateful to Professor David Kelsell, the Postgraduate student fund, and the QMUL research fund for funding for travel to conferences during my PhD.

I would like to finish by saying a big thank you to everyone that has given me advice, guidance, and support during the last four years. In the lab, I have learnt a lot from members of the Kelsell group: Phil Bland, Dr Diana Blaydon, Dr Matthew Brooke, Dr Anissa Chikh, Ben Fell, Dr Thiviyani Maruthappu, Daniela Nitoiu, Dr Claire Scott and Dr Charlotte Simpson. I would particularly like to thank Dr Diana Blaydon for support and advice during the PhD, Dr Daniel Tattersall, Dr Diana Blaydon and Dr Claire Scott for teaching at the beginning of the PhD, and Daniela Nitoiu for listening and providing problem solving advice both in the lab and during coffee breaks. Thanks also to the O'Toole lab group who have been supportive in discussing experiments and sharing supplies. Thank you to everyone who has supported me during the writing up process, David Kelsell for advice and feedback, and Dr Diana Blaydon, Daniela Nitoiu, Dr Anissa Chikh, Dr Thiviyani Maruthappu and Graham Littlewood for proof-reading the final chapters. Finally, thank you to everyone in CCR and the Blizard institute for making it a great place to work during the last four years.

List of Abbreviations

4E-BP	Eukaryotic initiation factor binding protein 4E
5-FU	5-fluorouracil
ADAM	A disintegrin and metalloproteinase
AJ	Adherens junction
APS	Ammonium persulphate
ARCI	Autosomal recessive ichthyosis
AREG	Amphiregulin
BCC	Basal cell carcinoma
bHLH	Basic-helix-loop-helix proteins
BMDM	Bone marrow derived macrophages
BSA	Bovine Serum Albumin
CAR	Calcium recognition site
CCR	Centre for Cutaneous Research
CD44, CD68	Cluster of differentiation 44 or 68
ChIP	Chromatin immunoprecipitation
CT	cycle threshold
DAB	Diaminobenzylene
DAG	Diacylglycerol
DAPI	4'-6-diamino-2-phenylindole
DMSO	dimethylsulphoxide
dNTP	deoxynucleotide triphosphates
DSC	Desmocollin
DSG	Desmoglein
DSP	Desmoplakin
dT	deoxythymine
DTT	Dithiothreitol
EA	Extracellular anchor
EC	Extracellular cadherin repeats
ECL	Enhanced chemiluminescence
EDTA	Ethylenediamine tetraacetic acid
EGF	Epidermal Growth Factor
EGFP	Enhanced Green Fluorescent Protein
EGFR	Epidermal Growth Factor Receptor
ELISA	Enzyme-Linked Immunosorbent Assay
EM	Electron microscopy
EMT	Epithelial mesenchymal transition
ER	Endoplasmic reticulum
ERAD	ER-associated degradation
ERK	Extracellular signal related kinase

FAK	Focal adhesion kinase
FCS	Foetal Calf Serum
FITC	Fluorescin isothyocyanate
FRET	Fluorescence resonance energy transfer
GAP	GTPase activating protein
GAPDH	Glyceraldehyde 3-phosphate dehydrogenase
GDP	Guanosine diphosphate
GFP	Green Fluorescent Protein
GJ	Gap junction
GOF	Gain-of-function
GPCR	G-Protein coupled receptor
Grb	Growth factor receptor bound protein
GRP	Gastrin-releasing peptide
GTP	Guanosine triphosphate
GUK	Guanylate Kinase
H&E	Haemotoxylin and Eosin stain
HB-EGF	Heparin-binding EGF
HI	Harlequin Ichthyosis
HIF	Hypoxia-inducible factor
HMW	High molecular weight
HNSCC	Head and neck squamous cell carcinoma
HPRT	Hypoxanthine-guanine phosphoribosyltransferase
HPV	Human papilloma virus
HRP	Horse-radish peroxidase
HSP	Heat shock protein
HUVEC	Human umbilical vein endothelial cells
IA	Intracellular anchor
ICC	Immunocytochemistry
ICD	Intracellular domain
ICS	Intracellular cadherin repeat sequence
IGF	Insulin-like growth factor
IGF-1R	Insulin-like growth factor 1 receptor
IgG	Immunoglobulin
IHC	Immunohistochemistry
IL	Interleukin
IPL	Intracellular proline-rich linker
IRF6	Interferon response factor 6
iRHOM	Inactive rhomboid protein
iRhom2-Cub	iRhom2-curly bare truncation mutation
IRS	Insulin receptor substrate
JAM	Junctional adhesion molecule

K1, K5, K9, K10, K14	Keratin proteins
KO	Knock-out
LOF	Loss-of-function
LPS	Lipopolysaccharide
LRP	low density lipoprotein receptor-related protein
MAG	Myelin-associated glycoprotein
MAM	Mastermind
MAPK	Mitogen-activated protein kinase
MDCK	Madine-Darby Kidney Cells
MeAc	Methanol-acetone
MEF	Mouse embryonic fibroblast
MHC	Major histocompatibility complex
miR	MicroRNA
MMC	Mitomycin C
MMP	Matrix metalloproteinase
mTOR	Mammalian Target of Rapamycin
mTORC	Mammalian Target of Rapamycin Complex
NF-κB	Nuclear factor kappa B
NICD	NOTCH Intracellular Domain
NRR	Negative regulatory region (NOTCH)
NSCLC	Non-small cell lung cancer
NTP	Non-targeting pool (siRNA)
OSCC	Oesophageal Squamous Cell Carcinoma
PBMC	Peripheral blood monocytes
PBS	Phosphate Buffered Saline
PDK1	3-phosphoinositide-dependent protein kinase 1
PEST	Protein sequence enriched in serine and threonine
PF	*Pemphigus foliaceus*
PFA	Paraformaldehyde
PG	Plakoglobin
PI	Propidium iodide
PI3K	Phosphoinositide-3 kinase
PIP_2 and PIP_3	Phosphatidyl inositol biphosphate
PKC	Protein kinase C
PKP	Plakophilin
PLC	Phospholipase C
PMA	Phorbol myristate acetate
PPK	Palmoplantar keratoderma
P/S	Penicillin/Streptomycin
PV	*Pemphigus vulgaris*
QMUL	Queen Mary, University of London

qPCR	Semi-quantitative reverse-transcriptase polymerase chain reaction
RACK	Receptor for activated C-kinase
RAPTOR	Regulatory associated protein of mTOR
RECK	Reversion-inducing-cysteine-rich protein with kazal motifs
RHEB	Ras homologue enriched in brain
Rho	Ras homologue gene family member
RICTOR	Rapamycin-insensitive companion of mTOR
ROCK	Rho-associated protein kinase
RT-PCR	Reverse Transcriptase-polymerase chain reaction
RSK	40S ribosomal protein S6 kinase
RTK	Receptor tyrosine kinase
RUD	Repeat unit domain
SCC	Squamous Cell Carcinoma
SDS	Sodium dodecyl sulphate
SDS-PAGE	SDS-polyacrylamide gel electrophoresis
shRNA	Short hairpin RNA
siRNA	Small interfering RNA
STAM	Signal transducing adaptor molecule
STAT	Signal transducer and activator of transcription
TAM	Tumour associated macrophage
TAPI-2	TNF protease inhibitor 2 ADAM17 inhibitor
TBS	Tris-buffered Saline
TBS-T	Tris-buffered Saline-Tween 20
TCF/LEF	Transcription factor/Lymphoid enhancing binding factor family
TEMED	*N,N,N,N*-tetramethylethylenediamine
TF	Transcription factor
TGF-α	Transforming Growth Factor-α
TJ	Tight junction
TLR	Toll-like receptor
TIMP3	Tissue inhibitor of metalloproteinase 3
TMD	Transmembrane domain
TNF-α	Tissue necrosis factor-α
TNFR	Tissue necrosis factor-α receptor
TOC	Tylosis with Oesophageal Cancer
TPA	12-O-tetradecanoyl-phorbol-13-acetate
Tris	Tris-hydroxymethylaminoethane
TSC2	Tuberous sclerosis complex 2
UPR	Unfolded protein response
UV	ultraviolet
VCAM	Vascular cell adhesion molecule
WT	Wild Type

Chapter 1: Introduction

Chapter 1: Introduction

1.1 The Skin

The skin is critical for functions including formation of the permeability barrier, innate immune defence, insulation and structural functions. The skin consists of three layers – the epidermis, dermis and hypodermis (figure 1.1 A; Chu, 2008). The hypodermis comprises mostly adipocytes, and is important in maintaining mechanical integrity, insulating the body and forming a reserve energy supply; the hypodermis also contains many blood vessels, lymphatic vessels and nerves. The dermis forms the bulk of the skin and is important for elasticity, tensile strength, and as the major structural element of the skin. The dermis also contains nerve endings, blood vessels, capillaries, and lymphatic vessels and a number of resident cells such as fibroblasts, macrophages and transient circulating immune cells (Chu, 2008).

The epidermis forms the permeability barrier and the outermost layer of the skin. It has key roles in adhesion, immune function and protection against ultraviolet (UV) radiation (Kalinin et al., 2001; Chu, 2008; Fuchs, 2009). The epidermis joins to the dermis via the dermal-epidermal junction, a semi-permeable basement membrane barrier important in providing resistance against external shearing forces, directing cytoskeletal organisation and developmental signals, and in determining the polarity of growth (Chu, 2008). The basement membrane allows epidermal keratinocytes to adhere through integrins, which form interactions between adjacent cells and components of the extracellular matrix. Keratinocytes of the basal epidermal layer express the integrins $\alpha_3\beta_1$ and $\alpha_6\beta_4$ which bind laminin V, a major component of the basement membrane (Kulukian and Fuchs, 2013).

1.1.1 The Epidermis

The epidermis has a stratified structure with four layers: the basal layer, spinous layer, granular layer and *stratum corneum* (figure 1.1 B). Keratinocytes account for approximately 80% of the epidermis, and are interspersed with other cell types including melanocytes, langerhans cells and merkel cells (Chu, 2008). Melanocytes produce the pigment of the skin in melanosomes, which are vacuoles that may be transferred to surrounding keratinocytes, and give skin its overall pigmentation (Haass and Herlyn, 2005). Langerhans cells are dendritic cells found predominantly in the suprabasal layer as well as in the spinous, granular and basal layers (Mutyambizia et al., 2009). They process antigens and present them to T-cells in the epidermis, and are therefore associated with allergic conditions such as atopic dermatitis. Merkel cells are slow-adapting mechanoreceptors found among keratinocytes of the basal layer in areas of

high-tactile sensitivity, with the majority of Merkel cells forming close associations with nerve endings (Halata et al., 2003).

The basal layer (*stratum basale)* comprises predominantly proliferating transit-amplifying cells: keratinocytes with a columnar shape that undergo a specific number of cell divisions before entering the differentiation pathway (Barrandon and Green, 1987; Fuchs and Raghavan, 2002). There is also a population of stem cells within the hair follicle that can contribute cells to the interfollicular epidermis, particularly during wound healing (Clayton et al., 2007; Mascré et al., 2012).

The suprabasal layer, or *stratum spinosum,* consists of cells with many desmosomal 'spines'. Desmosomes are cell surface modifications attached to the keratin intermediate filaments, and are important in cell-cell adhesion and providing resistance to mechanical stress (Fuchs, 2009). Spinous cells located closer to the basal layer have rounded nuclei and a polyhedral shape and as they differentiate, they develop a flatter shape and begin to produce lamellar granules and keratohyalin granules. Organelles found in cells of the granular layer contain precursors of lipids and proteins needed for formation of the cornified envelope in the *stratum corneum* (Candi et al., 2005; Fuchs, 2009).

1.1.1.1 Expression of keratins

Expression of keratins in the epidermis and other epithelia changes with the differentiation status of the cells (Fuchs and Green, 1980). Keratins form the intermediate filaments, which anchor the epidermis to the basement membrane at hemidesmosomes in the basal layer, and to neighbouring epidermal cells via desmosomes (Yin and Green 2004; Fuchs 2009). Proliferating basal cells express the smaller molecular weight keratins K5 and K14. Spinous cells retain keratins K5 and K14, but do not produce any more of these keratins under normal conditions. They begin to synthesise keratins K1 and K10, which are known as differentiation-specific keratins (Fuchs and Green, 1980; Fuchs, 1995; Blanpain and Fuchs, 2009). In hyperproliferative disorders, K1 and K10 are down-regulated and keratinocytes produce the K6 and K16 keratins (Fuchs, 1995). Specific keratins may be expressed in particular regions of skin, for example K9 expression is restricted to the palms and soles (Candi et al., 2005).

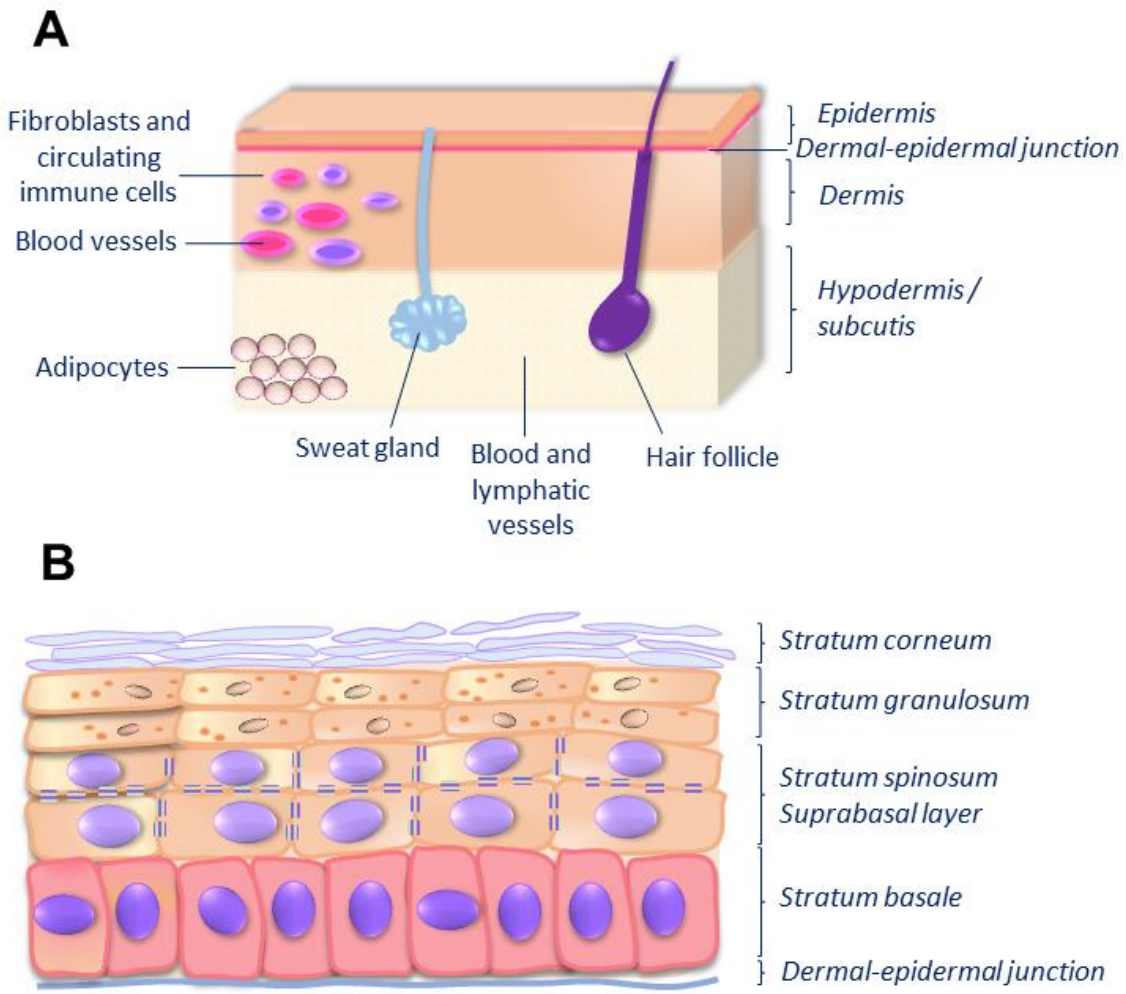

Figure 1.1 Structure of the skin and epidermis. The skin comprises three layers: the hypodermis; dermis and epidermis **(A).** The dermis attaches to the epidermis via the dermal epidermal junction, and contains fibroblasts, blood vessels, and circulating immune cells. **B:** The stratified structure of the epidermis, formed by the progressive differentiation of keratinocytes from the basal layer. The keratinocytes gain a flatter morphology as they move through the epidermal layers, and eventually undergo terminal differentiation. Expression of proteins, such as keratins, change during the differentiation process. The purple structures on the cells of the spinous layer, or *stratum spinosum*, are desmosomes, important for the mechanical integrity of the epidermis. Images are adapted from Chu, 2008

1.1.1.2 Differentiation

Keratinocytes in the epidermis follow a program of progressive differentiation with mitotically active cells in the basal layer developing into the terminally differentiated corneocytes of the *stratum corneum* (Fuchs, 1990). Proliferation in the basal layer is balanced by desquamation of the cornified cell layer at the cell surface in a process of epidermal homeostasis (Candi et al., 2005; Blanpain and Fuchs, 2009). Lineage tracing experiments in the epidermis have shown that the keratinocytes form vertical columns of progressively differentiating cells within the epidermis, with keratinocytes from the basal layer providing cells to the more differentiated upper layers of the epidermis (Clayton et al., 2007; Poulson and Lechler, 2010; Mascré et al., 2012). Stratification occurs through asymmetric cell divisions of the progenitor cells in the basal layer, with a balance of symmetric and asymmetric cell division maintaining epidermal development and homeostasis (Lechler and Fuchs, 2005; Clayton et al., 2007; Mascré et al., 2012). Around 80 % of basal cell divisions result in production of both a differentiating and a proliferating cell, thus maintaining the basal population (Clayton et al., 2007; Mascré et al., 2012).

1.1.1.3 Terminal differentiation and formation of the *stratum corneum*

Keratinocytes of the granular layer generate many of the structural proteins and lipids needed to form the *stratum corneum* (Candi et al., 2005; Fuchs, 2009). The cells contain basophilic keratohyalin granules containing predominantly profilaggrin, keratin filaments, loricrin and small proline rich proteins (SPR), components of the *stratum corneum* (Candi et al., 2005; Fuchs, 2009). Once profilaggrin is released from the keratohyalin granules, it is cleaved in a Ca^{2+}-dependent manner, and subsequently aggregates the keratin intermediate filaments, forming macrofilaments and resulting in the flattened structure of the upper epidermal cells (Candi et al., 2005). Filaggrin is eventually degraded into molecules such as urocanic acid and pyrrolidone carboxylic acid, which aid hydration of the stratum corneum and protect against UV rays (Chu, 2008).

Release of loricrin from keratohyalin granules allows it to bind to desmosomal structures. It is then cross-linked to the plasma membrane by tissue transglutaminases. Filaggrin and loricrin provide a scaffold for the cross-linking of other cornified envelope proteins, including involucrin, trichohyalin and SPRs (Candi et al., 2005). Complex cornified envelope lipids such as ceramides are also synthesised and covalently attached to cornified envelope proteins such as loricrin, reinforcing the barrier layer (Serre et al., 1991; Steinert, 1998). Corneocytes are attached to each other by corneodesmosomes, which are proteolytically degraded in the uppermost layers of the cornified envelope to allow desquamation (Serre et al., 1991; Simon et al., 1996; Candi et al., 2005).

1.2 Cell-cell adhesion and communication in the skin

The epidermis is subjected to high levels of mechanical stress, so cell-cell connectivity is critical for resisting mechanical forces and barrier function. Cell-cell adhesion and communication is mediated by adherens junctions (AJ) and tight junctions (TJ) which bind the actin cytoskeleton (Niessen, 2007); desmosomes, which bind the intermediate filament networks (Yin and Green 2004); and Gap junctions (GJs), which allow cells to communicate through transfer of small molecules and ions (Scott et al., 2012). The structures of the junctions are represented in figure 1.2. Further functions of cell-cell adhesion complexes in cell signalling include direct signalling via activity of junctional components. Junctions may also act as “landmarks” in the membrane for cell-signalling molecules (Niessen, 2007).

Junctional proteins have multiple, overlapping roles, but the major functional types include structural roles critical for initiation and maintenance of the junctions, plaque proteins which associate with the cytoskeleton, and proteins that regulate signalling and polarity (Niessen, 2007). Regulation of cell-cell junctions can occur via transcriptional mechanisms, and by post-translational and signalling modifications such as phosphorylation of junctional components by growth factor signalling, cleavage of junction molecules by proteases, and endocytosis (Niessen, 2007).

1.2.1 Gap junctions

GJs are channels that allow the passage of small molecules and ions between the cytoplasm of adjacent epithelial cells, thus mediating the chemical coupling of the cells (Scott et al., 2012). GJs form by the joining of two hexameric hemichannels at the surface of adjacent cells (figure 1.2 A). The hemichannels cluster to form cell surface plaques which contain several hemichannels, ranging in number from a few channels to thousands of hemichannels per plaque (Goodenough and Paul, 2009).

The hemichannels are formed by connexins, which are integral membrane proteins with four transmembrane domains (TMD); 6 connexins join to form the hexameric hemichannel (connexon), which can consist of a homomeric or heteromeric combination of connexins (Goodenough and Paul, 2009). There are 21 members of the connexin gene family named after their molecular weight, and most tissues express at least one type of connexin protein (Scott et al., 2012). The epidermis expresses a number of connexins, including connexins 26, 30, 30.3, 31, 37 and 43 (Wiszniewski et al., 2000; Di et al., 2001), and mutations in a number of these connexins are associated with syndromic and non-syndromic inherited skin diseases (Scott et al., 2012). The number of connexin channel subunits, and their homophilic or heterophilic assembly, results in an array of combinations that allow fine-tuning of the GJ channel properties

(Goodenough and Paul, 2009), such as charge selectivity and conductance (Bukauskas and Verselis, 2004; Rackauskas et al., 2007; Goodenough and Paul, 2009).

The opening and closing of the GJ channel may be regulated by a number of mechanisms including voltage gating, changing unitary conductance of single channels, or altering the channel open probability. These properties may also vary between the two hemichannel components of the GJ, providing further diversity in channel properties. Slower methods of regulating channel properties include controlling the number of channels at the cell surface, the rate of synthesis and assembly of the hemichannels; and channel degradation and turnover. A number of these steps are dependent on post-translational modifications such as phosphorylation, which can also stabilise the channels in a range of conductance states (Goodenough and Paul, 2009).

1.2.2 Tight junctions

Tight junctions are specialised structures that form a semi-permeable diffusion barrier between the apical and basolateral membrane domains of polarised cells (Niessen, 2007). A diagram representing the structure of TJs is shown in figure 1.2 B.

The major TJ proteins include junctional adhesion molecules (JAMs), claudins, occludins and the scaffolding proteins ZO-1 to 3 (Niessen, 2007). The precise role of occludins in tight junctions is unclear. TJs still form in the absence of occludins, however, loss of occludins in knock-out mice results in phenotypes associated with loss of barrier function (Saitou et al., 2000; Niessen, 2007). Furthermore, knock-down of occludins results in a number of changes in cell phenotype and TJ function in epithelial cells *in vitro* (Yu et al., 2005). There are at least 24 members of the claudin family (Angelow et al., 2008), which are expressed in a tissue-specific manner. Claudins appear to be able to initiate tight junction formation, as exogenous expression of claudins intiated Ca^{2+}-independent initiation of cell-cell adhesion (Furuse et al., 1998; Van Itallie et al., 2001; Nitta et al., 2003). Specific expression of these claudins regulates ion size and charge selectivity of the semipermeable junctions (Van Itallie et al., 2001), with charge selectivity regulated by differences in the isoelectric point in the claudin extracellular loop (Colegio et al., 2002).

JAM proteins include JAM-A, B and C, and some more distantly related JAM proteins such as adenovirus receptor, endothelial cell-selective molecule and JAM4 (Niessen, 2007). JAMs can form homo- or heterophilic interactions. JAM proteins are also found on the surface of cells that do not form TJ, such as leukocytes, to help mediate transendothelial migration (Ebnet et al., 2004). A role for JAM-4 has also been shown in recruiting polarity complexes (Gliki et al., 2004).

The cytoplasmic binding ZO proteins ZO-1 to 3 act as scaffolds for the formation of tight junctions (Niessen, 2007). The ZO family are membrane associated guanylate kinase-like homologues, containing 3 N-terminal PDZ domains, and SH3 domain and a guanylate kinase (GUK) domain. ZO proteins interact with occludins and claudins via the PDZ domain, while their C-terminus can associate with actin, forming a direct link with the cytoskeleton (Schneeberger and Lynch, 2004). ZO-1 localisation to TJ is largely dependent on its actin binding domain (Fanning et al., 2002). ZO-1 can interact with JAMS directly, and forms homodimers or heterodimers with ZO-2 or ZO-3. Furthermore, ZO-1 and 2, but not ZO-3 have been shown to be important for tight junction clustering, strand formation and barrier function. Other scaffolding proteins include MUPP1 and MAG1 proteins, which associate with the TJ cytosolic plaque (Schneeberger and Lynch, 2004). Cingulin, a non-PDZ TJ protein, interacts with ZO proteins, JAMs and actins via its head domain, while its central rod domain is required for homodimerization and interaction with myosin (Cordenonsi et al., 1999; Bazzoni et al., 2000; Guillemot et al., 2004), providing a further link to the cytoskeleton.

1.2.3 Adherens junctions

AJ are critical in the initiation and maintenance of cell-cell adhesion, and are dynamic complexes even in fully polarised epithelia (Niessen, 2007). A representation of the AJ structure is shown in figure 1.2 C. AJ comprise two major units – the cadherin-catenin complex, and the nectin-afadin complex, which likely interact via interactions between afadin, α-catenin and the actin cytoskeleton (Tachibana et al., 2000; Ooshio et al., 2010). The nectin-afadin complex is also necessary for the recruitment of tight junction proteins to the apical side of the AJ (Yamada et al., 2006; Ooshio et al., 2010).

There are four main nectin proteins (nectin 1-4), and also multiple splice variants of these proteins (Irie et al., 2004). Nectins are immunoglobulin (IgG)-like adhesion receptors containing a PDZ domain, which may provide the first scaffold for AJ and TJ formation (Irie et al., 2004; Niessen, 2007). Nectins form lateral homodimers and may also form intercellular interactions with other nectins in a homophilic or heterophilic manner, which varies depending on the individual nectin (Irie et al., 2004). Nectins form a unit with afadin, an actin binding protein also known as AF-6, which can also bind to the actin cytoskeleton (Irie et al., 2004).

The cadherin-catenin complex component of AJ comprises type 1 classical cadherins such as epithelial cadherin (E-cadherin), neuronal cadherin (N-cadherin) and P-cadherin, which contain a typical cadherin extracellular repeat (Niessen, 2007). There are a number of other members of the cadherin family including the desmosomal cadherins desmoglein and desmocollin (Getsios et al., 2004). The catenins p120-catenin

and β-catenin bind to the cadherins via their Armadillo repeat domains (Niessen, 2007). α-catenin connects to the complex via β-catenin. In addition to its role at the AJ, β-catenin is a critical mediator of the Wnt signalling pathway, it can mediate signal-induced changes in cadherin adhesive contacts, and can directly interact with signalling proteins including the epidermal growth factor receptor (EGFR; Nelson and Nusse 2004). Phosphorylation of β-catenin by EGFR can disrupt its binding to cadherins, allowing it to translocate to the nucleus and fulfil its signalling roles (Roura et al., 1999; Park et al., 2005).

P120-catenin is part of the subfamily of Armadillo-repeat containing proteins which includes the desomosomal plakophilins, with binding of p120-catenin regulating junctional stability by regulating endocytosis of the junctions (Xiao et al., 2007). P120-catenin also regulates and integrates intracellular signalling via Rho small GTPases (Anastasiadis, 2007).

Binding of α-catenin to actin or β-catenin is mutually exclusive (Drees et al., 2005), however actin polymerisation is partly dependent on α-catenin, and occurs close to the AJ (Drees et al., 2005; Gates and Peifer, 2005; Yamada et al., 2006). Afadin is another point at which AJ bind directly to the actin cytoskeleton (Niessen, 2007). Actin-binding proteins and other regulatory proteins may also associate with the AJ and regulate actin binding, for example, ZO-1, vinculin, spectrin and α-actinin (Gates and Peifer, 2005; Scott and Yap, 2006; Scott et al., 2006). Cadherin or nectin engagement can induce activity of Rho small GTPases, which are regulators of actin dynamics. The regulation of Rho GTPases may be via upstream Rap small GTPases and recruitment of guanine-nucleotide exchange factors (GEFs). RapGEFs interact with E-cadherin, which activates Rap, resulting in a positive loop reinforcing adhesion (Irie et al., 2004; Braga and Yap, 2005).

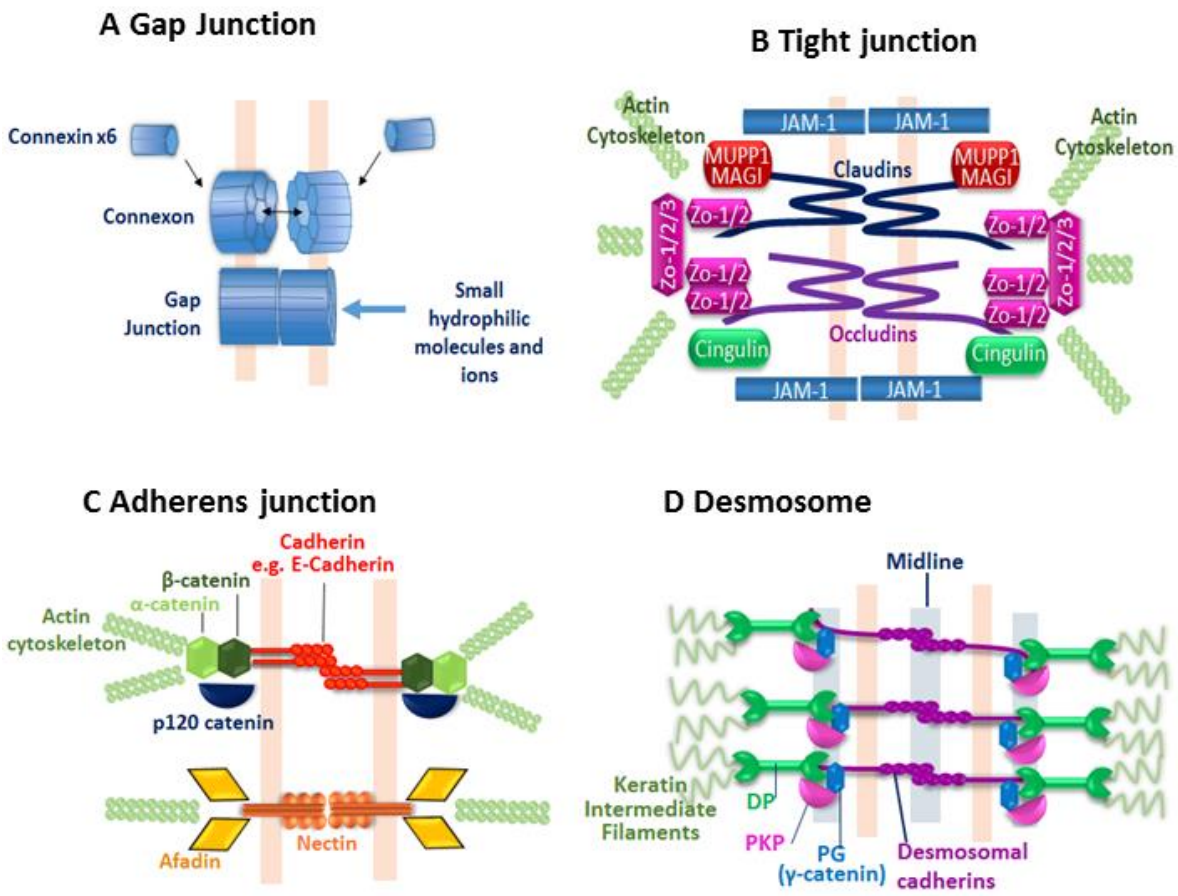

Figure 1.2 Cell-cell junctions in the epidermis. The components of cell-cell junctions and their assembly into **A:** Gap junctions, **B:** Tight junctions (adapted from Niessen 2007), **C:** Adherens junctions (adapted from Niessen 2007), and **D:** Desmosomes (adapted from Getsios et al 2004 and Thomason et al 2010).

1.2.4 Desmosomes

Desmosomes are found in many tissues and organs in the body, particularly in tissues that undergo high levels of mechanical stress, with the highest expression found in the skin and heart (Getsios et al. 2004; Yin and Green 2004; Garrod et al. 2002). Desmosomes are critical in functions including cell-cell adhesion and communication, and an increasing number of cell signalling roles are emerging for desmosomal proteins (Getsios et al., 2004; Thomason et al., 2010). Their function in both adhesion and signalling means disruption of desmosomal components or their regulatory proteins through genetic or environmental factors result in a range of diseases throughout the body.

Desmosomes comprise three main classes of protein: the cadherins; the armadillo-family proteins; and the plakin protein desmoplakin (Thomason et al., 2010; Brooke et al., 2012). Cadherins include desmogleins and desmocollins, while armadillo proteins include plakophilins and plakoglobin (PG). PG is also known as γ-catenin and can associate with AJ, although it has a stronger affinity for the desmosomes (Choi et al., 2009). Distinct expression of the desmosomal proteins is seen in different tissues, and in different layers of the epidermis (figure 1.3A; Borrmann et al. 2000; Getsios et al. 2004).

The desmosomal cell-cell contacts are formed by the desmosomal cadherins, with cadherins from neighbouring cells binding in a Ca^{2+}-dependent manner (Nollet, et al., 2000), as occurs with the classical cadherins in AJ. Once the desmosomes have formed, the dependence on Ca^{2+} is lost, with adhesion in mature desmosomes showing resistance to the extracellular Ca^{2+} concentration, or to Ca^{2+} chelation (Watt, 1984; Mattey and Garrod, 1986). Reversion of the Ca^{2+}-independence of desmosomes is seen upon wounding of confluent monolayers of cells. The process is rapid, occurring in around 15 min, and appears to depend on protein kinase C (PKC), as inhibition of PKC promotes Ca^{2+}-independence (Wallis et al., 2000; Garrod et al., 2005).

Electron microscopy has shown desmosomes to form dense plaques in regions of cell-cell contact. An electron-dense midline is visible in mature, hyperadhesive, Ca^{2+}-independent desmosomes, which is lost upon wounding both *in vitro* and *in vivo*, accompanied by a decrease in the size of the intracellular space (Garrod et al., 2005). A diagram showing the structure of the assembled desmosome is shown in figure 1.4. The thicker, inner dense plaque is visible below the cell surface, where PKPs link DSP and cadherins via PG, with an outer dense plaque formed where DSP binds to keratin intermediate filaments (Getsios et al., 2004).

1.2.4.1 Desmosomal Cadherins

Cadherins span the cell membrane, linking with cadherins from adjacent cells in the intracellular space to form the electron-dense midline seen in electron microscopy images of mature desmosomes (Garrod et al., 2005; Green and Simpson, 2007). There are three members of the desmocollin family (DSC1-3) and four members of the desmoglein family (DSG1-4). The structure of cadherin proteins shares about 30% similarity with each other and with the classical cadherins N-Cadherin and E-Cadherin (Garrod et al., 2002), allowing for variability and fine tuning of adhesion properties in different tissues. Desmocollins have two forms - 'a' and 'b' forms, that differ at the c-terminal as a result of alternative splicing. Cadherins are synthesised with a pro-peptide domain and signal sites in the N-terminus, which are cleaved during protein maturation (Collins et al., 1991; Getsios et al., 2004).

Cadherin structure is shown in figure 1.3 B. All cadherins contain four extracellular cadherin repeats (EC), including Ca^{2+} binding sites and a cell-adhesion recognition (CAR) site; extracellular anchor (EA); TMD; and intracellular anchor (IA) (Getsios et al., 2004; Thomason et al., 2010). The desmocollin a isoforms and desmogleins contain an intracellular cadherin repeat sequence (ICS) which binds PG. The shorter b form contains a shortened version of the ICS, which lacks the PG-binding domain (Collins et al., 1991). Desmogleins contain an additional region that includes an intracellular proline rich linker (IPL), repeat unit domain (RUD) and a DSG terminal domain (Garrod and Chidgey, 2008; Thomason et al., 2010).

DSG2 and DSC2 are expressed predominantly in the intestine and heart (Legan et al., 1994; Schäfer et al., 1996). They are expressed at low levels in the basal layer of stratified epithelia such as the epidermis (Schäfer et al., 1996; Garrod et al., 2002), with slightly stronger expression in skin of the palm in adults, and stronger basal layer DSG2 expression in neonatal epidermis (Mahoney et al., 2006). DSG1 and 3 are more strongly expressed in stratified epithelia (Mahoney et al., 2006; figure 1.3 A).

Binding between cadherins can be either homophilic or heterophilic (Marcozzi et al., 1998; Tselepis et al., 1998; Runswick et al., 2001; Garrod and Chidgey, 2008), and cadherins from the same cell can also bind each other in lateral interactions. Inter-cadherin interactions tend to form in cis on the same cell, or in trans with adjacent cells (Boggon et al., 2002; Getsios et al., 2004). Lateral interactions between different cadherin subtypes may also occur following Ca^{2+} depletion, for example between N-cadherin and desmosomal cadherins (Troyanovsky et al., 1999; Lorch et al., 2004).

The importance of the balance of desmosomal cadherin expression during and after development is shown by the effect of modulating their expression in mice: for example,

DSG2 knock-out mice die after implantation (Eshkind et al., 2002), while overexpression of DSG2 in the epidermis leads to hyperproliferation and formation of papillomas (Brennan et al., 2007), which will be discussed in more detail later. DSC3 knock-out leads to pre-implantation lethality in mice, despite being thought to be an epidermal specific cadherin (Den et al., 2006). However, truncated DSC1 lacking the PG and PKP binding tail was shown to be sufficient for a normal epidermal phenotype (Cheng et al., 2004).

1.2.4.2 Armadillo proteins

The Armadillo family of proteins contain a central domain containing a variable number of 42 amino acid repeats, or arm sequences, which have some variations in their sequences. PG contains 12 arm repeats, allowing its binding to desmosomes or AJ (figure 1.3 B; Choi et al. 2009). Within the desmosome structure, PG acts as an adaptor protein, binding to the desmosomal cadherins, DSP, PKP2 and 3, and p0071, an armadillo protein also known as PKP4 (Getsios et al 2004). The plakophilins PKP1-3 contain 9 arm repeats and a flexible bend-causing insert between repeats 5 and 6 (Choi et al., 2009), and can bind to DSP and cadherins (Getsios et al., 2004).

PG may play a role in the linking (lateral association) of desmosomes and AJ in cultured cells and regulating desmosome size (Palka and Green, 1997), with deletion of the C-terminus of PG leading to formation of large desmosomes. Furthermore, mice lacking PG showed mixing of desmosomal and AJ proteins in cardiac muscle (Ruiz et al., 1996). PG may mediate cross-talk between AJ and desmosomes. The structure of PG is also shown in figure 1.3B.

PKP1-3 are expressed in a tissue and differentiation-specific manner (Neuber et al., 2010). Alternative splicing of PKP1 and 2 results in two isoforms of these proteins (Mertens et al., 1996; Schmidt et al., 1997). PKP1-3 can all be expressed in the nucleus as well as in the desmosomes, with PKP1b found only in the nucleus. PKP1b is the longer isoform, so the additional sequence may contain a nuclear localisation signal (Schmidt et al., 1997; Garrod and Chidgey, 2008). PKPs may also be regulated and targeted to the membrane by 14-3-3 proteins which bind to phosphoserine motifs (Darling et al., 2005). Other desmosomal accessory components include p0071, sometimes referred to as PKP4 (Hatzfeld and Nachtsheim, 1996; Garrod and Chidgey, 2008), which can locate to desmosomes or AJ and may be involved in cross-talk between the two adhesion structures.

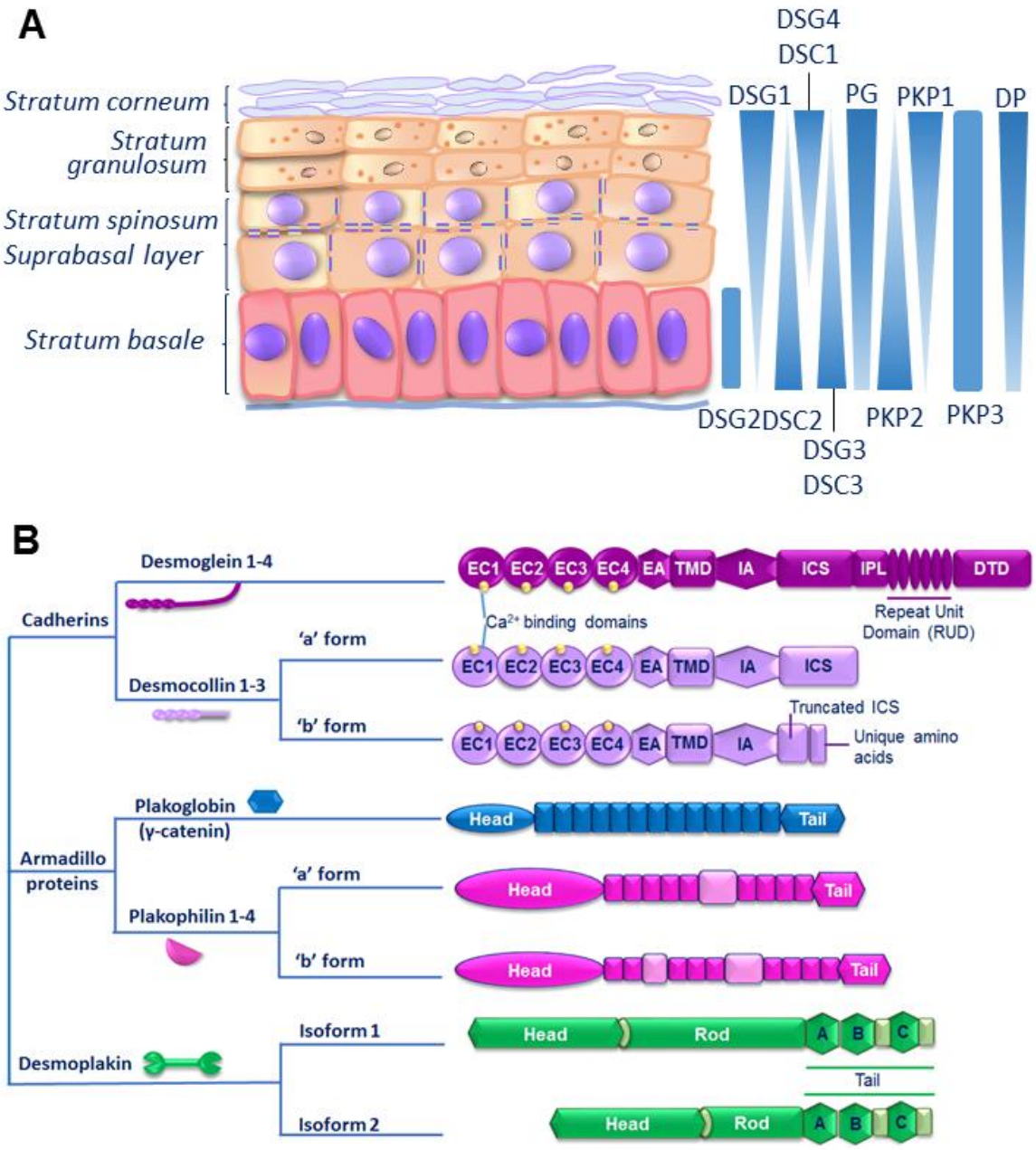

Figure 1.3 Desmosomal proteins in the skin. A: Diagram indicating relative expression levels of desmosomal components within the epidermis. **B:** Diagrams representing the approximate protein structure of the desmosomal components, including the cadherins, the armadillo proteins, and DSP. The different isoforms of the desmogleins, plakophilins and DSP are also indicated. Adapted from Getsios et al 2004, Garrod and Chidgey 2005, Thomason et al 2010 and Chu, 2008.

1.2.4.3 Desmoplakin

The plakin linker protein DSP is critical in anchoring the desmosome to the cytoskeleton via keratin intermediate filaments (Green et al., 1990), and is essential for desmosome formation (Getsios et al., 2004). Knock-out of DSP in mice is lethal by E6.5, with defects in desmosome assembly and/or stabilisation, and effects were seen on the tissue architecture (Gallicano et al., 1998), showing the importance of DSP and desmosomes in development.

There are two DSP isoforms, formed by alternative splicing (Green et al., 1990) and a minor isoform, DSP 1a, has also been identified (Cabral et al., 2010). DSPI and II are expressed at equal levels in stratified epithelia (Angst et al., 1990). Cabral et al (2012) showed decreased levels of PKP1, DSC2 and DSC3 but not of other desmosomal proteins in HaCaT keratinocytes after DSP1 or DSPI and II knock-down. They showed greater importance of isoform II in maintaining cell-cell adhesion in HaCaT monolayers after mechanical stretching and in dispase adhesion assays, and a reduced number of desmosomes with less well defined inner and outer dense plaques (Cabral et al., 2012).

The DSP structure comprises globular head and tail domains surrounding a coiled-coil rod region which is shorter in the DSPII isoform (figure 1.3 B). The coiled-coil rod region is thought to allow dimerization of DSP. The head is the plakin domain, which is important for protein-protein interactions, and which contains two pairs of spectrin repeats either side of a Src 3 homology domain (Jefferson et al., 2007; Garrod and Chidgey, 2008). The C-terminal tail has three plakin repeat domains (A, B and C) which each have 4 ½ copies of a 38 amino acid sequence. Repeats B and C are globular structures containing grooves that may allow binding of intermediate filament proteins (Choi et al., 2002). Association of DSP with intermediate filaments may be negatively regulated by a phosphorylation site in the glycine-serine-arginine rich domain at the C-terminal of DSP (Stappenbeck et al., 1994). In addition to anchoring the IFs, DSP associates with microtubule anchoring protein ninein, and plays an important role in differentiation-specific microtubule organisation (Lechler and Fuchs, 2005).

1.2.4.4 Other desmosomal proteins

Other plakin proteins include envoplakin and periplakin, whose expression are concentrated in the upper layers of the epidermis, particularly in the cornified envelope (Ruhrberg et al., 1996, 1997). Envoplakin and periplakin have a similar structure to desmoplakin, with the periplakin *N*-terminal localising to the desmosomal membranous space, and the *C*-terminal localising with keratin intermediate filaments when transfected into cells (DiColandrea et al., 2000). Envoplakin predominantly forms aggregates with the intermediate filaments, in a process mediated by its rod domain (DiColandrea et al.,

2000). The *C*-terminus of periplakin can stabilise the interaction of both periplakin and envoplakin with the intermediate filaments (Karashima and Watt, 2002).

Corneodesmosin, expressed in the upper layers of the epidermis, is a secreted glycoprotein that is added to desmosomes before they are converted into corneodesmosomes in the upper layers of the epidermis. Corneodesmosin is thought to act as an adhesion protein (Simon et al., 2001; Jonca et al., 2002; Garrod and Chidgey, 2008), and is necessary for desquamation.

Perp is a more recently identified desmosomal-associated protein (Ihrie et al., 2005; Marques et al., 2005), although it is debated whether it is a direct desmosomal component, or plays a regulatory role (Ihrie and Attardi, 2005; Ihrie et al., 2005). Perp does not appear to be necessary for the function of desmosomes in simple epithelia, but seems to be important in desmosomal regulation in stratified epithelia as a target of p63 (Ihrie et al., 2005). Perp has also been shown to play a role in apoptosis as a target of the p53-mediated apoptosis pathway (Attardi et al., 2000): in mouse embryonic fibroblasts (MEFs), expression of perp was sufficient to induce cell death.

1.2.4.5 Desmosome assembly

Desmosome formation in keratinocytes nearly always forms following AJ formation (Vasioukhin et al., 2000), with communication between the two types of adhesion junctions critical in mediating and regulating cell adhesion. Continuous assembly of hemi-desmosomes occurs in low calcium, and the hemi-desmosomes are constantly recycled by endocytosis (Demlehner et al., 1995). When extracellular Ca^{2+} concentrations increase, within 5 minutes, cell-cell contact is initiated mostly by AJ. E-Cadherin in the AJ can bind PKG/γ-catenin, p120-catenin, β-catenin or α-catenin at specific sites. Interactions with actin filaments are then formed (Pokutta and Weis, 2007).

PG is thought to mediate the initial communication, as it binds to both AJ and desmosomes (Lewis et al., 1997; Getsios et al., 2004). E-Cadherin and PG may then recruit PKP3 to the cell border to initiate desmosome formation (Gosavi et al., 2011), with these three proteins present at low levels at the cell membrane even in low levels of Ca^{2+} (Gosavi et al., 2011). This assembly step is followed by recruitment of the rest of the desmosomal components, for example, the plakophilins can recruit DSP to cell-cell borders (Kowalczyk et al., 1999; Bornslaeger et al., 2001; Bonné et al., 2003; Koeser et al., 2003; Getsios et al., 2004). Plakophilins may also mediate lateral interactions between desmosomal components (Kowalczyk et al., 1999).

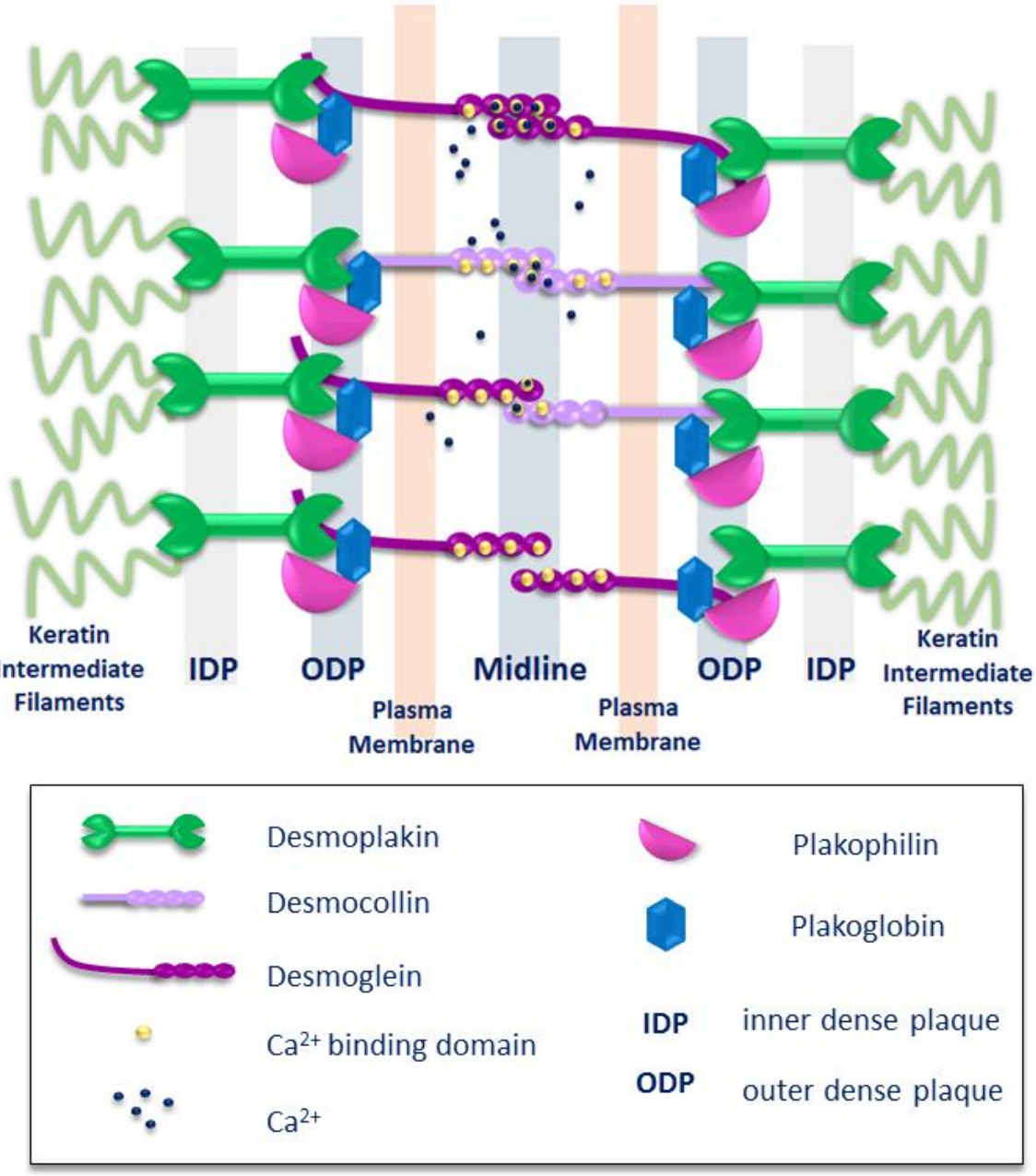

Figure 1.4 Structure of the desmosome and location of desmosomal proteins within the structure. This cartoon represents the structure of the desmosome, showing Ca^{2+}-dependent cell-cell adhesion mediated by homophilic or heterophilic binding of cadherins, which forms the electron-dense midline seen in electron microscopy images of mature desmosomes. The cytoplasmic tail of the cadherins is bound to the desmoplakin head domain via plakophilin and plakoglobin-mediated adhesion, forming the desmosomal outer dense plaque. The tail domain of desmoplakin binds to keratin intermediate filaments, forming the translucent outer dense desmosomal plaque and connecting the desmosomes to the cytoskeleton. Adapted from Getsios et al 2004, Garrod et al 2008 and Thomason et al 2010.

1.2.4.6 Desmosomal signalling

Desmosomes also regulate tissue organisation and morphogenesis, and an increasing number of signalling roles are being identified for desmosomal proteins Some examples include DSG1-mediated differentiation in the epidermis by suppression of EGFR-extracellular signal-related kinase (ERK)1/2 signalling (Getsios et al., 2009; Lin et al., 2010). PG also interacts with receptor tyrosine kinases (RTKs) including the EGFR; and RTK-mediated phosphorylation regulates the interaction of PG with AJ and desmosomes, and likely also downstream signalling events (Gaudry et al., 2001; Miravet et al., 2003).

PG (γ-catenin) can compensate for β-catenin at AJ (Wickline et al., 2013), however PG and β-catenin appear to have differing signalling roles. PG could not fulfil the roles of β-catenin in Wnt signalling in β-catenin knock-out mice or β-catenin null cells (Wickline et al., 2013). However, although it was not as effective as β-catenin, PG was able to regulate TCF/LEF transcription activity (Hu et al., 2003; Shimizu et al., 2008; Al-Jassar et al., 2013). Furthermore, overexpression of the two proteins in developing epidermis resulted in different outcomes: β-catenin induced a hyperproliferative phenotype with increased hair follicle differentiation, while PG overexpression suppressed both these phenotypes (Gat et al., 1998; Charpentier et al., 2000; Getsios et al., 2004).

The plakophilins also have important roles in cell signalling, with PKPs found in the nucleus as well as in junctions (Bonné et al., 1999, 2003). Their function has been related to that of p120-catenin, and include regulation of trafficking, stabilisation, clustering and recycling of cadherins at the cell surface. PKPs have also been associated with RNA Polymerase III and RNA binding proteins (Mertens et al., 1996; Müller et al., 2003; Garrod and Chidgey, 2008), and PKP2 has been suggested to play a role in regulating cell shape, which is also a function of p120-catenin (Getsios et al., 2004).

The wide range of adhesion and signalling roles of desmosomes mean that genetic mutations in the proteins result in a range of syndromic and non-syndromic phenotypes, in particular affecting the skin and the heart (Brooke et al., 2012; Nitoiu et al., 2014).

1.3 Inherited Skin Diseases

There are many inherited diseases affecting the skin and epidermis, which result from mutations in a number of genes, including those encoding proteins of the desmosome (Maruthappu et al., 2014; Nitoiu et al., 2014). Monogenic mutations may result in conditions such as keratodermas, ichthyoses, and blistering conditions, and result from mutations in a diverse range of genes via a number of mechanisms. These include barrier proteins such as filagrin and transglutaminase; structural and adhesion proteins

such as desmosomal components and collagens; cell-cell communication proteins such as the connexins; proteases and their inhibitors (Nagy and McGrath, 2010; Fine et al., 2014; Maruthappu et al., 2014; Nitoiu et al., 2014).

Inherited skin conditions can also be syndromic, for example loss of the metalloproteinase A Disintegrin and Metalloproteinase 17 (ADAM17) leads to inflammatory skin and bowel disease (Blaydon et al. 2011), and mutations in desmosomal proteins lead to an array of syndromic and non-syndromic conditions including arrhythmic right ventricular cardiomyopathy (Nitoiu et al., 2014). Tylosis with oesophageal cancer (TOC) is a form of palmoplantar keratoderma (PPK) associated with a high life-time risk of developing oesophageal cancer (Ellis et al., 1994; Hennies et al., 1995; Stevens et al., 1996).

1.3.1 Mutations in desmosomal proteins

A number of diseases arise from mutations in desmosomal proteins, including palmoplantar keratoderma (PPK), ectodermal dysplasia, hair disorders and cardiomyopathies, such as arrhythmic right ventricular cardiomyopathy (ARVC) (Brooke et al., 2012; Al-Jassar et al., 2013). The pathologies resulting from desmosomal mutations are complex – different mutations in the same desmosomal protein can cause different phenotypes, with no obvious clustering of mutations in the protein structure (Al-Jassar et al., 2013; Nitoiu et al., 2014).

The phenotype typically reflects tissue-specific expression and the adhesion properties of desmosomal components; phenotypes include acantholysis and blistering, thickening and epidermal hyperproliferation. However, desmosomal dysregulation may also result in disrupted intracellular organisation and signalling (Al-Jassar et al., 2013), reflecting the diverse roles of desmosomal proteins. For example, *PKP2* mutations have recently been linked to the dysregulated trafficking of sodium channels in cardiomyopathy and Brugada syndrome (Cerrone and Delmar, 2014).

There are a number of genetic mechanisms by which desmosomal mutations cause disease. For example, autosomal dominant mutations in *DSP* (Armstrong et al., 1999) and *DSG1* (Kljuic et al., 2003) were identified in striate PPK, with the conditions appearing to cause disease through a mechanism of haploinsufficiency. However, homozygous loss-of-function (LOF) mutations in *DSG1* resulted in a syndrome of severe dermatitis, allergies and metabolic wasting, with the patients' parents suffering from the less severe non-syndromic striate PPK resulting from heterozygous *DSG1* mutations (Samuelov et al., 2014).

Recessive *DSP* mutations are found in conditions such as Carvajal syndrome, which is characterised by ARVC with dilated cardiomyopathy, woolly hair, striate PPK and hyperkeratosis. The symptoms of Carvajal syndrome reflect the keratin binding properties of DSP, with hyperkeratosis occurring at sites of stress in the skin such as the joints, caused by loss of the keratin binding site affecting the intermediate filaments as well as cell adhesion (Norgett et al., 2000; Huen et al., 2002; Getsios et al., 2004). Loss of PG results in a reduction in the number of desmosomes, and loss of adhesion structures between keratinocytes in a lethal condition resulting from homozygous mutations in *JUP*, the gene encoding PG (Pigors et al., 2011). Recessive mutations in *JUP* were also found in patients with skin fragility, diffuse PPK and woolly hair, but these patients did not have any signs of ARVC (Cabral et al. 2010).

1.3.2 Mutations causing defects in protein folding

Cutaneous disease also arises from mutations in desmosomal regulatory proteins. Darier's disease results from mutations in the *ATP2A2* gene, which encodes the SERCA2 Ca^{2+} pump (Sakuntabhai et al., 1999). Symptoms of Darier's disease include acantholysis, abnormal keratinisation and mucosal lesions, with formation of papules and plaques in seborrheic regions (Beck et al., 1977; Sakuntabhai et al., 1999). SERCA2 maintains endoplasmic reticulum (ER) Ca^{2+} stores, which are required for post-translational processing, folding and export of proteins such as DSP to the plasma membrane upon cell-cell contact (Jamora and Fuchs, 2002). If the Ca^{2+} store is depleted, misfolded proteins accumulate in the ER, leading to induction of the unfolded protein response (UPR) (Yoshida, 2007).

The impaired adhesion and acantholysis associated with Darier's disease appear to result from impaired trafficking of DSP (Dhitavat et al., 2003; Hobbs et al., 2011; Celli et al., 2012), which was associated with dysregulation of AJ and other desmosomal proteins, and enhanced further by treatment with thapsigargin, a specific inhibitor of SERCA pumps (Thastrup et al., 1994). Keratinocytes from patients with Darier's disease showed constant activation of the UPR (Savignac et al., 2014), which could be reversed by treatment with α-glucosidase inhibitor Miglustat, allowing normal formation of AJ and desmosomes (Savignac et al., 2014).

The condition Erythrokeratoderma Variabilis (EKV) is caused by mutations in the Gap-junction proteins Connexin 31 and Connexin 30.3 (Richard et al., 1998; Wilgoss et al., 1999; Macari et al., 2000; Gottfried et al., 2002; Terrinoni et al., 2004). EKV also results from protein misfolding, defective trafficking and activation of the UPR (Di et al., 2002; Tattersall et al., 2009). EKV is characterised by fixed hyperkeratotic plaques, mainly on the extensor surfaces of the limbs, and transient erythematous patches. The

erythematous patches can last from a few hours to a few weeks and can sometimes migrate, when they are followed by fine white scaling. Around 50% of patients also suffer from PPK (Common et al., 2005). Activation of the UPR in HeLa cells and keratinocytes was shown by increased expression of UPR markers activating transcription factor 6 (ATF6), and ER chaperone GRP78, also known as BiP (binding protein; Tattersall et al., 2009). UPR activation results in up-regulation of factors to assist the cell with protein folding and alleviate the ER stress. However, if activation of the UPR does not resolve the ER stress, it eventually leads to cell death (Yoshida, 2007). Consistent with this, a high level of cell death was seen in cells transfected with EKV-causing mutant connexin 31 (Di et al., 2002; Diestel et al., 2002; Tattersall et al., 2009).

1.3.3 Ichthyoses, including Harlequin Ichthyosis

Ichthyoses are characterised by scaling of the skin, often covering the whole surface of the epidermis, hyperkeratosis, or a combination of both conditions, and may also present in a syndromic or non-syndromic manner (Oji et al., 2010). Identified genes associated with ichthyoses include *TGM*-1, encoding transglutaminase-1; *FLG,* encoding filagrin; *CYP4F22*, a member of the cytochrome p450 family; and *ALOX12B*, which codes for an epidermal-type lipoxygenase enzyme (Oji et al., 2010). Autosomal recessive ichthyoses (ARCI) comprise three main groups: ichthyosiform erythroderma; lamellar ichthyosis; and the most severe form of ichthyosis, Harlequin Ichthyosis (HI) (Maruthappu et al.. 2014). Babies with ARCI are often born with a collodion membrane, which is shed during the first months of life (Ahmed and O'Toole, 2014).

HI results from recessive LOF mutations in the lipid transporter *ABCA12* gene (Kelsell et al., 2005), which may be homozygous or compound heterozygous (Akiyama et al., 2006, 2007; Thomas et al., 2006). The type and position of the mutations affects the severity of the HI phenotype (Ahmed and O'Toole, 2014). At birth, babies born with HI have hard scale plate with deep fissures, eclabium, and bilateral ectropion, with a high perinatal mortality rate (Kelsell et al., 2005; Oji et al., 2010). Those that survive the perinatal period develop a severe, highly scaling erythroderma (Oji et al., 2010; Ahmed and O'Toole, 2014).

ABCA12 encodes the ATP-binding cassette family of transporters, and transports glucosylceramides through the lamellar granules to the extracellular space (Scott et al., 2013). As ABCA12 protein function is severely disrupted in HI, lamellar granules are distorted, reduced or absent, and the lipid layer is severely reduced (Ishida-Yamamoto et al., 2005; Akiyama et al., 2006; Akiyama, 2011; Scott et al., 2013). Severe hyperkeratosis occurs as a compensatory mechanism for the loss of lipids, and the skin barrier is impaired; this likely explains why HI is associated with increased incidence of

infection and dehydration (Radner and Fischer, 2014). Although HI is associated with a high mortality rate in the first few weeks of life, understanding and treatment of the condition are improving and survival rates are increasing (Ahmed and O'Toole, 2014).

1.3.4 Mutations in proteases and their inhibitors

Another form of Ichthyosis, Exfoliative Ichthyosis, results from mutations in the *CSTA* gene encoding protease inhibitor Cystatin A (Blaydon et al. 2011b). An increasing number of proteases and their regulatory proteins are being identified as the cause of cutaneous diseases and syndromes (Curtis and Kelsell, 2013). Exfoliative ichthyosis, also known as peeling skin syndrome, is an autosomal recessive condition characterised by peeling of the skin of the palms and soles and dry scaly skin (Blaydon et al. 2011b). Cystatin A inhibits proteases including the Cathepsins B, H and L (Pavlova et al., 2002; Jenko et al., 2003; Renko et al., 2010). The mechanism by which Cystatin A mutations lead to Exfoliative Ichthyosis appear to involve detachment of the skin in the basal and suprabasal layers, and knock-down of the Cystatin A protein *in vitro* in keratinocytes results in impaired adhesion, in particular following mechanical stress (Blaydon et al. 2011b).

Protease activity, including that of the Cathepsins, is also important for the barrier function of the skin and in wound healing (Brocklehurst and Philpott, 2013; Curtis and Kelsell, 2013; Martins et al., 2013). In addition, increases in protease activity are frequently associated with inflammatory disease (Curtis and Kelsell, 2013). Homozygous LOF mutations in *ADAM17,* the gene encoding ADAM17, were identified in two siblings suffering from an inflammatory skin and bowel disease. The boy has survived into adulthood and leads a relatively normal life. The girl died aged 12 from fulminant parvovirus B19-associated myocarditis, and the boy was later found to have left ventricular dilatation (Blaydon et al. 2011). The skin and bowel symptoms associated with loss of ADAM17 function include perioral and perianal lesions with a generalised pustular rash, flares of erythema and scaling, frequent skin and bowel *Staphylococcus aureus* infections, wiry and disorganised hair, and nail abnormalities (Blaydon et al. 2011).

ADAM17 is a metalloproteinase responsible for shedding of a wide range of substrates, including cell-cell adhesion proteins (Pruessmeyer and Ludwig, 2009), and will be described in more detail in section 1.5. In contrast to ADAM17 LOF in inflammatory skin and bowel disease (Blaydon et al. 2011), the autosomal dominantly inherited syndrome TOC, caused by gain of function (GOF) variants in the inactive rhomboid protein iRHOM2, appears to result from a gain of ADAM17 function (Blaydon et al., 2012; Brooke et al., 2014) and will form the focus of this thesis.

1.3.5 Tylosis with oesophageal cancer

Recently, our group identified mutations in the *RHBDF2* gene, which encodes the inactive Rhomboid protein iRHOM2, in patients with the syndrome Tylosis with Oesophageal Cancer (TOC; OMIM 148500; Blaydon et al., 2012). TOC is an autosomal dominant condition characterised by symptoms including PPK, oral leukoplakia (figure 1.5 A), follicular papules and nail abnormalities. The patients also suffer from oesophageal lesions and have up to a 95% life time risk of developing oesophageal squamous cell carcinoma (OSCC), which develops by age 65 (Ellis et al., 1994; Hennies et al., 1995; Stevens et al., 1996).

The TOC mutations were found in three families from the UK, the US, and Germany, with the UK and US families having large pedigrees. The c.557T>C (p.Ile186Thr) mutation was identified in both the UK and US families, and the mutation c.566C>T (p.Pro189Leu) was found in the German family (Blaydon et al., 2012). Subsequently, the c.562G>A (p.Asp188Asn) mutation was identified in a Finnish family suffering from TOC (Saarinen et al., 2012). The mutations occur within 9 base pairs of the *RHBDF2* gene, or four amino acids of the protein, in a region of the iRHOM2 protein that is highly conserved in a number of different species, and also conserved between iRHOM1 and iRHOM2 (figure 1.5 B; Blaydon et al. 2012).

1.4 Rhomboid proteins

Rhomboid proteins were first identified in drosophila and named due to the misshapen heads of mutant larvae (Urban et al., 2001). Drosophila Rhomboid protein (now known as Rhomboid-1 or dRho-1) was shown to be involved in EGFR signalling through cleavage of Spitz, an EGFR ligand and homologue of human TGF-α (Wassermanet al., 2000; Freeman, 2009). The rhomboid protein family is conserved in all eukaryotes and many prokaryotes, and involvement of the rhomboid proteases has been reported in processes such as quorum sensing in bacteria, invasion of host cells by parasites and in mitochondrial fusion and remodelling (Freeman, 2009). Rhomboids typically contain 7TMD and act as serine proteases, cleaving substrates in their transmembrane region.

There are four subgroups of mammalian rhomboids: Secretase A and B; PARL; and iRHOMs (Lemberg and Freeman, 2007b). Secretase-A type rhomboids are named for their predicted localisation in the secretory pathway. They have 7TMD and include dRho1 and human RHBDL2. Secretase-B, or basic rhomboids, have six TMD and include *E. coli* GlpG and Human RHBDL4. PARL-type rhomboids such as drosophila Rhomboid-7 and human Presenilin-Associated-Rhomboid Like (PARL) contain the 7TMD characteristic of rhomboid proteins, and are all predicted to be found in the

mitochondria. The final rhomboid group is the inactive rhomboids, iRHOM1 and 2, which are encoded by the genes *RHBDF1* and *RHBDF2* respectively (Lemberg and Freeman, 2007b; Freeman, 2009).

1.4.1 The Inactive Rhomboids

iRHOMs have the typical rhomboid 7TMD, with an extended N-terminus and large loop L1 (figure 1.5 C; Lemberg and Freeman 2007; Freeman 2008). The physiological role of the iRHOMs is just beginning to be understood, with the iRHOM2 mutations in TOC providing insight into the importance of iRHOM2 in the skin and oesophagus (Blaydon et al., 2012). A likely role for iRHOM2 in rheumatoid arthritis was also recently demonstrated (Issuree et al., 2013). iRHOM1 and iRHOM2 lack the catalytic residues present in active rhomboids proteases (Koonin et al., 2003; Nakagawa et al., 2005; Freeman, 2009; Adrain et al., 2011). Instead, iRHOMs contain a highly conserved proline residue *N*-terminal to the catalytic serine, with a critical sequence of GPx rather than the GxS motif found in active proteases (Zettl et al., 2011). Substituting the proline residue into the sequence of RHBDL2 significantly lowered its catalytic activity. Zettl et al (2011) also demonstrated the lack of catalytic activity of iRHOM1 and iRHOM2 in a proteolytic activity assay. The *N*-terminal of the iRHOMs does not appear to be similar to any other proteins; the *N*-terminal of iRHOM1 contains a PEST (protein domain enhanced in serine and threonine) domain which is likely to be used for rapid proteolytic degradation (Rechsteiner, 1988; Nakagawa et al., 2005).

iRHOM1 has been shown to be highly expressed in heart, lung, skeletal muscle and placenta with low levels in the colon, kidney and small intestine. It is barely detectable in the brain and peripheral blood monocytes (PBMCs) and not seen in any other tissues tested (Nakagawa et al., 2005). iRHOM2 appears most highly expressed in macrophages (Christova et al. 2013; Su et al. 2004, www.biogps.org/#goto=genereport&id=79651). Both iRHOMs are reported to localise to the ER and golgi in cultured cells (Nakagawa et al., 2005; Zou et al., 2009; Zettl et al., 2011; Hosur et al., 2014).

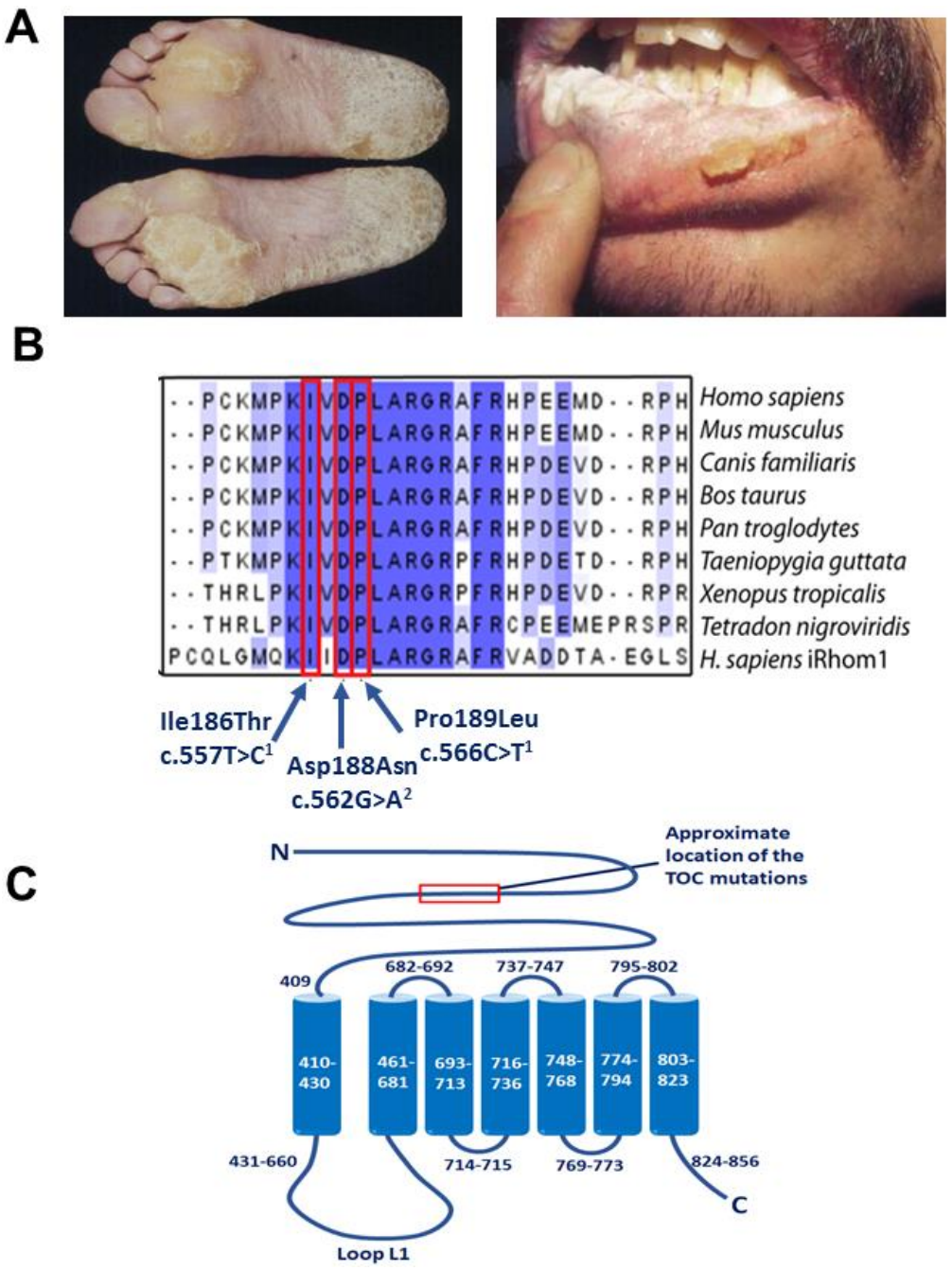

Figure 1.5 Tylosis with oesophageal cancer (TOC) is caused by mutations in *RHBDF2*, the gene encoding the inactive rhomboid protein iRHOM2. A: Pictures showing two of the clinical symptoms of TOC: plantar keratoderma and oral leukoplakia. **B:** Sequence alignment showing that the mutations in the *RHBDF2* gene are found in a highly conserved region of the iRHOM2 protein (Blaydon et al., 2012). **C:** The protein structure of iRHOM2, showing the 7TMD, large loop L1 and long N-terminus, which accounts for approximately half of the protein. The numbers on the diagram indicate the amino acid numbers for each predicted region of the iRHOM2 protein (Uniprot database; www.uniprot.org). References for *RHBDF2* mutations: 1. Blaydon et al 2012. 2. Saarinen et al., 2012.

Reflecting tissue-specific expression of the iRHOMs, murine knock-out of iRhom1 and 2 has very different consequences. iRhom1$^{-/-}$ mice were indistinguishable from their littermates at birth, but failed to gain weight and died within 9 days or 6 weeks of birth, depending on the background strain (Christova et al., 2013). The mixed background mice, who survived longer, suffered a number of phenotypic effects, including myocardial infarction which likely resulted from thrombi development. All iRhom1$^{-/-}$ mice suffered brain haemorrhages, and the mice also suffered bone marrow, spleen, thymus and pancreatic defects (Christova et al., 2013). In contrast, iRhom2 knock-out mice appear healthy, and are fertile with no morphological defects, showing only an altered response to infection despite a normal immune cell distribution (McIlwain et al., 2012). Double knock-out of both iRhoms was embryonic lethal (Christova et al., 2013).

1.4.2 Rhomboid Proteases

A number of studies have contributed to elucidation of the rhomboid protease mechanism (Lemberg and Freeman, 2007a). Two highly conserved residues critical for Rhomboid catalytic activity were first identified as Ser201 and His254 in the *E. coli* rhomboid GlpG (Wang et al., 2006) and in *H. influenzae* GlpG (Lemieux et al., 2007). Rhomboid substrate specificity involves recognition of a 'partially disordered conformation' caused by several helix de-stabilising residues, particularly glycines and alanines, found in the luminal region of the substrate TMD (Urban and Freeman, 2003).

1.4.2.1 RHBDL2

The expression profile of RHBDL2 shows variable levels of expression between different mammalian tissues (Adrain et al. 2011; Su et al. 2004, http://www.biogps.gnf.org/). Variation in expression levels of RHBDL2 was seen between tumour cell lines (Adrain et al., 2011), suggesting that there may be different modes of regulating EGFR signalling in different tissues. A role for the human rhomboid protease RHBDL2 in EGFR signalling has been demonstrated (Adrain et al., 2011), suggesting that at least some of its function is conserved from dRho1. RHBDL2 is activated by proteolytic cleavage in loop L1 by an unidentified protease, which is sensitive to high doses of the gamma-secretase sulphonamide inhibitor GS118, but not to other gamma secretase inhibitors (Lei and Li, 2009). In cultured cells, the N-terminal fragment translocates to the cell membrane following cleavage while the C-terminal portion seems to remain in the ER membrane. Staining of human cell lines demonstrated that RHBDL2 exists almost completely in the cleaved, activated state in those cell lines (Lei and Li, 2009). Substrates of RHBDL2 identified thus far contain an epidermal growth factor (EGF)-like domain and include EGF (Adrain et al., 2011), thrombomodulin (Lohi et al., 2004) and members of the Ephrin B family, in particular Ephrin B3 (Pascall and Brown, 2004).

1.4.2.1.1 RHBDL2 substrates - Thrombomodulin

Thrombomodulin is a type-1 transmembrane glycoprotein expressed on the surfaces of endothelial cells and epidermal keratinocytes (Esmon, 1995; Lager et al., 1995; Weiler and Isermann, 2003) and is involved in many physiological and pathophysiological processes. Lohi et al (2004) identified thrombomodulin as a potential substrate of RHBDL2 due to its EGF-like domain and because it contained a rhomboid recognition-like region (based on the protein conformation). They demonstrated a low-level of cleavage of thrombomodulin by RHBDL2 but not RHBDL1. Cleavage was unaffected by the metalloprotease inhibitor batimastat, and was dependent on the cytoplasmic domain of thrombomodulin (Lohi et al., 2004). The RHBDL2-thrombomodulin pathway has been demonstrated to be relevant to cutaneous wound healing (Cheng et al., 2011).

1.4.2.1.2 RHBDL2 substrates – Ephrin B3

Ephrins are ligands for the Eph tyrosine kinase receptors. Eph-Ephrin signalling is bi-directional, affecting both the signal-sending and signal-receiving cell. Eph-Ephrin signalling is involved in processes including cell-cell communication, adhesion and migration (Pasquale, 2005, 2008) and can be dysregulated in cancer (Pasquale, 2010). Pascall and Brown (2004) first identified Ephrin B2 as a potential substrate of RHBDL2 due to close sequence similarity in the luminal region with Spitz. Ephrin B1 and 3 do not contain this sequence but have many helix-destabilising alanines and glycines in the transmembrane region. RHBDL2 was shown to cleave a small amount of Ephrin B1, cleaved slightly higher levels of Ephrin B2 and showed robust cleavage of Ephrin B3. The cleavage of EphrinB3 appeared specific to RHBDL2 and dRho1, as no cleavage was seen in the presence of RHBDL1 or RHBDL4 (Pascall and Brown 2004). Ephrin B3 cleavage probably occurs in the transmembrane region of the protein, and was independent of the cytoplasmic domain, in contrast to thrombomodulin cleavage (Pascall and Brown 2004; Lohi et al. 2004).

1.4.2.1.3 RHBDL2 substrates - EGF

The third protein reported as a substrate of RHBDL2 is EGF, which binds to the EGFR. This is consistent with the EGFR signalling role of dRho1 in drosophila (Wasserman et al., 2000), indicating conservation of rhomboid function in mammals. EGFR signalling is critical in development and is dysregulated in many cancers (Salomon et al., 1995). Adrain et al. (2011) demonstrated cleavage of Myc-tagged EGF; only slight cleavage of betacellulin and rat Nrg1; and no cleavage of other EGF-like ligands. This indicates that RHBDL2 signalling has a degree of specificity in the EGFR pathway. These findings contrast with previous findings by Pascall and Brown (2004), who did not see cleavage of any mammalian EGF-like ligand. However, Adrain et al (2011) explained that this may

be because the chimeras used by Pascall and Brown (2004) were missing EGF residues in the juxtamembrane region needed for cleavage by RHBDL2.

EGF cleavage by RHBDL2 was independent of ADAM metalloproteinases, shown by experiments carried out in the presence and absence of the metalloprotease inhibitor BB94. The cleavage occurred at Ala1031, a different site to EGF cleavage by ADAM17. EGFR was also activated when ADAMs were inhibited, with a similar efficiency to ADAM17-mediated EGFR activation (Adrain et al., 2011). Cleavage of EGF by RHBDL2 was also possible when ADAM17 was active, indicating independent proximal pathways that lead to EGF cleavage and EGFR activation (Adrain et al., 2011). In addition, ADAM17-independent secretion of EGF was impaired in cells transduced with four different RHBDL2 shRNAs, but ADAM17 mediated cleavage was unaffected. A combination of BB94 and RHBDL2 shRNA blocked cleavage and secretion of EGF completely (Adrain et al., 2011).

1.4.3 iRHOM protein signalling

A role for iRHOM1 in EGFR signalling and the NOTCH signalling pathway was suggested by studies expressing iRHOM1 in drosophila (Nakagawa et al., 2005). The shorter 52KDa iRHOM1 resulted in a severe wing phenotype, resembling the phenotype seen with mutations in Notch (e.g. Rabinow & Birchler 1990), and expression of targets downstream of Notch such as *cut* was reduced (Nakagawa et al., 2005). Co-expression of iRHOM1 with heparin-binding EGF (HB-EGF) resulted in a more severe wing phenotype, providing further evidence for involvement of iRHOM1 in this pathway. No obvious effect was seen with full length iRHOM1, perhaps because another protein not present in drosophila was needed for its activity (Nakagawa et al., 2005). Drosophila expresses a single iRHOM, diRhom, expressed only in neuronal cells. Knock-out of diRhom in flies caused a ‘sleep-like’ phenotype, with a significant decrease in daytime activity but no change in the ability of the flies to move. In contrast to Nakagawa et al (2005), however, no change was seen in other developmentally significant pathways, including the Notch pathway (Zettl et al., 2011). This could be because human iRHOM1 has gained more functions compared to diRhom. The sleep-like phenotype seen with diRhom knock-out is consistent with increased activation of the EGFR pathway by transient overexpression of dRho1 and Star (Foltenyi et al., 2007), again suggesting that diRhom is involved in the regulation of this pathway.

iRHOM1 siRNA knock-down affected pathways downstream of EGFR, shown by reduced levels of phosphorylated extracellular signal-related kinase (phospho-ERK) and phospho-Akt in MDA-MDB-435 breast cancer cells and head and neck squamous cell carcinoma (HNSCC) 1483 cells (Yan et al., 2008). In addition, knock-down of iRHOM1

reduced levels of phospho-EGFR and its downstream target p44/p42 mitogen activated protein kinase (MAPK) following stimulation with gastrin-releasing peptide (GRP) (Zou et al., 2009). Basal levels of p44/p42 MAPK phosphorylation were also reduced as well as the ability of serum-starved HNSCC 1483 cells to migrate into matrigel in response to GRP (Zou et al., 2009).

Cutaneous keratinocytes from TOC patients were unresponsive to removal of exogenous EGF in proliferation and migration experiments (Blaydon et al., 2012). In control keratinocytes, both proliferation and migration were significantly reduced in the absence of exogenous EGF. This reduction in cell growth and wound healing was not seen in two cell lines derived from TOC cutaneous keratinocytes, which may suggest that the TOC keratinocytes are endogenously producing higher levels of EGFR ligands, so that the exogenous EGF does not affect their proliferation and migration. These findings also provide further evidence for a physiological role for iRHOM2 in EGF signalling (Blaydon et al., 2012). The hyperproliferative phenotype seen in the TOC cells is consistent with the hyperproliferative PPK and dysregulated wound healing seen in TOC patients.

Zettl et al (2011) also demonstrated direct regulation of EGF by human iRHOM1 and mouse iRhom2. Both iRHOM1 and iRhom2 reduced the release of co-expressed EGF and other EGF-family ligands in COS-7 cells, which have no endogenous rhomboid activity and also in HeLa cells, which do express RHBDL2 endogenously (Adrain et al., 2011). The ADAM family of metalloproteases was not inhibited in these experiments, and the release of control proteins prolactin and delta was unaffected. These findings suggest that iRHOMs act directly on rhomboid substrates rather than inhibiting the protease (Zettl et al., 2011). iRHOM-mediated reduction in EGF levels occurred through targeting the proteins for ER-associated degradation (ERAD) via the proteasome (Zettl et al., 2011). ERAD is a pathway often induced as a result of ER quality control mechanisms, especially following ER stress and induction of the UPR (Vembar and Brodsky, 2008). Furthermore, FLAG-tagged EGF co-immunoprecipitated with HA-tagged human iRHOM1 and mouse iRhom2 but not control proteins (Zettl et al., 2011).

Further regulation of EGFR signalling by iRHOMs also results through regulation of ADAM17 (Adrain et al., 2012; McIlwain et al., 2012; Christova et al., 2013), which cleaves a number of ligands for the EGFR (Pruessmeyer and Ludwig, 2009).

1.5 ADAM17

ADAM17 (also known as TNF-α converting enzyme; TACE), is a type 1 transmembrane protein first identified as the enzyme responsible for catalysing the cleavage and shedding of transmembrane TNF-α (Black, 2002). ADAM17 has since been identified as the sheddase for a wide range of substrates, including a number of ligands for the EGF receptor and cell-adhesion molecules; ADAM17 has also been shown to mediate ligand-independent cleavage of NOTCH (Bozkulak and Weinmaster, 2009; Pruessmeyer and Ludwig, 2009).

1.5.1 ADAM17 structure and expression

The ADAM17 protein comprises the pro-domain, the disintegrin domain, an EGF-like domain, TMD and the C-terminal cytoplasmic domain (figure 1.6 A; Black, 2002; Horiuchi, 2013). The disintegrin domain is thought to play a role in cell-cell adhesion through binding to the integrin $\alpha_5\beta_1$, while the EGF-like domain is thought to facilitate the activation of ADAM17 though removal of the pro-domain, and also regulates the substrate specificity of ADAM17 (Horiuchi et al., 2009). ADAM17 cleaves its substrates in the extracellular juxtamembrane region, and the metalloproteinase catalytic activity is dependent on the presence of zinc ions (Black, 2002; Horiuchi et al., 2007, 2009). The inhibitory pro-domain contains a cysteine residue thought to interact with the zinc of the active site; this must be displaced to allow ADAM17 metalloproteinase activity. This pro-domain is cleaved during ADAM17 maturation by furin proteases in the golgi (Schlondorff et al., 2000), activating ADAM17 before it is trafficked to the cell surface. Only active ADAM17 reaches the cell surface (Doedens and Black, 2000).

ADAM17 appears to be synthesised and activated constitutively in many tissues, but its activity usually requires stimulation, for example with physiological stimuli such as lipopolysaccharide (LPS) or pharmacologically with phorbol esters (Pruessmeyer and Ludwig, 2009). The stimulation occurs downstream of MAPK and constitutively active kinases such as PKC (Black, 2002), as MAPK inhibitors prevented the increase in ADAM17 sheddase activity seen upon stimulation (Fan and Derynck, 1999). ADAM17 appears to form multimers at the cell surface (Lorenzen et al., 2011), which are necessary for its catalytic activity: a dominant negative form of ADAM17 inhibited the activity of WT ADAM17. The association is dependent on the ADAM17 EGF-like domain (Lorenzen et al., 2011)

1.5.2 iRHOMs traffick ADAM17 from ER to Golgi

A role for iRHOM2 in the trafficking of ADAM17 and regulation of TNF-α shedding was demonstrated in iRhom2 knock-out mice (iRhom2$^{-/-}$) (Adrain et al., 2012; McIlwain et al., 2012), with the same role later demonstrated for iRhom1, also in knock-out mice (Christova et al., 2013). iRHOM2 expression is up-regulated in response to LPS stimulation, which mimics bacterial infection. LPS also increases expression of ADAM17 substrate, TNF-α (Adrain et al. 2012; McIlwain et al. 2012). TNF-α production was nearly completely abolished in iRhom2$^{-/-}$ mice, and there appeared to be an accumulation of TNF-α protein on the cell surface, which was mimicked by metalloprotease inhibitors (Adrain et al., 2012; McIlwain et al., 2012). LPS caused an increase in mRNA levels of iRhom2, ADAM17 and TNF-α in control cells, and levels of TNF-α and ADAM17 were increased even further in iRhom2$^{-/-}$ cells. No differences were seen in levels of other cytokines including IL-6 and IL-12 (McIlwain et al., 2012).

The location of ADAM17 in the secretory pathway was shown using its glycosylation status (Adrain et al., 2012). Under normal conditions, ADAM17 undergoes N-linked glycosylation, which is sensitive to Endo-H. It is then trafficked to the golgi, where the sugars are elaborated and the glycosylation becomes resistant to Endo-H before the inhibitory pro-domain is cleaved by Furin later in the trans-golgi network (Schlondorff et al., 2000). In WT and iRhom2$^{-/-}$ mice, most ADAM17 was located in the ER. However, ADAM17 never became resistant to endo-H in iRhom2$^{-/-}$ mice, suggesting that it did not reach the golgi. Furin-cleavage of the pro-domain was also abolished in iRhom2$^{-/-}$ cells, with no mature ADAM17 seen iRhom2$^{-/-}$ macrophages, splenocytes or Bone Marrow Derived Macrophages (BMDM) (Adrain et al., 2012; McIlwain et al., 2012). Conversely, overexpression of iRhom2 in HEK293T cells increased the amount of ADAM17 exiting the ER, as more furin-cleaved ADAM17 was present in cell lysates, suggesting that this function of iRhom2 is conserved between humans and mice (Adrain et al., 2012). A mislocalisation of ADAM17 was also seen in iRhom2$^{-/-}$ BMDMs to 'granular vesicular compartments', shown by confocal microscopy and a count of the number of cells with a granular appearance (McIlwain et al., 2012).

Interaction between iRhom2 and ADAM17 was seen in macrophages and mouse embryonic fibroblasts (MEFs) (Adrain et al., 2012; McIlwain et al., 2012). Interaction with both full length and mature ADAM17 was seen in both studies, but the interaction with mature, cleaved ADAM17 was weaker (Adrain et al., 2012; McIlwain et al., 2012). No interaction was seen between iRhom2 and other ADAM family members (McIlwain et al., 2012). Catalytically active ADAM17 was also found in iRhom2$^{-/-}$ cells, showing that its production and folding is not affected by the absence of iRhom2 (Adrain et al., 2012). Overall, these findings suggest that iRhom2 is required for the trafficking of ADAM17

from the ER to the golgi, where it is cleaved into its active form before it travels to the cell surface (Adrain et al., 2012). iRhom2 in macrophages also contains golgi-specific (Endo-H resistant) glycans, suggesting that it is itself trafficked beyond the ER (Adrain et al., 2012).

As iRHOM1 also trafficks ADAM17 and regulates its activation (Christova et al., 2013), the wider tissue distribution of iRHOM1 may explain why the phenotype of iRhom2$^{-/-}$ mice is much less severe than that of iRhom1$^{-/-}$ or ADAM17$^{-/-}$ mice (McIlwain et al., 2012; Christova et al., 2013; Hosur et al., 2014). However, there is a clear reduction in mature ADAM17 levels in iRhom2$^{-/-}$ mice in a number of tissues (McIlwain et al., 2012), which may suggest that further iRHOM1 and iRHOM2 functions are involved in the pathogenesis associated with iRhom1 knock-out.

1.5.3 ADAM17 substrates

ADAM17 cleaves its substrates proximal to the cell membrane in a process known as ectodomain shedding. ADAM17, and its most closely related metalloproteinase ADAM10 (Kuzubian or Kuz in drosophila) mediate a number of processes via cleavage of a diverse range of substrates (Pruessmeyer and Ludwig, 2009). The balance of the shedding and signalling of ADAM17 substrates is critical, as dysregulation of substrates such as EGFR ligands and TNF-α may have pathological consequences such as inflammation and cancer. Loss of ADAM17 function results in severe consequences, both in mice and humans (Peschon et al., 1998; Blaydon et al., 2011). ADAM17 signalling is therefore tightly regulated, including its expression via micro-RNAs (Schlondorff et al., 2000; Adrain et al., 2012; McIlwain et al., 2012), and also by protease inhibitors at the cell surface, such as tissue inhibitor of metalloproteinase 3 (TIMP3) (Amour et al., 1998).

1.5.3.1 Tumour Necrosis Factor-α (TNF-α)

TNF-α is targeted in a number of therapies for inflammatory conditions such as rheumatoid arthritis (Moss et al., 2008; Arribas and Esselens, 2009). Shedding of TNF-α by ADAM17 is stimulated by LPS, which mimics infection, and by PKC activator phorbol myristate acetate (PMA) (Black et al., 1997; Moss et al., 1997; Rosendahl et al., 1997). A role for iRHOM2 was also shown in regulating ADAM17 in the pathogenesis of rheumatoid arthritis (Issuree et al. 2013). The TNF receptor (TNFR) is also shed by ADAM17, resulting in production of soluble TNFR (sTNFR); an important mechanism of regulating the TNF pathway through reducing availability of the receptor to circulating TNF-α. The sTNFR also binds to circulating TNF-α thus sequestering the inflammatory molecule form binding to the cell surface (Pruessmeyer and Ludwig, 2009).

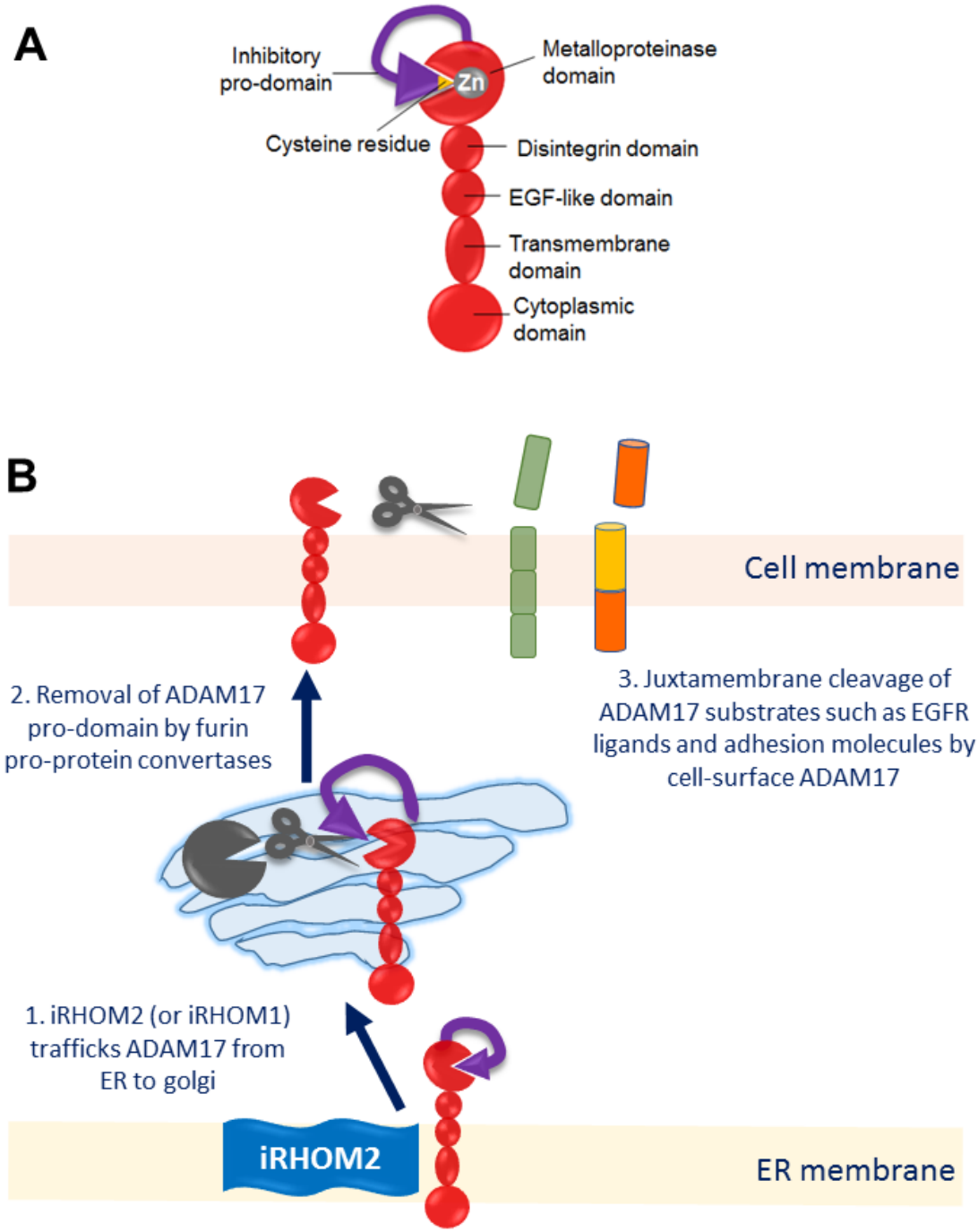

Figure 1.6. Activation of matrix metalloproteinase ADAM17 is dependent on iRHOM activity. The diagram shown in **A** indicates the structure of the ADAM17 protein, including the inhibitory pro-domain. The pro-domain contains a cysteine amino acid residue that interacts with the Zn^{2+} of the metalloproteinase domain. The diagram in **B** shows some of the steps required for ADAM17 processing and activation. iRHOM1 or 2 interact with ADAM17 in the ER, then facilitate its trafficking from the ER to the golgi, where its pro-domain is cleaved by furin-like pro-protein convertases. Cleavage of the protease activates the protein, allowing its trafficking to the cell surface where it cleaves substrates such as EGFR ligands and adhesion molecules.

1.5.3.2 Adhesion molecules

ADAM17-mediated shedding of adhesion molecules by ADAM17 may also result in regulation of pro-inflammatory effects, particularly in the vascular endothelium. Adhesion molecules shed by ADAM17 include vascular cell adhesion molecule 1 (VCAM1), JAM-A, and L-selectin. Shedding of L-selectin, for example, mediates recruitment of leukocytes to the blood vessel endothelium (Hafezi-Moghadam and Ley, 1999; Hafezi-Moghadam et al., 2001; Venturi et al., 2003). Desmosomal cadherin DSG2 is also a substrate of ADAM17, and appears to be cleaved in response to changes in EGFR signalling (Lorch et al., 2004; Bech-Serra et al., 2006). Another possible role for ADAM17 in cell-cell adhesion may include binding of ADAM17 to integrins via its disintegrin domain (Horiuchi et al., 2009).

1.5.3.3 EGFR ligands

EGFR ligands cleaved by ADAM17 include amphiregulin (AREG), transforming growth factor-α (TGF-α), heparin-binding EGF (HB-EGF), and epigen (Borrell-Pagès et al., 2003; Sahin et al., 2004; Sahin and Blobel, 2007; Pruessmeyer and Ludwig, 2009; Schneider and Wolf, 2009). ADAM10 is responsible for shedding of EGF itself, and also betacellulin (Sahin et al., 2004; Sanderson et al., 2005; Schneider and Wolf, 2009). Shedding of these EGFR ligands was shown to be induced by ligands for G-protein coupled receptors (GPCRs) (Gschwind et al., 2003; Hart et al., 2004).

Each ligand mediates different cellular effects in addition to spatio-temporal regulation of EGFR ligands through tissue-specific expression (Berasain and Avila, 2014). The ligands have different affinities for binding to the EGFR, for example, AREG has a lower affinity than EGF or TGF-α (Shoyab et al., 1989; Neelam et al., 1998). This seems to result in differential intensity and length of EGFR stimulation, which may affect the kinetics of downstream signalling pathways (Berasain and Avila, 2014): more transient EGFR activation, for example by AREG, may result in transient activation of downstream signalling components (Gilmore et al., 2008; Wilson et al., 2012), ultimately leading to differential biological effects (Andreu-Pérez et al., 2011). In support of this, TGF-α and HB-EGF stimulation resulted in different levels of phosphorylation and activation of the EGFR in Hep2 cells (Roepstorff et al., 2009).

1.5.3.3.1 Amphiregulin

AREG is synthesised as a type 1 transmembrane protein, known as pro-AREG, which is trafficked to the cell surface. AREG is expressed in a number of cell-types and tissues, and regulates cellular processes through binding to the EGFR, including proliferation, migration and apoptosis (Berasain and Avila, 2014). Mice lacking AREG have demonstrated a number of roles mediated by AREG, including mammary gland

development and aspects of the female reproductive system (Luetteke et al., 1999; Sternlicht and Sunnarborg, 2005; Schneider and Wolf, 2008), bone development (Qin et al., 2005), functions in the immune system (Zaiss et al., 2006), and also a role in epidermal homeostasis (Liu et al., 2008), including regulation of wound healing and production of antimicrobial peptides (Berasain and Avila, 2014).

The balance of AREG, and other growth factor signalling is critical, with its hyperactivity leading to diseases including asthma, where increased AREG levels were seen in airway epithelial cells and circulating basophils (Enomoto et al., 2009; Kim et al., 2009; Qi, et al., 2010; Hirota et al., 2012). Other conditions in which AREG has been implicated include rheumatoid arthritis (Yamane et al., 2008) and psoriasis (Cook et al., 1992, 2004; Bhagavathula et al., 2005). AREG dysregulation has also been seen in a wide range of cancers including liver, lung, breast, colon, and pancreatic cancer (e.g. Johnson et al. 1991; Funatomi et al. 1997; Hurbin et al. 2002; Shao et al. 2003; Willmarth & Ethier 2006).

1.5.3.3.2 Transforming Growth Factor Alpha

TGF-α was the second EGFR ligand to be discovered, and also has roles in a number of cellular processes, and a pathological role for TGF-α over-activity has been demonstrated, particularly in epithelial cancers (Singh and Coffey, 2014). The TGF-α knock-out mouse displays eye defects at birth and corneal inflammation, and most strikingly a wavy hair phenotype (Luetteke et al., 1993; Mann et al., 1993; Singh and Coffey, 2014). This phenotype resembles that of mice with mutations in the RTK domain of the EGFR (Luetteke et al., 1994), reflecting the role of TGF-α in EGFR signalling. A number of studies overexpressing TGF-α under a variety of promoters have demonstrated a role for TGF-α in mammary gland development, and in regulating cell proliferation, with overexpression of the EGFR ligand resulting in hyperplasia or metaplasia in tissues including the liver, stomach and gastrointestinal system (Jhappan et al., 1990; Matsui et al., 1990; Sandgren et al., 1990). Furthermore, a critical role for TGF-α in skin proliferation was demonstrated, by overexpression under the skin-specific K14 promoter, where psoriasis-like lesions, stunted hair growth and occasional papillomas were seen, indicating the oncogenic potential of overactive TGF-α signalling in the epidermis (Vassar and Fuchs, 1991; Singh and Coffey, 2014).

1.6 EGF receptor signalling

The role of ADAM17 in cleaving ligands for the EGFR makes it an important regulator of EGFR signalling. EGFR signalling is critical in development, growth and wound healing, and regulates a wide range of cellular signalling processes, including proliferation, migration, and cell survival (Jones and Rappoport, 2014). EGFR signalling is

dysregulated in many cancers (Salomon et al., 1995; Blobel, 2005), and also in TOC keratinocytes (Blaydon et al., 2012), consistent with a role for iRHOM2 in regulating EGFR signalling.

1.6.1 The EGFR / ErbB family of receptor tyrosine kinases

The EGFR, also known as ErbB1, is one of four members of the ErbB family of RTKs (Jones and Rappoport, 2014). The ErbB RTK structure contains an extracellular domain, single TMD and an intracellular domain. Soluble forms of EGFR lacking the TMD and intracellular domain (ICD) also exist, and can be biomarkers for cancer (Salomon et al., 1995; Jones and Rappoport, 2014). Following ligand stimulation, ErbB receptors at the plasma membrane form homo- or heterodimers (Tzahar et al., 1996; Olayioye et al., 2000). Each ICD then phosphorylates the other in a process of autophosphorylation (Zhang et al., 2006), resulting in activation of a wide range of downstream signalling cascades (Mendoza et al., 2011; Jones and Rappoport, 2014). Following activation and phosphorylation, the receptor is internalised by endocytosis and targeted for recycling or degradation, for example through ubiquitination (Eden et al., 2012; Jones and Rappoport, 2014).

The formation of homo- or hetero-dimers depends on the ligand, and on the complement of receptors expressed by a particular cell type. Each combination of receptors confers different properties to the RTK (Olayioye et al., 2000), providing one of the mechanisms of fine-tuning the signalling process depending on the specific situation (Jones and Rappoport, 2014). For example, in Hep2 laryngeal carcinoma cells, stimulation with TGF-α resulted in a weak phosphorylation and ubiquitination of EGFR, which resulted in complete recycling of the receptor, whereas HB-EGF or betacellulin stimulation caused persistant phosphorylation and ubiquitination of the receptor, leading to its degradation (Roepstorff et al., 2009). The method of internalisation may also be affected by the type of ligand, e.g. knock-down of clathrin inhibited internalisation of the receptor following stimulation with EGF, but caused only partial inhibition of the internalisation after stimulation with betacellulin or HB-EGF (Henriksen et al., 2013).

1.6.2 Signalling Pathways downstream of EGFR activation

Downstream signalling cascades activated by ligand binding to EGFR include MAPK, ERK, phosphoinositide-3-kinase (PI3K), Akt, Shc (p66), phospholipase C (PLC) γ, signal transducer adapter molecule (STAM), and Hrs, which may be activated through ligand binding at the plasma membrane (i.e. MAPK, ERK, Akt, Shc and PLCγ), or intracellularly following receptor internalisation (i.e. PI3K, ERk, Akt, STAM and Hrs) (Mendoza et al., 2011; Park et al., 2012; Jones and Rappoport, 2014). The downstream signalling may also affect the trafficking of EGFR, providing feedback signals to the pathway (Jones and

Rappoport, 2014). The MAPK-Erk, PI3K-Akt and PLCγ pathways are shown in figure 1.7. Other pathways include phosphorylation of caveolin, which regulates signalling through Grb7 (Lee et al., 2000), signal transducer and activator of transcription (STAT) signalling (Olayioye et al., 1999), and Src-focal adhesion kinase (FAK) signalling, which regulates cell migration (Biscardi et al., 1999; Ray et al., 2012).

1.6.2.1 MAPK/ERK signalling

A schematic of the major steps of ERK signalling are shown in (figure 1.7 A). ERK is a MAPK, and the major effector of the Ras oncoprotein, mediating and regulating cell survival, proliferation and motility (Mendoza et al., 2011). Ras belongs to the family of small GTPases, and stimulates ERK signalling via a cascade of kinase activity: MAPKKK, or MAP kinase kinase kinase (e.g. Raf), is a GTPase regulated kinase that phosphorylates MAPKK, or MAP kinase kinase (e.g. MEK), an intermediate kinase, which in turn phosphorylates a MAPK, or MAP kinase, i.e. ERK (Mendoza et al., 2011).

Following growth factor binding to EGFR/ErbB RTKs, dimerisation and autophosphorylation, the adaptor protein GRB2 (growth factor receptor-bound protein 2) and guanine nucleotide exchange factor SOS (son of sevenless) are recruited to the cell surface, promoting increased levels of GTP-bound Ras, which activates Raf, which phosphorylates and activates MEK, which phosphorylates and activates ERK. ERK then phosphorylates p90 S6 kinase (RSK), and activates transcription factors which lead to transcription of immediate early genes such as c-Fos and c-Myc. These in turn signal to up-regulate late responsive genes, which in combination with RSK activity, lead to cell survival, proliferation and motility (Mendoza et al., 2011).

Activated ERK also feeds back to earlier steps in the cascade to negatively regulate the pathway. Hormones, neurotransmitters or chemokines may bind to G-protein coupled receptors, leading to transactivation of ERK signalling via PKC and/or upstream RTKs. Phorbol esters, such as PMA which stimulates ADAM17 activity, mimic di-acyl glycerol (DAG), and bind and activate PKC. The signalling pathway may also be regulated through cross-talk with other signalling pathways such as the PI3K-Akt pathway (Mendoza et al., 2011).

1.6.2.2 The PI3K-Akt cell survival pathway

A PI3K-Akt cell-survival pathway (Rodrigues, 2000; Mendoza et al., 2011) schematic is shown in figure 1.7B. Growth factor stimulation of RTKs, for example by insulin and insulin-like growth factor 1 (IGF-1), leads to recruitment of insulin receptor substrate (IRS) and PI3K to the cell surface. PI3K then catalyses the conversion of phosphatidyl inositol biphosphate (PIP_2), to phosphatidyl inositol tri-phosphate (PIP_3) (Sengupta et al., 2010). In quiescent cells, the tumour suppressor PTEN maintains low levels of PIP_3

(Lemmon and Schlessinger, 2000). However, in the presence of PI3K, PIP_3 levels increase, leading to recruitment of the protein kinase Akt and PDK1 (3-phosphoinositide-dependent protein kinase 1) to the cell surface via pleckstrin homology domains (Sengupta et al., 2010; Mendoza et al., 2011). PDK1 activates Akt, which phosphorylates proteins needed for survival, proliferation and migration. Akt also phosphorylates tuberous sclerosis complex 2 (TSC2), a GTPase activating protein, or GAP. In quiescent cells, TSC2 and TSC1 maintain the GTPase RHEB (Ras homologue enriched in brain) in a primarily GDP-bound state. However, the phosphorylation of TSC2 releases this inhibition, allowing RHEB to activate mammalian target of rapamycin complex 1 (mTORC1) (Mendoza et al., 2011).

mTORC1 comprises mTOR (mammalian target of rapamycin), RAPTOR (regulatory associated protein of mTOR), and mammalian lethal with Sec13 protein 8 (mLST8). RAPTOR is a scaffolding protein, and tethers mTOR to substrates of mTORC1 (Alessi et al., 2009). mTORC1 phosphorylates and inhibits 4E-BP (eIF4E-binding protein; eIF4E is eukaryotic initiation factor binding protein 4E), preventing it from sequestering the eIF4E mRNA cap binding protein, which allows assembly of the cap-binding complex and initiation of translation (Mendoza et al., 2011). mTORC1 also phosphorylates S6K, resulting in its activation of transcription factors, ribosomal protein S6, RNA helicases, and other proteins involved in translation, initiation and elongation (Sengupta et al., 2010). The net effect of these phosphorylation steps is promotion of ribosomal biogenesis as well as translation of cell growth and division proteins such as c-Myc and cyclin D (Mendoza et al., 2011).

Akt may also be activated by mTORC2 (mammalian target of rapamycin complex 2), a second complex with which mTOR is associated, mTORC2 comprises mTOR, RICTOR (rapamycin-insensitive companion of mTOR), mLST8 and mSIN1 (mammalian stress-activated protein kinase interacting protein). RICTOR is a scaffolding protein that tethers mTOR to mTORC2 substrates, as RAPTOR does in mTORC1 (Alessi et al., 2009). mTORC2 activation is involved in cytoskeletal reorganisation, cell survival and lipid metabolism (Mendoza et al., 2011).

1.6.2.3 Cross-talk between the PI3K-Akt and Ras-MAPK/ERK pathways

The dynamics of the pathways downstream of EGFR/ErbB activation are regulated by a number of factors, including the amount of the growth factor, the expression and cell-surface localisation of the corresponding RTKs, and other RTK family members, and the co-expression of docking proteins (Lemmon and Schlessinger, 2000). Positive feed-forward loops, and negative feedback loops provide regulation within a pathway, for example the inhibitory action of ERK-mediated phosphorylation of Ras-GTP, Raf and

MEK (Dhillon et al., 2007). S6K also provides negative feedback in the PI3K-Akt pathway through inhibition of PIP_3 production by PI3K (Mendoza et al., 2011).

Cross-talk between the pathways may also include cross-inhibition, cross-activation, and pathway convergence. ERK, RSK, Akt and S6K, for example, phosphorylate a number of proteins involved in the core signalling pathways, in addition to their activation or inhibition of downstream effectors of processes such as cell survival, proliferation or motility (Mendoza et al., 2011).

1.6.2.4 PLCγ activation of PKC

EGFR signalling also affects Ca^{2+} signalling (Margolis 1989), which can occur via the PLCγ pathway (Jones and Rappoport, 2014). A brief schematic of this pathway is shown in figure 1.8 C, the pathway forms one component of the complex, multi-layered phospho-lipase signalling network (Park et al., 2012). Binding of an EGFR ligand to the EGFR results in recruitment and phosphorylation of PLCγ, leading to hydrolysis of PIP_2. This produces DAG and inositol triphosphate (IP_3). Lipid mediators such as IP_3 regulate a wide range of cellular processes, including actin cytoskeleton reorganisation, proliferation and migration (Suh et al. 2008; Wang et al. 2006; Park et al. 2012). DAG activates PKC (this effect is mimicked by PMA, another mechanism of cross-talk or feedback into the MAPK/ERK signalling pathway, while IP_3 leads to the release of intracellular Ca^{2+} and Ca^{2+} signalling (Park et al., 2012; Jones and Rappoport, 2014). Ca^{2+} is also required for the activation of PKC.

Ca^{2+} signalling is critical for a wide range of cellular processes, acting in part through activation of calmodulin, which acts on calcineurin (Park et al., 2012). Ultimately, this pathway results in activation of downstream proteins such as NFAT (Nuclear factor of activated T-cells) which provides a further mechanism of promoting cell growth and survival pathways (Park et al., 2012). DAG may also be phosphorylated by DAG kinase, producing the phospholipids phosphatidylserine, phosphatidylcholine and phosphatic acid, which ultimately result in production of prostaglandins and leukotrienes. The pathway also interacts with the Rho/ ROCK (Ras homologue/ Rho associated protein kinase) signalling pathway, which regulates cell migration via modulation of the actin cytoskeleton (Park et al., 2012).

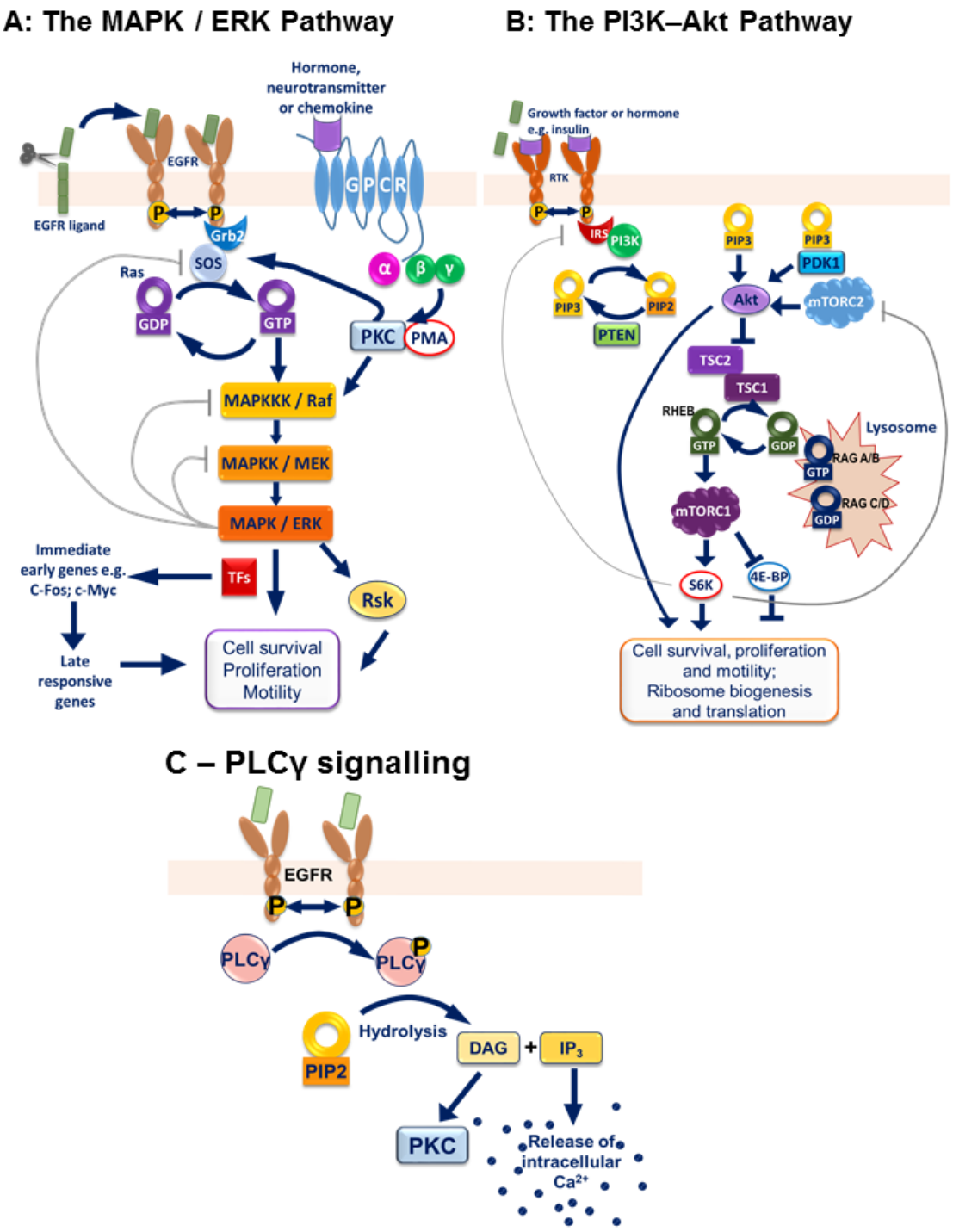

Figure 1.7 Three components of the EGFR signalling pathway. Binding of a ligand to EGFR, or another RTK, results in homo- or heterodimerisation of the RTK followed by autophosphorylation. An array of signalling cascades occur downstream of this event, with crosstalk and feedback occurring between the pathways. Three of the pathways are illustrated above: **A:** The MAPK/ERK pathway; **B:** PI3K-Akt signalling; and **C:** PLCγ signalling, which mediates intracellular Ca^{2+} release and signalling and activation of PKC, which may also transactivate the MAPK/ERK signalling pathway downstream of GPCR activation. Adapted from Mendoza et al 2011 and Jones and Rappaport 2014.

1.7 NOTCH signalling

NOTCH signalling is critical in a number of processes including development, regulation of proliferation, apoptosis and the cell cycle and in determining cell fate (Christian, 2012). NOTCH proteins were initially named after the wings of a female drosophila fly were described as being 'notched'; which turned out to result from a dominant haploinsufficiency in the *Notch* gene (Poulson, 1939; Greenwald, 2012). Knock-out of *Notch* in mice is embryonic lethal, and ablation of *Notch* in mice after birth leads to skin tumours and hair loss (Nicolas et al., 2003; Demehri et al., 2008). The complex and heterogeneous nature of NOTCH signalling in different tissue types, and the importance of NOTCH in processes such as development and differentiation, are illustrated by the wide range of LOF and GOF somatic mutations found in NOTCH in cancers from different tissues and organs (South, 2012), which will be discussed in Chapter 5.

1.7.1 NOTCH receptor Structure and Function

NOTCH family receptors are Type 1 transmembrane proteins with 29-36 extracellular EGF-like repeats, three LIN cysteine-rich repeats, a linking region between the intra- and extra-cellular regions of the protein (the negative regulatory region; NRR), then a cytoplasmic RAM23 (Rbp associated protein) domain, six ankyrin repeats and a PEST domain in the C-terminal (Bray, 2006; Katoh and Katoh, 2007). Ligands for the NOTCH receptor bind at EGF repeats 11 and 12. The RAM domain is important in binding of NOTCH to the CSL transcription factor in the nucleus, and also contains a nuclear localisation signal (Bray, 2006). The ankyrin repeats may also allow binding of the intracellular domain to transcription factors in the nucleus (Mosavi et al., 2004). The PEST domain is needed for rapid degradation of NOTCH to allow for fast regulation of this highly dynamic pathway.

Four NOTCH proteins have been identified in mammals (Ellisen et al., 1991; Weinmaster et al., 1991, 1992; Larsson et al., 1994; Li et al., 1998) and show specific cell-type specific expression patterns, for example NOTCH1 and NOTCH2 exhibit unique patterns of expression in human B-lineage cells (Bertrand et al., 2000). The four NOTCH proteins have different efficiencies at activating transcription (Bellavia et al., 2008), and induce different downstream genes (Bray, 2006; Ohashi et al., 2010; Wang, 2011). NOTCH3, for example, is important for HES5 induction in oesophageal differentiation (Ohashi et al., 2010), whereas HES1 is more predominant during epidermal differentiation (Blanpain et al., 2006). The different NOTCH isoforms can also work synergistically, for example, NOTCH1 and 3 co-ordinate in keratinocyte differentiation in the oesophagus (Ohashi et al., 2010). This provides considerable diversity in NOTCH signalling and downstream effects between different tissues (Bray, 2006).

1.7.2 The NOTCH Signalling Pathway

NOTCH signalling can be canonical (ligand-dependent) or non-canonical (ligand-independent), depending on the situation. In both cases, NOTCH activation is regulated by a number of processing steps (figure 1.8). Initially, the full-length NOTCH is cleaved by a furin-like convertase to remove the pro-domain (Logeat et al., 1998). This is known as S1 cleavage. NOTCH can then traffick to the cell surface where it is expressed as a heterodimer in canonical NOTCH signalling (Logeat et al., 1998). Whilst in the plasma membrane, NOTCH can be cleaved by ADAM10 or ADAM17 (S2 cleavage) (Brou et al., 2000; van Tetering et al., 2009), which allows for S3 cleavage by γ-secretase and release of the NOTCH intracellular domain (NICD) (Saxena et al., 2001; Okochi et al., 2002). The NICD then trafficks to the nucleus (Iso et al. 2003; Lubman et al. 2004), where it results in altered expression of a number of genes (Bray, 2006; Wang, 2011; Christian, 2012).

In the nucleus, the NICD binds to a complex which includes CSL (CBF-1, Su(H), LAG-1) and Mastermind (MAM) (Petcherski and Kimble, 2000; Wu et al., 2001). CSL is a DNA-binding protein complex, and MAM acts as a co-activator (Bray, 2006). In the absence of NOTCH, CSL proteins recruit co-repressor proteins to prevent inappropriate activation of NOTCH target genes (Bray, 2006). MAM also recruits histone acetylase p300, which promotes the assembly of initiation and elongation complexes and also controls the NICD turnover via the PEST domain (Fryer et al., 2004; Tsunematsu et al., 2004). NOTCH1 gene targets include E(spl)/HES class basic-helix-loop-helix (bHLH) proteins, which are well characterised NOTCH targets, although the response to NOTCH is dependent on the cell type and extracellular environment, and may be regulated through interactions with other pathways (Bray, 2006; Wang, 2011).

1.7.2.1 Canonical and non-canonical NOTCH signalling

Canonical NOTCH signalling is originated by binding of ligands on the signal-sending cell to NOTCH S1 on the signal receiving cell (Wang, 2011). Internalisation of the ligand then causes a conformational change in the NOTCH protein, allowing access of the ADAM metalloproteinases to the cleavage site at which S2 cleavage takes place (Brou et al., 2000; Wang, 2011). Canonical NOTCH signalling results in formation of the CSL-NICD complex. Activated by MAM family of co-activators, and leads to transcription of HES1, HES5, HES7, HEY1, HEY2 and HEYL genes, which encode the bHLH/orange domain transcriptional repressors (Bray, 2006). In development, canonical NOTCH signalling is important in regulating cell fate, which depends on whether a cell is a signal-sending cell expressing NOTCH ligands, or a signal receiving cell expressing the NOTCH receptor (Bray, 2006).

In non-canonical NOTCH signalling, alternative proteins may initiate NOTCH signalling in the absence of the typical ligands such as Delta-like and Jagged, with an increasing number of proteins are being discovered with roles in non-canonical NOTCH signalling (Wang, 2011). Some of these non-canonical ligands contain EGF repeat domains, similar to the canonical ligands, but others appear unrelated in structure (Wang, 2011). Mediators of non-canonical NOTCH signalling include thrombospondin 2 (Aho and Uitto, 1998; Meng et al., 2010), which is dependent on low density lipoprotein receptor-related protein 1 (LRP1) to mediate NOTCH signalling (Meng et al., 2010), and EGF-like domain 7 (EGFL7) (Schmidt et al., 2009), and Delta-Notch-like EGF-related receptor (Eiraku et al., 2005). In non-canonical signalling, the NICD may associate with CSL, NICD and Deltex instead of MAM. This results in amplification of a different group of target genes through MAG, a tissue-specific transcription factor, leading to terminal differentiation (Katoh and Katoh, 2007; Wang, 2011). The NOTCH NICD may also interact with p50 or c-Rcl in the nucleus to enhance the NF-κB pathway via p50 or c-Rcl (Shin et al., 2006).

1.7.3 Is S2 cleavage mediated by ADAM10 or ADAM17?

When NOTCH-S1 reaches the plasma membrane, its cleavage is regulated by the NRR, an internal inhibitory domain that prevents access of ADAM proteases to the S2 cleavage site (Bozkulak and Weinmaster, 2009; Gordon et al., 2009). A conformational change is required to reveal the S2 cleavage site and allow access by the ADAM proteases. This can be mediated by binding of ligands in neighbouring cells followed by endocytosis of the ligands, or by non-ligand mediated methods, which are less well understood but may result from changes in the cell microenvironment or through endocytosis of NOTCH, although this process is thought to be ADAM-independent (Bray, 2006; Wang, 2011; Christian, 2012).

Whether S2 cleavage of NOTCH is mediated by ADAM10 or ADAM17 has been debated (Christian, 2012). Deficiency in ADAM10 homologue Kuz in flies, or Adam10 in mouse, resulted in the same phenotype as Notch1 deficiency in these species, whilst a different phenotype is seen in ADAM17-deficient flies and mice (Sotillos et al., 1997; Lieber et al., 2002; Delwig and Rand, 2008), suggesting that ADAM10 is the major mediator of S2 proteolysis *in vivo,* particularly ligand-dependent cleavage (Delwig and Rand, 2008; Christian, 2012). Further, Adam10 is essential for Notch signalling in the cardiovascular system and epidermis in mouse (Weber et al., 2011), and Adam10 endothelial knock-out mice showed reduced expression of Notch1 target genes *Snail* (by 60 %) and Bmp2 (by 30%) (Zhang et al., 2010). It remains to determine whether the remaining 40 % expression was due to Notch cleavage by ADAM17 (Christian, 2012).

Bozkulak and Weinmeister (2009) showed that ADAM10 is needed for ligand-dependent Notch cleavage in mouse embryonic fibroblasts (MEFs) in the signal-receiving cell, and expression of ADAM17 does not rescue the phenotype, demonstrating that ADAM10 and not ADAM17 is the main metalloprotease in ligand-dependent Notch cleavage. This was confirmed by ADAM10 and ADAM17 siRNA knock-down in C2C12 cells, although the western blot shows much higher levels of ADAM10 processing than ADAM17 processing.

However, MEFs expressing a mutated form of ADAM17, lacking the Zinc-binding domain and therefore protease activity ($MEF^{\Delta Zn/\Delta Zn}$), showed a 2-3 fold reduction in CSL reporter activity compared with WT ADAM17 MEFs (Sotillos et al., 1997; Delwig and Rand, 2008). However, reporter activity was not reversed by either anti-ADAM17 siRNA, or overexpression of active ADAM17 in the $MEF^{\Delta Zn/\Delta Zn}$, so differences may be due to clonal variation in cell lines (Bozkulak and Weinmeister 2009). ADAM17 is likely to be the major mediator of ligand-independent NOTCH cleavage: cells treated with EDTA to destabilise the NRR showed increased CSL-reporter activity, which was reversed by metalloprotease inhibitor and siRNA against ADAM17 but not by ADAM10 siRNA (Bozkulak and Weinmaster, 2009).

Further supporting these findings, Kuz expression in cells lacking ADAM17 resulted in ligand-dependent Notch S2 cleavage, whereas high ADAM17 expression resulted in ligand-independent Notch cleavage in the same system (Sotillos et al., 1997; Lieber et al., 2002; Delwig and Rand, 2008).

1.7.4 Regulation of NOTCH

Other NOTCH regulators include Neuralised and Mindbomb in drosophila, and NEURL1/NEURL and NEURL2; MIB1 and MIB2 in humans and Mib1 and Mib2 in mouse (Katoh and Katoh, 2007). These proteins are E3-Ubiquitin Ligases, and are necessary for ligand activation at the cell surface (Lai, 2002; Le Borgne et al., 2005; Pitsouli and Delidakis, 2005; Bray, 2006). Other ubiquitin and E3 ligases that act on NOTCH include the Itch/NEDD4/Su(dx) family of HECT domain ubiquitin ligases, which may be involved in regulating NOTCH turnover and tend to negatively regulate NOTCH signalling (Qiu et al., 2000; Lai, 2002; Bray, 2006). Deltex is a RING finger protein and E3 ligase which positively regulates NOTCH in many tissues, including ligand-independent signalling (Matsuno et al., 1995; Hori et al., 2004; Bray, 2006). For example, in experiments with several genetically modified strains of yeast, Deltex was required for the presence of Notch in endocytic vesicles (Hori et al., 2004; Wilkin et al., 2004). In some cell types such as neurons, however, Deltex antagonises Notch (Sestan et al., 1999; Bray, 2006). Depending on a number of tissue and cell-dependent situation, the balance of negative

and positive NOTCH Regulators may determine the accessibility of NOTCH to ligands or γ-secretase, thus fine-tuning the rate of NOTCH signalling (Bray, 2006).

The EGF-like repeats on the NOTCH extracellular domain are sites for glycosylation. Glycosylation by enzymes such as those of the Fringe family is essential for correct NOTCH function, and allows for a number of combinations of glycosylated NOTCH to further regulate signalling. Removing *O-Fucosyltransferase,* the enzyme that adds the first fucose to Notch, from drosophila or mice results in phenotypes similar to those seen with loss of Notch signalling e.g. through loss of a member of the γ-secretase complex (Shi and Stanley, 2003). *O-Fucosyltransferase* is also important in the folding and trafficking of NOTCH (Okajima et al., 2005), and glycosylation regulates the affinity of ligands for the NOTCH EGF repeats: The presence of Fringe enhances Notch binding to DLL instead of serrate in dorsal drosophila wing cells (Johnston et al., 1997; Sasamura et al., 2003) and this effect is abrogated when the EGF-12 repeat is mutated – serrate can then bind to Notch even in the presence of Fringe.

1.7.4.1 NOTCH endocytosis and trafficking

Further regulation of the NOTCH pathway is mediated through NOTCH ligand endocytosis and trafficking, and therefore spatial regulation of the signalling components (Bray, 2006). A large fraction of NOTCH is found in the endocytic pathway, co-localising with small RAB GTPases RAB5 and RAB7 (Jékely and Rørth, 2003; Wilkin et al., 2004). The short half-life of the downstream transcription factor proteins such as CSL is also important to allow fast dynamics of the pathway, in addition to rapid NOTCH degradation via the PEST domain (Gupta-Rossi et al., 2001; Oberg et al., 2001; Wu et al., 2001; Bray, 2006). Further regulation may be mediated through regulation and modulation of the enzymes that cleave NOTCH, such as ADAM10 and ADAM17 and members of the γ-secretase complex.

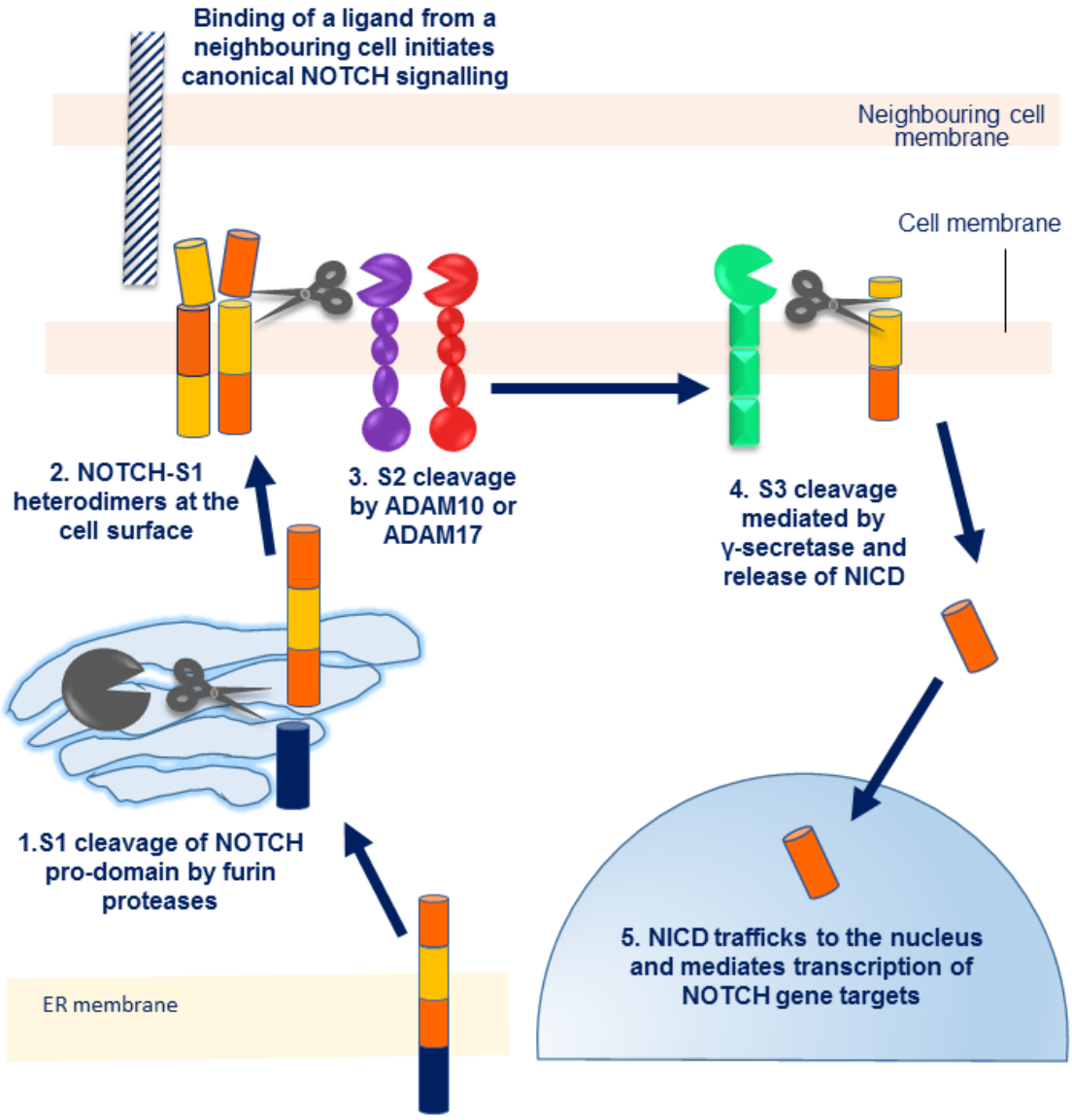

Figure 1.8 The NOTCH signalling pathway. A schematic showing the basic steps of the NOTCH signalling pathway, including the activation by cleavage of the pro-domain by furin proteases (S1 cleavage), followed by trafficking of heterodimeric NOTCH to the cell surface. At the cell surface, S2 cleavage is mediated by ADAM metalloproteinases ADAM10 and ADAM17, often following NOTCH binding to a ligand on a neighbouring cell, but ligand independent signalling is also possible. ADAM10 appears to be the predominant metalloproteinase for ligand-dependent signalling. Once S2 cleavage has taken place, S3 cleavage is mediated by γ-secretases, which release the intracellular domain (NICD). This can then translocate to the nucleus and regulate the expression of target genes. NOTCH signalling is tightly regulated, and the NICD is rapidly degraded after activation via its PEST domain (Bray, 2006; Wang, 2011; Christian, 2012).

1.7.5 NOTCH signalling in the skin and gastrointestinal tract

The multiple functions of NOTCH include self-renewal of stem cells, cell-fate determination of progenitor cells and initiating terminal differentiation of proliferating cells (Lowell et al., 2000; Nickoloff et al., 2002; Yamamoto et al., 2003; Blanpain et al., 2006; Ohashi et al., 2010). For example, activation of NOTCH1 signalling in the skin promotes exit of keratinocytes from the cell cycle and entry into the differentiation program (Rangarajan et al., 2001). Differences in the differentiation of different tissues, such as the skin and oesophagus, is in part mediated by tissue-specific expression of NOTCH and Delta-like and Jagged ligands and through interactions with other signalling pathways such as the EGFR pathway (Blanpain et al., 2006; Estrach et al., 2008; Ohashi et al., 2010; Nowell and Radtke, 2013).

1.7.5.1 NOTCH signalling in the epidermis

In the epidermis, NOTCH expression is highest in the suprabasal spinous and granular layers, where it appears to mediate both the initiation and maintenance of differentiation (Blanpain et al., 2006; Wang et al., 2008; Nowell and Radtke, 2013). Expression of NOTCH in specific cell clusters of the basal layer has also been identified (Lowell et al., 2000), suggesting a role for NOTCH in regulating stem cell homeostasis. Expression has been seen of NOTCH1-4, and the ligands Jagged-1 and Jagged-2; expression of Delta-like 1 has also been noted in stem cells in the basal layer, where it appears to negatively regulate NOTCH in stem cells, preventing early entry into the differentiation pathway whilst promoting differentiation of neighbouring cells (Lowell et al., 2000; Estrach et al., 2008). Notch1 appears to be the major Notch isoform in murine epidermis, as knock-out of Notch1 had severe epidermal consequences that were only slightly compensated by the Notch2-4 isoforms (Nicolas et al., 2003; Vauclair et al., 2005). A role for NOTCH has also been implicated in inflammatory skin conditions such as atopic dermatitis (Ambler and Watt, 2010; Ziegler and Artis, 2010; Nowell and Radtke, 2013).

In the basal layer, proliferation is driven by the activity of transcription factor p63, and also mediated by signalling pathways including the EGFR pathway (Nowell and Radtke, 2013). EGFR signalling promotes Activator protein 1 (AP-1) transcription factor activity via C-Jun, and AP-1 and c-Jun negatively regulate NOTCH and p53 in these conditions. Indeed, overactivity of EGFR in the suprabasal layers impairs NOTCH activity and differentiation (Kolev et al., 2008). The balance of EGFR signalling appears to be regulated by the transcription factor ctip2, which positively regulates either EGFR or NOTCH signalling depending on the Ca^{2+} concentration (Zhang et al., 2012). The AP-1 and NOTCH pathways appear to show reciprocal antagonism, as knock-out of Adam17 in mouse resulted in high AP-1 activity and abnormalities associated with loss of Notch (Guinea-viniegra et al., 2012), which also further demonstrates the importance of

ADAM17 in skin homeostasis and differentiation, and may suggest a role for the NOTCH pathway in the epidermis (Nowell and Radtke, 2013).

Following initiation of NOTCH signalling, which appears to be mediated predominantly by Jagged-1 (Estrach et al., 2006), the NOTCH pathway negatively regulates AP-1 (as just described) and also p63. NOTCH activity induces expression of the cell cycle inhibitor p21/CDKN1A (Rangarajan et al., 2001; Nguyen et al., 2006), which provides further inhibition of p63-induced proliferation. At the same time, NOTCH up-regulates or activates retinoic acid signalling, factors such as interferon response factor 6 (IRF6), and transcription of Hes/Hey transcriptional repressor proteins, in particular HES1 (Vauclair et al., 2005; Collins and Watt, 2008; Moriyama et al., 2008). In combination, these pathways promote differentiation in combination with other differentiation-promoting pathways (Nowell and Radtke, 2013)

1.7.5.2 NOTCH signalling in oesophageal differentiation

The oesophagus is also a stratified squamous epithelium, the structure of which will be discussed further in the next section. Oesophageal cells follow a similar pattern of differentiation to epidermal keratinocytes, which is dependent on NOTCH1 and NOTCH3 (Katoh and Katoh, 2007; Ohashi et al., 2010). NOTCH3 induction was essential for the differentiation of oesophageal keratinocytes, and downstream NOTCH targets were activated following Ca^{2+}-induced differentiation of telomerase-immortalised, non-transformed oesophageal keratinocyte cell line EPC2-hTERT: Increased luciferase reporter activity of CSL was seen, in addition to increased HES5 mRNA and increased levels of the differentiation markers involucrin and cytokeratin 13 (Ohashi et al., 2010). In contrast to the epidermis, where HES1 appears to be a major downstream mediator of NOTCH activation, in the oesophagus, HES5 appears to be the major mediator (Ohashi et al., 2010). In the *in vitro* 3D model of oesophageal differentiation, NOTCH3 expression was induced by the NOTCH1 NICD (Ohashi et al., 2010), suggesting that differentiation is initiated by NOTCH1, and that subsequent induction of NOTCH3 follows.

1.8 The Oesophagus

The morphology of normal oesophagus consists of three main layers – the basal layer, prickle cell layer, and superficial or functional layer (figure 1.9) (Hopwood, 1991; Kuo and Urma, 2006). The basal layer is clearly defined, comprising columnar-shaped basophilic cells, usually making up 10-15 % of the thickness of the epithelium. As in the skin, the basal layer of the oesophagus is important in regeneration, with a number of dividing cells scattered throughout the layer, and a few argyrophil cells, the number varying between individuals (Hopwood, 1991).

Above the basal layer is the prickle cell layer, and above that the superficial or functional cell layer. These two layers are difficult to distinguish in paraffin-embedded tissue sections such as those shown in chapter 5. The cells of the functional layer are flatter than those of the prickle cell layer, and the prickle cell layer has wide spaces between the cells with more desmosomes than the functional layer, or the basal layer which has a number of hemidesmosomes (Logan et al., 1978; Hopwood, 1991; Kuo and Urma, 2006).

The oesophagus has a distinct pattern of keratins in each layer, similar to the epidermis, but the pattern of keratin expression is different to that seen in the epidermis (Banks Schlegel and Harris, 1983). The morphology can depend on the depth at which the biopsy was taken, as the cells are differentially affected by acid reflux, which can cause the cells to become leakier and less electron dense. Oesophageal submucosal glands can be seen in regions of connective tissue. These glands contain mucous and serous secreting cells and myo-epithelial cells which are similar to salivary glands. In addition, a number of papillae carrying blood vessels project into the lower half of the oesophagus. As in the skin, a number of infiltrating cells can be seen by electron microscopy including lymphocytes, granulocytes, and langerhans cells (Yassin and Toner, 1976).

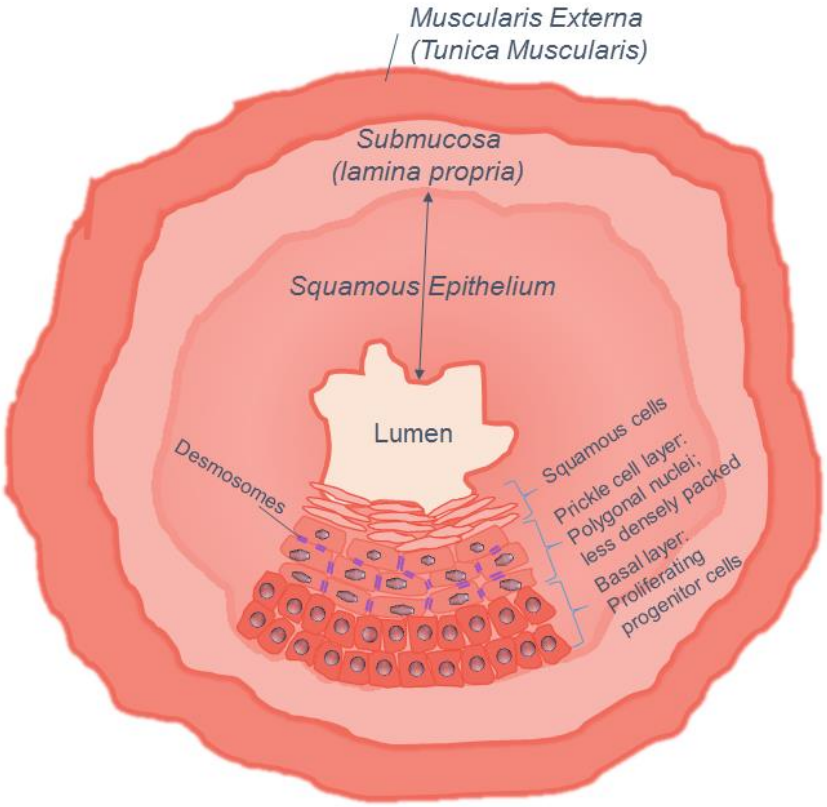

Figure 1.9. The structure of the oesophagus. The oesophagus comprises three main layers: the *muscularis externa*, or *tunica muscularis*, the muscular, functional layer of the oesophagus; the submucosa, or *lamina propria*, which comprises loosely packed connective tissue, focal lymphocytes can be found in this layer; and the mucosal layer, a stratified squamous epithelium that surrounds the oesophageal lumen. The squamous layer cells migrate from the basal layer to the squamous layer at the oesophageal lumen in a process of terminal differentiation, similar to the process that occurs in the skin. The prickle cell layer contains a large number of desmosomes (shown in purple). As cells progress through the differentiation pathway, they gain a flatter shape and eventually form the flattened, squamous cells found at the oesophageal lumen.

1. www.proteinatlas.org/dictionary/normal/esophagus+1, accessed 10.8.2014

2. Kuo and Urma 2006, *GI Motility Online* PART 1: Oral cavity, pharynx and oesophagus, http://www.nature.com/gimo/contents/pt1/full/gimo6.html, accessed 5.9.2014.

1.9 Oesophageal Cancer

Oesophageal cancer is currently one of most common cancers and causes of cancer mortality. According to estimates of global cancer incidence by the Globacan database in 2008 and 2012 (http://globocan.iarc.fr/Pages/fact_sheets_cancer.aspx accessed 15/2/14), oesophageal cancer is the 8th most common cancer worldwide, and the 6th most common cause of cancer-related deaths internationally (4.9 % worldwide) (Pennathur et al., 2013). In the UK in 2011, oesophageal cancer was the 8th most common cancer in men, and 14th most common in women (CRUK, http://publications.cancerresearchuk.org/downloads/product/CS_REPORT_INCIDENCE.pdf accessed 03.2014; office for national statistics, accessed 09.2014: http://www.ons.gov.uk/ons/rel/vsob1/cancer-statistics-registrations--england--series-mb1-/no--43--2012/index.html) and in 2012 was the 7th most common cancer in men and 14th most common in women worldwide, based on age-standardised incidence rates which adjust for variations in the populations' age structure (GLOBOCAN 2012, http://globocan.iarc.fr/Pages/fact_sheets_cancer.aspx accessed 03.2014).

Areas with higher levels of deprivation show highest incidence of oesophageal cancer across the world and in the UK (GLOBOCAN 2012 and 2008; (Bray et al., 2013; Ferlay et al., 2014). Risk factors include alcohol, tobacco and exposure to nitrosamines (Pennathur et al., 2013). Mortality rates of oesophageal cancer are particularly high, with a mortality to incidence ratio of 0.88, and a 5-year survival of approximately 13 % (CRUK website, accessed 02.2014). A particular challenge in oesophageal cancer is early detection, with many cases being diagnosed at an advanced stage, making treatment difficult. Furthermore, metastasis occurs early in oesophageal cancer development even with the presence of a superficial primary tumour (Altorki et al., 2008; Pennathur et al., 2009).

1.9.1 Oesophageal Squamous Cell Carcinoma

There are two major forms of oesophageal cancer: oesophageal adenocarcinoma, which originates in mucous-producing glandular cells lower in the oesophagus; and OSCC, which originates in the squamous cells lining the oesophagus. Together, these forms account for over 90 % of oesophageal cancer cases worldwide http://www.clevelandclinicmeded.com/medicalpubs/diseasemanagement/hematology-oncology/esophageal-cancer/; CRUK; accessed 03.2014). OSCC is usually found in the upper two layers of the oesophagus. A change in epidemiology of OSCC compared with adenocarcinoma has been seen, with a large increase in adenocarcinoma in the UK and US. Nevertheless, OSCC accounted for about 28 % of oesophageal cancer cases in the UK(http://www.cancerresearchuk.org/cancer-info/cancerstats/types/oesophagus/incide

nce/uk-esophageal-cancer-incidence-statistics#source1; 2008-2010;accessed 03.2014) and still accounts for a high proportion of cases worldwide (Pennathur et al., 2009).

The initial stages of OSCC development at a histological level are described in Wang et al (2005): In the normal oesophagus, the basal layer accounts for less than 15 % of the thickness of the epithelium. With the onset of oesophagitis, infiltration of neutrophils and eusinophils is seen, with thickening of the basal layer to more than 15 % of the epithelia, but the cells seen are typical for the region of the oesophagus. With the onset of dysplasia, atypical cells are seen, firstly in the lower third of the epithelium with mild dysplasia, then progressing to the lower two-thirds of the epithelium in moderate dysplasia and finally covering all thirds of the epithelium, but not reaching full thickness in severe dysplasia. Carcinoma *in situ* is diagnosed when a full-thickness spread of atypical cells is seen throughout the oesophageal epithelium, without any metastasis or lymph node spread (Kuwano et al., 2003; Wang et al., 2005). Squamous cell carcinoma is diagnosed with invasion of the cells into the lamina propria (Wang et al., 2005).

Lymph node metastasis is often seen early in the spread of OSCC due to the high number of lymphatic vessels found in the oesophagus (Kuwano et al., 2003; Pennathur et al., 2013). Other features of OSCC morphology can include glandular differentiation within the tumours, which is not normally seen in the oesophagus (Kuwano et al., 2003). Further, it is possible for multiple primary OSCC tumours to develop.

Genetic predisposition has previously been implicated in OSCC development, for example mutations in enzymes that metabolise alcohol such as aldehyde dehydrogenase-2 (*ALDH2*) and alcohol dehydrogenase 2 (*ADH2*) may increase OSCC risk in Japan and China (Yokoyama et al., 1996; Pennathur et al., 2013). However, iRHOM2 represents the first highly penetrant gene associated with OSCC, with up to a 95 % risk of developing the cancer associated with the condition (Stevens et al., 1996). iRHOM2 and other Rhomboid proteins and proteases are therefore of interest as targets for future research into oesophageal cancer and other forms of cancer. A role for iRHOM1 has also been demonstrated in breast cancer and head and neck SCC (HNSCC) (Yan et al., 2008; Zou et al., 2009; Zhou et al., 2014), and the ADAM17 and NOTCH pathways mediate pathogenesis of a range of cancers.

1.10 ADAM17 in Cancer

There are many examples of ADAM17 dysregulation in a number of cancer types. ADAM17 overexpression in non-small-cell lung cancer (NSCLC) was associated with tumour grade, size, lymph node metastasis and overall poor patient survival (Ni et al., 2013), and Warneke et al (2013) reported poor prognosis in gastric cancer patients associated with the EpCam pathway, in which EpCam is cleaved by ADAM17. Overexpression of ADAM17 has also been reported in ovarian, prostate, breast (Lendeckel et al., 2005; Sinnathamby et al., 2011; Narita et al., 2012), pancreatic (Ringel et al., 2006), colorectal, gastrointestinal (Blanchot-Jossic et al., 2005; Nakagawa et al., 2009), non-small-cell lung cancer (Zhou et al., 2006) and head and neck cancer (Stokes et al., 2010; Kornfeld et al., 2011). Normal colony shape and cell polarity were restored in breast cancer cells following ADAM17 shRNA treatment, along with reduced AREG and TGF-α secretion (Kenny and Bissell, 2007). Kenny and Bissell (2007) also showed that high levels of ADAM17 and TGF-α were indicators of poor survival in breast cancer patients.

1.11 NOTCH1 signalling in cancer

A wide range of somatic mutations in NOTCH in cancer illustrate the complex and heterogeneous nature of NOTCH signalling in different tissue types and the importance of NOTCH in processes such as development and differentiation. Mutations can be LOF or GOF in nature depending on the tissue type (Wang, 2011; South, 2012). While knock-out or mutation of Notch 1 or 2 in mice is embryonic lethal (Swiatek et al., 1994; Conlon, Reaume and Rossant, 1995; Hamada et al., 1999), ablation of Notch in mice after birth leads to hair loss, skin tumours susceptibility to chemical carcinogenesis (Nicolas et al., 2003; Demehri et al., 2008). Total epidermal knock-out of Notch caused impaired barrier formation leading to systemic B-lympheroproliferative disease and death (Demehri et al., 2008).

The first NOTCH1 mutations identified in cancer were found in T-cell acute lymphoblastic leukaemia (T-ALL), where over 50 % of patients have mutations in the NRR or PEST domains leading to increased NOTCH activity and reduced protein turnover (Ellisen et al., 1991; Weng et al., 2004). Other cancers resulting from activating NOTCH1 mutations include chronic lymphocytic leukemia and diffuse large B-cell lymphoma (Di Ianni et al., 2009; S. Lee et al., 2009; Fabbri et al., 2011; Puente et al., 2011). Furthermore, NOTCH1 mutations were associated with worse prognosis in B-Cell chronic Lymphocytic Leukaemia (B-CLL) (Sportoletti et al., 2010; Fabbri et al., 2011; Rasi et al., 2012). Activating mutations result in up-regulation of NOTCH1 target genes such as HES1,

which prevents transcription of the tumour suppressor gene PTEN (Malecki et al., 2006; Psyrri et al., 2013). In a comparison of activating NOTCH mutations on CSL reporter activity, NOTCH mutants had significantly higher reporter activity than wild type (WT) NOTCH, but there was variation between mutants. Processing of the mutants showed some dependency on ADAM10, but ADAM17 appeared to be the major metalloprotease in processing GOF-mutant NOTCH in T-ALL (Bozkulak and Weinmaster, 2009; van Tetering et al., 2009).

While in these situations NOTCH1 has a tumour promoting function, in other tissues NOTCH1 acts as a tumour suppressor (Nicolas et al., 2003; Demehri et al., 2008; South, 2012), with inactivating mutations found in cutaneous squamous cell carcinoma (SCC), lung cancer (Wang, 2011; South et al., 2014) and HNSCC (Agrawal et al., 2011; Stransky et al., 2011). Inactivating mutations were mostly found in the EGF-repeat, ankyrin-repeat or heterodimerization domains or caused truncations of the protein, resulting in disrupted ligand binding and inactivation of the signalling cascade (Agrawal et al., 2011; Wang, 2011). Further, inhibiting NOTCH signalling with γ-secretase inhibitors resulted in metaplasia in mouse goblet cells (Menke et al., 2010).

Notch signalling has also been implicated in oesophageal cancer development: 40 % of 3-month old transgenic mice expressing dominant-negative MAML1 (DN-MAML1; an inhibitor of Notch signalling), showed oesophageal basal cell hyperplasia/dysplasia, with a significantly higher Ki67 labelling index compared to the DNMAML1f/f and K14Cre generations of the mice. There was a reduction in involucrin staining and loss of filaggrin in keratohyalin granules in addition to loss of nuclear Notch3 staining (Ohashi et al., 2010) suggesting altered differentiation. In addition, high NOTCH1 expression is a predictor of poor prognosis in OSCC (Ogawa et al., 2013) and is implicated in resistance to 5-FU treatment in OSCC cell line KYSE70 (Liu et al., 2013). Inactivating mutations were seen in 21 % of OSCCs but not in oesophageal adenocarcinomas (Agrawal et al., 2012).

1.12 Aims

The inactive rhomboids are relatively recently discovered proteins, with little known about their physiological roles. As mutations in *RHBDF2,* the gene encoding iRHOM2, affect the skin in TOC, this work firstly aims to investigate the expression and localisation of iRHOM2 in the epidermis. Secondly, initial investigation into the signalling function of iRHOM2 in epidermal keratinocytes will be performed, particularly focussing on iRHOM2-mediated regulation of ADAM17 and EGF signalling and some potential downstream pathways. As *RHBDF2/*iRHOM2 is the first gene associated with highly penetrant inherited OSCC and as iRHOM2 regulates ADAM17 and EGFR signalling, the localisation and expression of iRHOM2 in OSCC and other SCCs will be investigated to see whether iRHOM2 dysregulation may be involved in the pathogenesis of sporadic cancers.

Chapter 2: Materials and Methods

Chapter 2: Materials and Methods

2.1 Cell Culture

Keratinocyte cell lines, isolated from control, unaffected, skin (K17, NEB1) and TOC patient skin (TYLK1 and TYLK2), and immortalised with Human-papilloma virus (HPV), were cultured in Dulbecco's Modified Eagle Medium (DMEM, Sigma-Aldrich, Gillingham, UK) supplemented with: Penicillin/Streptomycin (P/S; 1 %); L-glutamine (1 %; both from Invitrogen, Gillingham, UK); 10 % Foetal Calf Serum (FCS; Biosera, Boussens, France); and RM+ supplement (1 %; see below). Cells were cultured in a humidified incubator with 5 % CO_2 in air at 37°C.

TYLK1 and TYLK2 cells were isolated by Dr Andrew South, University of Dundee, as described in Blaydon et al., (2012): After gaining appropriate consent, primary keratinocyte cells were isolated from biopsies of affected papular skin from male (TYLK1) and female (TYLK2) tylosis patients. The primary keratinocytes were grown in the presence of a γ-irradiated 3T3 feeder-cell layer. Cells were immortalized with HPV16 (E6/E7) and passaged until they could grow independently of the feeder cell layer.

HeLa and HEK-293T cells were cultured in DMEM supplemented with 10 % FCS, 1 % L-glutamine and 1 % P/S and cultured in a humidified incubator at 5 % CO_2 in air at 37°C. The OSCC cell lines TE-4, TE-8, KYSE270 and KYSE410 were cultured in RPMI 1640 medium with 1 % L-glutamine and 10 % FCS at 37°C at 5 % CO_2 in air. HNSCC cell lines were kindly provided by Helena Emich and Dr Adrian Biddle (Centre for Cutaneous Research (CCR), Blizard Institute, QMUL), and used only to make protein lysates.

100X RM+ stock contains: EGF (1 µg/ml); transferrin (500 µg/ml); hydrocortisone (40 µg/ml); cholera toxin (84 ng/ml); insulin (500 µg/ml); L4 supplement (1.3 µg/ml). L4 was prepared from 3,3',5-Triiodo-L-thyronine sodium salt. All ingredients for RM+ were purchased from Sigma-Aldrich except EGF, which was purchased from ABD Serotec, (Kidlington, UK). Where cells were cultured in the absence of exogenous EGF, RM- supplement was included instead. RM- contains the same ingredients as RM+, but the EGF is omitted. All other cell culture equipment and consumables were purchased from Fisher Scientific (Loughborough, UK).

2.1.1 Cell Passaging

When cells reached approximately 90 % confluency, the medium was removed, cells washed with Phosphate-Buffered Saline (PBS; Sigma-Aldrich), and treated with trypsin-EDTA (Invitrogen) in PBS until all cells detached from the flask: 1X concentration (0.05 %) for HeLa, HEK293T cells and OSCC Cell lines; 3X concentration (0.15 %) for

cutaneous keratinocytes. The trypsin reaction was quenched with serum-containing medium, the cells transferred to a 15 ml falcon tube, and centrifuged at 1200 rpm for 5 min to pellet cells and allow complete removal of the trypsin. The supernatant was removed by aspiration, and the cells re-suspended in fresh medium. The required amount of cells was then seeded into a new flask with fresh medium. For example, for a 1 in 10 split, $1/10^{th}$ of the cell suspension was transferred into the new flask. The 'split', or the proportion of cells transferred to the new flask, was adjusted depending on the cell line and the growth rate of the cells.

2.2 Transfection of cell lines

2.2.1 Overexpression of DNA constructs

Overexpression of DNA constructs was performed with Fugene 6 Transfection reagent (Roche, Welwyn Garden City, UK). Prior to transfection, 0.5×10^5 cells were plated per well of a 12-well cell culture dish containing coverslips for immunofluorescence experiments, or at 1.8×10^5 cells per well of a 6-well plate to make protein lysates. Transfections of HeLa and HEK-293T cells were carried out the following day and transfection of keratinocytes was carried out on the same day.

Transfection complexes were formed in polystyrene tubes, as polypropylene decreases the activity of the Fugene 6 reagent. Per well of a 12-well dish, the reaction was set up as follows: 50 µl PBS was added to two separate tubes. 500 ng DNA was added to one tube and 1.5 µl Fugene added to the other. This was incubated for 5 min, and the DNA mixture transferred to the Fugene mixture and mixed by flicking. Reactions were incubated at room temperature for at least 20 min, then the DNA-fugene mixture added to the cells in a drop-wise manner. The cell culture medium was changed 6-24 h after transfection as the Fugene reagent can be toxic to the cells. This protocol was scaled up proportionately for transfection in a 6-well plate. Cells were used for experiments 48 h after transfection unless otherwise stated.

2.2.2. siRNA Transfections

Knock-down of *RHBDF2* (iRHOM2) and ADAM17 was carried out using OnTarget plus SmartPool siRNA and Dharmafect transfection reagent (Dharmacon, Fisher Thermoscientific). All work was carried out in RNase free sterile conditions with surfaces cleaned with RNaseZap® beforehand (Ambion-Invitrogen, Paisley, UK). siRNA was resuspended to a concentration of 20 µM in siRNA resuspension buffer (Fisher Thermoscientific) according to the manufacturer's instructions; aliquots were stored at -80°C.

Cells were plated into 6-well dishes at a density of 2 x 10^5 cells per well one day prior to transfection. For each well, 6 µl Dharmafect was added to 194 µl serum and antibiotic-free medium in a polystyrene transfection tube. In a separate tube, 10 µl siRNA was added to 190 µl serum and antibiotic free medium for each well of cells. These mixtures were incubated for 5 min at room temperature, and then the diluted siRNA was added to the Dharmafect mixture. This was incubated for 20 min at room temperature.

Antibiotic-free medium (1.6 ml; containing FCS) was added to the siRNA-Dharmafect complex, mixed by inverting, and added to the cells (2 ml per well). The transfection was left for a maximum of 24 h before medium was changed to complete medium containing antibiotics. It is important to change the medium within 24 h as the Dharmafect reagent can be toxic to the cells.

2.3 Staining

2.3.1 Immunocytochemistry (ICC)

Cells were seeded onto coverslips in 12-well dishes and fixed for immunofluorescence staining once they had reached the desired level of confluency. In experiments involving transient overexpression of plasmid DNA, cells were transfected as described above, and fixed after approximately 48 h or when expression of the construct was optimal.

Cells were fixed with either 4 % paraformaldehyde (PFA) in PBS for 30 min at room temperature, or in ice-cold methanol-acetone (1:1 mixture) at -20°C for 5 min. The following steps were all carried out at room temperature: cells were permeabilised with triton X100 (0.1 %) in PBS for 10 min, then blocked with Bovine Serum Albumin (BSA; 3 %) for 30 min. Cells were incubated with primary antibody diluted in the blocking solution for 1 h at room temperature as indicated in Table 2.1. After the primary antibody incubation, cells were washed at least 3X in PBS, and then incubated for 1 h at room temperature with the appropriate AlexaFluor® fluorescently-conjugated secondary antibody (Invitrogen, UK) diluted 1 in 1000 in PBS. The secondary antibody targets the immunoglobulins of the host species of the primary antibody. The fluorescence conjugates used were AlexaFluor® 488, which is shown in the green channel; and AlexaFluor® 568, which shows in the red channel.

Following incubation with the secondary antibody, the cells were washed thoroughly in PBS (at least 4 X 3 min), with 100 ng/ml 4',6-diamidino-2-phenylindole (DAPI) included in the second wash. Coverslips were then mounted onto slides with Shandon Immumount (Thermoscientific). Slides were left to set at 4°C, and then imaged on the Zeiss 510 Meta Confocal or the Zeiss LSM710 Meta Confocal microscope, as indicated.

2.3.2 Immunohistochemistry (IHC)

Frozen skin sections were air-dried for 30-60 min. In some cases, sections were fixed with ice-cold methanol-acetone (MeAc; 1:1 mixture), which was added to the sections after air-drying and left to air-dry for approximately another 20 min. For staining with goat anti-EphA2 antibody, sections were fixed for 10 min with 4 % PFA in PBS at the end of the air-drying step. For further details of the conditions used for individual antibodies please see Table 2.1.

Following drying and fixing, sections were permeabilised for 10 min in triton X100 (0.1 %), and blocked for 20 min in 3 % BSA in PBS. The primary antibody was diluted in the blocking solution and applied to the sections for an overnight incubation at 4°C. The following day, sections were washed in PBS, and then incubated for 1 h at room temperature with the appropriate Alexafluor® secondary antibody, diluted 1 in 800 in PBS unless otherwise indicated. The sections were washed at least 3X with PBS, with DAPI nuclear stain (100 ng/ml) included in the second wash. Coverslips were mounted with Shandon Immumount mounting medium (Thermoscientific).

2.3.3 Co-localisation

For co-localisation experiments, the primary antibodies used were from two different species to ensure that the antibodies do not bind to each other and give a false-positive signal. The secondary antibodies, AlexaFluor® 488 and AlexaFluor® 568 had non-overlapping emission spectra to minimise bleed-through between the channels and a false-positive result. In each experiment, the following control experiments were included:

i) Negative control treated only with rabbit secondary antibody, negative control treated with only mouse secondary, and negative control treated with both secondary antibodies to detect non-specific binding of the secondary antibodies to the section or blocking solution.

ii) Controls with each primary antibody stained individually and treated with the secondary targeting the host of that primary antibody only, which were used when choosing microscope settings, which were adjusted to avoid bleed-through.

iii) Controls with each primary antibody stained individually and treated with both secondary antibodies to ensure the secondary antibodies are binding only to their target antibody, and that there is no false-positive signal resulting from non-specific binding of one secondary antibody to the wrong primary antibody.

Protein	Species	Company	Staining Conditions	Western Blot Conditions
β-catenin	Mouse	BD Transduction Labs	MeAc fix, 1in100 IHC	n/a
ADAM17 - pro	Rabbit	AbCam	n/a	10%, Milk block, 1in1000
ADAM17 - total	Rabbit	AbCam	n/a	10%, Milk block, 1in2000
Anti-GFP	Mouse	AbCam	1in500 ICC	n/a
Anti-GFP	Rabbit	AbCam	1in500 ICC	n/a
CD68	Mouse	AbCam	MeAc fix, 1in500 IHC	n/a
Desmocollin 2	Mouse	ProGen	MeAc fix, 1in500 ICC and IHC	10%, Milk block, 1in1000
Desmocollin 3	Mouse	ProGen	MeAc fix, 1in50 ICC and IHC	10%, Milk block, 1in250
Desmoglein 1	Mouse	ABD Serotec	MeAc fix, 1in100 ICC and IHC	n/a
Desmoglein 1 and 2 (3.10)	Mouse	ProGen	1in200 ICC and IHC	n/a
Desmoglein 2 10D2	Mouse	Kindly Provided by Pr My Mahoney	1in50 ICC and IHC	n/a
Desmoglein 2 Ab10	Rabbit	Kindly Provided by Pr My Mahoney	n/a	10%, BSA block, 1in10,000
Desmoplakin 11-5F	Mouse	Kindly provided by Pr David Garrod	MeAc fix1in100 ICC and IHC	HMW protocol, Milk Block, 1in250
E-Cadherin	Mouse	AbCam	MeAc fix1in100 ICC	n/a
EphA2	Goat	R&D Systems	PFA fix, 1in50	10%, Milk block, 1in500
EphA4	Rabbit	AbCam	1in50	10%, Milk block, 1in500
EphA4 (phospho-EphA4)	Rabbit	R&D Systems	1in50, use TBS instead of PBS at all steps	n/a
Ephrin A1 V18	Rabbit	Kindly provided by Dr Spiro Getsios	1in50 IHC	12%, Milk block, 1in1000, 25KDa band
GRP78 (ET-21)	Rabbit	AbCam	PFA fix, 1in100	n/a
iRHOM1 / RHBDF1	Rabbit	AbCam	1in100 IHC	n/a
iRHOM2 / RHBDF2	Rabbit	Sigma	MeAc fix, 1in100 ICC and IHC	10%, Milk block, 1in500
iRHOM2 / RHBDF2	Rabbit	Custom-made by Harlan laboratories, Oxon, UK	MeAc fix, 1i in 100 IHC	n/a
NOTCH1 (ChIP grade)	Rabbit	AbCam	MeAc fix 1in50 ICC	HMW protocol, BSA block, 1in500
NOTCH1 (mN1A)	Mouse	AbCam	MeAc fix 1in50 ICC	n/a
NOTCH1 (Val1744)	Rabbit	AbCam	MeAc fix 1in50 ICC	n/a
Plakoglobin	Mouse	ABD Serotec	MeAc fix 1in25 ICC and IHC	10%, Milk block, 1in100
Plakophilin 1	Mouse	ProGen	MeAc fix1in50 ICC and IHC	10%, Milk block, 1in100
Plakophilin 2	Mouse	ProGen	MeAc fix1in25 ICC and IHC	10%, Milk block, 1in250
RHBDL2-N Terminal	Rabbit	AbCam	1in50 IHC	n/a
Thrombomodulin	Rabbit	AbCam	1in100 IHC	n/a
Tubulin	Mouse	AbCam	1in750	n/a

Table 2.1 Table of antibodies and conditions for staining and western blots

2.3.4 Confocal microscopy

Images were taken using the Zeiss 510 Meta Confocal or the Zeiss LSM 710 Meta Confocal microscopes using the LSM or Zen software respectively. Once the microscope system was running, the appropriate lasers were selected to detect the required wavelengths: 405 nm (DAPI), 488 nm (FITC) and 543 nm or 561 nm for the 510 and 710 microscopes respectively (red channel). The laser power was set to 2.0% for each laser for each image on the LSM 710 micropscope. On the 510 microscope, the 488 nm laser was set to 12.0% and the 405 nm laser to 10.0%. Once the sample was identified using the eyepiece at a 10X magnification, the objective was changed to 40X, 63X or 100X as indicated with oil applied to the sample coverslip for all oil immersion lenses.

With the Zen software for the 710 microscope, initial settings were determined using the Auto Exposure setting, while settings from a previous image were used as a starting point on the LSM 510 microscope. The focus was adjusted so that the region of brightest staining was in focus for each image. The pinhole was set to 1 airy unit (1 AU) for each channel; the detectors were aligned and the digital offset and gain settings were adjusted for each channel to avoid under- or overexposed pixels and to ensure the image was within the dynamic range of the detectors. The scanning parameters were then set: The frame size was 1024 x 1024 pixels; the scan speed was set to 7; data depth was 16 bit; and the scan average was set to 8. A single slice image was taken for each image. Microscope settings were kept the same for all images within an experiment to allow comparison between samples.

2.4 Western Blotting

2.4.1 Preparation of cell lysate

Cells were lysed in 2X Laemelli buffer (0.1 M Tris-HCL (pH 6.8), 4 % sodium dodecyl sulphate (SDS), 20 % Glycerol, 0.001 % Bromophenol Blue, 1.44 M β-mercaptoethanol). Laemelli buffer is a denaturing buffer, making protein epitopes available to the probing antibodies. The SDS in the buffer gives the protein a negative charge, thereby allowing it to migrate through the gel in response to electrical charge. β-mercaptoethanol is a reducing agent, removing disulphide bridges from proteins and enabling them to move through the gel according to their size. Glycerol is included in the buffer to increase the density of the sample helping even loading of the gel. Bromophenol blue allows detection of the movement of the protein through the gel as it migrates through the gel faster than the other components of the sample.

Before the lysis, the cell culture dish was placed on ice and the cells washed twice with PBS. The 2X Laemelli buffer was heated at 95°C for 5 min on a heat block, the PBS

removed from the cells and 150-250 µl heated 2X Laemelli buffer added to each well of a 6-well plate. A cell scraper was used to ensure the cells were detached from the plate, and the cell lysate transferred to a 1.5 ml eppendorf tube. The lysate was placed on the heat block at 95°C for 5 min and then immediately put back onto ice. The lysates were centrifuged at 13,000 rpm for 5-10 min and the supernatant transferred to a fresh ice-cold tube (avoiding any pellet formed by the centrifugation, as this contains cell debris). If the supernatant was viscous, it was sonicated with the Soniprep 150 sonicator (MSE, Sydenham, UK) for 10-20 s. Protein lysates were stored at -80˚C.

2.4.2 Electrophoresis

2.4.2.1 SDS-PAGE

Sodium-dodecyl Sulphate-polyacrylamide gel electrophoresis (SDS-PAGE) was carried out using equipment from Bio-Rad (Hemel Hempsted, UK). All equipment was cleaned with hot water and 100 % ethanol before use. SDS-PAGE gels were prepared with an appropriate polyacrylamide percentage for the protein being detected (see Table 2.2), with higher percentage gels used for lower molecular weights. iRHOM2 is around 90 KDa in size, so an 8 % gel was used for this antibody initially, then later, 10 % gels were used to allow visualisation of the 'doublet' seen in higher percentage gels. The resolving gel was made up first according to the recipe in Table 2.3. The basic ingredients are double distilled H_2O (ddH_2O), 30 % polyacrylamide mix (Protogel), tris (1.5 M, pH 8.8), SDS (10 %), ammonium persulphate (APS, 10 %; Sigma-Aldrich) and *N,N,N,N*-tetramethylethylenediamine (TEMED; Sigma-Aldrich). APS and TEMED act as polymerising agents in the gel. After pouring the gel, isopropanol was added to level the top of the gel and remove air bubbles. The gel was then left to set for around 20 min. The resolving gel has a higher resistance, so protein migration through the gel is slower, allowing separation of the proteins by size. As the gel percentage increases, the resistance also increases, allowing greater protein separation, and visualisation of smaller differences in size.

Once the resolving gel was set, the isopropanol was removed and the top of the gel washed with ddH_2O. The stacking gel was then prepared. The stacking gel has a lower resistance than the resolving gel, allowing the proteins to 'stack up' at the same point before entering the more resistant resolving gel. Each 5 ml stacking gel contained: 3.4 ml ddH_2O; 0.8 ml 30 % polyacrylamide mix; 0.63 ml Tris (1 M, pH6.8), 0.05 ml SDS (10 %), 0.05 ml APS (10 %) and 5 µl TEMED. The gel was poured around 10 or 15-well combs which form the loading wells at the top of the gel, avoiding the formation of air bubbles. This was left to set for approximately 30 min.

Once the gels had set, they were fitted into the tank and the combs removed. Running buffer (0.3 % Tris, 1.44 % Glycine and 0.1 % SDS in ddH_2O) was poured in between the gels and outside the gel but without it touching to prevent a short circuit. The wells of the gel were rinsed to remove any gel debris or un-polymerised gel using a 1 ml pipette and running buffer. Protein samples were heated to 95°C or 5 min and then cooled on ice and spun at 13,000 rpm for 5 min in a bench top centrifuge before loading into the gels. Rainbow ladder (GE Healthcare) or HiMark high molecular weight protein ladder (Invitrogen) was also included in at least one well per gel to allow identification of protein size. The gel was then run for approximately 1 ½ h at 12 mA per gel until the dye front from the bromophenol blue in the loading buffer reached the bottom of the gel. The protein has a negative charge (from the SDS in the loading buffer), causing the protein to migrate from negative charge towards positive charge when the electrical current is run through the tank.

2.4.2.2 Tris-acetate gradient gel electrophoresis

DSP and NOTCH1 western blots were run on a pre-cast 3-8 % tris-hydroxymethyl amino ethane (TRIS)-acetate gradient gel (Invitrogen) due to their high molecular weight (HMW). The gels were prepared according to manufacturer's instructions, and run with tris-acetate running buffer comprising: tricine (0.9 %), tris base (0.6 %) and SDS (1 %). HiMark HMW protein ladder (Invitrogen) was included in at least one well as a size marker.

Protein size (kDa)	**Gel percentage (%)**
4-40	20
12-45	15
10-70	12.5
15-100	10
25-200	8

Table 2.2 SDS-PAGE gels

Reagent	**8 %**	**10 %**	**12 %**
H_2O	4.6 ml	4.0 ml	3.3 ml
30 % Acrylamide Mix	2.7 ml	3.3 ml	4.0 ml
1.5 M Tris (pH 8.8)	2.5 ml	2.5 ml	2.5 ml
10 % SDS	100 µl	100 µl	100 µl
10 % APS	100 µl	100 µl	100 µl
TEMED	4 µl	4 µl	4 µl

Table 2.3 Recipes for 10 ml resolving gel at 8 %, 10 % and 12 %

2.4.3 Transfer

The next step was to transfer the proteins from the gel onto a nitrocellulose membrane (GE Healthcare, Buckinghamshire, UK), which has a high affinity for proteins, allowing them to be retained during antibody incubation. For the transfer process, blotting paper, sponge pads and a piece of nitrocellulose membrane were soaked in transfer buffer (0.3 % tris, 1.4 % glycine, 20 % methanol in ddH_2O). A cassette was used to sandwich in order: a sponge pad, two pieces of blotting paper, the gel, the nitrocellulose membrane, two pieces of blotting paper and another sponge pad, taking care to avoid air bubbles by rolling over the blotting paper on top of the gel and membrane with a 5 ml pipette. As with gel electrophoresis, the negatively charged protein migrates from negative charge towards positive charge when an electrical current is run through the tank. The gel was therefore placed towards the negative side of the tank and the membrane at the positive side. The tank was filled with transfer buffer, and an ice pack added to prevent overheating. A current of 300 mA for a 1½-2 h transfer, or 100 mA for overnight transfer, was run through the tank. HMW proteins were always transferred overnight at 100 mA using a buffer comprising: tris base (0.6 %), glycine (0.2 %) and methanol (5 %), without SDS.

2.4.4 Blocking

Once the transfer was complete, the nitrocellulose membranes were blocked in either 10 % milk or 5 % BSA in tris-buffered saline-Tween (TBS-T) as indicated in table 2.1 for 1 h, at room temperature. TBS-T comprises: Tris-HCl (0.2 %; Fisher Thermoscientific); NaCl (0.8 %) and Tween-20 (0.1 %; Sigma-Aldrich) in ddH_2O. The pH was adjusted to 7.5 in the 10X stock solution with concentrated hydrochloric acid (Sigma-Aldrich).

2.4.5 Antibody incubation

Primary antibodies were diluted in 5 % milk in TBS-T, or in 5 % BSA depending on the blocking solution. The conditions used for each antibody are shown in table 2.1. The membrane was incubated in the antibody overnight at 4°C, or for 2 h at room temperature where overnight transfer was carried out. A house-keeping gene of a different molecular weight to the protein of interest, such as glyceraldehyde 3-phosphate dehydrogenase (GAPDH), β-actin or vinculin, was included as a loading control to show whether the loading of proteins was equal.

Following the primary antibody incubation, the membranes were washed in TBS-T, then incubated for 2 h in horseradish-peroxidase (HRP)-conjugated secondary antibody

(Dako, Ely, Cambridgeshire, UK) at a dilution of 1 in 3000 (swine-anti-rabbit secondary antibody), 1 in 2000 (rabbit-anti-mouse secondary antibody), or 1 in 2000 (rabbit-anti-goat secondary antibody). Following the incubation with secondary antibody, membranes were washed at least 3X 5 min in TBS-T, and visualised using ECL plus or prime chemiluminescent reagent according to the manufacturer's instructions (GE Healthcare) or Immobilon western chemiluminescence reagent (Millipore), also according to the manufacturer's instructions.

Chemiluminescence works using HRP conjugated to the secondary antibody, combined with peroxide, to catalyse the oxygenation of a lumigen substrate such as the PS-3 Acridan substrate found in ECL plus. This generates acridinium ester intermediates which produce a sustained chemiluminescence in combination with the peroxidase and slightly alkaline conditions. The membranes were placed in a cassette and, in a dark room with only red light, photographic film (GE Healthcare) was exposed to the membrane for the appropriate amount of time to develop clear bands, then fixed and developed using the Compact X4 automated developing system (Xograph Imaging Systems, Gloucestershire, UK).

2.4.6 Densitometry analysis

Densitometrical analysis was carried out using Image J software (Rasband, W.S., Image J, U. S. National Institutes of Health, Maryland, USA) and Image Studio Lite software version 3.1 (LI-COR, Cambridge, UK). Film was scanned and images saved in JPEG format before importing into Image J or Image Studio Lite.

For analysis with Image Studio Lite: The image was saved as a single colour file, and cropped to the appropriate size. Boxes were drawn around each band, and the integrated density calculated by the software as a measure of the intensity of the signal. The software measures the intensity of each pixel in the box, plotting a line graph of pixel number against intensity of the signal, giving a curve for each band. The software then measures the area under the curve to take into account the area and intensity of the band as integrated density. Any free rotations were carried out after the densitometry to avoid unwanted manipulation of the data.

Analysis with Image J works in a similar way. JPEG files were imported into the programme and the images cropped and rotated in right angles to the right orientation. The 'Analyse Gels' tool was used: A box was drawn around each band, plots of the band intensity against pixel number generated and the area under the curve was measured.

The same process was carried out for GAPDH or other loading control bands in both software packages. The final band intensity is shown as a percentage of loading control signal to control for uneven protein loading.

2.5 Phospho-Receptor Tyrosine Kinase arrays

Phospho-RTK arrays were purchased from R&D systems and carried out according to the manufacturer's instructions. Briefly, membranes were blocked with the blocking buffer provided. 500 µg protein from lysates of TYLK1 and TYLK2 TOC cells and NEB1 control cells was diluted in 2 ml blocking buffer and applied to the membranes overnight at 4°C. Membranes were washed using the wash buffer provided, then incubated with a phospho-specific secondary antibody for 2 h at room temperature. Membranes were washed again with the buffer provided, and developed using ECL plus reagent (Amersham, GE Healthcare).

2.6 ELISA

2.6.1 Sample collection

KYSE270, KYSE410 and TE-4 cells were plated in 12-well plates at a density of 3 x 10^5 cells per well. The following day, once the cells had attached to the wells, the cells were washed with PBS and 1 ml fresh medium (RPMI 1640 with FCS, P/S, L-glutamine and RM+) added to each well of cells. Medium was collected immediately for the 0 h time point, then at 3 h, 6 h, 12 h, 24 h and 48 h time points. The medium was stored at -80°C until needed. At the 24 h time point, mRNA was also extracted from the cells with the RNeasy mini kit, protocol described in section 2.8.1.

2.6.2 ELISA

Enzyme-Linked Immunosorbent Assays (ELISAs) were carried out with the DuoSet ELISA development system (R&D Systems, Abingdon, UK) according to kit instructions. Briefly, the capture antibody was diluted to the working concentration specified by the manufacturer's instructions (2 µg/ml for AREG; 0.4 µg/ml for TGF-α) and 100 µl added to each well of a 96-well ELISA plate. The plate was sealed and incubated at room temperature overnight.

The following day, the wells were washed three times with wash buffer (0.05 % Tween-20 in PBS; pH 7.2-7.4) and the wells dried by blotting the plate onto paper towels. Plates were blocked for 1 h at room temperature with 300 µl reagent diluent (1 % BSA in PBS; pH 7.2-7.4; 0.2 µm filtered), then the plate washed three times as described above. Standards were prepared by diluting in reagent diluent according to instructions for the particular kit: A high standard of 1000 pg/ml was used for AREG and 500 pg/ml for

TGF-α. Two-fold serial dilutions were then carried out to form a 7-point standard curve. Samples were diluted 1 in 4 for AREG ELISAs and 1 in 2 for TGF-α ELISAs in reagent diluent. Samples or standards were added to each well, 100 µl per well, each sample in duplicate. The samples and standards were incubated for 2 h at room temperature.

Plates were washed 3 times, and detection antibody diluted in reagent diluent according to kit instructions. The diluted antibody was added to each well, 100 µl per well. This was incubated for a further 2 h at room temperature, then the wash step repeated. Further steps were carried out avoiding exposure to direct light. Firstly, 100 µl of the 1 in 200 working dilution of streptavidin-HRP was added to each well and incubated for 20 min. The wash step was repeated, and 100 µl substrate solution added to each well. Substrate solution comprises a 1:1 mixture of colour reagent A (Hydrogen peroxide; H_2O_2) and colour reagent B (Tetramethylbenzidine). Stop solution (50 µl; 2 N sulphuric acid (H_2SO_4)) was then added and the optical density measured at 450 nm with a Synergy HT plate reader. Readings at 540 nm were subtracted from the readings to correct for background from the plate.

2.6.3 ELISA analysis

Data was imported into Microsoft Excel, and a standard curve generated from the absorbance of the standard protein concentration. A polynomial trend line was added with the order best fitting the data and achieving an R^2 value as close to 1 as possible. The equation generated was used to determine protein concentrations in the individual samples. As each sample was run in duplicate, an average of the two readings was taken, and then an average of the triplicates for each condition calculated to determine the final protein reading for each experiment. The cells were counted at the 24 h timepoint and the concentration of AREG or TGF-α expressed as pg/ml/10^5 cells.

2.7 Reverse-Transcriptase PCR

2.7.1 mRNA extraction

mRNA was extracted from cells using the RNeasy mini kit according to the manufacturer's instructions (Qiagen, Crawley, UK). Cells were lysed directly in the cell culture dish using 350 µl buffer RLT with 3 µl β-mercaptoethanol included to inactivate endogenous RNases. Cells were removed from the cell culture dish with a cell scraper (Fisher Scientific), passed through a 20-gauge needle at least 5 times and transferred to an RNase/DNase-free tube. One volume of 70 % ethanol was added to the tube and mixed by pipetting. The lysate was then transferred to the RNeasy spin column and spun at 8,000 *g* for 30 s. Ethanol provides optimal conditions for the RNA to bind to the silica spin column. The flow-through from the spin was discarded, and the column washed with

700 µl buffer RW1 and spun at 8,000 *g* for 30 s. Two washes were then performed with buffer RPE, centrifuged for 30 s at 8,000 *g* for the first wash, then at 8,000 *g* for 2 min for the second wash. The column was transferred to a clean RNase/DNase-free tube, and centrifuged without solution for 1 min at maximum speed (~16,000 *g*) to remove all traces of ethanol, which can inhibit the elution step. Finally, the mRNA was then eluted in 30 µl RNase-free water and the concentration measured using the nanodrop spectrophotometer (Thermo Scientific).

2.7.2 cDNA synthesis

cDNA synthesis was performed with Superscript II reverse transcriptase enzyme (Invitrogen). Two tubes were included for each mRNA sample, one in which the reverse transcriptase enzyme is present (RT+) and one in which the enzyme is omitted (RT-). The RT- sample acts as a negative control, showing that there is no DNA or RNA contamination in the sample or reagents. For each sample, to make 20 µl cDNA, the following was added to a 0.2 ml RNase-free thin-walled PCR tube: 8 µl RNase free H_2O, 1 µl oligodT (short sequence of deoxy-thymine residues), 0.5 µl random primers/hexamers, 1 µl deoxynucleotide triphosphates (dNTP), and 1.5 µl RNA (diluted to 100 ng/µl). This mixture was incubated at 65˚C for 5 min and transferred quickly to ice. 5X first-strand buffer (4 µl), 2 µl dithiothrietol (DTT; 0.1 M) and RNase Out (1 µl) were then added and the tube incubated at 42˚C for 2 min. Finally, 1 µl Superscript II enzyme was added to each RT+ sample and 1 µl RNase free H_2O added to each RT- sample and the tubes were incubated at 42˚C for 50 min. A polymerase chain reaction (PCR) for house-keeping gene hypoxanthine-guanine phosphoribosyltransferase (HPRT) was then carried out to check the quality of the cDNA and check for contamination in the RT- samples.

2.7.3 PCR

Polymerase chain reactions (PCR) were carried out using either BioTaq DNA polymerase (Bioline, UK) or GoTaq DNA polymerase (Promega, UK) as indicated in Table 2.4. PCRs were carried out using primers from Sigma Genosys (UK). Primers were designed by Dr Diana Blaydon. The primer sequences, PCR conditions, annealing temperatures and the size of the PCR product are indicated in Table 2.4.

A mastermix was prepared for each set of reactions. BioTaq mastermix contained: 10X buffer (2 µl); $MgCl_2$ (50 mM; 0.6 µl); dNTP (0.4 µl); 0.2 µl each of forward and reverse primers and Taq polymerase (0.2 µl). Mastermix for reactions with GoTaq polymerase contained: 5X GoTaq buffer (4 µl); $MgCl_2$ (25 mM; 1.2 µl); dNTP (0.4 µl); 0.2 µl each of forward and reverse primers; and Taq polymerase (0.2 µl). The primer stock solutions were at a concentration of 10 µM. Dimethylsulphoxide (DMSO) was added as indicated

in Table 2.4 to increase the specificity of some reactions. Finally, ddH_2O was added to a total volume of 19.5 µl per reaction. Once the mastermix was prepared, it was transferred to separate 0.2 ml thin-walled PCR tubes or to the wells of a PCR plate, and 0.5 µl cDNA added to each well or tube. 0.5 µl ddH_2O was added to one well/tube per reaction to act as a negative control and rule out contamination from the components of the PCR reaction.

The tubes or plates were then put into a DNA engine Tetrad 2 Peltier thermocycler (MJ Research) and put through the following programme: 95°C for 30 s initial melting, followed by 35 cycles of the following: 95°C for 30 s to melt the double stranded DNA, exposing the bases for the primers to bind; X°C for 15 s to allow the primers to bind to the DNA – this annealing step was carried out at the temperature indicated in Table 2.4. An extension step of 1 min at 72°C was then carried out to allow further nucleotides to be added to the forming DNA strand. Finally, once the 35 cycles were complete, a final extension of 72°C for 10 min was carried out to ensure that all the PCR products were complete.

Once the PCR cycle was finished, a 1 % agarose gel was prepared by boiling a solution of agarose in Tris-Borate-EDTA buffer (TBE) in a microwave until the agarose dissolved. The agarose solution was then cooled until comfortable to touch, then 0.5 µg/ml ethidium bromide was added. The gel was poured into a tray with a comb to form wells for loading the PCR products. The products were mixed in a 1:1 ratio with loading dye and run through the gel in a DNA electrophoresis tank (Horizon 11.14, Gibco BRL). Because DNA is negatively charged, when a current is run through the gel, the DNA migrates away from the negative charge at one side of the gel towards the positive charge at the other end of the gel. Smaller proteins will migrate faster through the gel, allowing separation of the PCR products by size. The 1 Kb plus DNA ladder (Invitrogen) was included in at least one well of each gel as a size marker. The ethidium bromide in the gel interchelates with the DNA and fluoresces under UV light when it is bound to the double stranded DNA allowing visualisation of the PCR products. Pictures of the gels were taken with the UviDoc system (Uvitec).

2.7.4 qPCR

Semi-quantitative real-time PCR (qPCR) was carried out using Taqman technology and the Rotorgene Q thermocycler (Qiagen). Taqman chemistry works using a sequence-specific probe. The probe is fused to a fluorescent reporter at the 5’ end and a quencher at the 3’ end. When the probe is in its unbound state, the quencher and reporter are in close proximity, so that any fluorescent energy emitted by the reporter is absorbed by the quencher by fluorescence resonance energy transfer (FRET) (Holland et al., 1991).

This prevents detection of any signal from the reporter. However, when the probe binds to its target sequence, the 3' and 5' ends are separated, so the quencher is too far from the reporter to absorb the signal. When the samples are exposed to light, signal from the reporters of any bound probes may be detected by the machine. Thus as the target sequence is amplified by gene-specific primers, the amount of probe bound to the target sequence increases, as does the signal detected from the reporter.

To set up the reactions, a mastermix was made using the Multiplex PCR Mastermix Kit (Qiagen). The mastermix contains the necessary ingredients for the qPCR including HotStarTaq DNA polymerase. The following was added for each reaction: Multiplex mastermix (10 µl); nuclease free H2O (6.5 µl); forward primer (10 µM, 1 µl); reverse primer (10 µM, 1 µl); Taqman probe (0.5 µl). The mastermix was transferred into individual 0.02 ml thin-walled PCR machines tailored for the rotorgene (19 µl per tube). Work was carried out on ice and nuclease-free conditions to preserve the enzyme, cDNA samples and other ingredients. cDNA was then added at a volume of 1 µl to give a total reaction volume of 20 µl. The qPCR reaction was carried out in triplicate for each sample, and a corresponding control reaction with RT- cDNA was included for each sample. Primers and probes against AREG, TGF-α and GAPDH were kindly provided by Dr Matthew Brooke, ordered from Sigma-Aldrich. The primer sequences are shown in table 2.4. The reaction was run on the RotorGene Q qPCR machine (Qiagen). An initial denaturing step was carried out at 95°C for 10 min, followed by 45 cycles consisting of a 15 s denaturing step at 95°C and 50 s at 60°C for annealing and extension.

qPCR results were analysed using the Rotorgene Q series software. Levels of each gene were expressed relative to housekeeping gene GAPDH using the ΔCT (change in cycle threshold) method (Livak and Schmittgen, 2001). A threshold was set using the software and the cycle number at which the signal for each sample crossed the threshold (the CT value) was recorded. The CT value for the gene of interest (AREG or TGF-α) was subtracted from the CT value for GAPDH to give the ΔCT value. This value was then expressed as 2 ΔCT to give a reading of the gene expression.

PCR	Forward Primer	Reverse Primer	Conditions	Annealing Temperature	Product Size (bp)
RHBDF2 isoforms 1 and 2	**RHBDF2ex2F** GGGCAAACT CAGACTCGA AG	**RHBDF2ex5R** CGCTGACTCC AAACCACTG	Bioline Taq 5 % DMSO	65°C	429 and 336
RHBDF2 isoform 1	**RHBDF2ex4F** AGAAAAGCC AGCCCAGGA C	**RHBDF2ex6R** AGGAGGTGAG GGACAGGACT	GoTaq 10 % DMSO	58°C	492
RHBDF2 isoform 2	**RHBDF2ex3/4 -F** CAGCATGCT GCCTGAGAG GA	**RHBDF2ex6R** AGGAGGTGAG GGACAGGACT	Bioline Taq 5 % DMSO	60°C	443
AREG (For qPCR)	**AREG qPCR** Forward AAGGACCAA TGAGAGCCC CG	**AREG qPCR** Reverse TAATGGCCTG AGCCGAGTAT C	**qPCR Probe** 6FAM-GCCGGCGC CGGTGGTG CTGT-BHQ1	60°C (Green channel)	
TGFα (For qPCR)	**TGFa qPCR Forward** AGCATGTGT CTGCCATTC TG	**TGFa qPCR Reverse** TGTGATGATA AGGACAGCCA GG	**qPCR Probe** 6FAM-TGGCCGTG GTGGCTGC CAGCCA-BHQ1	60°C (6FAM = Green channel reporter)	
GAPDH (For qPCR)	**GAPDH qPCR Forward** TGGCCCCTC CGGGAAACT GT	**GAPDH qPCR Reverse** CCTTGCCCAC AGCCTTGGCA	**qPCR Probe** HEX-GCGTGATG GCCGCGG GGCTCTCC A-BHQ1	60°C (HEX = Yellow channel reporter)	

Table 2.4 PCR primers and reaction conditions. Anti-*RHBDF2* primers were kindly provided by Dr Diana Blaydon, and qPCR primers provided by Dr Matthew Brooke.

2.8 Migration assays

Cells were plated in 6-well plates in triplicate for each cell line and condition and grown until confluent. Cells were incubated for 2 h at 37°C, 5 % CO_2 with or without mitomycin C (MMC; 10 µg/mL; Sigma-Aldrich) which irreversibly inhibits proliferation, thus ensuring

that differences seen are due only to migration of the cells. Cells were washed 3X with PBS to remove the MMC, then two scratches placed perpendicular to each other to form a cross shape. The centre of the cross forms a guide to ensure images are taken at the same location in the scratch at each time point. Cells were again washed 3 times with PBS to remove any dead cells and cell debris formed by the scratch and medium without exogenous EGF (RM- medium) added to the cells. Images were then taken to show the scratch wounds at the 0 h time point with the Nikon Eclipse TE2000-5 microscope and Nikon digital Sight DSL1. Four pictures were taken of each well at the four regions adjoining the centre point of the scratches in each well. Further pictures were taken every 24 h until the scratch was closed.

2.9 Flow Cytometry

NEB1 or HeLa cells were plated in 6-well dishes and transfected with Fugene 6 transfection reagent as described in section 2.2. Cells were transfected with green fluorescent protein (GFP)-tagged wild type (WT) and mutant Connexin 31 or iRHOM2 constructs. Approximately 48 h after transfection, the medium was collected and stored in a 15 ml falcon tube. The cells were washed with PBS and the PBS transferred to the falcon tube. The medium and PBS from the wash step were kept to allow collection of any dead cells that had detached from the culture dish. Next, 500 µl trypsin-EDTA in PBS was added to each well of cells (0.05 % for HeLa cells, 0.15 % for keratinocytes) and the plates incubated at 37°C until the cells had detached from the dish. The trypsin was neutralised with warm serum-containing medium, and the medium and cells transferred to the falcon tube. The tube was centrifuged at 1200 rpm to collect the cells, the medium removed and the cells re-suspended in 500 µl PBS with 1 % FCS.

Flow cytometry (FC) was carried out using the BD FACS Canto II machine at the BICMS core FACS facility with Dr Luke Gammon (CCR, QMUL). Immediately prior to FC, one drop of propidium iodide (PI; 500 µg/ml) was added to the cells and mixed with a Pasteur pipette, which also resuspended any pelleted cells. PI preferentially enters dead cells and fluoresces at approximately 600 nm upon binding nucleic acids within the cells (Nicoletti et al., 1991). Cells were then transferred to a polystyrene tube of the appropriate size for flow cytometry. At least 10,000 events were recorded for each sample, and each transfection was carried out in duplicate.

For each experiment and each cell line, control tubes were prepared including:

1) Untransfected cells to allow exclusion of any cell fragments or clusters. Cell size can be determined using the forward scatter and side scatter measurements and a gate set to include only cells of the desired size.

2) Untransfected cells plus PI to allow compensation for any bleed-through from the red (PI) channel into the green channel (known as the FITC, or fluorescein isothyocyanate channel, which detects emission signals at the GFP emission wavelength).
3) Cells transfected with plasmids coding for enhanced green fluorescent protein (pEGFP), to allow a gate to be set for GFP-positive cells and compensation set to avoid recording any bleed-through from the green channel into the red channel.
4) pEGFP transfected cells plus PI to allow gates to be set for detection of GFP-positive cells.

2.9.1 Flow Cytometry Analysis

A plot of forward scatter vs side scatter was generated. Forward scatter detects cell size, and side scatter measures cell density, allowing detection of distinct cell populations. In this case, a gate was drawn to select single cells and exclude any cell debris and clumps of cells from the analysis. A plot of GFP / FITC intensity vs side scatter was then drawn using GFP-transfected control cells to allow determination of GFP-positive and negative populations, and the same performed for PI-positive and negative populations. Quadrants were then drawn to show:

1) GFP-negative, PI-negative populations (untransfected, alive cells)
2) GFP-negative, PI-positive populations (untransfected, dead cells)
3) GFP-positive, PI-negative populations (transfected, alive cells)
4) GFP-positive, PI-positive populations (transfected, dead cells)

Compensation was carried out to account for any bleed-through from GFP into the red channel and from PI into the green channel. Gates were adjusted slightly for each sample to account for subtle differences in fluorescence intensity as distinct populations were visible. Finally, the percentage of transfected, dead cells was calculated for each sample. For analysis of iRHOM2-GFP transfected cells, the green fluorescent intensity of PI-negative cells was also taken into account, with the mean intensity plotted against cell number.

Chapter 3: iRHOM2 expression and localisation in the skin

Chapter 3: iRHOM2 localisation and expression in normal and TOC Skin

3.1 Introduction and Aims

The inactive rhomboid protein iRHOM2 (and its homologue iRHOM1) are members of a relatively recently discovered family of proteins and are not well characterised in the skin and other squamous tissues. The iRHOMs are predicted to be localised to the ER, and an ER and golgi localisation has been seen in cultured cells (Nakagawa et al., 2005; Zou et al., 2009; Zettl et al., 2011; McIlwain et al., 2012), with the highest iRHOM2 expression levels reported in macrophages (Adrain et al., 2012; McIlwain et al., 2012). We recently identified germline mutations in iRHOM2 as the underlying cause of autosomal dominant inherited condition TOC (Blaydon et al., 2012). This chapter aims to investigate iRHOM2 localisation and expression in normal and TOC skin and keratinocytes, to look at the desmosomal structure of TOC skin via electron microscopy (EM) imaging, and to investigate the protein expression and localisation of desmosomal proteins.

3.2 Results

3.2.1 iRHOM2 localisation in the skin

To study the epidermal localisation of iRHOM2, IHC was performed in frozen skin sections and MeAc fixed keratinocytes.

3.2.1.1 iRHOM2 in the epidermis

iRHOM2 in normal skin sections was localised predominantly to the cell periphery, suggesting a plasma membranous localisation (figure 1 A and B), unlike the previously predicted ER localisation of iRHOM2 in cultured cells. Some fainter punctate intracellular staining was also seen, which could represent ER-iRHOM2 localisation. iRHOM2 staining could also be seen in individual cells within the dermis.

In NEB1 keratinocytes cultured in monolayer, the localisation of iRHOM2 appeared more intracellular, with punctate staining, particularly in the perinuclear region of the cells (figure 3.2.1 C), suggesting an ER-localisation of iRHOM2. Some cell-surface staining was sometimes also visible in NEB1 keratinocytes (figure 3.2.1 C), but the appearance of the membranous staining varied between experiments, perhaps suggesting that iRHOM2 localisation varies within the cell depending on the situation. Further evidence for cell-surface iRHOM2 is suggested by overexpression of GFP-tagged iRHOM2 in NEB1 keratinocytes (figure 3.2.1 D), which shows cell-surface staining in addition to fainter intracellular staining which sometimes appeared punctate in nature.

Negative control staining in which the primary antibody was omitted did not show any positive staining, indicating that staining was not due to non-specific binding of the secondary antibody to proteins in the skin or cells (figure 3.2.1 Aii, Bii and Cii). In addition, a similar cell-surface iRHOM2 localisation was seen in staining with another antibody against iRHOM2 in frozen skin sections (appendix A1), suggesting that the staining pattern does not result from non-specific binding of the anti-iRHOM2 antibody. Furthermore, western blotting of protein lysate from NEB1 keratinocytes showed a band at around 90 KDa which was of a reduced intensity in lysates from cells treated with siRNA targeting iRHOM2 (figure 3.2.1 E). The full length western blot is shown in appendix A1, including two faint additional bands at approximately 150 KDa and 52 KDa, which will be discussed later in the chapter.

3.2.1.2 iRHOM2 is expressed in infiltrating macrophages

iRHOM2 has previously been shown to be predominantly expressed in murine macrophages (Adrain et al., 2012; McIlwain et al., 2012). As some individual cells in the human epidermis stained brightly for iRHOM2, co-localisation was performed with antibodies against iRHOM2 and macrophage marker cluster of differentiation 68 (CD68) to confirm whether the individual iRHOM2-expressing cells in the dermis were indeed macrophages. CD68 staining in normal frozen skin sections was seen in a number of individual cells in the dermis and epidermis, which often had a spindle-like shape (figure 3.2.2 A). iRHOM2 expression was seen adjacent to CD68 staining in many of the cells (figure 3.2.2 B-D), suggesting that iRHOM2 was expressed in the same cells as CD68 in the dermis, which are likely to be infiltrating macrophages. The iRHOM2 and CD68 staining sometimes appeared to co-localise in the perinuclear region of the cells, but in general, the staining was distinct, with iRHOM2 appearing perinuclear and CD68 staining closer to the cell surface in most cells. This suggests iRHOM2 may be found in the ER in human macrophages, consistent with the localisation reported in the mouse.

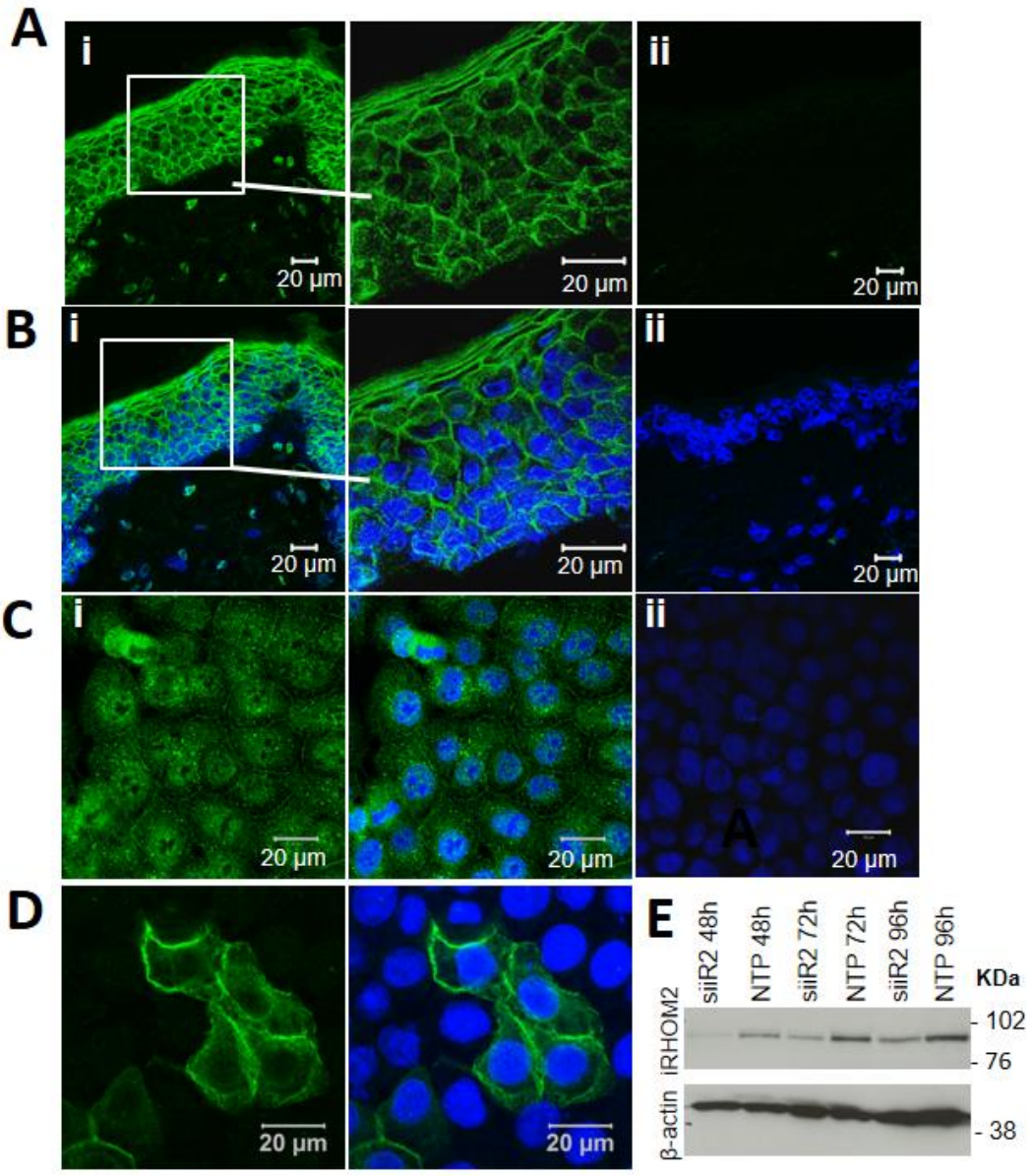

Figure 3.2.1 iRHOM2 has a plasma membrane and perinuclear localisation in human epidermis and keratinocytes. A and **B:** iRHOM2 IHC in frozen skin sections from facelift skin in the absence **(A)** and presence **(B)** of DAPI nuclear stain. Images were taken at 40X magnification (n=6), and the regions marked with white boxes at 100X (n=1), shown to the right. **C:** ICC of iRHOM2 in NEB1 keratinocytes in the presence **(ii)** and absence **(i)** of DAPI (n=6). Negative controls are shown in Aii, Bii and Cii. **D:** NEB1 cells overexpressing GFP-tagged iRHOM2-WT, fixed with MeAc and stained with anti-GFP antibody (n=3). Imaging of frozen skin sections was carried out on the LSM510 confocal microscope, and of NEB1 cells on the Zeiss Meta 710 confocal microscope. iRHOM2 staining is shown in green, DAPI nuclear staining in blue. **E:** Western blots showing iRHOM2 protein in NEB1 keratinocytes after treatment with iRHOM2 siRNA or non-targeting pool siRNA.

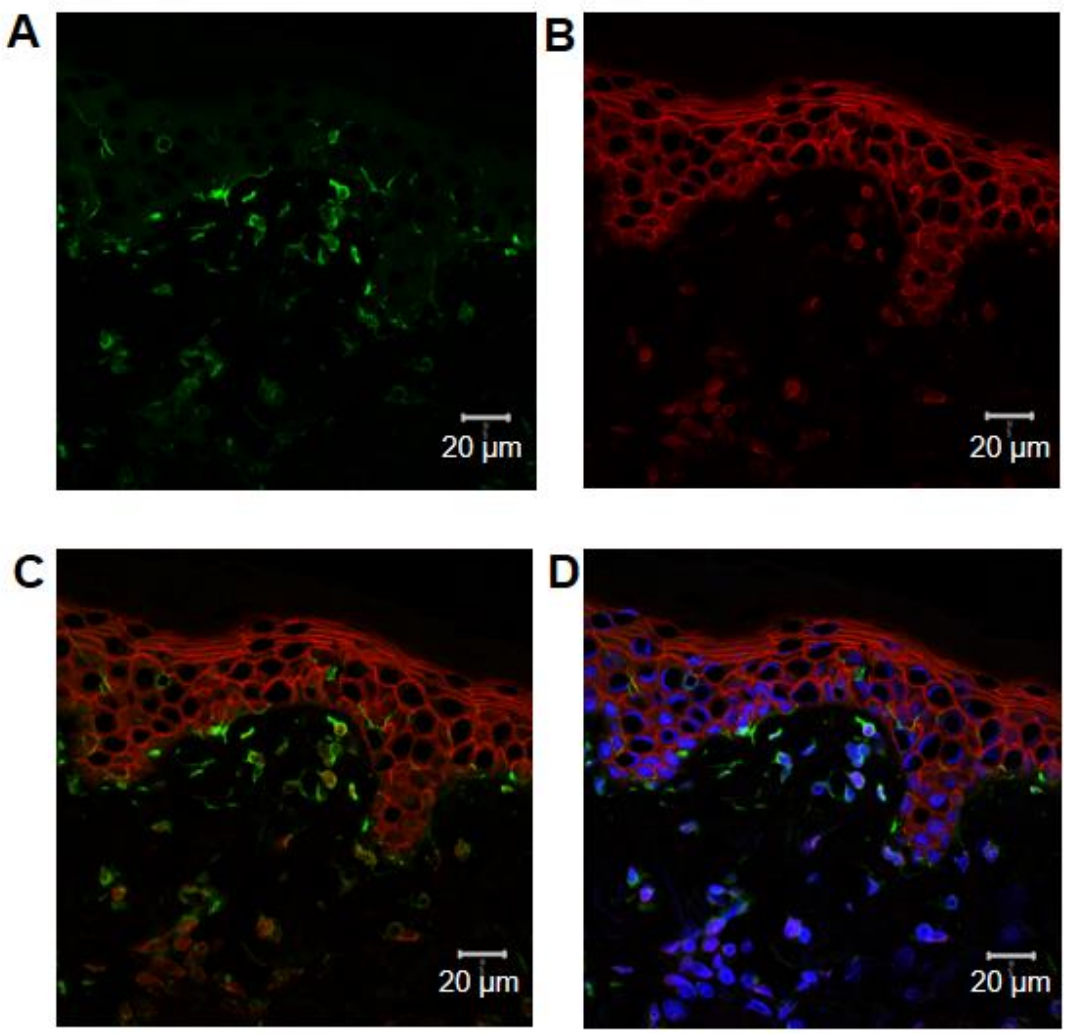

Figure 3.2.2 iRHOM2 is expressed in macrophages in normal skin. Co-localisation of iRHOM2 and macrophage marker CD68 in normal frozen breast skin sections (n=3). **A:** Green channel, showing CD68 staining, **B:** Red channel showing anti-iRHOM2 staining **C:** CD68 and iRHOM2 (red and green channel merge). **D:** Merge of iRHOM2, CD68 and DAPI nuclear stain, shown in blue. Images were taken with the Zeiss LSM 710 Confocal microscope. Please see Appendix A2 for control staining performed at the same time as the above experiment.

3.2.1.3 iRHOM2 localisation in the oesophagus

The localisation of iRHOM2 in the oesophagus was also investigated. IHC against iRHOM2 in normal oesophagus was performed by Dr Laura Gay, Centre for Digestive Diseases, QMUL. iRHOM2 also appeared to show a cell-surface expression in the oesophagus (figure 3.2.3), perhaps with some intracellular staining in some cells. This is consistent with iRHOM2 localisation in the epidermis, and suggests that iRHOM2 may be predominantly at the cell-surface in stratified squamous epithelia.

3.2.2 iRHOM2 mRNA expression in keratinocytes

The mRNA expression of iRHOM2 was investigated in a panel of human cells lines, including NEB1, HaCaT and N/TERT human keratinocyte cell lines, primary human keratinocytes (1˚HK), HeLa and HEK293T cells, to further confirm iRHOM2 expression in the skin. The *RHBDF2* gene is 19 exons long and has two splice variants, isoforms 1 and 2, which differ by 85 base pairs (bp) missing from the beginning of exon 4 in isoform 2 (figure 3.2.4 A). Primers targeting *RHBDF2* exons 2-5, spanning the region that differs between isoforms, produced two PCR products at around 336 bp and 423 bp, the sizes predicted for *RHBDF2* isoforms 1 and 2 (figure 3.2.4 B). The RT-PCR was not quantitative, but, the smaller band likely representing isoform 2 appeared more intense in all the cell lines tested, with lower expression in N/TERT cells compared with the other cell lines. The 423 bp band for isoform 1 varied in intensity between the cell lines, with stronger expression in HaCaT, 1ºHK and HeLa cells and a faint band present in NEB1 cells.

To confirm these results, primers specific to isoforms 1 and 2 were designed. The isoform 2 PCR produced robust bands at approximately the correct size (443 bp) in all cell lines tested (figure 3.2.4 D), and showed lower isoform 2 levels in N/TERT cells, consistent with figure 3.2.4 B. A second faint band was visible in HeLa and HEK293T cells, however, suggesting detection of a non-specific product during the PCR. The isoform 1 PCR was less robust, but showed variable expression of *RHBDF2* isoform 1 between cell lines (figure 3.2.4 C), also consistent with the PCR of both isoforms (figure 3.2.4 B). A band was also present at around 1 Kb in some samples. Overall, these results suggest that isoform 2 is the major isoform in keratinocytes, with isoform 1 expression more variable.

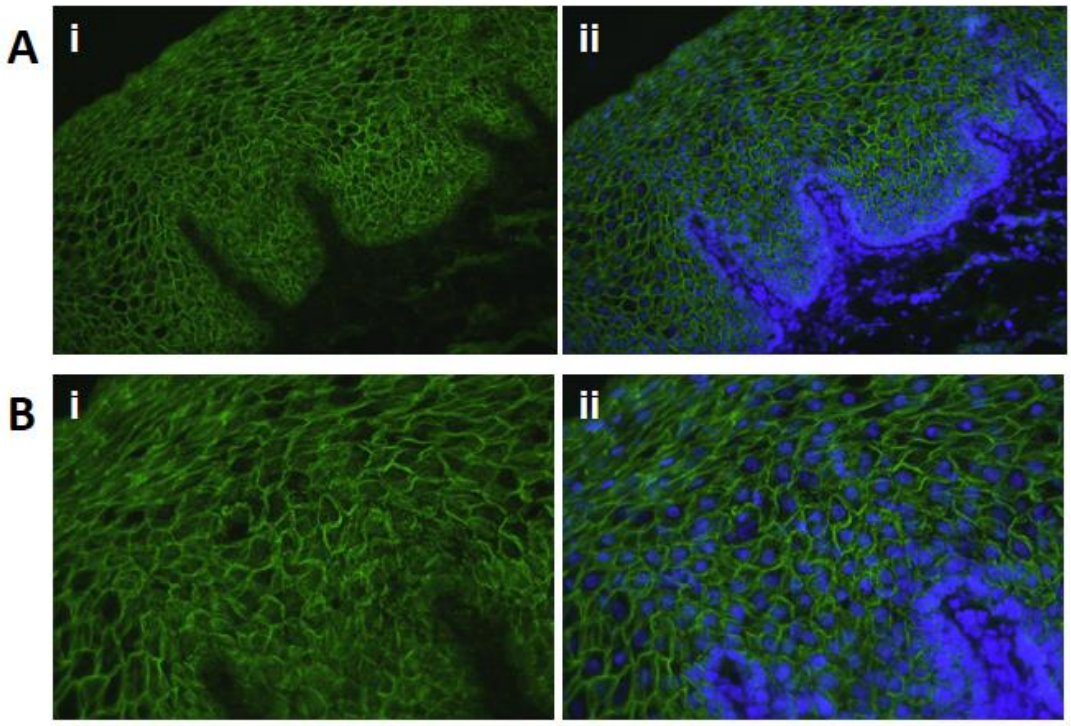

Figure 3.2.3 iRHOM2 localisation in normal oesophagus. Plasma membranous staining of iRHOM2 in normal oesophagus at magnifications of 20X (**A**) and 40X (**B**) in the presence (i) and absence (ii) of DAPI nuclear stain, shown in blue. Images were taken by Dr Laura Gay. Brightness and contrast increased by 10 % from original image.

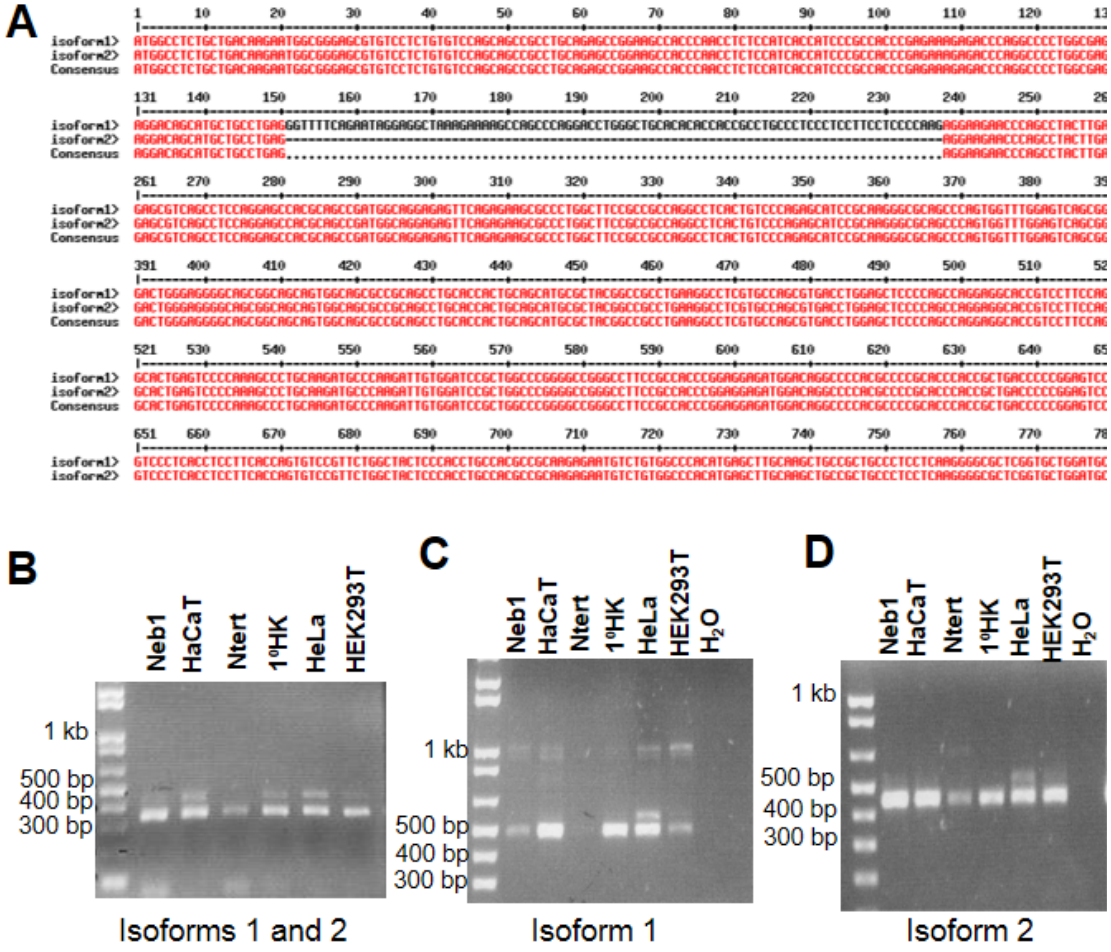

Figure 3.2.4 Variable expression of iRHOM2 isoforms 1 and 2 at the mRNA level in human keratinocytes. A: An alignment of the first section of the cDNA sequence of iRHOM2 isoforms 1 and 2 was performed (Multiple sequence alignment with hierarchical clustering; Corpet 1988, http://multalin.toulouse.inra.fr/multalin/). **B:** RT-PCR was carried out with primers detecting both isoforms 1 and 2 of iRHOM2 (B; n=1)), isoform 1 specific primers (C; n=2)) and isoform 2 specific primers (D; n=2).

3.2.3 iRHOM2 localisation in Tylosis with Oesophageal Cancer

IHC was performed against iRHOM2 in TOC frozen skin biopsies to determine whether the *RHBDF2* mutations affect the localisation of the iRHOM2 protein. Initial IHC experiments were carried out in an older frozen skin biopsy from a TOC patient, who will be referred to as patient 4. (The majority of IHC in this thesis was performed in three newer biopsies.) iRHOM2 in normal facelift skin stained at the same time showed the same plasma membranous localisation seen previously, with some fainter intracellular staining and expression in the macrophages (figure 3.2.5 A). In TOC patient 4, however, the intensity of iRHOM2 at the cell surface was reduced and much more intracellular staining was seen (figure 3.2.5 B), suggesting that iRHOM2 localisation is altered in TOC.

The IHC was repeated in newer biopsies from three female TOC patients from three generations of the same family. Patient 1 is the mother of patient 2 and grandmother of patient 3; patient 2 is the mother of patient 3. In contrast to patient 4, IHC in TOC patients 2 and 3 (figure 3.2.6 C and D) showed a localisation of iRHOM2 very similar to that seen in normal epidermis (figure 3.2.6 A), with plasma-membranous staining and fainter punctate intracellular staining. Patient 1, however, had dysregulated iRHOM2 staining, with less staining at the cell surface and increased intracellular staining which appeared more diffuse (figure 3.2.6 B), similar to the localisation seen in patient 4.

3.2.3.1 iRHOM2 co-localises with β-catenin at the cell surface in normal and TOC skin

IRHOM2 co-localisation experiments were performed with β-catenin to assess protein expression at the cell surface (figure 3.2.7). In normal epidermis, β-catenin appeared at the plasma membrane, with some intracellular staining in a couple of cells, but this was absent from most epidermal cells (figure 3.2.7 A and B). β-catenin appeared to co-localise with iRHOM2, shown by yellow plasma-membranous staining where the signal from both secondary antibodies was emitted from the same region of the tissue. Control staining is shown in appendix A3, showing that the signal was not a result of non-specific binding of the anti-mouse secondary antibody to the iRHOM2 primary antibody, or vice versa, and that there was no signal in the negative control.

In the epidermis of TOC skin, iRHOM2 still appeared to co-localise with β-catenin, particularly in patients 2 and 3 (figure 3.2.7 D and E), with strong yellow staining seen at the plasma membrane. In epidermis from patient 1, which showed dysregulated iRHOM2 staining, there still appeared to be some faint co-localisation at the cell surface (figure 3.2.7 C), but the staining was much weaker and the signal from the co-localisation appeared more orange in colour. This indicates that iRHOM2 still reaches the plasma

membrane in TOC when iRHOM2 is dysregulated, but suggests that cell-surface levels of iRHOM2 are reduced.

3.2.3.2 iRHOM2 expression in macrophages appears unaffected in TOC

To see whether iRHOM2 expression in the macrophages was affected by the TOC *RHBDF2* mutations, co-localisation with macrophage marker CD68 was performed in TOC skin (figure 3.2.8). There were no clear differences in CD68 or iRHOM2 staining in the macrophages of TOC skin compared with normal skin, and iRHOM2 still appeared to be found in the same cells as CD68. Perhaps iRHOM2 staining appeared a little more diffuse in the macrophages in patient 1 epidermis (figure 3.2.8 B).

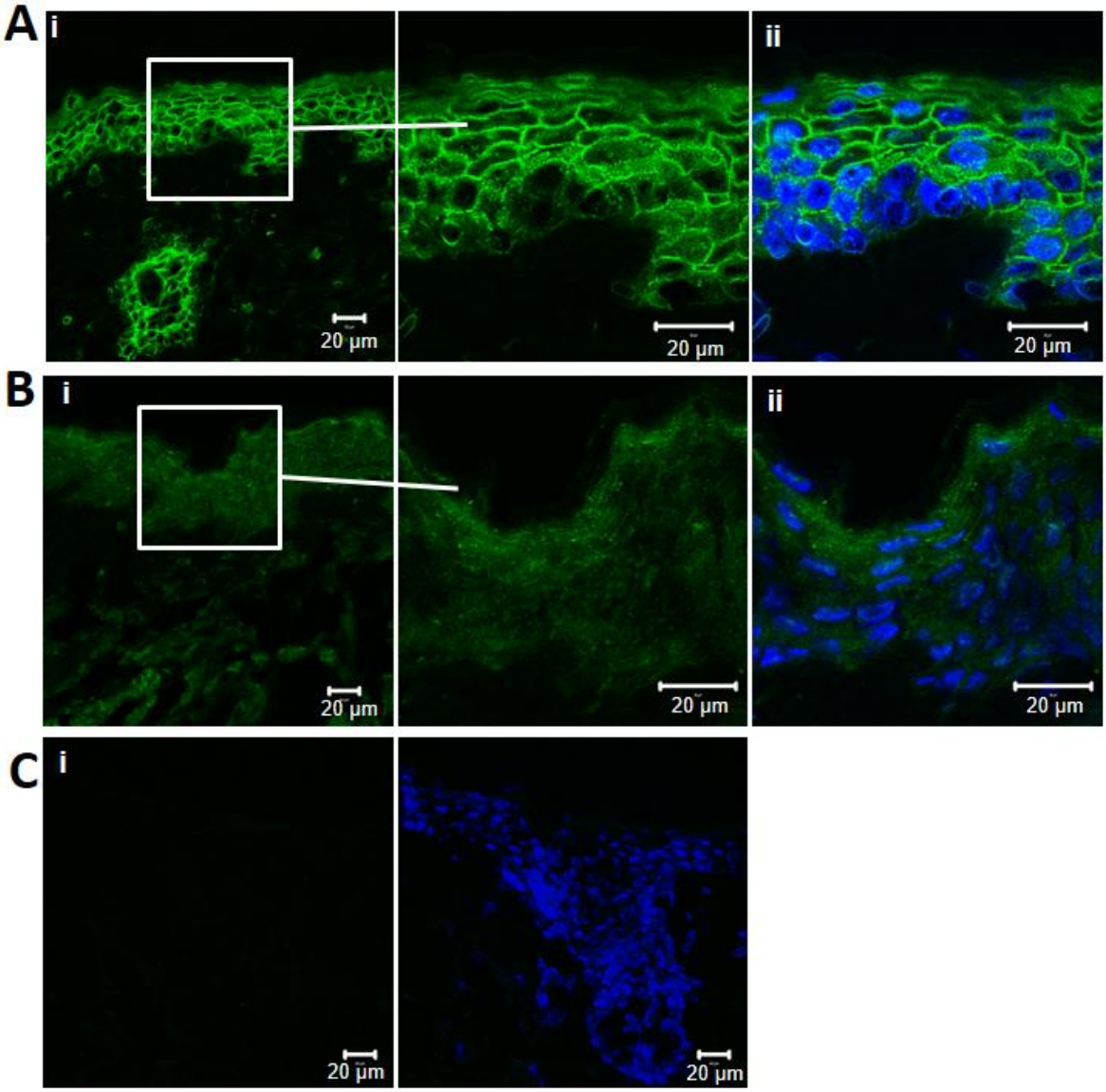

Figure 3.2.5 Variable iRHOM2 localisation and lower expression TOC skin. IHC of iRHOM2 in normal frozen sections from facelift skin. **A:** Normal skin and **B:** TOC skin (patient 4). Images were taken initially at 40X (n=4), then the regions indicated by white boxes imaged at 100X (n=1), shown on the right, and in the presence of DAPI nuclear stain in Aii and Bii. **C:** Negative control shown in the absence (i) and presence (ii) of DAPI nuclear stain. Images were taken on the LSM 510 confocal microscope. iRHOM2 staining is shown in green and DAPI nuclear stain in blue.

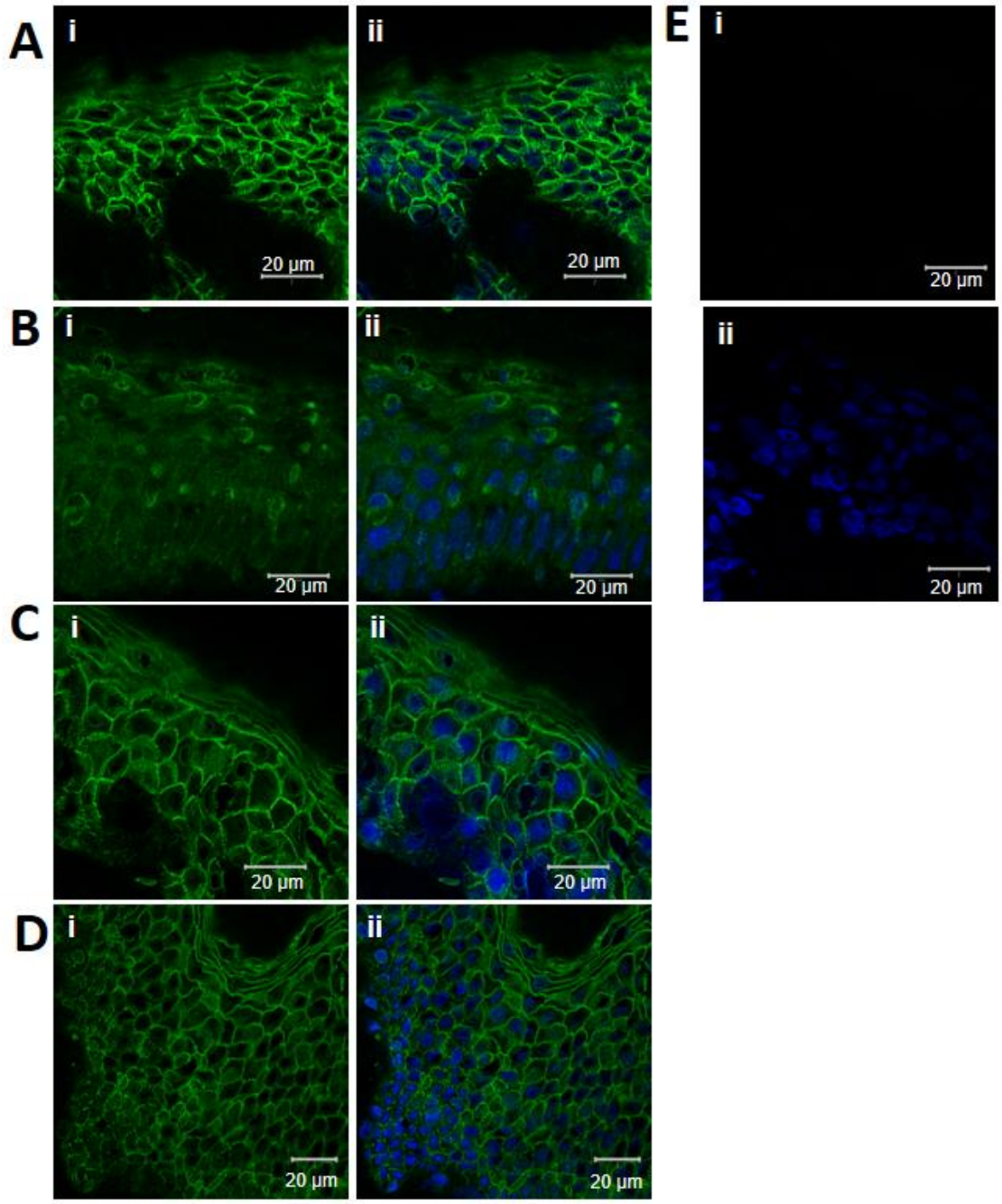

Figure 3.2.6 Variable iRHOM2 localisation in TOC skin, part 2. IHC of iRHOM2 in three TOC frozen skin biopsies taken at a later date than the original biopsy. iRHOM2 staining is shown in the absence (i) and presence (ii) of DAPI nuclear stain. **A:** Normal frozen facelift skin **B:** TOC patient 1 (n=2), **C:** TOC patient 2 (n=3), **D:** TOC patient 3 (n=2). **E:** Negative control. Images were taken on the Zeiss Meta 710 confocal microscope. iRHOM2 staining is shown in green and DAPI nuclear stain in blue.

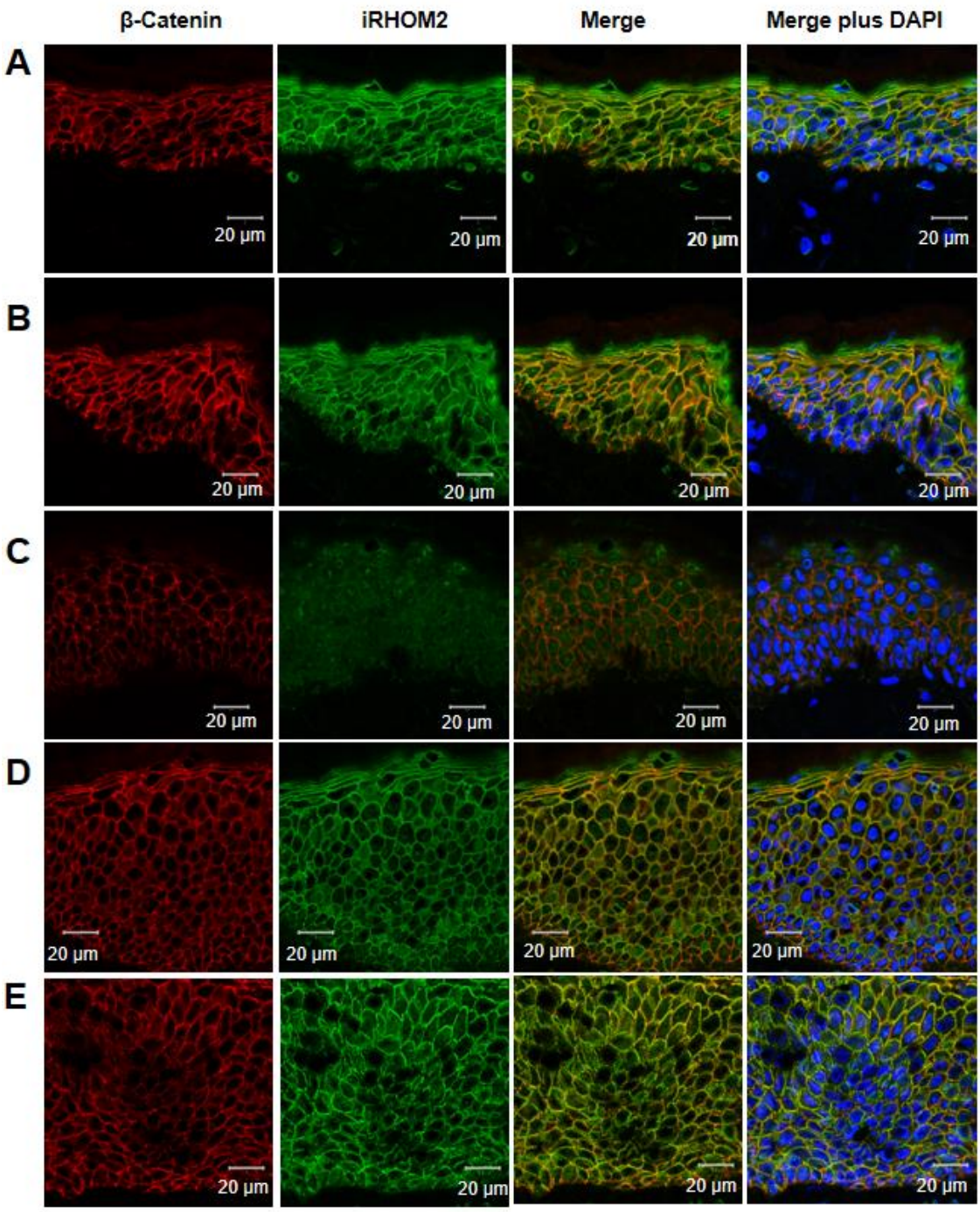

Figure 3.2.7 iRHOM2 still reaches the cell surface in TOC skin. Co-localisation of iRHOM2 and β-Catenin in TOC frozen skin sections compared to control skin (n=2). **A:** Normal skin (same settings as TOC patient 2 in E) **B:** Normal skin (same settings as TOC patients 1 and 3 in C and D). **C:** TOC patient 1, **D:** TOC patient 3, **E:** TOC patient 2. iRHOM2 staining is shown in green, β-catenin is shown in red, DAPI nuclear stain is shown in blue. Images were taken on the Zeiss Meta 710 confocal microscope. Control staining can be seen in Appendix A3.

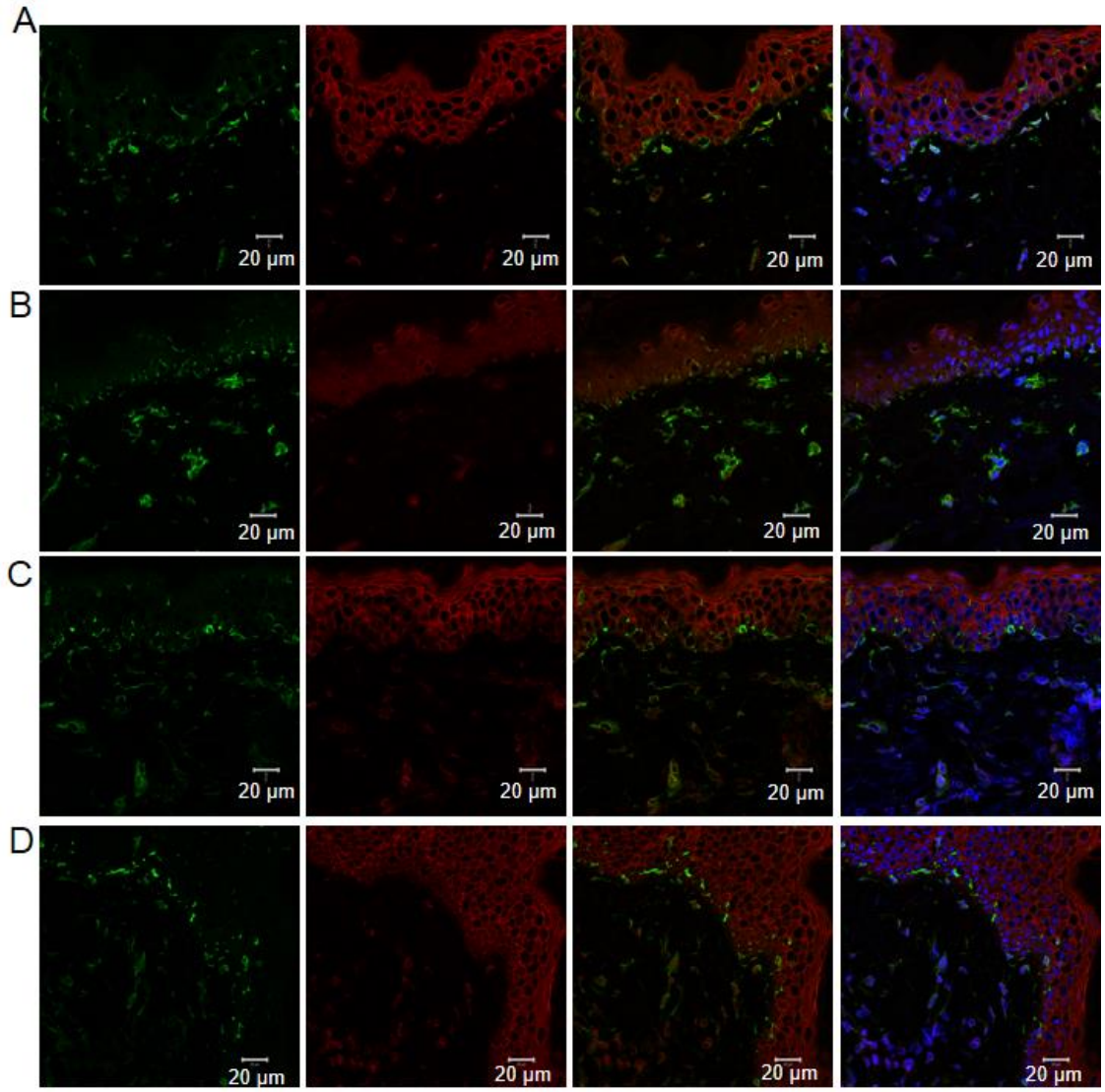

Figure 3.2.8 iRHOM2 appears unaffected in macrophages in TOC skin. IHC showing co-localisation of iRHOM2 and CD68 as indicated in **A:** Normal skin, **B:** TOC patient 1, **C:** TOC patient 2, **D:** TOC patient 3. CD68 is shown in green, iRHOM2 in red, and DAPI nuclear staining in blue. N=1. Please see Appendix A4 for control images. Images were taken on the Zeiss Meta 710 confocal microscope.

3.2.3.3 iRHOM2 localisation in TOC keratinocytes

The localisation of iRHOM2 in cutaneous keratinocytes was also investigated by ICC (figure 3.2.9). ICC was highly variable between a number of staining experiments, as seen in staining of NEB1 keratinocytes, so this figure represents one example. The variation may suggest that small changes in culture conditions and perhaps cell confluence levels can impact on iRHOM2 localisation, which may reflect changes in its activity in different situations. This may also reflect the differentiation status of the cells, as the cells were cultured in high Ca^{2+} medium.

As described in section 3.2.1, in NEB1 control keratinocytes, iRHOM2 showed a predominantly punctate perinuclear localisation, which was consistent between different experiments. Some faint plasma membranous staining can be seen here (figure 3.2.9 A), which occurred in many but not all experiments. Staining in K17 control keratinocytes was also punctate and predominantly perinuclear, with some even fainter cell-surface staining, but the intensity of the staining appeared reduced. TYLK1 and TYLK2 keratinocytes also showed punctate iRHOM2 staining, but this appeared to be found throughout the cell, reaching to the plasma membrane. Staining was also seen in the plasma membrane in TYLK1 but not TYLK2 cells (figure 3.2.9), although again, there was variation in the plasma membranous staining between different experiments.

Figure 3.2.9 B shows the staining at a higher magnification, allowing clearer visualisation of the cell-surface staining. Negative control staining is shown in figure 3.2.9 C. K17, TYLK1 and TYLK2 cells were perhaps at a lower confluence level than NEB1 cells for this experiment, and did not form the same block-like morphology, possibly explaining some variation within this experiment.

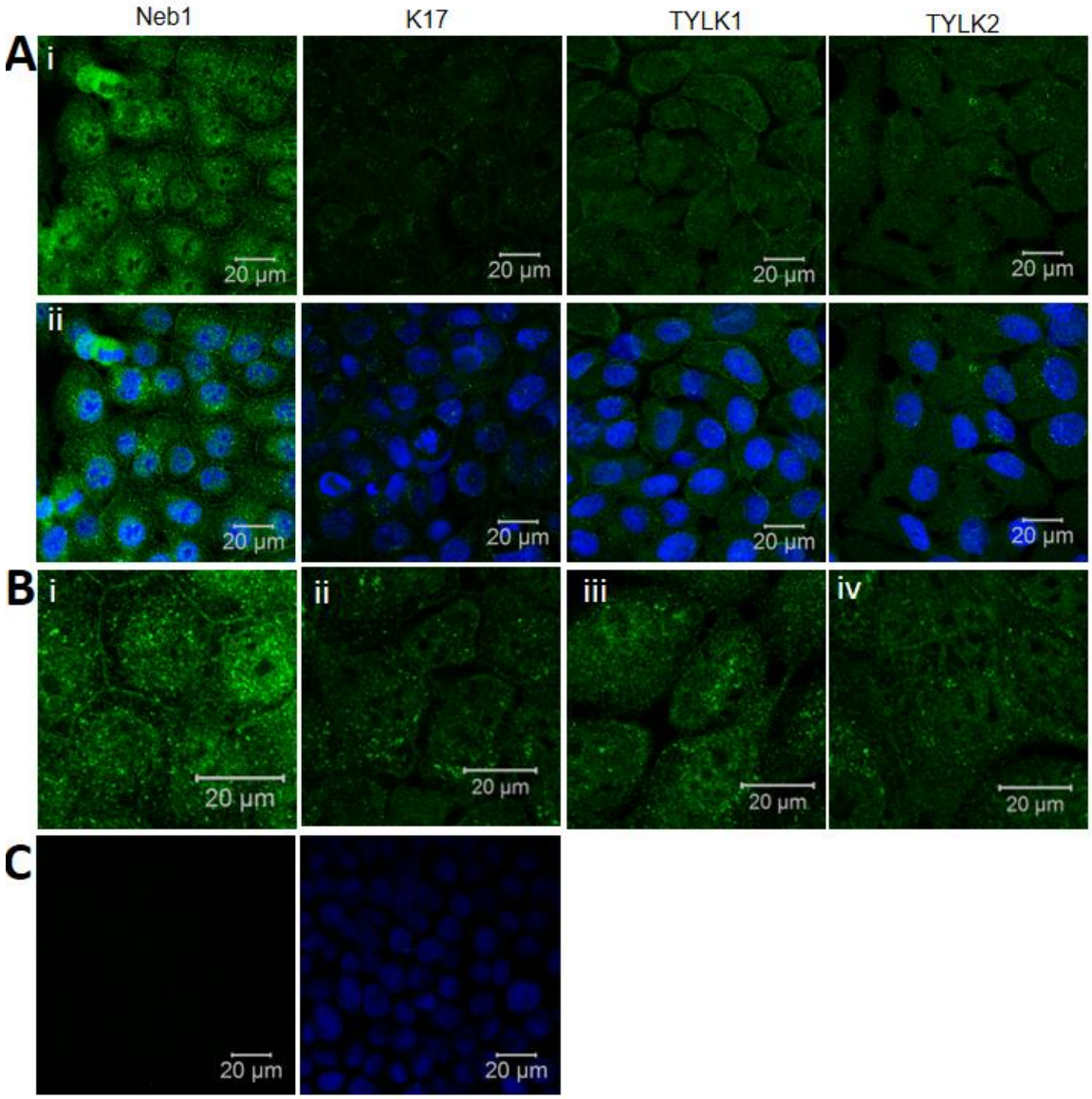

Figure 3.2.9 iRHOM2 localisation in TOC and control keratinocytes. A: An example of ICC of iRHOM2 in control and TOC keratinocytes as indicated in the absence (i) and presence (ii) of DAPI nuclear stain (n=5). **B:** Control and TOC cells at a higher digital zoom. **C:** Negative control. Images were taken on the Zeiss Meta 710 confocal microscope.

3.2.4 iRHOM2 expression appears reduced in TOC

IHC in frozen skin sections appeared reduced in TOC epidermis compared with control epidermis (figures 3.2.5-3.2.8). It is difficult to accurately determine expression levels from immunofluorescence, but similar results were seen in western blots with lysates from NEB1 cells overexpressing WT and TOC-mutant GFP-tagged iRHOM2, (figure 3.2.10 A), where the intensity of the higher band representing GFP-tagged iRHOM2 was much lower for both iRHOM2-I186T and iRHOM2-P189L. Repeats of this experiment are shown in appendix A5. The expression levels of iRHOM2-GFP were variable between experiments, but the overall trend appears consistent in NEB1 cells. Interestingly, the same difference was not seen in HEK293T cells overexpressing iRHOM2 (appendix A5).

Flow cytometry was performed on NEB1 cells overexpressing both isoforms of iRHOM2. Flow cytometry counts individual cells, allowing selection of all GFP-expressing keratinocytes and exclusion of untransfected cells. Flow cytometry measurements were performed with the help of Dr Luke Gammon, Centre for Cutaneous Research, QMUL. Consistent with the western blotting results in figure 3.2.10 A, the fluorescence intensity appeared slightly lower in mutant iRHOM2-expressing cells than WT overexpressing cells (figure 3.2.10 B). Interestingly, the fluorescence intensity of isoform 2-transfected cells appeared slightly higher than the intensity of cells transfected with isoform 1, which would be consistent with the intensity of the RT-PCR bands for iRHOM2 mRNA levels in figure 3.2.4.

Cells were stained with PI immediately before flow cytometry analysis to determine cell-death levels in the cells, and whether cell death was the cause of the lower overexpression levels seen. There was a slight trend towards increased cell death in cells overexpressing isoform 2 (figure 3.2.10 C) shown by the percentage of cells positive for propidium iodide, which could explain some of the difference seen. However, flow cytometry measures individual cells and the cells included in the analysis for fluorescence were negative for propidium iodide. Furthermore, increased cell death was not seen in cells overexpressing mutant iRHOM2 compared to cells overexpressing wild type iRHOM2, so cell death does not appear to account for the reduced intensity. Cells transfected with Connexin 31 WT and the C86S mutant were included as negative and positive controls for cell death. Connexin 31 C86S is a *GJB3* mutation associated with autosomal dominant erythrokeratoderma variabilis (EKV), and its expression causes activation of the UPR and cell death (Tattersall et al., 2009).

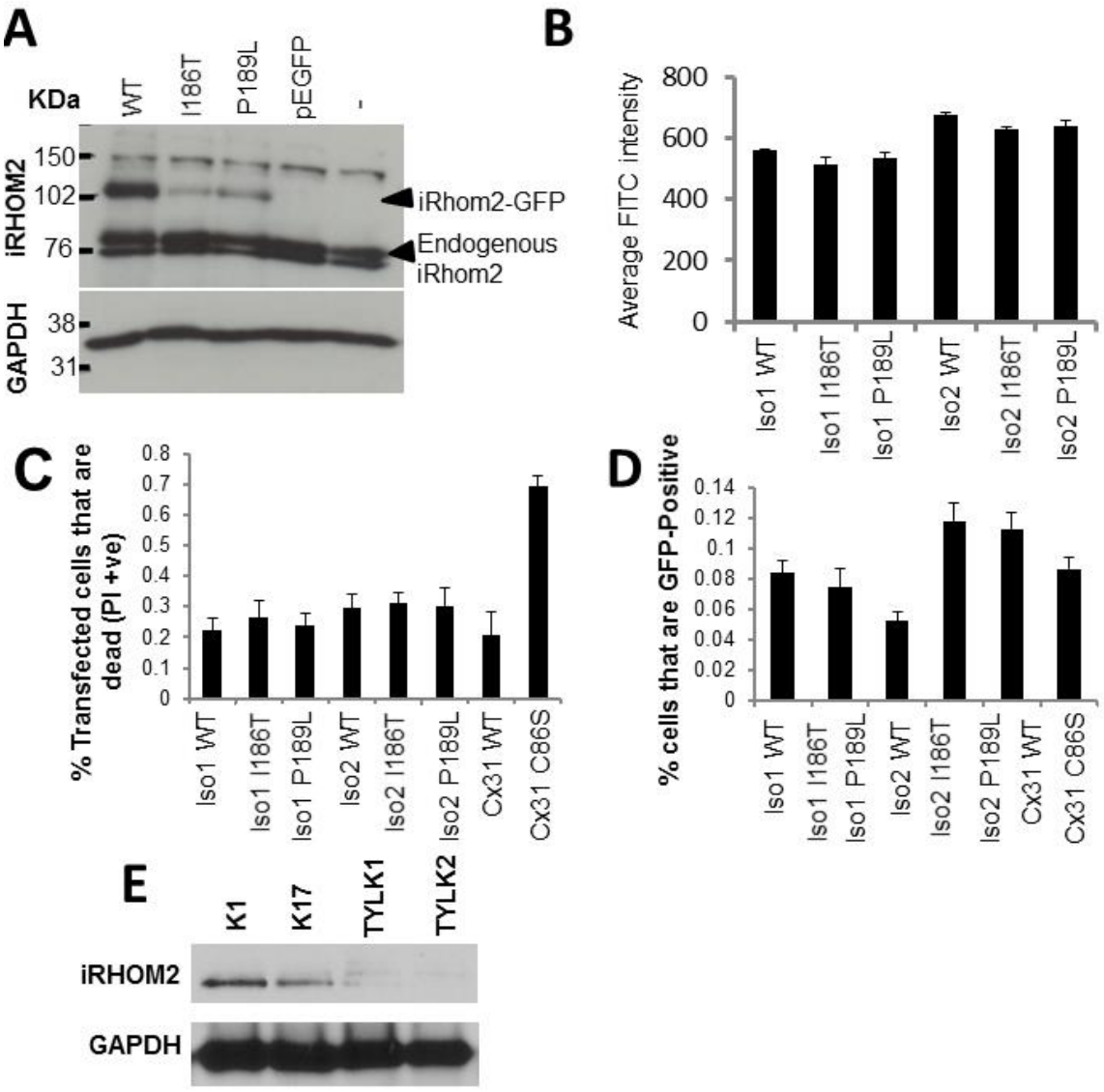

Figure 3.2.10 iRHOM2 harbouring TOC mutations expresses at a lower level when overexpressed in NEB1 keratinocytes. NEB1 cells were transfected as indicated with iRHOM2 WT or TOC mutant, pEGFP, or were untransfected control cells. **A:** Western blot showing expression of iRHOM2-GFP isoform 2, and endogenous iRHOM2 (n=3). **B:** Graph of a flow cytometry experiment showing average FITC intensity for each event for cells overexpressing isoform 1 and isoform 2 of iRHOM2 (n=3). **C:** Percentage of cells in flow cytometry experiments that are positive for PI staining, i.e. dead cells (n=3). Connexin 31 WT and EKV-mutant expressing cells were included as positive and negative controls for cell death. **D:** Graph showing the percentage of GFP-positive cells of all the total events in flow cytometry experiments (n=3). **E:** Western blot showing iRHOM2 and GAPDH loading control in lysates from 3D raft cultures with control (K1 and K17) and TOC (TYLK1 and TYLK2) keratinocytes (n=1). 3D cultures and western blot was performed by Dr Nihal Kaplan and Dr Spiro Getsios, Northwestern University, Chicago, US.

It is also possible that the differences seen by western blot could have resulted from lower transfection efficiency with mutant iRHOM2. To determine whether this was the case, the transfection efficiency in the flow cytometry experiments was estimated by the percentage of GFP-positive cells in the population (figure 3.2.10 C). The transfection efficiency did appear to be slightly greater for isoform 2, and also appeared to be lower for iRHOM2-P189L isoforms 1 and 2. However, the reduction in transfection efficiency does not appear to correlate closely with the reduction in protein expression in figure 3.2.10 A, particularly for iRHOM2-I186T. The flow cytometry experiments measure the intensity of individual cells that have taken up the GFP-tagged plasmid, which should in part control for this possibility unless there was a large variation in the number of plasmids taken up by the cells in each experiment.

Further evidence for a reduction in iRHOM2 expression in TOC is shown by western blots in lysates from 3D raft cultures with the TOC keratinocytes by Dr Spiro Getsios and Dr Nihal Kaplan, Northwestern University, Chicago (figure 3.2.10 E), which show reduced levels of iRHOM2 in raft cultures from TOC keratinocytes compared with control keratinocytes. Interestingly, western blots of TOC keratinocytes grown in monolayer culture did not always show reduced levels of iRHOM2, which will be discussed further later in this chapter and in the next chapter.

3.2.5 Is expression of iRHOM2 specific to keratinocytes?

Overexpression of GFP-tagged WT and mutant iRHOM2 constructs in both NEB1 and HeLa cells showed variable distributions of iRHOM2 (figure 3.2.11). In NEB1 keratinocytes (figure 3.2.11 A), iRHOM2 appeared to localise predominantly to cell-cell borders, as seen in normal epidermis (figure 3.2.1) with some intracellular localisation particularly in the perinuclear region of the cells. There was perhaps a slight increase in perinuclear localisation of iRHOM2 in some cells expressing iRHOM2-P189L, but there were no striking differences in WT and mutant iRHOM2 localisation.

In HeLa cells (figure 3.2.11 B), both WT and mutant iRHOM2 appeared to be present throughout the cell (figure 3.4A), with some aggregation of iRHOM2 in the perinuclear areas of some cells. This may suggest that there is something specific to keratinocytes that leads to iRHOM2 localisation at the plasma membrane. However, HeLa cells were derived from cervical cancer, and have been passaged many times so do not represent a normal non-keratinocyte cell line. Therefore, overexpression in a wider range of cell lines and staining in endogenous tissues could be performed. Other groups have also shown an ER-localisation of iRhom2 in non-keratinocyte cells including COS-7 cells (Zettl et al 2011), L929 cells (McIlwain et al 2012 supplementary information) and MEFs

(Hosur et al 2014). Furthermore, iRHOM1 does not go to the plasma membrane in keratinocytes (chapter 4), suggesting that cell-surface localisation of iRHOM2 in keratinocytes and squamous tissue is specific to iRHOM2. The cell surface localisation of iRHOM2 in the epidermis and in the oesophagus will be discussed further later in the thesis.

To confirm that iRHOM2-GFP is indeed reaching the cell surface, co-localisation of iRHOM2-GFP with the cell-surface proteins E-Cadherin and PG was performed (figure 3.2.12). Though the level of cell-surface iRHOM2 expression appeared variable, where it reached the plasma membrane, co-localisation was seen with both E-Cadherin and PG. Negative controls and repeats with the iRHOM TOC mutants not shown in figure 3.2.12 can be seen in Appendix A6.

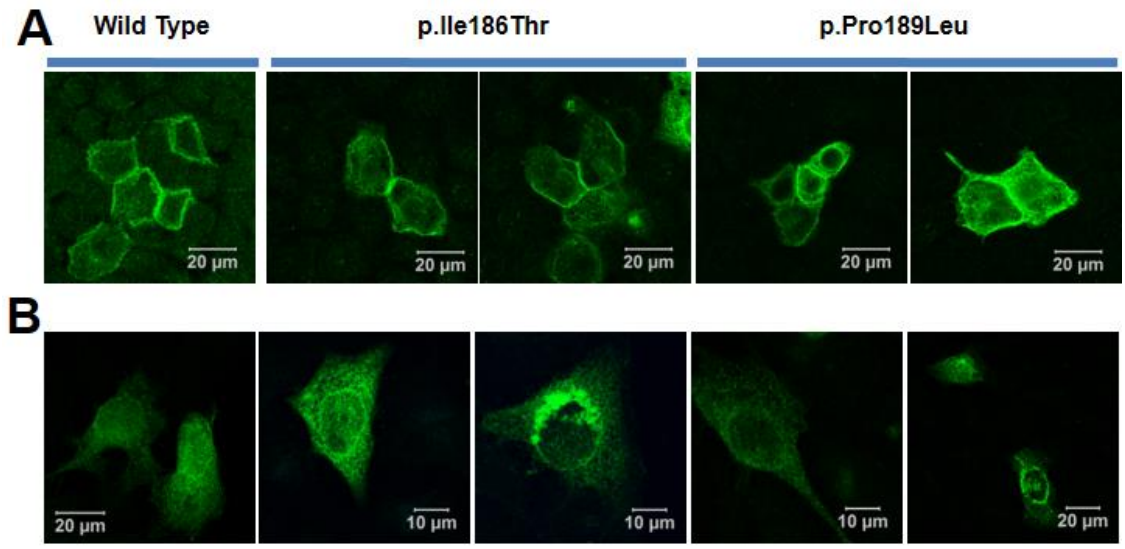

Figure 3.2.11 Expression of iRHOM2-GFP at cell-cell borders in keratinocytes but not HeLa cells is unaffected by mutations found in TOC. GFP-tagged WT and TOC-mutant iRHOM2 was overexpressed in **A:** NEB1 keratinocytes (n=3) **B:** HeLa cells (n=1). Imaging was performed on the Zeiss Meta 710 Confocal Microscope.

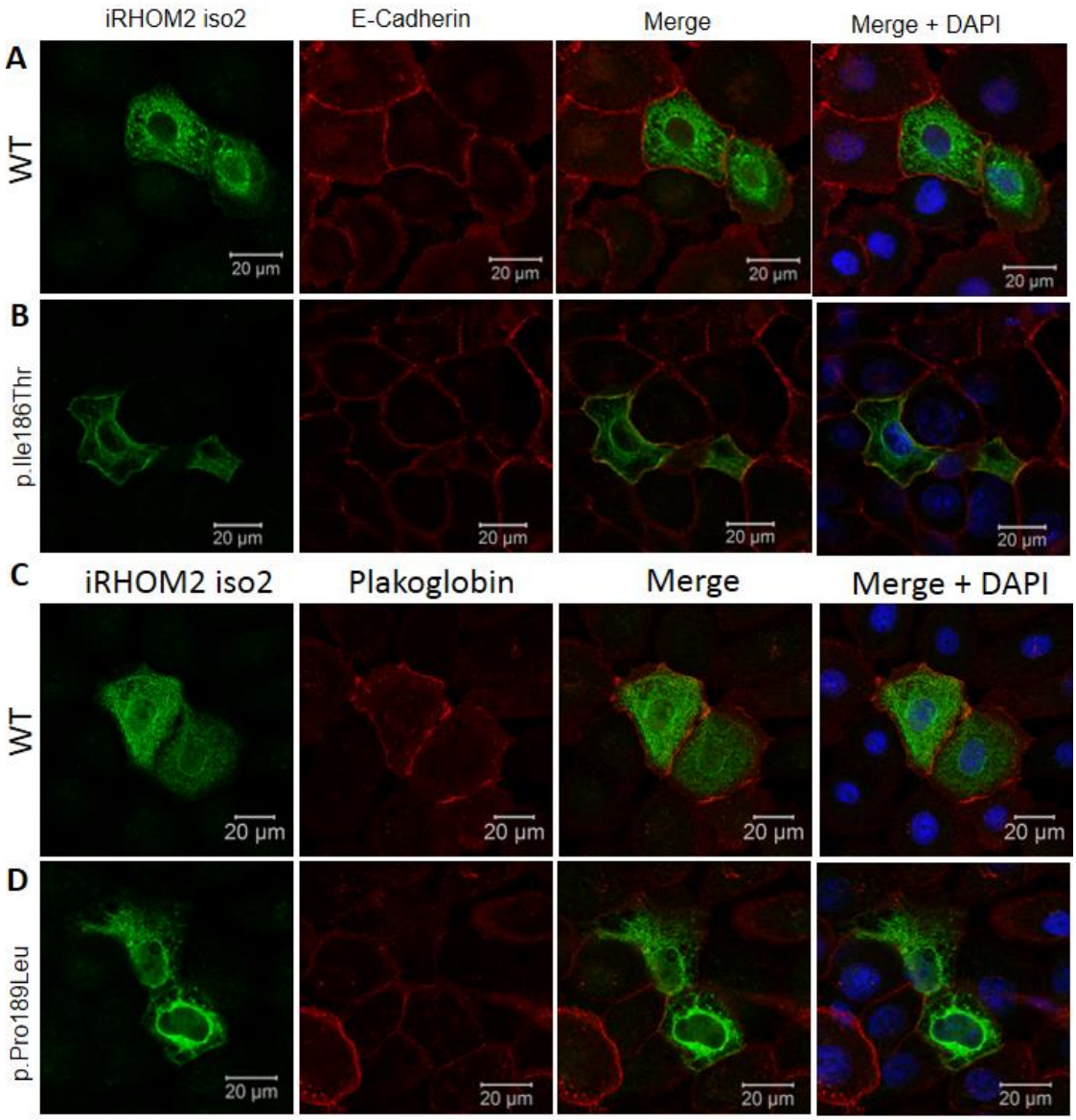

Figure 3.2.12 Co-localisation of overexpressed iRHOM2 with membrane protein E-Cadherin and membrane-associated desmosomal protein PG. A and **B:** Co-localisation in NEB-1 cells of overexpressed iRHOM-WT-GFP (**A**) and iRHOM2-I186T-GFP (**B**) with membrane protein E-cadherin (n=1); **C** and **D:** Co-localisation of iRHOM2-WT-GFP (**C**) and iRHOM2-P189L-GFP (**D**) with PG, which can associate with both desmosomes and AJ at the cell-surface (n=1). Images were taken on the Zeiss Meta 710 LSM confocal microscope. iRHOM2-GFP is shown in green, E-Cadherin and PG are shown in red, DAPI nuclear staining is shown in blue.

3.2.6 Desmosomes are dysregulated in TOC

To look more closely at the structure of TOC epidermis and investigate epidermal structures such as the desmosomes, biopsies from TOC patients 1, 2 and 3 were fixed in gluteraldehyde. The biopsies were processed for electron microscopy by Mr Graham McPhail, Pathology department, Barts and the London School of Medicine and Dentistry. Electron microscopy was performed by Professor Akemi Ishida-Yamamoto, Tokyo, Japan.

Desmosomes in all layers of TOC epidermis lacked the electron-dense midline seen in mature desmosomes in normal epidermis (figure 3.2.13), suggesting that they are in the immature form seen in wound healing (Garrod et al 2005). To look further at which desmosomal proteins were affected, western blotting was performed in lysates of control (NEB1 and K17), and TOC (TYLK1 and TYLK2) keratinocytes after culture in the presence and absence of exogenous EGF (figure 3.2.14), as desmosomal proteins are regulated by EGF signalling (Lorch et al., 2004; Klessner et al., 2009). A summary of all western blots and GAPDH loading control are shown in appendix A7.

There was some variation in expression of desmosomal proteins between the different cell lines, but the majority of the proteins did not show a distinction in expression between control and TOC keratinocytes. The exception was DSG2, which was consistently reduced in TOC keratinocytes after culture in the absence of EGF, but this difference was much less clear after culture in the presence of EGF (figure 3.2.14). Increased expression of PKP1, PKP2 and PG was seen in NEB1 cells after culture in the absence of EGF relative to the other three cell lines. Western blots of lysates from the absence and presence of EGF were carried out separately, however, and so cannot be compared directly.

DSP isoforms I and II, PG, both DSC2 isoforms and DSG2 appeared at approximately the size expected. PKP1 and PKP2 appeared slightly lower than the expected size (PKP1 was ~70-76 KDa compared with the predicted 87 KDa, and PKP2 was ~76 KDa, while it was predicted to be 97 KDa). Some of the size differences may be explained by uneven running of the gel, but it is surprising that PKP1 and 2 appeared ~15 KDa smaller. PKP2 appeared closer to 100 kDa after culture in RM-, suggesting that the size difference may be an issue with the marking of the ladder used in the western blots.

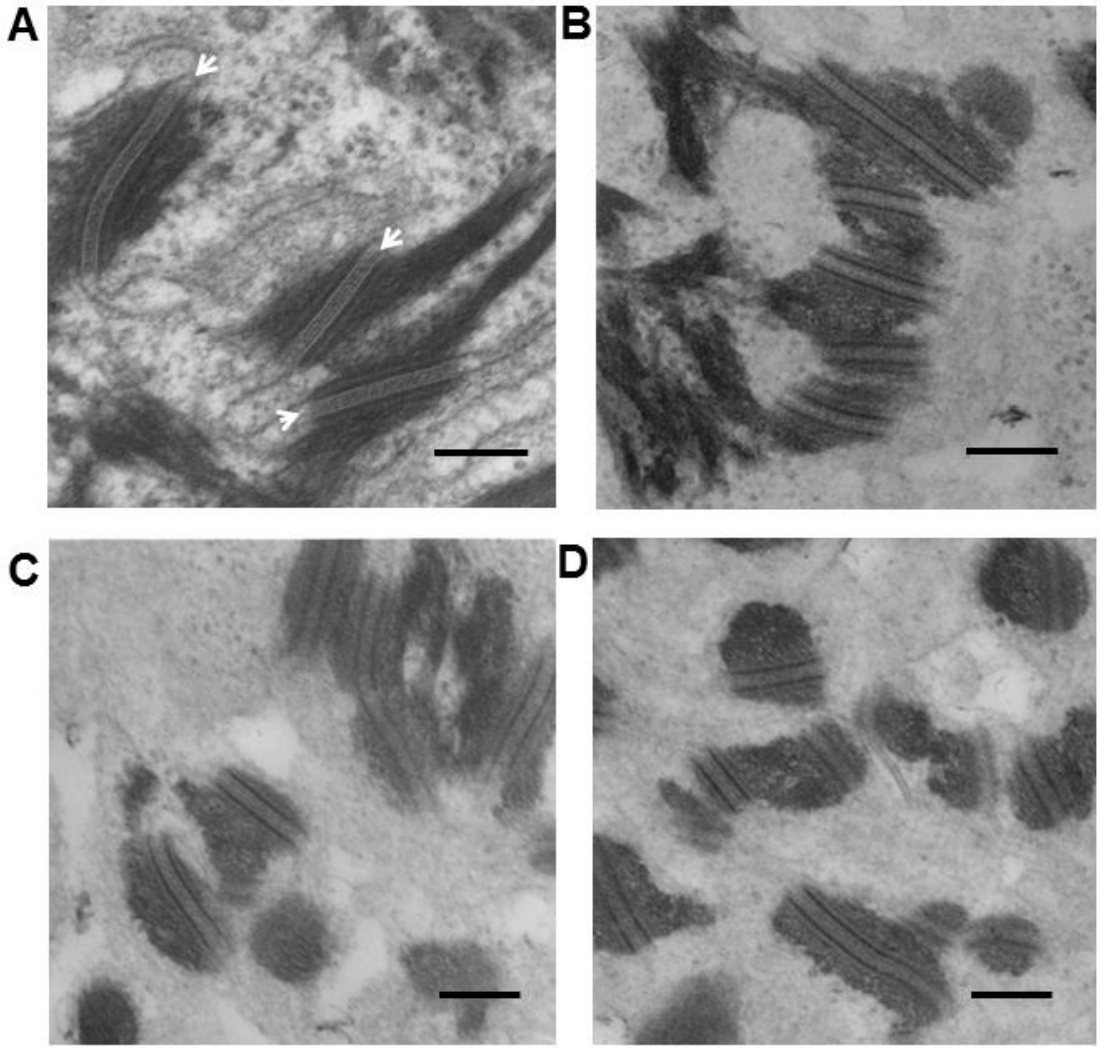

Figure 3.2.13 TOC skin lacks mature desmosomes. Electron microscopy showing desmosomes in **A:** Normal skin and **B-D:** Three TOC patients. White arrows in **A** indicate electron dense midlines seen in desmosomes of normal skin but not TOC skin. Scale bars represent 200 nm. Electron microscopy was performed by Dr Akemi Ishida-Yamamoto, Asahikawa Medical University, Japan.

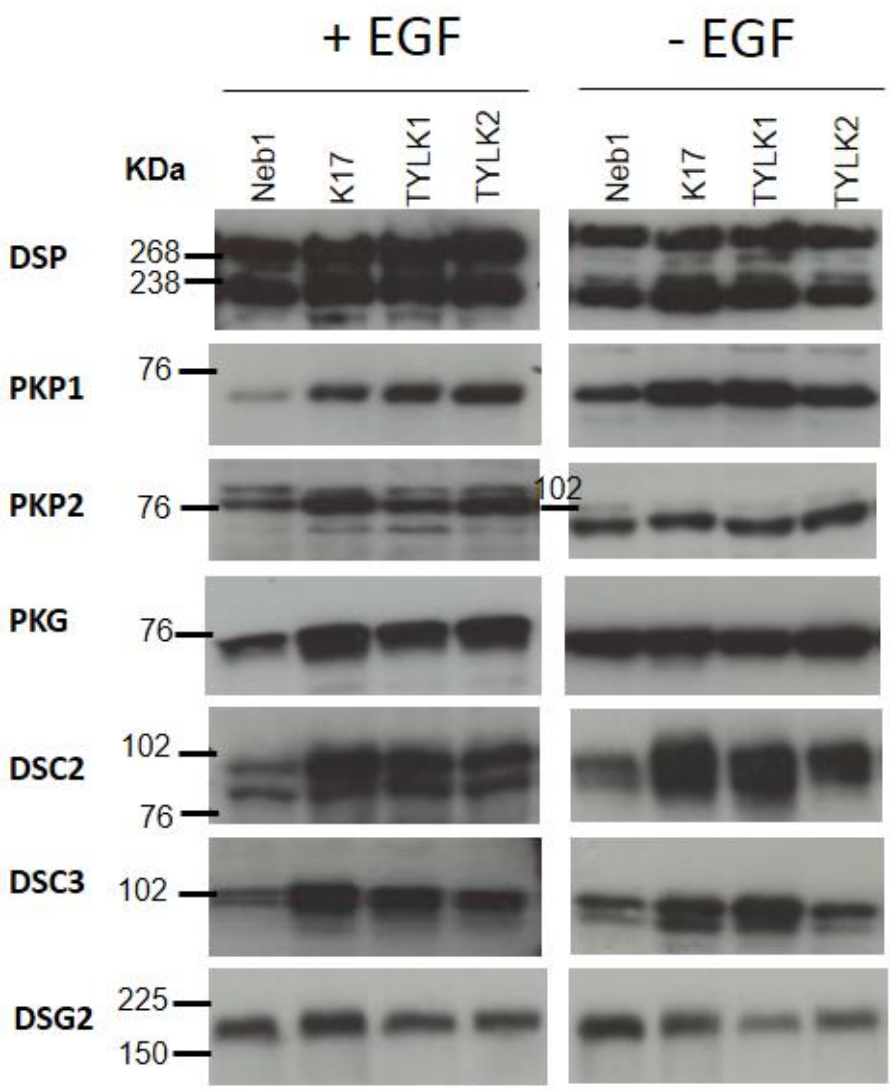

Figure 3.2.14 Variable expression of desmosomal proteins in control and TOC keratinocytes. Western blots showing levels of several desmosomal proteins in control and TOC keratinocytes after culture in the presence and absence of exogenous EGF, as indicated. Please see appendix A7 for repeats of the western blots in two more sets of protein lysates.

3.2.6.1 Increased desmoglein 2 processing in TOC

As levels of full-length DSG2 protein appeared reduced in TOC keratinocytes after culture in the absence of EGF, and DSG2 is of interest as a substrate of ADAM17 (Lorch et al., 2004; Bech-Serra et al., 2006), the DSG2 western blots were analysed further. The antibody used to detect DSG2 protein is Ab10, a polyclonal antibody raised against the extracellular domain of DSG2 closest to the membrane (Brennan and Mahoney, 2009). DSG2 is cleaved by ADAM17 in the juxtamembrane region to give a 100 KDa fragment, the intensity of which is reduced in the presence of siRNA targeting ADAM17 (Klessner et al., 2009). The 100 KDa fragment comprises the entire DSG2 cytoplasmic tail, transmembrane domain, and an extracellular juxtamembrane domain.

The anti-DSG2 western blot detected fragments at approximately the reported sizes for full-length and ADAM17-cleaved DSG2 (Klessner et al., 2009) (figure 3.2.15 A). There were no clear differences in the intensity of the bands for cleaved DSG2 in control and TOC keratinocytes after culture in the presence of exogenous EGF, as described for full-length DSG2 in the previous figure. However, the reduction in full-length DSG2 in TOC keratinocytes after culture in the absence of EGF was accompanied by an increase in the intensity of the 100 KDa band representing cleaved DSG2, particularly in TYLK1 cells (figure 3.2.15 A). The other bands seen may represent DSG2 cleavage products mediated by other enzymes such as ADAM10 (Klessner et al., 2009). Graphs showing densitometry analysis of three repeats of the experiments are shown in figure 3.2.15 B. There is some variation between experiments, but there is a clear trend, and the findings are consistent with further repeats by Dr Matthew Brooke, and with increased ADAM17 activity in TOC which is discussed in the next chapter.

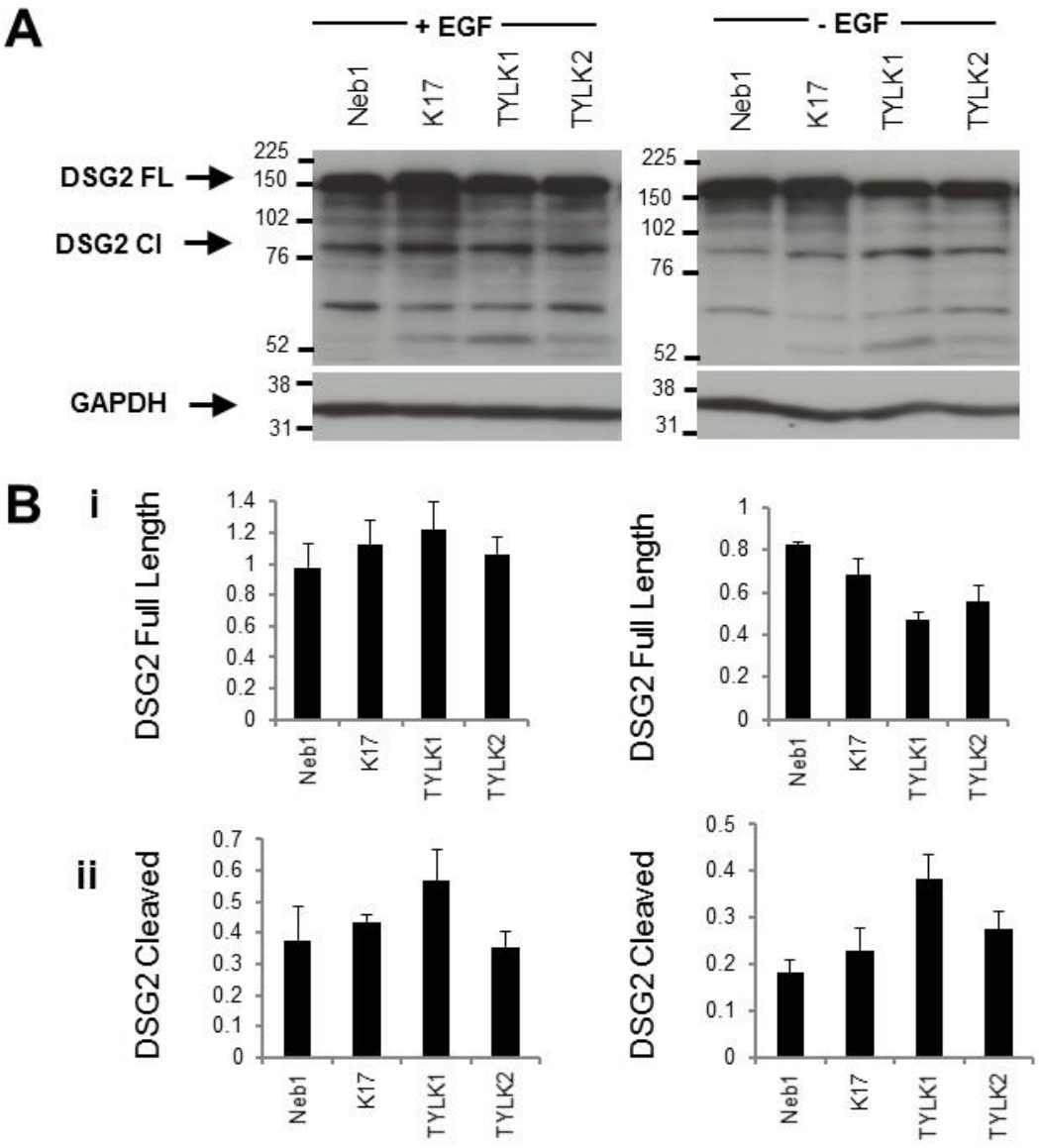

Figure 3.2.15 Reduced levels of ADAM17 substrate DSG2 in TOC cells. Control and TOC cells were cultured in the presence and absence of exogenous EGF. **A:** Western blots of DSG2, including full length DSG2 (DSG2 FL), cleaved DSG2 and GAPDH loading control in the control and TOC cells. The band thought to represent ADAM17-cleaved DSG2 (Klessner et al., 2009) is indicated as 'DSG2 Cl'. **B:** Densitometry of DSG2 FL **(i)** and DSG2 Cl **(ii)** in cells after culture in the presence and absence of EGF, n = 3. Densitometry was carried out with Image J.

3.2.6.2 DSG2 localisation in monolayer keratinocytes

ICC of DSG2 in keratinocytes after culture in the presence and absence of EGF is shown in figure 3.2.16. After culture in the presence of EGF, DSG2 appeared to be localised in a thin line around the plasma membrane (figure 3.2.16A) with no clear differences between control and TOC cells. There was also punctate staining throughout the cell, which may have been due to inclusion of the cell surface in the confocal image. After culture in the absence of EGF (figure 3.2.16 B), the plasma membrane localisation appeared slightly different, with projections crossing the membrane in some cells as if the cells were being 'stitched together' by DSG2, which would be consistent with increased desmosome formation in the absence of EGF, and the formation of desmosomal links between cells. Again, there were no clear differences between control and TOC keratinocytes.

The cells were confluent in both experiments, but may have been more tightly packed after culture in the presence of EGF, which could influence DSG2 localisation. ICC of DSG2 was performed with the monoclonal antibody 10D2, which recognises a specific region of DSG2 EC1 region (Keim et al., 2008), so staining with Ab10 would be of interest for future work to see whether a change in DSG2 localisation is seen in TOC keratinocytes. Further repeats are needed to confirm whether there is a consistent difference. A z-stack, or whole cell imaging and co-localisation with a cell-surface, or lipid raft marker, would also allow collection of a complete picture of DSG2 localisation in control and TOC keratinocytes in future imaging.

IHC of DSG2 in TOC frozen skin sections was also performed with antibody 10D2. However, the staining was very faint and difficult to see and therefore not shown. DSG2 has been reported to be expressed at low levels in the basal layer of the epidermis (Brennan and Mahoney, 2009), which could explain why little staining was seen in skin sections. Keratinocyte cell lines are proliferative and represent cells of the basal layer, perhaps explaining why differences in DSG2 were seen in monolayer. One example of DSG2 IHC with antibody 10D2 is shown in appendix figure A8, which shows intracellular DSG2 staining in the epidermis and cell-surface DSG2 in the hair follicle of the same tissue section, so future work staining DSG2 with 10D2, and perhaps Ab10 IHC would be of interest to determine DSG2 localisation in the epidermis.

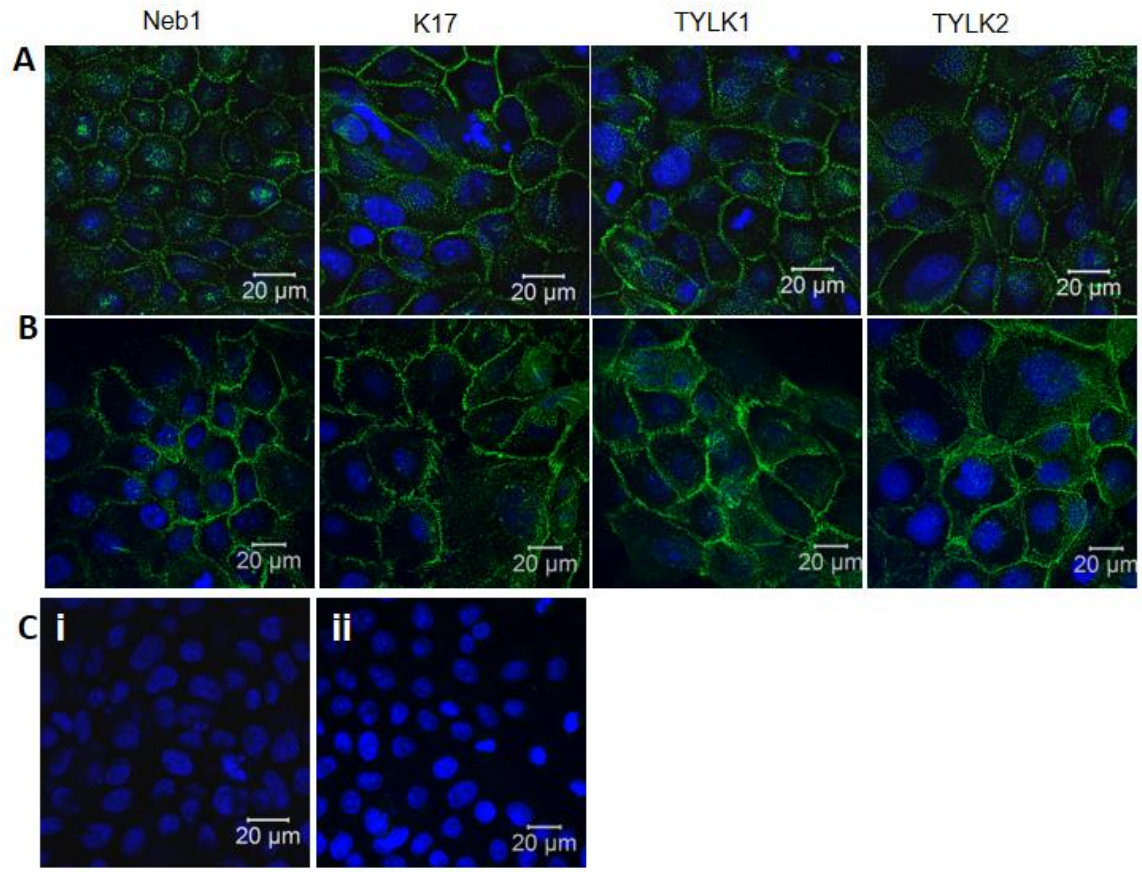

Figure 3.2.16 DSG2 localisation in cells cultured in the presence and absence of exogenous EGF. ICC of DSG2 in cells after culture in RM+, with EGF (**A**) (n=2) and RM- (n=2), without EGF (**B**). A and B were carried out in separate staining and imaging experiments. **C:** Negative controls for A are shown in (i) and B are shown in (ii). Images were taken on the Zeiss Meta 710 Confocal microscope. DSG2 is shown in green, DAPI nuclear stain shown in blue.

3.2.6.3 Localisation of desmosomal proteins in normal and TOC skin

These findings may suggest that another cadherin is affected in the upper layers of the epidermis, so IHC of a panel of desmosomal proteins was also performed in skin biopsies (figure 3.2.17 and appendix A9-A22). IHC in control skin and patient 1 is shown in figure 3.2.17. There were no clear differences in the localisation of most of the desmosomal proteins stained. There were perhaps some subtle differences in staining intensity in patient 1, for example staining of DSG1 and 2, PG and DSP was possibly slightly reduced in patient 1 (figure 3.2.17 B, D and F) and perhaps PKP1 was slightly increased in the upper epidermal layers, which was also seen in the other TOC patients (figure 3.2.17 E and appendix A20). Interestingly, DSC2 appeared up-regulated in patient 2, but not patients 1 or 3 (figure 3.2.17 G). The localisation did not appear to be significantly altered, shown in figure 3.2.17 H, which has increased digital zoom and reduced gain to allow visualisation of the localisation.

3.2.6.3.1 Desmosomal proteins in cell monolayer

The localisation of desmosomal proteins was also investigated in keratinocyte monolayers by ICC after culture in the presence of EGF (figure 3.2.18 parts A and B). There did not appear to be any striking differences in the localisation of any of the desmosomal components between control and TOC keratinocytes, although there was some variation in the staining. DSG1 appeared at lower intensity in NEB1 keratinocytes, with little membranous staining in TYLK2 cells (figure 3.2.18 A), but it would perhaps be expected at low levels in the basal layer and monolayer keratinocytes. There perhaps appeared to be less membranous staining of DSC2 in TYLK1 cells (figure 3.2.18 B), but NEB1 cells appeared at a higher density than the other cell lines. DSC3 membranous staining appeared variable, with perhaps lower intensity in NEB1 cells as seen by western blotting. PG membranous staining perhaps appeared more diffuse in TOC keratinocytes (figure 3.2.18 D), but again, NEB1 cells were more densely packed in staining of PG, which could affect desmosomal proteins. Very low staining levels of PKP1 were seen in all cell lines (figure 3.2.18 E), perhaps because it is expressed minimally in the basal layer. No clear differences could be seen in PKP2 or DSP staining (figure 3.2.18 F and G).

Overall, more work is needed to investigate desmosomal proteins in TOC. Perhaps future experiments after culture in the absence of EGF would highlight any subtle differences, as was the case for DSG2. Culture was in high Ca^{2+} medium, which should encourage the formation of cell-cell adhesion complexes and desmosomes.

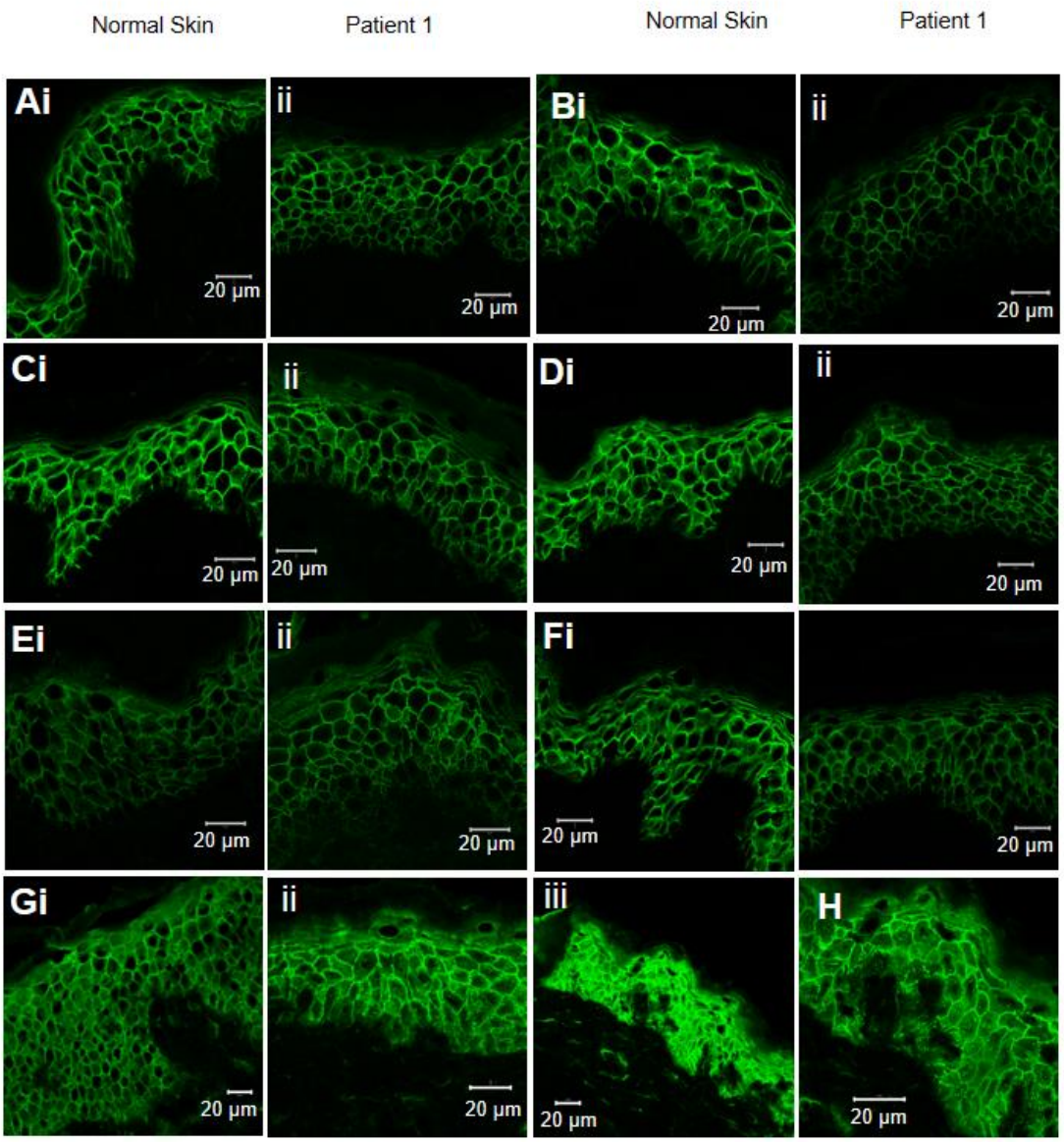

Figure 3.2.17 Localisation of desmosomal proteins in normal and TOC skin. IHC was performed against a panel of desmosomal proteins in frozen skin sections from normal (i) and TOC (ii) skin. **A-F:** Staining in normal skin and patient 1 of **A:** DSG1 (n=2), **B:** DSG1 and 2 (DSG3.10 antibody) (n=2) **C:** DSC3 (n=1), **D:** PG (n=1), **E:** PKP1 (n=2), **F:** DSP (n=2). **G:** DSC2 (n=1) in normal skin from breast (i); patient 1 (ii), patient 2 (iii), **H,** DSC2 in patient 2 at lower digital gain and exposure to allow visualisation of protein localisation. Further staining of the desmosomal proteins in all three patients can be seen in appendix A9-B22.

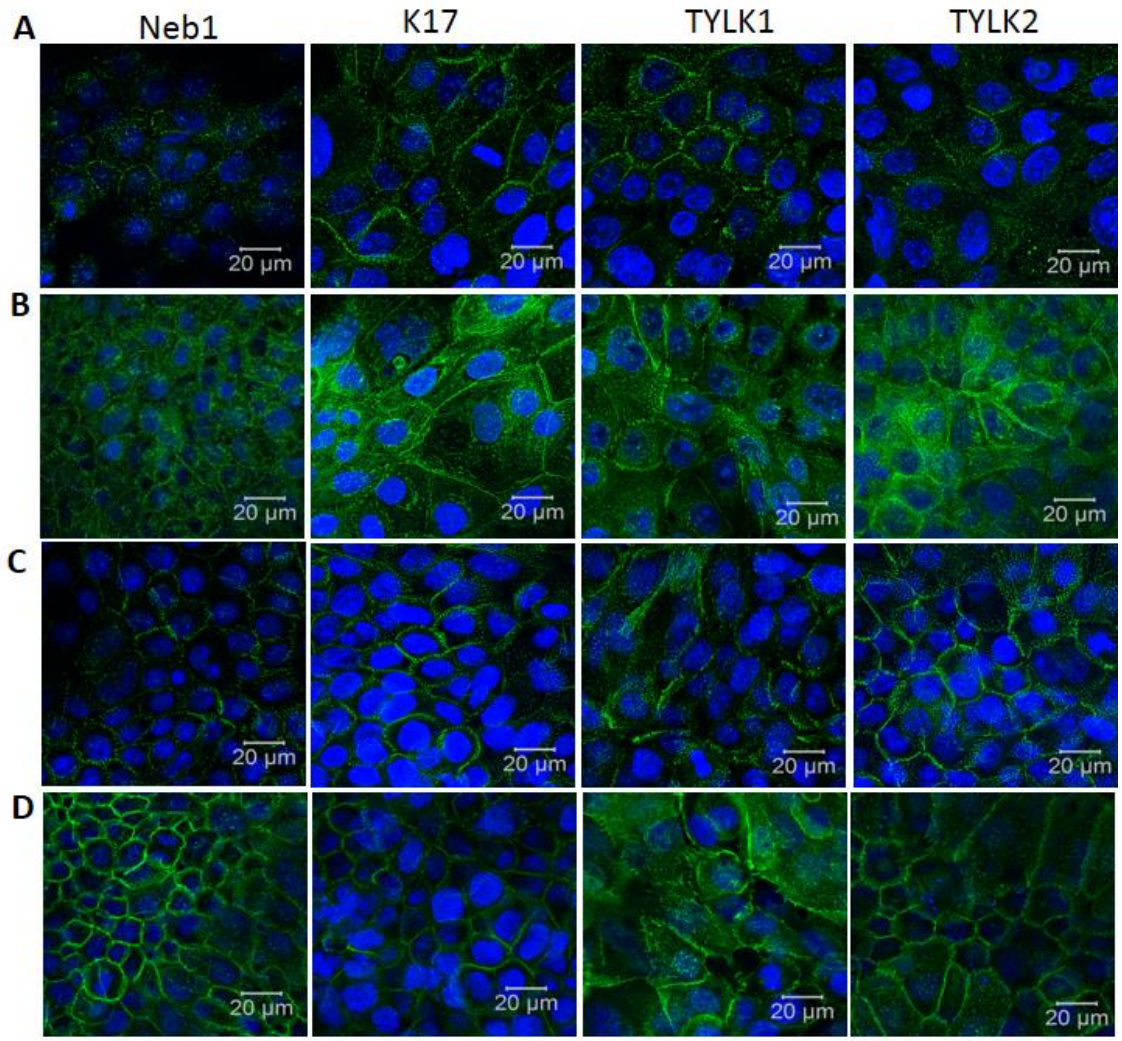

Figure 3.2.18 part 1: Desmosomal proteins in control and TOC cells. ICC showing desmosomal proteins in control (NEB1 and K17) and TOC (TYLK1 and TYLK2) cell lines (n=1). **A:** DSG1**, B:** DSC2, **C:** DSC3**, D:** PG**.** Images were taken on the Zeiss Meta 710 Confocal microscope. Desmosomal proteins are shown in green and DAPI nuclear stain in blue.

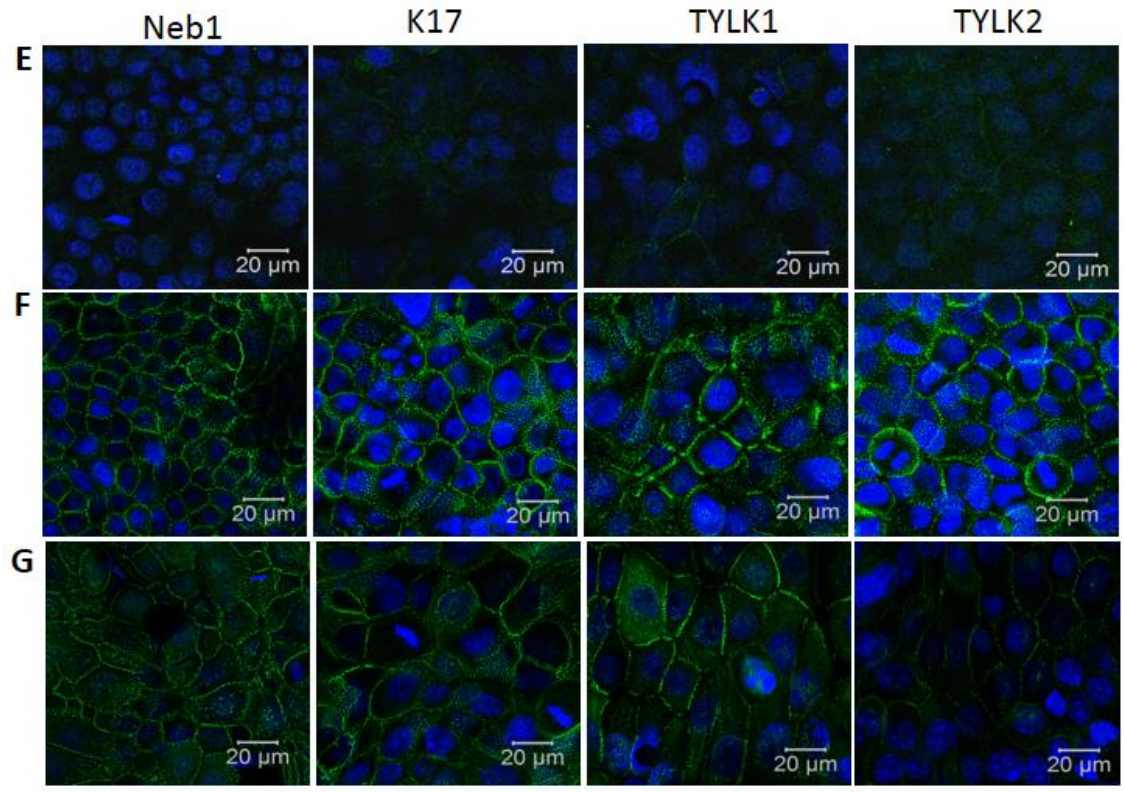

Figure 3.2.18 part 2: Desmosomal proteins in control and TOC cells. E: PKP1 (n=1), **F:** PKP2 (n=1), **G:** DSP (n=3). Images were taken on the Zeiss Meta 710 Confocal microscope. Desmosomal proteins are shown in green and DAPI nuclear stain in blue.

3.3 Discussion

3.3.1 Summary of results:

1) iRHOM2 is localised at the cell-surface in the skin and oesophagus
2) iRHOM2 localisation may be dysregulated in some instances in TOC
3) iRHOM2 expression may be reduced in TOC
4) Desmosomes in TOC epidermis lack electron-dense midlines
5) There appears to be increased processing of desmosomal cadherin DSG2 in TOC keratinocytes

3.3.2 iRHOM2 at the cell-surface

iRHOM2 was predicted to be an ER-membrane protein, and previously described functions of iRHOM2, including targeting of EGF for ERAD and trafficking of ADAM17, appear to be performed primarily from an ER localisation. However, IHC in the skin and oesophagus has not previously been described, and iRHOM2 appeared to show a predominantly plasma-membranous localisation in these tissues. The role of iRHOM2 at the cell surface in keratinocytes of the epidermis and oesophagus is unknown and could reflect an additional unknown function of iRHOM2. Another theory could be that excess iRHOM2 is 'stored' at the cell surface, which would be consistent with the variation in cell-surface iRHOM2 between overexpression experiments (figure 3.2.1D and 3.2.12), where there is likely to be more iRHOM2 than is needed in the cell. During imaging of cells strongly expressing iRHOM2 at the plasma membrane, fainter intracellular staining may have been missed as the microscope settings were adjusted for the bright staining seen at the plasma membrane. The often punctate localisation of iRHOM2 could also suggest localisation to a particular region of the cell membrane such as lipid rafts, where desmosomes are located, and/or in vesicles in intracellular staining.

Staining of monolayer keratinocytes did appear to show a mostly perinuclear punctate localisation, suggesting ER-localised iRHOM2 with some faint cell-surface staining. iRHOM2 did not co-localise with ER markers, however, but appeared 'next to' staining with ER markers (work by Dr Daniel Tattersall). iRHOM2 has 7TMD and a long *N*-terminus and loop L1, so the antibody could be recognising a portion of the iRHOM2 protein outside of the ER. The antibody epitope is shown in appendix A1. The cells shown in figure 3.2.1 were quite confluent, so perhaps cell contact or contact inhibition are affecting the appearance of cell-surface iRHOM2.

Previous studies reporting ER-localisation of iRHOM2 have predominantly been performed in monolayer culture using tagged versions of overexpressed iRHOM2 (Zettl et al., 2011). Some tumour biopsies shown in chapter 5 show cell-surface localisation, for example lung carcinoma, also suggesting that iRHOM2 may show plasma membrane localisation in other squamous tissues. iRHOM2 localisation in cancer will be discussed further in chapter 5.

The striking cell-surface staining seen in the skin and oesophagus (keratinocytes) perhaps suggests that something specific to these cells encourages a cell-surface localisation of iRHOM2. The protein unique to keratinocytes is keratin. A yeast-two-hybrid screen was performed with the *N*-terminal of iRHOM2, and results included three type I keratin proteins. This is currently being followed up by Dr Thiviyani Maruthappu in the group, so it will be interesting to see whether a link with keratins turns out to be a reason for cell-surface iRHOM2 localisation.

Also, perhaps there is a further link between iRHOM2 and the desmosomes additional to processing by ADAM17: DSP is the anchor protein that links the keratin cytoskeleton to the plasma membrane. In one experiment, DSP knock down in HaCaT keratinocytes resulted in a striking up-regulation of iRHOM2 (appendix A24). This result was not shown in this chapter as further repeats did not produce the same results, although the knock down was effective. Perhaps something specific to the conditions in the first experiment (e.g. there was a lot of cell death) could have caused up-regulation of iRHOM2. The appearance of cell-surface iRHOM2 in staining of keratinocyte monolayers was highly variable, and iRHOM2 localisation appears to be dynamic and to depend on the cell conditions.

3.3.3 iRHOM2 processing (Different iRHOM2 fragments in western blotting)

Nakagawa et al (2005) showed that iRHOM1 undergoes proteolytic cleavage to give a fragment around 52 KDa and likely an undetectable *N*-terminal cleaved fragment, which may be degraded due to the presence of the PEST sequence. A band potentially representing a processed form of iRhom2 was also detected in co-immunoprecipitation experiments (McIlwain et al., 2012) suggesting that iRHOMs themselves may be regulated by proteolytic cleavage. Processing of active rhomboid protease RHBDL2 has been shown – RHBDL2 is cleaved, then the *N*-terminus goes to the cell surface while the *C*-terminal portion remains in the ER membrane (Lei and Li, 2009).

iRHOM2 western blots often showed a band at approximately 52 KDa in cutaneous keratinocytes, which was also seen in HNSCC cells (chapter 5). This band was

sometimes increased in intensity in cells overexpressing iRHOM2, although this was again variable. Co-immunoprecipitation experiments also suggested iRHOM1 exists as a homodimer or oligomer (Nakagawa et al., 2005). An additional band at approximately 150 KDa was also often seen in iRHOM2 western blots which could reflect an iRHOM2 dimer or complex, although perhaps the molecular weight would be expected to be slightly higher. Also, this band was not affected by siRNA against iRHOM2, but a reduction in protein levels after siRNA transfection is dependent on the half-life of the protein, so an iRHOM2 dimer could be a more stable form of the protein less susceptible to degradation.

3.3.4 iRHOM2 isoforms

Additionally, there are two isoforms of iRHOM2 that may behave in slightly different ways. The two isoforms have not previously been discussed in detail in the literature. RT-PCR appeared to suggest that isoform 2 is the dominantly expressed isoform in most cutaneous keratinocyte cell lines, with more variable expression of isoform 1. This could suggest that isoform 1 is less stable or more tightly regulated than isoform 2. However, isoform 2 was focussed on in overexpression experiments as it appeared to be the major isoform of iRHOM2. Future work to improve the RT-PCR technique and avoid the non-specific bands seen would be of interest, and qPCR could be performed to quantify the differences in expression. Further investigation of both isoforms and their roles in the epidermis and different tissues would be interesting - DSP, for example, has two isoforms, which have different roles in different tissues, with isoform II being the critical isoform for adhesion in the epidermis (Cabral et al., 2010).

3.3.5 Desmosome dysregulation in TOC

There appeared to be a general dysregulation of desmosomes in TOC epidermis, including increased processing of DSG2. The 100 KDa DSG2 fragment detected in western blots is likely detecting DSG2 after endocytosis. Lorch et al (2004) also detected a 60 KDa fragment in the supernatant, representing the extracellular portion of DSG2. Further processing of DSG2, producing other cleavage fragments, has also been reported (Klessner et al. 2009; Nava et al., 2007). Future work with ELISA assays for DSG2, or western blotting of the supernatant would determine whether this fragment was found in medium from TOC cells.

Otherwise, there appeared to be subtle changes in desmosomal proteins but no clear differences in each patient as was seen in the electron-dense midline in the desmosomes of all three patients in the same biopsies. This perhaps suggests general dysregulation of desmosomes in TOC epidermis rather than a dramatic effect on one or two desmosomal components. There are some drawbacks of the IHC analysis: staining is

not easily quantifiable; there could be variation in the point in the section the confocal image was taken (although the image was focussed at the point of brightest staining for all sections); MeAc fixation may have masked some cytoplasmic staining. Western blotting of monolayer keratinocytes does not represent all of the epidermal layers and may therefore miss some differences.

Perhaps DSG1 or 3, or DSC1, which were not tested by western blotting are affected - DSC1 and DSG1 are associated with differentiation, although there was no clear difference in DSG1 specific IHC. Cadherins form the electron dense midline, so it seems likely that a cadherin is affected. Desmosomal dysregulation could be mediated through increased DSG2 cleavage by ADAM17 and/or increased EGFR signalling. The lack of midlines in TOC desmosomes is indicative of desmosomes in a wound healing state (as described in Garrod et al. 2005), and suggests that there may be accelerated wound healing in TOC.

3.3.5.1 ADAM17

Staining with an antibody against DSG1 and 2 in skin from a patient homozygous for LOF mutations in ADAM17 showed an increase in staining intensity, implying a reduction in DSG2 shedding by ADAM17 in this patient (Blaydon et al., 2011). In contrast, TOC appears to result in increased processing and activity of ADAM17, and increased EGFR signalling (Chapter 4, Brooke et al., 2014; Blaydon et al., 2012). Loss of the electron-dense midline in TOC desmosomes is consistent with desmosomes in a wound-healing state (Garrod et al., 2005), and appeared to be accompanied by increased processing of DSG2 in TOC cutaneous keratinocytes, which could be mediated by ADAM17 and EGFR signalling (Lorch et al., 2004; Getsios et al., 2009; Klessner et al., 2009) causing alterations in desmosomal composition and Ca^{2+}-dependence.

The increased DSG1 and 2 staining in epidermis with homozygous LOF mutations in ADAM17 was seen throughout the epidermis, despite previous reports of DSG2 expression being restricted to the basal layer (Brennan and Mahoney, 2009). This is consistent with staining in patient 1 (figure 3.2.17) and patient 4 (appendix A24) showing reduced DSG1 and 2 throughout the epidermis, but no obvious difference in DSG1 staining. The staining is very weak in the basal layer, which may suggest that the antibody is recognising predominantly DSG1. It is possible that MeAc fixation before staining masked signal from cytoplasmic DSG2 in the basal layer. There could also be differences in expression levels of the desmosomal proteins between skin from different body sites, and recognition of different forms of the desmogleins by different antibodies raised against different epitopes.

3.3.5.2 EGFR regulation of desmosomes

EGFR signalling results in phosphorylation of desmosomal cadherins followed by subsequent cleavage and endocytosis, e.g. DSG2 (Lorch et al., 2004; Klessner et al., 2009). Internalisation of other adhesion complex proteins can occur in clathrin-dependent and independent manners, for example E-cadherin internalisation (Le et al., 1999; Paterson et al., 2003; Bryant and Stow, 2004; Ivanov et al., 2004; D'Souza-Schorey, 2005; Bryant et al., 2007), with the many internalisation and trafficking pathways contributing to its regulation of the proteins through degradation or recycling (Bryant and Stow, 2004). Less is known about desmosomal trafficking.

EGFR inhibition increases adhesion between cells (Lorch et al., 2004; Brennan and Mahoney, 2009; Klessner et al., 2009) and results in accumulation of ADAM17 at the cell-surface in the highly invasive SCC68 cell line (Klessner et al., 2009). As there is increased EGFR signalling in TOC (Blaydon et al., 2012) and increased ADAM17 processing and activity (Brooke et al., 2014; chapter 4), it suggests that desmosomal dysregulation in TOC may be mediated by EGFR signalling.

Furthermore, an increase in a 100 KDa cleavage fragment of DSG2 was seen in SCC8 cells, which was inhibited by ADAM17 siRNA, but not ADAM10 siRNA (Klessner et al., 2009). This is consistent with the findings in this chapter (published in Brooke et al., 2014) which suggest increased levels of a 100 KDa DSG2 fragment in TOC keratinocytes potentially resulting from increased DSG2 cleavage by ADAM17. In SCC8 cells, the pool of DSG2 was shifted away from the ADAM17-rich cell compartment upon EGFR inhibition, reducing DSG2 cleavage despite increased levels of the protease (Klessner et al., 2009). Interestingly, siRNA knock down of ADAM10 in the SCC68 cells increased levels of the 100 KDa fragment, suggesting that ADAM10 may further regulate DSG2 downstream of ADAM17 cleavage (Klessner et al., 2009).

In contrast to Klessner et al (Santiago-Josefat et al., 2007; Klessner et al., 2009), Santiago-Josefat et al (2007) saw stabilisation of ADAM17 protein following EGF treatment in the cell lines T47D and A431, resulting in increased protein levels of mature ADAM17 at the cell surface (Bech-Serra et al., 2006). Santiago-Josefat et al (2007) also saw an increase in DSG2 cleavage products associated with the increase in ADAM17 protein levels, which was reduced by metalloproteinase inhibition, consistent with the findings in this chapter, and with Klessner et al (2009).

3.3.5.3 EGFR signalling in diseases targeting desmogleins

Further evidence for involvement of EGFR signalling in desmosome regulation comes from the autoimmune disease pemphigus. *Pemphigus* pathology is mediated by auto-antibodies which target desmogleins, resulting in severe blistering phenotypes.

Pemphigus foliaceus (PF) occurs due to autoantibodies against DSG1 (Koulu et al., 1984; Stanley et al., 1986; Eyre and Stanley, 1988; Ishii et al., 2000), while *Pemphigus vulgaris (PV)* results from auto-antibodies against DSG3 (Amagai et al., 1991), or against both DSG1 and DSG3 (Ding et al., 1997). The disease can switch from PV to PF or vice versa, which is accompanied by a change in the autoantibodies in patient serum (Komai et al., 2001; Harman et al., 2002).

The phenotype of *PV* and *PF* correlate with tissue-specific expression of DSG1 and 3 and with the epidermal layers in which DSG1 and 3 are expressed (Amagai et al., 1991; Payne et al., 2004; Mahoney et al., 2006): *PV* is characterised by blistering of both the skin and mucous membranes, particularly at the suprabasal layers, and epidermal cell-cell detachment (acantholysis) occurs in these layers due to loss of cell-cell contact. *PF* causes superficial blisters and scales resulting from acantholysis in the granular layer of the epidermis, with no blistering in the mucous membranes (Amagai and Stanley, 2012; Kitajima, 2013). DSG1 and 3 can compensate for each other in the epidermal layers in which they are co-expressed (Shirakata et al., 1998; Mahoney et al., 1999).

There are three main theories to describe the mechanism of pemphigus autoantibodies disrupting desmosomal integrity: Steric hindrance, where the antigen causes desmosome splitting (Iwatsuki et al., 1989; Shimizu et al., 2004); the non-assembly and depletion hypothesis (e.g. Calkins et al. 2006; Oktarina et al. 2011); and desmosome remodelling impairment where DSG is internalised and sequestered from reassembly into the desmosome (Kitajima, 2013). However, a number of lines of evidence now point away from the steric hindrance model (Koch et al., 1997; Chernyavsky et al., 2007; Aoyama et al., 2010; Kitajima, 2013).

3.3.5.3.1 Non-assembly and depletion hypothesis

The non-assembly and depletion hypothesis suggests that sequestration of DSGs prevents desmosome assembly, leading to the depletion of the desmosomal proteins (e.g. Calkins et al., 2006; Oktarina et al., 2011). *PV*-IgG disrupts the desmosome structure, followed by internalisation of desmosomal components into intracellular vesicles and retraction of intermediate filaments, resulting in decreased cell-cell adhesion (Calkins et al., 2006; Yamamoto et al., 2007). PG co-internalised with DSG3 after *PV*-IgG treatment, and DSG3 total levels were specifically reduced (Calkins et al., 2006). Depletion of DSG3 by PV-IgG appeared to prevent Ca^{2+}-induced desmosome assembly, and DSG3 was detected in early endosomes (Mao et al., 2009). DSG3 sequestration in the cytoplasm means it is unavailable for reassembly into the desmosome (Mao et al., 2009).

3.3.5.3.2 Desmosome-remodelling impairment

There is increasing evidence that the internalisation and sequestration of DSG and depletion of desmosomal components after binding of pemphigus IgG is mediated through an outside-in signalling cascade. The final model for *Pemphigus* pathology is of desmosomal remodelling due to a cascade of signalling events resulting from *PV*-IgG binding, including DSG3 phosphorylation, the Ca^{2+}/PKC pathway, apoptosis signalling, PG modulation, p38MAPK, EGFR and heat shock protein (HSP) 27 (Kitajima, 2013).

The Ca^{2+}-dependent form of desmosomes is required for internalisation upon *PV*-IgG binding (Eyre and Stanley, 1987; Cirillo, et al. 2010; Spindler et al., 2014). The Ca^{2+}-dependent depletion is dependent on PKC (Osada et al., 1997; Cirillo et al., 2010; Spindler et al., 2014). Schulze et al (2012) showed that AK23, a pathogenic anti-DSG3 antibody, activates EGFR, leading to increased Myc levels causing proliferation and acantholysis in injected mice (Schulze et al., 2012). They hypothesised that binding of the *PV*-IgG and/or DSG3 depletion interferes with the cross-talk between AJ and desmosomes, impairing the control of desmosome remodelling (Schulze et al., 2012). Some insight into the order of signalling events following *PV*-IgG binding in keratinocytes was gained by time-course studies showing peak activation of Src 30 min after *PV*-IgG binding, EGFR 60 min after EGFR binding, and p38 MAPK after 240 min (Chernyavsky et al., 2007).

A number of studies have demonstrated a role for p38MAPK in regulating retraction of the cytoskeleton and mediating *Pemphigus* pathology (Berkowitz et al., 2005, 2006; Chernyavsky et al., 2007; Berkowitz et al., 2008; Berkowitz et al., 2008; Lee et al., 2009; Jolly et al., 2010), which is perhaps mediated via blocking RhoA (Waschke et al., 2006). Inhibition of p38MAPK prevented DSG3 internalisation and depletion of DSG3 in both detergent soluble and insoluble cell fractions in human keratinocytes (Jolly et al., 2010) and also prevented retraction of the cytoskeleton (Lee et al., 2009).

Lee et al (2009) also saw increased apoptosis in mouse skin after injection with PF-IgG, and in human keratinocytes. P38MAPK has also been shown to regulate apoptosis in the skin (Hildesheim et al., 2002; Laethem et al., 2004) as have DSG2 and desmosomal regulator Perp (Attardi et al., 2000). Nguyen et al (Nguyen et al., 2009) showed that PERP is internalised with DSG3 and PG upon treatment with PV-IgG in human keratinocytes. Loss of PERP enhances adhesion defects in response to PV-IgG (Bektas and Rubenstein, 2009; Nguyen et al., 2009).

These pathways may be of interest in future work to determine the mechanism of desmosome dysregulation and whether it is mediated by EGFR signalling. A blistering phenotype is not seen in TOC, despite alterations in desmosomes, suggesting that a

more subtle dysregulation of the desmosomes is taking place, and that cell-cell adhesion is not dramatically affected in TOC. Further investigation of the emerging signalling roles of desmosomes may also be interesting in relation to iRHOM2, EGFR signalling and TOC.

3.3.6 Conclusion

iRHOM2 appears to be localised at the plasma membrane in the epidermis and oesophagus, although it was previously reported to be an ER protein. TOC mutant iRHOM2 is able to traffick to the plasma membrane, but appears to be dysregulated/ re-localised in some instances, as shown in frozen skin biopsies from 2 out of 4 TOC patients. iRHOM2 localisation was variable in keratinocytes cultured in monolayer. Furthermore, iRHOM2 expression appears reduced in TOC IHC, flow cytometry, and western blots of NEB1 cells overexpressing iRHOM2, consistent with reduced iRHOM2 expression seen in 3D cultures. Desmosomes in TOC skin lack the electron-dense midline usually formed by binding of cadherins from adjacent cells, suggesting a wound-healing phenotype. This appeared to be accompanied by increased processing of DSG2, which may be mediated by metalloproteinase ADAM17.

Chapter 4: iRHOM2 signalling pathways in the skin

Chapter 4: iRHOM2 signalling pathways in the skin

4.1 Introduction

In the previous chapter, EM imaging showed that TOC skin lacks the electron-dense midline formed by cadherins in mature desmosomes in normal skin, which could be associated with increased processing of the desmosomal cadherin DSG2 in TOC keratinocytes (chapter 3; Brooke et al., 2014). Increased DSG2 processing could result from a combination of ADAM17-mediated DSG2 shedding (Lorch et al., 2004; Klessner et al., 2009), and/or desmosomal remodelling resulting from changes in EGFR signalling (Lorch et al., 2004; Brennan and Mahoney, 2009; Getsios et al., 2009; Klessner et al., 2009).

Previously described functions of iRHOM2 (and iRHOM1) include a role in EGFR signalling through targeting of EGF for ERAD (Zettl et al., 2011), and trafficking of ADAM17 from the ER to the golgi (Adrain et al., 2012; McIlwain et al., 2012) where it is activated. Further regulation of ADAM17-mediated shedding by iRHOM2 has also been demonstrated through direct regulation of ADAM17 substrates (Maretzky et al., 2013), including EGFR ligands. Dysregulation of EGFR signalling has also been implicated in TOC by our group (Blaydon et al., 2012), shown by increased proliferation and migration in TOC keratinocytes, especially after culture in the absence of exogenous EGF.

ADAM17 has also been shown to cleave NOTCH at the S2 stage of processing, predominantly in a ligand-independent manner (Bozkulak and Weinmaster, 2009). NOTCH signalling plays an important role in differentiation in squamous tissues such as the skin and oesophagus (Rangarajan et al., 2001; Ohashi et al., 2010), and inactivating mutations in NOTCH underlie a number of SCCs (Agrawal et al., 2011; Stransky et al., 2011; Wang, 2011; South, 2012). A role for iRHOM1 in NOTCH signalling was suggested by studies expressing a 52 KDa truncated version of iRhom1 in drosophila, causing a wing phenotype resembling that associated with Notch mutations. The phenotype was associated with reduced expression of downstream Notch targets such as *cut,* although no obvious effect was seen when full length iRHOM1 was expressed (Nakagawa et al., 2005). Zettl et al (2011) did not see any genetic interactions between drosophila iRhom and Notch.

4.1.1 Aims

This chapter aimed to investigate the iRHOM2-ADAM17 pathway in normal and TOC epidermis, TOC plus tissue from a patient harbouring homozygous LOF mutations in ADAM17. Investigation of how downstream signalling is affected in TOC was also carried out, including a protein array against phosphorylated RTKs and preliminary investigations into the Eph/Ephrin pathway and NOTCH1 expression. Finally, IHC was performed against iRHOM1, rhomboid protease RHBDL2 and its substrate thrombomodulin to determine how mutations in iRHOM2 may affect localisation/function of these other rhomboid proteins in the skin.

4.2 Results

4.2.1 Increased migration in TOC cells in the absence of EGF

We previously demonstrated an increased rate of migration in TOC keratinocytes, particularly in the absence of exogenous EGF, in experiments performed by Dr Andrew South, University of Dundee (Blaydon et al., 2012). However, a slight increase in the rate of proliferation was also seen in these cells, which could account in part for some of the increased scratch-wound closure seen. Therefore, to confirm that the scratch-wound closure was due to migration of the cells, scratch-wound assays were performed in the absence of exogenous EGF, with and without pre-treatment with MMC, which irreversibly inhibits proliferation (figure 4.2.1).

Consistent with previous findings, TYLK1 TOC keratinocytes migrated faster than control K17 keratinocytes, covering more of the scratch than K17 cells after 24 h, and completely closing the scratch wound at the 48 h time point. The increased migration was seen in TOC cells with and without pre-treatment with MMC (figure 4.2.1), confirming that the results seen in previous scratch assays were due to migration, and not a result of increased proliferation in these cell lines.

4.2.2 Regulation of ADAM17 and iRHOM2 expression may be linked

IHC was performed against iRHOM2 in skin from a patient homozygous for LOF mutations in ADAM17 (figure 4.2.2) to see how loss of ADAM17 impacts on iRHOM2 expression and localisation. iRHOM2 in LOF ADAM17 skin was localised to the plasma-membrane as seen in normal epidermis. However, the intensity of the staining appeared reduced, suggesting that loss of ADAM17 expression and/or activity results in a reduction of iRHOM2 expression levels.

Figure 4.2.4 A shows western blots against iRHOM2 and ADAM17 in control and TOC keratinocytes after treatment with non-targeting pool (NTP), ADAM17 or iRHOM2 siRNA. Levels of iRHOM2 and ADAM17 were reduced by the respective siRNA treatments (figure 4.2.3 B and C), though there was some variability in the efficiency of the knock down, particularly for iRHOM2 (shown in figure 4.2.3 B). The upper band of the iRHOM2 doublet appeared to be preferentially knocked down, though the lower band also appeared reduced with iRHOM2 knock down in a number of the samples.

ADAM17 knock down also appeared to lower iRHOM2 protein levels in control (NEB1 and K17) and TOC (TYLK1 and TYLK2) keratinocytes compared to keratinocytes treated with NTP siRNA (figure 4.2.3 A and B). In some cases, the reduction appeared greater than that seen after treatment with iRHOM2 siRNA. This is consistent with reduced iRHOM2 expression in ADAM17 LOF patient skin, and suggests that regulation of iRHOM2 and ADAM17 expression may be related.

4.2.3 iRHOM2 processes ADAM17 in normal and TOC skin

siRNA knock down of iRHOM2 appeared to result in reduced levels of mature ADAM17 in all four cell lines (figure 4.2.3 A and C; appendix B1). In K17 cells in two experiments, and NEB1 cells in one experiment, the reduction in mature ADAM17 also appeared to be accompanied by a slight increase in pro-ADAM17 protein, but expression of pro-ADAM17 appeared to stay at a relatively similar level in the other NEB1 cells and was variable in TYLK1 and TYLK2 cells. Surprisingly, iRHOM2 protein expression appeared to be slightly increased in the TOC cells compared to NEB1 cells, in contrast to findings in chapter 3 and Blaydon et al (2012), which will be discussed further later in the chapter. Although there was high variability between samples, perhaps relating to variability in the efficiency of the knock down, the reduction of mature ADAM17 levels were consistent with additional western blots performed by Dr Matthew Brooke (Brooke et al., 2014). ANOVA analysis comparing the cell lines did not show a significant difference in mature ADAM17, perhaps due to the variation in results. However, including the further repeats by Dr Brooke showed that anti-iRHOM2 siRNA significantly reduced mature ADAM17 levels in TYLK1 and TYLK2 cells ($p<0.01$ for both cell lines) (Brooke et al., 2014).

4.2.3.1 Increased ADAM17 processing in TOC

Increased levels of mature ADAM17 in TOC epidermis (figure 4.2.3) is supported by the observed increased levels of mature ADAM17 and the free ADAM17 pro domain in TOC keratinocyte monolayers compared to NEB1 cells (figure 4.2.4 A; Dr Matthew Brooke), and in 3D raft cultures of TOC keratinocytes compared to K17 rafts (figure 4.2.4 B; Dr Nihal Kaplan and Dr Spiro Getsios, Northwestern University, Chicago). Immunofluorescence experiments also showed increased cell-surface ADAM17 in

monolayer and 3D culture (figure 4.2.4 C and D, Brooke et al. 2014). Together, the data suggest that the mutations in iRHOM2 found in TOC are GOF in nature and lead to increased trafficking, processing and activation of ADAM17.

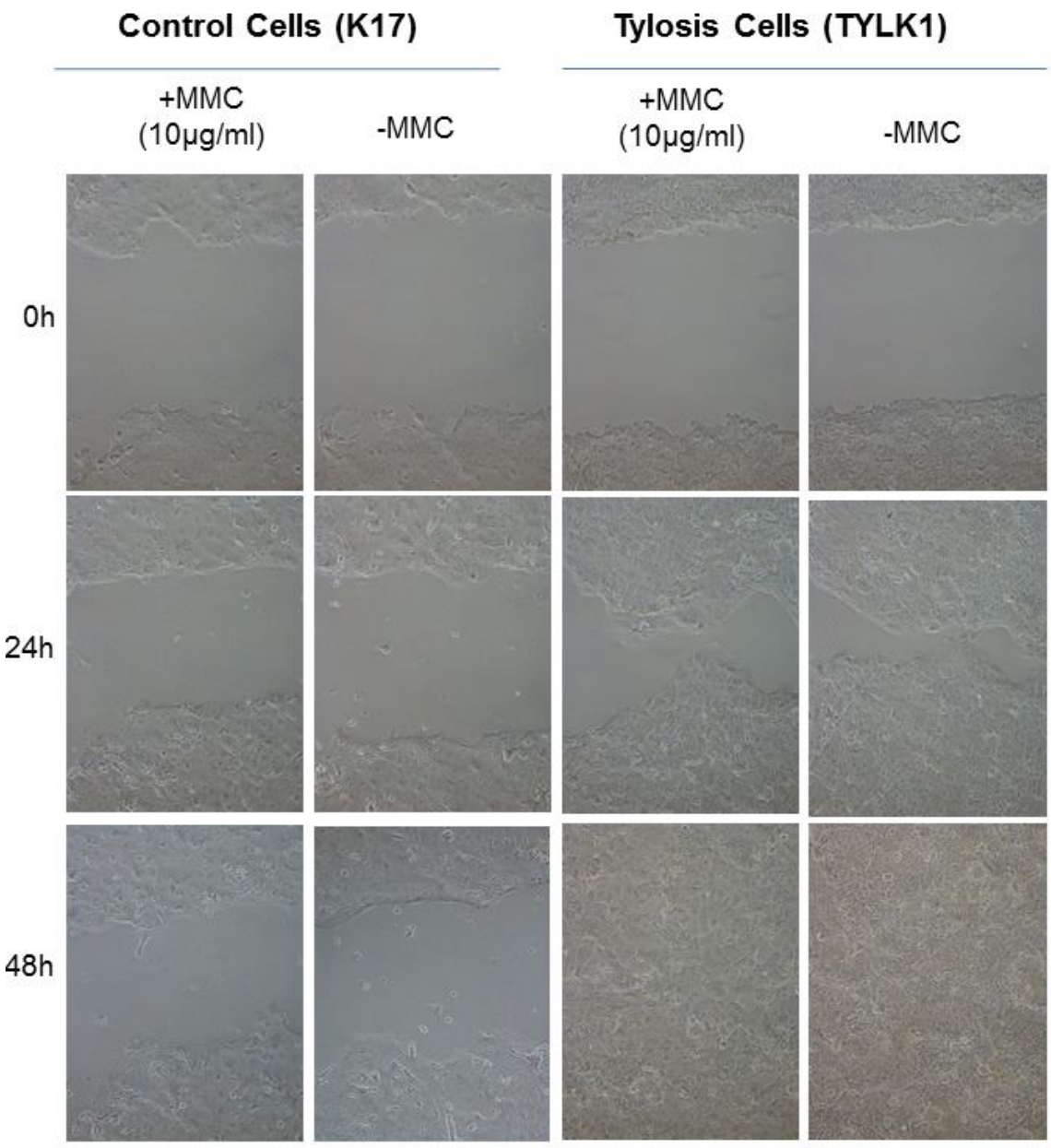

Figure 4.2.1 Accelerated wound closure in TOC cells is independent of proliferation Scratch-wound migration assays were performed in control (K17) and TOC (TYLK1) cell lines in the absence of exogenous EGF (n=2). Cells were incubated with MMC (10 µg/ml) or vehicle (H_2O) as indicated prior to scratch wounding. MMC irreversibly inhibits proliferation.

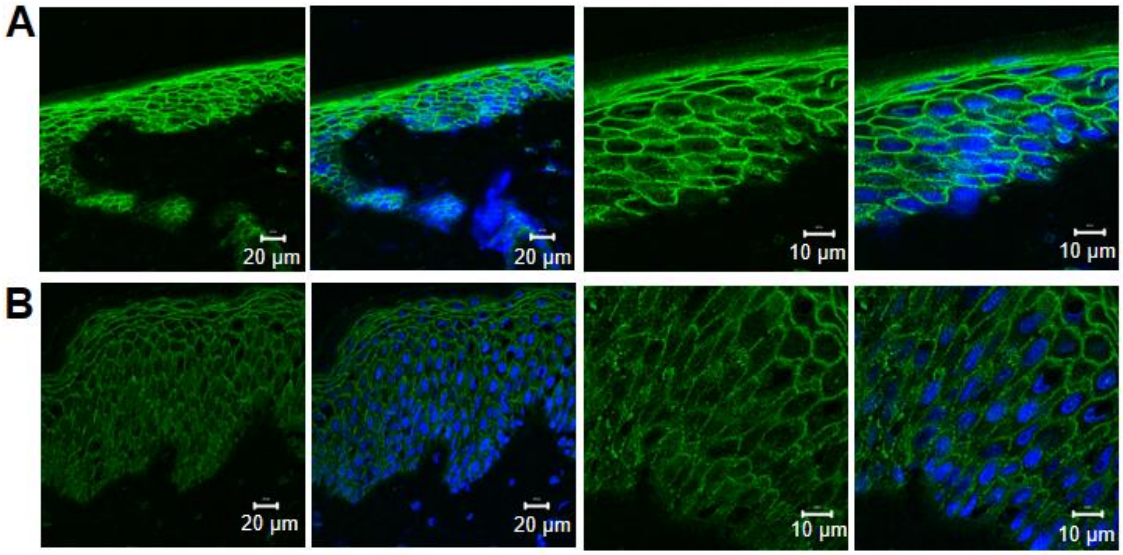

Figure 4.2.2 Reduced iRHOM2 staining in a patient with a homozygous Loss of Function ADAM17 mutations IHC of iRHOM2 in frozen sections from normal skin **(A)** and in skin from a patient with homozygous LOF mutation in ADAM17 **(B).** n=1 due to low availability of the sample. iRHOM2 staining is shown in green, DAPI nuclear stain in blue. Images were taken with the LSM510 confocal microscope at magnifications of 40X (left-hand images) and 100X (right hand images).

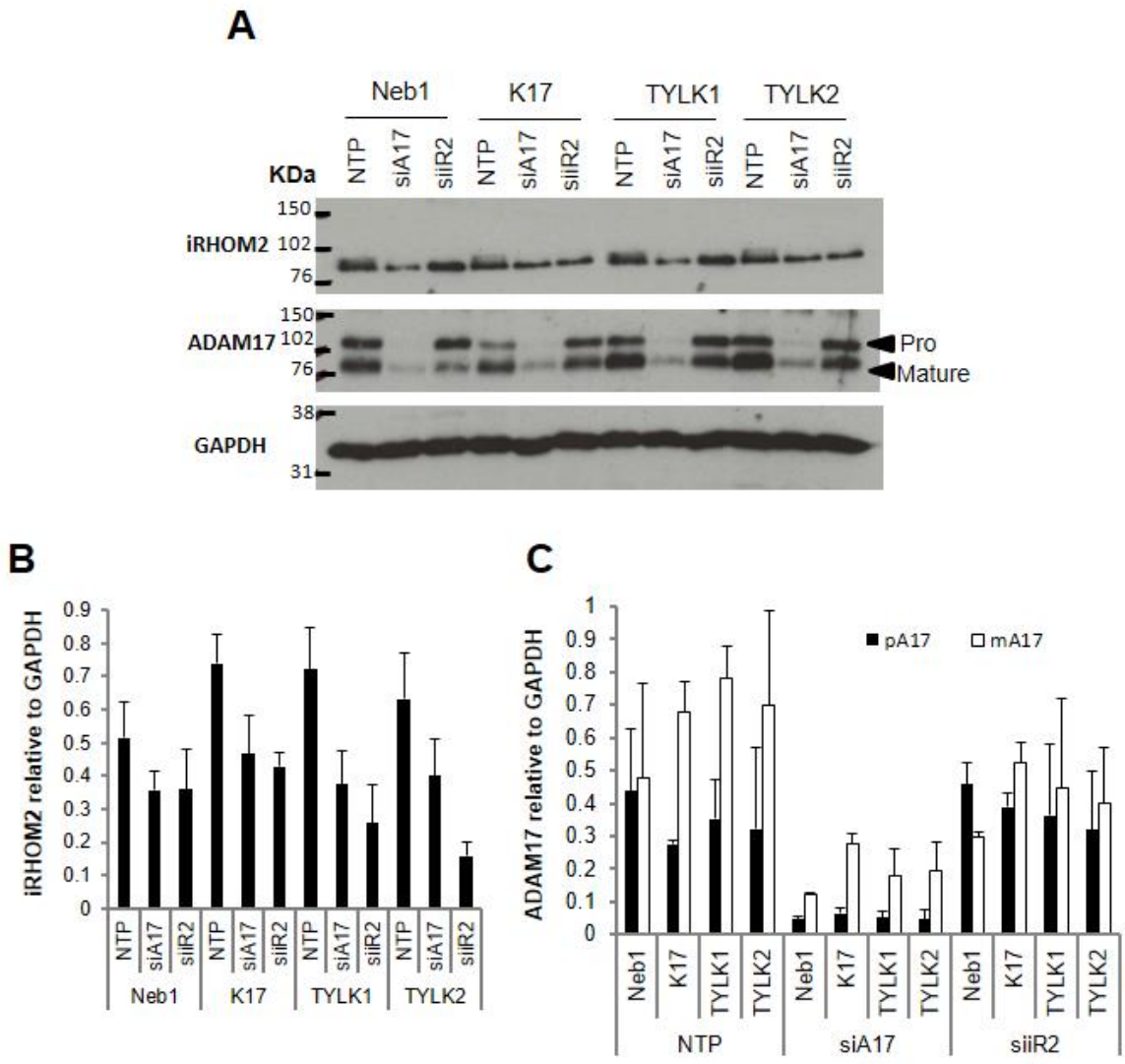

Figure 4.2.3 iRHOM2 knock down reduces ADAM17 processing in normal and TOC keratinocytes, and ADAM17 knock down reduces iRHOM2 protein levels. A: Western blots against iRHOM2, total ADAM17 and GAPDH loading control were performed with lysates from normal and TOC keratinocytes after treatment with ADAM17, iRHOM2 or Non-targeting pool (NTP) control siRNA (n=3). **B-C:** Bar graphs showing densitometry (relative to GAPDH) for iRHOM2 **(B)** and pro- and mature ADAM17 **(C)** as indicated. Densitometry was performed with Image J software. Both bands of the iRHOM2 doublet were included in analysis in B.

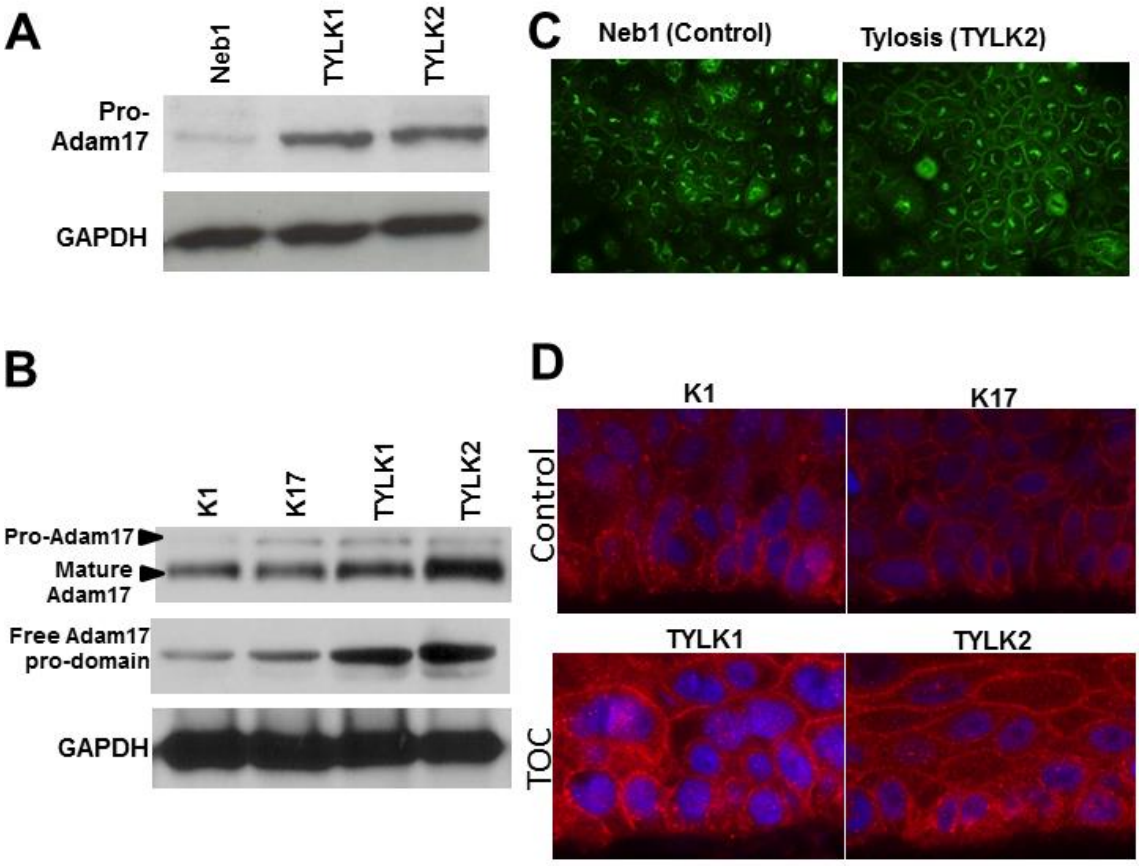

Figure 4.2.4 iRHOM2 mutations in TOC result in increased processing of ADAM17. Western blots and IHC of ADAM17 were performed in keratinocyte monolayers and 3D cultures. **A:** Western blot showing the free ADAM17 pro-domain and GAPDH loading control in protein lysates from control (NEB1) and TOC (TYLK1 and TYLK2) keratinocyte monolayers. **B:** Western blots in control (K1 and K17) and TOC (TYLK1 and TYLK2) 3D raft cultures, showing total ADAM17, the free ADAM17 pro-domain and GAPDH loading control. **C:** IHC showing total ADAM17 staining in NEB1 control cells and TYLK2 TOC keratinocyte monolayers, showing increased ADAM17 levels at the cell surface in TYLK2 cells. **D:** Total ADAM17 staining in 3D raft cultures with control (K1 and K17) and TOC (TYLK1 and TYLK2) keratinocytes, also showing elevated cell-surface ADAM17 in TOC (magnification 63X). Monolayer IHC and western blots were performed by Dr Matthew Brooke. 3D raft cultures and associated staining and western blots were performed by Dr Nihal Kaplan and Dr Spiro Getsios, Northwestern University, Chicago, US.

4.2.4 Protein array against phosphorylated Receptor Tyrosine Kinases (RTKs)

To investigate the effects of increased ADAM17 processing and dysregulated EGFR signalling in TOC (Blaydon et al., 2012; Brooke et al., 2014), a protein array was performed against phosphorylated RTKs to begin to identify which signalling pathways are affected downstream of EGFR (figure 4.2.5). The array was performed in lysates from TYLK1 and TYLK2 TOC keratinocytes and NEB1 control cells in collaboration with Dr Diana Blaydon (figure 4.2.5 A). Densitometry was performed on phospho-EGFR and the three proteins that showed striking differences between NEB1 control cells and the TOC keratinocytes relative to the control proteins included in the corners of the array. There was perhaps a slight increase in phospho-EGFR levels according to the densitometry analysis (figure 4.2.5 B) although the signal was very strong, which is likely to affect the accuracy of the densitometry measurements so further experiments would therefore be needed to confirm this.

Clear differences were seen in three proteins between TOC and NEB1 keratinocytes: phospho-Insulin Receptor (figure 4.2.5 C) and phospho-IGF1R (Insulin-like Growth Factor 1 receptor; figure 4.2.5 D) were both up-regulated in TYLK1 and TYLK2 cells; and a decrease was seen in phosphorylation of the EphA4 receptor (figure 4.2.5 E). The Eph/Ephrin pathway was selected for further investigation.

The Eph receptor family is the largest family of RTKs, with EphA receptors binding predominantly GPI-anchored Ephrin A ligands, while EphB receptors bind mostly Ephrin B ligands (Kullander and Klein, 2002). EphA4 is an exception, and binds both Ephrin A and B ligands, including Ephrin B3 (e.g. Gale et al. 1996; Bergemann et al. 1998; Kullander & Klein 2002), which is a substrate of rhomboid protease RHBDL2 (Pascall and Brown, 2004). EphA2 and its ligand Ephrin A1 were also chosen for further investigation as targets of EGFR signalling (Macrae et al., 2005; Larsen et al., 2007; Menges and McCance, 2008) and because the EphA2-EphrinA1 signalling axis is important in differentiation in the skin (Lin et al., 2010).

4.2.5 EphA2 and EphA4 receptor expression may be affected downstream of EGFR in TOC keratinocytes and skin

To investigate EphA2 and EphA4 expression in TOC keratinocytes, cells were cultured in the presence and absence of exogenous EGF, then lysates collected for western blot analysis. Protein levels of EphA4 (figure 4.2.6 A) and EphA2 (figure 4.2.6 B) appeared to be lower in NEB1 cells after culture with exogenous EGF compared with TOC control cells. However, after culture in the absence of EGF (RM-), levels of both EphA4 and EphA2 appeared reduced in control cells, but were reduced to a lesser extent in the

TYLK1 and TYLK2 cells, suggesting that the increased EGFR signalling in TOC keratinocytes may affect downstream EphA2 and EphA4 expression.

The findings were highly variable, however, perhaps due to variation in cell density affecting EphA2 and EphA4 expression, although confluent monolayers were used each time, control cells grow more slowly than TOC cells in the absence of exogenous EGF and so may not have been as densely packed. The strong signal associated with the EphA2 western blot may also have affected the densitometry results, particularly after culture in the presence of EGF (figure 4.2.6 B) where there was also a strong signal below the western blot which likely results from processing of EphA2. Increased EphA2 expression was also seen by Dr Spiro Getsios in 3D cultures of the TOC cells compared to 3D cultures of both K1 and K17 control keratinocytes (figure 4.2.6 F).

Unfortunately, western blots for phospho-EphA4 did not work well (my findings, and personal communication from Dr Spiro Getsios) – this would have been useful to confirm the findings of the phospho-array. Expression of EphA2 ligand Ephrin A1 appeared to be variable between cell lines after culture in the presence and absence of EGF (figure 4.2.6 E), perhaps suggesting that it is not directly affected in TOC keratinocyte monolayers. Ephrin A1 expression did not appear to be affected in the TOC keratinocyte 3D cultures (figure 4.2.6 F).

4.2.5.1 EphA2 and EphA4 in the skin

To further investigate EphA2 and EphA4 in the skin, IHC for EphA2, total EphA4 and phospho-EphA4 was performed in frozen skin biopsies from control and TOC skin, and in a number of other skin diseases, to see whether any changes in this pathway were specific to TOC skin.

4.2.5.1.1 EphA4 localisation

IHC against EphA4 in frozen skin biopsies is shown in figure 4.2.7. In normal skin, EphA4 could be seen throughout the cell in the upper layers of the epidermis, with stronger plasma membrane staining in the upper epidermal layers, particularly the *stratum granulosum.* Staining was of brighter intensity in the basal layer, where the localisation appeared more cytoplasmic. Some small puncta could be seen in some cells, which appeared to co-localise with the DAPI staining, suggesting a nuclear localisation.

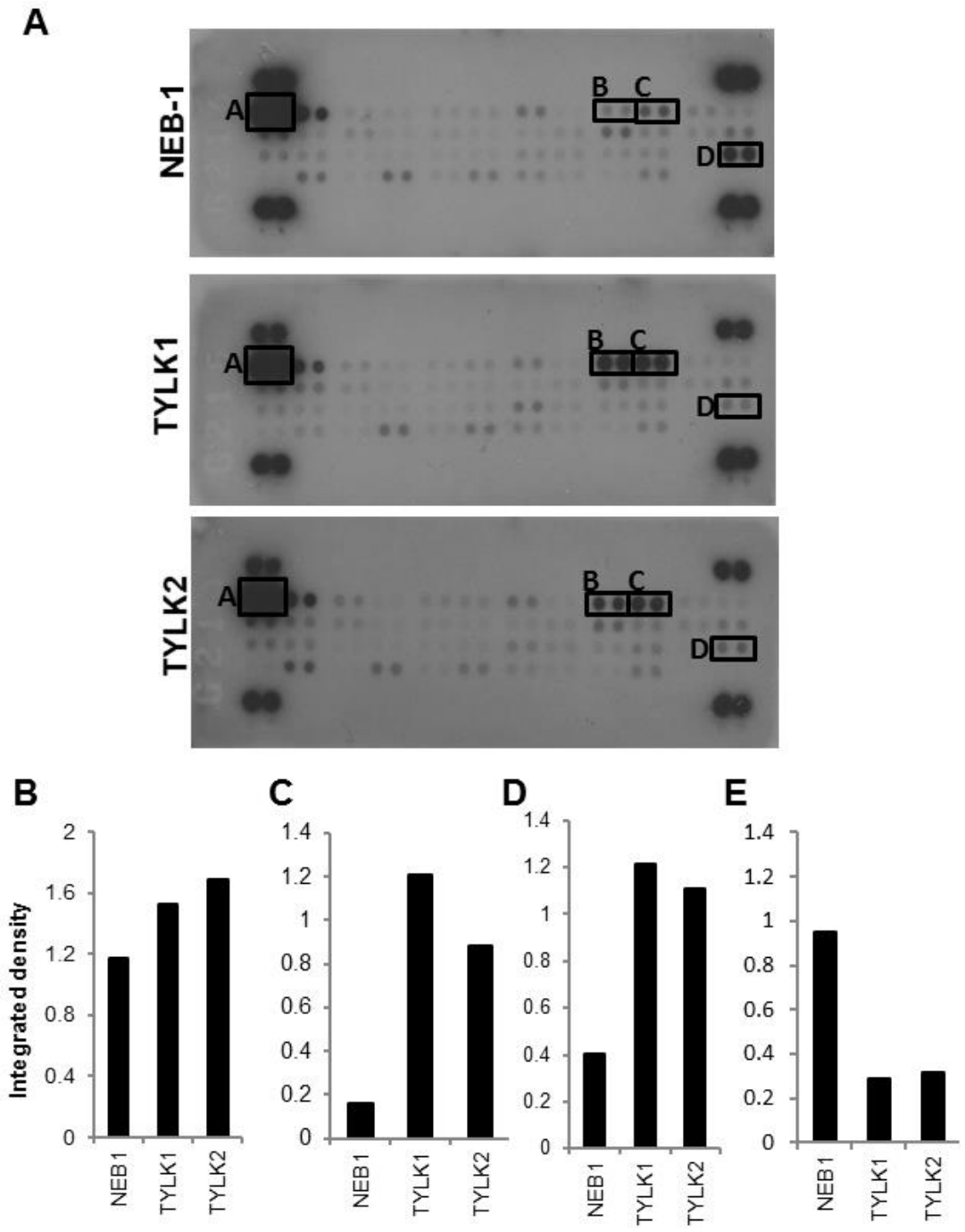

Figure 4.2.5 Protein array against phosphorylated Receptor Tyrosine Kinases in TOC keratinocytes compared to NEB1 controls. A: The three phospho-arrays performed with NEB1 control lysates and TYLK1 and TYLK2 TOC cell lysates (n=1). **B-E:** Bar graphs showing densitometry of the spots representing phospho-EGFR **(B)** and the three proteins with the clearest differences are shown in **C-E:** Phospho-Insulin Receptor **(C);** phospho-IGF1-R **(D);** and Phospho EphA4 **(E).** Densitometry was carried out with the Image J Software. Densitometry of each phospho-protein is shown in Appendix B2.

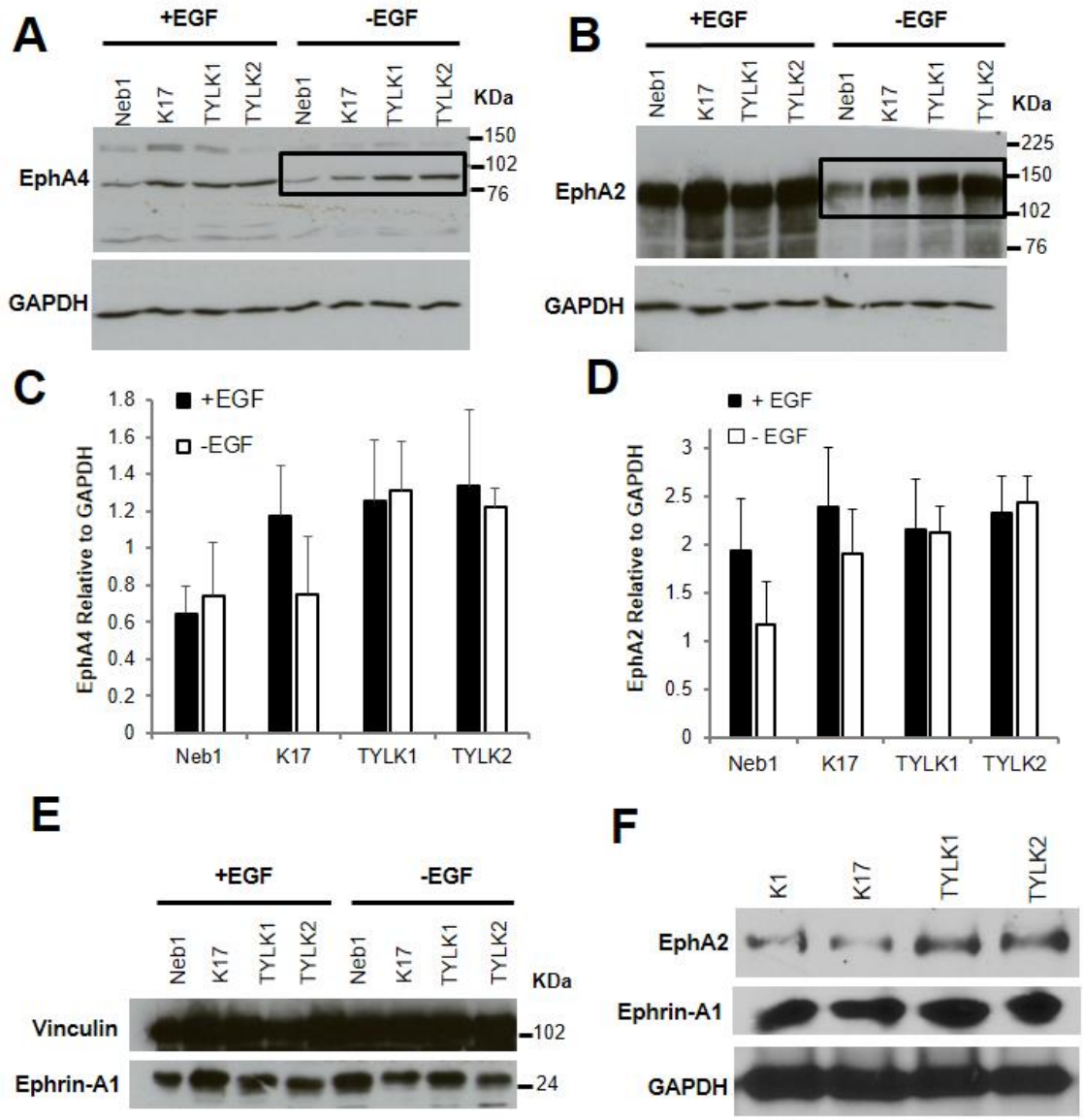

Figure 4.2.6 Expression of Eph Receptors EphA2 and EphA4 and EphA2 ligand Ephrin A1. Cells were cultured in the presence and absence of exogenous EGF, and western blots were carried out against **A:** EphA4 receptor, **B:** EphA2 receptor. Densitometry was carried out with Image J Software of **C:** EphA4 (NEB1, TYLK1, TYLK2 n=3; K17 n=2 (due to a broken gel for GAPDH)), **D:** EphA2 (n=3). **E:** Western blot showing EphA2 ligand Ephrin A1 and vinculin loading control in control and TOC cells after culture in the presence and absence of EGF (n=1). **F:** Western blots against EphA2, Ephrin A1 and GAPDH loading control in 3D cultures of control (K1 and K17) and TOC (TYLK1 and TYLK2) keratinocytes. 3D cultures and western blots shown in F were by Dr Spiro Getsios and Dr Nihal Kaplan.

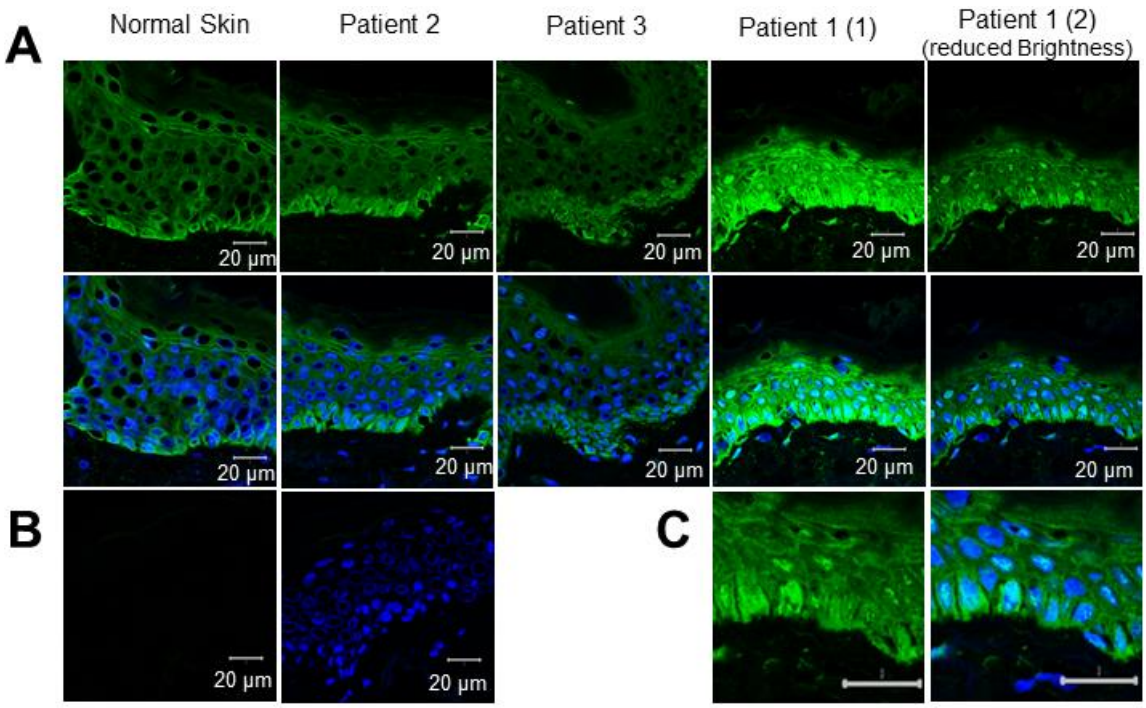

Figure 4.2.7 EphA4 receptor expression up-regulated, with nuclear translocation in the skin of a TOC patient with dysregulated iRHOM2 localisation. A: IHC of total EphA4 protein in normal skin from breast tissue (n=4), and TOC patients 2, 3 and 1 as indicated (n=1). Patient 1 is shown twice: 1) at the same settings as normal skin and patients 2 and 3 to allow comparison of staining intensity with normal skin; and 2) at reduced brightness to allow clearer visualisation of EphA4 localisation. Skin from patient 1 showed altered iRHOM2 localisation, whereas patients 2 and 3 had cell-surface iRHOM2. **B:** Negative control staining. **C:** Digitally zoomed in images of EphA4 localisation in patient 1. EphA4 is shown in green and DAPI nuclear staining in blue. Images were taken on the Zeiss Meta 710 Confocal microscope.

In TOC patients 2 and 3, a similar staining pattern of EphA4 was seen, with larger puncta with potential localisation in patient 3. The stronger cell-surface staining perhaps appeared in lower epidermal layers in patient 2. The most striking differences in EphA4 expression and localisation were seen in patient 1 (the patient showing dysregulated iRHOM2 localisation): EphA4 staining intensity was dramatically higher when imaged at the same settings as the other sections. This also appears to be the case in the dermal macrophages, visible below the epidermis in figure 4.2.8 A, which could be confirmed by co-localisation with macrophage marker CD68, as in Chapter 3.

Imaging with a lower exposure in the green channel to allow clearer visualisation of the localisation showed clear cell-surface staining throughout the upper layers of the skin, reaching the suprabasal layers. EphA4 in the basal layer appeared nuclear and perinuclear, and membranous staining was less clear. Bright nuclear staining was also visible and appeared to co-localise with the DAPI stain. This nuclear staining was seen in all epidermal layers in patient 1, whereas it was only seen in the upper layers of the epidermis in normal skin and patients 2 and 3. The nuclear 'puncta' were much larger than in normal skin and patient 2, but more consistent with the size of the puncta in patient 3.

IHC was also performed against phospho-EphA4 (figure 4.2.8). In normal skin, the phospho-EphA4 staining pattern was diffuse throughout the cells, with perhaps a slight increase in staining intensity in the basal layer (less difference than that seen for total EphA4 receptor). No nuclear puncta were visible. Phospho-EphA4 localisation in skin from TOC patient 2 showed a similar staining pattern to normal skin. Patient 3 showed the same diffuse staining throughout the cells of the epidermis, with increased staining intensity in the basal layer. A striking increase in phospho-EphA4 staining was seen in patient 1, however, consistent with the differences seen in expression and localisation of the total EphA4 receptor in this patient. A change in the localisation of phospho-EphA4 was also seen in this patient: while diffuse staining throughout the cell and plasma membrane was seen in normal skin and in patients 1 and 3, EphA4 did not reach the plasma membrane in skin from patient 1. Furthermore, large puncta were visible with a nuclear or perinuclear localisation.

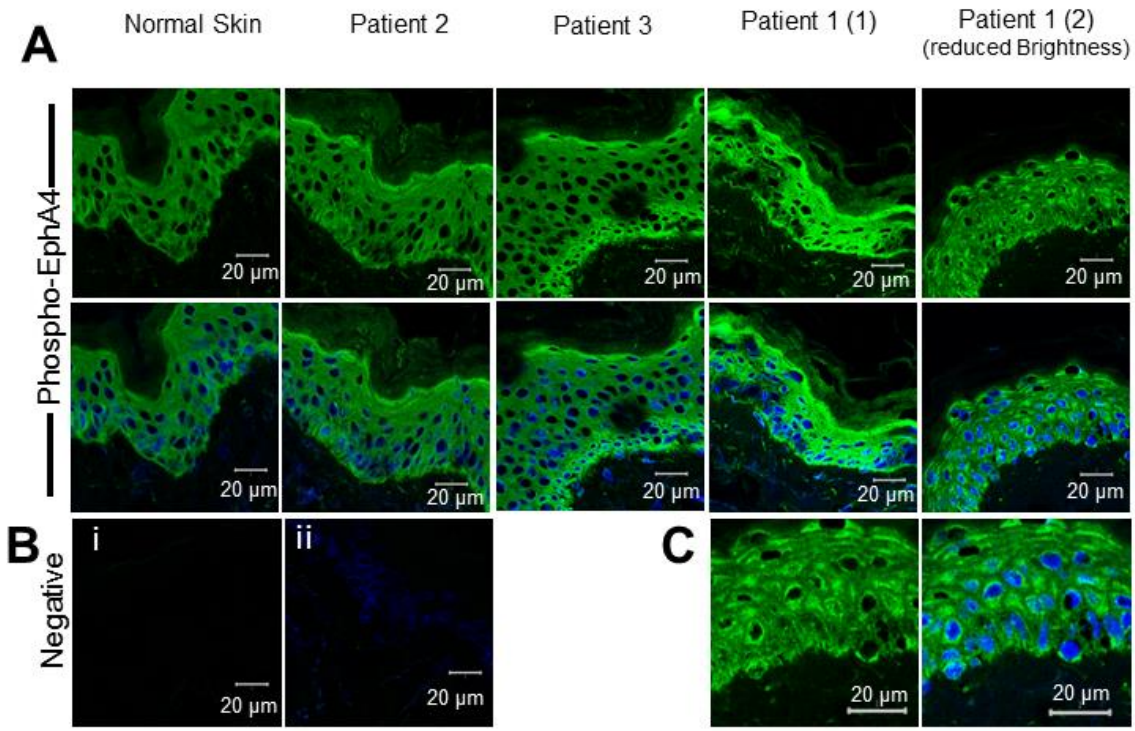

Figure 4.2.8 Variable localisation of phospho-EphA4 in TOC skin. IHC was performed against phospho-EphA4 in frozen skin sections (n=2). **A:** phospho-EphA4 in frozen skin sections from normal breast skin, and TOC skin from patients 2, 3 and 1. As in the previous figure, patient 1 is shown twice at two different exposures to allow both comparison of staining intensity with normal skin (1), and clearer visualisation of localisation (2). Patient 1 showed the most altered iRHOM2 localisation. **B:** Negative control staining. **C:** Phospho-EphA4 staining in Patient 1 digitally zoomed to allow clearer visualisation of the localisation. Images were taken on the Zeiss Meta 710LSM confocal microscope. Phospho-EphA4 staining is shown in green, DAPI nuclear staining in blue.

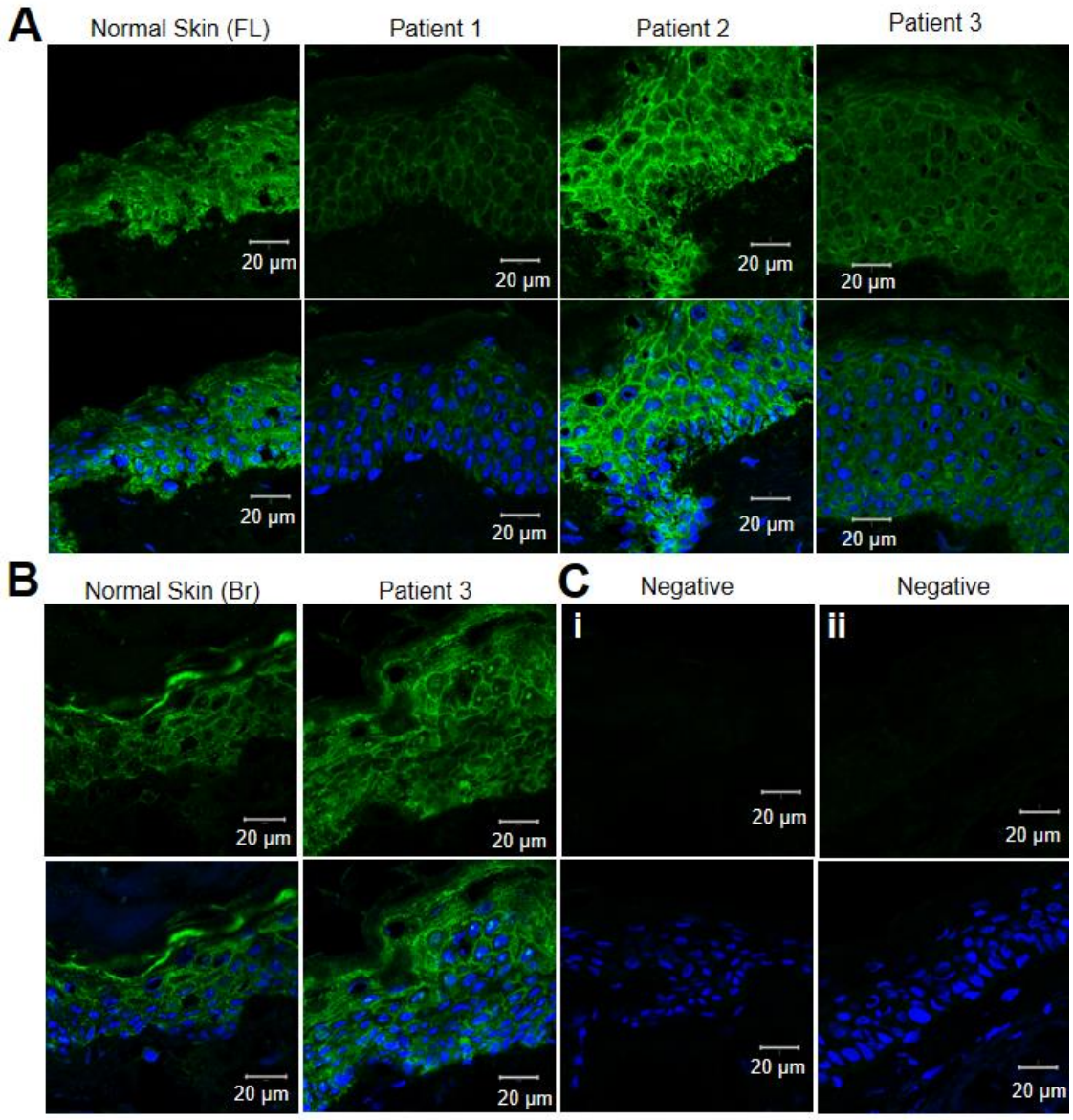

Figure 4.2.9 EphA2 localisation in normal and TOC skin. IHC of EphA2 in frozen skin sections from normal skin and TOC skin showing variable staining intensity. **A:** Experiment 1 – EphA2 staining in normal skin from facelift, and TOC patients 1-3. **B:** Experiment 2 – EphA2 staining in normal skin from breast, and TOC patient 3. Normal skin sections from two different body sites were stained in case of variation in EphA2 localisation between body sites, **C:** Negative control staining in experiment 1 (i) and experiment 2 (ii). EphA2 is shown in green, DAPI nuclear stain in blue. Images were taken on the Zeiss Meta 710LSM confocal microscope.

4.2.5.1.2 EphA2 localisation

EphA2 appeared to be localised to the plasma membrane with some cytoplasmic staining in normal and TOC skin, with some small nuclear or perinuclear puncta as seen for EphA4 in normal skin (figure 4.2.9). Two separate staining experiments are shown to allow comparison of EphA2 in normal skin from facelift and breast. EphA2 in normal skin from facelift appeared to be expressed throughout the epidermis, but with lower expression in the upper epidermal layers (figure 4.2.9 A). In contrast, expression of EphA2 was seen throughout the epidermis in normal skin from breast (figure 4.2.9 B; see also figure 4.2.12 A) suggesting body-site-specific EphA2 expression patterns in the skin. The intensity of EphA2 staining was variable between different sections, but also between different staining experiments (n=3), so it is not possible to determine expression levels of EphA2 from this data.

4.2.5.2 EphA2 and EphA4 in keratinocytes

ICC against EphA2 and EphA4 was also performed in control and TOC keratinocytes after culture in the absence of EGF (figure 4.2.10). Strong membranous staining of EphA2 was seen in NEB1 and K17 control keratinocytes, and TYLK2 TOC keratinocytes (n = 2, also see appendix B3), with fainter cytoplasmic and perinuclear staining. There was no clear difference in EphA2 localisation between control and TOC cells.

EphA4 appeared to be localised predominantly to the nucleus in control and TOC keratinocytes, with a punctate staining pattern. Some faint plasma membranous staining was visible, and also weaker punctate cytoplasmic staining which could perhaps represent EphA4 in trafficking vesicles. Staining intensity appeared lower in K17 cells, perhaps related to higher confluency of the cells in this experiment.

4.2.5.3 Ephrin A1

IHC was also performed against Ephrin A1 in normal and TOC frozen skin sections (figure 4.2.11). Ephrin A1 was expressed throughout the epidermis in normal skin, with more intense perinuclear staining in the basal layer. Staining in the upper layers of the epidermis appeared diffuse throughout the cell and plasma membrane, with some possible nuclear staining in some cells. In TOC patients 1 and 2, more epidermal cells appeared to show nuclear (or perinuclear) Ephrin A1. The staining was faint, and some of the sections appeared to contain holes around the nucleus, likely resulting from the freezing process. Some cell-surface Ephrin A1 was seen in the upper epidermal layers in patient 3. TOC skin also appeared to show nuclear staining in a greater number of basal cells in addition to perinuclear staining in the basal layer, particularly in patients 1 and 2.

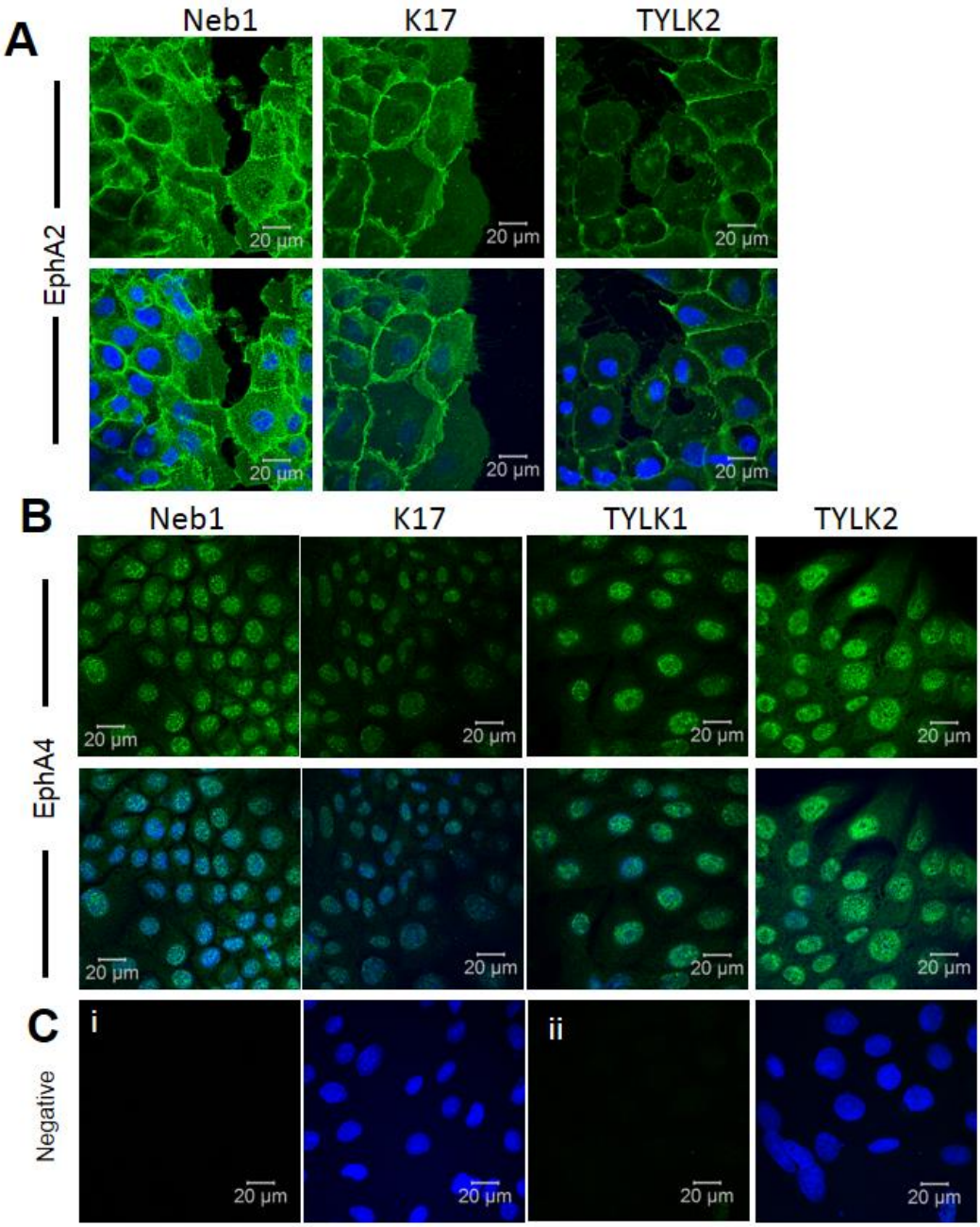

Figure 4.2.10 EphA2 and EphA4 localisation unaffected in control and TOC keratinocytes in the absence of EGF. ICC was carried out after culture in the absence of EGF (RM-). **A:** EphA2 in NEB1, K17 and TYLK2 cells as indicated (n=2). **B:** EphA4 in NEB1, K17, TYLK1 and TYLK2 cells as indicated (n=3). **C:** Negative controls for EphA4 with anti-rabbit secondary antibody (i) and for EphA2 with anti-Goat secondary antibody (ii). EphA2 and EphA4 staining is shown in green, DAPI nuclear staining is shown in blue. Images were taken on the Zeiss Meta 710 LSM confocal microscope.

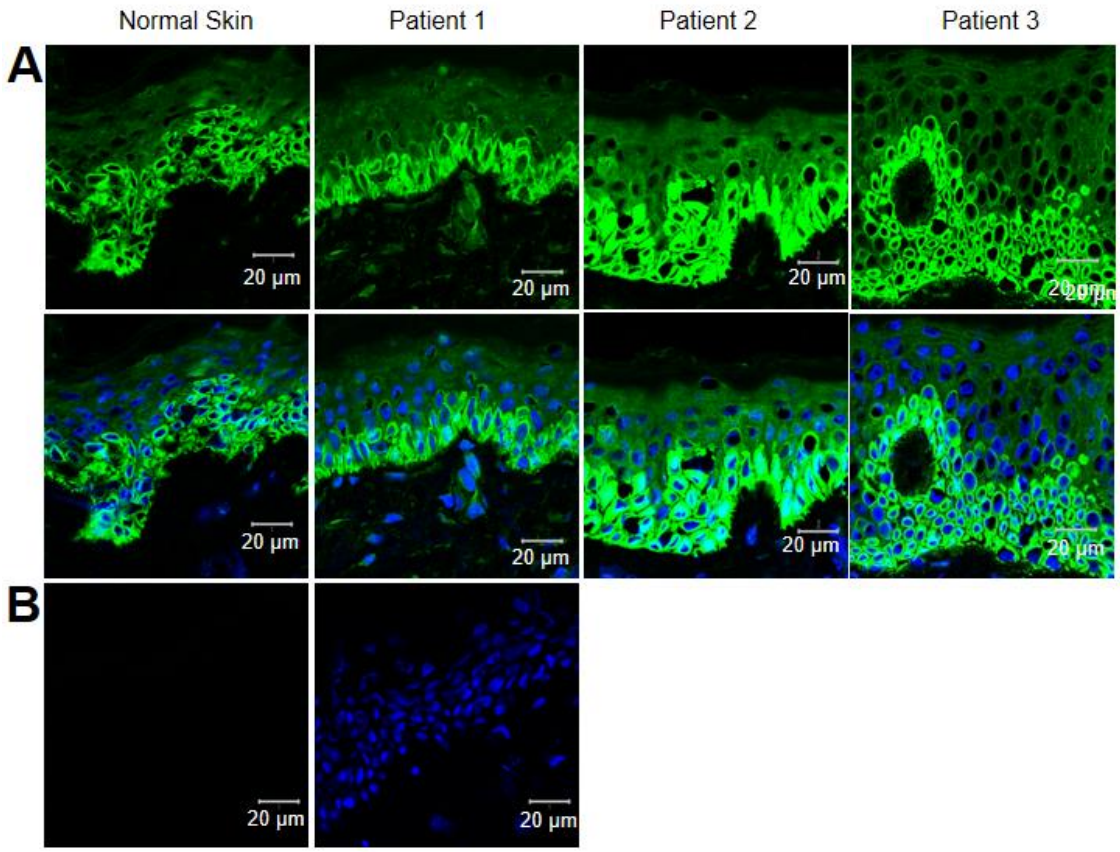

Figure 4.2.11 Ephrin A1 localisation appears unaffected in TOC skin. **A**: IHC against EphA2 ligand Ephrin A1 in frozen skin sections from normal and TOC patient skin as indicated (n=2). **B:** Negative control staining. Ephrin A1 is shown in green, DAPI nuclear stain in blue. Images were taken on the Zeiss Meta 710 confocal microscope.

4.2.5.4 EphA2 and Ephrin A1 in other genetic skin disease

EphA2 and its ligand Ephrin A1 were also stained in frozen skin biopsies from the following genetic skin diseases: recessive inflammatory skin/bowel disease (ADAM17); dominant EKV (Cx31) and recessive Harlequin Ichthyosis (ABCA12) (figure 4.2.12 and 4.2.13 C, D and E respectively).

There was no clear difference in EphA2 localisation between normal skin and skin from the panel of different genodermatoses (figure 4.2.12). Ephrin A1 also showed a similar localisation in all the sections stained (figure 4.2.13), with stronger perinuclear staining in the basal layer and fainter, more diffuse staining in the upper epidermal layers. In the patient with homozygous LOF ADAM17 mutations, the strong perinuclear staining appeared to extend into the suprabasal layers of the epidermis, with strong nuclear staining seen in the basal layer (figure 4.2.13 C). As Ephrin A1 is associated with inhibiting differentiation, this could be consistent with a reduction in barrier function and increased incidence of infection associated with ADAM17 LOF (Blaydon et al., 2011; Brooke et al., 2014).

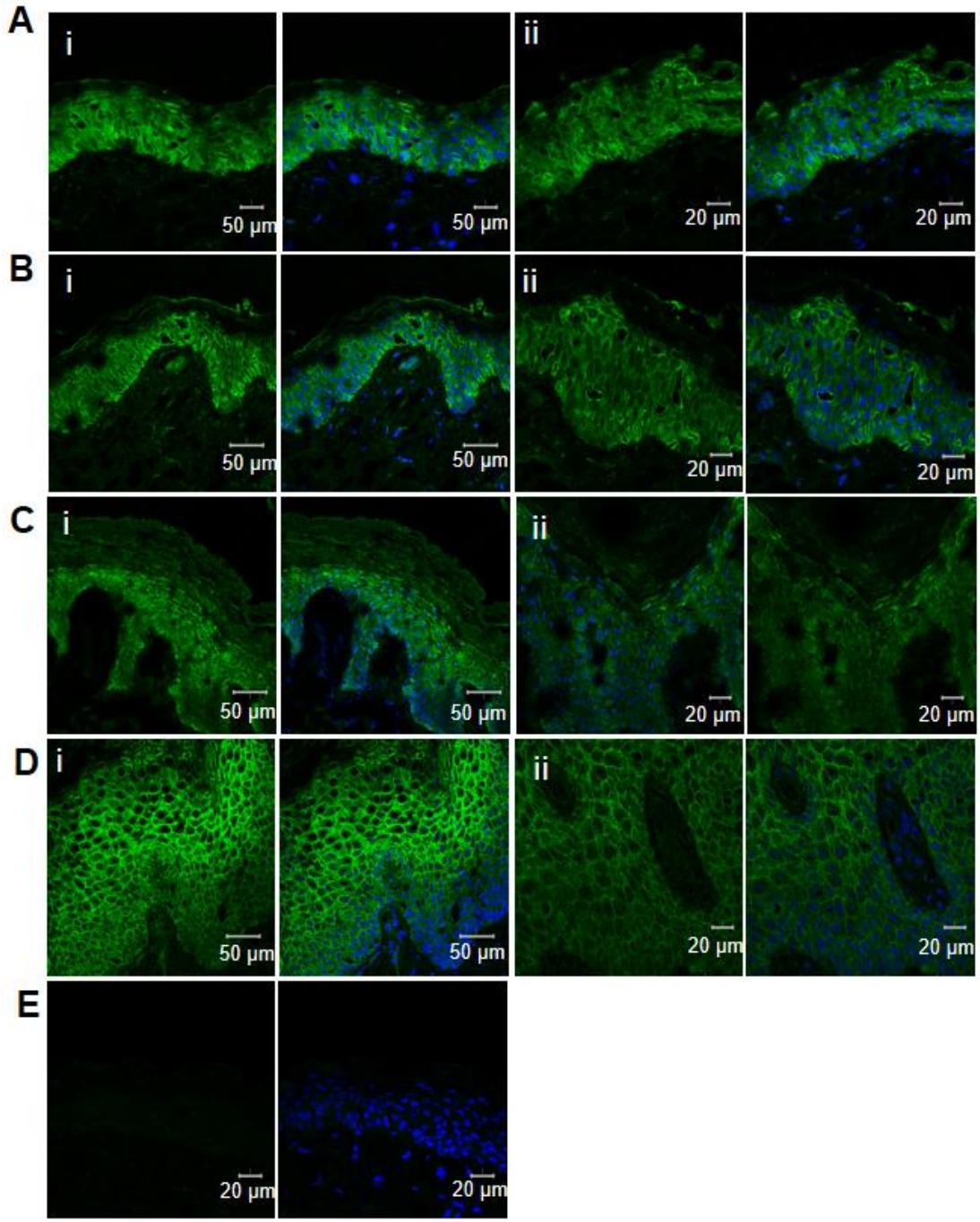

Figure 4.2.12 Localisation of EphA2 in a panel of genetic skin diseases. IHC against EphA2 in frozen skin sections, taken at magnifications of 40X (i) and 63X (ii). **A:** Control Skin, **B:** recessive inflammatory skin/bowel disease (ADAM17) (n=1); **C:** dominant EKV (Cx31) (n=1) and **D:** recessive Harlequin Ichthyosis (ABCA12) (n=1). Negative control staining is shown in **E.** Images are shown with and without DAPI nuclear stain (shown in blue), with EphA2 staining shown in green. Images were taken on the Zeiss Meta 710 Confocal microscope.

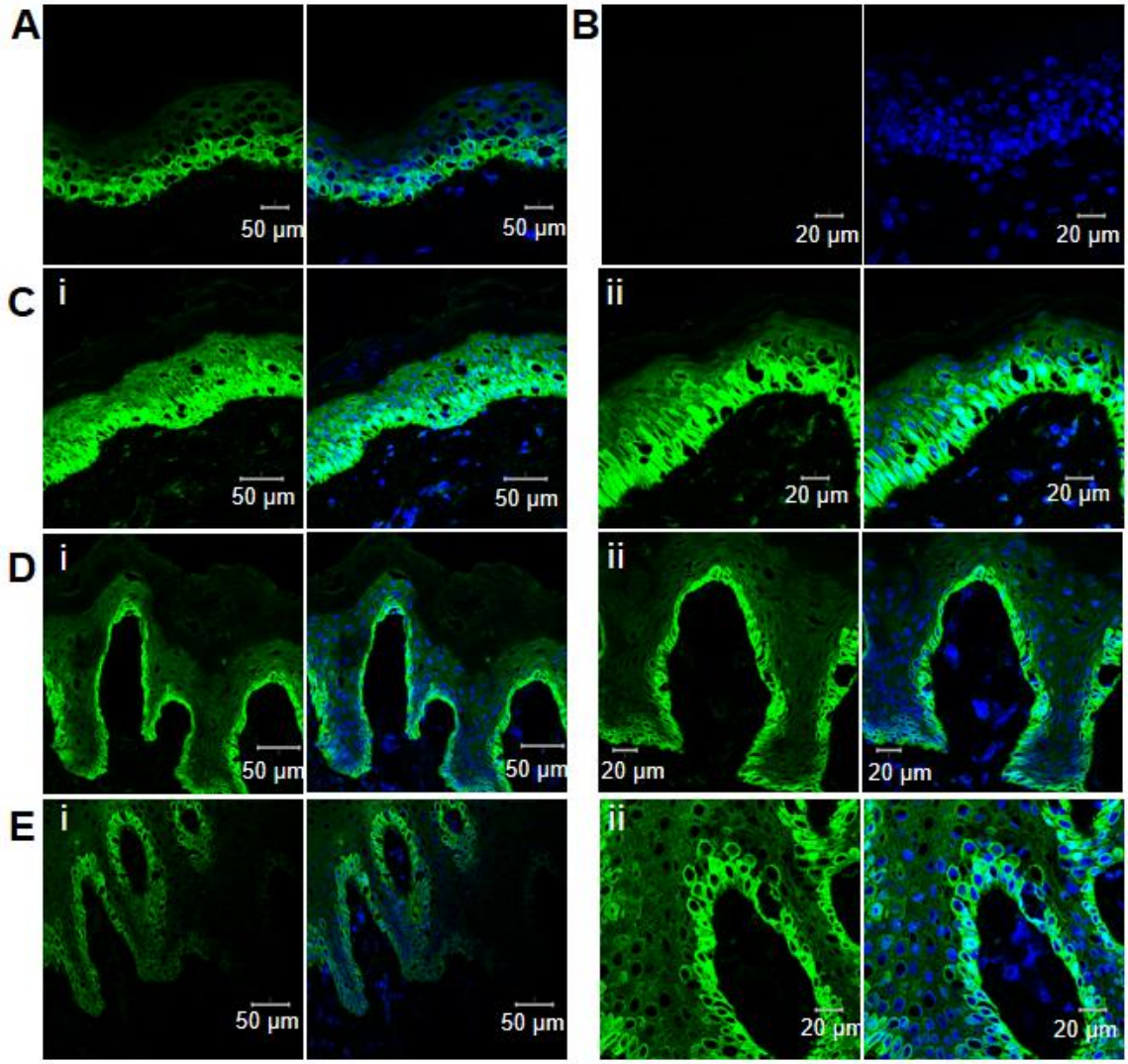

Figure 4.2.13 Localisation of EphrinA1 in a panel of genetic skin diseases: LOF ADAM17 mutations may be associated with increased suprabasal Ephrin A1 staining. Staining of EphA2 ligand EphrinA1 in frozen skin sections from control skin and genetic skin diseases taken at magnifications of 40X (i) and 63X (ii): **A:** Control skin, **B:** negative control with primary antibody omitted, **C:** recessive inflammatory skin/bowel disease (ADAM17), **D:** dominant EKV, **E:** Harlequin Ichthyosis (ABCA12). Ephrin A1 staining is shown in green, and DAPI nuclear stain is shown in blue. Images were taken on the Zeiss Meta 710 Confocal microscope. Staining was only performed once due to limited availability of the frozen sections.

4.2.6 NOTCH1 expression

In contrast to ADAM17 LOF skin, increased Transglutaminase 1 activity indicative of increased barrier function was seen in TOC (Brooke et al., 2014). An important mediator of differentiation is NOTCH, which can be cleaved by ADAM17 in the ligand-independent S2 cleavage step. Therefore, western blots, ICC and IHC were performed against NOTCH1 in control and TOC keratinocytes frozen skin biopsies.

4.2.6.1 NOTCH1 protein expression

Western blots against NOTCH1 in three sets of lysates are shown in figure 4.2.14 A. This was performed with the Abcam Chromatin immunoprecipitation (ChIP)-grade antibody, which recognises the whole NOTCH1 protein and detects full-length NOTCH1 at around 460 KDa (not seen in these western blots), activated S1-cleaved NOTCH1 at around 250 KDa (both bands of this doublet were measured for densitometry); and cleaved NOTCH1, seen at approximately 118-110 KDa, which includes S2-NOTCH1 cleaved by ADAM10 or ADAM17, and S3-NOTCH1 cleaved by γ-secretase. The lower band at approximately 80 KDa is reported as non-specific (Abcam website: http://www.abcam.com/notch1-antibody-chip-grade-ab27526-references.html; accessed 09.2014).

Levels of NOTCH1 S1 fragment appeared to be increased in TYLK1 and TYLK2 TOC keratinocytes in lysate sets 2 and 3, and in TYLK1 cells in lysate set 1 (figure 4.2.14 A), suggesting increased overall NOTCH1 expression and activation. Densitometry was performed on lysate sets 1 and 2 (figure 4.2.14 B). Particularly in TYLK1 cells, the densitometry suggests increased expression of the NOTCH1 S1 fragment, with some increase in NOTCH1 expression in TYLK2 cells. However, the GAPDH loading control signal is strong with a lot of background in the first lane which may have affected the densitometry analysis. Lysate set 3 was excluded from analysis as the GAPDH signal was too strong for accurate densitometry. The signal did appear consistent between the cell lines, however, suggesting approximately equal protein loading.

Cleaved NOTCH1 also appeared to be increased in expression in TOC keratinocytes (figure 4.2.14 A), which was again seen more strongly in TYLK1 cells, but a slight increase appeared in TYLK2 cells compared to NEB1 and K17 control keratinocytes. Densitometry for lysate sets 1 and 2 is shown in figure 4.2.14 C, supported elevated processing of NOTCH1 in TOC compared to controls although more experiments are needed to confirm this.

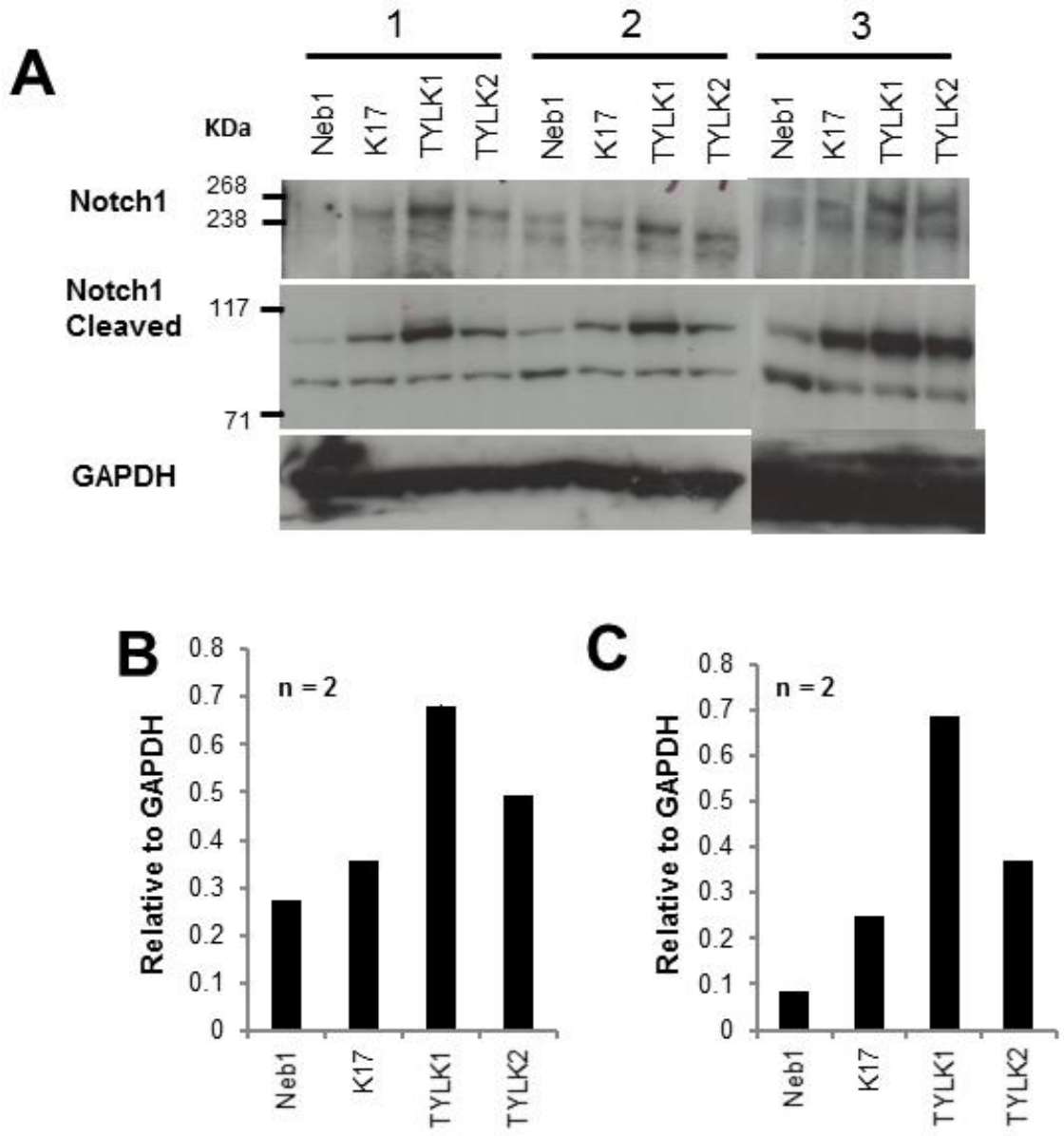

Figure 4.2.14 NOTCH1 expression and processing may be increased in TOC keratinocytes. A: Western blots showing full length and cleaved NOTCH1 in lysates taken from three sets of keratinocytes (labelled 1 to 3). Each sample set included NEB1 and K17 control cell lines and TYLK1 and TYLK2 TOC cell lines. **B:** Densitometry of NOTCH1 S1 fragment, **C:** Densitometry of cleaved NOTCH1 (S2-S4 fragments). Densitometry was performed on lysate sets 1 and 2 because the GAPDH was too bright to get meaningful results in the third set of samples. The third experiment does, however, also suggest increased levels of NOTCH1 S1 and perhaps cleaved NOTCH1 in the TOC cell lines. Densitometry was carried out using Image J Software.

4.2.6.2 NOTCH1 localisation in keratinocyte cell lines

Staining of total and cleaved NOTCH1 was carried out in confluent monolayers of TOC keratinocytes after culture in the presence of EGF. ICC with the ChIP grade antibody recognising total NOTCH1 showed punctate intracellular staining, with some staining at the cell surface, and larger puncta that appear to co-localise with DAPI nuclear staining (figure 4.2.15). The cell-surface staining appeared to be more intense in many areas of the monolayers in TOC keratinocytes compared to control cells, where plasma-membranous staining was more difficult to locate during imaging (n=2). The increase was particularly clear in TYLK1 monolayers, shown at a higher zoom level in figure 4.2.15 B alongside K17 control keratinocytes, consistent with western blotting of the S1 fragment, which would be expected to be found at the plasma membrane.

A similar result was seen with ICC with the mN1A antibody, which recognises S1 cleaved NOTCH1 (figure 2.16). Staining with the mN1A antibody gave a similar punctate staining pattern to the ChIP grade antibody, again showing slightly increased NOTCH1 at the cell surface in TOC keratinocytes compared to control cells although the differences are more subtle than those seen with the ChIP grade antibody.

The antibody Val1744 recognises NOTCH1 cleaved at amino acid residue Val1744, a stable form of the NICD. ICC with this antibody showed a ‘speckled’ appearance throughout the cell, including in the nucleus (figure 4.2.17), with smaller more diffuse puncta than those seen in staining with the ChIP grade or mN1A antibodies. There appeared to be more intense staining in TOC keratinocytes than control keratinocytes, particularly in the nucleus. This was more pronounced in TYLK1 cells, also consistent with levels of cleaved NOTCH1 in the western blot in figure 2.14.

4.2.6.3 Variability in localisation between NOTCH1 antibodies

Although these findings suggest that it may be interesting to look further at NOTCH1 localisation in TOC keratinocytes, it is not possible to reach a conclusion due to the low number of repeats and inconsistencies in the staining patterns between the different antibodies.

For example, staining with the mN1A antibody showed weak staining at cell borders compared with the ChIP grade antibody although the S1 and S2 cell-surface fragments would be expected to be at the same levels and to be recognised by both antibodies. The staining pattern of the NICD also appeared much more diffuse with the NICD-specific antibody compared to intracellular staining with the ChIP grade and mN1A antibodies. Further work is therefore needed to confirm the localisation of the different processed forms of NOTCH1 fragments within control and TOC cells e.g. with cell fractionation and additional antibodies.

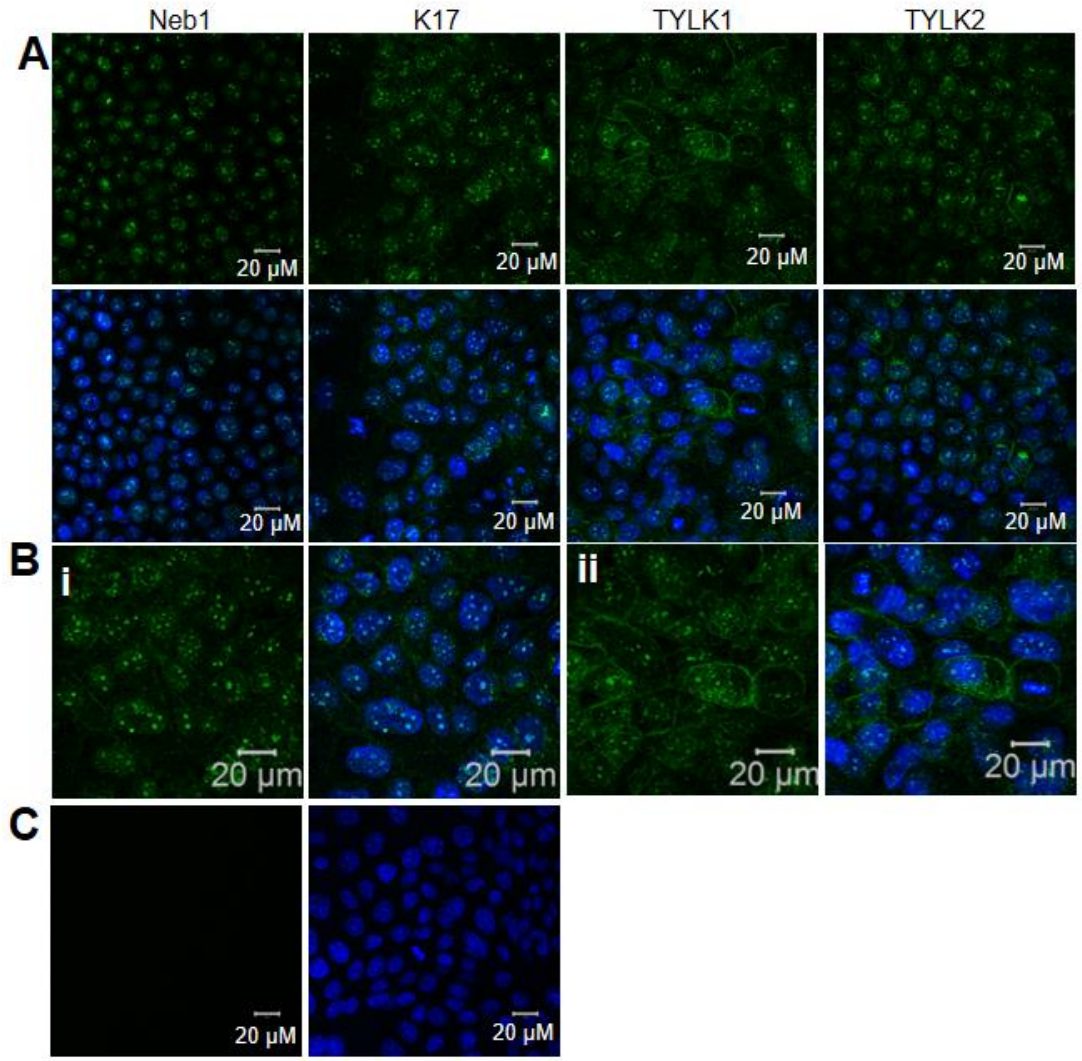

Figure 4.2.15 Cell-surface NOTCH1 may be increased in TOC cutaneous keratinocytes. A: ICC in control (NEB1, K17) and TOC (TYLK1 and TYLK2) keratinocytes with an antibody recognising total NOTCH1 protein (AbCam ChIP-grade antibody) (n=1), **B:** Higher power images of cell-surface NOTCH1 staining in i) K17 control cells and ii) TYLK1 TOC keratinocytes. NOTCH1 is shown in green, DAPI nuclear stain is shown in blue. Images were taken on the Zeiss Meta 710 Confocal Microscope.

4.2.6.3 NOTCH1 in the epidermis

IHC was also performed in normal and TOC skin with the same antibodies to investigate NOTCH1 in differentiated epidermis. IHC with the mN1A antibody (figure 2.18) showed a punctate intracellular localisation in normal skin from breast and abdomen, similar to that seen in staining of keratinocyte monolayers with the same antibody. Some faint plasma-membranous staining was seen in the upper epidermal layers. The staining intensity of NOTCH1 was variable between IHC experiments and within IHC experiments: in experiment 1 (figure 2.18 A), TOC patients 1 and 2 appeared to show increased overall expression of NOTCH1, compared to normal breast skin stained and imaged in the same experiment, however, this was not replicable in experiment two. In experiment 2, staining of normal skin from breast and abdomen was performed, showing variability in staining intensity between skin biopsies taken from different body sites (figure 2.18 left hand side). Cell-surface expression of NOTCH1 was particularly faint in this experiment. This time, patient two appeared to have a similar staining intensity to that of normal breast skin (figure 4.2.18 B), with a similar localisation. Patient 3 showed the greatest differences in staining with this antibody, with increased staining intensity, and strong cell-surface staining in the upper epidermal layers (figure 4.2.18 C).

Staining with the ChIP grade antibody was very faint in IHC, with no clear differences in the staining (appendix B4), so further optimisation may be required in future experiments, or perhaps the antibody is not suitable for use in IHC with frozen sections.

Staining of cleaved NOTCH1 with the Val1744 antibody in normal and TOC skin (figure 4.2.19) was more consistent with the western blotting data, with greater staining intensity in all three TOC biopsies compared to normal skin from breast and abdomen in two separate staining experiments. The staining was diffuse and cytoplasmic in both normal and TOC skin, and interestingly did not appear to be localised to the nucleus in many of the cells of the epidermis in contrast to staining of monolayer keratinocytes. Staining was much fainter in the basal layer of the epidermis with strong staining in the suprabasal layers in normal skin and TOC, perhaps consistent with increased NOTCH1 activity in differentiating keratinocytes. However, the variability and inconsistency in the staining means that the data should perhaps be interpreted with caution and confirmed by other methods, for example in 3D keratinocyte cultures and cell fractionation.

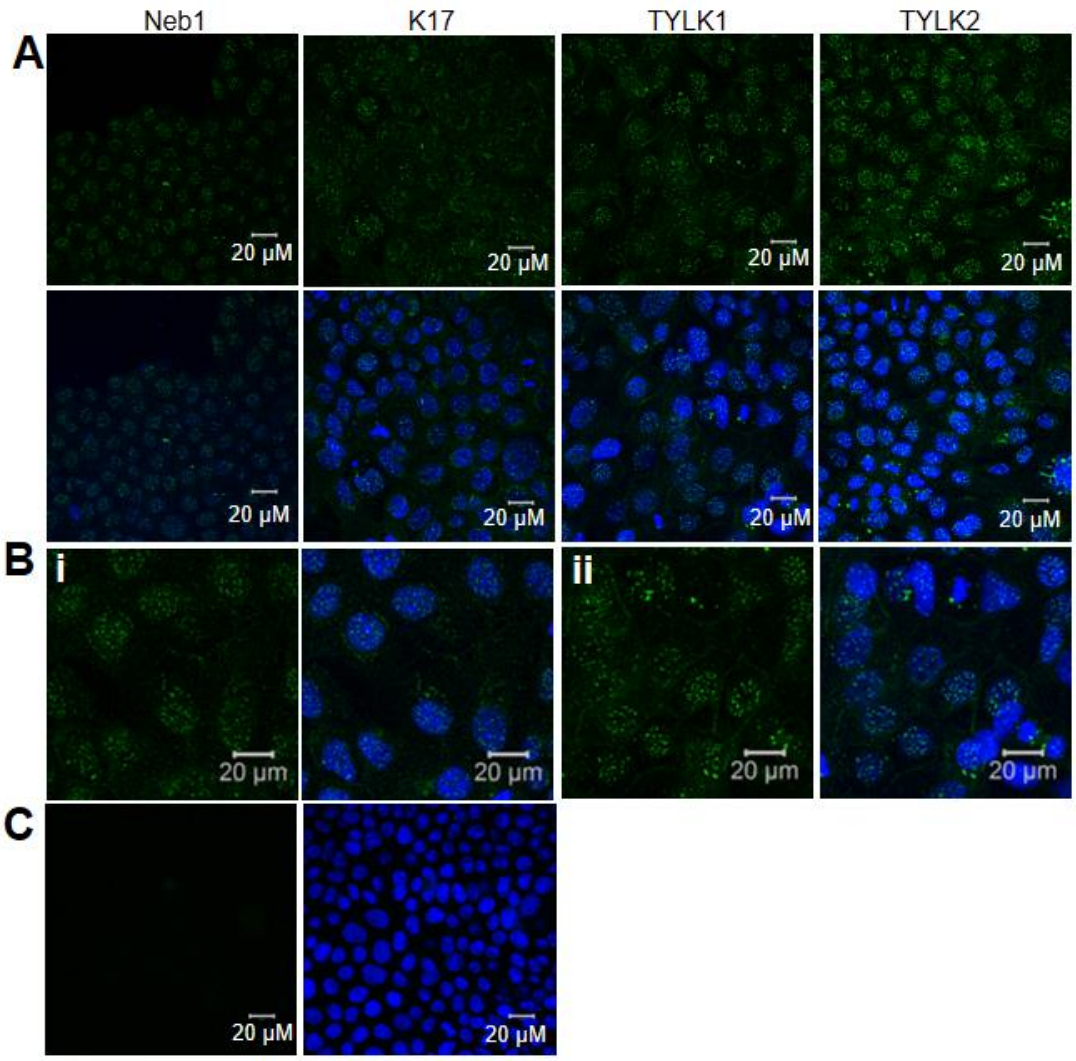

Figure 4.2.16 Increased processing of NOTCH1 may be taking place in TOC keratinocytes. A and B: ICC of NOTCH1 with an antibody that recognises NOTCH1 after S1 cleavage (mN1A) (n=1). **B:** NOTCH1 mN1A staining shown at a higher zoom level in (i) K17 control and (ii) TYLK1 TOC keratinocytes. **C:** Negative control staining. NOTCH1 is shown in green, DAPI nuclear stain is shown in blue. Images were taken on the Zeiss Meta 710 Confocal Microscope.

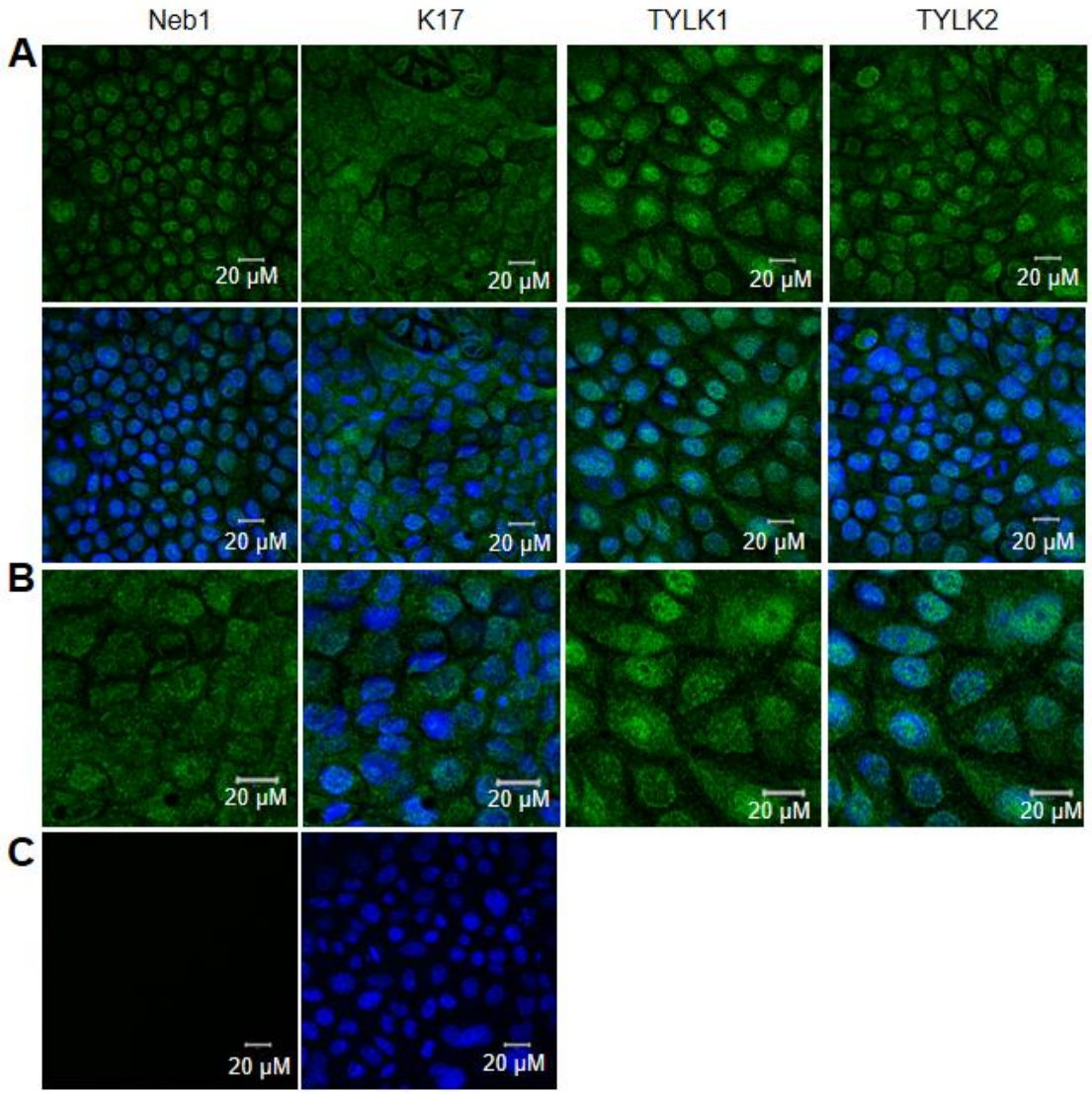

Figure 4.2.17 Increased staining intensity and nuclear localisation of NOTCH1 NICD in TOC keratinocytes. A: ICC in control (NEB1, K17) and TOC (TYLK1 and TYLK2) keratinocytes with an antibody that specifically recognises NOTCH1 cleaved at Valine residue 1744 – the NICD**. B:** K17 (i) and TYLK1 (ii) stained with anti Val1744 at a higher magnification. **C:** Negative control staining**.** NOTCH1 is shown in green, DAPI nuclear stain is shown in blue. Images were taken on the Zeiss Meta 710 confocal microscope. Please note that this is preliminary data from one experiment only.

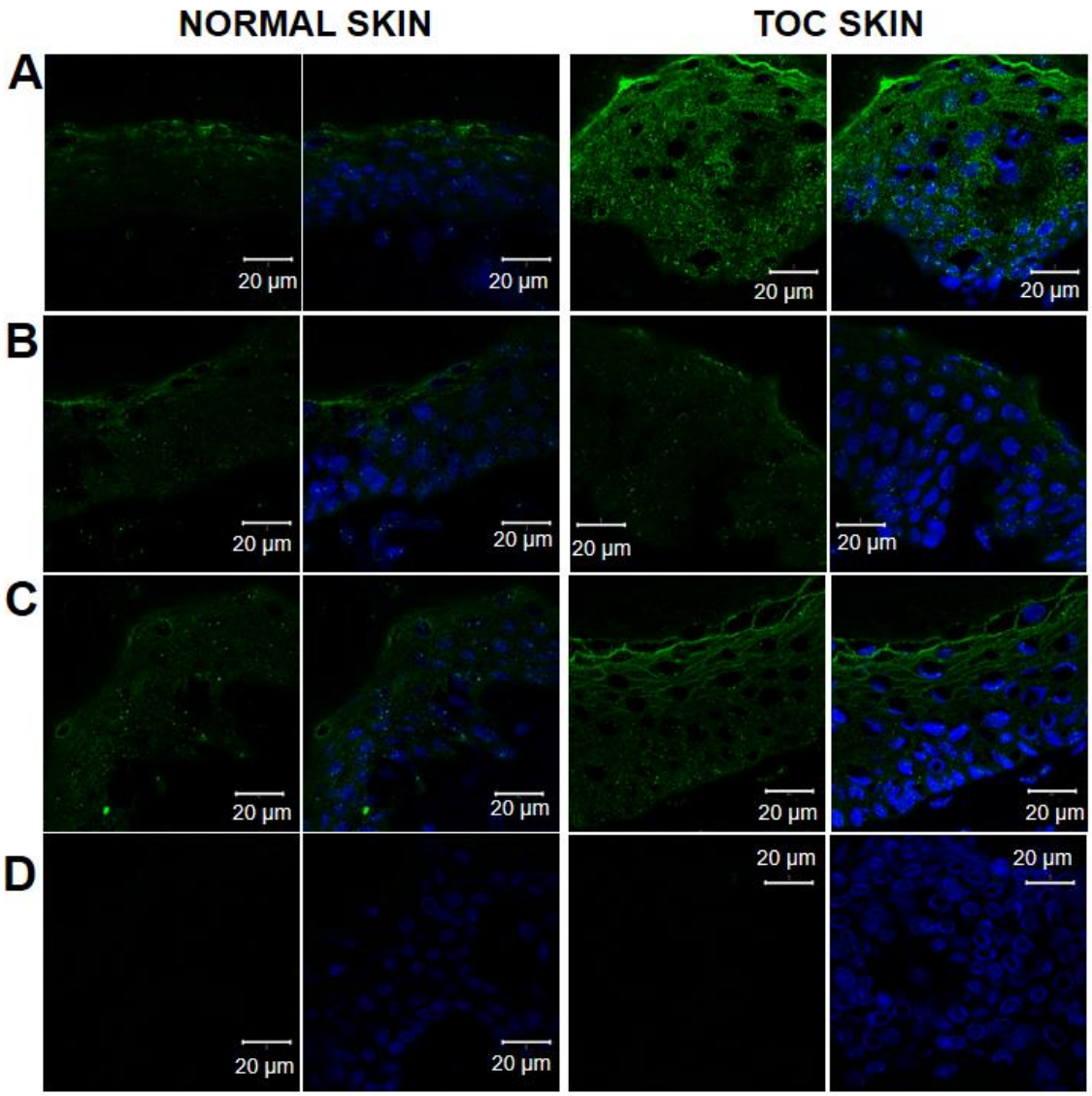

Figure 4.2.18 NOTCH1 S1 fragment localisation is variable in TOC skin. IHC against S1 cleaved NOTCH1 (mN1A antibody) in frozen sections from normal and TOC skin**. A:** Experiment 1 – Normal breast skin and TOC patient 1, staining carried out in the same staining session. **B** and **C:** Experiment 2 (All sections shown in **B** and **C** were stained at the same time). **B:** Normal skin from breast tissue, TOC patient 2. **C:** Normal skin from abdomen, TOC patient 3. **D:** Negative control staining in experiment 1 (i) and experiment 2 (ii)**.** NOTCH1 is shown in green, DAPI nuclear stain is shown in blue. Images were taken on the Zeiss Meta 710 Confocal Microscope, and all images in this figure were taken with the same settings, although imaging for experiments 1 and 2 was performed on different days.

4.2.7 Are other rhomboid family proteins dysregulated in TOC?

As rhomboid proteins are a relatively recently discovered family of proteins, little is known about their regulation and localisation in the skin. Preliminary IHC experiments were therefore performed against iRHOM1, RHBDL2 and the RHBDL2 substrate thrombomodulin. RHBDL2 was selected as it cleaves EGF, and because it has been shown to be important in wound healing *in vitro.* Thrombomodulin is also important in wound healing and is tightly regulated during differentiation. (Ephrin B3, another RHBDL2 substrate, may also have been interesting, but IHC was not consistent in frozen tissue sections.)

iRHOM1 IHC in normal and TOC skin is shown in figure 4.2.20. In contrast to the plasma-membranous iRHOM2 staining seen in the skin, iRHOM1 appeared to have a more cytoplasmic or perinuclear localisation, with more intense staining in the basal layer and some faint cell-surface staining in the granular layer. A similar localisation of iRHOM1 was seen in skin from TOC patients, with the intense basal-layer staining appearing to reach further into the suprabasal layers, perhaps due to the hyperproliferative nature of TOC skin. In patients 2 and 3, the cell-surface staining in the *stratum granulosum* appeared more intense, and in patient 1, which shows the strongest alteration in iRHOM2 localisation, some individual cells in the suprabasal layer appeared to show cell-surface staining (figure 4.2.20). IHC of RHBDL2 is shown in figure 4.2.21. IHC and western blotting were both inconsistent with this antibody. The experiment shown is the result of one experiment, with normal skin from facelift and TOC skin from patient 4, an older TOC skin biopsy. The staining in normal skin showed a diffuse localisation throughout the cell and plasma membrane (and in the macrophages), with brighter nuclear or perinuclear staining. In TOC patient 4 in this experiment, the staining appeared more cytoplasmic, with no staining at the cell surface, and much brighter, compact perinuclear staining was seen, perhaps consistent with a golgi-like localisation. This localisation was seen in normal skin to a lesser extent in one experiment.

In normal frozen skin, thrombomodulin staining appeared diffuse throughout the cytoplasm and plasma membrane in the lower epidermal layers, and more cytoplasmic in the upper layers. In the frozen sections, there was perhaps some nuclear/stronger perinuclear staining in some cells of the basal layer, in contrast to IHC in paraffin-embedded skin sections (figure 4.2.22; Raife et al. 1994; Lager et al. 1995), showing cell-surface staining in the spinous and granular epidermal layers. Patients 2 and 3 appeared to show stronger perinuclear staining in the basal layer, but otherwise showed a similar localisation and staining intensity to normal skin with increased cytoplasmic staining in the upper layers of the epidermis.

Some plasma membrane staining was seen in Patient 1 sections, which appeared to show a reduced staining intensity compared to normal skin and the other TOC patients, particularly in the basal layer which would be more consistent with the normal skin staining reported by Lager et al. (1995). In the upper layer, the diffuse staining appeared to be of lower intensity, with some plasma membrane staining seen in these layers. The differences between patient 1 and the other patients and normal skin could suggest that RHBDL2 and thrombomodulin are affected by the altered iRHOM2-ADAM17-EGF signalling in TOC, but the inconsistencies with previous work (Lager et al., 1995) suggest that these findings may need to be repeated in paraffin-embedded skin. These findings are very preliminary, and further investigations of the rhomboid signalling pathway in the skin are warranted.

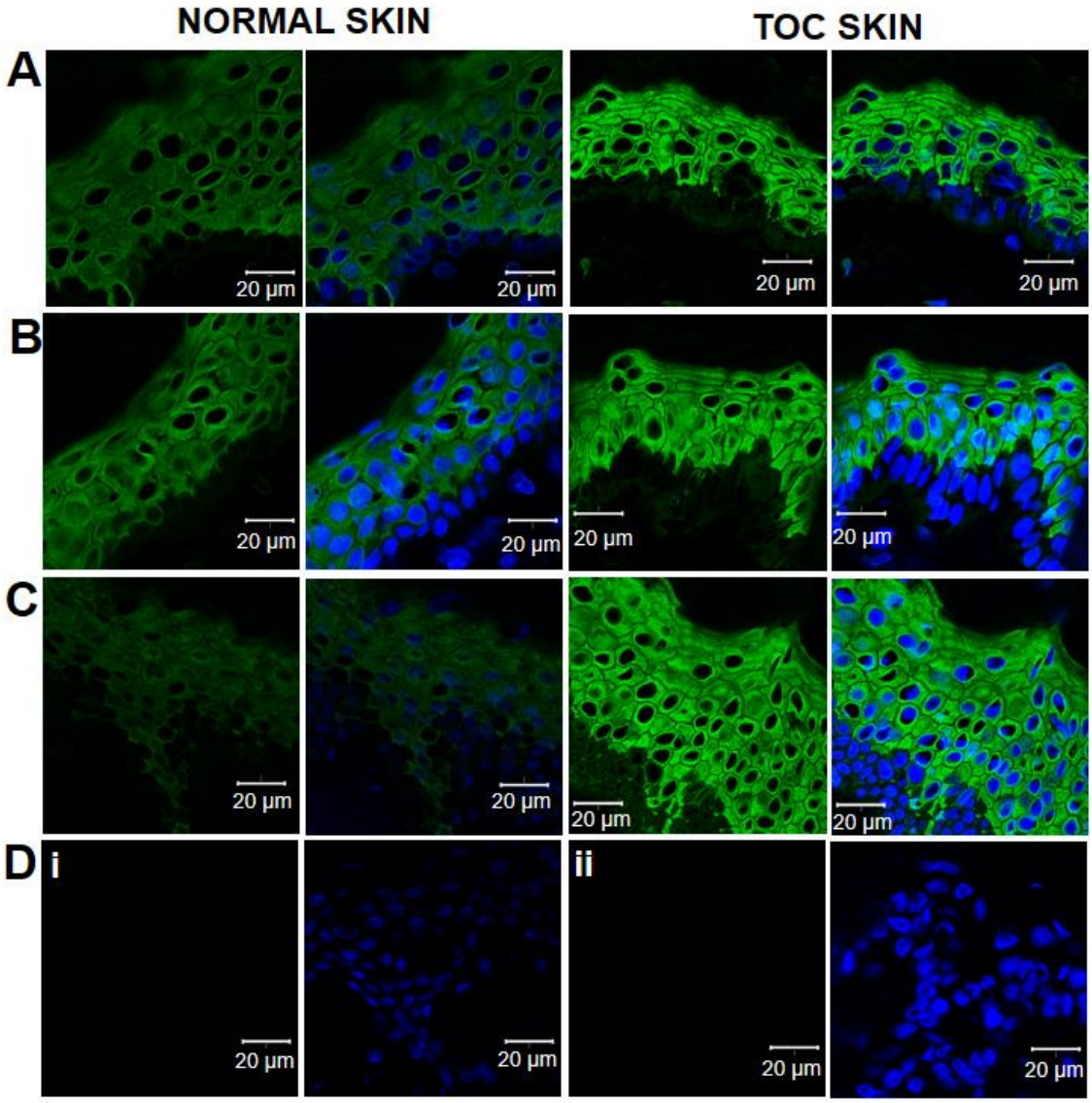

Figure 4.2.19 NOTCH1 NICD expression is increased in TOC skin. IHC against NOTCH1 cleaved at Val1744 (NICD) in frozen sections from normal and TOC skin**. A:** Experiment 1; normal breast skin and TOC patient 1. **B and C:** Experiment 2 (All sections shown in **B** and **C** were stained at the same time). **B:** Staining from normal skin from breast tissue and TOC patient 2. **C:** Normal skin from abdomen and TOC skin from patient 3. **D:** Negative control staining in experiment 1 (i) and experiment 2 (ii)**.** NOTCH1 is shown in green, DAPI nuclear stain is shown in blue. Images were taken on the Zeiss Meta 710 Confocal Microscope, and all images in this figure were taken with the same settings, although imaging for experiments 1 and 2 was performed on different days.

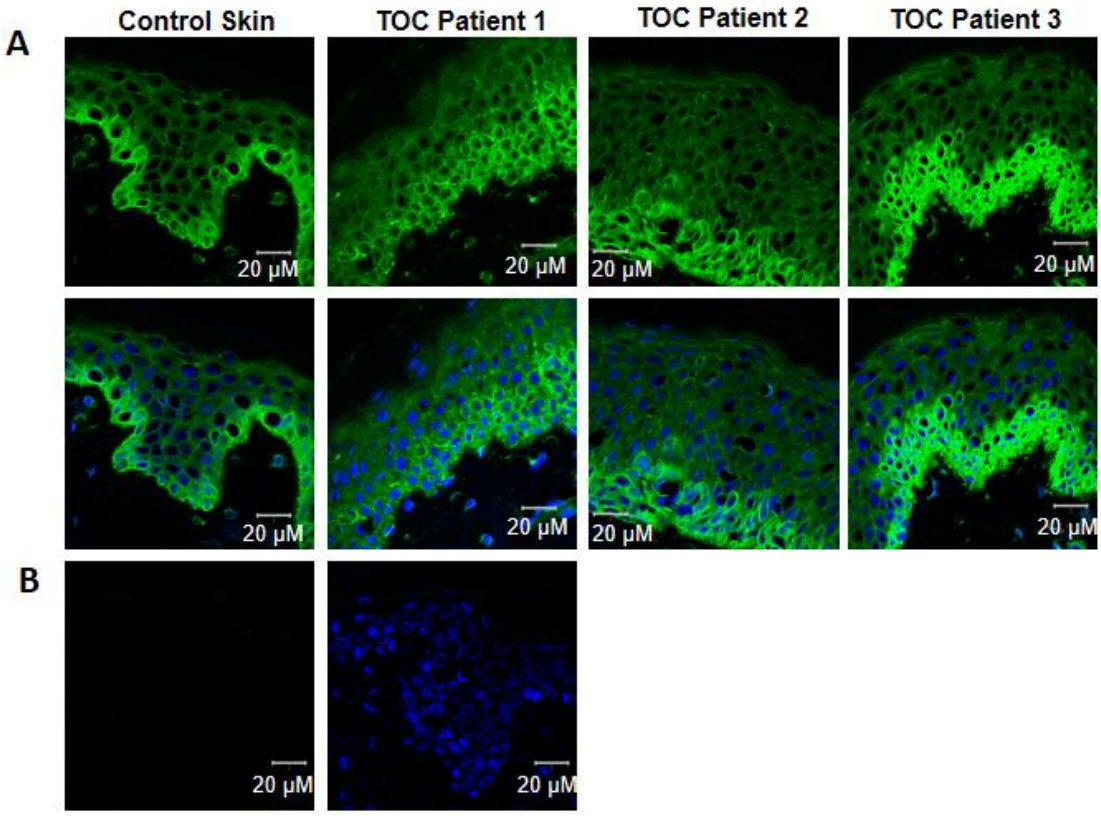

Figure 4.2.20 iRHOM1 localisation in normal and TOC skin. A: IHC in frozen skin sections from normal and TOC skin. **B:** negative control. iRHOM1 staining is shown in green, and DAPI nuclear stain is shown in blue. Staining was carried out on the Zeiss Meta 710 Confocal Microscope. N=2.

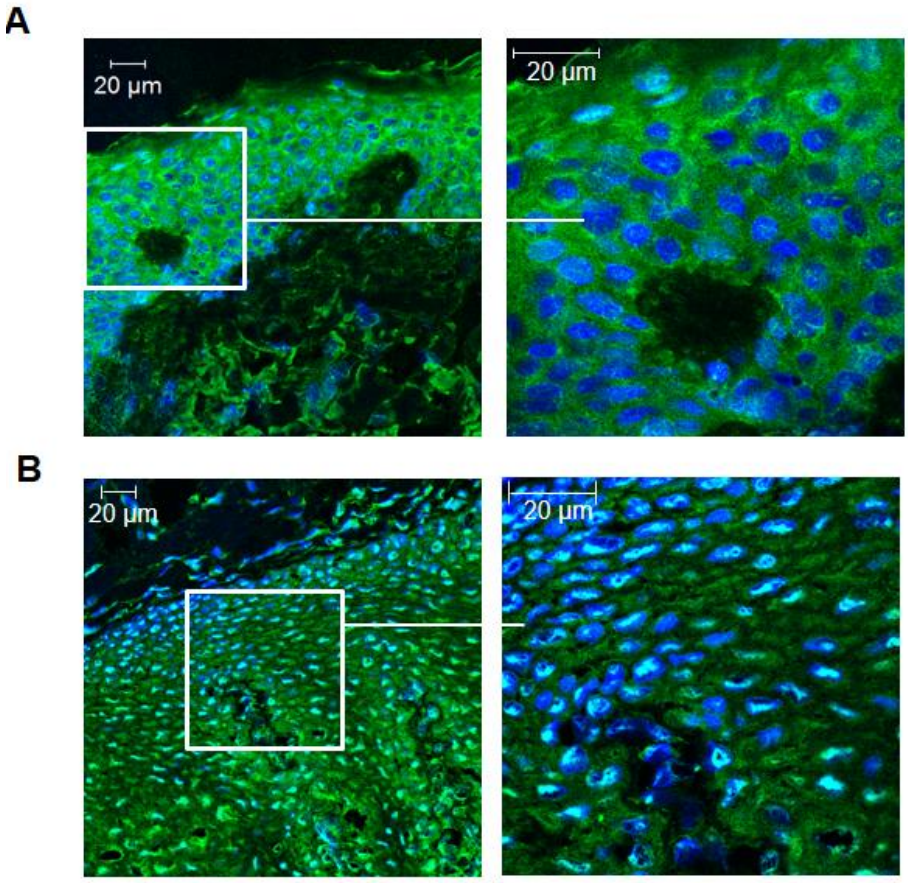

Figure 4.2.21 Rhomboid protease RHBDL2 in normal and TOC skin. IHC of RHBDL2 in normal facelift skin (**A**) and TOC skin from patient 4 (**B**). Images were taken on the 510 Meta LSM confocal microscope. RHBDL2 staining is shown in green, and DAPI nuclear stain in blue. Please note that staining results varied between experiments, and this result was seen only once this strikingly, and less clearly one other time in the same frozen sections despite a number of repeats. Further information is included in the results text.

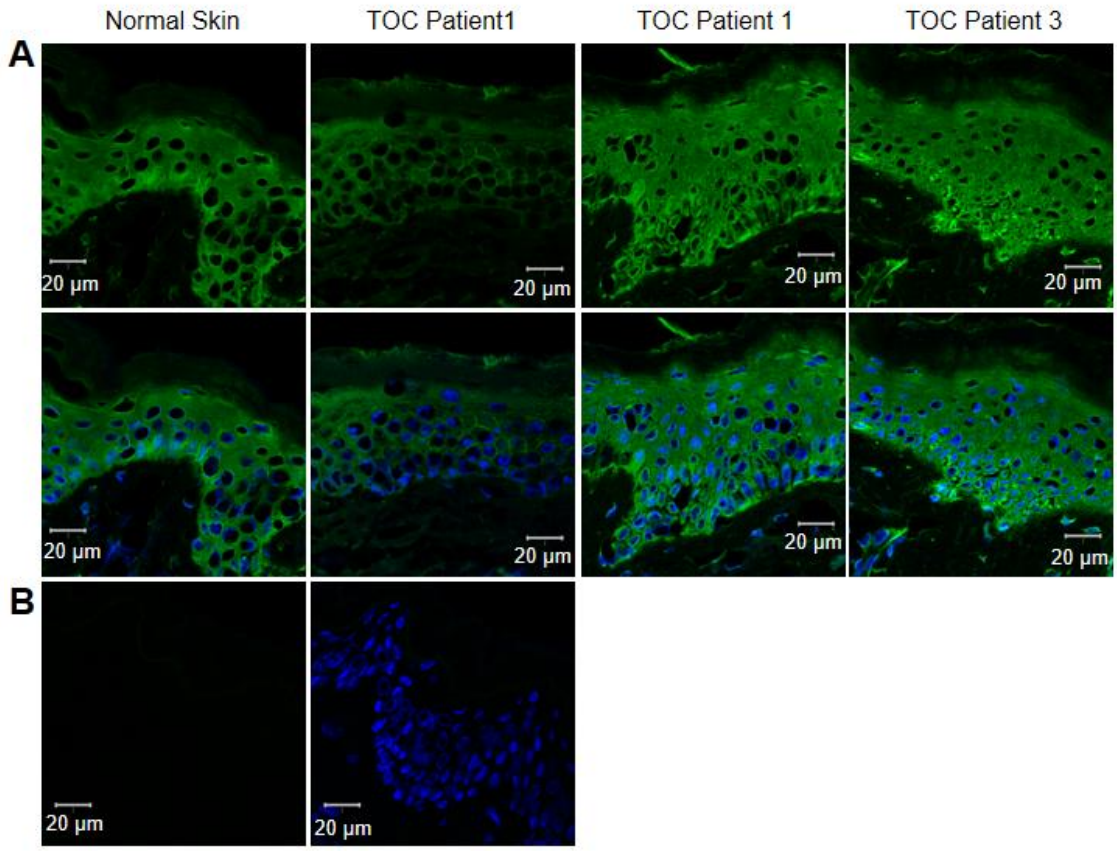

Figure 4.2.22 Localisation of RHBDL2 substrate thrombomodulin in normal and TOC skin. IHC on frozen skin sections from normal and TOC skin **(A),** with negative control staining shown in **B.** Images were taken on the Zeiss Meta 710 microscope, Thrombomodulin staining is shown in green, and DAPI nuclear staining in blue. Staining was repeated twice for each biopsy.

4.3 Discussion

This chapter investigated the iRHOM2-ADAM17 pathway in TOC and the effect of increased EGFR signalling on downstream pathways including Eph/Ephrin and NOTCH1 signalling. Finally, preliminary investigation of other rhomboid proteins was performed.

4.3.1 Summary of Results

1) Increased migration in TOC cells appears to be independent of proliferation, shown by scratch assays carried out in the presence and absence of MMC.

2) iRHOM2 appears to be important in processing metalloproteinase ADAM17 in cutaneous keratinocytes, shown by reduced mature ADAM17 levels after iRHOM2 knock down.

3) TOC mutations appear to increase ADAM17 processing, shown by increased cell-surface ADAM17 and increased mature ADAM17 levels in TOC keratinocyte monolayers and 3D cultures (collaborative data).

4) iRHOM2 expression may be partly regulated by ADAM17, as iRHOM2 protein levels appeared reduced after ADAM17 siRNA knock down, and the staining intensity of iRHOM2 appeared reduced in skin from a patient with a homozygous LOF ADAM17 mutation.

5) Eph-Ephrin signalling may be a downstream target of increased EGF signalling in TOC, shown by western blotting and IHC of EphA2 and EphA4 and a protein array against phospho-RTKs.

6) NOTCH1 expression and processing appear increased in confluent TOC cells compared to control cell lines.

7) Other rhomboid signalling pathways may also show some subtle dysregulation in TOC, shown by IHC of iRHOM1, RHBDL2 and thrombomodulin.

4.3.2 Increased ADAM17 processing and EGFR signalling in TOC

iRHOM2 mutations in TOC result in increased EGFR signalling (Figure 4.2.1; (Blaydon et al., 2012; Brooke et al., 2014), likely mediated by increased iRHOM2-dependent ADAM17 activation (figures 4.2.2-4.2.4; Brooke et al. 2014) and increased processing of EGFR ligands by ADAM17 (figure 4.2.4; Brooke et al. 2014).

4.3.2.1 ADAM17 processing

Reduced mature ADAM17 levels after iRHOM2 knock down is consistent with results in human monocytes by Issuree et al. (2013) and with the role of iRHOM2 in ADAM17 processing; collaborative data also shows increased mature ADAM17 levels and cell-surface ADAM17 in TOC keratinocyte monolayers and 3D cultures. Furthermore, ELISA assays show increased shedding of a number of EGFR ligands in TOC keratinocytes including AREG and TGF-α (Brooke et al. 2014; shown in figure 4.2.4). There was some variation in the western blotting data shown in figure 4.2.3 between sets of lysates, but results appear consistent with other methods used and with the literature showing iRHOM2-mediated ADAM17 processing (Adrain et al., 2012; McIlwain et al., 2012).

4.3.2.2 Increased TOC keratinocyte migration and EGF signalling

Increased proliferation and migration was seen in the TOC cells, which was particularly apparent after culture in the absence of exogenous EGF (figure 4.2.1; Blaydon et al. 2012). ADAM17 has been shown to be required for keratinocyte migration, for example FGF7-stimulated migration was blocked by ADAM17 siRNA and EGFR inhibition (Maretzky et al., 2011). The process was also dependent on ADAM17 substrate HB-EGFR, as the migration was blocked by mutant diphtheria toxin CRM197, which selectively inhibits EGF. Furthermore, recent data in the group by Dr Matthew Brooke showed reduced migration in TOC keratinocytes after treatment with an ADAM17 inhibitor (*GW280264X)* but not with an ADAM10 inhibitor, further suggesting that increased ADAM17-mediated shedding of EGFR ligands may be the mechanism for increased migration in TOC keratinocytes.

Further research into the role of RHBDL2 would also be of interest, as RHBDL2 has also been shown to cleave EGF (Adrain et al., 2011) and RHBDL2 and its substrate thrombomodulin have been implicated in wound-healing (Cheng et al., 2011). IHC shown in this chapter is very preliminary and not easily reproduced, but if the dramatic re-localisation seen was 'real', it perhaps suggests that this pathway may be affected in TOC and would be interesting for future research into EGF signalling, migration and wound healing in the skin. Adrain et al. (2011) showed that EGF cleavage by RHBDL2 was independent of ADAM17 in experiments carried out in the presence and absence of the metalloproteinase inhibitor BB94, and that RHBDL2-mediated cleavage of EGF could occur while ADAM17 was active or inhibited. EGFR was activated when ADAMs were inhibited with a similar efficiency to ADAM17-mediated EGFR activation (Adrain et al., 2011) demonstrating an additional pathway for regulation of EGFR signalling, and suggesting that this pathway would be interesting for further research in the skin.

4.3.2.3 Eph-Ephrin Signalling affected downstream of EGFR signalling

Effectors of migration downstream of EGF signalling may include members of the Eph/Ephrin family of RTKs and ligands. The Eph/Ephrin family is involved in a number of cellular processes, including proliferation, adhesion, cell survival and differentiation (e.g. Guo et al., 2006; Yamada et al., 2008; Egawa et al., 2009; Furne et al., 2010; Genander et al., 2010; Genander and Frisén 2010; Lin et al., 2010; Kaplan et al., 2012), and a number of studies have implicated Eph/Ephrin signalling in migration (Larsen et al., 2007; Fukai et al., 2008; Miao et al., 2009; Hiramoto-Yamaki et al., 2010; Larsen, Stockhausen and Poulsen, 2010; Kaplan et al., 2012).

4.3.2.3.1 EphA4 and EphA2 signalling in migration

EphA4 has been shown to promote migration and proliferation in glioma cell lines (Fukai et al., 2008), inhibit migration in lung adenocarcinoma (Saintigny et al., 2012), and regulates migration in many processes in the nervous system, for example inhibiting Schwann Cell migration in peripheral nerve regeneration (Wang et al., 2013). Both EphA4 and EphA2 regulate migration through Rho-GTPase-dependent mechanisms (Fukai et al., 2008; Hiramoto-Yamaki et al., 2010).

The Ephrin A1-EphA2 signalling axis is better characterised, particularly in the skin. EphA2 can act in a ligand (Ephrin A1)-dependent or independent manner (Miao et al., 2009; Hiramoto-Yamaki et al., 2010), and appears to be constitutively active (Larsen et al., 2007) in contrast to other Eph receptors such as EphA4 (Binns et al., 2000; Wybenga-Groot et al., 2001). The role of Ephrin A1 includes regulating EphA2 turnover at the plasma membrane.

Ligand-independent EphA2 activation appears to stimulate migration, while Ephrin A1 mediated activation of EphA2 results in phosphorylation, followed by internalisation and down-regulation of EphA2 and an inhibitory effect on migration (Larsen et al., 2007; Miao et al., 2009; Hiramoto-Yamaki et al., 2010; Larsen et al., 2010). Ligand-independent action of EphA2 stimulated serum-induced chemotaxis in glioma and prostate cancer cells, which was dependent on phosphorylation at S897 by Akt (Miao et al., 2009). The Ephrin A1/EphA2 pathway is also relevant to wound healing in the cornea, where elevated Ephrin A1 expression was seen in diabetic corneal cells and in corneal cells cultured in high glucose, and was associated with impaired migration and wound healing mediated by inhibition of Akt (Kaplan et al., 2012).

4.3.2.3.2 EphA4 and EphA2 in TOC

Decreased phospho-EphA4 was seen in a phospho-protein array against RTKs carried out with lysates from cells cultured in the presence of EGF in addition to changes in IGF-1R and Insulin-R. Further pathways could potentially be identified after culture without

exogenous EGF, as potential (although variable) differences in total EphA2 and EphA4 receptor expression were seen in TOC keratinocytes after culture without exogenous EGF but not after culture in the presence of EGF. The findings were supported by increased EphA2 in 3D cultures of TOC keratinocytes compared to control keratinocyte 3D cultures (figure 4.2.6). Insulin-R and IGF-1R signalling have also been implicated in migration, proliferation and differentiation in the skin (Benoliel et al., 1997; Wertheimer et al., 2000; Sadowski and Dietrich, 2003; Sadagurski et al., 2006), and may be of interest in future investigations.

IHC in frozen skin biopsies suggested increased EphA4 and phospho-EphA4 protein in patient 1, but not in the other TOC patients, suggesting that EphA4 may be affected downstream of dysregulated iRHOM2, but not in 'normal' circumstances. Some possible nuclear EphA4 was seen in some cells in patient 1 epidermis, and in ICC, perhaps suggesting an additional role for EphA4 in the skin. EphA2 appeared to be in the nucleus in serum-starved HEK293T cells (Miao et al., 2009), but EphA4 in mouse skin appeared to show a more intracellular localisation (Egawa et al., 2009), and IHC against EphA4 by Yamada et al (2008) in skin sections showed stronger expression at the plasma membrane. This could suggest variable EphA4 localisation between species and different body sites in human; recognition of cleavage products of EphA4 (for example, EphA4 is cleaved by Caspase 3 in adult neurogenesis, where it acts as a dependence receptor (Furne et al., 2010); or could represent inconsistencies between protocols and antibodies, so this requires further investigation, for example, by cell fractionation.

An increase in phospho-EphA4 contrasts with the findings of the phospho-array, perhaps due to the different conditions in monolayer culture compared with differentiating cells in the upper layers of the epidermis. Further, the phospho-EphA4 antibody did not work well for western blotting (my experience and personal communication from Dr Spiro Getsios), so it is possible that the staining is non-specific. Changes were only in patient 1, consistent with the results seen with the total EphA4 antibody, however, suggesting that this pathway may be affected. Further work will be required to confirm these findings, perhaps including *in vivo* and 3D wound healing assays, and IHC in involved TOC skin.

4.3.2.3.3 Effect of growth factors on EphA2

Alterations in EphA2 expression downstream of EGF signalling have previously been shown in cancer cell lines with both ligand-dependent EGFR signalling and constitutively active EGFR mutant EGFRvIII (Larsen et al., 2007). This induction of expression was partly dependent on MEK and src family kinases (Larsen et al., 2007; 2010), and was dependent on cell adhesion and proteins of the extracellular matrix (Larsen et al., 2010). Furthermore, co-immunoprecipitation experiments in a number of cell lines showed increased association of EphA2 with EGFR upon stimulation of the cells with EGF,

suggesting that activation of EGFR is required for the association of the two RTKs to occur (Larsen et al., 2007). Growth-factor stimulation of cancer cell lines also induced phosphorylation of EphA2 residue S897, which was required for EphA2 localisation at the leading edge of the cell, and for cell polarisation (Miao et al., 2009).

Growth factors and cytokines associated with psoriasis have been shown to affect epidermal morphology (Johnston et al., 2010; Gordon et al., 2013). Keratinocyte organisation in 3D cultures was disrupted in the basal and spinous layers by treatment with EGF and IL-1α, associated with a reduced number of keratohyalin granules and expanded stratum corneum and reduced expression of differentiation markers K10, DSG1, and loricrin (Johnston et al., 2010; Gordon et al., 2013). These changes were accompanied by up-regulation of members of the RTK family, including EphA2. More minor morphological changes were seen with TNF-α and IL17-α treatment despite similar changes in EphA2 (Gordon et al., 2013). Enhanced IL-1 expression and proliferation was seen in the skin of mice where Ephrin B2 was knocked out perinatally (Egawa et al., 2009).

4.3.2.3.4 RHBDL2 and thrombomodulin in epidermal wound healing

Expression of RHBDL2 substrate thrombomodulin is closely regulated in epidermal wound healing (e.g. Raife et al., 1994; Lager et al., 1995; Raife et al., 1996; Mizutani et al. 1994; Senet et al., 1997) and may be interesting to study in future investigations. Thrombomodulin is cleaved by a number of proteases, and soluble thrombomodulin is released extracellularly; furthermore, recombinant thrombomodulin acts as a mitogenic factor (Hamada et al., 1995; Shi et al., 2005).

Increased expression of soluble thrombomodulin and RHBDL2 was seen after wounding in HaCat cells and in mice after transdermal incision surgery (Peterson et al., 1999; Cheng et al., 2011). The increase in soluble thrombomodulin release in HaCaT cells was dependent on RHDL2, as its release was prevented by the non-specific serine protease inhibitor 3,4-dichloroisocoumarin (DCI) and also by shRNA directed against RHBDL2. Migration and proliferation were also reduced by RHBDL2 knock down, and the effects reversed by treatment with recombinant soluble thrombomodulin. Conversely, overexpression of RHBDL2 increased release of soluble thrombomodulin (Cheng et al., 2011). These findings lead to the hypothesis that RHBDL2 cleaves thrombomodulin after wounding, releasing soluble thrombomodulin to induce proliferation and migration in keratinocytes to close the wound (Cheng et al., 2011).

4.3.3 ADAM17-dependent regulation of iRHOM2 expression

Two pieces of data from this chapter support ADAM17-mediated regulation of iRHOM2 expression in the skin: reduced iRHOM2 protein after ADAM17 knock down, and

reduced iRHOM2 staining intensity in skin from a patient with a homozygous LOF ADAM17 mutation. Furthermore, a relationship between iRHOM2 and ADAM17 expression is consistent with data in OSCC and HNSCC cell lines, which will be shown in the next chapter. The data contrasts with findings of Issuree et al (2013), who did not see down-regulation of iRHOM2 upon treatment with anti-ADAM17 siRNA in human monocytes. The result was seen at the mRNA level, however, so the regulation could take place at the post-translational level, or the time points of the experiments could have been different (the time point for sample collection was not stated in (Issuree et al., 2013). Alternatively, different regulatory pathways could be active in these tissues compared with the pathways dominant in immune cells, and the presence of iRHOM1 in keratinocytes may affect iRHOM2 regulation due to the overlapping functions of the two proteins. Other functions of the iRHOMs may play a role in regulating their expression, for example targeting EGF for ERAD (Zettl et al., 2011). Christova et al. (2013) also saw reduced ADAM17 levels in iRHOM double knock-out mouse cells, suggesting that iRHOM2 levels affect pro-ADAM17 expression, as well as the reverse situation shown here.

4.3.3.1 iRHOM2 expression in TOC

In IHC in the previous chapter, western blots of overexpressed iRHOM2 and 3D keratinocyte cultures appeared to show reduced iRHOM2 levels in TOC. However, in figure 4.2.3 in this chapter, iRHOM2 levels appeared higher in TYLK1 and TYLK2 cells than in control keratinocytes. There is no clear explanation for this inconsistency. The differences might reflect subtle differences in culture conditions such as the confluency of the cells when protein lysates were made, or interpretation of bands on western blot. iRHOM2 appears to be a highly dynamic protein, so subtle changes in conditions could cause variation in iRHOM2 activity. In addition to regulating ADAM17 processing, targeting EGF for ERAD (Zettl et al., 2011) and controlling substrate selectivity of ADAM17 (Maretzky et al., 2013), iRHOM2 may have a further undiscovered functions that could affect its expression, localisation and processing.

As discussed in the previous chapter, the appearance of iRHOM2 as a doublet in western blots may be interesting. The iRHOM2 knock down appeared fairly weak, and to primarily affect the upper band of the doublet, whilst having a clear impact on ADAM17 processing. However, some reduction in the lower band was seen after knock down in some lysates, and after ADAM17 knock down. This suggests either a non-specific effect of the siRNA, or that the lower band is a more stable form of iRHOM2. Alternatively, if the lower band represents isoform 2 of iRHOM2 and the upper band isoform1, perhaps the iRHOM2 pool of siRNAs preferentially targets isoform 1. Future work breaking down

the pool of siRNAs would be useful, and would confirm the specificity of the iRHOM2 siRNA.

4.3.4 NOTCH Signalling in TOC

Expression of NOTCH1 S1 and cleaved NOTCH1 appeared increased in TOC keratinocytes. A potential increase in cell-surface total NOTCH1 in TOC keratinocytes (shown by two separate antibodies) and in the upper layers of skin from TOC patient 3 were also seen. Furthermore, there appeared to be an increase in cleaved NOTCH1 in the nucleus in TOC keratinocytes and increased staining of cleaved NOTCH1 in the upper layers of TOC skin. However, the staining was not nuclear as seen in the cells, and as might be expected for NOTCH NICD. Expression in the upper layers of the epidermis would be consistent with a role of NOTCH in differentiation. However, further work is needed to confirm these preliminary results.

NOTCH gene transcription has been reported to be negatively regulated by EGFR signalling (via suppression of p53 by c-jun; Kolev et al., 2008), so it is perhaps a little surprising to see increased NOTCH1 in TOC where increased shedding of EGFR ligands is seen. The increase in NOTCH1 expression could be a compensatory mechanism to balance the increase in EGFR signalling, or increased processing may be mediated by increased ligand-independent S2 cleavage by ADAM17. There is some evidence for a positive feedback loop in NOTCH expression, shown by reduced levels of Notch in zebrafish and mouse Notch pathway mutants (Del Monte et al., 2007). Positive feedback loops have also been suggested in the NOTCH pathway in several previous studies (e.g. de Celis et al. 1997; Deftos et al. 1998). This could mean that increased NOTCH1 processing in TOC is leading to positive feedback and increased overall NOTCH1 expression in some situations.

4.3.5 Differentiation and skin barrier

EphA4 staining appeared stronger in the upper epidermal layers in some of the TOC patients, with some variability in EphA2 IHC. There were no clear differences in Ephrin A1 in TOC, while there was perhaps an increase in Ephrin A1 associated with LOF ADAM17 mutations in the suprabasal layers, which could potentially be related to impaired differentiation. Ephrin A1 treatment has been shown to activate and down-regulate EphA2 leading to colony compaction, stratification, and differentiation in keratinocytes cultured in low Ca^{2+} medium (Lin et al., 2010). The mechanism occurred via induction of DSG1 expression, which induces further differentiation including up-regulation of keratin 10 and DSC1 a and b isoforms (Lin et al., 2010). EphA4 has also been shown to be up-regulated upon differentiation (Gordon et al., 2013).

In psoriasis, which is associated with abnormal differentiation of keratinocytes (Tschachler, 2007; Elder et al., 2010; Guttman-Yassky, Nograles and Krueger, 2011), changes were seen in the expression profile of Eph receptors and Ephrin ligands (Kulski et al., 2005; Piruzian et al., 2009; Jabbari et al., 2012; Gordon et al., 2013). EphA2 and EphA4 were both up-regulated compared to normal skin, while Ephrin A1 was down-regulated (Gordon et al., 2013). This was replicated in 3D raft cultures after treatment with EGF ligands, where impaired induction of differentiation-associated proteins was seen. Treatment with the Ephrin A1-Fc peptide improved expression of many differentiation markers, including DSG1, DSC1 and K10, and rescued the disrupted morphology associated with treatment with EGF or IL-1α (Gordon et al., 2013). Interestingly, Gordon et al saw less disruption in epidermal morphology after treatment with TNF-α or IL-17a, suggesting that increased EphA2 expression alone is not enough to disrupt epidermal morphology. This may also explain why the epidermal morphology in TOC is not so disrupted, although it is often thicker due to hyperproliferation.

Expression of RHBDL2 substrate thrombomodulin is also tightly regulated in differentiation as well as in wound healing (Mizutani et al., 1994; Raife et al., 1994; Lager et al., 1995; Raife, Demetroulis and Lentz, 1996; Senet et al., 1997). The exact role of thrombomodulin in this process is not well known, but thrombomodulin is up-regulated in keratinocytes by differentiation-inducing retinoic acid, and down-regulated by TNF-α in endothelial cells but not in keratinocytes (Raife et al., 1996).

In addition, an increase was seen in transglutaminase 1 (TGM1) activity in TOC skin and 3D cultures of TOC keratinocytes (Brooke et al., 2014), suggesting altered differentiation in TOC. Conversely, ADAM17 knock-out mouse epidermis had impaired TGM activity, impaired barrier function and atopic dermatitis, which was which was improved by topical treatment with TGF-α (Franzke et al 2012) showing that TGM activity is regulated by the ADAM17-EGFR pathway. Further, reduced expression of TGM1 (Blaydon et al., 2011) and reduced TGM activity (unpublished data by Matthew Brooke) was associated with homozygous LOF ADAM17 mutations in human epidermis. This suggests that increased TGM1 activity in TOC skin may improve barrier function.

4.3.5.1 The iRHOM2-ADAM17 pathway in infection

Decreased TGM1 expression and activity in LOF ADAM17 skin is associated with an increased incidence of infection, suggesting that increased ADAM17 and TGM1 activity in TOC skin and keratinocytes may infer resistance to attack by pathogens. Consistent with this, a reduction in the adhesion and invasion efficiency of *S. aureus* was seen in TOC keratinocytes compared with control cells (Brooke et al. 2014, data by Dr Charlotte Simpson). ADAM17 knock down increased the efficiency of *S. aureus* adhesion and invasion in both control and TOC keratinocytes.

Furthermore, a physiological role for murine iRhom2 in the immune response was demonstrated (McIlwain et al., 2012). iRhom2$^{-/-}$ mice were protected against septic shock and liver damage, which was mimicked by co-injection of LPS and galactosamine (GalN). The mice had much reduced serum TNF-α levels following injection but normal levels of other cytokines, and also lower levels of CD62L-negative granulocytes in the spleen and blood. The knock-out mice had a less disrupted liver architecture than WT mice, and were much less likely to die in the 48 hours after treatment (McIlwain et al., 2012). However, defence against the bacterium *Listeria monocytogenes* was impaired in the iRhom2 knock-out mice, as the mice had higher levels of liver granulomas and succumbed to the infection much more quickly than WT mice, even at low titres of infection (McIlwain et al., 2012).

4.3.6 Conclusion

The data in this chapter and in Brooke et al (2014) suggest that the TOC mutations in iRHOM2 are GOF in nature and result in increased ADAM17 processing and ADAM17-mediated shedding of EGFR ligands. This appears to lead to effects on EGFR signalling in TOC keratinocytes, and potentially the downstream Eph/Ephrin pathways. In addition, there appeared to be an increase in NOTCH1 expression in TOC keratinocytes and epidermis. The changes appear to affect migration and perhaps differentiation in TOC skin and may have a favourable effect on barrier function and resistance to *S. aureus* infection. Other members of the rhomboid protein family may be of interest for future investigation into EGFR signalling, differentiation and wound healing in the skin.

Chapter 5:
A role for the iRHOM2-ADAM17 pathway in Cancer

Chapter 5: A role for the iRHOM2-ADAM17 pathway in Cancer

5.1 Introduction

iRHOM2 / *RHBDF2* is the first gene associated with high-penetrance inherited OSCC (Blaydon et al., 2012; Saarinen et al., 2012), and iRHOM1 has previously been associated with HNSCC and breast cancers in cell lines, *in vivo* xenograft tumour experiments and breast cancer tumours (Yan et al., 2008; Zou et al., 2009). iRHOM2 and iRHOM1 are important for the processing of ADAM17 (Adrain et al., 2012; McIlwain et al., 2012; Christova et al., 2013), which is a sheddase with substrates including EGFR ligands and cell adhesion molecules (Gschwind et al., 2003; Sahin et al., 2004; Bech-Serra et al., 2006; Klessner et al., 2009; Pruessmeyer and Ludwig, 2009).

ADAM17 has been implicated in the pathogenesis of a wide range of cancers, including non-small-cell lung cancer (NSCLC) (Ni et al. 2013; Zhou et al. 2006), ovarian, prostate, breast (Lendeckel et al., 2005; Sinnathamby et al., 2011; Narita et al., 2012), colorectal, gastrointestinal (Blanchot-Jossic et al., 2005; Nakagawa et al., 2009) and head and neck cancer (Stokes et al., 2010; Kornfeld et al., 2011). ADAM17-mediated shedding of AREG and TGF-α was also indicative of poor survival in breast cancer patients (Kenny and Bissell, 2007).

NOTCH signalling has also been reported to be regulated by ADAM17 (Bozkulak and Weinmaster, 2009), and appeared dysregulated in TOC keratinocytes in the previous chapter. NOTCH acts as a tumour suppressor in a number of epithelia (Nicolas et al., 2003; Demehri et al., 2008; South, 2012), with LOF mutations frequently found in cutaneous SCC, lung cancer (Wang, 2011; South et al., 2014) and HNSCC (Stransky et al. 2011; Agrawal et al. 2011). In addition, inactivating NOTCH mutations were seen in 21 % of OSCCs but not in oesophageal adenocarcinomas (Agrawal et al., 2011), and whole exome sequencing revealed NOTCH1 mutations in further OSCC samples (Song et al., 2014). NOTCH1 has also been implicated in resistance to 5-FU treatment in OSCC cell line KYSE70 (Liu et al., 2013).

5.1.2 Aims

This chapter aimed to investigate the iRHOM2-ADAM17 pathway in OSCC, focussing in particular on protein expression of iRHOM2, ADAM17 and NOTCH1 in OSCC and HNSCC cell lines. Further aims included investigation of iRHOM2 localisation in a wider range of cancer tissues by IHC, in particular to determine whether localisation was predominantly membranous or cytoplasmic and whether iRHOM2 localisation is dysregulated in different tumours. Finally, the catalogue of somatic mutations in cancer (COSMIC) database was searched for iRHOM1 and iRHOM2 mutations to determine the incidence of iRHOM mutation in different cancers.

5.2 Results

5.2.1 ADAM17 and iRHOM2 expression in OSCC biopsies and cell lines

IHC for total ADAM17 and iRHOM2 was performed in adjacent TOC and sporadic OSCC sections by the BICMS core pathology facility. Protein levels appeared to vary between the stromal and tumour tissue in both TOC (figure 5.2.1 A) and sporadic (figure 5.2.1 B and C) OSCC sections, with both iRHOM2 and ADAM17 staining appearing to be of low intensity in stromal regions and of stronger intensity in the tumour tissue of the biopsies, for example in figure 5.2.1 B.

To further investigate the link between iRHOM2 and ADAM17 in OSCC, western blots of iRHOM2 and ADAM17 were carried out in four commercially available OSCC cell lines: KYSE270; KYSE410; TE-4 and TE-8, which were kindly provided by Dr Janet Risk, University of Liverpool. The KYSE270 cell line was originally isolated from a well-differentiated OSCC from a 79-year-old male Japanese patient and KYSE410 from a poorly-differentiated OSCC from a 51-year-old male Japanese patient (http://www.phe-culturecollections.org.uk). TE-4 cells were isolated from a 48-year old male (http://cancer.sanger.ac.uk/cosmic/sample/overview?id=735828) but the differentiation status of the tumour is unknown. The TE-8 cell line originated from a moderately differentiated OSCC (Sakai et al., 2009). Mutations in EGFR have been reported in KYSE270 cells (Kato et al., 2013), while TE-4 and TE-8 cells have both been reported to not harbour EGFR mutations (Kimura et al. 2006; Sudo et al. 2007; COSMIC database).

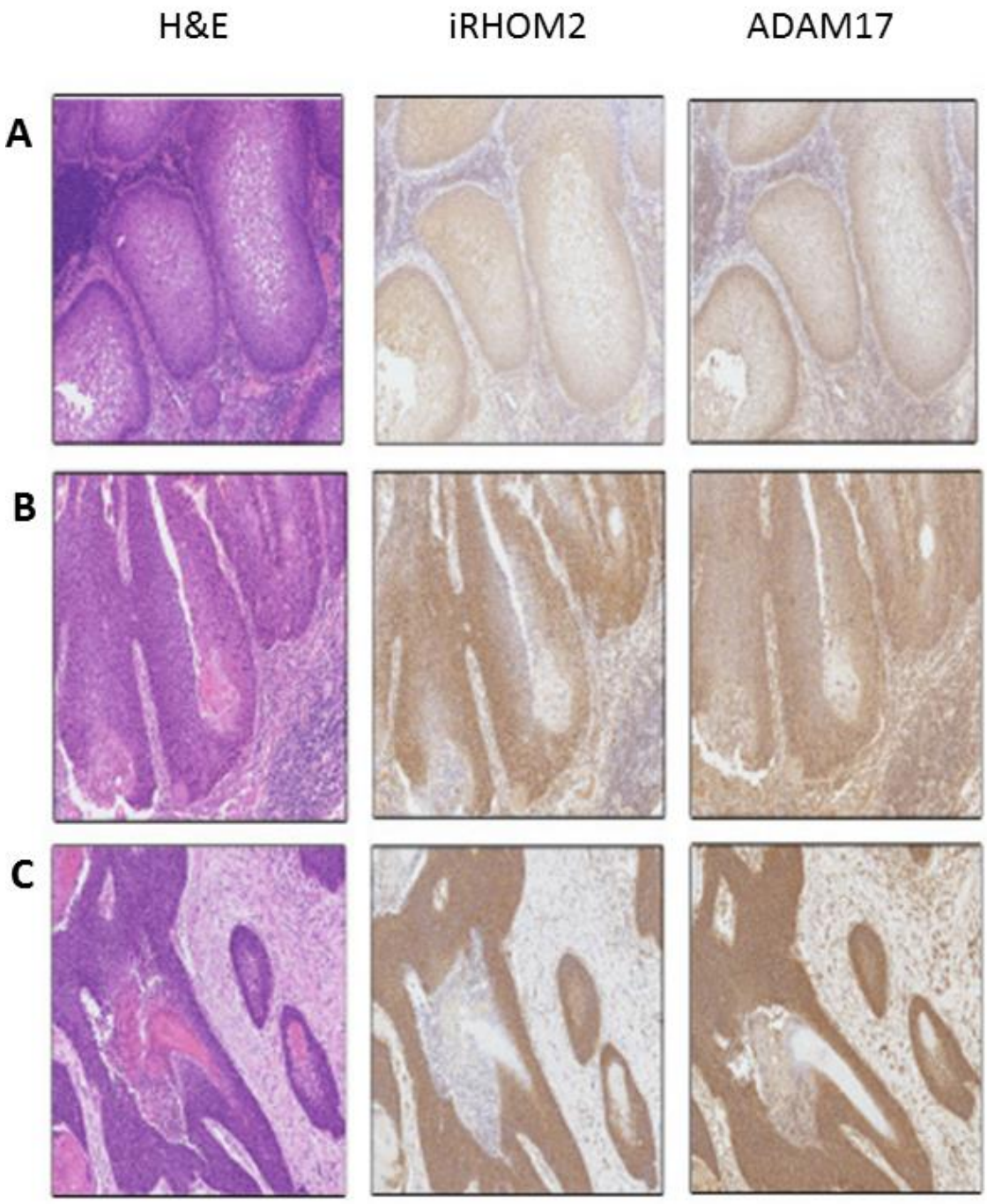

Figure 5.2.1 ADAM17 expression mirrors iRHOM2 expression in tylotic and sporadic Oesophageal Squamous Cell Carcinoma. Sections cut from paraffin-embedded oesophageal SCC (OSCC) biopsies were stained with Haematoxylin and Eosin (H&E) and diaminobenzylene (DAB) staining against iRHOM2 and ADAM17 as indicated. **A:** Tylotic OSCC, **B** and **C:** Sporadic OSCC. Staining was carried out by the Core Pathology Facility. ***Please note that this image was originally in JPEG format and is therefore of reduced quality.***

During cell culture, KYSE270 cells grew with a block-like morphology similar to cutaneous keratinocytes, and grew the fastest of the four cell lines. KYSE410 cells had a spindle-like morphology. TE-8 cells grew with the spindle-like or epitheloid morphology of KYSE410 cells, but there appeared to be a fairly high level of cell death.

5.2.1.1 iRHOM2 in OSCC cells:

Western blots for iRHOM2 showed a wide range of expression between the four cell lines (figure 5.2.2 Ai), with particularly high expression in the KYSE270 cell line. As in cutaneous keratinocyte cell lines, the iRHOM2 band appeared as a 'doublet' with two bands at around 90 KDa. Densitometry (taking into account both bands; figure 5.2.2 C) showed moderate iRHOM2 expression in TE-4 and TE-8 cells, low expression in KYSE410 cells and the highest expression in KYSE270 cells. There was some variability between sample sets, perhaps due to differing exposure times between western blots. The upper band of iRHOM2 often appeared at a slightly higher molecular weight in TE-4 cells compared to the other cell lines (figure 5.2.2 Ai), perhaps suggesting post-translational modification. KYSE410 and TE-8 cell lysates appeared to have a greater proportion of the lower band of the iRHOM2 doublet.

5.2.1.2 ADAM17 in OSCC cells:

The intensity of bands representing ADAM17 also varied between the four cell lines (figure 5.2.2 Aii), with particularly high ADAM17 levels seen in the KYSE270 cell line corresponding with high iRHOM2 levels. The mature ADAM17 band was of particularly high intensity in KYSE270 cells, consistent with increased iRHOM2-mediated ADAM17 processing. TE-8 cells showed lower total ADAM17 expression compared to TE-4 cells, despite similar levels of iRHOM2 expression (figure 5.2.2 D). KYSE410 cells had similar total ADAM17 levels to TE-4 cells, but the proportion of mature ADAM17 was lower (figure 5.2.2 D and E), corresponding with lower overall iRHOM2 protein expression, and a higher proportion of the lower iRHOM2 band (figure 5.2.2 Ai). This may suggest that the upper band of the 'doublet' may be important in ADAM17 processing, as it was strongly expressed in KYSE270 cells.

The mature ADAM17 band consistently appeared at a slightly higher molecular weight in KYSE270 cells, perhaps due to *N*-linked glycosylation which has previously been reported for ADAM17 (Issuree et al., 2013; Chavaroche et al., 2014).

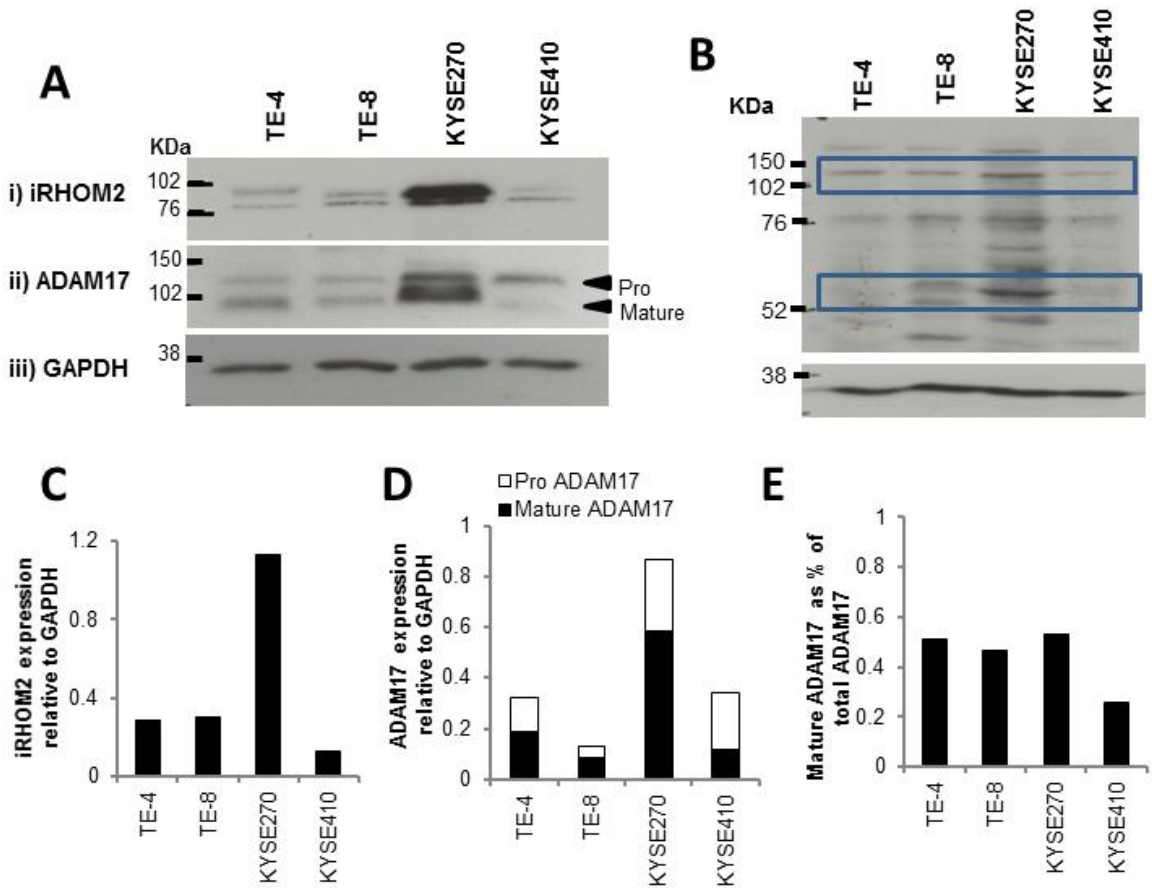

Figure 5.2.2 Variable iRHOM2 and ADAM17 levels in OSCC cell lines. A: Western blots against iRHOM2 and ADAM17 in four OSCC cell lines. **B:** Western blot against the pro-domain of ADAM17. The blue boxes indicate the bands of interest: the top band represents full length pro-ADAM17; the bottom band represents the free pro-domain. **C-E:** Graphs representing densitometry analysis of the bands in the western blots in part A: **C-D:** Densitometry analysis was carried out to analyse the proportion of pro- and mature ADAM17 in each cell line in relation to the iRHOM2 expression. **C**: iRHOM2 densitometry; **D:** Stacked bar graph showing ADAM17 densitometry. The band representing mature ADAM17 is shown in black and the band representing pro-ADAM17 shown in white. **E:** The percentage of total ADAM17 protein accounted for by the band representing mature ADAM17 in each cell line. N = 2 for each densitometry analysis, but the same results were also seen in a third set of lysates for which no loading control is available. Densitometry was carried out with Image Studio Lite software.

Figure 5.2.2 B shows a western blot against pro-ADAM17 in the four OSCC cell lines. The antibody recognises the free pro-domain of ADAM17 and unprocessed pro-ADAM17 (both highlighted by blue boxes), in addition to some non-specific bands. TOC cutaneous keratinocytes showed increased levels of the free ADAM17 pro-domain compared to control cutaneous keratinocytes (see Chapter 4). The OSCC cells did not appear to retain the free pro-domain to the same extent as cutaneous keratinocytes, however slightly elevated levels of the free pro-domain were seen in KYSE270 cells, along with slightly higher unprocessed pro-ADAM17 levels (figure 5.2.2 B).

5.2.3 Correlation between iRHOM2 and ADAM17 expression in Head and Neck Squamous Cell Carcinoma cell lines

Western blots in a panel of ten HNSCC cell lines isolated from primary tumour tissue were performed to study the potential relationship between iRHOM2 and ADAM17 expression in another cancer type. The cell lines were made by Dr Helena Emich, Centre for Cutaneous Research, QMUL.

5.2.3.1 iRHOM2 in HNSCC cell lines

As seen in the OSCC cells, iRHOM2 levels varied between the different HNSCC cell lines in preliminary western blots (figure 5.2.3 A), with particularly high iRHOM2 levels in LUC4, 24n, NA and 50(2), and the lowest levels in Mkn, 57n, TUM57 and TUM59. As in keratinocytes and OSCC cells, a ‘doublet’ was often seen at around 90 KDa. In most cases the lower band of the doublet appeared more prominent, with the exception of TUM59 cells. There was some variability in the size of the iRHOM2 band at ~90 KDa in the cell lines, with a slightly smaller lower band present in NA cells accompanied by another fragment at approximately 76 KDa.

The full length western blot of iRHOM2 in the HNSCC cell lines is shown in figure 5.2.3 B. As mentioned in Chapter 3, some extra bands were detected by the anti-iRHOM2 antibody: one around 150 KDa, and one around 55 KDa. The intensity of these bands also varied between the HNSCC cell lines, with the 150 KDa band particularly strong in NA, LK and 24n cells, and the 55 KDa band particularly bright in NA, LM, 24n and LUC4 cells; another band at around 50 KDa was seen in 57n cells (figure 5.2.3 B). These data could suggest non-specific binding of the anti-iRHOM2 antibody, as discussed in chapter 3, or could potentially show different processing of iRHOM2 between the cell lines.

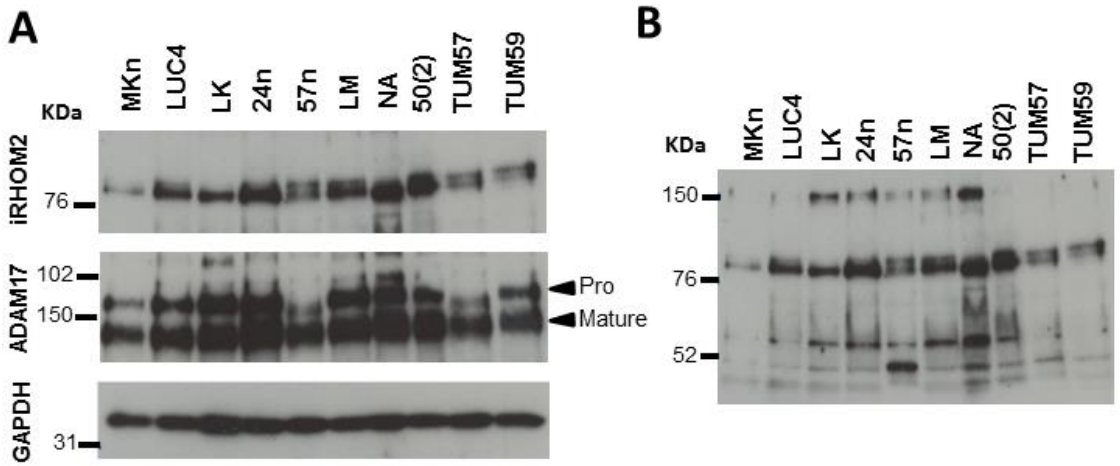

Figure 5.2.3 Variable expression of iRHOM2 and ADAM17 in HNSCC cell lines. A: Western blotting of iRHOM2 and ADAM17 in a panel of ten Head and Neck SCC (HNSCC) cell lines**. B:** Full length western blot of iRHOM2 to show all the bands present, perhaps indicating different processing of iRHOM2 between cell lines. Please note that this is preliminary data from one western blot of each protein.

5.2.3.2 Correlation between iRHOM2 and ADAM17 expression in HNSCC cell lines

Preliminary western blots for ADAM17 in the HNSCC cell lines are shown in figure 5.2.3 A, although this was only performed once in one set of lysates. ADAM17 expression was variable between cell lines, with higher levels appearing in cell lines with higher iRHOM2 (figure 5.2.3 A). iRHOM2 and ADAM17 protein levels were analysed relative to GAPDH and plotted in a scattergraph with iRHOM2 protein expression on the X axis and ADAM17 protein expression on the Y axis (figure 5.2.4). A polynomial best-fit curve was plotted, with the Pearson's correlation coefficient, or r^2 value, calculated using Microsoft Excel. An r^2 value of 1 indicates a perfect positive correlation, a value of -1 indicates a perfect negative correlation and a value of 0 indicates that there is no correlation between the data sets.

When iRHOM2 expression was plotted against total ADAM17 protein expression, there appeared to be a strong positive correlation between the levels of the two proteins (figure 5.2.4 A), with an r^2 value of 0.932 associated with the data. One outlier was excluded from the analysis - the LK cell line, shown in red. LK cells had low iRHOM2 and relatively high ADAM17 expression. The correlation appeared less strong when only pro-ADAM17 levels were taken into account (figure 5.2.4 B), with an r^2 value of 0.7239 associated with the curve when LK cells were excluded. However, taking into account the intensity of bands for mature, processed ADAM17 (figure 5.2.4 C), which is reliant on the action of iRHOM2, the r^2 correlation value reached 0.918 excluding the LK cell line, and 0.8357 including the LK cells: this indicates that the proportion of pro-ADAM17 in LK cells was higher than that of mature ADAM17, perhaps because the lower iRHOM2 levels meant reduced processing of ADAM17.

Figure 5.2.4 D shows expression of both pro- and mature- ADAM17 in order of increasing iRHOM2 expression, showing the suggested trend toward increasing ADAM17 levels with iRHOM2 levels and the high proportion of pro-ADAM17 in outlier cell line LK. Interestingly, LK cells did not appear to express the upper band of the iRHOM2 doublet (figure 5.2.3 A), consistent with findings in OSCC cell lines (figure 5.2.2) suggesting that expression of the upper iRHOM2 band is required for production of mature ADAM17.

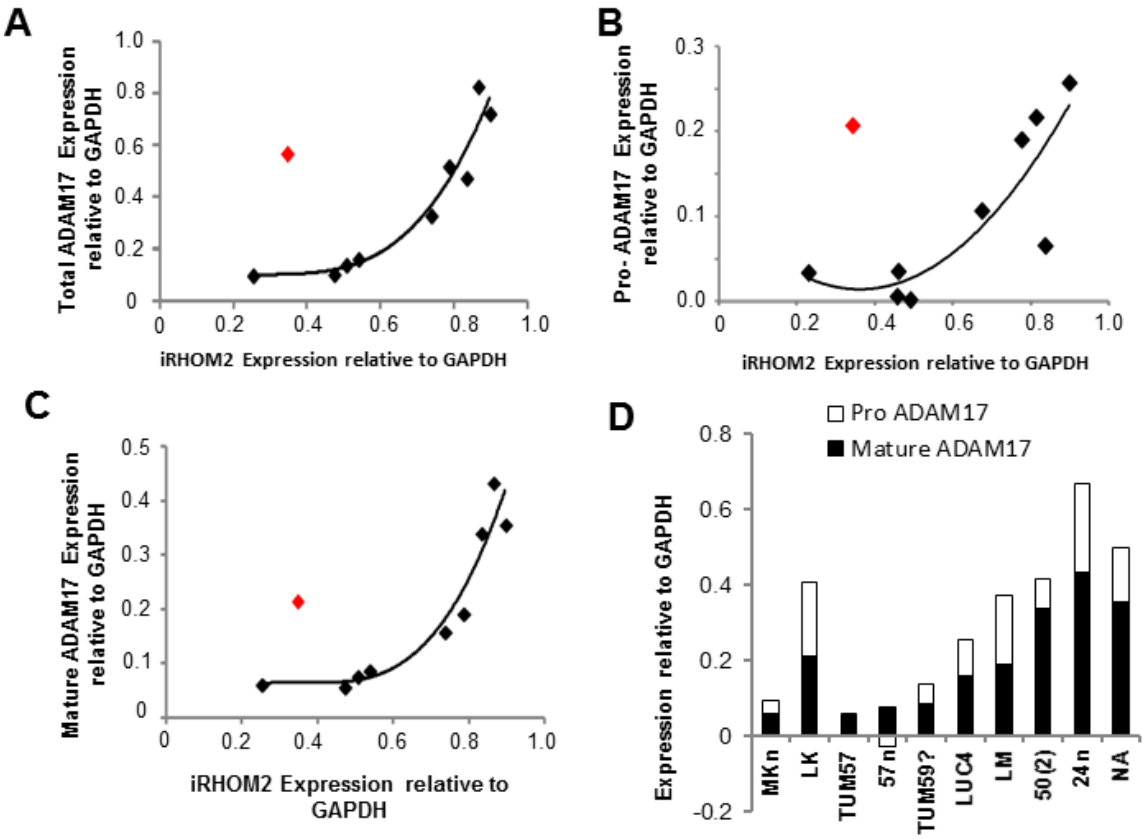

Figure 5.2.4 iRHOM2 and ADAM17 expression appears to correlate in HNSCC cell lines. Expression levels of iRHOM2 and ADAM17 protein were measured by densitometry relative to a GAPDH loading control. **A-C:** Scattergraphs showing iRHOM2 protein expression on the X-axis against total levels of ADAM17 **(A)**, pro-ADAM17 **(B)** and mature ADAM17 **(C)** on the Y-axis. **D:** Relative levels of pro-ADAM17 (white) and mature ADAM17 (black). Cell lines are presented in order of increasing iRHOM2 expression. Densitometry was carried out with Image Studio Lite software. Please note that this is preliminary data from one western blot of each protein.

5.2.3.3 iRHOM2 levels and tumour characteristics

Table 5.2.1 shows the cell lines in order of increasing iRHOM2 expression, alongside the characteristics of the original tumours. All the cell lines were from moderately differentiated, moderate to poorly differentiated, or poorly differentiated tumours, or from lymph node metastasis. The sample size was too small to determine a link between tumour stage and / or characteristics, but observational analysis suggested that there was not a clear correlation between iRHOM2 expression levels and differentiation status, tumour depth, perineural invasion or extracapsular spread.

Two cell lines expressing fairly high iRHOM2 (LM and 50(2); 3rd and 4th highest iRHOM2 expression) showed a cohesive invasion front while cell lines expressing lower iRHOM2 had a discohesive invasion front. The two cell lines expressing highest iRHOM2 (24n and NA) had different properties: NA cells had a discohesive but infiltrative invasion front; and 24n cells were from a lymph node metastasis so invasion front was not applicable. Again, the sample size is much too small to form a conclusion from this, but further investigation of iRHOM2 and ADAM17 in invasion would be interesting, particularly as ADAM17 has previously been implicated in tumour invasion (Chen et al., 2013; Doberstein et al., 2013; Giricz et al., 2013).

Increasing iRHOM2 expression

Cell line	iRHOM2	Grade	Depth (mm)	Perineural invasion	Lymphovasc	Extracaps spread	Invasion Front
MKn	0.254	Lymph node	n/a	n/a	n/a	Y	n/a
LK	0.349	Moderately diff	10	N	N	N/a	Discohesive
TUM57	0.472	Poorly diff	20	Y	N	Y	Discohesive
57n	0.506	Lymph node	n/a	n/a	n/a	Y	n/a
TUM59?	0.538	Unknown					
LUC4	0.737	Moderate to poorly	23.5	Y	N	Y	Discohesive
LM	0.785	Moderately diff	20	N	N	Y	Cohesive
50(2)	0.833	Moderately diff	8	N	N	n/a	Cohesive
24n	0.865	Lymph node	n/a	n/a	n/a	N	n/a
NA	0.896	Moderate to poorly	7	Y	N	N	Discohesive, infiltrative

Table 5.2.1 iRHOM2 expression does not appear to correlate with tumour characteristics in HNSCC cell lines. Table showing cell lines in increasing order of iRHOM2 expression according to densitometry analysis against tumour grade, depth, perineural invasion, lymphovascular spread, extracapsular spread and invasion front. Please note that this is preliminary data from one set of lysates.

5.2.4 ADAM17 activity in OSCC cell lines

To see whether active ADAM17 levels are related to shedding of ADAM17 substrates, ELISA assays were performed to measure shedding of AREG and TGF-α into the cell culture medium over a time period of 0 to 48 h. Semi-quantitative RT-PCR (qPCR) was performed on mRNA extracted at the 24 h time point to measure expression levels relative to housekeeping gene GAPDH. There was variation between levels of AREG and TGF-α in the medium from the three cell lines (figure 5.2.5 A and B respectively), but this did not appear to correspond with levels of mature ADAM17 in lysates from the cells.

KYSE270 cells shed the lowest level of AREG (figure 5.2.5 A), despite having the greatest level of mature ADAM17 protein. KYSE410 cells had the lowest iRHOM2 and mature ADAM17 protein of the three cell lines, but medium from KYSE410 cells had an AREG concentration approximately 3.5X higher than medium from KYSE270 cells after 48 h (figure 5.2.5 A). TE-4 cells shed particularly high levels of AREG (figure 5.2.5 A), while expressing moderate levels of mature ADAM17 protein. The results could in part be explained by the mRNA levels of AREG (figure 5.2.5 B), which were particularly high in KYSE410 cells. However, TE-4 cells, which shed the highest levels of AREG, had a moderate AREG expression at the mRNA level. Further investigation into regulation of AREG and ADAM17 expression will be required to explain these findings.

TGF-α is shed by OSCC cells (and cutaneous keratinocytes; Brooke et al. 2014) at a much lower level than AREG (Figure 5.2.5 C). Variability was also seen in the shedding of TGF-α between the three cell lines, although the pattern was different to that of AREG: while TE-4 again shed the highest levels of TGF-α (associated with moderate mRNA expression), the TGF-α concentration was higher in medium from KYSE270 cells than KYSE410 cells (figure 5.2.5 C). This corresponded with higher mRNA levels of TGF-α and high mature ADAM17 protein levels in KYSE270 cells (figure 5.2.5 D). KYSE410 cells showed a much lower mRNA expression of TGF-α than KYSE270 cells (combined with low iRHOM2/ADAM17 levels). Interestingly, the level of TGF-α decreased in medium from KYSE270 cells between the 24 h and 48 h time points (figure 5.2.5 C).

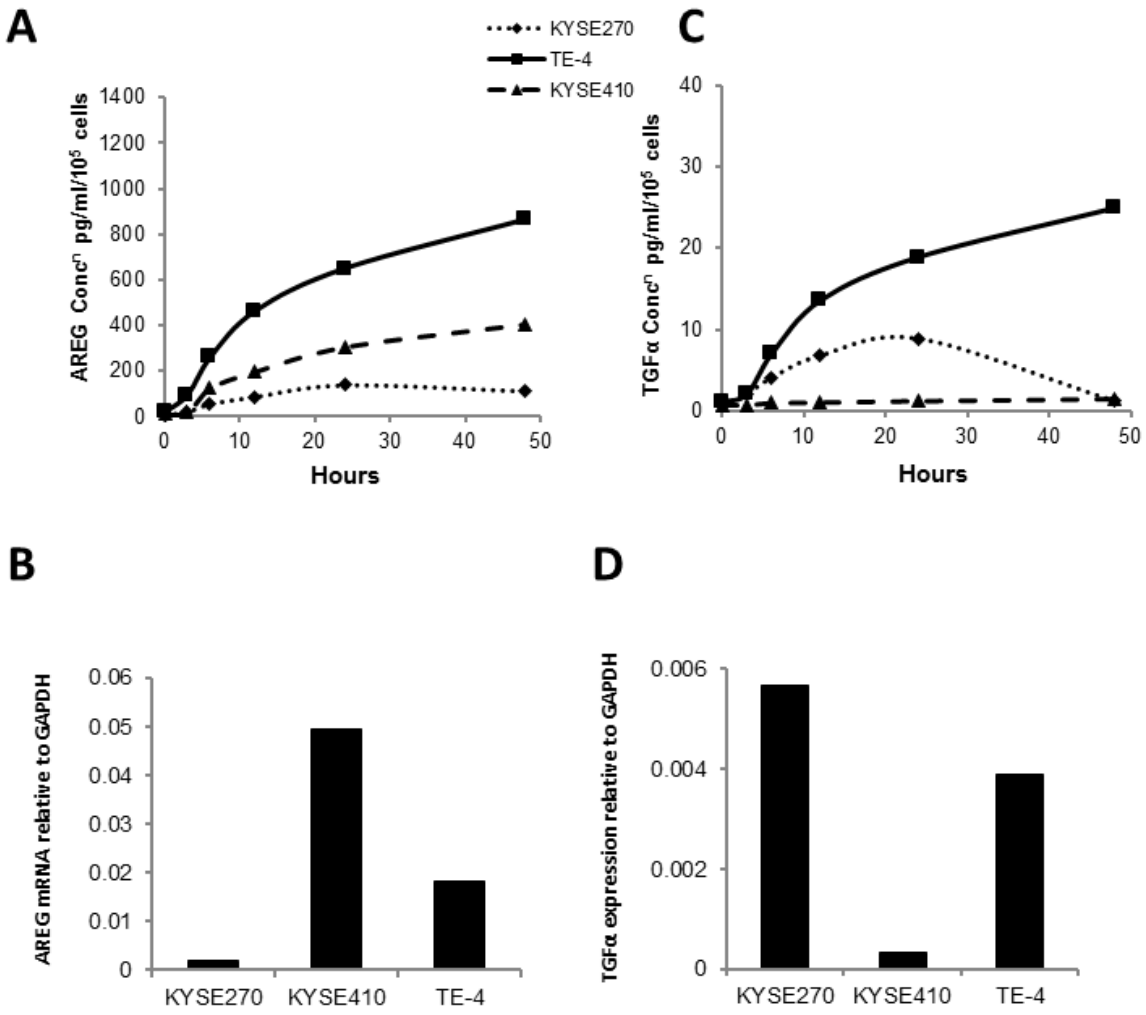

Figure 5.2.5 Variable shedding of ADAM17 substrates AREG and TGF-α in OSCC cell lines may be linked with differential mRNA expression
Cells were cultured for up to 48 h, and the medium collected at a number of timepoints for ELISA analysis of AREG and TGF-α protein concentration. mRNA was extracted from cells at the 24 h timepoint and qPCR performed to estimate mRNA levels of AREG and TGF-α. N=2 for all experiments. **A:** Chart showing concentration of AREG in medium from KYSE-270, KYSE-410 and TE-4 cells, measured by ELISA (n=2). **B:** Semi-quantitative RT-PCR (qPCR) showing relative mRNA levels of AREG (n=1). **C:** Protein concentrations of TGFα in medium from the three OSCC cell lines measured by ELISA (n=2). **D:** qPCR showing mRNA levels of TGF-α relative to GAPDH (n=1). Similar results were seen at 24 h and 48 h in preliminary ELISA experiments.

5.2.5 iRHOM2 and downstream proteins in OSCC and Oesophagitis

To look further at iRHOM2 in OSCC, preliminary IHC experiments were carried out in paraffin-embedded oesophageal biopsies from a patient suffering from oesophagitis, OSCC from a TOC patient, and sporadic OSCC (figure 5.2.6 A-C respectively). IHC was carried out by the BICMS core pathology facility and images taken and selected by Dr Laura Gay and Professor David Kelsell.

iRHOM2 staining was seen throughout the layers of the oesophagus, with the most intense staining in the basal layer and the faintest staining in the middle layers. Although it is more difficult to determine localisation in DAB-stained paraffin-embedded biopsies, iRHOM2 appeared to show a cell-surface localisation In the upper, more differentiated functional layers of the oesophagus, consistent with staining at the plasma membrane and with fluorescence staining of iRHOM2 in a normal frozen oesophageal tissue section in chapter 3 (figure 3.1.4). In the paraffin section, iRHOM2 appeared at lower levels in the middle prickle cell layer, where it appeared to show a more perinuclear localisation, perhaps consistent with iRHOM2 located in the ER (figure 5.2.6 A). The basal layer appeared to show intracellular iRHOM2 staining at a stronger intensity than the other oesophageal layers.

In the sections from TOC and sporadic OSCC, the distinct morphology of the oesophagus was lost, with smaller, more compact cells consistent with increased proliferation in the cancer, particularly in the TOC OSCC (figure 5.2.5 B and C). iRHOM2 staining was of variable intensity throughout the sections, consistent with staining in OSCC biopsies in figure 5.2.1. iRHOM2 staining in the upper oesophageal layers appeared to be more diffuse than that in control oesophagus, with no clear plasma membranous staining (figure 5.2.5 B and C), although this is a small number of samples and it is difficult to distinguish iRHOM2 localisation.

5.2.5.1 Ephrin B3 in OSCC sections

As Eph/Ephrin signalling was implicated by the phospho-RTK array and western blotting in TOC cutaneous keratinocytes (Chapter 4), IHC was performed against Ephrin B3, a substrate of RHBDL2. In oesophagitis, Ephrin B3 staining was very faint throughout the section, perhaps with slightly more intense staining in the basal layers of the oesophagus and some faint cell-surface staining in the upper layers (figure 5.2.6 A). In the TOC and sporadic OSCC sections, Ephrin B3 staining appeared at higher intensity than in control oesophagus, with a diffuse, cytoplasmic-like localisation (figure 5.2.6 B and C). Again, this is a small, preliminary sample set and the localisation of Ephrin B3 is difficult to distinguish, particularly in OSCC biopsies.

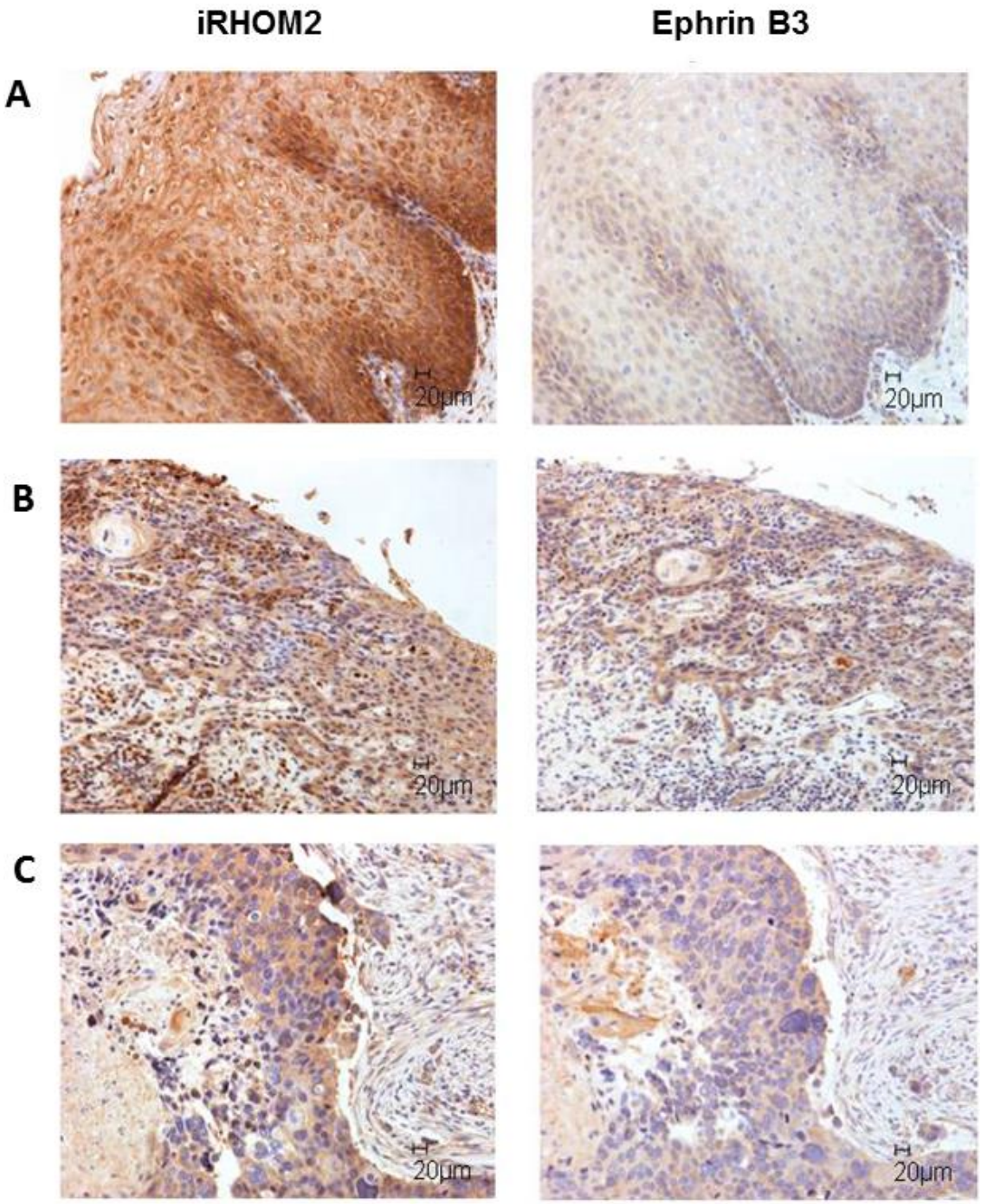

Figure 5.2.6 Altered localisation of iRHOM2 and expression of RHBDL2 substrate Ephrin B3 in Tylotic and Sporadic Oesophageal SCC. Sections from paraffin-embedded TOC stained with iRHOM2 (Left panel) and Ephrin B3 (Right panel) in **A:** control oesophagus from a patient suffering from oesophagitis, **B:** oesophageal SCC (OSCC) from a TOC patient, **C:** Sporadic OSCC. IHC was kindly performed by the Core Pathology Facility.

5.2.6 A possible link between NOTCH1 expression and the iRHOM2-ADAM17 pathway in OSCC and HNSCC cell lines

As LOF somatic mutations in NOTCH 1 are prevalent in SCC and NOTCH1 expression appeared up-regulated in TOC keratinocytes, western blots were carried out with an antibody against total NOTCH1 in OSCC and HNSCC cell lines with the AbCam ChIP grade antibody which recognises total NOTCH1.

5.2.6.1 NOTCH1 in OSCC cell lines

In OSCC and HNSCC cell lines where iRHOM2 and ADAM17 levels appeared higher, levels of full length and cleaved NOTCH1 also appeared increased (figure 5.2.7). Of the OSCC cell lines TE-4, KYSE270 and KYSE410 (figure 5.2.7 A), KYSE270 cells had the highest level of the NOTCH1 S1 and S2/S3 fragments, correlating with high iRHOM2 and active ADAM17 protein expression seen in figure 5.2, while lower levels of NOTCH1 S1 and S2/S3 fragments seen in KYSE410 cells were associated with the low iRHOM2 and mature ADAM17 expression. TE-4 cells had no visible NOTCH1 S1, but interestingly had a higher level of NOTCH1 S2/S3 (figure 5.2.7 A) with a relatively high proportion of mature ADAM17 (figure 5.2.7 A).

Another faint band is also visible in the NOTCH1 western blot in the OSCC cell lines at about 170 KDa in the two KYSE cell lines (figure 5.2.7 A), which is absent in the TE-4 cell line and not seen in any other NOTCH1 western blots, perhaps indicating a non-specific band or a differently processed but stable form of NOTCH1. However, the sample size is too small to determine a correlation between iRHOM2 and NOTCH1 expression.

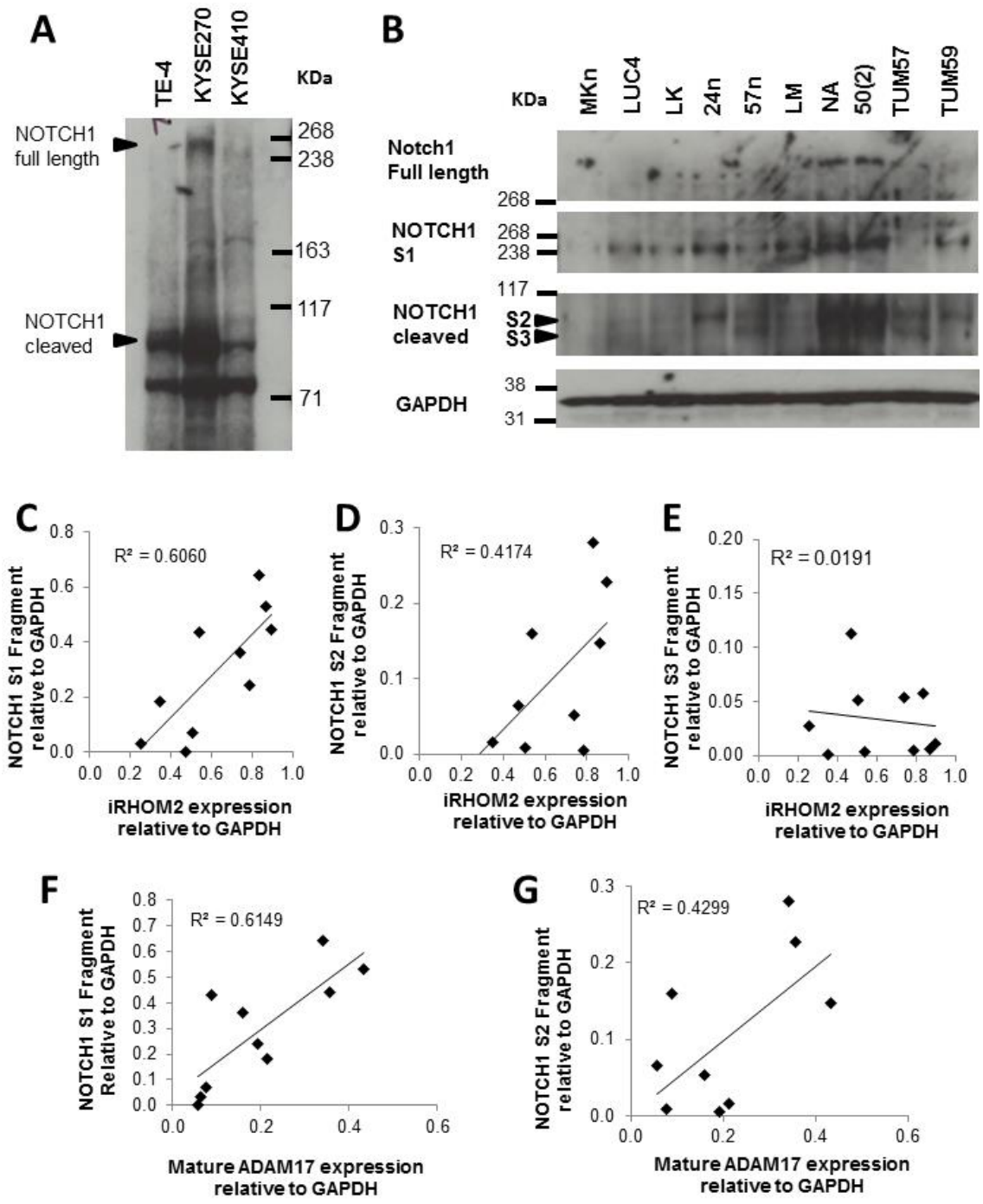

Figure 5.2.7 NOTCH1 expression appears to correlate with iRHOM2 and ADAM17 levels in HNSCC cell lines. Western blots with an antibody against total NOTCH1 (AbCam ChIP grade) in **A:** Oesophageal SCC cell lines, **B:** HNSCC cell lines. **C-E:** Densitometry analysis of western blots in HNSCC cell lines shown in B: The integrated density of iRHOM2 in the HNSCC cell lines (western blot shown fig 5.2.4) was plotted against the integrated density of bands representing NOTCH1 S1 fragment **(C)**, NOTCH1 S2 fragment **(D)** and NOTCH1 S3 fragment **(E)**, all shown relative to GAPDH loading control. **F-G:** Densitometry of mature ADAM17 against NOTCH1 fragments S1 **(F)** and S2 **(G) (**also from fig 5.2.4**).** Densitometry was performed with Image Studio Lite software. Please note that this is preliminary data from one western blot.

5.2.6.2 NOTCH1 in HNSCC cell lines

There also appeared to be a possible correlation between iRHOM2 and NOTCH1 levels in the HNSCC cells in a preliminary western blot (figure 5.2.7 B-D), with cell lines with the highest levels of iRHOM2 (50(2), 24n and NA) also showing the highest levels of NOTCH1 S1 and S2 fragments. In this western blot, perhaps because of the running conditions or protein loading, the S2 and S3 bands appeared to be visible separately, allowing densitometry of the individual S2 and S3 fragments.

A band at the predicted molecular weight as full length NOTCH1 was also visible in some cell lines, shown in figure 5.2.7 B, although there was high background, and transfer of high molecular weight proteins may not have been consistent. Two out of three of the cell lines with highest iRHOM2 (NA and 50(2) but not 24n) had clear bands at this size, however, much weaker bands or no bands were visible at this size in the other cell lines, perhaps suggesting a correlation between total NOTCH1 expression and iRHOM2 expression.

When iRHOM2 expression (from the western blot shown in figure 5.2.4) was plotted on the X-axis against the NOTCH1 S1 fragment (~260 KDa) on the Y axis, the data fitted a linear trendline with an r^2 value of 0.6060 indicating a moderate positive correlation (figure 5.2.7 C). There also appeared to be a less strong correlation between NOTCH1 S2 and iRHOM2 expression (figure 5.2.7 D) with an associated r^2 value of 0.4174. Interestingly, the correlation between NOTCH1 S1 and S2 appeared linear, suggesting that the link between the proteins may be indirect, or depend on other factors, perhaps including γ-secretase activity. The correlation was not seen when iRHOM2 expression was plotted against the band that likely represents the NOTCH1 S3 fragment (figure 5.2.7 E), which had an r^2 value of 0.0191 when a linear trend-line was plotted.

This preliminary work was in a small number of samples with only one set of lysates, and needs further investigation to confirm the findings, but overall could suggest that expression of the NOTCH1 S1 and S2 fragments but not the S3 fragment may be dependent on iRHOM2 expression. This would also be consistent with ADAM17-mediated S2 cleavage of NOTCH1 being dependent on iRHOM2 expression and activity levels.

Scattergraphs showing densitometry of mature ADAM17 against NOTCH1 S1 and S2 fragments also fitted linear trendlines with a similar correlation between mature ADAM17 and NOTCH1 S1 (r^2=0.6149, figure 5.2.7F), suggesting a moderate correlation. The relationship between mature ADAM17 and NOTCH1 S2 also showed a linear, although slightly less strong correlation (r^2=0.4299). Further investigation of this would be interesting as ADAM17 may be expected to cleave NOTCH1 at the S2 stage. The scatter

graph also appeared to show two distinct populations with low and high mature ADAM17 expression. This may be due to the small sample size, and further investigation is needed, but overall these data support further correlation between NOTCH1 expression and the iRHOM2-ADAM17 pathway.

5.2.7 iRHOM2 localisation in frozen cancer sections

5.2.7.1 Cutaneous SCC

Symptoms of TOC include hyperproliferation in the skin, particularly of the palms and soles. Furthermore, cutaneous SCCs frequently show chromosomal imbalance or LOH on Chromosome 17q (Purdie et al., 2007), the location of the *RHBDF2* gene. Therefore, IHC for iRHOM2 was performed in a panel of frozen tissue sections from sporadic cutaneous SCC, kindly provided by Dr Karin Purdie, Centre for Cutaneous Research, QMUL (figure 5.2.8). Sections D, E, I and J showed loss of chromosome 17, while chromosomes F, G and H had normal chromosome 17 copy numbers.

The cutaneous SCCs seemed to retain a plasma-membranous localisation of iRHOM2, with higher levels of punctate intracellular staining in some sections such as sections C, E and I. This may be because the surface of some cells was included in the confocal image and is often seen in normal skin. The overall staining intensity of iRHOM2 appeared reduced compared to normal skin, with particularly low intensity in sections F and J, although it is difficult to judge expression levels from immunofluorescence.

5.2.7.2 iRHOM2 Localisation in Frozen Tumour Biopsies

To see whether iRHOM2 localisation or expression was affected in a number of other sporadic cancers, IHC was performed on frozen tissue sections from breast carcinoma, breast ductal carcinoma, breast lobular carcinoma, neuroblastoma, endometrial adenocarcinoma, cervical SCC and lung SCC kindly provided by the Core Pathology facility. Initially, images were taken with the same microscope settings to allow some comparison of the iRHOM2 staining intensity. Unfortunately, matched normal tissue sections from the correct body sites were not available for control staining in the same tissue. Additional staining not shown in this chapter can be seen in appendix figures C1-C5.

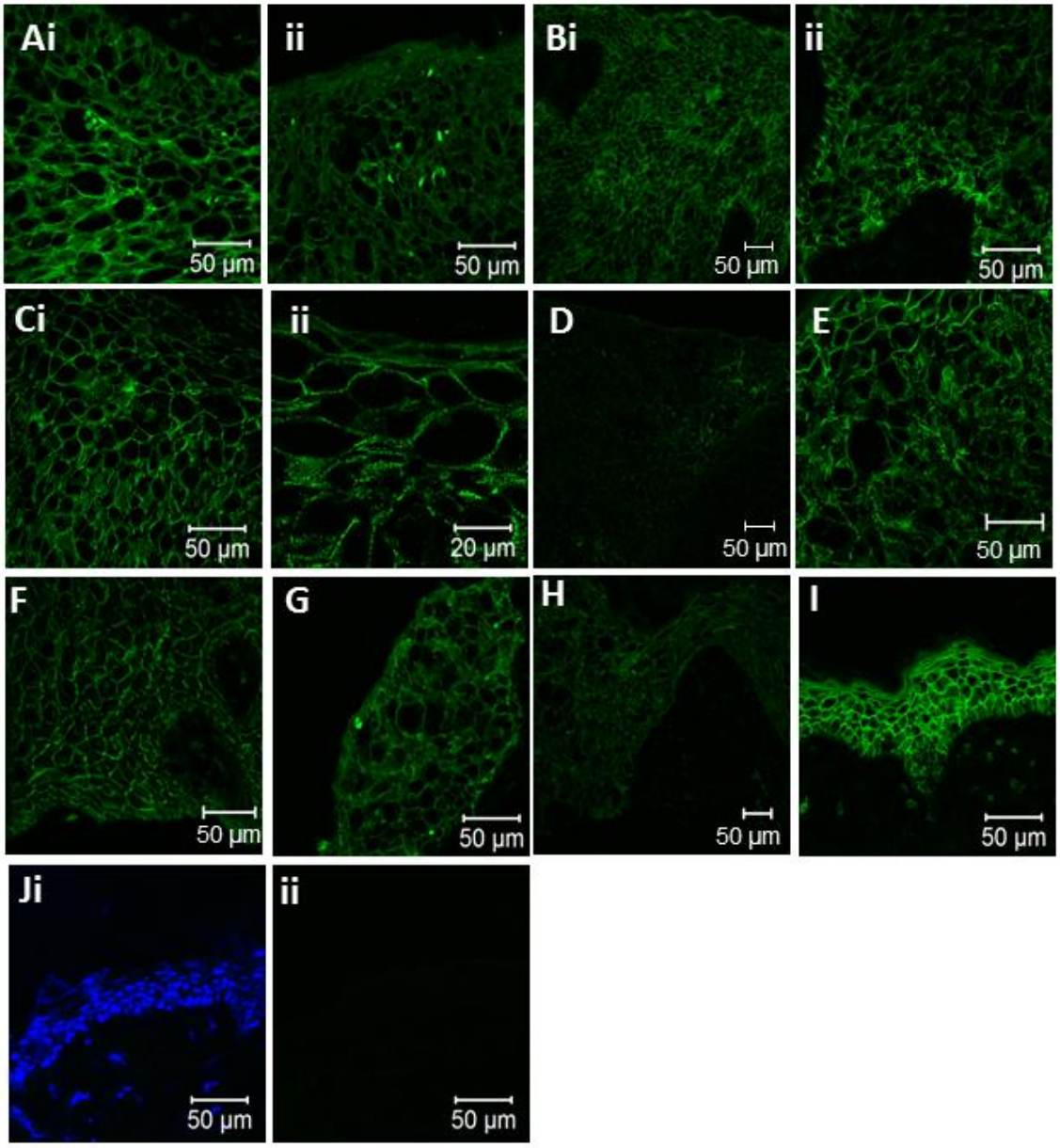

Figure 5.2.8 iRHOM2 shows cell-surface localisation and variable staining intensity in cutaneous Squamous Cell Carcinomas (SCCs). IHC of iRHOM2 was carried out in a panel of SCCs and normal skin. Images were taken on the LSM 510 confocal microscope at magnifications of 20X, 40X and 100X. The settings were kept the same for each image to allow comparison. Sections were labelled alphabetically. **Ai-ii:** section C; **Bi-ii** section D; **Ci-ii:** section E; **E:** section F; **F:** section G; **G:** section H; **H:** section I; **I:** Normal skin, image taken at 40X. **J** shows the negative control in which primary antibody was omitted. N=2 for each biopsy. iRHOM2 staining is shown in green, DAPI nuclear staining in the negative control is shown in blue **(J ii)**.

Plasma membranous staining was seen in distinct regions in a number of the tumour sections (figure 5.2.11, indicated by white arrows) with particularly clear membranous staining seen in regions of breast carcinoma (figure 5.2.11 A, B) and lung SCC (figure 5.2.11 C). Some less clear cell-surface staining was also seen in breast ductal carcinoma (figure 5.11 D) and neuroblastoma (figure 5.11 E). Where there was plasma membranous staining, there was still strong intracellular staining.

In tumour regions without plasma-membranous iRHOM2 staining, the localisation appeared diffuse throughout the cells/tissue, perhaps including a lower level of plasma membranous staining. Cells in regions of some sections included brighter perinuclear staining, for example neuroblastoma (figure 5.2.11 F) and breast lobular carcinoma (figure 5.2.11 G), which could suggest an ER-localisation of iRHOM2. In the cervical SCC (figure 5.12 A-D), regions with lower levels of iRHOM2 staining also showed a patchier staining pattern, perhaps indicating faint perinuclear staining.

A few sections showed brighter iRHOM2 staining at the tissue edges, indicated by orange arrows in the figures, for example in breast duct carcinoma (figure 5.2.11 H) and endometrial carcinoma (figure 5.2.11 I, J).

5.2.7.2.1 High iRHOM2 expression in infiltrating immune cells.

In regions of the cervical SCC with fainter iRHOM2 staining, several individual cells showed bright iRHOM2 staining (figure 5.2.12 A, B), perhaps representing infiltrating macrophages as iRHOM2 is expressed predominantly in immune cells (Su et al., 2004), as seen in the dermis of the skin (Chapter 3). Some individual cells with brighter iRHOM2 staining could be seen to a lesser extent in endometrial adenocarcinoma (figure 5.12 C), and a small number of infiltrating-like cells could perhaps be seen in lung Carcinoma (figure 5.12 D) although this staining is less distinct and has a lower intensity than in the cervical SCC section. Breast carcinoma sections also contained cells with particularly high iRHOM2 staining intensity (figure 5.12 E).

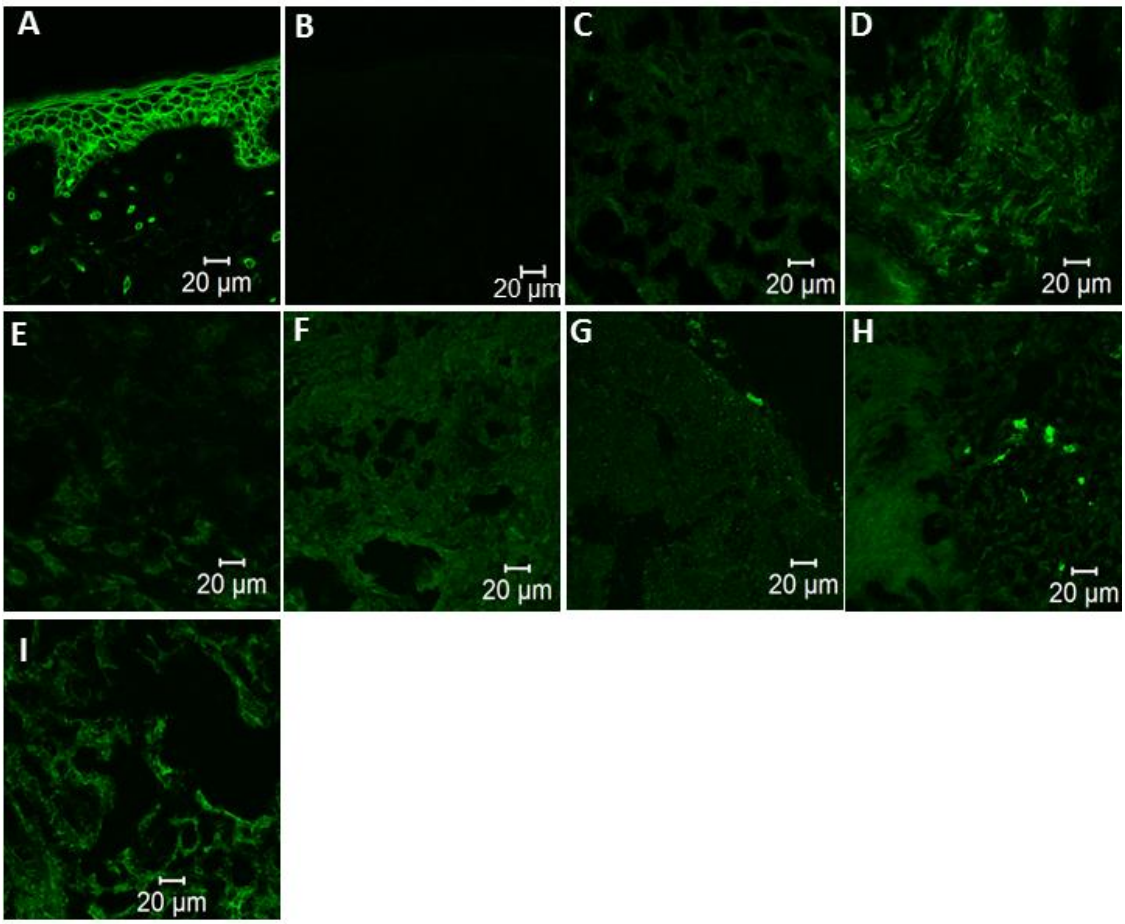

Figure 5.2.9 Variable iRHOM2 expression (staining intensity) in a panel of frozen tumour sections compared to normal skin. IHC against iRHOM2 in frozen sections from **A**: normal facelift skin, **B**: negative control (normal skin; no primary antibody), **C**: breast carcinoma, **D**: breast duct carcinoma, **E:** breast lobular carcinoma, **F**: neuroblastoma, **G**: endometrial adenocarcinoma, **H:** cervical SCC, **I**: lung carcinoma. Images were taken on the LSM 510 Confocal microscope. Settings were the same as those used for normal skin. N=2 for each biopsy.

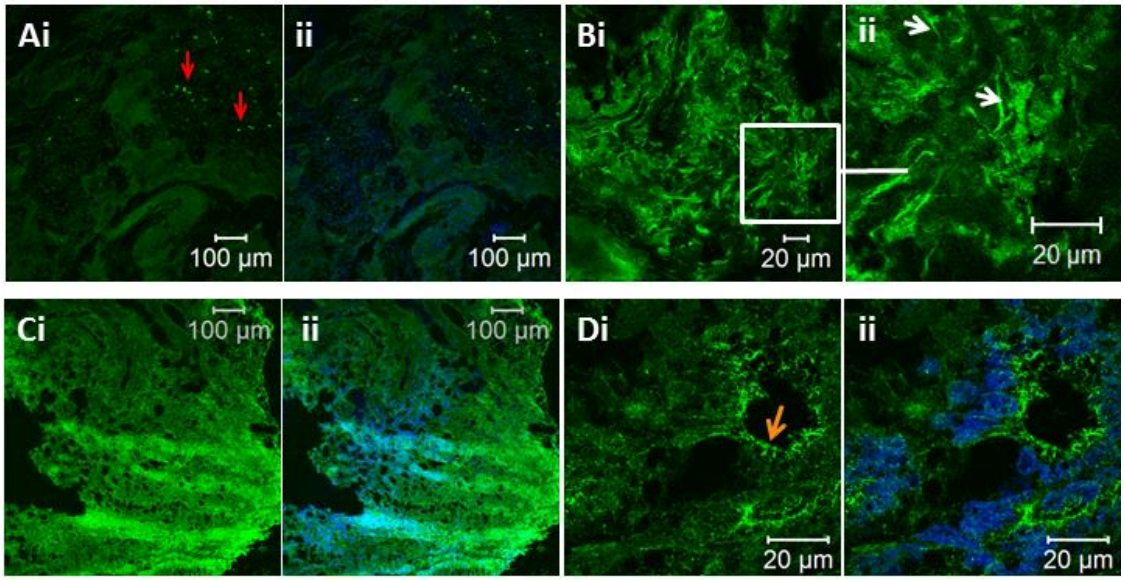

Figure 5.2.10 iRHOM2 expression varies between distinct tumour regions. IHC of iRHOM2 in frozen sections from **A:** cervical SCC, **B:** breast ductal carcinoma, **C:** neuroblastoma, **D**: endometrial adenocarcinoma. Images were taken on the LSM510 confocal microscope. iRHOM2 is shown in green and blue staining represents DAPI nuclear staining. N=2 for each biopsy.

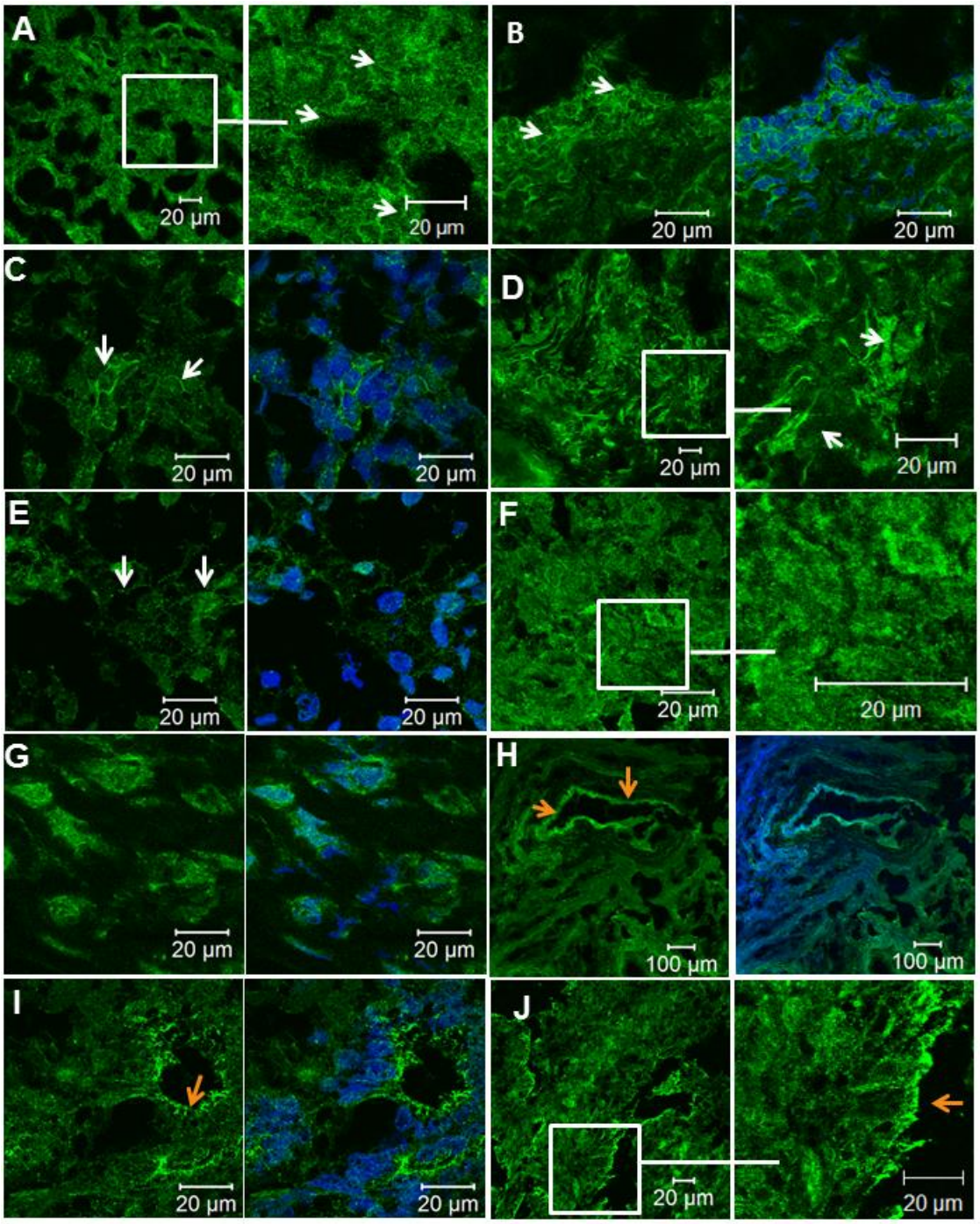

Figure 5.2.11 Membranous, cytoplasmic and perinuclear localisation of iRHOM2 is seen in different tumour sections. IHC of iRHOM2 in breast carcinoma **(A, B)**, lung carcinoma **(C)**, breast ductal carcinoma **(D)**, neuroblastoma (**E** and **F; F** focuses on brighter perinuclear staining). **G:** breast lobular carcinoma **H:** breast ductal Carcinoma, **I-J:** breast ductal carcinoma. iRHOM2 staining is shown in green, DAPI nuclear stain in blue. Images were taken with the LSM 510 Confocal microscope. White arrows indicate plasma membranous staining, orange arrows indicate brighter iRHOM2 staining at the tissue edge. N=2 for each biopsy.

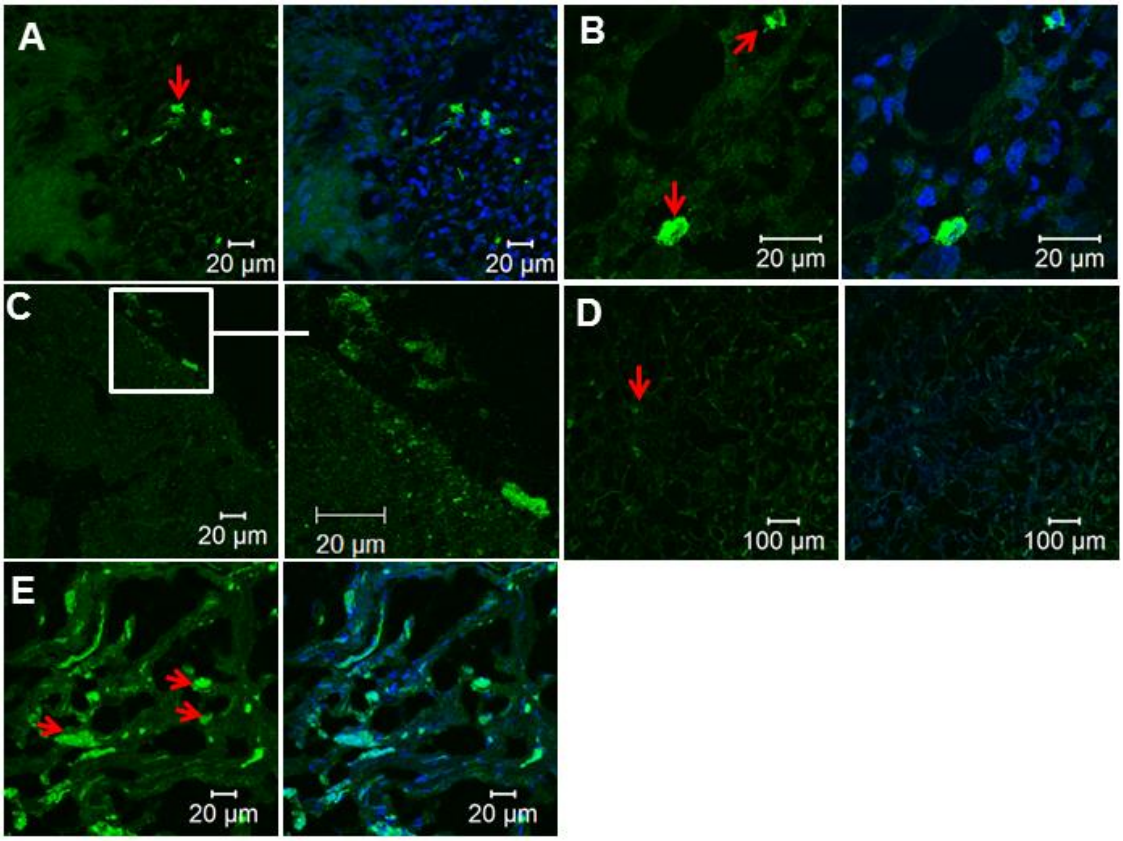

Figure 5.2.12 iRHOM2 is strongly expressed in infiltrating cells in tumours. IHC of iRHOM2 in Cervical SCC **(A, B)**, Endometrial adenocarcinoma **(C)**, Lung carcinoma **(D)** Breast carcinoma **(E)**. Red arrows indicated brightly stained individual cells that may be infiltrating macrophages, or tumour-associated macrophages (TAM). iRHOM2 is shown in green, DAPI nuclear stain in blue. Images were taken on the LSM 510 confocal microscope. N=2 for each biopsy.

5.2.8 Somatic mutations in iRHOM1 and iRHOM2

The COSMIC database (Catalogue of Somatic Mutations in Cancer; http://www.sanger.ac.uk/resources/databases/cosmic.html) stores the currently known information on somatic mutations across the genome, and information about the tumours in which the mutations were found. The location of mutations throughout the iRHOM1 and iRHOM2 structures was studied, as well as the tissue distribution of the mutations. Coding mutations were selected and compared with the Exome Variant Server (EVS) to eliminate single nucleotide polymorphisms (SNPs; appendix C6 and C7). Somatic mutations were marked onto the sequence of iRHOM1 and iRHOM2, and the Uniprot protein database http://www.uniprot.org/ used to determine the approximate distribution of the mutations throughout the predicted regions of the iRHOM1 and iRHOM2 protein structures.

A number of mutations/sequence variants were found throughout the sequence of both iRHOM1 and iRHOM2 (figure 5.2.13), with a similar number of variations found in both iRHOM1 and iRHOM2: 22 and 25 mutations respectively (figure 5.2.14 B). The mutations were predominantly missense mutations, but five LOF mutations were found: three frameshift mutations (one in iRHOM1 and two in iRHOM2), and one nonsense stop mutation in each protein.

5.2.8.1 Distribution of mutations throughout the protein structure

The approximate distribution of mutations throughout the structure of iRHOM1 and iRHOM2 is shown in figure 5.14 A, with the number of mutations in each protein region shown in figure 5.14 B. Approximately half of the mutations were found in the characteristic long N-termini of the proteins (figure 5.14 C), which account for around half the amino acid sequence. No mutations were seen in the conserved region of the *N*-terminal in which the TOC mutations are found in iRHOM2. A number of mutations were found in the extended loop L1: 8 mutations in iRHOM2, including both frameshift mutations and the nonsense mutation; and 4 mutations in iRHOM1 including the frameshift mutation. Two mutations were found in the TMD of iRHOM1, 5 in iRHOM2 TMD, and 1 mutation in loop L6 of iRHOM2. iRHOM2 lacked mutations in the C-terminal, whereas 3 mutations were found in this region of iRHOM1, which comprises 30 amino acids.

5.2.8.2 Tissue distribution of mutations:

Mutations in iRHOM1 and iRHOM2 were found in a number of tissues (figure 5.15). iRHOM1 mutations were particularly concentrated in large intestine (13 mutations, 1.86 % of samples tested) and lung (9 mutations, 1 % of samples tested). One mutation was found in cervical cancer samples out of 14 samples tested (7.14 %), and one in soft tissue out of 15 samples tested (6.7 %). iRHOM2 mutations were most prevalent in lung (8 mutations, 0.96 of samples tested); large intestine (5 mutations, 1.76 of samples tested); breast (5 mutations, 0.52 % of samples tested), and prostate (4 mutations, 1.25 % of samples tested).

Interestingly, three mutations were seen in iRHOM1 in oesophageal cancer (1.73 % of samples tested), but no somatic mutations in iRHOM2 have yet been reported (Weaver et al., 2014). The LOF nonsense and frameshift mutations in iRHOM1 were both found in the large intestine. In iRHOM2, one frameshift deletion mutation in was found in large intestine, the other in ovary; the nonsense mutation in iRHOM2 was found in breast.

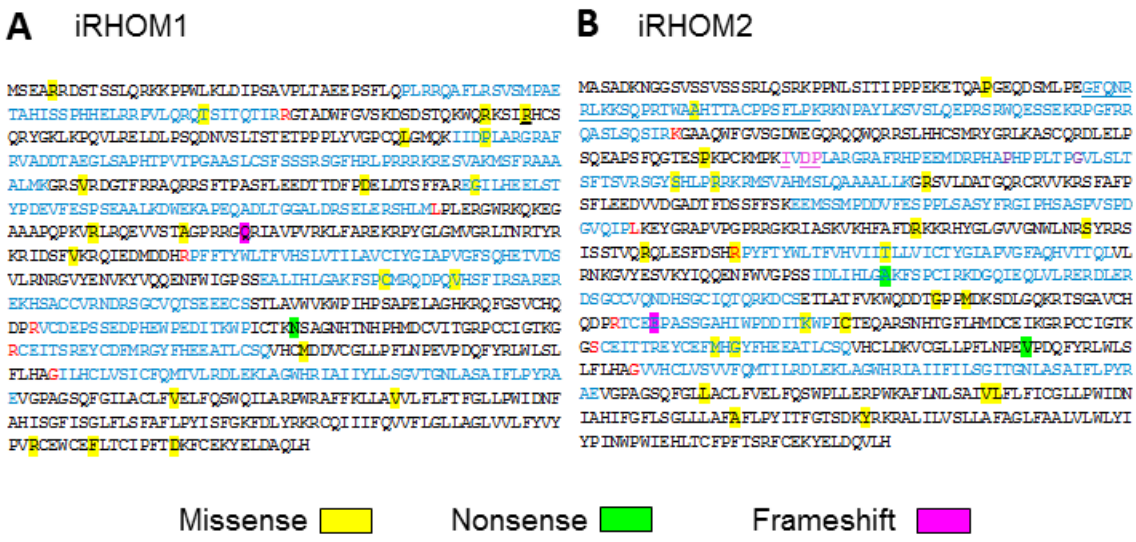

Figure 5.2.13 Somatic mutations in iRHOM1 and iRHOM2 are distributed throughout the protein structure. Somatic mutations in iRHOM1 and 2 were extracted from the Collection of Somatic Mutations in Cancer (COSMIC) database. Amino acid residues affected by Mutations in COSMIC, and not found on the Exome Variant Server (EVS) are highlighted in the sequence of iRHOM1 (A) and iRHOM2 (B). Missense mutations are highlighted in yellow, frameshift mutations in green and Nonsense mutations in pink. R107 on the second line of iRHOM1 is underlined, as two mutations were found in this residue: R107C and R107H. Red letters indicate residues already identified as variants in ENSEMBL. Bold, purple letters indicate COSMIC mutations found on the EVS. Blue letters highlight alternative exons, the long underline indicates the residues absent in isoform 2 of iRHOM2, and the pink underlined letters show the TOC mutations.

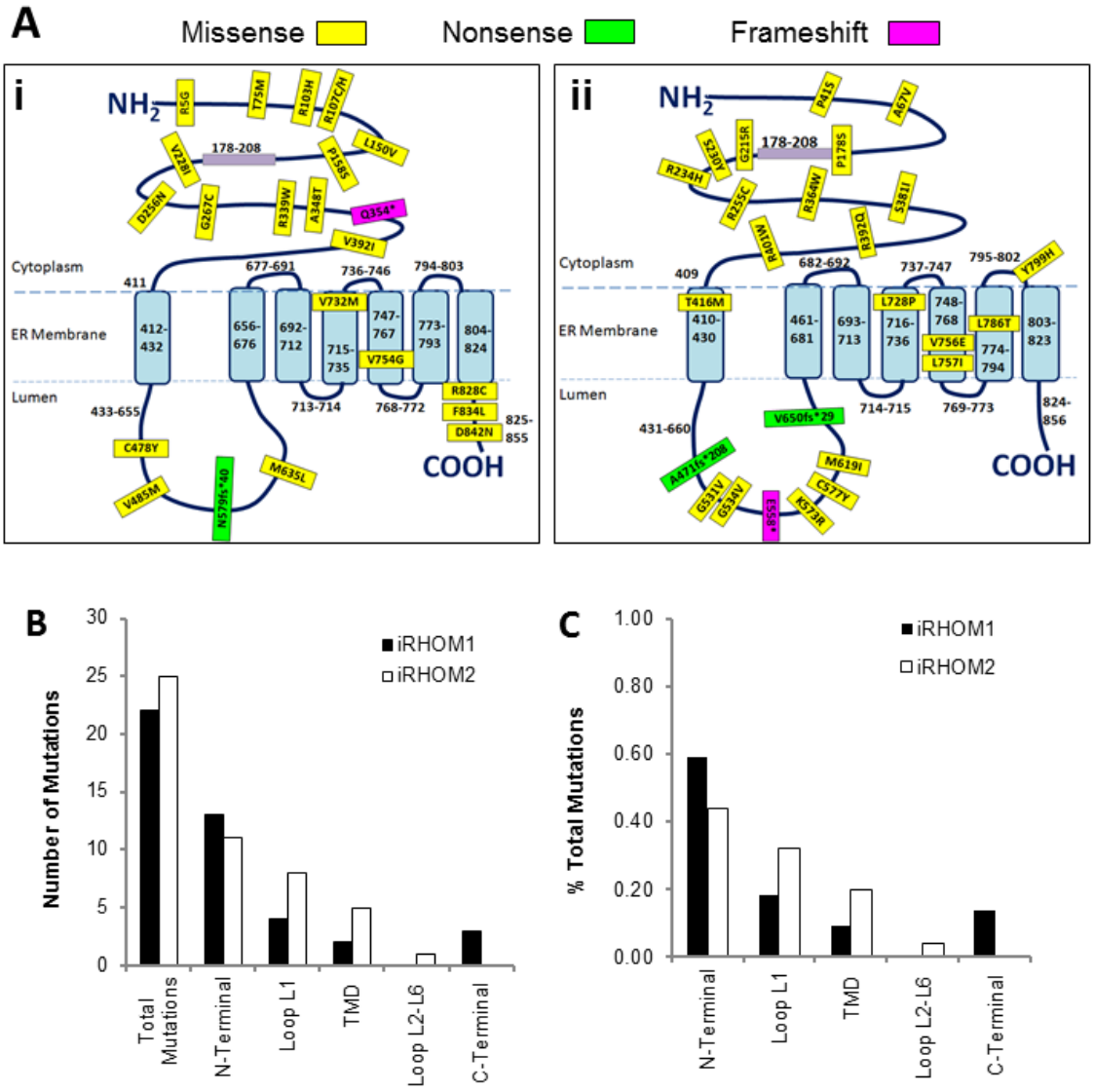

Figure 5.2.14 Location of somatic mutations throughout the structure of iRHOM1 and iRHOM2. A: Schematic showing structures of iRHOM1 **(i)** and iRHOM2 **(ii)** in the ER membrane. Approximate locations of the somatic mutations listed in the collection of somatic mutations in cancer (COSMIC) database are indicated: missense mutations by yellow rectangles; frameshift mutations by green rectangles; and nonsense mutations by pink rectangles. The rough location of the region in which TOC mutations are found in iRHOM2 are indicated on both proteins with a purple rectangle. Amino acid residue numbers are written in black. **B:** Bar chart indicating the number of mutations in iRHOM1 and 2 in the different regions of the proteins. **C:** The percentage of the total mutations found in each region of iRHOM1 and iRHOM2.

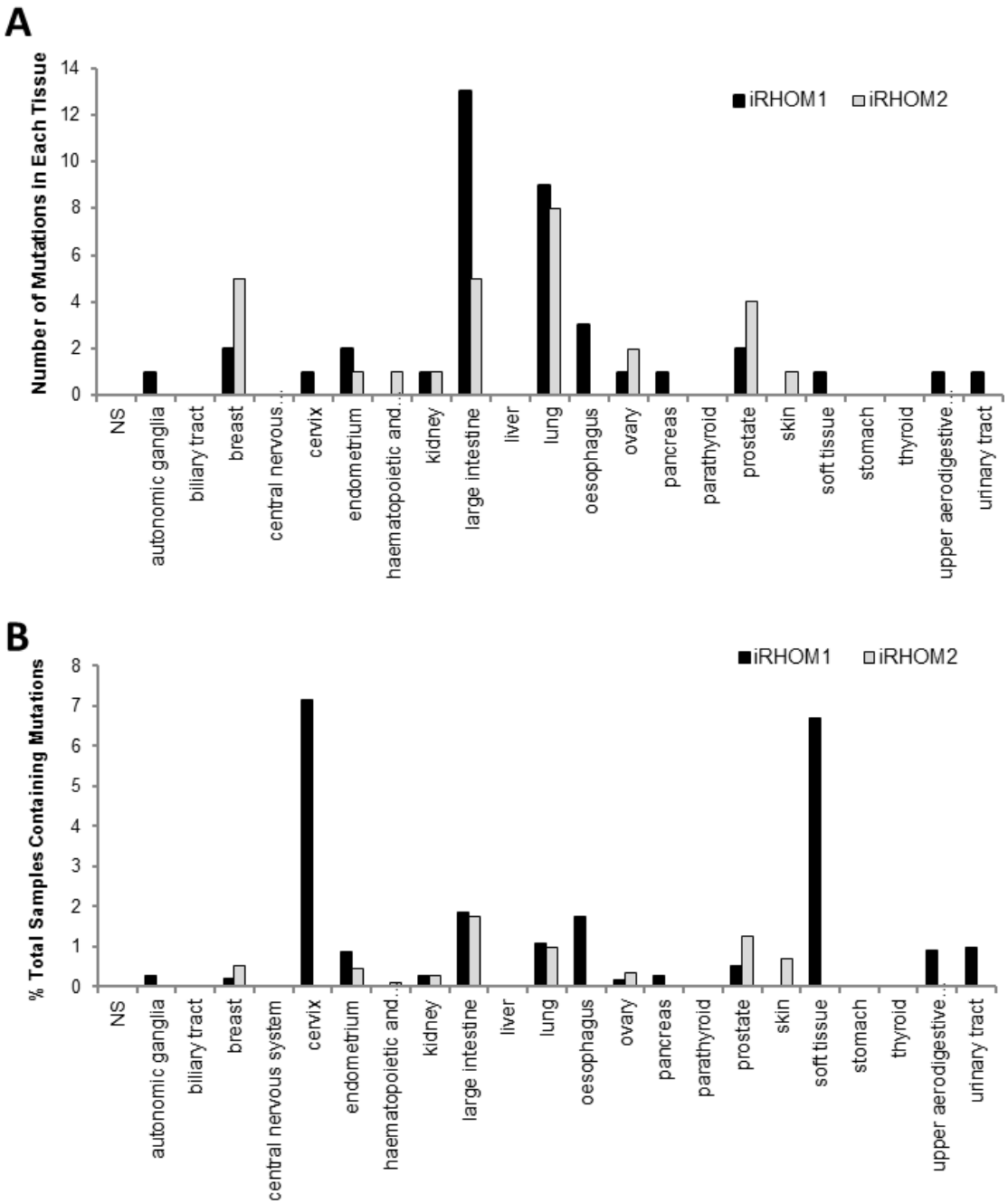

Figure 5.2.15 Tissue distribution of somatic mutations in iRHOM1 and iRHOM2. The tissues in which mutations were found in iRHOM1 and iRHOM2 in the collection of somatic mutations in cancer (COSMIC) database are shown. **A:** Number of mutations found in each tissue. **B:** Percentage of total samples of each tissue containing mutations in iRHOM1 or iRHOM2.

5.3 Discussion

5.3.1 Summary of Findings

The main findings from this chapter are as follows:

1) iRHOM2 and ADAM17 expression levels are variable between different tumours, shown by western blotting of OSCC and HNSCC cell lines, and IHC of TOC and sporadic OSCC tumours
2) iRHOM2 showed a variable localisation and expression pattern, both between tumours and within individual tumours, shown by preliminary IHC experiments in a panel of frozen tumour sections
3) ADAM17 and NOTCH1 expression appeared to correlate with iRHOM2 protein levels in OSCC biopsies and cell lines, and in HNSCC cell lines
4) The ligand Ephrin B3, which is a substrate of rhomboid protease RHBDL2, appeared to be up-regulated in OSCC in sporadic and TOC tumours
5) Somatic mutations in iRHOM2 and its homologue iRHOM1 reported in the COSMIC database were found throughout the structure of iRHOM1 and 2 and in tumours originating from a number of different tissues, with highest frequencies in large intestine and lung

5.3.2 iRHOM2 localisation in cancer

In this preliminary work, IHC showed variable localisation and expression of iRHOM2 in several frozen tumour biopsy sections including neuroblastoma, cervical SCC, lung and breast cancer. A major drawback is the lack of a normal control sample for comparison of iRHOM2 localisation (and expression) at the particular body site, particularly as little is known about the tissue-specific localisation of iRHOM2. Nevertheless, iRHOM2 localisation appeared to be variable between different tumours and also within individual tumour sections, perhaps indicating some dysregulation in cancer, or cell-specific iRHOM2 activity.

A stronger staining intensity was seen at the edges of some sections. ADAM17 expression has been reported at the invasion front in glioblastoma stem cells (Chen et al., 2013), and a role for ADAM17 in invasion and metastasis was reported in a number of studies (e.g. Chen et al. 2013; Doberstein et al. 2013; Giricz et al. 2013; Lu et al. 2013). As iRHOM2 and ADAM17 expression appeared to correlate in keratinocytes, OSCC and HNSCC cell lines (Chapter 4 and figure 5.2.4), this expression pattern in

cancer may suggest a particular role for the iRHOM2-ADAM17 pathway in invasion (and/or migration) in these tumour regions.

Staining of iRHOM2 and ADAM17 in paraffin-embedded TOC and sporadic OSCC biopsies potentially suggested a more cytoplasmic localisation of iRHOM2 compared to control oesophagus in some tumour regions (figures 5.2.1 and 5.2.6). The quality of the iRHOM2 staining in paraffin-embedded sections was fairly low, however, and the biopsies were a number of years old, which may have impacted on the staining quality. In addition, the number of tumours studied was small, but as a preliminary result, it suggests that further research into iRHOM2 localisation in OSCC and other cancers may be of interest.

5.3.2.1 Tumour-Associated Macrophages

iRHOM2 was predicted to be an ER-membrane protein with high expression in macrophages. There was indeed some bright staining in individual cells, particularly in cervical SCC (figure 5.2.12), indicative of infiltrating macrophages as seen in the dermis of normal and TOC skin (chapter 3). This could be confirmed in future by co-staining with macrophage marker CD68. Strong iRHOM2 staining in macrophages is consistent with previous reports of iRHOM2 expression (Adrain et al., 2012; McIlwain et al., 2012; Issuree et al., 2013), and with co-localisation of iRHOM2 and CD68 in the dermis of normal and TOC frozen skin biopsies in Chapter 3.

Macrophages have been shown to play a particular role in tumour development, with a change in phenotype to Tumour Associated Macrophages (TAM). The cells seen may therefore represent classically activated (M1) macrophages, which play important cytotoxic anti-tumour roles, or tumour-associated macrophages (TAMs) which can be found at various stages towards the alternatively activated (M2) macrophages, which have a wound healing phenotype and pro-cancer properties (Biswas and Lewis, 2010; Biswas and Mantovani, 2010; Rego, Helms and Dréau, 2014).

TAMs in breast cancer have been associated with worse clinical outcome (Finak et al., 2008; Beck et al., 2009), and many ADAM17 substrates shed by cancer cells are important in recruiting macrophages to the tumour tissue (Kenny and Bissell, 2007; Talmadge, Donkor and Scholar, 2007; Scheller et al., 2011) and in driving the change in phenotype to pro-tumour M2 macrophages. These ligands include colony-stimulating factor (CSF-1), TNF-α, intercellular adhesion molecule 1 (ICAM1), Vascular Cell Adhesion Molecule 1 (VCAM1), soluble IL-6 receptor, AREG and TGF-α (Rego, Helms and Dréau, 2014). Pro-tumour roles of TAMs include promotion of angiogenesis, ECM degradation, promotion of tumour cell invasion, and suppression of anti-tumour immune responses (e.g. Lin et al. 2001; Lin et al. 2006; Ojalvo et al. 2009; Erreni et al. 2011).

TAMs are recruited to specific regions of the tumour microenvironment, and macrophages with different protein profiles are found in different tumour regions depending on local stimuli such as hypoxia and level of vascularisation (Lewis et al., 2000; Mantovani et al., 2002; Biswas and Mantovani, 2010). Inflitration of macrophages into specific tumour areas is consistent with the localisation seen in the cervical SCC biopsy, with brightly-stained macrophages in regions of lower iRHOM2 expression.

5.3.3 Correlation between iRHOM2 and ADAM17 levels in cancer cell lines

iRHOM2 and ADAM17 both appeared at variable levels in OSCC and HNSCC cancer cell lines, consistent with variable iRHOM1 expression levels seen in HNSCC cell lines (Yan et al., 2008). Variation in iRHOM2 staining intensity was also seen in cutaneous SCC sections, although this could result from different processing of the biopsies, or bleaching of some sections during microscopy.

Results in chapter 4 and this chapter suggest a correlation between iRHOM2 and ADAM17 expression: reduced iRHOM2 in cutaneous keratinocytes treated with ADAM17 siRNA; higher ADAM17 and iRHOM2 staining in the same regions of OSCC tumour biopsies; reduced iRHOM2 in a patient with homozygous LOF mutations in ADAM17; and western blots of iRHOM2 and ADAM17 protein levels in OSCC and HNSCC cell lines. Ideally, a larger number of samples would be used, particularly of OSCC cell lines, to allow testing for the correlation between iRHOM2 and ADAM17 expression levels. Results for the HNSCC cell lines were also limited to one set of lysates. However, although preliminary, the data are consistent from several experiments, and because iRHOM2 is critical in the processing of ADAM17 (Adrain et al., 2012; McIlwain et al., 2012), it would be logical for regulation of the expression of the two proteins to be linked.

The lack of a normal control cell line for OSCC and HNSCC makes determination of normal iRHOM2 levels impossible in these tissues. However, there was clear variability in expression between cell lines. OSCC cells were all grown in RPMI 1640 medium with RM+ keratinocyte supplement. This may not have been optimal for the TE-8 cell line, as some cell death was seen, but was kept the same to allow comparison between the cell lines after culture in the same conditions. The addition of RM+ supplement may also have been unnecessary for cancer cells, but it would have been necessary to supplement at least EGF had we acquired a normal oesophageal cell line. These factors could be considered for future culture of these cell lines.

As iRHOM2 levels vary between regions in tumours from a number of tissues, the variability could reflect the area of the tumours from which the cell lines originated, for example from fibroblasts or keratinocytes. This could further indicate organ or tissue-

specific expression of iRHOM2. Christova et al., (2013) reported particularly high iRHOM2 mRNA expression in the skin and lungs of wild-type mice, which also correlated with ADAM17 mRNA expression levels in these tissues, consistent with the results in this chapter and chapter 4.

In general, iRhom1 was expressed at higher levels than iRhom2, and the highest levels of all three proteins were seen in the skin, lungs, large intestine and stomach (Christova et al., 2013). Interestingly, the greatest number of somatic mutations in iRHOM1 and iRHOM2 reported in the COSMIC database were in the large intestine and lung, with both LOF mutations in iRHOM1 found in large intestine, and one of the three LOF mutations in iRHOM2 found in cancer of the large intestine. As ADAM17 deletion causes a gut phenotype in humans (Blaydon et al., 2011), it may suggest that this pathway is important in the gut, particularly the large intestine. This data may also highlight the tissue-specific expression of iRHOM2.

The KYSE270 OSCC cell line, which showed particularly high iRHOM2 and ADAM17 levels, originated from a well-differentiated tumour (Shimada et al., 1992). This may suggest an important role for iRHOM2 early in tumour development, which would be consistent with elevated iRHOM1 levels in breast cancer at stage 1 and 4 tumours, but not in stage 2 and 3 tumours (Yan et al., 2008).

5.3.4 ADAM17 Activity

ELISAs showed variable secretion of AREG and TGFα into culture medium between TE-4, KYSE270 and KYSE410 cells, and also variable mRNA expression of the proteins. The qPCRs had very little signal in RT- samples, and strong signal in samples where reverse transcriptase was included, suggesting that results were specific and not due to contamination. Use of ADAM17 inhibitors in future studies may help to clarify the variation seen between mature ADAM17 protein and AREG and TGF-α mRNA levels and shedding.

The variability seen in AREG and TGF-α shedding is consistent with previous studies showing variable expression of TGF-α, AREG and other ADAM17 ligands between different cancers. For example, TGF-α up-regulation was seen in breast-cancer associated fibroblasts (Gao et al., 2013), and invasion of triple-negative breast cancer cells was mediated by ADAM17 shedding of TGF-α (Giricz et al., 2013). Another explanation for variability could come from further regulation of ADAM17 activity, such as by microRNAs (Ostenfeld et al., 2010; Chen and Chang, 2013) or by protein disulphide isomerase (PDI) which has been reported to reduce ADAM17 enzymatic activity by catalysing the formation of disulphide bonds in the membrane proximal region (Düsterhöft et al., 2013).

5.3.5 NOTCH1

Consistent with the increased expression of full-length and cleaved NOTCH1 in TOC cutaneous keratinocytes described in Chapter 4, a positive correlation between iRHOM2, ADAM17 and NOTCH1 protein expression was seen in HNSCC cell lines. There is a high level of background in the NOTCH1 western blot, which could affect densitometry analysis. However, the Image Studio Lite software used for the analysis corrects for background.

The correlation may imply regulation of NOTCH1 via ADAM17-mediated cleavage (likely ligand-independent cleavage), and NOTCH1 expression appeared to correlate with iRHOM2 and ADAM17 expression up to the S2 cleavage stage in the HNSCC cell lines. However, the correlation between mature ADAM17 and NOTCH1 appeared to be weaker than the iRHOM2-NOTCH1 and iRHOM2-ADAM17 correlations. This could reflect inaccuracies in densitometry measurements, as the pro- and mature ADAM17 bands are fairly close together. Alternatively, it could perhaps reflect an indirect association with Notch signalling. Future work using ADAM17 inhibitors may help to determine whether ADAM17 is directly affecting NOTCH1 expression. Investigation of ADAM10 in these cells would also be useful to determine whether its expression and activity is also related to NOTCH signalling.

High NOTCH1 expression was also seen in the KYSE270 OSCC cell line, which expressed high iRHOM2 and mature ADAM17, consistent with the correlation seen in HNSCC cell lines, although the sample size was again very small and no loading control was included in this experiment. However, the differences between NOTCH1 in the cell lines are quite pronounced, and the same sets of lysates gave consistent loading in ADAM17-iRHOM2 western blots.

The COSMIC cell line project has records of NOTCH1 substitution mutations in KYSE270 cells (http://cancer.sanger.ac.uk/cell_lines/sample/overview?id=753574; c.1393G>C, p.A465P; c.1393G>C, p.A465P) and two non-protein changing mutations). No NOTCH1 mutations were reported in KYSE410 (http://cancer.sanger.ac.uk/cell_lines/sample/overview?id=753574; accessed 19.4.14) or TE-4 cells (http://cancer.sanger.ac.uk/cell_lines/sample/overview?id=1503371; accessed 19.4.14). Two NOTCH1 mutations were reported in TE-8 cells (http://cancer.sanger.ac.uk/cell_lines/sample/overview?id=753574; both c.1318T>C, p.C440R). However, most reported somatic NOTCH1 mutations in SCCs are LOF rather than missense mutations (e.g. Weaver et al. 2014). Further investigation of a wider range of OSCC cell lines and study of iRHOM2/ADAM17 inhibition on cell properties such as migration and invasion would be interesting.

5.3.6 Ephrin B3 in cancer

Ephrin B3 appeared up-regulated in TOC and sporadic OSCC in IHC experiments. However, the staining was carried out on a small sample set, and western blots did not appear to work with this antibody. Increased Ephrin B3 expression in OSCC would be consistent with findings in epithelial ovarian cancer (Castellano et al., 2006), where arteriole-specific Ephrin B3 staining was seen in normal ovarian epithelial tissue and no staining in stromal cells, but increased Ephrin B3 staining intensity in cancerous tissue. The localisation was partly at the cell membrane and in the cytoplasm in the ovarian tumours, with some nuclear staining visible (Castellano et al., 2006); the staining in figure 5.2 appeared to show Ephrin B3 staining throughout the cell in the tumour samples. In epithelial ovarian cancers, expression of the Ephrin B3-EphB4 ligand pair was associated with worse survival (Castellano et al., 2006).

A role for Ephrin B3 in glioma cell migration and invasion was shown, with Ephrin B3 required for EphB2/Fc-mediated migration in glioma cell lines via Rac1, an important regulator of cell motility (Nakada et al., 2006). Furthermore, increased Ephrin B3 phosphorylation correlated with tumour grade in glioma specimens (Nakada et al., 2006). Knock down of Ephrin B3 in non-small-cell lung cancer (NSCLC) cells affected proliferation and cell morphology (Ståhl et al., 2011, 2013), and Ephrin B3 expression was associated with EphA2 phosphorylation at Ser-897, downstream of Akt phosphorylation in NSCLC (Ståhl et al., 2011). Further study of the wider Eph/Ephrin signalling pathway would be of interest in TOC and OSCC in association with iRHOM2-ADAM17 signalling, as EphA2 and EphA4 appeared to be altered in TOC cutaneous keratinocytes.

5.3.7 Conclusion

Taken together, these findings show variation in iRHOM2 expression and localisation in a number of cancer tissues and cell lines, particularly OSCC and HNSCC, perhaps suggesting that iRHOM2 may be dysregulated in these cancers. Furthermore, the iRHOM2-ADAM17 pathway may play a role in modulating the immune response to cancer, as high expression of iRHOM2 was seen in infiltrating macrophage-like cells in cervical cancer and breast cancer, and ADAM17 and its substrates have been implicated in the tumour immune response in a number of previous studies. The results are preliminary and performed on a small number of samples, but suggest that iRHOM2 may be of interest for further investigation in cancer progression as a regulator of ADAM17, EGFR and growth factor signalling, and perhaps the NOTCH signalling pathway.

Chapter 6: Discussion

Chapter 6: Discussion

This work began with investigation of the localisation and expression of iRHOM2 in normal and TOC skin. Following electron microscopy imaging of TOC epidermis showing desmosomal dysregulation, the expression and localisation of desmosomal proteins was investigated, including ADAM17 substrate DSG2. The function of iRHOM2 in relation to trafficking and activation of metalloproteinase ADAM17 was studied and preliminary work carried out to look at the pathways that may be affected in TOC downstream of ADAM17-EGFR signalling. Finally, preliminary work investigating the expression and localisation of iRHOM2, and expression of ADAM17 and NOTCH1 was carried out in OSCC and HNSCC cell lines and OSCC biopsies.

6.1 Overview of findings

Missense mutations in the *N*-terminus of iRHOM2 associated with the autosomal dominant condition TOC appear to be GOF in nature, resulting in increased processing and activation of metalloproteinase ADAM17. This leads to increased levels of cell-surface ADAM17, and increased cleavage of ADAM17 substrates including EGFR ligands and DSG2. A schematic summarising this mechanism and possible downstream effects is shown in figure 6.1 A and B.

Increased ADAM17-mediated cleavage of EGFR ligands including AREG and TGF-α leads to amplified EGFR signalling. This causes a wound healing phenotype in TOC epidermis, features of which include increased migration of TOC keratinocytes and desmosomal re-modelling. Increased migration may be mediated in part by changes in Eph/Ephrin signalling, and is also associated with increased proliferation of TOC keratinocytes (Blaydon et al., 2012). In the basal layer of the epidermis, desmosomal remodelling may also be mediated by increased processing of DSG2 by ADAM17, further affecting the formation and maintenance of desmosomes. Desmosomal remodelling may also be associated with effects on cell-cell adhesion.

Increased ADAM17 activity also appears to result in increased activity of TGM1, leading to increased barrier formation in TOC epidermis, and reduced levels of infection (Brooke et al., 2014), which may be associated with changes in NOTCH1 activity.

Further work is needed to determine why the TOC iRHOM2 mutations lead specifically to oesophageal SCC. The oesophagus is subjected to high levels of physical and chemical stress (e.g. alcohol, smoking and hot drinks), and ADAM17 and EGFR signalling are associated with the development and progression of a number of cancers,

as are Eph/Ephrin signalling and desmosomal dysregulation. Future investigation into these pathways may uncover some of the reasons for the occurrence of OSCC in TOC.

6.2 How do iRHOM2 mutations lead to increased ADAM17 processing?

The main mechanism by which the mutations in the *N*-terminus of iRHOM2 affect its signalling appears to be increased stability of the iRHOM2 protein, resulting in increased iRHOM2 activity. Hosur et al (2014) recently demonstrated increased stability of iRHOM2 *p.I186T*, and showed increased stability of murine iRhom2 with an *N*-terminal truncation mutation found in mice suffering from a phenotype including hair loss, accelerated wound healing and tumour formation. The mutation, known as *Cub* (curly-bare), was previously described in Johnson et al (2003), and is caused by splicing of *Rhbdf2* exons 1-7, resulting in production of an approximately 63.5 KDa protein, as the next start ATG is in exon 8.

There was a greater reduction in iRHOM2 immunoreactivity of COS-7 cells overexpressing WT human iRHOM2 than in cells expressing either iRHOM2-*p.I186T* or the iRhom2-*cub* mutation following treatment with protein synthesis inhibitor cyclohexamide. Hosur et al (2014) also suggested that WT iRHOM2 itself may be regulated by targeting for ERAD (in addition to its targeting EGF for ERAD) as the half-life ($t_{1/2}$) of iRHOM2-WT was increased by treatment with proteasomal inhibitor MG-132, but the $t_{1/2}$ of iRHOM2-*cub* was not affected.

iRHOM1 has also been shown to be an unstable protein (Nakagawa et al 2005), with a PEST domain located in its N-terminal region. A PEST domain is a 12-60 amino acid long region rich in proline (P), glutamic acid (E), serine (S) and threonine (T), often flanked by positively charged amino acids (Rogers et al., 1986; Rechsteiner, 1988; Rechsteiner and Rogers, 1996), although the sequence itself does not contain positively charged amino acids. PEST domains are found in proteins such as enzymes and signalling molecules for which rapid changes in concentration are required (Rechsteiner, 1988; Rechsteiner and Rogers, 1996), including NOTCH1 (Öberg et al., 2001; Weng et al., 2004; Bray, 2006). Interestingly, DSG1 also contains a PEST region (Garrod and Chidgey, 2008), likely relating to a signalling function of the cadherin such as its role in cell death.

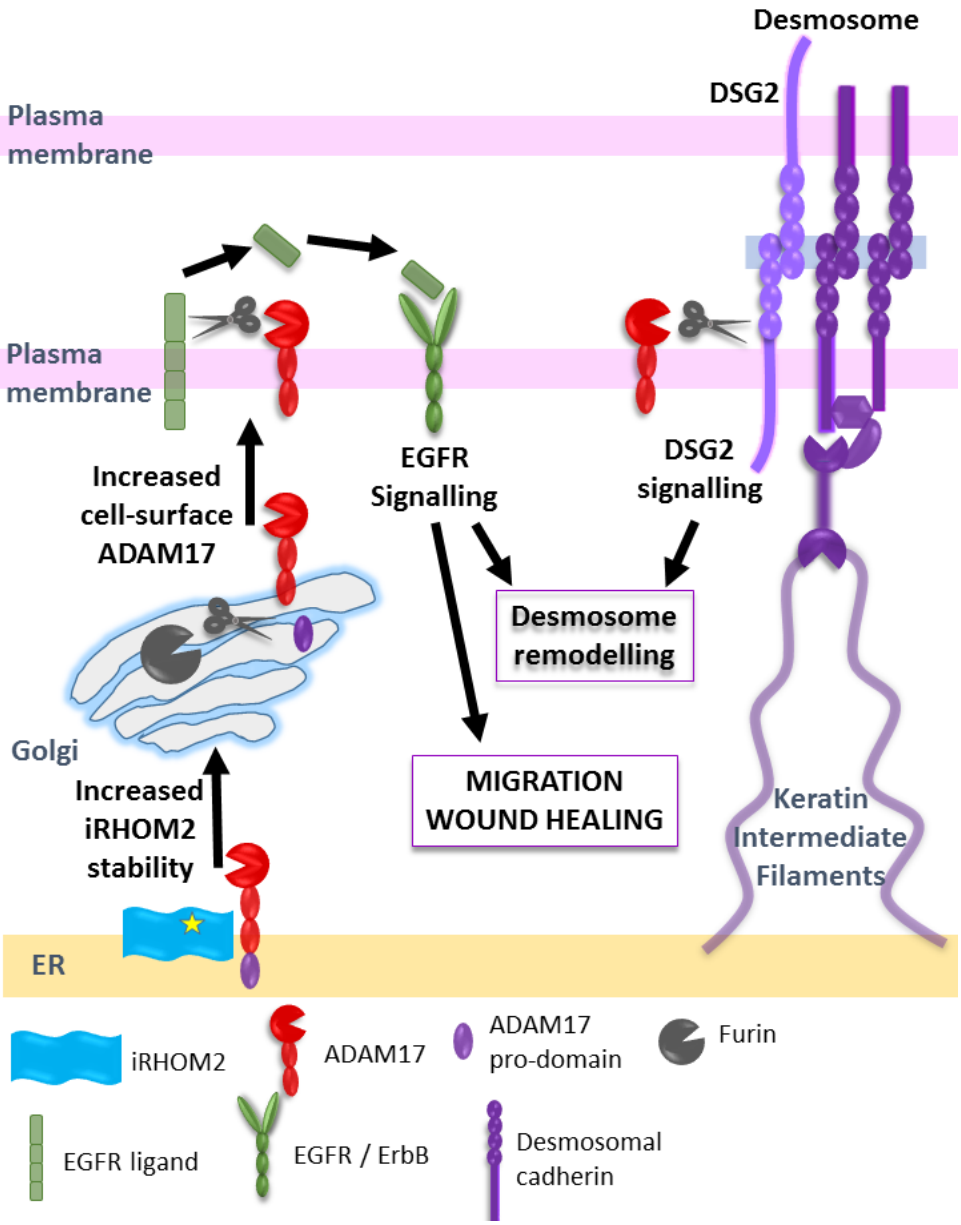

Figure 6.1 A: Schematic showing hypothesis for the mechanism of iRHOM2 mutations effect in TOC. Increased stabilisation of iRHOM2 results in its greater availability for trafficking of ADAM17 from the ER to the golgi, and ultimately increased levels of active ADAM17 at the cell surface. This results in enhanced shedding of ADAM17 substrates including EGFR ligands and desmosomal cadherin DSG2. Increases in EGFR signalling result in enhanced migration and hyperactive wound healing, and may also lead to desmosomal re-modelling, which is an important part of the wound healing response. Desmosomal remodelling may also be enhanced by ADAM17-mediated cleavage of DSG2, for example in the basal layers of the epidermis. There may also be some differences in downstream desmosomal signalling.

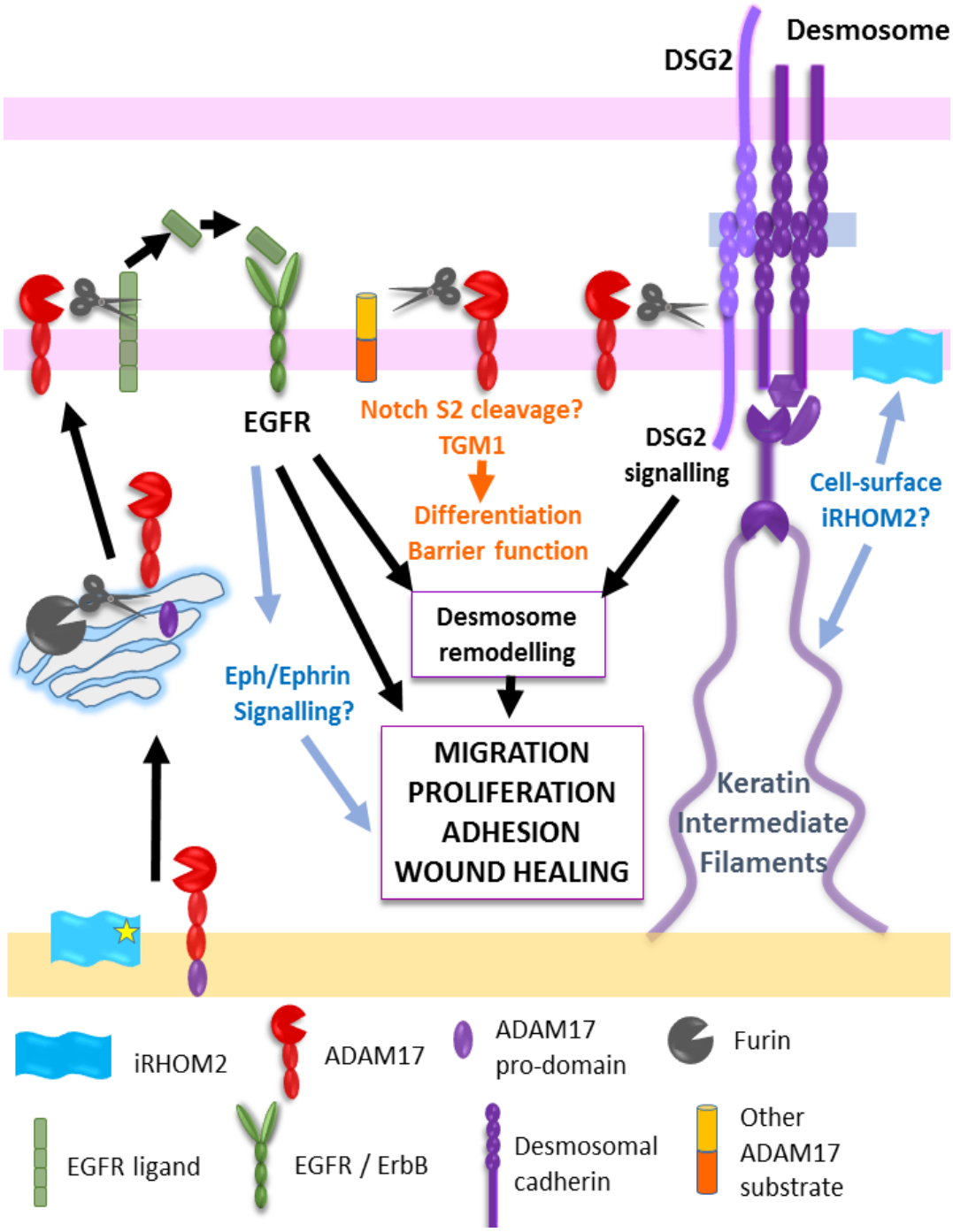

Figure 6.1 B: Pathways that may be affected downstream of enhanced EGFR signalling in TOC. Pathways affected in TOC, and affecting migration, proliferation, and likely adhesion may include Eph/Ephrin signalling, possibly mediated by EphA2 and EphA4; increased transglutaminase activity and potentially NOTCH signalling, leading to enhanced barrier function and protection from infection. A major question remaining is the role of iRHOM2 at the cell-surface in squamous tissues, and whether this may involve interaction with and/or regulation of keratins.

Increased iRHOM2 stability is consistent with the apparent increase in iRHOM2 protein expression seen in some sets of lysates from TOC keratinocytes compared with control cells in the siRNA knock down experiments presented in Chapter 4. However, some results in this thesis suggested reduced levels of iRHOM2 protein in TOC (Chapter 3). This could perhaps result from signalling feedback and other regulatory mechanisms needed to tightly control iRHOM2 and ADAM17 expression and activity, which could mean that slight changes in conditions result in changes in iRHOM2 expression (and localisation), perhaps explaining some of the variability seen in results in the results shown this thesis.

Hosur et al (2014) also demonstrated that iRhom2-*cub* was a GOF mutation of iRHOM2. They generated an *Rhbdf2* knock-out mouse, which did not show a phenotype and had normal hair growth (consistent with the findings of McIlwain et al. 2012). They crossed the *Rhbdf2* knock-out mice with *Rhbdf2*$^{cub/cub}$ mice to generate compound mutant mice. These mice had sparse hair, showing that expression of *Rhbdf2*^{cub} rather than loss of the protein is the cause of the phenotype.

6.2.1 The effect of increased iRHOM2 stability on EGFR signalling

Increased ADAM17 trafficking resulting from *N*-terminal mutant iRHOM2 stability leads to elevated shedding of EGFR ligands by ADAM17. This leads to increased EGFR signalling, which is reflected in the TOC hyperproliferative phenotype (Blaydon et al., 2012; Brooke et al., 2014). The *Rhbdf2*$^{Cub/Cub}$ truncation also resulted in increased migration and accelerated wound healing in MEFs and mouse ear punch wounds (Hosur et al., 2014). Increased proliferation was seen in *Rhbdf2*$^{cub/cub}$ MEFs (Hosur et al., 2014), consistent with increased proliferation and migration of TOC keratinocytes (Blaydon et al. 2012; Brooke et al. 2014; Chapter 4), and with hyperproliferation and thickening of skin in response to stress (Ellis et al., 1994; Hennies, Hagedorn and Reis, 1995; Stevens et al., 1996).

The *Rhbdf2*$^{Cub/Cub}$ phenotype of accelerated wound healing was associated with increased phosphorylation of proteins of the EGFR signalling pathway, including Akt, mTOR, and p38MAPK, and also with increased EGFR internalisation, consistent with increased activation of the pathway (Hosur et al., 2014). This is also consistent with the findings in TOC (Blaydon et al. 2012; Brooke et al. 2014; Chapter 4). Interestingly, *Rhbdf2*$^{+/cub}$ heterozygotes also showed accelerated wound healing, without the defects in hair growth and coat formation (Hosur et al., 2014), consistent with the dominant mode of inheritance of the iRHOM2 mutations in TOC (Blaydon et al., 2012).

A large proportion of the wound healing phenotype seen in *Rhbdf2*$^{Cub/cub}$ mice appears to be mediated by Areg: a LOF point mutation was identified in *Areg,* known as *Areg*^{MCub}*,* which affects a splice site in exon 1. This results in gain of 22 extra nucleotides, disrupting the coding frame and adding a premature stop codon. Homozygous *Areg*^{MCub} reduced the hyperactive EGFR signalling and wound closure, while a single copy of the *Areg*^{MCub} gene prevented the hair loss phenotype seen in *Rhbdf2*^{cub} mice. This genetic combination resulted in a wavy hair phenotype, suggesting that remaining phenotypic differences result from other changes in the EGFR pathway (Hosur et al., 2014).

The accelerated wound healing phenotype in *Rhbdf2*$^{cub/cub}$ mice with *N*-terminal truncations of iRHOM2 therefore appear to result from increased Areg shedding rather than solely on ADAM17-EGFR ligand signalling, suggesting that increased AREG levels may also mediate the accelerated wound healing phenotype in TOC. Further evidence for the importance of growth factor balance in the skin and gastrointestinal system are demonstrated by the overlapping phenotypes associated with ADAM17 LOF mutation (Blaydon et al., 2011) and a LOF mutation in EGFR recently reported by Campbell et al (Campbell et al., 2014) in a patient suffering from an inflammatory bowel, lung and cutaneous syndrome, which resulted in death caused by infection at the age of two and a half.

Overall, these findings suggest that iRHOM2 mutations in TOC stabilise the protein as seen with *N*-terminal truncation *Cub* mutation, but still allow trafficking of ADAM17, which is augmented through the increased longevity of iRHOM2 (Brooke et al., 2014; Hosur et al., 2014). Trafficking of ADAM17 appears to depend on the *N*-terminal of iRHOM2, as *Rhbdf2*$^{Cub/cub}$ mice showed defects in ADAM17 trafficking, but increased Areg secretion (Hosur et al., 2014).

6.3 Regulation of iRHOM2 and ADAM17 expression

In this work there appeared to be a correlation between iRHOM2 and ADAM17 protein expression levels, consistent with the findings of Christova et al (2013) in the mouse. The mechanisms of iRHOM regulation are beginning to be uncovered, with protein stability appearing to be a major factor regulating expression of both iRHOM1 and iRHOM2 (Nakagawa et al., 2005; Hosur et al., 2014). Expression could be further regulated by control of transcription and translation, regulatory proteins such as micro-RNAs (miRNAs), and through feedback from various signalling pathways such as those downstream of EGFR signalling.

Regulation of ADAM17 expression appears to vary depending on the cell type and situation. Two major pathways reported to be involved in up-regulation and activation of

ADAM17 include: TNF-α/ TLR-4–induced up-regulation of ADAM17, for example in response to LPS (e.g. Scott et al. 2011; Chanthaphavong et al. 2012); and hypoxia, which has been reported in conditions including rheumatoid arthritis and cancer (Charbonneau et al., 2007; Szalad et al., 2009; Wang, Feng and Li, 2013).

6.3.1 Hypoxia-induced ADAM17 up-regulation

ADAM17, along with TNF-α, is up-regulated by hypoxia through hypoxia-inducible factor-1α (HIF-1α) in a number of cell types, including synovial cells (Charbonneau et al., 2007), vascular smooth muscle cells (VSMC) (Obama et al. 2014), the U87 glioma cell line (Szalad et al., 2009) and hepatocellular carcinoma cell lines (Wang, Feng and Li, 2013). Hypoxia results in up-regulation or activation of a number of transcription factors, including NF-κB (Koong, Chen and Giaccia, 1994) and HIF-1α (Wang and Semenza, 1995; Wang et al., 1995).

HIF-1α is usually degraded in normoxic conditions by oxygen-dependent prolyl hydroxylation, leading to ubiquitination and proteasomal degradation (Bruick and McKnight, 2001). In hypoxia, HIF-1α is regulated by RACK1, which forms a complex with Elongin C and E3 ubiquitin ligases, also leading to HIF-1α degradation. The molecular chaperone HSP90, however, competes with RACK1 for binding to HIF-1α, and when bound, stabilises HIF-1α (Liu et al. 2008). This allows it to be targeted to the nucleus where it regulates gene transcription in association with HIF-1β (Liu and Semenza, 2007; Liu et al., 2008), which is present constitutively in normoxic and hypoxic conditions (Wang and Semenza, 1995).

Hypoxia-mediated regulation of ADAM17 appears in part to be mediated by iRHOM activity. iRHOM1 was recently shown to regulate HIF-1α in breast cancer, and its expression is associated with poor response to treatment (Zhou et al., 2014), suggesting the development of drug resistance with iRHOM1 expression. iRHOM1 was shown to regulate HIF-1α by binding RACK1, sequestering it from HIF-1α, and therefore preventing RACK1-mediated HIF-1α degradation. Zhou et al (2014) therefore suggested that iRHOM1 is part of a molecular switch controlling HIF-1α stability.

This provides further insight into the link between regulation of iRHOM and ADAM17 expression. The similarity in protein sequence and overlapping functions of iRHOM1 and 2 suggest that this pathway, or a similar pathway, may be regulated by iRHOM2 and may be an area for future investigation.

6.3.2 Micro-RNA regulation of ADAM17 expression

Micro-RNAs are emerging as important regulators of ADAM17. miR-122 and miR-145, for example, have been shown to be important in regulating ADAM17 expression in a number of cancer cell lines (Tsai et al., 2009; Chen and Chang, 2013). Micro-RNAs are highly conserved non-coding RNAs of approximately 20 nucleotides in length and predominantly function to regulate expression of a vast array of proteins by binding to the 3' UTR of the mRNA (Ebert and Sharp, 2012).

Hydroquinone-induced miRNA-122 down-regulation in human leukaemia cells caused up-regulation of ADAM17, likely via ERK activation (Chen and Chang, 2013); miR-122 was also down-regulated in hepatocellular carcinoma with local intrahepatic metastases (Tsai et al., 2009). Restoring miR-122 expression *in vitro* or *in vivo* reduced invasion and migration of cell lines; and *in vivo*, reduced tumourigenesis, angiogenesis and development of intrahepatic metastases. Knock down of ADAM17 produced similar results, suggesting that this pathway may be a future therapeutic target (Tsai et al., 2009).

Yu et al (2013) demonstrated that miR-145 reduces expression of both ADAM17 and the SOX9 (SRY-box containing gene 9) transcription factor. ChIP assays demonstrated that SOX9 binds to the ADAM17 promoter (Yu et al., 2013), suggesting that it may be involved in mediating the effects of miR-145 on ADAM17 expression. Furthermore, miR-145 expression was reduced in head and neck cancer, affecting proliferation, sphere formation and tumour volume (Yu et al., 2013).

Recently, miR-152 was also shown to negatively regulate ADAM17 expression in human umbilical vein endothelial cells (HUVEC; Wu et al. 2014), reducing both proliferation and migration. A decrease in miR-152 expression may contribute to (or result from) the increase in ADAM17 expression in hypoxia, as miR-152 expression was decreased while ADAM17 mRNA and protein expression increased in hypoxic conditions. Furthermore, there was a reduction of circulating miR-152 in patients with atherosclerosis, while miR-145 expression was unaffected, suggesting that the relationship between miR-152 and ADAM17 expression may be important in the pathogenesis of atherosclerosis (Wu et al., 2014).

6.4 Other functions of the iRHOMs

Previously described functions of the iRHOMs include targeting of EGF for ERAD (Zettl et al., 2011), regulating substrate selectivity of protease substrates such as AREG and TGF-α (Nakagawa et al., 2005; Maretzky et al., 2013), and as described in the previous section, iRHOM1 has been shown to regulate HIF-1α stability (Zhou et al., 2014). This is

interesting as it suggests a further role for iRHOM1 in regulating ADAM17 expression and activity in addition to regulating ADAM17 trafficking.

6.4.1 Substrate selectivity

Both iRHOM1 and iRHOM2 have been shown to control substrate selectivity of EGFR ligands for shedding. iRHOM1 interaction with the unprocessed forms of TGF-α, with only a weak association with the mature, *N*-glycosylated TGF-α, was previously described by Nakagawa et al (2005). Interaction of iRHOM1 with one isoform of transmembrane HB-EGF and with Spitz was also seen in transfected cells (Nakagawa et al., 2005). Interestingly, drosophila Star, which is needed for trafficking of Spitz in drosophila (Lee et al., 2001), co-localised with iRHOM1, but no interaction was seen between the two proteins (Nakagawa et al., 2005). No homologue of Star has been identified in the mammalian genome. As drosophila expresses a single iRHOM, it suggests that iRHOM1 and 2 may have adapted to take the role of Star in mammalian cells, regulating EGFR ligand availability at the cell surface and providing a further mechanism for fine-tuning EGF signalling in different cell types.

Maretzky et al (2013) identified the substrate selectivity of iRhom2, demonstrating in mouse embryonic fibroblasts (MEFs) that shedding of ligands including Hbegf, Areg, epiregulin and Kit ligand 2 is dependent on iRhom2, as shedding of these ligands was reduced in iRhom2 knock-out MEFs. Shedding of some other ADAM17 substrates such as TGF-α is dependent on iRhom1 (Maretzky et al., 2013). PMA-stimulated shedding of HB-EGF, which is needed for GPCR-mediated cross-talk with the EGFR/ERK1/2 signalling axis (Prenzel et al., 1999; Maretzky et al., 2011), was almost completely abrogated in iRhom2 knock-out MEFS compared with WT controls, although mature ADAM17 was present in both WT and knock-out MEFs. iRhom2 did not appear to be involved with regulation of ADAM10-mediated ligand shedding (Maretzky et al., 2013).

The difference in ligand shedding was seen in PMA-stimulated cells, but no great differences were seen in constitutive shedding in iRhom2 knock-out MEFs, or upon overexpression of iRhom2 although small differences may have been missed. This suggests that iRHOM2 is important in controlling substrate selectivity under stimulated conditions (Maretzky et al., 2013), and may act to regulate cellular response to specific situations, allowing fine tuning of signalling processes.

Regulation of substrate selectivity was dependent on the *N*-terminal domain of iRhom2 (Maretzky et al., 2013). Furthermore, Areg/AREG selectivity appeared to be controlled by iRHOM2 independently of ADAM17, as human or mouse *Rhbdf2-Cub* with the *N*-terminal truncation was able to increase shedding of Areg, but was not able to traffick ADAM17 (Hosur et al., 2014). Expression of iRHOM2 *p.I186T* in HEK293T cells also

resulted in greater levels of AREG in conditioned medium and lower intracellular levels compared with Human WT iRHOM2 (Hosur et al., 2014).

The regulation of Areg appears to be dependent on the rhomboid peptidase domain (Hosur et al., 2014), which is active in rhomboid proteases, but catalytically inactive in the iRHOMs (Lemberg and Freeman, 2007b; Adrain and Freeman, 2012). Deletion of the peptidase domain of Human iRHOM2 with the *Cub* N-terminal truncation diminished AREG secretion. Hosur et al (2014) also showed that the increased secretion of AREG and HB-EGF was dependent on the amino acid residues Glu-426 and Cys-432 in TMD 4; and His-366 and His-475 in TMD2 and 6 respectively. These residues were also critical for the suppression of EGF via targeting for ERAD (Hosur et al., 2014).

6.5 How might iRHOM2 dysregulation lead to cancer?

iRHOM2 is involved in EGFR signalling through multiple mechanisms, including: direct regulation of ADAM17 activation; targeting EGF for ERAD (Zettl et al., 2011); and regulating ADAM17 substrate selectivity, including ADAM17-independent regulation of AREG (Maretzky et al., 2013). Increased EGFR signalling is known to mediate development and progression of many cancers, and ADAM17 has been implicated in a number of cancers through functions including shedding of EGFR ligands and adhesion proteins, and modulation of the immune response. The role of ADAM17 in cancer will be discussed further in the next section. It also seems likely that additional functions of iRHOM2 will be uncovered in future, which could provide further insight into the role of iRHOM2 in cancer.

GOF in iRHOM2 resulted in increased susceptibility to tumour formation in a mouse model of human familial adenomatous polyposis (Hosur et al., 2014). $Apc^{Min/+}$ mice heterozygous for $iRhom2^{cub/cub}$ showed decreased survival, as well as an increase in the number of polyps and tumour area. No increased incidence of cancer was seen in *Rhbdf* knock-out mice over two years, consistent with the *Cub* and TOC mutations being GOF in nature. Overall, this suggests that the more stable iRHOM2 increases the growth of epithelial tumours, but does not result in spontaneous incidence of cancer, i.e. provides a “conducive environment for, but does not drive” tumour development (Hosur et al., 2014).

This is consistent with the life-time risk of developing OSCC in TOC, which tends to occur by the age of 65, rather than patients developing oesophageal tumours early as seen with other cancer-driving mutations. The findings of Hosur et al. (2014), with regard to the effect of iRhom2 GOF on tumour development, provide further insight into the TOC

phenotype, and support the hypothesis of accelerated and dysregulated wound healing in tissues subjected to stress.

6.5.1 ADAM17 in cancer development and progression

As described in Chapter 1, ADAM17 expression and activity is dysregulated in a number of cancer types including NSCLC (Zhou et al., 2006; Ni et al., 2013), gastric cancer (Warneke et al., 2013), ovarian, prostate, breast (Lendeckel et al., 2005; Kenny and Bissell, 2007; Sinnathamby et al., 2011; Narita et al., 2012), pancreatic (Ringel et al., 2006), colorectal, gastrointestinal (Blanchot-Jossic et al., 2005; Nakagawa et al., 2005), and head and neck cancer (Stokes et al., 2010; Kornfeld et al., 2011). ADAM17 is also associated with tumour progression through immune modulation and recruitment of TAMs (e.g. Talmadge et al. 2007; Kenny & Bissell 2007; Scheller et al. 2011; Das et al. 2012).

ADAM17 has also been implicated in enhancing communication between tumour and stromal cells, thus mediating tumour progression. Cancer-associated fibroblasts isolated from breast tumours secreted higher levels of TGF-α than normal fibroblasts, and conditioned medium from the cells promoted growth of TGF-α-negative breast cancer cells (Gao et al., 2013). ADAM17, as well as ADAM10, may have a role in dampening the immune response by shedding major histocompatibility complex (MHC) class 1 molecules required for tumour cell recognition by the immune system (Chitadze et al., 2013).

Recently, a role for ADAM17 in regulating stemness was also reported (Kamarajan et al., 2013; Hong et al., 2014). In HNSCC cell line UM-SCC-14A, orasphere formation (a marker of stemness) was inhibited by metalloprotease inhibitor TAPI-2 and by ADAM17 shRNA, likely by inhibiting ADAM17-mediated cleavage of CD44. ADAM17 shRNA also reduced tumour incidence and volume (Kamarajan et al., 2013). RECK also inhibited expression of stemness markers in gastric cancer cells by suppressing ADAM17-mediated NOTCH activation (Hong et al., 2014). In contrast, Guinea-Viniegra et al. (2012) reported suppression of skin cancer by ADAM17 through NOTCH-mediated differentiation.

6.5.2 Eph/Ephrin signalling in cancer

Results shown in chapters 4 and 5 suggested changes in EphA2 and EphA4 in TOC epidermis and keratinocytes, as well as a potential up-regulation of Ephrin B3 in preliminary IHC of OSCC biopsies. Further study of the wider Eph/Ephrin signalling pathway would be of interest in TOC and OSCC in association with iRHOM2-ADAM17 signalling and downstream pathways. The Eph/Ephrin pathway has been implicated in proliferation, angiogenesis, invasion and metastasis in a number of cancers; Eph

receptors and Ephrin ligands also play complex roles in signalling and cross-talk with other pathways (Chen, 2012).

EphA4 and EphA2 expression was reported as a prognostic factor in gastric cancer (Miyazaki et al., 2013), with high expression correlating with poor survival. In contrast, Giaginis et al. (2014) reported better survival associated with EphA4 expression in NSCLC patients, where expression was seen in low-grade tumours and associated with inflammation. The outcome of Eph receptor signalling may depend on the Ephrin ligands present, for example, Ephrin B3 inhibits the pro-apoptotic functions of EphA4 in adult neurogenesis (Furne et al., 2010), while Ephrin A1 acts antagonistically to EphA2 in the skin (Lin et al., 2010).

A further potential tumour-suppressive role was described for EphA4 in regulating EMT and adhesion via the β1-integrin pathway in hepatoma cells (Yan et al., 2013): EphA4 was down-regulated by MiR-10a, which was overexpressed in cancerous hepatoma tissues. Different effects of MiR-10a overexpression were seen in invasion and metastasis *in vitro* and in metastasis *in vivo*, perhaps relating to effects of EphA4 on the extracellular matrix (Yan et al., 2013). Yan et al. did not comment on the presence of Ephrin B3 or other Ephrin ligands, which could affect EphA4 signalling. This may also explain some of the differences seen between *in vitro* and *in vivo* effects of MiR-10a overexpression.

EphA2 is perhaps the best studied Eph receptor in cancer, with high expression of this receptor frequently correlating with poor prognosis, for example in NSCLC, breast and pancreatic cancer (e.g. Duxbury et al. 2004; Brannan et al. 2009; Faoro et al., 2010; Kinch et al., 2003; Martin et al., 2008; Zhuang et al., 2010; Brantley-Sieders, 2012). In contrast to many findings of poor prognosis associated with EphA2 expression, favourable survival of patients expressing EphA2 and Ephrin A1 mRNA was reported in stage 1 NSCLC patients (Ishikawa et al., 2012). Higher EphA2 expression was reported more commonly in women, non-smokers and in tumours carrying EGFR mutations (Ishikawa et al., 2012). This is consistent with EphA2 as a target of EGFR signalling, but contrasts with the findings of Brannan et al (2009) who found higher EphA2 expression in smokers with K-ras but not EGFR mutations in NSCLC, and saw an association between increased EphA2 expression and poor prognosis. This indicates a tumour-suppressor role for the Ephrin A1 ligand, demonstrating the different effects of ligand-dependent and independent Eph/Ephrin signalling. Consistent with this, EphA2 and Ephrin A1 expression was shown to be mutually exclusive in breast cancer cell lines (Macrae et al., 2005).

EphA2 has been implicated in tumour initiation and progression (e.g. Zelinski et al. 2001; Duxbury et al. 2004; Brantley-sieders et al. 2008; Martin et al. 2008; Zhuang et al. 2010). Pro-tumour EphA2 signalling appears to be mediated in a mostly ligand independent manner (Brantley-sieders et al., 2008; Yang et al., 2011); Ephrin A1-dependent activation of EphA2 suppressed growth of prostate cancer cell line PC3 via inhibition of the Akt-mTORC1 pathway (Yang et al., 2011). This was consistent with the findings of Ishikawa et al (2012) in NSCLC. Knock down of EphA2 in glioma cell lines inhibited stem-cell like properties, including self-renewal and stem cell marker expression, and also inhibited tumorigenesis of the cells *in vivo.* Stemness of the cells was inhibited by disrupting cross-talk with the Akt pathway, but this did not reduce tumorigenesis (Miao et al., 2014). As a role for ADAM17 in stemness was also described in HNSCC (Kamarajan et al., 2013; Hong et al., 2014), future investigation of a link between the ADAM17-EGFR-EphA2 signalling in cancer progression and stemness may be interesting.

The different associations between EphA2 and EphA4 expression in terms of outcome or survival in different cancers demonstrate the complex and varying roles of Eph/Ephrin signalling. They may also indicate differential roles for EphA2 depending on the stage of tumour development and progression, and on the presence of Ephrin ligands. This also highlights the complexity of developing any potential therapies targeting the Eph/Ephrin pathway. However, targeting of EphB4 in a mouse model of oesophageal cancer appeared to be promising in preventing tumour progression (Hasina et al., 2013). Furthermore, inhibition of Ephrin B3 in NSCLC combined with ionising radiation treatment resulted in senescence, activation of cell-death pathways and alteration of the Akt pathway, a mechanism implicated in combined treatment with ionising radiation and staurosporine analogue PKC-142 to target radiation-resistant NSCLC cells (Ståhl et al., 2013).

As discussed in Chapter 5, EphB4 has been studied in cancer as a binding partner of Ephrin B3. In addition, EphB4 overexpression was identified in a number of cancers, including breast cancer (Wu et al., 2004), prostate cancer (Lee et al., 2005; Xia et al., 2005), bladder cancer (Xia et al., 2006) and ovarian cancer (Kumar et al., 2007). EphB4 mediated tumour cell survival, migration and invasion *in vitro* in addition to promoting tumour growth in a xenograft mouse model of breast cancer (Kumar et al., 2007). This likely occurred via ligand-independent signalling, as the presence of Ephrin B2 inhibited the viability of breast cancer cells. EphB4 is a substrate of ADAM17, and interestingly, its PMA-induced shedding was abrogated in iRhom2$^{-/-}$ MEFs (Maretzky et al., 2013) suggesting a further role for iRhom2 in regulating Eph/Ephrin signalling via ADAM17. EphB4 also appeared to be regulated by EGFR signalling in bladder cancer cell lines

and xenograft models, with EphA4 knock down reducing tumour volume by almost 80 %, and reducing *in vitro* migration, migration and angiogenesis (Xia et al., 2006).

Increased expression of EphB4 was seen in OSCC and oesophageal adenocarcinoma (Hasina et al., 2013), as well as a correlation with the grade of the tumour. Hasina et al. (2013) also identified an increased gene copy number of EphB4 in a number of OSCC and adenocarcinoma tumour samples. EphB4-targeting siRNA and a small molecule inhibitor of EphB4 (AZ12489875-002) both inhibited proliferation and migration of OSCC and adenocarcinoma cell lines, and also reduced tumour growth in a chemically-induced oesophageal cancer mouse model. The development of the tumours in the mouse model was also associated with an increase in EphB4 expression (Hasina et al., 2013), consistent with a role for EphB4 in tumour growth.

6.5.3 IGF-1 Receptor

IGF-1R has also been implicated as a potential target for treatment of oesophageal and gastrointestinal cancer (Piao et al., 2008; Adachi et al., 2014), and increased phosphorylation of IGF-1R in TOC keratinocytes compared to NEB1 control cells was seen in phospho-arrays shown in Chapter 4. Ligand binding and activation of IGF-1R results in downstream phosphorylation and activation of pathways including Akt and MAPK (Chitnis et al., 2008). IGF-1R expression is increased in a number of cancers (Baserga, 1994; Chitnis et al., 2008; Werner, 2012), including in a high percentage of oesophageal cancer samples (Ouban et al., 2003; Imsumran et al., 2007; Adachi et al., 2014), and has been associated with Akt-mediated resistance to chemotherapy (Imsumran et al., 2007; Kyula et al., 2010; Adachi et al., 2014).

IGF-1R is an important mediator of malignant transformation in many cells, often facilitating cancer progression after a 'first hit' driver event has occurred (Chitnis et al., 2008; Werner, 2012). A number of clinical trials of therapies targeting IGF-1R in cancer are underway (http://www.clinicaltrials.gov/ct2/results?term=IGF-1R&Search=Search; accessed 21/7/14), including one phase II trial in oesophageal cancer testing IGF-1R-targeting monoclonal antibody cuxitumumab in combination with chemotherapeutic agent paclitaxel (www.clinicaltrials.gov ref NCT01142388). However, targeting of IGF-1R can be complicated by its high homology to the insulin receptor (Imsumran et al., 2007).

6.5.4 Desmosomes in cancer

Dysregulation of adhesion molecules and cell-cell junctions is a critical step in the progression of cancer, with roles for proteins of AJ, TJ, connexins and desmosomes demonstrated in a wide range of cancers (Reynolds and Roczniak-Ferguson, 2004; Carneiro et al., 2012; Valenta et al., 2012; Ding et al., 2013; Gall and Frampton, 2013; Kwon, 2013; Runkle and Mu, 2013; Martin et al., 2014). Many desmosomal proteins have

been shown to be involved in intracellular signalling (Green and Simpson, 2007; Thomason et al., 2010), and desmosomes appeared dysregulated in TOC epidermis, which could suggest that dysregulation of desmosomal adhesion could be one of the mechanisms involved in development of OSCC in TOC.

Desmosomes play a variety of roles in cancer through adhesion-dependent and independent processes. The increased processing of DSG2 by ADAM17 (Chapter 3; Brooke et al. 2014) could therefore play a role in OSCC development or progression. Alternatively, depletion of other desmosomal proteins due to DSG2 processing and/or increased EGFR signalling may have further downstream effects. DSG2 and PG play a role in mediating apoptosis and cell survival, for example (Brennan et al., 2007; Nava et al., 2007; Ryan et al., 2012).

A role for DSG2 has been shown in a number of cutaneous cancers. Up-regulation of DSG2 was seen in basal cell carcinoma (BCC), SCC, sweat gland carcinoma and adenocarcinoma (Brennan and Mahoney, 2009). Re-localisation of DSG2 from the membrane to the cytoplasm and nucleus was seen in cutaneous SCC (Kurzen et al. 2003; Brennan and Mahoney, 2009) and nuclear and cytoplasmic DSG2 was seen in mice overexpressing Dsg2 (Brennan et al., 2007). Furthermore, DSG2 was expressed more frequently in high-risk SCCs than low-risk SCCs (Kurzen et al., 2003), perhaps suggesting a role in cancer progression outside of adhesion in the desmosome.

DSG2 overexpression in the suprabasal layers of transgenic mouse skin caused alteration in cytoskeletal organisation, cornified envelope hyperplasia and hyperproliferation. Over half of the mice developed benign papillomas by 6 weeks to 3 months of age, and the mice were much more susceptible to chemical-induced carcinogenesis, although no increase in the invasiveness of the tumours was seen (Brennan et al., 2007).

Other desmosomal proteins are also dysregulated in a number of other cancers, acting as tumour suppressors or mediating cancer development through adhesion-dependent and independent mechanisms (Brooke et al., 2012; Al-Jassar et al., 2013). Some recent examples include the following: Reduced expression of DSG3 correlated with worse survival in oesophageal SCC (Fang et al., 2014) with protein levels correlating with those of PG and DSP. Overexpression of DSG3 in Head and Neck cancer primary tumours and cell lines correlated with tumour stage, depth and extracapsular spread in lymph nodes (Chen et al., 2007), while DSG3 knock down resulted in PG translocation to the nucleus in head and neck cancer cell lines, where it regulated cell migration, invasion and cell growth via the TCF/LEF transcription factors (Chen et al., 2013).

Reduced PG mRNA was seen in prostate cancer samples (Shiina et al., 2005) resulting from methylation, partial methylation and LOH mechanisms. Down-regulation of desmocollins has also been reported in a number of cancers (e.g. Cui et al. 2011; Cui et al. 2012a; Cui et al. 2012b; Kolegraff et al. 2011) and loss of DSC3 due to promoter methylation was a predictor of poor clinical outcome in colon cancer (Cui et al., 2011). DSP was also shown to act as a tumour suppressor by inhibiting the Wnt/β-catenin pathway in human lung cancer (Yang et al., 2012).

A switch between DSG2 and DSG3 expression was seen in OSCC (Teh et al., 2011), suggesting that further investigation of DSG expression and processing in the oesophagus may be of interest, particularly as increased DSG2 processing was seen in TOC keratinocytes (Chapter 3; Brooke et al. 2014). Isoform switching was also reported for desmocollins in colon cancer and colorectal dysplasia (Khan et al., 2006). The p53/p63 target gene Perp, which is required for desmosomal assembly (Attardi et al., 2000; Ihrie et al., 2005), may also play a role in tumour development, as $Perp^{fl/fl}$ mice were resistant to papilloma development after treatment with TPA (Marques et al., 2005).

6.5.5 iRHOM1 in cancer

Roles for iRHOM1 have been demonstrated in breast cancer and HNSCC. siRNA knock down of iRHOM1 affected pathways downstream of EGFR, shown by reduced levels of the phospho-ERK and phospho-Akt in MDA-MDB-435 breast cancer cells and HNSCC 1483 cells (Yan et al., 2008). In addition, knock down of iRHOM1 reduced levels of phospho-EGFR and its downstream target p44/p42 MAPK following stimulation with GRP (Zou et al., 2009). Basal levels of p44/p42 MAPK phosphorylation were reduced, as well as the ability of serum-starved HNSCC 1483 cells to migrate into matrigel in response to GRP (Zou et al 2009).

siRNA knock down of iRHOM1 in MDA-MB-435 breast cancer cell lines reduced growth and proliferation and increased levels of apoptosis. Similarly, in HNSCC cell line 1483, siRNA against iRHOM1 caused a reduction in proliferation and an increase in autophagy (Yan et al., 2008). In addition, delivery of iRHOM1 siRNA to xenograft tumours made with MDA-MDB-435 cells or HNSCC 1483 cells significantly inhibited tumour growth (Yan et al., 2008). iRHOM1 levels were reduced by around 50 % in the tumours.

As discussed in section 6.4.2, iRHOM1 regulates HIF-1α stability in breast cancer (Zhou et al., 2014). Increased *RHBDF1*/iRHOM1 expression correlated with increases in HIF-1α expression, and was associated with worse prognosis, faster progression, and poor response to chemotherapy (Zhou et al., 2014). Targeting of iRHOM1 and HSP90 may therefore be a possible way to overcome drug resistance in cancer, which is often

associated with hypoxia. Further investigation of the role of both iRHOM proteins in hypoxia may be of interest in future studies of cancer progression.

6.5.6 Why do iRHOM2 mutations specifically cause Oesophageal SCC?

While the data presented in this thesis and that described in Hosur et al (2014) support the hypothesis of iRHOM2-TOC and iRHOM2-*cub* GOF mutations being associated with dysregulated, accelerated wound healing in tissues subjected to stress, the oesophagus is not the only area of the GI tract subjected to high levels of stress, and incidence of other cancers does not appear to be increased in TOC (Ellis et al., 1994; Stevens et al., 1996).

This suggests that tissue-specific variation in expression of iRHOM2 and other tissue-specific factors may play a role in OSCC development in TOC. Some examples may include tissue-specific regulators of iRHOM2/ADAM17 expression such as miRNAs, downstream mediators of the signalling pathways affected, and the balance of growth factor signalling in the tissues.

Tissue specific expression of other proteins may also play a role. For example, the presence or absence of Ephrin ligands affects the function of Eph receptors which may function in ligand-dependent or independent manners. Expression of specific desmosomal cadherins such as DSG2 may also be a factor that could affect adhesion and cellular signalling, and isoform switching of DSG2 and 3 has been demonstrated in oesophageal cancer (Teh et al., 2011). Results in chapter 4 suggest that NOTCH signalling may also be dysregulated in TOC. NOTCH is known to act as a tumour suppressor in some tissues, but as an oncogene in others (South, 2012), so disruption of the balance of this signalling pathway could contribute to tissue-specific effects at different stages of cancer development and progression.

6.6 ADAM17 as a therapeutic target

Due to its wide range of substrates, and its role in regulating and mediating a number of signalling processes such as shedding of inflammatory molecule TNF-α, ADAM17 was identified as a promising target for the development of small molecule inhibitors. These compounds were developed for treatment of a number of conditions, including rheumatoid arthritis and cancer, and were developed with varying degrees of specificity: many also target MMPs and other ADAM family members (Moss, Sklair-Tavron and Nudelman, 2008; Arribas and Esselens, 2009; Rose-John, 2013). Inhibition of ADAM17 proved promising in pre-clinical studies and animal models, but results from early clinical

trials have given disappointing results with respect to both efficacy and toxicity (Moss et al., 2008).

6.6.1 The effect of ADAM17 loss-of-function in mice and humans

A major concern in targeting ADAM17 is the high risk of toxicity and adverse events. ADAM17 knock-out in mouse is lethal (Peschon et al., 1998). Horiuchi et al. (2009) generated a conditional ADAM17 knock-out mouse using the SOX9 promoter to specifically knock-out ADAM17 in non-haematopoietic cells. The mice survived 6-9 months (into adulthood), suffering from growth retardation, infertility, skin defects, bone loss and osteoporosis-like symptoms. The mice also suffered defects in the haematopoietic system, which did not result from lack of ADAM17 in haematopoietic cells (Horiuchi et al., 2009). This also suggests that ADAM17 inhibition may have severe consequences, particularly in long-term chronic therapy.

As described previously, loss of ADAM17 function in humans appears to result in a less severe phenotype (Blaydon et al., 2011), although ADAM17 LOF does result in severe inflammatory skin and bowel disease, and a high incidence of infection (Blaydon et al., 2011), again suggesting that there are likely to be a number of adverse events associated with ADAM17 inhibition. A number of the effects of ADAM17 inhibition are likely mediated through reduced EGFR signalling, as a similar phenotype was associated with a LOF mutation in EGFR (Campbell et al., 2014).

6.6.2 ADAM17 therapy in cancer

As described earlier in this chapter, ADAM17 is overexpressed in a number of cancers including breast cancer (Borrell-Pagès et al., 2003), and is associated with poor prognosis and disease progression (e.g. Sinnathamby et al., 2011; Stokes et al., 2010; Zhou et al., 2006; Narita et al., 2012; Ringel et al., 2006; Kornfeld et al., 2011; Chen et al., 2013; Hong et al., 2014; Kamarajan et al., 2013). The role of ADAM17 in many different aspects of cancer development and progression (section 6.6.1), such as migration and invasion (Chen et al., 2013; Giricz et al., 2013; Gao et al., 2013; Wang et al., 2013; Das et al., 2012), angiogenesis (Blanchot-Jossic et al., 2005; Tsai et al., 2009) and immune cell recruitment and modulation (e.g. Lin et al., 2001; Lin et al., 2006; Kenny and Bissell 2007; Talmadge et al., 2007; Ojalvo et al., 2009; Erreni et al., 2011; Scheller et al., 2011), may suggest that inhibition of ADAM17 would provide a multi-faceted approach to targeting tumours. Furthermore, the nature of cancer, and more acute therapeutic strategy, may suggest a greater tolerability to adverse events than in a chronic condition such as arthritis (Arribas and Esselens, 2009).

ADAM17 has been successfully targeted in a number of cancer cell models *in vitro* and *in vivo* (Kenny & Bissell 2007; Chen et al. 2013; Das et al. 2012; Giricz et al. 2013).

Sinnathamby et al (Sinnathamby et al., 2011) also identified ADAM17 as a target for immunotherapy in breast, prostate and ovarian cancers through specific processing of an ADAM17 HLA-A2 restricted epitope by cancer cells but not normal cells (Sinnathamby et al., 2011). INCB3619 has been shown to work synergistically with chemotherapeutic agent paclitaxel to reduce tumour volume in a mouse model of NSCLC (Zhou et al., 2006) and Richards et al (2012) reported a specific anti-ADAM17 antibody, D1(A12), which showed anti-tumour effects in an *in vivo* ovarian cancer mouse model.

ADAM17 has also been associated with acquired resistance to chemotherapy and therapies targeting the EGFR pathways. Some examples include resistance to cisplatin in hepatocellular carcinoma via EGFR/PI3K/Akt signalling (Wang et al., 2013); resistance to gefitnib in NSCLC via up-regulation of HER-3 and Akt (Zhou et al., 2006); and resistance to 5-fluorouracil (5-FU) in *in vitro* and *in vivo* models of colorectal cancer (Kyula et al., 2010). This ADAM17-mediated 5-FU resistance in colorectal cancer cells was also associated with up-regulation of HER-3, although ADAM17 siRNA only appeared to result in a small reduction in HER-3 levels. ADAM17 siRNA did help to reduced tumour volume in a xenograft model and reduce phosphorylation of $EGFR^{Y1068}$, however (Kyula et al., 2010). These findings suggest that combining EGFR tyrosine kinase inhibitors with ADAM17 inhibition may help to overcome one mechanism of resistance (Arribas and Esselens, 2009). In support of this, combined EGFR and ADAM17 inhibition therapy in breast cancer cells *in vitro* and in *in vivo* xenograft models resulted in synergistic inhibition of cell and tumour growth (Witters et al., 2008), including reducing levels of phosphorylated HER-3 and Akt, which are associated with chemotherapy resistance (Witters et al., 2008).

6.6.3 Could targeting the iRHOMs represent an alternative method of targeting ADAM17?

Targeting of tissue-specific downstream effectors, or ADAM17 regulators such as the iRHOMs, or perhaps miRNAs, may provide a more targeted, tissue-specific approach and reduce side effects associated with ADAM17-targeting therapy. iRHOM1 knock-out in mouse had severe consequences, resulting in death approximately 6 weeks after birth (Christova et al., 2013). However, although associated with severe inflammatory syndromes in humans, knock-out of ADAM17 and EGFR appears less severe (Blaydon et al., 2011; Campbell et al., 2014), so the same could be true of iRHOM1 as it regulates many of the same pathways. iRHOM2 knock-out mice appear generally healthy (McIlwain et al., 2012; Hosur et al., 2014), although response to infection was altered (McIlwain et al., 2012). Tissue-specific blocking of iRHOM2 would lead to specific

inhibition of ADAM17 maturation in the immune cells, but iRHOM1 would allow processing of at least some ADAM17 in other tissues (Rose-John, 2013).

iRHOM2 appears to play an important role in modulating the immune system. As discussed in chapter 4.3, iRhom2$^{-/-}$ mice were protected against septic shock and liver damage (McIlwain et al., 2012), consistent with Mohler et al (1994) who showed protection against septic shock with ADAM17 inhibition, However, the defence of the iRhom2$^{-/-}$ mice against *L. monocytogenes* was impaired, with mice succumbing to the infection much more quickly than WT mice (McIlwain et al., 2012). Furthermore, TOC keratinocytes showed reduced adhesion and invasion of *S. aureus*, which was reversed by ADAM17 inhibition (Brooke et al., 2014) and interestingly, PMA stimulation of TOC PBMCs, but not LPS stimulation, produced a dramatic increase in shedding of TNF-α. Overall, this suggests that iRHOM2 may be a potential target for treatment of septic shock, but that inhibiting iRHOM2 may result in greater susceptibility to other types of infection. Indeed, anti-TNF-α therapies for treating rheumatoid arthritis were shown to be associated with increased incidence of infection in a meta-analysis of clinical trials and publications relating to TNF-α therapy (Bongartz et al., 2006).

The tissue-specific expression of iRHOM1 and iRHOM2, with absence of iRHOM1 in immune cells, means that rheumatoid arthritis is another potential target for ADAM17 inhibition. Issuree et al (2013) demonstrated a role for iRHOM2 in mediating rheumatoid arthritis, as mice lacking iRHOM2 were protected against K/BxN inflammatory arthritis, which was associated with increased iRhom2/ADAM17-dependent shedding of TNF-α. iRHOM2 may also therefore provide a tissue-specific target for modulation of ADAM17 activity in the tumour immune response, as modulation of iRHOM2 may be compensated by iRHOM1 activity in non-haematopoietic tissues. Furthermore, the rheumatoid joint is hypoxic, and iRHOM1 mediates hypoxia-induced responses in breast cancer (Zhou et al., 2014), suggesting that research into iRHOM2 in hypoxia may provide further insight into its role in rheumatoid arthritis, and also in cancer, where iRHOM1 and ADAM17 are known to mediate hypoxia and HIF-1α-induced resistance to chemotherapy (Zhou et al., 2014).

6.7 Future Work

A number of findings in this work suggest further investigation and follow-up studies may be of interest, as well as performing further repeats of the experiments presented to confirm the findings, many of which are preliminary. Areas for further investigation include the localisation of iRHOM2, uncovering further binding partners and roles for iRHOM2, and further investigation of the Eph/Ephrin and NOTCH signalling pathways in keratinocyte migration, proliferation and adhesion. Further investigation of these pathways in oesophageal cancer and other squamous cell cancers such as HNSCC would also be of interest.

6.7.1 iRHOM2 localisation

During ICC experiments presented in this thesis, the localisation of iRHOM2 appeared variable, and in both IHC and ICC, the staining had a punctate appearance. To further investigate the localisation of iRHOM2, further co-localisation of iRHOM2 could be performed with markers of cell compartments such as the ER, golgi and vesicular markers, as well as further cell-surface markers and a marker of lipid rafts such as caveolin to further dissect the precise subcellular localisation of iRHOM2. Future IHC and ICC studies could include isotype-matched negative controls where the sections or cells are incubated with an IgG to ensure that the antibody is not binding non-specifically to cell-surface proteins via the IgG domain. This could be further confirmed biochemically with subcellular fractionation, for example sucrose gradients.

Further confirmation of co-localisation with iRHOM2 binding partners could include techniques such as fluorescence-resonance energy transfer (FRET) or the DuoLink® assay (Olink bioscience, Uppsalla, Sweden; Gullberg et al. 2010), another method of measuring the distance between two proteins and whether they are likely to interact. DuoLink® is a proximity ligation assay in which cells are treated with two probes against one or two primary antibodies. The probes are detected only if they are within a certain proximity of one another, thus confirming co-localisation. Co-immunoprecipitation with ADAM17 and any other binding partners could also be performed to see whether iRHOM2 protein-protein interactions are affected in TOC, and to determine whether the stability of the iRHOM2-ADAM17 interaction is also enhanced in TOC.

Live cell imaging experiments with tagged iRHOM2, ADAM17 and any other iRHOM2 binding partners identified would show more about iRHOM2 regulation and trafficking in different conditions, for example whether iRHOM2 is recycled, and how quickly WT and mutant iRHOM2 is degraded in human skin (compared with the findings of Hosur et al. 2014)

Finally, further investigation of the tissue-specific localisation of iRHOM2 would be of interest, for example in cancerous and adjacent normal tissue, and how this compares with the localisation of iRHOM1. Investigation of the cell-surface localisation of iRHOM2 in squamous tissues is an important question currently being addressed (Dr Thiviyani Maruthappu, CCR, Blizard Institute, QMUL) in addition to identification of iRHOM2 binding partners such as type I keratins following a yeast two hybrid screen, which may uncover further functions of iRHOM2.

6.7.2 Migration and wound healing

To further investigate the downstream pathways mediating the change in the rate of migration in TOC keratinocytes, i*n vitro* scratch and proliferation assays could be performed in the presence and absence of siRNA and inhibitors of various cell pathways, such as members of the Eph/Ephrin family (including EphA2, EphA4 and EphB4), Insulin-R and IGF-1R. Migration assays with ADAM17 and ADAM10 inhibitors have been carried out by Dr Matthew Brooke, confirming that the increased migration is largely dependent on ADAM17. Transwell migration (and invasion) assays could be performed to look further at the migration phenotype in TOC, and in OSCC and HNSCC cancer cell lines with high and low iRHOM2 and ADAM17 expression.

Experimental tools to further these findings may include development of stable cell lines as transient transfection efficiency of iRHOM2 was low in this work; wound healing assays in 3D skin and oesophagus equivalents; and potentially *in vivo* wound healing assays in a mouse model overexpressing the iRHOM2-TOC mutations. This could perhaps be compared with iRhom2$^{-/-}$ and iRhom2$^{cub/cub}$ mice if they were available. As changes appear to be mediated by AREG (Brooke et al., 2014; Hosur et al., 2014), treatment of cells with exogenous AREG, or conditioned medium from TOC cells with or without AREG, iRHOM2 or ADAM17 siRNA could determine how much of the effect in TOC is due to AREG shedding. This could further determine how much of the AREG shedding is independent of ADAM17, which often needs a stimulus such as PMA/ionomycin or LPS for its activity to increase above basal levels, including in ADAM17 overexpressing mice (Yoda et al., 2013).

As iRHOM2 expression appeared concentrated at the edge of some tumour tissues, staining of iRHOM2 and ADAM17 at the edge of scratches in wound-healing assays in keratinocytes and OSCC cell lines would be of interest; in addition to invasion assays with and without iRHOM2 and ADAM17 siRNA or inhibitors.

6.7.3 Adhesion and desmosomal dysregulation

As the desmosomes were dysregulated in TOC, and the Eph/Ephrin pathway has also been associated with cellular adhesion, further investigation of adhesion in TOC would be interesting. Initially, further experiments to investigate DSG2 processing could be performed, to increase the number of experiments, and to determine how much of the dysregulation depends on the change in EGFR signalling by using EGFR and ADAM17 inhibitors, and iRHOM2 siRNA.

To look further at desmosomal regulation in TOC, it would also be interesting to investigate expression and localisation of the desmosomal cadherins DSG1 and 3 and DSC1, which were not investigated in this thesis. Due to their expression predominantly in the upper epidermal layers, this could be performed in 3D raft cultures to determine whether their expression differs in a 3D stratified tissue structure. EM of 3D cultures with TOC keratinocytes with and without ADAM17 inhibitors or siRNA or inhibitors could be performed to look at the desmosomal midline. This could also be performed following treatment with ADAM17 and EGFR inhibitors. Processing of DSG2 and other cadherins could be studied with western blotting, to determine whether the lack of midline is a direct effect of EGFR signalling, or also dependent on other iRHOM2-dependent pathways.

Dispase and adhesion assays could be performed *in vitro* to measure cell-cell adhesion in the different conditions, and the adhesion of TOC and control cells to the cell culture dish could also be tested. Stretching of the cells in monolayer followed by dispase assays and light microscopy could be a way to see whether subjecting the cells to mechanical stress stimulates an increase in wound healing behaviour of the cells, as hyperproliferation is seen in areas of stressed skin in TOC. ELISA assays to look at shedding of ADAM17 substrates could help determine which molecules may be mediating the response. Live cell imaging with tagged desmosomal proteins co-transfected with WT and mutant iRHOM2 (or in stable cell lines) to investigate trafficking and assembly of desmosomes and how this is affected by the TOC mutations. Exogenous AREG or EGF could be applied to the cells during the imaging and the time course of any remodelling captured, with or without EGFR inhibitors.

6.7.4 iRHOM2-ADAM17 regulation of expression and activity

Regulation of iRHOM2 appears to occur at least in part through ADAM17, as ADAM17 knock down also reduced levels of iRHOM2. It would be interesting to look at levels of iRHOM1 in the HNSCC cell lines, as iRHOM1 can also traffick ADAM17 from ER to golgi, and has been shown to be altered in HNSCC cell lines and breast cancer.

ChIP assays are currently being performed by Dr Anissa Chikh to look at which transcription factors bind to the promoters of iRHOM2, ADAM17 and iRHOM1. This could

be followed by treatment of the cells with transcription factors in combination with a luciferase reporter assay for ADAM17 and iRHOM2 (and iRHOM1) to directly measure transcription and look further at regulation of their expression. This could be performed in the presence and absence of siRNA targeting the iRHOMs and ADAM17, and could be performed in control and TOC keratinocytes to determine how the mutations in iRHOM and increased activity affect regulation of the expression of proteins in this pathway.

Further investigation of post-transcriptional regulation of iRHOM2 and ADAM17 would also be of interest, for example, screening to identifty which microRNAs regulate iRHOM2 and ADAM17 expression in the skin and oesophagus. Proteins that regulate ADAM17 protein activity could also be investigated, such as TIMP3. This could also be investigated in the OSCC cell lines, and may explain some of the variability seen in ELISA assays presented in chapter 5.

6.7.5 NOTCH1 signalling

Preliminary data suggested enhanced NOTCH1 signalling in TOC, and a potential correlation between NOTCH1, iRHOM2 and ADAM17 expression in cancer cell lines. Further characterisation of NOTCH1 signalling in TOC and control keratinocytes could include subcellular fractionation and western blotting of total NOTCH1 and NOTCH NICD in the presence and absence of ADAM17 and ADAM10 inhibitors to confirm NOTCH1 localisation, which would also be useful to look at iRHOM2 and ADAM17 localisation. Use of ADAM17 and ADAM10 inhibitors followed by western blotting of NOTCH1 NICD and total NOTCH1 would determine whether NOTCH processing is in part mediated by enhanced ADAM17 activity. This is also being performed by Dr Anissa Chikh, CCR, Blizard Institute, QMUL.

qPCR and western blotting of downstream NOTCH genes, e.g. slug. In the presence and absence of EGFR inhibitors, and investigation of feedback between EGFR and NOTCH signalling in control and TOC keratinocytes may also reveal more about the role of NOTCH signalling in TOC. The Ctip2 transcription factor, for example, controls EGFR and NOTCH expression (Zhang et al., 2012).

It would be of interest to investigate other members of the NOTCH family in TOC skin and oesophagus, and to look at ADAM10 in these cells to determine whether its expression is also related to NOTCH signalling, and also whether ADAM10 activity and expression are affected by enhanced ADAM17 activity in TOC. Hosur et al (2014) reported decreased mRNA levels of ADAM10 substrate egf in iRhom2$^{cub/cub}$ mice. Investigation of NOTCH ligand expression and the effect of siRNA targeting NOTCH1 would also be interesting to determine whether ligand-dependent or independent

signalling or a combination of the two is modified in TOC (as ADAM10 has previously been reported to be the major regulator of ligand-dependent signalling and ADAM17 implicated in ligand-dependent signalling; Bozkulak & Weinmaster 2009). Further, determination of how NOTCH signalling is affected by the changes in EGFR signalling in TOC would also be interesting.

6.7.6 Further investigation of iRHOM2-ADAM17 in cancer

Further, *in vivo* assays could be performed to assess tumourigenesis and to investigate how increases in the iRHOM2-ADAM17 pathway enhance development and progression of cancer. ADAM17 has also been implicated in angiogenesis and the tumour immune response, so further investigation of these pathways would be of interest. Looking at expression of and the effect of inhibiting PI3K-Akt-mTOR signalling and the relationship with ADAM17-EGFR signalling in TOC in cancer cell lines, perhaps in relation to drug resistance, would also be interesting, as well as investigating how iRHOM1 is involved, and whether iRHOM2 also plays a role in mediating hypoxia-response and drug resistance.

Investigation of tumourigenesis and angiogenesis *in vivo* could also be performed, e.g. Xenografts experiments with stable cell lines overexpressing WT and mutant iRHOM2 could be performed in the presence and absence of ADAM17 inhibitors or siRNA against iRHOM1 or iRHOM2. Chemical carcinogenesis studies in mice overexpressing ADAM17 (Yoda et al., 2013) may also be interesting, and further research of the role of AREG, as ADAM17 overexpressing mice did not appear to have increased ADAM17 expression in all tissues (Yoda et al., 2013).

Investigation of iRHOM1 and iRHOM2 expression in primary tumours, and their association with poor survival / drug resistance (as in Zhou et al. 2014), particularly OSCC tumours, could help determine the stages of cancer development at which iRHOM2 is important. Further study of the Eph/Ephrin and NOTCH signalling pathways in OSCC may also be logical, as both these pathways have been widely implicated in cancer. The IGF2-IGF2R ligand-receptor pair was also associated with worse prognosis in epithelial ovarian cancer (Sayer et al., 2005), and may be of interest in OSCC research, as IGF-1R has been associated with oesophageal cancer.

6.7.7 Other potential future studies

ADAM17 activity has been implicated in a number of other diseases and conditions. The potential link with ADAM17 and Insulin-R / IGF-1R signalling and in mediating insulin resistance suggest that this pathway may be relevant to diabetes. Further investigation of iRHOM2 in diabetes models may therefore be of interest. Other functions of the

iRHOMs, such as ERAD, would also be interesting in TOC, and could be studied with proteasome inhibitors, as in Hosur et al (2014) for example.

Active rhomboid protease RHBDL2 also regulates EGF signalling, and many inactive protease-family enzymes regulate the same pathways as their active counterparts (Adrain and Freeman, 2012). This suggests that there may be some feedback between RHBDL2 and iRHOM activity. Furthermore, preliminary IHC suggested there may be some dysregulation of RHBDL2 in TOC, so this may be another avenue of future investigation. Further investigation of the effect of enhanced iRHOM2 stability in TOC on feedback to iRHOM1 expression and signalling would also be interesting, as iRHOM is involved in the regulation of ADAM17 trafficking.

6.8 Summary and Conclusions

Mutations in the inactive rhomboid protein iRHOM2 cause TOC, which is associated with enhanced ADAM17 trafficking and shedding of EGFR ligands, and desmosomal dysregulation (Blaydon et al., 2012; Brooke et al., 2014). This leads to enhanced migration and proliferation and an accelerated wound healing response in TOC keratinocytes. This work also suggested potential dysregulation in Eph/Ephrin signalling and the NOTCH signalling pathway, and enhanced barrier function and protection from infection have also been associated with TOC (Brooke et al., 2014). The iRHOM2 mutations appear to result from enhanced iRHOM2 stability, leading to increased availability and may also lead to enhanced shedding of AREG (Brooke et al., 2014; Hosur et al., 2014). Regulatory mechanisms of iRHOM2 and ADAM17 expression also appear to be related, including in cancer cell lines, and a role for this pathway in both OSCC and HNSCC has been suggested. Some points for future investigation include the role of iRHOM2 at the cell surface, determining which proteins and pathways are mediating the downstream effect of enhanced migration, and why TOC is specifically associated with oesophageal cancer.

References

Adachi, Y., Ohashi, H., Imsumran, A., Yamamoto, H., Matsunaga, Y., Taniguchi, H., Nosho, K., Suzuki, H., Sasaki, Y., Arimura, Y., Carbone, D. P., Imai, K. and Shinomura, Y. (2014) "The effect of IGF-I receptor blockade for human esophageal squamous cell carcinoma and adenocarcinoma" *Tumour biology* 35(2): 973–85.

Adrain, C. and Freeman, M. (2012) "New lives for old: evolution of pseudoenzyme function illustrated by iRhoms" *Nature reviews. Molecular cell biology*. 13(8): 489–98.

Adrain, C., Strisovsky, K., Zettl, M., Hu, L., Lemberg, M. K. and Freeman, M. (2011) "Mammalian EGF receptor activation by the rhomboid protease RHBDL2.," *EMBO reports*. 12(5): 421–7.

Adrain, C., Zettl, M., Christova, Y., Taylor, N. and Freeman, M. (2012) "Tumor necrosis factor signaling requires iRhom2 to promote trafficking and activation of TACE," *Science*, 335(6065): 225–228.

Agrawal, N., Frederick, M. J., Pickering, C. R., Chang, K., Li, R. J., Fakhry, C., Xie, T., Zhang, J., Wang, J., Zhang, N., El-naggar, A. K., Jasser, S. A., Weinstein, J. N., Treviño, L., Drummond, J. A., Muzny, D. M., Wu, Y., Wood, L. D., Hruban, R. H., Westra, W. H., Koch, W. M., Califano, J. A., Richard, A., Sidransky, D., Vogelstein, B., Velculescu, V. E., Wheeler, D. A., Kinzler, K. W., Myers, J. N. and Street, N. W. (2011) "Exome Sequencing of Head and Neck Squamous Cell Carcinoma Reveals Inactivating Mutations in NOTCH1," *Science*, 333(6046):1154–1157.

Agrawal, N., Jiao, Y., Bettegowda, C., Hutfless, S., Wang, Y., David, S., Cheng, Y., Twaddell, W., Latt, N., Shin, E., Wang, L.-D., Wang, L., Yang, W., Velculescu, V., Vegelstein, B., Papadopoulos, N., Kinzler, K. and Meltzer, S. (2012) "Comparative genomic analysis of esophageal adenocarcinoma and squamous cell carcinoma," *Cancer discovery*, 2(10): 899–905.

Ahmed, H. and O'Toole, E. a (2014) "Recent advances in the genetics and management of harlequin ichthyosis." *Pediatric dermatology*, 31(5): 539–46.

Aho, S. and Uitto, J. (1998) "Two-hybrid analysis reveals multiple direct interactions for thrombospondin 1." *Matrix Biology*, 17(6): 401–412.

Akiyama, M. (2011) "The roles of ABCA12 in keratinocyte differentiation and lipid barrier formation in the epidermis." *Dermato-endocrinology*, 3(2): 107–12.

Akiyama, M., Sakai, K., Sugiyama-Nakagiri, Y., Yamanaka, Y., McMillan, J. R., Sawamura, D., Niizeki, H., Miyagawa, S. and Shimizu, H. (2006) "Compound heterozygous mutations including a de novo missense mutation in ABCA12 led to a case of harlequin ichthyosis with moderate clinical severity." *The Journal of investigative dermatology*, 126(7): 1518–23.

Akiyama, M., Titeux, M., Sakai, K., McMillan, J. R., Tonasso, L., Calvas, P., Jossic, F., Hovnanian, A. and Shimizu, H. (2007) "DNA-based prenatal diagnosis of harlequin ichthyosis and characterization of ABCA12 mutation consequences.," *The Journal of investigative dermatology*, 127(3): 568–73.

Alessi, D. R., Pearce, L. R. and García-Martínez, J. M. (2009) "New insights into mTOR signaling: mTORC2 and beyond.," *Science signaling*, 2(67): e27.

Al-Jassar, C., Bikker, H., Overduin, M. and Chidgey, M. (2013) "Mechanistic basis of desmosome-targeted diseases.," *Journal of molecular biology*. 425(21): 4006–22.

Altorki, N. K., Lee, P. C., Liss, Y., Meherally, D., Korst, R. J., Christos, P., Mazumdar, M. and Port, J. L. (2008) “Multifocal neoplasia and nodal metastases in T1 esophageal carcinoma: implications for endoscopic treatment.,” *Annals of surgery*, 247(3): 434–9.

Amagai, M., Klaus-Kovtun, V. and Stanley, J. R. (1991) “Autoantibodies against a novel epithelial cadherin in pemphigus vulgaris, a disease of cell adhesion.” *Cell*, 67(5): 869–77.

Amagai, M. and Stanley, J. R. (2012) “Desmoglein as a target in skin disease and beyond.,” *The Journal of investigative dermatology*. 132(3 Pt 2): 776–84.

Ambler, C. A. and Watt, F. M. (2010) “Adult epidermal Notch activity induces dermal accumulation of T cells and neural crest derivatives through upregulation of jagged 1.,” *Development*, 137(21): 3569–79.

Amour, A., Slocombe, P. M., Webster, A., Butler, M., Knight, C. G., Smith, B. J., Stephens, P. E., Shelley, C., Hutton, M., Knäuper, V., Docherty, a J. and Murphy, G. (1998) “TNF-alpha converting enzyme (TACE) is inhibited by TIMP-3.,” *FEBS letters*, 435(1): 39–44.

Anastasiadis, P. Z. (2007) “p120-ctn: A nexus for contextual signaling via Rho GTPases.,” *Biochimica et biophysica acta*, 1773(1): 34–46

Andreu-Pérez, P., Esteve-Puig, R., de Torre-Minguela, C., López-Fauqued, M., Bech-Serra, J. J., Tenbaum, S., García-Trevijano, E. R., Canals, F., Merlino, G., Avila, M. A. and Recio, J. A. (2011) “Protein arginine methyltransferase 5 regulates ERK1/2 signal transduction amplitude and cell fate through CRAF.,” *Science signaling*, 4(190): ra58.

Angelow, S., Ahlstrom, R. and Yu, A. S. L. (2008) “Biology of claudins.,” *American journal of physiology. Renal physiology*, 295(4): F867–76.

Angst, B. D., Nilles, L. a and Green, K. J. (1990) “Desmoplakin II expression is not restricted to stratified epithelia.,” *Journal of cell science*, 97 (Pt 2; 1986): 247–57.

Aoyama, Y., Nagai, M. and Kitajima, Y. (2010) “Binding of pemphigus vulgaris IgG to antigens in desmosome core domains excludes immune complexes rather than directly splitting desmosomes.,” *The British journal of dermatology*, 162(5): 1049–55.

Armstrong, D. K., McKenna, K. E., Purkis, P. E., Green, K. J., Eady, R. A., Leigh, I. M. and Hughes, A. E. (1999) “Haploinsufficiency of desmoplakin causes a striate subtype of palmoplantar keratoderma.,” *Human molecular genetics*, 8(1): 143–8.

Arribas, J. and Esselens, C. (2009) “ADAM17 as a therapeutic target in multiple diseases,” *Current pharmaceutical design*, 15: 2315–2335.

Attardi, L., Reczek, E., Cosmas, C., Demicco, E., McCurrach, M., Lowe, S. and Jacks, T. (2000) “PERP, an apoptosis-associated target of p53, is a novel member of the PMP-22/gas3 family,” *Genes & Development*, 14: 704–718.

Banks-Schlegel, S. and Harris, C. (1983) “Tissue-specific expression of keratin proteins in human esophageal and epidermal epithelium and their cultured keratinocytes,” *Experimental cell research*, 146(2): 271–80.

Barrandon, Y. and Green, H. (1987) “Cell migration is essential for sustained growth of keratinocyte colonies: the roles of transforming growth factor-alpha and epidermal growth factor.,” *Cell*, 50(7): 1131–7.

Baserga, R. (1994) “Oncogenes and the strategy of growth factors,” *Cell*, 79(6): 927–930.

Bazzoni, G., Martinez-Estrada, O. M., Orsenigo, F., Cordenonsi, M., Citi, S. and Dejana, E. (2000) “Interaction of junctional adhesion molecule with the tight junction components ZO-1, cingulin, and occludin.,” *The Journal of biological chemistry*, 275(27): 20520–6.

Bech-Serra, J. J., Santiago-Josefat, B., Esselens, C., Saftig, P., Baselga, J., Arribas, J. and Canals, F. (2006) “Proteomic identification of desmoglein 2 and activated leukocyte cell adhesion molecule as substrates of ADAM17 and ADAM10 by difference gel electrophoresis.,” *Molecular and cellular biology*, 26(13): 5086–95.

Beck, A. H., Espinosa, I., Edris, B., Li, R., Montgomery, K., Zhu, S., Varma, S., Marinelli, R. J., van de Rijn, M. and West, R. B. (2009) “The macrophage colony-stimulating factor 1 response signature in breast carcinoma.,” *Clinical cancer research : an official journal of the American Association for Cancer Research*, 15(3): 778–87.

Beck, A. J., Finocchio, A. and White, J. (1977) “Darier’s disease: a kindred with a large number of cases,” *British Journal of …*, 97(3), pp. 335–339.

Bektas, M. and Rubenstein, D. S. (2009) “Perp and pemphigus: a disease of desmosome destabilization.,” *The Journal of investigative dermatology*. 129(7): 1606–8.

Bellavia, D., Checquolo, S., Campese, a F., Felli, M. P., Gulino, a and Screpanti, I. (2008) “Notch3: from subtle structural differences to functional diversity.,” *Oncogene*, 27(38): 5092–8.

Benoliel, A. M., Kahn-Perles, B., Imbert, J. and Verrando, P. (1997) “Insulin stimulates haptotactic migration of human epidermal keratinocytes through activation of NF-kappa B transcription factor.,” *Journal of cell science*, 110 (Pt 1): 2089–97.

Berasain, C. and Avila, M. a (2014) “Amphiregulin.,” *Seminars in cell & developmental biology*, 28: 31–41.

Bergemann, a D., Zhang, L., Chiang, M. K., Brambilla, R., Klein, R. and Flanagan, J. G. (1998) “Ephrin-B3, a ligand for the receptor EphB3, expressed at the midline of the developing neural tube.,” *Oncogene*, 16(4): 471–80.

Berkowitz, P., Chua, M., Liu, Z., Diaz, L. A. and Rubenstein, D. S. (2008) “Autoantibodies in the autoimmune disease pemphigus foliaceus induce blistering via p38MAPK-dependent signalling in the skin,” *The American journal of pathology*, 173(6): 1628–1636.

Berkowitz, P., Diaz, L. a, Hall, R. P. and Rubenstein, D. S. (2008) “Induction of p38MAPK and HSP27 phosphorylation in pemphigus patient skin.,” *The Journal of investigative dermatology*, 128(3): 738–40.

Berkowitz, P., Hu, P., Liu, Z., Diaz, L. a, Enghild, J. J., Chua, M. P. and Rubenstein, D. S. (2005) “Desmosome signaling. Inhibition of p38MAPK prevents pemphigus vulgaris IgG-induced cytoskeleton reorganization.,” *The Journal of biological chemistry*, 280(25): 23778–84.

Berkowitz, P., Hu, P., Warren, S., Liu, Z., Diaz, L. a and Rubenstein, D. S. (2006) “p38MAPK inhibition prevents disease in pemphigus vulgaris mice.,” *Proceedings of the National Academy of Sciences of the United States of America*, 103(34): 12855–60.

Bertrand, F. E., Eckfeldt, C. E., Lysholm, a S. and LeBien, T. W. (2000) “Notch-1 and Notch-2 exhibit unique patterns of expression in human B-lineage cells.,” *Leukemia*, 14(12): 2095–102.

Bhagavathula, N., Nerusu, K., Fisher, G., Liu, G., Thakur, A., Gemmell, L., Kumar, S., Xu, Z., Hinton, P., Tsurushita, N., Londolif, N., Voorhees, J. and Varani, J. (2005) “Amphiregulin and epidermal hyperplasia: amphiregulin is required to maintain the psoriatic phenotype of human skin grafts on severe combined immunodeficient,” *The American journal of pathology*, 166(4): 1009–1016.

Binns, K. L., Taylor, P. P., Sicheri, F., Pawson, T. and Holland, S. J. (2000) “Phosphorylation of tyrosine residues in the kinase domain and juxtamembrane region regulates the biological and catalytic activities of Eph receptors.,” *Molecular and cellular biology*, 20(13): 4791–805.

Biscardi, J. S., Maa, M.-C., Tice, D. a., Cox, M. E., Leu, T.-H. and Parsons, S. J. (1999) “c-Src-mediated Phosphorylation of the Epidermal Growth Factor Receptor on Tyr845 and Tyr1101 Is Associated with Modulation of Receptor Function,” *Journal of Biological Chemistry*, 274(12): 8335–8343.

Biswas, S. K. and Lewis, C. E. (2010) “NF-κB as a central regulator of macrophage function in tumors.,” *Journal of leukocyte biology*, 88(5): 877–84.

Biswas, S. K. and Mantovani, A. (2010) “Macrophage plasticity and interaction with lymphocyte subsets: cancer as a paradigm.,” *Nature immunology*. 11(10): 889–96.

Black, R. a (2002) “Tumor necrosis factor-alpha converting enzyme.,” *The international journal of biochemistry & cell biology*, 34(1): 1–5.

Black, R. A., Rauch, C. T., Kozlosky, C. J., Peschon, J. J., Slack, J. L., Wolfson, M. F., Castner, B. J., Stocking, K. L., Reddy, P., Srinivasan, S., Nelson, N., Boiani, N., Schooley, K. A., Gerhart, M., Davis, R., Fitzner, J. N., Johnson, R. S., Paxton, R. J., March, C. J. and Cerretti, D. P. (1997) “A metalloproteinase disintegrin that releases tumour-necrosis factor-alpha from cells.,” *Nature*, 385(6618): 729–33.

Blanchot-Jossic, F., Jarry, A., Masson, D., Bach-Ngohou, K., Paineau, J., Denis, M. G., Laboisse, C. L. and Mosnier, J.-F. (2005) “Up-regulated expression of ADAM17 in human colon carcinoma: co-expression with EGFR in neoplastic and endothelial cells.,” *The Journal of pathology*, 207(2): 156–63.

Blanpain, C. and Fuchs, E. (2009) “Epidermal homeostasis: a balancing act of stem cells in the skin,” *Nature reviews Molecular cell biology*, 10(3): 207–217.

Blanpain, C., Lowry, W. E., Pasolli, H. A. and Fuchs, E. (2006) “Canonical notch signaling functions as a commitment switch in the epidermal lineage.,” *Genes & development*, 20(21): 3022–35.

Blaydon, D., Biancheri, P., Di, W., Plagnol, V., Cabral, R., Brooke, M., van Heel, D., Ruschendorf, F., Toynbee, M., Walne, A., O’Toole, E., Martin, J., Lindley, K., Vulliamy, T., Abrams, D., MacDonald, T., Harper, J. and Kelsell, D. (2011) “Inflammatory skin and bowel disease linked to ADAM17 deletion,” *New England Journal of Medicine*, 365(16): 1503–1508.

Blaydon, D. C., Etheridge, S. L., Risk, J. M., Hennies, H.-C., Gay, L. J., Carroll, R., Plagnol, V., McRonald, F. E., Stevens, H. P., Spurr, N. K., Bishop, D. T., Ellis, A., Jankowski, J., Field, J. K., Leigh, I. M., South, A. P. and Kelsell, D. P. (2012) “RHBDF2 mutations are associated with tylosis, a familial esophageal cancer syndrome.,” *American journal of human genetics*. The American Society of Human Genetics, 90(2): 340–6.

Blaydon, D. C., Nitoiu, D., Eckl, K.-M., Cabral, R. M., Bland, P., Hausser, I., van Heel, D. a, Rajpopat, S., Fischer, J., Oji, V., Zvulunov, A., Traupe, H., Hennies, H. C. and Kelsell, D. P. (2011) “Mutations in CSTA, encoding Cystatin A, underlie exfoliative ichthyosis and reveal a role for this protease inhibitor in cell-cell adhesion.,” *American journal of human genetics*. 89(4): 564–71.

Blobel, C. P. (2005) “ADAMs: key components in EGFR signalling and development.,” *Nature reviews. Molecular cell biology*, 6(1): 32–43.

Boggon, T. J., Murray, J., Chappuis-Flament, S., Wong, E., Gumbiner, B. M. and Shapiro, L. (2002) “C-cadherin ectodomain structure and implications for cell adhesion mechanisms.,” *Science*, 296(5571): 1308–13

Bongartz, T., Sutton, A., Sweeting, M., Buchan, I., Matteson, E. and Montori, V. (2006) “Anti-TNF antibody therapy in rheumatoid arthritis and the risk of serious infections and malignancies: systematic review and meta-analysis of rare harmful effects in randomized,” *Jama*, 295(19): 2275–2285.

Bonné, S., Gilbert, B., Hatzfeld, M., Chen, X., Green, K. J. and van Roy, F. (2003) “Defining desmosomal plakophilin-3 interactions.,” *The Journal of cell biology*, 161(2): 403–16.

Bonné, S., van Hengel, J., Nollet, F., Kools, P. and van Roy, F. (1999) “Plakophilin-3, a novel armadillo-like protein present in nuclei and desmosomes of epithelial cells.,” *Journal of cell science*, 112 (Pt 1): 2265–76.

Le Borgne, R., Remaud, S., Hamel, S. and Schweisguth, F. (2005) “Two distinct E3 ubiquitin ligases have complementary functions in the regulation of delta and serrate signaling in Drosophila.,” *PLoS biology*, 3(4): e96.

Bornslaeger, E. a, Godsel, L. M., Corcoran, C. M., Park, J. K., Hatzfeld, M., Kowalczyk, a P. and Green, K. J. (2001) “Plakophilin 1 interferes with plakoglobin binding to desmoplakin, yet together with plakoglobin promotes clustering of desmosomal plaque complexes at cell-cell borders.,” *Journal of cell science*, 114(Pt 4): 727–38.

Borrell-Pagès, M., Rojo, F., Albanell, J., Baselga, J. and Arribas, J. (2003) “TACE is required for the activation of the EGFR by TGF-alpha in tumors.,” *The EMBO journal*, 22(5): 1114–24.

Borrmann, C. M., Mertens, C., Schmidt, a, Langbein, L., Kuhn, C. and Franke, W. W. (2000) “Molecular diversity of plaques of epithelial-adhering junctions.,” *Annals of the New York Academy of Sciences*, 915: 144–50.

Bozkulak, E. C. and Weinmaster, G. (2009) “Selective use of ADAM10 and ADAM17 in activation of Notch1 signaling.,” *Molecular and cellular biology*, 29(21): 5679–95.

Braga, V. M. and Yap, A. S. (2005) “The challenges of abundance: epithelial junctions and small GTPase signalling.,” *Current opinion in cell biology*, 17(5): 466–74.

Brannan, J. M., Dong, W., Prudkin, L., Behrens, C., Lotan, R., Bekele, B. N., Wistuba, I. and Johnson, F. M. (2009) “Expression of the receptor tyrosine kinase EphA2 is increased in smokers and predicts poor survival in non-small cell lung cancer.,” *Clinical cancer research*, 15(13): 4423–30.

Brantley-Sieders, D. (2012) “Clinical relevance of Ephs and ephrins in cancer: lessons from breast, colorectal, and lung cancer profiling,” *Seminars in cell & developmental biology*, 23(1): 102–108.

Brantley-sieders, D. M., Zhuang, G., Hicks, D., Fang, W. Bin, Hwang, Y., Cates, J. M. M., Coffman, K., Jackson, D., Bruckheimer, E., Muraoka-cook, R. S. and Chen, J. (2008) “The receptor tyrosine kinase EphA2 promotes mammary adenocarcinoma tumorigenesis and metastatic progression in mice by amplifying ErbB2 signaling,” *The Journal of clinical investigation*, 118(1): 64–78.

Bray, F., Ren, J.-S., Masuyer, E. and Ferlay, J. (2013) “Global estimates of cancer prevalence for 27 sites in the adult population in 2008.,” *International journal of cancer.* 132(5): 1133–45.

Bray, S. J. (2006) “Notch signalling: a simple pathway becomes complex.,” *Nature reviews. Molecular cell biology*, 7(9): 678–89.

Brennan, D., Hu, Y., Joubeh, S., Choi, Y. W., Whitaker-Menezes, D., O’Brien, T., Uitto, J., Rodeck, U. and Mahoney, M. G. (2007) “Suprabasal Dsg2 expression in transgenic mouse skin confers a hyperproliferative and apoptosis-resistant phenotype to keratinocytes.,” *Journal of cell science*, 120(Pt 5): 758–71.

Brennan, D. and Mahoney, M. (2009) “Increased expression of Dsg2 in malignant skin carcinomas,” *Cell Adhesion and Migration*, 3(2): 148–154

Brocklehurst, K. and Philpott, M. P. (2013) “Cysteine proteases: mode of action and role in epidermal differentiation.,” *Cell and tissue research*, 351(2), pp. 237–44.

Brooke, M. A., Etheridge, S. L., Kaplan, N., Simpson, C., O’Toole, E. A., Ishida-Yamamoto, A., Marches, O., Getsios, S. and Kelsell, D. P. (2014) “iRHOM2-dependent regulation of ADAM17 in cutaneous disease and epidermal barrier function.,” *Human molecular genetics*, 23(15): 4064–76.

Brooke, M. A., Nitoiu, D. and Kelsell, D. P. (2012) “Cell-cell connectivity: desmosomes and disease.,” *The Journal of pathology*, 226(2): 158–71.

Brou, C., Logeat, F., Gupta, N., Bessia, C., LeBail, O., Doedens, J. R., Cumano, A., Roux, P., Black, R. a and Israël, a (2000) “A novel proteolytic cleavage involved in Notch signaling: the role of the disintegrin-metalloprotease TACE.,” *Molecular cell*, 5(2): 207–16.

Bruick, R. K. and McKnight, S. L. (2001) “A conserved family of prolyl-4-hydroxylases that modify HIF.,” *Science*, 294(5545): 1337–40.

Bryant, D. M., Kerr, M. C., Hammond, L. A., Joseph, S. R., Mostov, K. E., Teasdale, R. D. and Stow, J. L. (2007) “EGF induces macropinocytosis and SNX1-modulated recycling of E-cadherin.,” *Journal of cell science*, 120(Pt 10): 1818–28.

Bryant, D. M. and Stow, J. L. (2004) “The ins and outs of E-cadherin trafficking.,” *Trends in cell biology*, 14(8): 427–34

Bukauskas, F. and Verselis, V. (2004) “Gap junction channel gating,” *Biochimica et Biophysica Acta,* 1662: 1–35.

Cabral, R. M., Liu, L., Hogan, C., Dopping-Hepenstal, P. J. C., Winik, B. C., Asial, R. a, Dobson, R., Mein, C. a, Baselaga, P. a, Mellerio, J. E., Nanda, A., Boente, M. D. C., Kelsell, D. P., McGrath, J. a and South, A. P. (2010) “Homozygous mutations in the 5’ region of the JUP gene result in cutaneous disease but normal heart development in children.,” *The Journal of investigative dermatology*, 130(6): 543–50.

Cabral, R. M., Tattersall, D., Patel, V., McPhail, G. D., Hatzimasoura, E., Abrams, D. J., South, A. P. and Kelsell, D. P. (2012) “The DSPII splice variant is crucial for desmosome-mediated adhesion in HaCaT keratinocytes.,” *Journal of cell science*, 125(Pt 12): 2853–61.

Cabral, R. M., Wan, H., Cole, C. L., Abrams, D. J., Kelsell, D. P. and South, A. P. (2010) “Identification and characterization of DSPIa, a novel isoform of human desmoplakin.,” *Cell and tissue research*, 341(1): 121–9.

Calkins, C. C., Setzer, S. V, Jennings, J. M., Summers, S., Tsunoda, K., Amagai, M. and Kowalczyk, A. P. (2006) “Desmoglein endocytosis and desmosome disassembly are coordinated responses to pemphigus autoantibodies.,” *The Journal of biological chemistry*, 281(11): 7623–34.

Campbell, P., Morton, P. E., Takeichi, T., Salam, A., Roberts, N., Proudfoot, L. E., Mellerio, J. E., Aminu, K., Wellington, C., Patil, S. N., Akiyama, M., Liu, L., McMillan, J. R., Aristodemou, S., Ishida-Yamamoto, A., Abdul-Wahab, A., Petrof, G., Fong, K., Harnchoowong, S., Stone, K. L., Harper, J. I., McLean, W. H. I., Simpson, M. A., Parsons, M. and McGrath, J. A. (2014) “Epithelial Inflammation Resulting from an Inherited Loss-of-Function Mutation in EGFR.,” *The Journal of investigative dermatology*. 134(10): 1–9.

Candi, E., Schmidt, R. and Melino, G. (2005) “The cornified envelope: a model of cell death in the skin.,” *Nature reviews. Molecular cell biology*, 6(4), pp. 328–40. doi: 10.1038/nrm1619.

Carneiro, P., Fernandes, M. S., Figueiredo, J., Caldeira, J., Carvalho, J., Pinheiro, H., Leite, M., Melo, S., Oliveira, P., Simões-Correia, J., Oliveira, M. J., Carneiro, F., Figueiredo, C., Paredes, J., Oliveira, C. and Seruca, R. (2012) "E-cadherin dysfunction in gastric cancer--cellular consequences, clinical applications and open questions.," *FEBS letters*, 586(18): 2981–9.

Castellano, G., Reid, J. F., Alberti, P., Carcangiu, M. L., Tomassetti, A. and Canevari, S. (2006) "New potential ligand-receptor signaling loops in ovarian cancer identified in multiple gene expression studies.," *Cancer research*, 66(22): 10709–19.

De Celis, J. F., Bray, S. and Garcia-Bellido, A. (1997) "Notch signalling regulates veinlet expression and establishes boundaries between veins and interveins in the Drosophila wing.," *Development*, 124(10): 1919–28.

Celli, A., Mackenzie, D., Zhai, Y., Tu, C.-L., Bikle, D., Walter, H., Uchida, Y. and Mauro, T. (2012) "SERCA2-Controlled Ca2+-Dependent Keratinocyte Adhesion and Differentiation Is Mediated via the Sphingolipid Pathway: A Therapeutic Target for Darier's," *Journal of Investigative Dermatology*, 132(4): 1188–1195.

Cerrone, M. and Delmar, M. (2014) "Desmosomes and the sodium channel complex: implications for arrhythmogenic cardiomyopathy and Brugada syndrome.," *Trends in cardiovascular medicine*. Elsevier, 24(5): 184–90.

Chanthaphavong, R. S., Loughran, P. a, Lee, T. Y. S., Scott, M. J. and Billiar, T. R. (2012) "A role for cGMP in inducible nitric-oxide synthase (iNOS)-induced tumor necrosis factor (TNF) α-converting enzyme (TACE/ADAM17) activation, translocation, and TNF receptor 1 (TNFR1) shedding in hepatocytes.," *The Journal of biological chemistry*, 287(43): 35887–98.

Charbonneau, M., Harper, K., Grondin, F., Pelmus, M., McDonald, P. P. and Dubois, C. M. (2007) "Hypoxia-inducible factor mediates hypoxic and tumor necrosis factor alpha-induced increases in tumor necrosis factor-alpha converting enzyme/ADAM17 expression by synovial cells.," *The Journal of biological chemistry*, 282(46): 33714–24.

Charpentier, E., Lavker, R. M., Acquista, E. and Cowin, P. (2000) "Plakoglobin suppresses epithelial proliferation and hair growth in vivo.," *The Journal of cell biology*, 149(2): 503–20.

Chavaroche, A., Cudic, M., Guilianotti, M., Houghten, R., Fields, G. and Minond, D. (2014) "Glycosylation of a disintegrin and metalloprotease 17 affects its activity and inhibition," *Analytical Biochemistry*, 449: 68–75.

Chen, J. (2012) "Regulation of tumor initiation and metastatic progression by Eph receptor tyrosine kinases," *Advances in cancer research*, 114: 1–20.

Chen, X., Chen, L., Chen, J., Hu, W., Gao, H. and Xie, B. (2013) "ADAM17 promotes U87 glioblastoma stem cell migration and invasion," *Brain research*, 1538: 151–158.

Chen, Y. and Chang, L. (2013) "Hydroquinone-induced miR-122 down-regulation elicits ADAM17 up-regulation, leading to increased soluble TNF-α production in human leukemia cells with expressed Bcr/Abl," *Biochemical pharmacology*, 86: 620–631.

Chen, Y.-J., Chang, J. T., Lee, L., Wang, H.-M., Liao, C.-T., Chiu, C.-C., Chen, P.-J. and Cheng, a-J. (2007) "DSG3 is overexpressed in head neck cancer and is a potential molecular target for inhibition of oncogenesis.," *Oncogene*, 26(3): 467–76.

Chen, Y.-J., Lee, L.-Y., Chao, Y.-K., Chang, J. T., Lu, Y.-C., Li, H.-F., Chiu, C.-C., Li, Y.-C., Li, Y.-L., Chiou, J.-F. and Cheng, A.-J. (2013) "DSG3 facilitates cancer cell growth and invasion through the DSG3-plakoglobin-TCF/LEF-Myc/cyclin D1/MMP signaling pathway.," *PloS one*, 8(5): e64088.

Cheng, T.-L., Wu, Y.-T., Lin, H.-Y., Hsu, F.-C., Liu, S.-K., Chang, B.-I., Chen, W.-S., Lai, C.-H., Shi, G.-Y. and Wu, H.-L. (2011) "Functions of rhomboid family protease RHBDL2 and thrombomodulin in wound healing.," *The Journal of investigative dermatology*. 131(12): 2486–94.

Cheng, X., Mihindukulasuriya, K., Den, Z., Kowalczyk, A. P., Calkins, C. C., Ishiko, A., Shimizu, A. and Koch, P. J. (2004) "Assessment of splice variant-specific functions of desmocollin 1 in the skin.," *Molecular and cellular biology*, 24(1): 154–63.

Chernyavsky, A. I., Arredondo, J., Kitajima, Y., Sato-Nagai, M. and Grando, S. A. (2007) "Desmoglein versus non-desmoglein signaling in pemphigus acantholysis: characterization of novel signaling pathways downstream of pemphigus vulgaris antigens.," *The Journal of biological chemistry*, 282(18): 13804–12.

Chitadze, G., Lettau, M., Bhat, J., Wesch, D., Steinle, A., Fürst, D., Mytilineos, J., Kalthoff, H., Janssen, O., Oberg, H.-H. and Kabelitz, D. (2013) "Shedding of endogenous MHC class I-related chain molecules A and B from different human tumor entities: heterogeneous involvement of the 'a disintegrin and metalloproteases' 10 and 17.," *International journal of cancer.* 133(7): 1557–66.

Chitnis, M. M., Yuen, J. S. P., Protheroe, A. S., Pollak, M. and Macaulay, V. M. (2008) "The type 1 insulin-like growth factor receptor pathway.," *Clinical cancer research : an official journal of the American Association for Cancer Research*, 14(20): 6364–70.

Choi, H.-J., Gross, J. C., Pokutta, S. and Weis, W. I. (2009) "Interactions of plakoglobin and beta-catenin with desmosomal cadherins: basis of selective exclusion of alpha- and beta-catenin from desmosomes.," *The Journal of biological chemistry*, 284(46): 31776–88.

Choi, H.-J., Park-Snyder, S., Pascoe, L. T., Green, K. J. and Weis, W. I. (2002) "Structures of two intermediate filament-binding fragments of desmoplakin reveal a unique repeat motif structure.," *Nature structural biology*, 9(8): 612–20.

Christian, L. (2012) "The ADAM family: insights into Notch proteolysis," *Fly*, 6(1): 30-34.

Christova, Y., Adrain, C., Bambrough, P., Ibrahim, A. and Freeman, M. (2013) "Mammalian iRhoms have distinct physiological functions including an essential role in TACE regulation.," *EMBO reports*. 14(10): 884–90.

Chu, D. H. (2008) "Development and Structure of Skin," in Wolff, K., Katz, S., Gilchrest, B., Paller, A., and Leffell, D. (eds) *Fitzpatrick's Dermatology in General Medicine*. McGraw Hill, pp. 57–73.

Cirillo, N., Lanza, A. and Prime, S. S. (2010) "Induction of hyper-adhesion attenuates autoimmune-induced keratinocyte cell-cell detachment and processing of adhesion molecules via mechanisms that involve PKC.," *Experimental cell research*. Elsevier B.V., 316(4): 580–92.

Clayton, E., Doupé, D. P., Klein, A. M., Winton, D. J., Simons, B. D. and Jones, P. H. (2007) "A single type of progenitor cell maintains normal epidermis.," *Nature*, 446(7132): 185–9.

Colegio, O. R., Van Itallie, C. M., McCrea, H. J., Rahner, C. and Anderson, J. M. (2002) "Claudins create charge-selective channels in the paracellular pathway between epithelial cells.," *American journal of physiology. Cell physiology*, 283(1): C142–7.

Collins, C. a and Watt, F. M. (2008) "Dynamic regulation of retinoic acid-binding proteins in developing, adult and neoplastic skin reveals roles for beta-catenin and Notch signalling.," *Developmental biology*. Elsevier Inc., 324(1): 55–67.

Collins, J. E., Legan, P. K., Kenny, T. P., MacGarvie, J., Holton, J. L. and Garrod, D. R. (1991) "Cloning and sequence analysis of desmosomal glycoproteins 2 and 3 (desmocollins): cadherin-like desmosomal adhesion molecules with heterogeneous cytoplasmic domains.," *The Journal of cell biology*, 113(2): 381–91.

Common, J. E., O'Toole, E. A, Leigh, I. M., Thomas, A., Griffiths, W. a D., Venning, V., Grabczynska, S., Peris, Z., Kansky, A. and Kelsell, D. P. (2005) "Clinical and genetic heterogeneity of erythrokeratoderma variabilis.," *The Journal of investigative dermatology*, 125(5): 920–7

Conlon, R. A., Reaume, A. G. and Rossant, J. (1995) "Notch1 is required for the coordinate segmentation of somites.," *Development (Cambridge, England)*, 121(5): 1533–45.

Cook, P. W., Brown, J. R., Cornell, K. a and Pittelkow, M. R. (2004) "Suprabasal expression of human amphiregulin in the epidermis of transgenic mice induces a severe, early-onset, psoriasis-like skin pathology: expression of amphiregulin in the basal epidermis is also associated with synovitis.," *Experimental dermatology*, 13(6): 347–56.

Cook, P. W., Pittelkow, M. R., Keeble, W. W., Graves-deal, R., Coffey, R. J. and Shipley, G. D. (1992) "Amphiregulin Messenger RNA Is Elevated in Psoriatic Epidermis and Gastrointestinal Carcinomas Advances in Brief Amphiregulin Messenger RNA Is Elevated in Psoriatic Epidermis and Gastrointestinal Carcinomas," *Cancer research*, 52: 3224–3227.

Cordenonsi, M., D'Atri, F., Hammar, E., Parry, D. A., Kendrick-Jones, J., Shore, D. and Citi, S. (1999) "Cingulin contains globular and coiled-coil domains and interacts with ZO-1, ZO-2, ZO-3, and myosin.," *The Journal of cell biology*, 147(7), pp. 1569–82.

Corpet, F. (1988) "Multiple sequence alignment with hierarchical clustering," *Nucleic acids research*, 16(22): 10881–10890.

Cui, T., Chen, Y., Yang, L., Knösel, T., Huber, O., Pacyna-Gengelbach, M. and Petersen, I. (2012) "The p53 target gene desmocollin 3 acts as a novel tumor suppressor through inhibiting EGFR/ERK pathway in human lung cancer.," *Carcinogenesis*, 33(12): 2326–33.

Cui, T., Chen, Y., Yang, L., Knösel, T., Zöller, K., Huber, O. and Petersen, I. (2011) "DSC3 expression is regulated by p53, and methylation of DSC3 DNA is a prognostic marker in human colorectal cancer.," *British journal of cancer*, 104(6): 1013–9.

Cui, T., Chen, Y., Yang, L., Mireskandari, M., Knösel, T., Zhang, Q., Kohler, L. H., Kunze, A., Presselt, N. and Petersen, I. (2012) "Diagnostic and prognostic impact of desmocollins in human lung cancer.," *Journal of clinical pathology*, 65(12): 1100–6.

Curtis, M. a and Kelsell, D. P. (2013) "Current insights into protease dynamics in human epithelial disease and barrier function.," *Cell and tissue research*, 351(2): 213-5.

D'Souza-Schorey, C. (2005) "Disassembling adherens junctions: breaking up is hard to do.," *Trends in cell biology*, 15(1): 19–26.

Darling, D., Yingling, J., Wynshaw, and Boris, A. (2005) "Role of 14–3–3 proteins in eukaryotic signaling and development," *Current topics in developmental Biology*, 68: 281–315.

Das, S., Czarnek, M., Bzowska, M., Mężyk-Kopeć, R., Stalińska, K., Wyroba, B., Sroka, J., Jucha, J., Deneka, D., Stokłosa, P., Ogonek, J., Swartz, M. a, Madeja, Z. and Bereta, J. (2012) "ADAM17 silencing in mouse colon carcinoma cells: the effect on tumoricidal cytokines and angiogenesis.," *PloS one*, 7(12): e50791.

Deftos, M., He, Y., Ojala, E. and Bevan, M. (1998) "Correlating notch signaling with thymocyte maturation," *Immunity*, 9(6): 777–786.

Delwig, A. and Rand, M. (2008) "Kuz and TACE can activate Notch independent of ligand," *Cellular and Molecular Life Sciences*, 65(14): 2232–2243.

Demehri, S., Liu, Z., Lee, J., Lin, M.-H., Crosby, S. D., Roberts, C. J., Grigsby, P. W., Miner, J. H., Farr, A. G. and Kopan, R. (2008) "Notch-deficient skin induces a lethal systemic B-

lymphoproliferative disorder by secreting TSLP, a sentinel for epidermal integrity.," *PLoS biology*, 6(5): e123.

Demlehner, M. P., Schäfer, S., Grund, C. and Franke, W. W. (1995) "Continual assembly of half-desmosomal structures in the absence of cell contacts and their frustrated endocytosis: a coordinated Sisyphus cycle.," *The Journal of cell biology*, 131(3): 745–60.

Den, Z., Cheng, X., Merched-Sauvage, M. and Koch, P. J. (2006) "Desmocollin 3 is required for pre-implantation development of the mouse embryo.," *Journal of cell science*, 119(Pt 3): 482–9.

Dhillon, A. S., Hagan, S., Rath, O. and Kolch, W. (2007) "MAP kinase signalling pathways in cancer.," *Oncogene*, 26(22): 3279–90.

Dhitavat, J., Cobbold, C., Leslie, N., Burge, S. and Hovnanian, A. (2003) "Impaired trafficking of the desmoplakins in cultured Darier's disease keratinocytes," *Journal of investigative Dermatology*, 121: 1349–1355.

Di, W. L., Rugg, E. L., Leigh, I. M. and Kelsell, D. P. (2001) "Multiple epidermal connexins are expressed in different keratinocyte subpopulations including connexin 31.," *The Journal of investigative dermatology*, 117(4): 958–64.

Di, W.-L., Monypenny, J., Common, J. E. a, Kennedy, C. T. C., Holland, K. a, Leigh, I. M., Rugg, E. L., Zicha, D. and Kelsell, D. P. (2002) "Defective trafficking and cell death is characteristic of skin disease-associated connexin 31 mutations.," *Human molecular genetics*, 11(17): 2005–14.

DiColandrea, T., Karashima, T., Määttä, a and Watt, F. M. (2000) "Subcellular distribution of envoplakin and periplakin: insights into their role as precursors of the epidermal cornified envelope.," *The Journal of cell biology*, 151(3): 573–86.

Diestel, S., Richard, G., Döring, B. and Traub, O. (2002) "Expression of a connexin31 mutation causing erythrokeratodermia variabilis is lethal for HeLa cells.," *Biochemical and biophysical research communications*, 296(3): 721–8.

Ding, L., Lu, Z., Lu, Q. and Chen, Y.-H. (2013) "The claudin family of proteins in human malignancy: a clinical perspective.," *Cancer management and research*, 5: 367–75.

Ding, X., Aoki, V., Mascaro, J. J., Lopez-Swiderski, A., Diaz, L. and Fairley, J. (1997) "Mucosal and mucocutaneous (generalized) pemphigus vulgaris show distinct autoantibody profiles," *Journal of investigative dermatology*, 109(4): 592–596.

Doberstein, K., Steinmeyer, N., Hartmetz, A., Eberhardt, W., Mittelbronn, M., Harter, P. N., Juengel, E., Blaheta, R., Pfeilschifter, J. and Gutwein, P. (2013) "MicroRNA-145 Targets the Metalloprotease ADAM17 and Is Suppressed in Renal Cell Carcinoma Patients 1," 15(2): 218–230.

Doedens, J. R. and Black, R. A. (2000) "Stimulation-induced Down-regulation of Tumor Necrosis Factor-alpha Converting Enzyme," *Journal of Biological Chemistry*, 275(19): 14598–14607.

Drees, F., Pokutta, S., Yamada, S., Nelson, W. J. and Weis, W. I. (2005) "Alpha-catenin is a molecular switch that binds E-cadherin-beta-catenin and regulates actin-filament assembly.," *Cell*, 123(5): 903–15.

Düsterhöft, S., Jung, S., Hung, C.-W., Tholey, A., Sönnichsen, F. D., Grötzinger, J. and Lorenzen, I. (2013) "Membrane-proximal domain of a disintegrin and metalloprotease-17 represents the putative molecular switch of its shedding activity operated by protein-disulfide isomerase.," *Journal of the American Chemical Society*, 135(15): 5776–81.

Duxbury, M. S., Ito, H., Zinner, M. J., Ashley, S. W. and Whang, E. E. (2004) “EphA2: a determinant of malignant cellular behavior and a potential therapeutic target in pancreatic adenocarcinoma.,” *Oncogene*, 23(7): 1448–56.

Ebert, M. S. and Sharp, P. a (2012) “Roles for microRNAs in conferring robustness to biological processes.,” *Cell*. 149(3): 515–24.

Ebnet, K., Suzuki, A., Ohno, S. and Vestweber, D. (2004) “Junctional adhesion molecules (JAMs): more molecules with dual functions?,” *Journal of cell science*, 117(Pt 1):19–29.

Eden, E., Huang, F., Sorkin, A. and Futter, C. (2012) “The role of EGF receptor ubiquitination in regulating its intracellular traffic,” *Traffic*, 13(2): 329–337.

Egawa, G., Osawa, M., Uemura, A., Miyachi, Y. and Nishikawa, S.-I. (2009) “Transient expression of ephrin b2 in perinatal skin is required for maintenance of keratinocyte homeostasis.,” *The Journal of investigative dermatology*., 129(10): 2386–95.

Eiraku, M., Tohgo, A., Ono, K., Kaneko, M., Fujishima, K., Hirano, T. and Kengaku, M. (2005) “DNER acts as a neuron-specific Notch ligand during Bergmann glial development.,” *Nature neuroscience*, 8(7): 873–80.

Elder, J. T., Bruce, A. T., Gudjonsson, J. E., Johnston, A., Stuart, P. E., Tejasvi, T., Voorhees, J. J., Abecasis, G. R. and Nair, R. P. (2010) “Molecular dissection of psoriasis: integrating genetics and biology.,” *The Journal of investigative dermatology*, 130(5): 1213–26.

Ellis, A., Field, J. K., Field, E. A., Friedmann, P. S., Fryer, A., Howard, P., Leigh, I. M., Risk, J., Shaw, J. M. and Whittaker, J. (1994) “Tylosis associated with carcinoma of the oesophagus and oral leukoplakia in a large Liverpool family--a review of six generations.,” *European journal of cancer. Part B, Oral oncology*, 30B(2): 102–12.

Ellisen, L. W., Bird, J., West, D. C., Soreng, a L., Reynolds, T. C., Smith, S. D. and Sklar, J. (1991) “TAN-1, the human homolog of the Drosophila notch gene, is broken by chromosomal translocations in T lymphoblastic neoplasms.,” *Cell*, 66(4): 649–61.

Enomoto, Y., Orihara, K., Takamasu, T., Matsuda, A., Gon, Y., Saito, H., Ra, C. and Okayama, Y. (2009) “Tissue remodeling induced by hypersecreted epidermal growth factor and amphiregulin in the airway after an acute asthma attack.,” *The Journal of allergy and clinical immunology*. 124(5): 913–20.e1–7.

Erreni, M., Mantovani, A. and Allavena, P. (2011) “Tumor-associated Macrophages (TAM) and Inflammation in Colorectal Cancer.,” *Cancer microenvironment : official journal of the International Cancer Microenvironment Society*, 4(2): 141–54.

Eshkind, L., Tian, Q., Schmidt, A., Franke, W. W., Windoffer, R. and Leube, R. E. (2002) “Loss of desmoglein 2 suggests essential functions for early embryonic development and proliferation of embryonal stem cells.,” *European journal of cell biology*, 81(11): 592–8.

Esmon, C. (1995) “Thrombomodulin as a model of molecular mechanisms that modulate protease specificity and function at the vessel surface.,” *The FASEB journal*, 9: 946–955.

Estrach, S., Ambler, C. a, Lo Celso, C., Hozumi, K. and Watt, F. M. (2006) “Jagged 1 is a beta-catenin target gene required for ectopic hair follicle formation in adult epidermis.,” *Development*, 133(22): 4427–38.

Estrach, S., Cordes, R., Hozumi, K., Gossler, A. and Watt, F. M. (2008) “Role of the Notch ligand Delta1 in embryonic and adult mouse epidermis.,” *The Journal of investigative dermatology*, 128(4): 825–32.

Eyre, R. and Stanley, J. (1987) “Human autoantibodies against a desmosomal protein complex with a calcium-sensitive epitope are characteristic of pemphigus foliaceus patients.,” *The Journal of experimental medicine*, 165: 1–6.

Eyre, R. W. and Stanley, J. R. (1988) “Identification of pemphigus vulgaris antigen extracted from normal human epidermis and comparison with pemphigus foliaceus antigen.,” *The Journal of clinical investigation*, 81(3): 807–12.

Fabbri, G., Rasi, S., Rossi, D., Trifonov, V., Khiabanian, H., Ma, J., Grunn, A., Fangazio, M., Capello, D., Monti, S., Cresta, S., Gargiulo, E., Forconi, F., Guarini, A., Arcaini, L., Paulli, M., Laurenti, L., Larocca, L. M., Marasca, R., Gattei, V., Oscier, D., Bertoni, F., Mullighan, C. G., Foá, R., Pasqualucci, L., Rabadan, R., Dalla-Favera, R. and Gaidano, G. (2011) “Analysis of the chronic lymphocytic leukemia coding genome: role of NOTCH1 mutational activation.,” *The Journal of experimental medicine*, 208(7): 1389–401.

Fan, H. and Derynck, R. (1999) “Ectodomain shedding of TGF-alpha and other transmembrane proteins is induced by receptor tyrosine kinase activation and MAP kinase signaling cascades.,” *The EMBO journal*, 18(24): 6962–72.

Fang, W.-K., Gu, W., Liao, L.-D., Chen, B., Wu, Z.-Y., Wu, J.-Y., Shen, J., Xu, L.-Y. and Li, E.-M. (2014) “Prognostic significance of desmoglein 2 and desmoglein 3 in esophageal squamous cell carcinoma.,” *Asian Pacific journal of cancer prevention : APJCP*, 15(2): 871–6.

Fanning, A., Ma, T. and Anderson, J. (2002) “Isolation and functional characterization of the actin binding region in the tight junction protein ZO-1,” *The FASEB Journal*, 16(13):1835-1837.

Faoro, L., Singleton, P. a, Cervantes, G. M., Lennon, F. E., Choong, N. W., Kanteti, R., Ferguson, B. D., Husain, A. N., Tretiakova, M. S., Ramnath, N., Vokes, E. E. and Salgia, R. (2010) “EphA2 mutation in lung squamous cell carcinoma promotes increased cell survival, cell invasion, focal adhesions, and mammalian target of rapamycin activation.,” *The Journal of biological chemistry*, 285(24), 18575–85.

Ferlay, J., Soerjomataram I, I., Dikshit, R., Eser, S., Mathers, C., Rebelo, M., Parkin, D. M., Forman D, D. and Bray, F. (2014) “Cancer incidence and mortality worldwide: sources, methods and major patterns in GLOBOCAN 2012.,” *International journal of cancer.*

Finak, G., Bertos, N., Pepin, F., Sadekova, S., Souleimanova, M., Zhao, H., Chen, H., Omeroglu, G., Meterissian, S., Omeroglu, A., Hallett, M. and Park, M. (2008) “Stromal gene expression predicts clinical outcome in breast cancer.,” *Nature medicine*, 14(5): 518–27.

Fine, J.-D., Bruckner-Tuderman, L., Eady, R. a J., Bauer, E. a, Bauer, J. W., Has, C., Heagerty, A., Hintner, H., Hovnanian, A., Jonkman, M. F., Leigh, I., Marinkovich, M. P., Martinez, A. E., McGrath, J. a, Mellerio, J. E., Moss, C., Murrell, D. F., Shimizu, H., Uitto, J., Woodley, D. and Zambruno, G. (2014) “Inherited epidermolysis bullosa: updated recommendations on diagnosis and classification.,” *Journal of the American Academy of Dermatology*. 70(6): 1103–26.

Foltenyi, K., Greenspan, R. J. and Newport, J. W. (2007) “Activation of EGFR and ERK by rhomboid signaling regulates the consolidation and maintenance of sleep in Drosophila.,” *Nature neuroscience*, 10(9): 1160–7.

Freeman, M. (2008) “Rhomboid proteases and their biological functions.,” *Annual review of genetics*, 42: 191–210.

Freeman, M. (2009) “Rhomboids: 7 years of a new protease family.,” *Seminars in cell & developmental biology*, 20(2): 231–9.

Fryer, C. J., White, J. B. and Jones, K. a (2004) “Mastermind recruits CycC:CDK8 to phosphorylate the Notch ICD and coordinate activation with turnover.,” *Molecular cell*, 16(4): 509–20.

Fuchs, E. (1990) “Mini-Review Epidermal Differentiation : The Bare Essentials,” *The Journal of cell biology*, 111(6): 2807–2814.

Fuchs, E. (1995) “Keratins and the skin.,” *Annual review of cell and developmental biology*, 11: 123–53.

Fuchs, E. (2009) “Finding One’s Niche in the Skin,” *Cell Stem Cell*, 4(6): 499–502.

Fuchs, E. and Green, H. (1980) “Changes in keratin gene expression during terminal differentiation of the keratinocyte,” *Cell*, 19:1033–1042.

Fuchs, E. and Raghavan, S. (2002) “Getting under the skin of epidermal morphogenesis.,” *Nature reviews. Genetics*, 3(3): 199–209.

Fukai, J., Yokote, H., Yamanaka, R., Arao, T., Nishio, K. and Itakura, T. (2008) “EphA4 promotes cell proliferation and migration through a novel EphA4-FGFR1 signaling pathway in the human glioma U251 cell line.,” *Molecular cancer therapeutics*, 7(9): 2768–78.

Funatomi, H., Itakura, J., Ishiwata, T., Pastan, I., Thompson, S. a, Johnson, G. R. and Korc, M. (1997) “Amphiregulin antisense oligonucleotide inhibits the growth of T3M4 human pancreatic cancer cells and sensitizes the cells to EGF receptor-targeted therapy.,” *International journal of cancer.* 72(3): 512–7.

Furne, C., Ricard, J., Cabrera, J. R., Pays, L., John, R., Mehlen, P. and Liebl, D. J. (2010) “EphrinB3 is an Anti-apoptotic Ligand that Inhibits the Dependence Receptor Functions of EphA4 Receptors during adult neurogenesis,” *Biochimica et biophysica acta*, 1793(2): 231–238.

Furuse, M., Sasaki, H., Fujimoto, K. and Tsukita, S. (1998) “A single gene product, claudin-1 or -2, reconstitutes tight junction strands and recruits occludin in fibroblasts.,” *The Journal of cell biology*, 143(2), pp. 391–401.

Gale, N. W., Holland, S. J., Valenzuela, D. M., Flenniken, a, Pan, L., Ryan, T. E., Henkemeyer, M., Strebhardt, K., Hirai, H., Wilkinson, D. G., Pawson, T., Davis, S. and Yancopoulos, G. D. (1996) “Eph receptors and ligands comprise two major specificity subclasses and are reciprocally compartmentalized during embryogenesis.,” *Neuron*, 17(1): 9–19.

Gall, T. M. H. and Frampton, A. E. (2013) “Gene of the month: E-cadherin (CDH1).,” *Journal of clinical pathology*, 66(11): 928–32.

Gallicano, G. I., Kouklis, P., Bauer, C., Yin, M., Vasioukhin, V., Degenstein, L. and Fuchs, E. (1998) “Desmoplakin is required early in development for assembly of desmosomes and cytoskeletal linkage.,” *The Journal of cell biology*, 143(7): 2009–22.

Gao, M., Kim, B., Kang, S., Choi, Y., Yoon, J. and Cho, N. (2013) “Human breast cancer-associated fibroblasts enhance cancer cell proliferation through increased TGF-α cleavage by ADAM17,” *Cancer letters*, 336: 240–246.

Garrod, D. and Chidgey, M. (2008) “Desmosome structure, composition and function.,” *Biochimica et biophysica acta*, 1778(3): 572–87.

Garrod, D. R., Berika, M. Y., Bardsley, W. F., Holmes, D. and Tabernero, L. (2005) “Hyper-adhesion in desmosomes: its regulation in wound healing and possible relationship to cadherin crystal structure.,” *Journal of cell science*, 118(Pt 24): 5743–54.

Garrod, D. R., Merritt, A. J. and Nie, Z. (2002) “Desmosomal cadherins.,” *Current opinion in cell biology*, 14(5): 537–45.

Gat, U., DasGupta, R., Degenstein, L. and Fuchs, E. (1998) “De Novo hair follicle morphogenesis and hair tumors in mice expressing a truncated beta-catenin in skin.,” *Cell*, 95(5): 605–14.

Gates, J. and Peifer, M. (2005) “Can 1000 reviews be wrong? Actin, alpha-Catenin, and adherens junctions.,” *Cell*, 123(5): 769–72.

Gaudry, C. a, Palka, H. L., Dusek, R. L., Huen, a C., Khandekar, M. J., Hudson, L. G. and Green, K. J. (2001) “Tyrosine-phosphorylated plakoglobin is associated with desmogleins but not desmoplakin after epidermal growth factor receptor activation.,” *The Journal of biological chemistry*, 276(27): 24871–80.

Genander, M. and Frisén, J. (2010) “Eph receptors tangled up in two: Independent control of cell positioning and proliferation.,” *Cell cycle*, 9(10): 1865–6.

Genander, M., Holmberg, J. and Frisén, J. (2010) “Ephrins negatively regulate cell proliferation in the epidermis and hair follicle,” *Stem Cells*, 28: 1196–1205.

Getsios, S., Amargo, E. V, Dusek, R. L., Ishii, K., Sheu, L., Godsel, L. M. and Green, K. J. (2004) “Coordinated expression of desmoglein 1 and desmocollin 1 regulates intercellular adhesion.,” *Differentiation; research in biological diversity*. 72(8): 419–33.

Getsios, S., Huen, A. C. and Green, K. J. (2004) “Working out the strength and flexibility of desmosomes.,” *Nature reviews. Molecular cell biology*, 5(4): 271–81.

Getsios, S., Simpson, C. L., Kojima, S., Harmon, R., Sheu, L. J., Dusek, R. L., Cornwell, M. and Green, K. J. (2009) “Desmoglein 1-dependent suppression of EGFR signaling promotes epidermal differentiation and morphogenesis.,” *The Journal of cell biology*, 185(7): 1243–58.

Giaginis, C., Tsoukalas, N., Bournakis, E., Alexandrou, P., Kavantzas, N., Patsouris, E. and Theocharis, S. (2014) “Ephrin (Eph) receptor A1, A4, A5 and A7 expression in human non-small cell lung carcinoma: associations with clinicopathological parameters, tumor proliferative capacity and patients’ survival.,” *BMC clinical pathology*, 14(1): 8.

Gilmore, J., Scott, J., Bouizar, Z., Robling, A., Pitfield, S. and Riese II, D. (2008) “Amphiregulin-EGFR signaling regulates PTHrP gene expression in breast cancer cells,” *Breast cancer research treatments*, 110(3): 493–505.

Giricz, O., Calvo, V., Peterson, E. a, Abouzeid, C. M. and Kenny, P. A. (2013) “TACE-dependent TGFα shedding drives triple-negative breast cancer cell invasion.,” *International journal of cancer.* 133(11): 2587–95.

Gliki, G., Ebnet, K., Aurrand-Lions, M., Imhof, B. a and Adams, R. H. (2004) “Spermatid differentiation requires the assembly of a cell polarity complex downstream of junctional adhesion molecule-C.,” *Nature*, 431(7006): 320–4.

Goodenough, D. a and Paul, D. L. (2009) “Gap junctions.,” *Cold Spring Harbor perspectives in biology*, 1(1): a002576.

Gordon, K., Kochkodan, J. J., Blatt, H., Lin, S. Y., Kaplan, N., Johnston, A., Swindell, W. R., Hoover, P., Schlosser, B. J., Elder, J. T., Gudjonsson, J. E. and Getsios, S. (2013) “Alteration of the EphA2/Ephrin-A signaling axis in psoriatic epidermis.,” *The Journal of investigative dermatology*. 133(3): 712–22.

Gordon, W. R., Roy, M., Vardar-Ulu, D., Garfinkel, M., Mansour, M. R., Aster, J. C. and Blacklow, S. C. (2009) “Structure of the Notch1-negative regulatory region: implications for normal activation and pathogenic signaling in T-ALL.,” *Blood*, 113(18): 4381–90.

Gosavi, P., Kundu, S. T., Khapare, N., Sehgal, L., Karkhanis, M. S. and Dalal, S. N. (2011) "E-cadherin and plakoglobin recruit plakophilin3 to the cell border to initiate desmosome assembly.," *Cellular and molecular life sciences : CMLS*, 68(8): 1439–54.

Gottfried, I., Landau, M., Glaser, F., Di, W.-L., Ophir, J., Mevorah, B., Ben-Tal, N., Kelsell, D. P. and Avraham, K. B. (2002) "A mutation in GJB3 is associated with recessive erythrokeratodermia variabilis (EKV) and leads to defective trafficking of the connexin 31 protein.," *Human molecular genetics*, 11(11): 1311–6.

Green, K. J. and Simpson, C. L. (2007) "Desmosomes - New perspectives on a classic," *Journal of investigative dermatology*, 127: 2499–2515.

Green, K., Parry, D., Steinert, P., Wagner, R., Angst, B. and Nilles, L. (1990) "Structure of the human desmoplakins. Implications for function in the desmosomal plaque.," *Journal of Biological Chemistry*, 265(19): 2603–2612.

Greenwald, I. (2012) "Notch and the awesome power of genetics.," *Genetics*, 191(3): 655–69.

Gschwind, A., Hart, S., Fischer, O. M. and Ullrich, A. (2003) "TACE cleavage of proamphiregulin regulates GPCR-induced proliferation and motility of cancer cells.," *The EMBO journal*, 22(10): 2411–21.

Guillemot, L., Hammar, E., Kaister, C., Ritz, J., Caille, D., Jond, L., Bauer, C., Meda, P. and Citi, S. (2004) "Disruption of the cingulin gene does not prevent tight junction formation but alters gene expression.," *Journal of cell science*, 117(Pt 22): 5245–56.

Guinea-viniegra, J., Zenz, R., Scheuch, H., Jiménez, M., Bakiri, L., Petzelbauer, P. and Wagner, E. F. (2012) "Differentiation-induced skin cancer suppression by FOS , p53 , and TACE / ADAM17," *Journal of Clinical investigation*, 122(8): 2898–2910.

Gullberg, M., Huang, S. and Andersson, A. (2010) "Analyzing human epidermal growth factor receptor family dimerization and activation using Duolink® ADVERTISING FEATURE," *Nature Publishing Group*. 7(12): an10–an11.

Guo, H., Miao, H., Gerber, L., Singh, J., Denning, M. F., Gilliam, A. C. and Wang, B. (2006) "Disruption of EphA2 receptor tyrosine kinase leads to increased susceptibility to carcinogenesis in mouse skin.," *Cancer research*, 66(14): 7050–8.

Gupta-Rossi, N., Le Bail, O., Gonen, H., Brou, C., Logeat, F., Six, E., Ciechanover, a and Israël, a (2001) "Functional interaction between SEL-10, an F-box protein, and the nuclear form of activated Notch1 receptor.," *The Journal of biological chemistry*, 276(37): 34371–8.

Guttman-Yassky, E., Nograles, K. E. and Krueger, J. G. (2011) "Contrasting pathogenesis of atopic dermatitis and psoriasis--part II: immune cell subsets and therapeutic concepts.," *The Journal of allergy and clinical immunology*. 127(6): 1420–32.

Haass, N. K. and Herlyn, M. (2005) "Normal human melanocyte homeostasis as a paradigm for understanding melanoma.," *The journal of investigative dermatology. Symposium proceedings / the Society for Investigative Dermatology, Inc. [and] European Society for Dermatological Research*, 10(2): 153–63.

Hafezi-Moghadam, A. and Ley, K. (1999) "Relevance of L-selectin shedding for leukocyte rolling in vivo.," *The Journal of experimental medicine*, 189(6): 939–48.

Hafezi-Moghadam, A., Thomas, K. L., Prorock, A. J., Huo, Y. and Ley, K. (2001) "L-selectin shedding regulates leukocyte recruitment.," *The Journal of experimental medicine*, 193(7): 863–72.

Halata, Z., Grim, M. and Bauman, K. I. (2003) “Friedrich Sigmund Merkel and his ‘Merkel cell’, morphology, development, and physiology: review and new results.,” *The anatomical record. Part A, Discoveries in molecular, cellular, and evolutionary biology*, 271(1): 225–39.

Hamada, H., Ishii, H., Sakyo, K., Horie, S., Nishiki, K. and Kazama, M. (1995) “The epidermal growth factor-like domain of recombinant human thrombomodulin exhibits mitogenic activity for Swiss 3T3 cells.,” *Blood*, 86(1): 225–33.

Hamada, Y., Kadokawa, Y., Okabe, M., Ikawa, M., Coleman, J. R. and Tsujimoto, Y. (1999) “Mutation in ankyrin repeats of the mouse Notch2 gene induces early embryonic lethality.,” *Development*, 126(15): 3415–24.

Harman, K. E., Gratian, M. J., Shirlaw, P. J., Bhogal, B. S., Challacombe, S. J. and Black, M. M. (2002) “The transition of pemphigus vulgaris into pemphigus foliaceus: a reflection of changing desmoglein 1 and 3 autoantibody levels in pemphigus vulgaris.,” *The British journal of dermatology*, 146(4): 684–7.

Hart, S., Fischer, O. M. and Ullrich, A. (2004) “Cannabinoids Induce Cancer Cell Proliferation via Tumor Necrosis Factor α -Converting Enzyme (TACE / ADAM17) -Mediated Transactivation of the Epidermal Growth Factor Receptor Advances in Brief Cannabinoids Induce Cancer Cell Proliferation via Tumor Necr,” *Cancer research*, 64: 1943–1950.

Hasina, R., Mollberg, N., Kawada, I., Mutreja, K., Kanade, G., Yala, S., Surati, M., Liu, R., Li, X., Zhou, Y., Ferguson, B. D., Nallasura, V., Cohen, K. S., Hyjek, E., Mueller, J., Kanteti, R., El Hashani, E., Kane, D., Shimada, Y., Lingen, M. W., Husain, A. N., Posner, M. C., Waxman, I., Villaflor, V. M., Ferguson, M. K., Varticovski, L., Vokes, E. E., Gill, P. and Salgia, R. (2013) “Critical role for the receptor tyrosine kinase EPHB4 in esophageal cancers.,” *Cancer research*, 73(1): 184–94.

Hatzfeld, M. and Nachtsheim, C. (1996) “Cloning and characterization of a new armadillo family member, p0071, associated with the junctional plaque: evidence for a subfamily of closely related proteins.,” *Journal of cell science*, 109 (Pt 1), pp. 2767–78.

Hennies, H. C., Hagedorn, M. and Reis, A. (1995) “Palmoplantar keratoderma in association with carcinoma of the esophagus maps to chromosome 17q distal to the keratin gene cluster.,” *Genomics*, 29(2): 537–40.

Henriksen, L., Grandal, M. V., Knudsen, S. L. J., van Deurs, B. and Grøvdal, L. M. (2013) “Internalization mechanisms of the epidermal growth factor receptor after activation with different ligands.,” *PloS one*, 8(3), p. e58148.

Hildesheim, J., Bulavin, D. and Anver, M. (2002) “Gadd45a protects against UV irradiation-induced skin tumors, and promotes apoptosis and stress signaling via MAPK and p53,” *Cancer Research*, 62, pp. 7305–7315.

Hiramoto-Yamaki, N., Takeuchi, S., Ueda, S., Harada, K., Fujimoto, S., Negishi, M. and Katoh, H. (2010) “Ephexin4 and EphA2 mediate cell migration through a RhoG-dependent mechanism.,” *The Journal of cell biology*, 190(3): 461–77.

Hirota, N., Risse, P., Novali, M., Mcgovern, T., Al-alwan, L., Mccuaig, S., Proud, D., Hayden, P., Hamid, Q. and Martin, J. G. (2012) “Histamine may induce airway remodeling through release of epidermal growth factor receptor ligands from bronchial epithelial cells,” *FASEB journal :* 26: 1704–1716.

Hobbs, R. P., Amargo, E. V, Somasundaram, A., Simpson, C. L., Prakriya, M., Denning, M. F. and Green, K. J. (2011) “The calcium ATPase SERCA2 regulates desmoplakin dynamics and intercellular adhesive strength through modulation of PKCα signaling.,” *FASEB journal*, 25(3): 990–1001.

Holland, P. M., Abramson, R. D., Watson, R. and Gelfand, D. H. (1991) “Detection of specific polymerase chain reaction product by utilizing the 5’----3' exonuclease activity of Thermus aquaticus DNA polymerase.,” *Proceedings of the National Academy of Sciences of the United States of America*, 88(16): 7276–80.

Hong, K.-J., Wu, D.-C., Cheng, K.-H., Chen, L.-T. and Hung, W.-C. (2014) “RECK inhibits stemness gene expression and tumorigenicity of gastric cancer cells by suppressing ADAM-mediated Notch1 activation.,” *Journal of cellular physiology*, 229(2): 191–201.

Hopwood, D. (1991) “The oesophageal lining,” in, pp. 4–11.

Hori, K., Fostier, M., Ito, M., Fuwa, T. J., Go, M. J., Okano, H., Baron, M. and Matsuno, K. (2004) “Drosophila deltex mediates suppressor of Hairless-independent and late-endosomal activation of Notch signaling.,” *Development*, 131(22): 5527–37.

Horiuchi, K. (2013) “A Brief History of Tumor Necrosis Factor α – converting Enzyme: An Overview of Ectodomain Shedding,” *The Keio Journal of Medicine*, 62(1): 29–36.

Horiuchi, K., Gall, S., Schulte, M., Yamaguchi, T., Reiss, K., Murphy, G., Toyama, Y., Hartmann, D., Saftig, P. and Blobel, C. (2007) “Substrate selectivity of epidermal growth factor-receptor ligand sheddases and their regulation by phorbol esters and calcium influx,” *Molecular biology of the cell*, 18(1): 176–188.

Horiuchi, K., Kimura, T., Miyamoto, T., Miyamoto, K., Akiyama, H., Takaishi, H., Morioka, H., Nakamura, T., Okada, Y., Blobel, C. P. and Toyama, Y. (2009) “Conditional inactivation of TACE by a Sox9 promoter leads to osteoporosis and increased granulopoiesis via dysregulation of IL-17 and G-CSF.,” *Journal of immunology*, 182(4): 2093–101.

Hosur, V., Johnson, K. R., Burzenski, L. M., Stearns, T. M., Maser, R. S. and Shultz, L. D. (2014) “Rhbdf2 mutations increase its protein stability and drive EGFR hyperactivation through enhanced secretion of amphiregulin.,” *Proceedings of the National Academy of Sciences of the United States of America*, 111(21):E2200-209

Hu, P., Berkowitz, P., O’Keefe, E. J. and Rubenstein, D. S. (2003) “Keratinocyte adherens junctions initiate nuclear signaling by translocation of plakoglobin from the membrane to the nucleus.,” *The Journal of investigative dermatology*, 121(2): 242-51

Huen, A. C., Park, J. K., Godsel, L. M., Chen, X., Bannon, L. J., Amargo, E. V, Hudson, T. Y., Mongiu, A. K., Leigh, I. M., Kelsell, D. P., Gumbiner, B. M. and Green, K. J. (2002) “Intermediate filament-membrane attachments function synergistically with actin-dependent contacts to regulate intercellular adhesive strength.,” *The Journal of cell biology*, 159(6): 1005–17.

Hurbin, A., Dubrez, L., Coll, J.-L. and Favrot, M.-C. (2002) “Inhibition of apoptosis by amphiregulin via an insulin-like growth factor-1 receptor-dependent pathway in non-small cell lung cancer cell lines.,” *The Journal of biological chemistry*, 277(51): 49127–33.

Di Ianni, M., Baldoni, S., Rosati, E., Ciurnelli, R., Cavalli, L., Martelli, M., Marconi, P., Screpanti, I. and Falzetti, F. (2009) “A new genetic lesion in B-CLL: a NOTCH1 PEST domain mutation,” *British journal of haematology*, 146(6): 689–691.

Ihrie, R. A., Marques, M. R., Nguyen, B. T., Horner, J. S., Papazoglu, C., Bronson, R. T., Mills, A. a and Attardi, L. D. (2005) “Perp is a p63-regulated gene essential for epithelial integrity.,” *Cell*, 120(6): 843–56.

Ihrie, R. and Attardi, L. (2005) “A new Perp in the lineup: linking p63 and desmosomal adhesion,” *Cell Cycle*, 4(7): 873–876.

Imsumran, A., Adachi, Y., Yamamoto, H., Li, R., Wang, Y., Min, Y., Piao, W., Nosho, K., Arimura, Y., Shinomura, Y., Hosokawa, M., Lee, C.-T., Carbone, D. P. and Imai, K. (2007) “Insulin-like

growth factor-I receptor as a marker for prognosis and a therapeutic target in human esophageal squamous cell carcinoma.," *Carcinogenesis*, 28(5): 947–56.

Irie, K., Shimizu, K., Sakisaka, T., Ikeda, W. and Takai, Y. (2004) "Roles and modes of action of nectins in cell-cell adhesion.," *Seminars in cell & developmental biology*, 15(6): 643–56.

Ishida-Yamamoto, A., Deraison, C., Bonnart, C., Bitoun, E., Robinson, R., O'Brien, T. J., Wakamatsu, K., Ohtsubo, S., Takahashi, H., Hashimoto, Y., Dopping-Hepenstal, P. J. C., McGrath, J. a, Iizuka, H., Richard, G. and Hovnanian, A. (2005) "LEKTI is localized in lamellar granules, separated from KLK5 and KLK7, and is secreted in the extracellular spaces of the superficial stratum granulosum.," *The Journal of investigative dermatology*, 124(2): 360–6

Ishii, K., Amagai, M., Ohata, Y., Shimizu, H., Hashimoto, T., Ohya, K. and Nishikawa, T. (2000) "Development of pemphigus vulgaris in a patient with pemphigus foliaceus: antidesmoglein antibody profile shift confirmed by enzyme-linked immunosorbent assay.," *Journal of the American Academy of Dermatology*, 42(5 Pt 2): 859–61.

Ishikawa, M., Miyahara, R., Sonobe, M., Horiuchi, M., Mennju, T., Nakayama, E., Kobayashi, M., Kikuchi, R., Kitamura, J., Imamura, N., Huang, C.-L. and Date, H. (2012) "Higher expression of EphA2 and ephrin-A1 is related to favorable clinicopathological features in pathological stage I non-small cell lung carcinoma.," *Lung cancer*. 76(3): 431–8.

Iso, T., Kedes, L. and Hamamori, Y. (2003) "HES and HERP families: multiple effectors of the Notch signaling pathway.," *Journal of cellular physiology*, 194(3): 237–55.

Issuree, P. D. a, Maretzky, T., McIlwain, D. R., Monette, S., Qing, X., Lang, P. a, Swendeman, S. L., Park-Min, K.-H., Binder, N., Kalliolias, G. D., Yarilina, A., Horiuchi, K., Ivashkiv, L. B., Mak, T. W., Salmon, J. E. and Blobel, C. P. (2013) "iRHOM2 is a critical pathogenic mediator of inflammatory arthritis.," *The Journal of clinical investigation*, 123(2): 928–32.

Van Itallie, C., Rahner, C. and Anderson, J. M. (2001) "Regulated expression of claudin-4 decreases paracellular conductance through a selective decrease in sodium permeability.," *The Journal of clinical investigation*, 107(10): 1319–27.

Ivanov, A., Nusrat, A. and Parkos, C. (2004) "Endocytosis of Epithelial Apical Junctional Proteins by a Clathrin-mediated Pathway into a Unique Storage Compartment," *Molecular biology of the cell*, 15:176–188.

Iwatsuki, K., Takigawa, M., Imaizumi, S. and Yamada, M. (1989) "In vivo binding site of pemphigus vulgaris antibodies and their fate during acantholysis," *J Am Acad Dermatol*, 20(4): 578–582.

Jabbari, A., Suárez-Fariñas, M., Dewell, S. and Krueger, J. G. (2012) "Transcriptional profiling of psoriasis using RNA-seq reveals previously unidentified differentially expressed genes.," *The Journal of investigative dermatology*, 132(1): 246–9.

Jamora, C. and Fuchs, E. (2002) "Intercellular adhesion, signalling and the cytoskeleton.," *Nature cell biology*, 4(4): E101–8.

Jefferson, J., Ciatto, C., Shapiro, L. and Liem, R. (2007) "Structural analysis of the plakin domain of bullous pemphigoid antigen1 (BPAG1) suggests that plakins are members of the spectrin superfamily," *Journal of molecular biology*, 366(2): 244–257.

Jékely, G. and Rørth, P. (2003) "Hrs mediates downregulation of multiple signalling receptors in Drosophila.," *EMBO reports*, 4(12): 1163–8.

Jenko, S., Dolenc, I., Gunčar, G., Doberšek, A., Podobnik, M. and Turk, D. (2003) "Crystal Structure of Stefin A in Complex with Cathepsin H: N-terminal Residues of Inhibitors can Adapt to the Active Sites of Endo- and Exopeptidases," *Journal of Molecular Biology*, 326(3): 875–885.

Jhappan, C., Stahle, C., Harkins, R. N., Fausto, N., Smith, G. H. and Merlino, G. T. (1990) "TGFalpha Over-expression in Transgenic Mice Induces Liver Neoplasia and Abnormal Development of the Mammary Gland and Pancreas," *Cell*, 61: 1137–1146.

Johnson, G., Saeki, T., Auersperg, N., Gordon, A., Shoyab, M., Salomon, D. and Stromberg, K. (1991) "Response to and expression of amphiregulin by ovarian carcinoma and normal ovarian surface epithelial cells: nuclear localization of endogenous amphiregulin," *Biochem Biophys Res Commun*, 180(2): 481–488.

Johnson, K. R., Lane, P. W., Cook, S. a, Harris, B. S., Ward-Bailey, P. F., Bronson, R. T., Lyons, B. L., Shultz, L. D. and Davisson, M. T. (2003) "Curly bare (cub), a new mouse mutation on chromosome 11 causing skin and hair abnormalities, and a modifier gene (mcub) on chromosome 5," *Genomics*, 81(1): 6–14.

Johnston, A., Gudjonsson, J., Aphale, A., Guzman, A., Stoll, S. and Elder, J. (2010) "EGFR and IL-1 signaling synergistically promote keratinocyte antimicrobial defenses in a differentiation-dependent manner," *Journal of Investigative Dermatology*, 131(2): 329–337.

Johnston, S. H., Rauskolb, C., Wilson, R., Prabhakaran, B., Irvine, K. D. and Vogt, T. F. (1997) "A family of mammalian Fringe genes implicated in boundary determination and the Notch pathway.," *Development*, 124(11): 2245–54.

Jolly, P. S., Berkowitz, P., Bektas, M., Lee, H.-E., Chua, M., Diaz, L. a and Rubenstein, D. S. (2010) "p38MAPK signaling and desmoglein-3 internalization are linked events in pemphigus acantholysis.," *The Journal of biological chemistry*, 285(12), 8936–41.

Jonca, N., Guerrin, M., Hadjiolova, K., Caubet, C., Gallinaro, H., Simon, M. and Serre, G. (2002) "Corneodesmosin, a component of epidermal corneocyte desmosomes, displays homophilic adhesive properties.," *The Journal of biological chemistry*, 277(7): 5024–9.

Jones, S. and Rappoport, J. Z. (2014) "Interdependent epidermal growth factor receptor signalling and trafficking.," *The international journal of biochemistry & cell biology*. 51: 23–8.

Kalinin, A., Marekov, L. N. and Steinert, P. M. (2001) "Assembly of the epidermal cornified cell envelope.," *Journal of cell science*, 114(Pt 17): 3069–70.

Kamarajan, P., Shin, J., Qian, X., Matte, B., Zhu, J. and Kapila, Y. (2013) "ADAM17-mediated CD44 cleavage promotes orasphere formation or stemness and tumorigenesis in HNSCC," *Cancer medicine*, 2(6): 793–802.

Kaplan, N., Fatima, A., Peng, H., Bryar, P. J., Lavker, R. M. and Getsios, S. (2012) "EphA2/Ephrin-A1 signaling complexes restrict corneal epithelial cell migration.," *Investigative ophthalmology & visual science*, 53(2): 936–45. Karashima, T. and Watt, F. M. (2002) "Interaction of periplakin and envoplakin with intermediate filaments," *Journal of Cell Science*, 115(24), pp. 5027–5037.

Kato, H., Arao, T., Matsumoto, K., Fujita, Y., Kimura, H., Hayashi, H., Nishiki, K., Iwama, M., Shiraishi, O., Yasuda, A., Shinkai, M., Imano, M., Imamoto, H., Yasuda, T., Okuno, K., Shiozaki, H. and Nishio, K. (2013) "Gene amplification of EGFR, HER2, FGFR2 and MET in esophageal squamous cell carcinoma.," *International journal of oncology*, 42(4): 1151–8.

Katoh, M. and Katoh, M. (2007) "Notch signaling in gastrointestinal tract (review).," *International journal of oncology*, 30(1): 247–51.

Keim, S. a, Johnson, K. R., Wheelock, M. J. and Wahl, J. K. (2008) "Generation and characterization of monoclonal antibodies against the proregion of human desmoglein-2.," *Hybridoma (2005)*, 27(4): 249–58.

Kelsell, D. P., Norgett, E. E., Unsworth, H., Teh, M.-T., Cullup, T., Mein, C. a, Dopping-Hepenstal, P. J., Dale, B. a, Tadini, G., Fleckman, P., Stephens, K. G., Sybert, V. P., Mallory, S. B., North,

B. V, Witt, D. R., Sprecher, E., Taylor, A. E. M., Ilchyshyn, A., Kennedy, C. T., Goodyear, H., Moss, C., Paige, D., Harper, J. I., Young, B. D., Leigh, I. M., Eady, R. a J. and O'Toole, E. a (2005) "Mutations in ABCA12 underlie the severe congenital skin disease harlequin ichthyosis.," *American journal of human genetics*, 76(5): 794–803.

Kenny, P. and Bissell, M. (2007) "Targeting TACE-dependent EGFR ligand shedding in breast cancer," *Journal of Clinical Investigation*, 117(2): 337–345.

Khan, K., Hardy, R., Haq, a, Ogunbiyi, O., Morton, D. and Chidgey, M. (2006) "Desmocollin switching in colorectal cancer.," *British journal of cancer*, 95(10): 1367–70.

Kim, K. W., Jee, H. M., Park, Y. H., Choi, B. S., Sohn, M. H. and Kim, K.-E. (2009) "Relationship between amphiregulin and airway inflammation in children with asthma and eosinophilic bronchitis.," *Chest*, 136(3): 805–10.

Kimura, T., Maesawa, C., Ikeda, K., Wakabayashi, G. and Masuda, T. (2006) "Mutations of the epidermal growth factor receptor gene in gastrointestinal tract tumor cell lines.," *Oncology reports*, 15(5): 1205–10.

Kinch, M., Moore, M. and Harpole, D. (2003) "Predictive value of the EphA2 receptor tyrosine kinase in lung cancer recurrence and survival," *Clinical cancer research*, 9: 613–618.

Kitajima, Y. (2013) "New insights into desmosome regulation and pemphigus blistering as a desmosome-remodeling disease.," *The Kaohsiung journal of medical sciences*. 29(1): 1–13.

Klessner, J. L., Desai, B. V, Amargo, E. V, Getsios, S. and Green, K. J. (2009) "EGFR and ADAMs Cooperate to Regulate Shedding and Endocytic Trafficking of the Desmosomal Cadherin Desmoglein 2," *Molecular Biology of the Cell*, 20: 328–337.

Kljuic, A., Gilead, L., Martinez-Mir, A., Frank, J., Christiano, A. M. and Zlotogorski, A. (2003) "A nonsense mutation in the desmoglein 1 gene underlies striate keratoderma.," *Experimental dermatology*, 12(4): 523–7.

Koch, P. J., Mahoney, M. G., Ishikawa, H., Pulkkinen, L., Uitto, J., Shultz, L., Murphy, G. F., Whitaker-Menezes, D. and Stanley, J. R. (1997) "Targeted disruption of the pemphigus vulgaris antigen (desmoglein 3) gene in mice causes loss of keratinocyte cell adhesion with a phenotype similar to pemphigus vulgaris.," *The Journal of cell biology*, 137(5): 1091–102.

Koeser, J., Troyanovsky, S. M., Grund, C. and Franke, W. W. (2003) "De novo formation of desmosomes in cultured cells upon transfection of genes encoding specific desmosomal components," *Experimental Cell Research*, 285(1): 114–130.

Kolegraff, K., Nava, P., Helms, M. N., Parkos, C. a and Nusrat, A. (2011) "Loss of desmocollin-2 confers a tumorigenic phenotype to colonic epithelial cells through activation of Akt/β-catenin signaling.," *Molecular biology of the cell*, 22(8): 1121–34.

Kolev, V., Mandinova, A., Guinea-Viniegra, J., Hu, B., Lefort, K., Lambertini, C., Neel, V., Dummer, R., Wagner, E. and Dotto, V. (2008) "EGFR signaling as a negative regulator of Notch1 gene expression: a differentiation/apoptosis control mechanism for proliferating keratinocytes and cancer," *Nature cell biology*, 10(8): 902–911.

Komai, A., Amagai, M., Ishii, K., Nishikawa, T., Chorzelski, T., Matsuo, I. and Hashimoto, T. (2001) "The clinical transition between pemphigus foliaceus and pemphigus vulgaris correlates well with the changes in autoantibody profile assessed by an enzyme-linked immunosorbent assay.," *The British journal of dermatology*, 144(6): 1177–82.

Koong, A. C., Chen, E. Y. and Giaccia, A. J. (1994) "Hypoxia Causes the Activation of Nuclear Factor κ B through the Phosphorylation of I κ B α on Tyrosine Residues Advances in Brief," *Cancer research*, 54: 1425–1430.

Koonin, E. V, Makarova, K. S., Rogozin, I. B., Davidovic, L., Letellier, M.-C. and Pellegrini, L. (2003) “The rhomboids: a nearly ubiquitous family of intramembrane serine proteases that probably evolved by multiple ancient horizontal gene transfers.,” *Genome biology*, 4(3): R19.

Kornfeld, J.-W., Meder, S., Wohlberg, M., Friedrich, R. E., Rau, T., Riethdorf, L., Löning, T., Pantel, K. and Riethdorf, S. (2011) “Overexpression of TACE and TIMP3 mRNA in head and neck cancer: association with tumour development and progression.,” *British journal of cancer*, 104(1): 138–45.

Koulu, L., Kusumi, A., Steinberg, M., Klaus-Kovtun, V. and Stanley, J. (1984) “Human autoantibodies against a desmosomal core protein in pemphigus foliaceus,” *The Journal of experimental medicine*, 160: 1509–1518.

Kowalczyk, A. P., Hatzfeld, M., Bornslaeger, E. a., Kopp, D. S., Borgwardt, J. E., Corcoran, C. M., Settler, A. and Green, K. J. (1999) “The Head Domain of Plakophilin-1 Binds to Desmoplakin and Enhances Its Recruitment to Desmosomes: IMPLICATIONS FOR CUTANEOUS DISEASE,” *Journal of Biological Chemistry*, 274(26): 18145-18148.

Kullander, K. and Klein, R. (2002) “Mechanisms and functions of Eph and ephrin signalling.,” *Nature reviews. Molecular cell biology*, 3(7), pp. 475–86.

Kulski, J. K., Kenworthy, W., Bellgard, M., Taplin, R., Okamoto, K., Oka, A., Mabuchi, T., Ozawa, A., Tamiya, G. and Inoko, H. (2005) “Gene expression profiling of Japanese psoriatic skin reveals an increased activity in molecular stress and immune response signals.,” *Journal of molecular medicine*, 83(12), pp. 964–75.

Kulukian, A. and Fuchs, E. (2013) “Spindle orientation and epidermal morphogenesis.,” *Philosophical transactions of the Royal Society of London. Series B, Biological sciences*, 368(1629): 20130016.

Kumar, S. R., Masood, R., Spannuth, W. a, Singh, J., Scehnet, J., Kleiber, G., Jennings, N., Deavers, M., Krasnoperov, V., Dubeau, L., Weaver, F. a, Sood, a K. and Gill, P. S. (2007) “The receptor tyrosine kinase EphB4 is overexpressed in ovarian cancer, provides survival signals and predicts poor outcome.,” *British journal of cancer*, 96(7):1083–91.

Kuo, B. and Urma, D. (2006) *PART 1: Oral cavity, pharynx and esophagus*, *GI Motility Online*. Available at: http://www.nature.com/gimo/contents/pt1/full/gimo6.html, accessed 5.9.2014.

Kurzen, H., Munzing, I. and Hartschuh, W. (2003) “Kurzen et al 2003 Expression of desmosomal proteins in SCCs of the skin,” *Journal of cutaneous pathology*, 30: 621-630.

Kuwano, H., Nakajima, M., Miyazaki, T. and Kato, H. (2003) “Distinctive clinicopathological characteristics in esophageal squamous cell carcinoma.,” *Annals of thoracic and cardiovascular surgery : official journal of the Association of Thoracic and Cardiovascular Surgeons of Asia*, 9(1): 6–13.

Kwon, M. J. (2013) “Emerging roles of claudins in human cancer.,” *International journal of molecular sciences*, 14(9): 18148–80.

Kyula, J. N., Van Schaeybroeck, S., Doherty, J., Fenning, C. S., Longley, D. B. and Johnston, P. G. (2010) “Chemotherapy-induced activation of ADAM-17: a novel mechanism of drug resistance in colorectal cancer.,” *Clinical cancer research : an official journal of the American Association for Cancer Research*, 16(13): 3378–89.

Laethem, A. Van, Kelst, S. Van, Lippens, S., Declercq, W., Vandenabeele, P., Janssens, S., Vandenheede, J. R., Garmyn, M. and Agostinis, P. (2004) “Activation of p38 MAPK is required for Bax translocation to mitochondria, cytochrome c release and apoptosis induced by UVB irradiation in human keratinocytes,” *FASEB journal,* 33(1): 1–33.

Lager, D. J., Callaghan, E. J., Worth, S. F., Raife, T. J. and Lentz, S. R. (1995) “Cellular localization of thrombomodulin in human epithelium and squamous malignancies.,” *The American journal of pathology*, 146(4): 933–43.

Lai, E. C. (2002) “Protein degradation: four E3s for the notch pathway.,” *Current biology : CB*, 12(2): R74–8.

Larsen, A. B., Pedersen, M. W., Stockhausen, M.-T., Grandal, M. V., van Deurs, B. and Poulsen, H. S. (2007) “Activation of the EGFR gene target EphA2 inhibits epidermal growth factor-induced cancer cell motility.,” *Molecular cancer research,* 5(3): 283–93.

Larsen, A. B., Stockhausen, M.-T. and Poulsen, H. S. (2010) “Cell adhesion and EGFR activation regulate EphA2 expression in cancer.,” *Cellular signalling*. 22(4): 636–44.

Larsson, C., Lardelli, M., White, I. and Lendahl, U. (1994) “The Human NOTCH1,2 and 3 Genes Are Located at Chromosome Positions 9q34, 1p13-p11, and 19p13. 2-p13. 1 in Regions of Neoplasia-Associated Translocation,” *Genomics*, 24: 253–258.

Le, T. L., Yap, A. S. and Stow, J. L. (1999) “Recycling of E-cadherin: a potential mechanism for regulating cadherin dynamics.,” *The Journal of cell biology*, 146(1): 219–32.

Lechler, T. and Fuchs, E. (2005) “Asymmetric cell divisions promote stratification and differentiation of mammalian skin,” *Nature*, 437(7056), pp. 275–280. Available at: http://www.nature.com/nature/journal/v437/n7056/abs/nature03922.html (Accessed: September 07, 2014).

Lee, H. E., Berkowitz, P., Jolly, P. S., Diaz, L. a, Chua, M. P. and Rubenstein, D. S. (2009) “Biphasic activation of p38MAPK suggests that apoptosis is a downstream event in pemphigus acantholysis.,” *The Journal of biological chemistry*, 284(18): 12524–32.

Lee, H., Volonte, D., Galbiati, F., Iyengar, P., Lublin, D. M., Bregman, D. B., Wilson, M. T., Campos-Gonzalez, R., Bouzahzah, B., Pestell, R. G., Scherer, P. E. and Lisanti, M. P. (2000) “Constitutive and growth factor-regulated phosphorylation of caveolin-1 occurs at the same site (Tyr-14) in vivo: identification of a c-Src/Cav-1/Grb7 signaling cassette.,” *Molecular endocrinology*, 14(11): 1750–75.

Lee, J. R., Urban, S., Garvey, C. F. and Freeman, M. (2001) “Regulated Intracellular Ligand Transport and Proteolysis Control EGF Signal Activation in Drosophila,” *Cell*, 107: 161–171.

Lee, S., Kumano, K., Nakazaki, K., Sanada, M., Matsumoto, A., Yamamoto, G., Nannya, Y., Suzuki, R., Ota, S., Ota, Y., Izutsu, K., Sakata-Yanagimoto, M., Hangaishi, A., Yagita, H., Fukayama, M., Seto, M., Kurokawa, M., Ogawa, S. and Chiba, S. (2009) “Gain-of-function mutations and copy number increases of Notch2 in diffuse large B-cell lymphoma,” *Cancer Science*, 100(5): 920–926.

Lee, Y.-C., Perren, J. R., Douglas, E. L., Raynor, M. P., Bartley, M. a, Bardy, P. G. and Stephenson, S.-A. (2005) “Investigation of the expression of the EphB4 receptor tyrosine kinase in prostate carcinoma.,” *BMC cancer*, 5: 119.

Legan, P., Yue, K. and Chidgey, M. (1994) “The Bovine Desmocollin Family: A New Gene and Expression Patterns Reflecting Epithelial Cell Proliferation and Differentiation.,” *The Journal of cell biology*, 126(2): 507–518.

Lei, X. and Li, Y.-M. (2009) “The processing of human rhomboid intramembrane serine protease RHBDL2 is required for its proteolytic activity.,” *Journal of molecular biology*, 394(5): 815–25.

Lemberg, M. K. and Freeman, M. (2007a) “Cutting proteins within lipid bilayers: rhomboid structure and mechanism.,” *Molecular cell*, 28(6): 930–40.

Lemberg, M. K. and Freeman, M. (2007b) “Functional and evolutionary implications of enhanced genomic analysis of rhomboid intramembrane proteases.,” *Genome research*, 17(11): 1634–46.

Lemieux, M. J., Fischer, S. J., Cherney, M. M., Bateman, K. S. and James, M. N. G. (2007) “The crystal structure of the rhomboid peptidase from Haemophilus influenzae provides insight into intramembrane proteolysis.,” *Proceedings of the National Academy of Sciences of the United States of America*, 104(3): 750–4.

Lemmon, M. and Schlessinger, J. (2000) “Cell signaling by receptor tyrosine kinases,” *Cell*, 141(7): 1117–1134.

Lendeckel, U., Kohl, J., Arndt, M., Carl-McGrath, S., Donat, H. and Röcken, C. (2005) “Increased expression of ADAM family members in human breast cancer and breast cancer cell lines.,” *Journal of cancer research and clinical oncology*, 131(1): 41–8.

Lewis, J. E., Wahl, J. K., Sass, K. M., Jensen, P. J., Johnson, K. R. and Wheelock, M. J. (1997) “Cross-talk between adherens junctions and desmosomes depends on plakoglobin.,” *The Journal of cell biology*, 136(4): 919–34.

Lewis, J. S., Landers, R. J., Underwood, J. C., Harris, a L. and Lewis, C. E. (2000) “Expression of vascular endothelial growth factor by macrophages is up-regulated in poorly vascularized areas of breast carcinomas.,” *The Journal of pathology*, 192(2), pp: 150–8.

Li, L., Huang, G. M., Banta, a B., Deng, Y., Smith, T., Dong, P., Friedman, C., Chen, L., Trask, B. J., Spies, T., Rowen, L. and Hood, L. (1998) “Cloning, characterization, and the complete 56.8-kilobase DNA sequence of the human NOTCH4 gene.,” *Genomics*, 51(1): 45–58.

Lieber, T., Kidd, S. and Young, M. W. (2002) “kuzbanian-mediated cleavage of Drosophila Notch.,” *Genes & development*, 16(2): 209–21.

Lin, E. Y., Li, J.-F., Gnatovskiy, L., Deng, Y., Zhu, L., Grzesik, D. a, Qian, H., Xue, X. and Pollard, J. W. (2006) “Macrophages regulate the angiogenic switch in a mouse model of breast cancer.,” *Cancer research*, 66(23): 11238–46.

Lin, E. Y., Nguyen, a V, Russell, R. G. and Pollard, J. W. (2001) “Colony-stimulating factor 1 promotes progression of mammary tumors to malignancy.,” *The Journal of experimental medicine*, 193(6): 727–40.

Lin, S., Gordon, K., Kaplan, N. and Getsios, S. (2010) “Ligand targeting of EphA2 enhances keratinocyte adhesion and differentiation via desmoglein 1,” *Molecular biology of the cell*, 21: 3902–3914.

Liu, B., Xia, X., Zhu, F., Park, E., Carbajal, S., Kiguchi, K., DiGiovanni, J., Fischer, S. M. and Hu, Y. (2008) “IKKalpha is required to maintain skin homeostasis and prevent skin cancer.,” *Cancer cell*, 14(3): 212–25.

Liu, J., Fan, H., Ma, Y., Liang, D., Huang, R., Wang, J., Zhou, F., Kan, Q., Ming, L., Li, H., Giercksky, K.-E., Nesland, J. M. and Suo, Z. (2013) “Notch1 is a 5-fluorouracil resistant and poor survival marker in human esophagus squamous cell carcinomas.,” *PloS one*, 8(2): e56141.

Liu, Y. V, Baek, J. H., Zhang, H., Diez, R., Cole, R. N. and Semenza, L. (2008) “RACK1 Competes with HSP90 for Binding to HIF-1α and is Required for O2 -independent and HSP90 Inhibitor-induced Degradation of HIF-1α,” *Mol Cell.*, 25(2): 207–217.

Liu, Y. V and Semenza, G. L. (2007) “RACK1 vs. HSP90,” *Cell Cycle*, 6(6): 656–659.

Livak, K. J. and Schmittgen, T. D. (2001) “Analysis of relative gene expression data using real-time quantitative PCR and the 2(-Delta Delta C(T)) Method.,” *Methods (San Diego, Calif.)*, 25(4): 402–8.

Logan, K., Hopwood, D. and Milne, G. (1978) “Cellular junctions in human oesophageal epithelium.,” *Journal of Pathology*, 126(3): 157–63.

Logeat, F., Bessia, C., Brou, C., LeBail, O., Jarriault, S., Seidah, N. G. and Israël, a (1998) “The Notch1 receptor is cleaved constitutively by a furin-like convertase.,” *Proceedings of the National Academy of Sciences of the United States of America*, 95(14): 8108–12.

Lohi, O., Urban, S. and Freeman, M. (2004) “Diverse substrate recognition mechanisms for rhomboids; thrombomodulin is cleaved by Mammalian rhomboids.,” *Current biology*, 14(3): 236–41.

Lorch, J. H., Klessner, J., Park, J. K., Getsios, S., Wu, Y. L., Stack, M. S. and Green, K. J. (2004) “Epidermal growth factor receptor inhibition promotes desmosome assembly and strengthens intercellular adhesion in squamous cell carcinoma cells.,” *The Journal of biological chemistry*, 279(35): 37191–200.

Lorenzen, I., Trad, A. and Grötzinger, J. (2011) “Multimerisation of A disintegrin and metalloprotease protein-17 (ADAM17) is mediated by its EGF-like domain.,” *Biochemical and biophysical research communications*. 415(2): 330–6.

Lowell, S., Jones, P., Le Roux, I., Dunne, J. and Watt, F. M. (2000) “Stimulation of human epidermal differentiation by delta-notch signalling at the boundaries of stem-cell clusters.,” *Current biology :* 10(9): 491–500.

Lu, Y., Chopp, M., Zheng, X., Katakowski, M., Buller, B. and Jiang, F. (2013) “MiR-145 reduces ADAM17 expression and inhibits in vitro migration and invasion of glioma cells.,” *Oncology reports*, 29(1): 67–72.

Lubman, O., Korolev, S. and Kopan, R. (2004) “Anchoring Notch genetics and biochemistry: structural analysis of the ankyrin domain sheds light on existing data,” *Molecular cell*, 13: 619–626.

Luetteke, C., Qiu, T., Peiffer, R., Oliver, P., Smithies, O. and Lee, D. (1993) “TGF alpha Deficiency Results in Hair Follicle and Eye Abnormalities in Targeted and Waved-1 mice,” *Cell*, 73: 263–278.

Luetteke, N. C., Phillips, H. K., Qiu, T. H., Copeland, N. G., Earp, H. S., Jenkins, N. a and Lee, D. C. (1994) “The mouse waved-2 phenotype results from a point mutation in the EGF receptor tyrosine kinase.,” *Genes & development*, 8(4): 399–413.

Luetteke, N. C., Qiu, T. H., Fenton, S. E., Troyer, K. L., Riedel, R. F., Chang, a and Lee, D. C. (1999) “Targeted inactivation of the EGF and amphiregulin genes reveals distinct roles for EGF receptor ligands in mouse mammary gland development.,” *Development*, 126(12): 2739–50.

Macari, F., Landau, M., Cousin, P., Mevorah, B., Brenner, S., Panizzon, R., Schorderet, D. F., Hohl, D. and Huber, M. (2000) “Mutation in the gene for connexin 30.3 in a family with erythrokeratodermia variabilis.,” *American journal of human genetics*, 67(5): 1296–301.

Macrae, M., Neve, R. M., Rodriguez-Viciana, P., Haqq, C., Yeh, J., Chen, C., Gray, J. W. and McCormick, F. (2005) “A conditional feedback loop regulates Ras activity through EphA2.,” *Cancer cell*, 8(2): 111–8.

Mahoney, M. G., Hu, Y., Brennan, D., Bazzi, H., Christiano, A. M. and Wahl, J. K. (2006) “Delineation of diversified desmoglein distribution in stratified squamous epithelia: implications in diseases.,” *Experimental dermatology*, 15(2): 101–9.

Mahoney, M. G., Wang, Z., Rothenberger, K., Koch, P. J., Amagai, M. and Stanley, J. R. (1999) “Explanations for the clinical and microscopic localization of lesions in pemphigus foliaceus and vulgaris.,” *The Journal of clinical investigation*, 103(4): 461–8.

Malecki, M. J., Sanchez-Irizarry, C., Mitchell, J. L., Histen, G., Xu, M. L., Aster, J. C. and Blacklow, S. C. (2006) “Leukemia-associated mutations within the NOTCH1 heterodimerization domain fall into at least two distinct mechanistic classes.,” *Molecular and cellular biology*, 26(12): 4642–51.

Mann, G., Fowler, K., Gabriel, A. and Nice, E. (1993) “Mice with a null mutation of the TGFα gene have abnormal skin architecture, wavy hair, and curly whiskers and often develop corneal inflammation,” *Cell*, 73: 249–261.

Mantovani, A., Sozzani, S., Locati, M., Allavena, P. and Sica, A. (2002) “Macrophage polarization: tumor-associated macrophages as a paradigm for polarized M2 mononuclear phagocytes.,” *Trends in immunology*, 23(11): 549–55.

Mao, X., Choi, E. J. and Payne, A. S. (2009) “Disruption of desmosome assembly by monovalent human pemphigus vulgaris monoclonal antibodies.,” *The Journal of investigative dermatology*, 129(4): 908–18.

Marcozzi, C., Burdett, I. D., Buxton, R. S. and Magee, a I. (1998) “Coexpression of both types of desmosomal cadherin and plakoglobin confers strong intercellular adhesion.,” *Journal of cell science*, 111 (Pt 4): 495–509.

Maretzky, T., Evers, A., Zhou, W., Swendeman, S., Wong, P.-M., Rafii, S., Reiss, K. and Blobel, C. (2011) “Migration of FGF7-stimulated epithelial cells and VEGF-A-stimulated HUVECs depends on EGFR transactivation by ADAM17,” *Nature communications*, 2: 229.

Maretzky, T., McIlwain, D. R., Issuree, P. D. a, Li, X., Malapeira, J., Amin, S., Lang, P. a, Mak, T. W. and Blobel, C. P. (2013) “iRhom2 controls the substrate selectivity of stimulated ADAM17-dependent ectodomain shedding.,” *Proceedings of the National Academy of Sciences of the United States of America*, 110(28): 11433–8.

Marques, M. R., Horner, J. S., Ihrie, R. A., Bronson, R. T. and Attardi, L. D. (2005) “Mice Lacking the p53/p63 Target Gene Perp Are Resistant to Papilloma Development,” *Cancer research*, 65: 6551–6556.

Martin, K. J., Patrick, D. R., Bissell, M. J. and Fournier, M. V (2008) “Prognostic breast cancer signature identified from 3D culture model accurately predicts clinical outcome across independent datasets.,” *PloS one*, 3(8): e2994.

Martin, P. E., Easton, J. a, Hodgins, M. B. and Wright, C. S. (2014) “Connexins: sensors of epidermal integrity that are therapeutic targets.,” *FEBS letters*. Federation of European Biochemical Societies, 588(8): 1304–14.

Martins, V. L., Caley, M. and O’Toole, E. a (2013) “Matrix metalloproteinases and epidermal wound repair.,” *Cell and tissue research*, 351(2): 255–68.

Maruthappu, T., Scott, C. A. and Kelsell, D. P. (2014) “Discovery in genetic skin disease: the impact of high throughput genetic technologies.,” *Genes*, 5(3): 615–34.

Mascré, G., Dekoninck, S., Drogat, B., Youssef, K. K., Broheé, S., Sotiropoulou, P. a, Simons, B. D. and Blanpain, C. (2012) “Distinct contribution of stem and progenitor cells to epidermal maintenance.,” *Nature*, 489(7415), 257–62.

Matsui, Y., Halter, S. A., Holt, J. T., Hogan, B. L. M. and Coffey, R. J. (1990) “Development of Mammary in MMTV-TGFalpha Transgenic Hyperplasia Mice and Neoplasia,” *Cell*, 61(29): 1147–1155.

Matsuno, K., Diederich, R. J., Go, M. J., Blaumueller, C. M. and Artavanis-Tsakonas, S. (1995) “Deltex acts as a positive regulator of Notch signaling through interactions with the Notch ankyrin repeats.,” *Development (Cambridge, England)*, 121(8): 2633-44.

Mattey, D. L. and Garrod, D. R. (1986) “Splitting and internalization of the desmosomes of cultured kidney epithelial cells by reduction in calcium concentration.,” *Journal of cell science*, 85: 113–24.

McIlwain, D. R., Lang, P. a, Maretzky, T., Hamada, K., Ohishi, K., Maney, S. K., Berger, T., Murthy, A., Duncan, G., Xu, H. C., Lang, K. S., Häussinger, D., Wakeham, A., Itie-Youten, A., Khokha, R., Ohashi, P. S., Blobel, C. P. and Mak, T. W. (2012) “iRhom2 regulation of TACE controls TNF-mediated protection against Listeria and responses to LPS.,” *Science*, 335(6065): 229–32.

Mendoza, M. C., Er, E. E. and Blenis, J. (2011) “The Ras-ERK and PI3K-mTOR pathways: cross-talk and compensation.,” *Trends in biochemical sciences*: 36(6): 320–8.

Meng, H., Zhang, X., Lee, S. J., Strickland, D. K., Lawrence, D. a and Wang, M. M. (2010) “Low density lipoprotein receptor-related protein-1 (LRP1) regulates thrombospondin-2 (TSP2) enhancement of Notch3 signaling.,” *The Journal of biological chemistry*, 285(30): 23047–55.

Menges, C. W. and McCance, D. J. (2008) “Constitutive activation of the Raf-MAPK pathway causes negative feedback inhibition of Ras-PI3K-AKT and cellular arrest through the EphA2 receptor.,” *Oncogene*, 27(20): 2934–40.

Menke, V., van Es, J. H., de Lau, W., van den Born, M., Kuipers, E. J., Siersema, P. D., de Bruin, R. W. F., Kusters, J. G. and Clevers, H. (2010) “Conversion of metaplastic Barrett’s epithelium into post-mitotic goblet cells by gamma-secretase inhibition.,” *Disease models & mechanisms*, 3(1-2): 104–10.

Mertens, C., Kuhn, C. and Franke, W. W. (1996) “Plakophilins 2a and 2b: constitutive proteins of dual location in the karyoplasm and the desmosomal plaque.,” *The Journal of cell biology*, 135(4): 1009–25.

Miao, H., Gale, N. W., Guo, H., Qian, J., Petty, a, Kaspar, J., Murphy, a J., Valenzuela, D. M., Yancopoulos, G., Hambardzumyan, D., Lathia, J. D., Rich, J. N., Lee, J. and Wang, B. (2014) “EphA2 promotes infiltrative invasion of glioma stem cells in vivo through cross-talk with Akt and regulates stem cell properties.,” *Oncogene*: Feb 3 [Epub ahead of print].

Miao, H., Li, D., Mukherjee, A., Guo, H. and Petty, A. (2009) “EphA2 mediates ligand-dependent inhibition and ligand-independent promotion of cell migration and invasion via a reciprocal regulatory loop with Akt,” *Cancer cell*, 16(1): 9–20.

Miravet, S., Piedra, J., Castaño, J., Raurell, I., Francí, C., Duñach, M. and García de Herreros, A. (2003) “Tyrosine phosphorylation of plakoglobin causes contrary effects on its association with desmosomes and adherens junction components and modulates beta-catenin-mediated transcription.,” *Molecular and cellular biology*, 23(20): 7391-402.

Miyazaki, K., Inokuchi, M., Takagi, Y., Kato, K., Kojima, K. and Sugihara, K. (2013) “EphA4 is a prognostic factor in gastric cancer.,” *BMC clinical pathology*. BMC Clinical Pathology, 13(1): 19.

Mizutani, H., Hayashi, T., Nouchi, N., Ohyanagi, S., Hashimoto, K., Shimizu, M. and Suzuki, K. (1994) “Functional and immunoreactive thrombomodulin expressed by keratinocytes,” *Journal of investigative dermatology*, 103(6): 825–828.

Mohler, K., Sleath, P., Fitzner, J., Cerretti, D., Alderson, M., Kerwar, S., Torrance, D., Otten-Evans, C., Greenstreet, T., Weerawarna, K., Kronheim, S., Petersen, M., Gerhart, M., Kozlosky, C., March, C. and Black, R. (1994) “Protection against a lethal dose of endotoxin by an inhibitor of tumour necrosis factor processing,” *Nature*, 370(6486): 218–220.

Del Monte, G., Grego-Bessa, J., González-Rajal, A., Bolós, V. and De La Pompa, J. L. (2007) “Monitoring Notch1 activity in development: evidence for a feedback regulatory loop.,” *Developmental dynamics : an official publication of the American Association of Anatomists*, 236(9): 2594–614.

Moriyama, M., Durham, A.-D., Moriyama, H., Hasegawa, K., Nishikawa, S., Radtke, F. and Osawa, M. (2008) “Multiple roles of Notch signaling in the regulation of epidermal development.,” *Developmental cell*, 14(4): 594–604.

Mosavi, L. K., Cammett, T. J., Desrosiers, D. C. and Peng, Z.-Y. (2004) “The ankyrin repeat as molecular architecture for protein recognition.,” *Protein science:* 13(6): 1435-48.

Moss, M. L., Jin, S. L., Becherer, J. D., Bickett, D. M., Burkhart, W., Chen, W. J., Hassler, D., Leesnitzer, M. T., McGeehan, G., Milla, M., Moyer, M., Rocque, W., Seaton, T., Schoenen, F., Warner, J. and Willard, D. (1997) “Structural features and biochemical properties of TNF-alpha converting enzyme (TACE).,” *Journal of neuroimmunology*, 72(2): 127–9.

Moss, M. L., Sklair-Tavron, L. and Nudelman, R. (2008) “Drug insight: tumor necrosis factor-converting enzyme as a pharmaceutical target for rheumatoid arthritis.,” *Nature clinical practice. Rheumatology*, 4(6): 300–9.

Müller, J., Ritt, D., Copeland, T. and Morrison, D. (2003) “Functional analysis of C-TAK1 substrate binding and identification of PKP2 as a new C-TAK1 substrate,” *The EMBO journal*, 22(17): 4431–4442

Mutyambizia, K., Bergera, C. L. and Edelson, R. L. (2009) “The balance between immunity and tolerance: The role of Langerhans cells,” *Cell Mol Life Sci*, 66(5): 831–840.

Nagy, N. and McGrath, J. a (2010) “Blistering skin diseases: a bridge between dermatopathology and molecular biology.,” *Histopathology*, 56(1): 91–9.

Nakada, M., Drake, K. L., Nakada, S., Niska, J. a and Berens, M. E. (2006) “Ephrin-B3 ligand promotes glioma invasion through activation of Rac1.,” *Cancer research*, 66(17): 8492–500.

Nakagawa, M., Nabeshima, K., Asano, S., Hamasaki, M., Uesugi, N., Tani, H., Yamashita, Y. and Iwasaki, H. (2009) “Up-regulated expression of ADAM17 in gastrointestinal stromal tumors: coexpression with EGFR and EGFR ligands.,” *Cancer science*, 100(4): 654–62.

Nakagawa, T., Guichard, A., Castro, C. P., Xiao, Y., Rizen, M., Zhang, H.-Z., Hu, D., Bang, A., Helms, J., Bier, E. and Derynck, R. (2005) “Characterization of a human rhomboid homolog, p100hRho/RHBDF1, which interacts with TGF-alpha family ligands.,” *Developmental dynamics:* 233(4): 1315–31.

Narita, D., Seclaman, E., Ursoniu, S. and Anghel, A. (2012) “Increased expression of ADAM12 and ADAM17 genes in laser-capture microdissected breast cancers and correlations with clinical and pathological characteristics.,” *Acta histochemica*. 114(2): 131–9.

Nava, P., Laukoetter, M., Hopkins, A., Laur, O., Gerner-Smidt, K., Green, K., Parkos, C. and Nusrat, A. (2007) “Desmoglein-2: a novel regulator of apoptosis in the intestinal epithelium,” *Molecular biology of the cell*, 18: 4565–4578.

Neelam, B., Richter, a, Chamberlin, S. G., Puddicombe, S. M., Wood, L., Murray, M. B., Nandagopal, K., Niyogi, S. K. and Davies, D. E. (1998) “Structure-function studies of ligand-induced epidermal growth factor receptor dimerization.,” *Biochemistry*, 37(14): 4884–91.

Nelson, W. J. and Nusse, R. (2004) “Convergence of Wnt, beta-catenin, and cadherin pathways.,” *Science*, 303(5663): 1483–7.

Neuber, S., Mühmer, M., Wratten, D., Koch, P. J., Moll, R. and Schmidt, A. (2010) “The desmosomal plaque proteins of the plakophilin family.,” *Dermatology research and practice*, 2010: 101452.

Nguyen, B., Dusek, R. L., Beaudry, V. G., Marinkovich, M. P. and Attardi, L. D. (2009) “Loss of the desmosomal protein perp enhances the phenotypic effects of pemphigus vulgaris autoantibodies.,” *The Journal of investigative dermatology*. 129(7): 1710–8.

Nguyen, B.-C., Lefort, K., Mandinova, A., Antonini, D., Devgan, V., Della Gatta, G., Koster, M. I., Zhang, Z., Wang, J., Tommasi di Vignano, A., Kitajewski, J., Chiorino, G., Roop, D. R., Missero, C. and Dotto, G. P. (2006) “Cross-regulation between Notch and p63 in keratinocyte commitment to differentiation.,” *Genes & development*, 20(8): 1028–42.

Ni, S.-S., Zhang, J., Zhao, W.-L., Dong, X.-C. and Wang, J.-L. (2013) “ADAM17 is overexpressed in non-small cell lung cancer and its expression correlates with poor patient survival.,” *Tumour biology : the journal of the International Society for Oncodevelopmental Biology and Medicine*, 34(3): 1813–8.

Nickoloff, B. J., Qin, J.-Z., Chaturvedi, V., Denning, M. F., Bonish, B. and Miele, L. (2002) “Jagged-1 mediated activation of notch signaling induces complete maturation of human keratinocytes through NF-kappaB and PPARgamma.,” *Cell death and differentiation*, 9(8): 842–55.

Nicolas, M., Wolfer, A., Raj, K., Kummer, J. A., Mill, P., van Noort, M., Hui, C., Clevers, H., Dotto, G. P. and Radtke, F. (2003) “Notch1 functions as a tumor suppressor in mouse skin.,” *Nature genetics*, 33(3): 416–21.

Nicoletti, I., Migliorati, G., Pagliacci, M., Grignani, F. and Riccardi, C. (1991) “A rapid and simple method for measuring thymocyte apoptosis by propidium iodide staining and flow cytometry,” *Journal of Immunological Methods.*, 139(2): 271–279.

Niessen, C. M. (2007) “Tight junctions/adherens junctions: basic structure and function.,” *The Journal of investigative dermatology*, 127(11): 2525–32.

Nitoiu, D., Etheridge, S. L. and Kelsell, D. P. (2014) “Insights into Desmosome Biology from Inherited Human Skin Disease and Cardiocutaneous Syndromes,” *Cell Communication and Adhesion*, 21(3): 129–140.

Nitta, T., Hata, M., Gotoh, S., Seo, Y., Sasaki, H., Hashimoto, N., Furuse, M. and Tsukita, S. (2003) “Size-selective loosening of the blood-brain barrier in claudin-5-deficient mice.,” *The Journal of cell biology*, 161(3): 653–60.

Nollet, F., Kools, P. and van Roy, F. (2000) “Phylogenetic analysis of the cadherin superfamily allows identification of six major subfamilies besides several solitary members.,” *Journal of molecular biology*, 299(3): 551–72.

Norgett, E. E., Hatsell, S. J., Carvajal-Huerta, L., Cabezas, J. C., Common, J., Purkis, P. E., Whittock, N., Leigh, I. M., Stevens, H. P. and Kelsell, D. P. (2000) “Recessive mutation in desmoplakin disrupts desmoplakin-intermediate filament interactions and causes dilated cardiomyopathy, woolly hair and keratoderma.,” *Human molecular genetics*, 9(18): 2761–6.

Nowell, C. and Radtke, F. (2013) “Cutaneous Notch Signaling in Health and Disease,” *Cold Spring Harbor Perspectives in Medicine*, 1;3(12):a017772

Obama, T., Takayanagi, T., Kobayashi, T., Bourne, A. M., Elliott, K. J., Charbonneau, M., Dubois, C. M. and Eguchi, S. (2014) “Vascular Induction of a Disintegrin and Metalloprotease 17 by Angiotensin II Through Hypoxia Inducible Factor 1α,” *American journal of hypertension* May 28 [Epub ahead of print].

Oberg, C., Li, J., Pauley, a, Wolf, E., Gurney, M. and Lendahl, U. (2001) “The Notch intracellular domain is ubiquitinated and negatively regulated by the mammalian Sel-10 homolog.,” *The Journal of biological chemistry*, 276(38): 35847–53.

Öberg, C., Li, J., Pauley, A., Wolf, E., Gurney, M. and Lendahl, U. (2001) "The Notch Intracellular Domain Is Ubiquitinated and Negatively Regulated by the Mammalian Sel-10 Homolog," *Journal of Biological Chemistry* , 276 (38): 35847–35853.

Ogawa, R., Ishiguro, H., Kimura, M., Funahashi, H., Wakasugi, T., Ando, T., Shiozaki, M. and Takeyama, H. (2013) "NOTCH1 Expression Predicts Patient Prognosis in Esophageal Squamous Cell Cancer," *European Surgical Research*, 51(3-4): 101–107.

Ohashi, S., Natsuizaka, M., Yashiro-Ohtani, Y., Kalman, R. a, Nakagawa, M., Wu, L., Klein-Szanto, A. J., Herlyn, M., Diehl, J. A., Katz, J. P., Pear, W. S., Seykora, J. T. and Nakagawa, H. (2010) "NOTCH1 and NOTCH3 coordinate esophageal squamous differentiation through a CSL-dependent transcriptional network.," *Gastroenterology*, 139(6): 2113–23.

Ojalvo, L. S., King, W., Cox, D. and Pollard, J. W. (2009) "High-density gene expression analysis of tumor-associated macrophages from mouse mammary tumors.," *The American journal of pathology*, 174(3): 1048–64.

Oji, V., Tadini, G., Akiyama, M., Blanchet Bardon, C., Bodemer, C., Bourrat, E., Coudiere, P., DiGiovanna, J. J., Elias, P., Fischer, J., Fleckman, P., Gina, M., Harper, J., Hashimoto, T., Hausser, I., Hennies, H. C., Hohl, D., Hovnanian, A., Ishida-Yamamoto, A., Jacyk, W. K., Leachman, S., Leigh, I., Mazereeuw-Hautier, J., Milstone, L., Morice-Picard, F., Paller, A. S., Richard, G., Schmuth, M., Shimizu, H., Sprecher, E., Van Steensel, M., Taïeb, A., Toro, J. R., Vabres, P., Vahlquist, A., Williams, M. and Traupe, H. (2010) "Revised nomenclature and classification of inherited ichthyoses: results of the First Ichthyosis Consensus Conference in Sorèze 2009.," *Journal of the American Academy of Dermatology*, 63(4): 607–41.

Okajima, T., Xu, A., Lei, L. and Irvine, K. D. (2005) "Chaperone activity of protein O-fucosyltransferase 1 promotes notch receptor folding.," *Science*, 307(5715): 1599–603.

Okochi, M., Steiner, H., Fukumori, A., Tanii, H., Tomita, T., Tanaka, T., Iwatsubo, T., Kudo, T., Takeda, M. and Haass, C. (2002) "Presenilins mediate a dual intramembranous gamma-secretase cleavage of Notch-1.," *The EMBO journal*, 21(20): 5408–16.

Oktarina, D. a M., van der Wier, G., Diercks, G. F. H., Jonkman, M. F. and Pas, H. H. (2011) "IgG-induced clustering of desmogleins 1 and 3 in skin of patients with pemphigus fits with the desmoglein nonassembly depletion hypothesis.," *The British journal of dermatology*, 165(3): 552–62.

Olayioye, M. a., Beuvink, I., Horsch, K., Daly, J. M. and Hynes, N. E. (1999) "ErbB Receptor-induced Activation of Stat Transcription Factors Is Mediated by Src Tyrosine Kinases," *Journal of Biological Chemistry*, 274(24): 17209–17218.

Olayioye, M., Neve, R., Lane, H. and Hynes, N. (2000) "The ErbB signaling network: receptor heterodimerization in development and cancer," *The EMBO journal*, 19(13): 3159–3167.

Ooshio, T., Kobayashi, R., Ikeda, W., Miyata, M., Fukumoto, Y., Matsuzawa, N., Ogita, H. and Takai, Y. (2010) "Involvement of the interaction of afadin with ZO-1 in the formation of tight junctions in Madin-Darby canine kidney cells.," *The Journal of biological chemistry*, 285(7): 5003–12.

Osada, K., Seishima, M. and Kitajima, Y. (1997) "Pemphigus IgG activates and translocates protein kinase C from the cytosol to the particulate/cytoskeleton fractions in human keratinocytes," *Journal of investigative dermatology*, 108(4): 482–487.

Ostenfeld, M. S., Bramsen, J. B., Lamy, P., Villadsen, S. B., Fristrup, N., Sørensen, K. D., Ulhøi, B., Borre, M., Kjems, J., Dyrskjøt, L. and Orntoft, T. F. (2010) "miR-145 induces caspase-dependent and -independent cell death in urothelial cancer cell lines with targeting of an expression signature present in Ta bladder tumors.," *Oncogene*, 29(7): 1073–84.

Ouban, A., Muraca, P., Yeatman, T. and Coppola, D. (2003) “Expression and distribution of insulin-like growth factor-1 receptor in human carcinomas,” *Human Pathology*, 34(8): 803–808.

Palka, H. L. and Green, K. J. (1997) “Roles of plakoglobin end domains in desmosome assembly.,” *Journal of cell science*, 110 (Pt 1): 2359–71.

Park, J. B., Lee, C. S., Jang, J.-H., Ghim, J., Kim, Y.-J., You, S., Hwang, D., Suh, P.-G. and Ryu, S. H. (2012) “Phospholipase signalling networks in cancer.,” *Nature reviews. Cancer*. Nature Publishing Group, 12(11): 782–92.

Park, J.-I., Kim, S. W., Lyons, J. P., Ji, H., Nguyen, T. T., Cho, K., Barton, M. C., Deroo, T., Vleminckx, K., Moon, R. T. and McCrea, P. D. (2005) “Kaiso/p120-catenin and TCF/beta-catenin complexes coordinately regulate canonical Wnt gene targets.,” *Developmental cell*, 8(6): 843–54.

Pascall, J. C. and Brown, K. D. (2004a) “Intramembrane cleavage of ephrinB3 by the human rhomboid family protease, RHBDL2.,” *Biochemical and biophysical research communications*, 317(1): 244–52.

Pascall, J. C. and Brown, K. D. (2004b) “ScienceDirect - Biochemical and Biophysical Research Communications : Intramembrane cleavage of ephrinB3 by the human rhomboid family protease, RHBDL2,” *Biochemical and biophysical research communications*, 317(1): 244–52.

Pasquale, E. (2010) “Eph receptors and ephrins in cancer: bidirectional signalling and beyond,” *Nature Reviews Cancer*, 10(3): 165–180.

Pasquale, E. B. (2005) “Eph receptor signalling casts a wide net on cell behaviour.,” *Nature reviews. Molecular cell biology*, 6(6): 462–75.

Pasquale, E. B. (2008) “Eph-ephrin bidirectional signaling in physiology and disease.,” *Cell*, 133(1): 38–52.

Paterson, A. D., Parton, R. G., Ferguson, C., Stow, J. L. and Yap, A. S. (2003) “Characterization of E-cadherin endocytosis in isolated MCF-7 and chinese hamster ovary cells: the initial fate of unbound E-cadherin.,” *The Journal of biological chemistry*, 278(23): 21050–7.

Pavlova, A., Estrada, S. and Björk, I. (2002) “The role of the second binding loop of the cysteine protease inhibitor, cystatin A (stefin A), in stabilizing complexes with target proteases is exerted predominantly by Leu73,” *European Journal of Biochemistry*, 269(22): 5649–5658.

Payne, A. S., Hanakawa, Y., Amagai, M. and Stanley, J. R. (2004) “Desmosomes and disease: pemphigus and bullous impetigo.,” *Current opinion in cell biology*, 16(5): 536-43

Pennathur, A., Farkas, A., Krasinskas, A., Ferson, P., Gooding, W., Gibson, M., Schuchert, M., Landreneau, R. and Luketich, J. (2009) “Esophagectomy for T1 esophageal cancer: outcomes in 100 patients and implications for endoscopic therapy,” *The Annals of thoracic surgery*, 87:1048–1055.

Pennathur, A., Gibson, M. K., Jobe, B. a and Luketich, J. D. (2013) “Oesophageal carcinoma.,” *Lancet*. Elsevier Ltd, 381(9864): 400–12.

Peschon, J., Slack, J., Reddy, P., Stocking, K., Synnarborg, S., Lee, D., Russell, W., Castner, B., Johnson, R., Fitzner, J., Boyce, R., Nelson, N., Kozlosky, C., Wolfson, M., Charles, T., Cerretti, D., Paxton, R., March, C. and Black, R. (1998) “An Essential Role for Ectodomain Shedding in Mammalian Development,” *Science*, 282(5392): 1281-1284.

Petcherski, A. G. and Kimble, J. (2000) “Mastermind is a putative activator for Notch.,” *Current biology* 10(13): R471–3.

Peterson, J. J., Rayburn, H. B., Lager, D. J., Raife, T. J., Kealey, G. P., Rosenberg, R. D. and Lentz, S. R. (1999) “Expression of thrombomodulin and consequences of thrombomodulin deficiency during healing of cutaneous wounds.,” *The American journal of pathology*, 155(5): 1569–75.

Piao, W., Wang, Y., Adachi, Y., Yamamoto, H., Li, R., Imsumran, A., Li, H., Maehata, T., Ii, M., Arimura, Y., Lee, C.-T., Shinomura, Y., Carbone, D. P. and Imai, K. (2008) “Insulin-like growth factor-I receptor blockade by a specific tyrosine kinase inhibitor for human gastrointestinal carcinomas.,” *Molecular cancer therapeutics*, 7(6): 1483–93.

Pigors, M., Kiritsi, D., Krümpelmann, S., Wagner, N., He, Y., Podda, M., Kohlhase, J., Hausser, I., Bruckner-Tuderman, L. and Has, C. (2011) “Lack of plakoglobin leads to lethal congenital epidermolysis bullosa: a novel clinico-genetic entity.,” *Human molecular genetics*, 20(9): 1811–9.

Piruzian, E. S., Sobolev, V. V, Abdeev, R. M., Zolotarenko, a D., Nikolaev, a a, Sarkisova, M. K., Sautin, M. E., Ishkin, a a, Piruzyan, A. L., Ilyina, S. a, Korsunskaya, I. M., Rahimova, O. Y. and Bruskin, S. a (2009) “Study of Molecular Mechanisms Involved in the Pathogenesis of Immune-Mediated Inflammatory Diseases, using Psoriasis As a Model.,” *Acta naturae*, 1(3): 125–35.

Pitsouli, C. and Delidakis, C. (2005) “The interplay between DSL proteins and ubiquitin ligases in Notch signaling.,” *Development (Cambridge, England)*, 132(18): 4041–50.

Pokutta, S. and Weis, W. I. (2007) “Structure and mechanism of cadherins and catenins in cell-cell contacts.,” *Annual review of cell and developmental biology*, 23: 237–61.

Poulson, D. F. (1939) “Effects of Notch deficiencies.,” *Drosophila Information Service*, 12: 64.

Poulson, N. D. and Lechler, T. (2010) “Robust control of mitotic spindle orientation in the developing epidermis.,” *The Journal of cell biology*, 191(5): 915–22.

Prenzel, N., Zwick, E., Daub, H., Leserer, M., Abraham, R., Wallasch, C. and Ullrich, a (1999) “EGF receptor transactivation by G-protein-coupled receptors requires metalloproteinase cleavage of proHB-EGF.,” *Nature*, 402(6764): 884–8.

Pruessmeyer, J. and Ludwig, A. (2009) “The good, the bad and the ugly substrates for ADAM10 and ADAM17 in brain pathology, inflammation and cancer.,” *Seminars in cell & developmental biology*, 20(2): 164–74.

Psyrri, A., Seiwert, T. Y. and Jimeno, A. (2013) “Molecular pathways in head and neck cancer: EGFR, PI3K, and more.,” *American Society of Clinical Oncology educational book / ASCO. American Society of Clinical Oncology. Meeting*: 246–55.

Puente, X. S., Pinyol, M., Quesada, V., Conde, L., Ordóñez, G. R., Villamor, N., Escaramis, G., Jares, P., Beà, S., González-Díaz, M., Bassaganyas, L., Baumann, T., Juan, M., López-Guerra, M., Colomer, D., Tubío, J. M. C., López, C., Navarro, A., Tornador, C., Aymerich, M., Rozman, M., Hernández, J. M., Puente, D. a, Freije, J. M. P., Velasco, G., Gutiérrez-Fernández, A., Costa, D., Carrió, A., Guijarro, S., Enjuanes, A., Hernández, L., Yagüe, J., Nicolás, P., Romeo-Casabona, C. M., Himmelbauer, H., Castillo, E., Dohm, J. C., de Sanjosé, S., Piris, M. a, de Alava, E., San Miguel, J., Royo, R., Gelpí, J. L., Torrents, D., Orozco, M., Pisano, D. G., Valencia, A., Guigó, R., Bayés, M., Heath, S., Gut, M., Klatt, P., Marshall, J., Raine, K., Stebbings, L. a, Futreal, P. A., Stratton, M. R., Campbell, P. J., Gut, I., López-Guillermo, A., Estivill, X., Montserrat, E., López-Otín, C. and Campo, E. (2011) “Whole-genome sequencing identifies recurrent mutations in chronic lymphocytic leukaemia.,” *Nature*, 475(7354): 101–5.

Purdie, K., Lambert, S., Teh, M.-T., Chaplin, T., Molloy, G., Raghavan, M., Kelsell, D., Leigh, I., Harwood, C., Proby, C. and Young, B. (2007) “Allelic imbalances and microdeletions affecting the PTPRD gene in cutaneous squamous cell carcinomas detected using single nucleotide polymorphism microarray,” *Genes, Chromosomes and Cancer*, 46(7): 661–669.

Qi, Y., Operario, D. and Oberholzer, C. (2010) “Human basophils express amphiregulin in response to T cell–derived IL-3,” *Journal of Allergy and clinical immunity*, 126(6): 1260–1266.

Qin, L., Tamasi, J., Raggatt, L., Li, X., Feyen, J. H. M., Lee, D. C., Dicicco-Bloom, E. and Partridge, N. C. (2005) “Amphiregulin is a novel growth factor involved in normal bone development and in the cellular response to parathyroid hormone stimulation.,” *The Journal of biological chemistry*, 280(5): 3974–81.

Qiu, L., Joazeiro, C., Fang, N., Wang, H. Y., Elly, C., Altman, Y., Fang, D., Hunter, T. and Liu, Y. C. (2000) “Recognition and ubiquitination of Notch by Itch, a hect-type E3 ubiquitin ligase.,” *The Journal of biological chemistry*, 275(46): 35734–7.

Rabinow, L. and Birchler, J. (1990) “Interactions of vestigial and scabrous with the Notch locus of Drosophila melanogaster.,” *Genetics*, 125: 41–50.

Rackauskas, M., Kreuzberg, M. M., Pranevicius, M., Willecke, K., Verselis, V. K. and Bukauskas, F. F. (2007) “Gating properties of heterotypic gap junction channels formed of connexins 40, 43, and 45.,” *Biophysical journal*, 92(6): 1952–65.

Radner, F. P. W. and Fischer, J. (2014) “The important role of epidermal triacylglycerol metabolism for maintenance of the skin permeability barrier function.,” *Biochimica et biophysica acta*. Elsevier B.V., 1841(3): 409–15.

Raife, T. J., Demetroulis, E. M. and Lentz, S. R. (1996) “Regulation of thrombomodulin expression by all-trans retinoic acid and tumor necrosis factor-alpha: differential responses in keratinocytes and endothelial cells.,” *Blood*, 88(6): 2043–9.

Raife, T., Lager, D., KC, M., Piette, W., Howard, E., Sturm, M., Chen, Y. and Lentz, S. (1994) “Thrombomodulin expression by human keratinocytes. Induction of cofactor activity during epidermal differentiation.,” *Journal of Clinical investigation*, 93: 184-1851.

Rangarajan, A., Talora, C., Okuyama, R., Nicolas, M., Mammucari, C., Oh, H., Aster, J. C., Krishna, S., Metzger, D., Chambon, P., Miele, L., Aguet, M., Radtke, F. and Dotto, G. P. (2001) “Notch signaling is a direct determinant of keratinocyte growth arrest and entry into differentiation.,” *The EMBO journal*, 20(13): 3427–36.

Rasi, S., Monti, S., Spina, V., Foà, R., Gaidano, G. and Rossi, D. (2012) “Analysis of NOTCH1 mutations in monoclonal B-cell lymphocytosis.,” *Haematologica*, 97(1): 153–4.

Ray, R., Li, C., Bhattacharya, S., Naren, A. and Johnson, L. (2012) “Spermine, a molecular switch regulating EGFR, integrin β3, Src, and FAK scaffolding,” *Cellular signalling*, 24(4): 931–942.

Rechsteiner, M. (1988) “Regulation of enzyme levels by proteolysis: the role of pest regions,” *Advances in enzyme regulation*, 27: 135–51.

Rechsteiner, M. and Rogers, S. W. (1996) “PEST sequences and regulation by proteolysis.,” *Trends in biochemical sciences*, 21(7): 267–71.

Rego, S. L., Helms, R. S. and Dréau, D. (2014) “Tumor necrosis factor-alpha-converting enzyme activities and tumor-associated macrophages in breast cancer.,” *Immunologic research*, 58(1): 87–100.

Renko, M., Požgan, U., Majera, D. and Turk, D. (2010) “Stefin A displaces the occluding loop of cathepsin B only by as much as required to bind to the active site cleft.,” *The FEBS journal*, 277(20): 4338–45.

Reynolds, A. B. and Roczniak-Ferguson, A. (2004) “Emerging roles for p120-catenin in cell adhesion and cancer.,” *Oncogene*, 23(48): 7947–56.

Richard, G., Smith, L. E., Bailey, R. a, Itin, P., Hohl, D., Epstein, E. H., DiGiovanna, J. J., Compton, J. G. and Bale, S. J. (1998) “Mutations in the human connexin gene GJB3 cause erythrokeratodermia variabilis.,” *Nature genetics*, 20(4): 366–9.

Richards, F. M., Tape, C. J., Jodrell, D. I. and Murphy, G. (2012) “Anti-tumour effects of a specific anti-ADAM17 antibody in an ovarian cancer model in vivo.,” *PloS one*, 7(7): e40597.

Ringel, J., Jesnowski, R., Moniaux, N., Lüttges, J., Ringel, J., Choudhury, A., Batra, S. K., Klöppel, G. and Löhr, M. (2006) “Aberrant expression of a disintegrin and metalloproteinase 17/tumor necrosis factor-alpha converting enzyme increases the malignant potential in human pancreatic ductal adenocarcinoma.,” *Cancer research*, 66(18): 9045–53.

Rodrigues, G.A., Falasca M., Zhang, Z., Ong, S.H., Schlessinger, J (2000). A Novel Positive Feedback Loop Mediated by the Docking Protein Gab1 and Phosphatidylinositol 3-Kinase in Epidermal Growth Factor Receptor Signaling. Molecular and Cellular Biology 2000;20: 1448–59

Roepstorff, K., Grandal, M. V., Henriksen, L., Knudsen, S. L. J., Lerdrup, M., Grøvdal, L., Willumsen, B. M. and van Deurs, B. (2009) “Differential effects of EGFR ligands on endocytic sorting of the receptor.,” *Traffic*, 10(8): 1115–27.

Rogers, S., Wells, R. and Rechsteiner, M. (1986) “Amino acid sequences common to rapidly degraded proteins: the PEST hypothesis.,” *Science,* 234(4774): 364–8.

Rose-John, S. (2013) “ADAM17, shedding, TACE as therapeutic targets.,” *Pharmacological research*, 71: 19–22.

Rosendahl, M. S., Ko, S. C., Long, D. L., Brewer, M. T., Rosenzweig, B., Hedl, E., Anderson, L., Pyle, S. M., Moreland, J., Meyers, M. a., Kohno, T., Lyons, D. and Lichenstein, H. S. (1997) “Identification and Characterization of a Pro-tumor Necrosis Factor- -processing Enzyme from the ADAM Family of Zinc Metalloproteases,” *Journal of Biological Chemistry*, 272(39): 24588–24593.

Roura, S., Miravet, S., Piedra, J., Garcia de Herreros, A. and Dunach, M. (1999) “Regulation of E-cadherin/Catenin Association by Tyrosine Phosphorylation,” *Journal of Biological Chemistry*, 274: 36734–36740.

Ruhrberg, C., Hajibagheri, M.A., Parry, D. A. and Watt, F. M. (1997) “Periplakin, a novel component of cornified envelopes and desmosomes that belongs to the plakin family and forms complexes with envoplakin.,” *The Journal of cell biology*, 139(7): 1835–49.

Ruhrberg, C., Hajibagheri, M. a, Simon, M., Dooley, T. P. and Watt, F. M. (1996) “Envoplakin, a novel precursor of the cornified envelope that has homology to desmoplakin.,” *The Journal of cell biology*, 134(3): 715–29.

Ruiz, P., Brinkmann, V., Ledermann, B., Behrend, M., Grund, C., Thalhammer, C., Vogel, F., Birchmeier, C., Günthert, U., Franke, W. W. and Birchmeier, W. (1996) “Targeted mutation of plakoglobin in mice reveals essential functions of desmosomes in the embryonic heart.,” *The Journal of cell biology*, 135(1): 215–25.

Runkle, E. A. and Mu, D. (2013) “Tight junction proteins: from barrier to tumorigenesis.,” *Cancer letters*. Elsevier Ireland Ltd, 337(1): 41–8.

Runswick, S. K., O’Hare, M. J., Jones, L., Streuli, C. H. and Garrod, D. R. (2001) “Desmosomal adhesion regulates epithelial morphogenesis and cell positioning.,” *Nature cell biology*, 3(9): 823–30.

Ryan, K. R., Lock, F. E., Heath, J. K. and Hotchin, N. a (2012) “Plakoglobin-dependent regulation of keratinocyte apoptosis by Rnd3.,” *Journal of cell science*, 125(Pt 13): 3202–9.

Saarinen, S., Vahteristo, P., Lehtonen, R., Aittomäki, K., Launonen, V., Kiviluoto, T. and Aaltonen, L. a (2012) “Analysis of a Finnish family confirms RHBDF2 mutations as the underlying factor in tylosis with esophageal cancer.,” *Familial cancer*, 11(3): 525–8.

Sadagurski, M., Yakar, S., Weingarten, G., Holzenberger, M., Rhodes, C. J., Breitkreutz, D., Leroith, D. and Wertheimer, E. (2006) “Insulin-Like Growth Factor 1 Receptor Signaling Regulates Skin Development and Inhibits Skin Keratinocyte Differentiation,” *Molecular and cellular biology*, 26(7): 2675–2687.

Sadowski, T. and Dietrich, S. (2003) “Matrix metalloproteinase 19 regulates insulin-like growth factor-mediated proliferation, migration, and adhesion in human keratinocytes through proteolysis of insulin-,” *Molecular biology of the cell*, 14: 4569–4580

Sahin, U. and Blobel, C. P. (2007) “Ectodomain shedding of the EGF-receptor ligand epigen is mediated by ADAM17.,” *FEBS letters*, 581(1): 41–4.

Sahin, U., Weskamp, G., Kelly, K., Zhou, H.-M., Higashiyama, S., Peschon, J., Hartmann, D., Saftig, P. and Blobel, C. P. (2004) “Distinct roles for ADAM10 and ADAM17 in ectodomain shedding of six EGFR ligands.,” *The Journal of cell biology*, 164(5): 769–79.

Saintigny, P., Peng, S., Zhang, L., Sen, B., Wistuba, I. I., Lippman, S. M., Girard, L., Minna, J. D., Heymach, J. V and Johnson, F. M. (2012) “Global evaluation of Eph receptors and ephrins in lung adenocarcinomas identifies EphA4 as an inhibitor of cell migration and invasion.,” *Molecular cancer therapeutics*, 11(9): 2021–32.

Saitou, M., Furuse, M., Sasaki, H., Schulzke, J. D., Fromm, M., Takano, H., Noda, T. and Tsukita, S. (2000) “Complex phenotype of mice lacking occludin, a component of tight junction strands.,” *Molecular biology of the cell*, 11(12): 4131–42.

Sakai, M., Kato, H., Sano, A., Tanaka, N., Inose, T., Kimura, H., Sohda, M., Nakajima, M. and Kuwano, H. (2009) “Expression of lysyl oxidase is correlated with lymph node metastasis and poor prognosis in esophageal squamous cell carcinoma.,” *Annals of surgical oncology*, 16(9): 2494–501.

Sakuntabhai, A., Ruiz-Perez, V., Carter, S., Jacobsen, S., Burge, S., Monk, S., Smith, M., Munro, C., O’Donavan, M., Craddock, N., Kucherlapati, R., Rees, J., Owen, M., Lathrop, G., Monaco, A., Strachan, T. and Hovnavian, A. (1999) “Mutations in ATP2A2, encoding a Ca2+ pump, cause Darier disease,” *Nature genetics*, 21: 271–277.

Salomon, D. S., Brandt, R., Ciardiello, F. and Normanno, N. (1995) “Epidermal growth factor-related peptides and their receptors in human malignancies.,” *Critical reviews in oncology/hematology*, 19(3):183–232.

Samuelov, L., Sarig, O., Harmon, R. M., Rapaport, D., Ishida-, A., Isakov, O., Koetsier, J. L., Gat, A. and Goldberg, I. (2014) “Desmoglein 1 deficiency results in severe dermatitis, multiple allergies and metabolic wasting,” *Nature genetics*, 45(10): 1244-1248.

Sanderson, M. P., Erickson, S. N., Gough, P. J., Garton, K. J., Wille, P. T., Raines, E. W., Dunbar, A. J. and Dempsey, P. J. (2005) “ADAM10 mediates ectodomain shedding of the betacellulin precursor activated by p-aminophenylmercuric acetate and extracellular calcium influx.,” *The Journal of biological chemistry*, 280(3): 1826–37.

Sandgren, E., Luetteke, N., Palmiter, R., Brinster, R. and Lee, D. (1990) “Overexpression of TGFα in transgenic mice: induction of epithelial hyperplasia, pancreatic metaplasia, and carcinoma of the breast,” *Cell*, 61: 1121–1135.

Santiago-Josefat, B., Esselens, C., Bech-Serra, J. J. and Arribas, J. (2007) “Post-transcriptional up-regulation of ADAM17 upon epidermal growth factor receptor activation and in breast tumors.,” *The Journal of biological chemistry*, 282(11): 8325–31.

Sasamura, T., Sasaki, N., Miyashita, F., Nakao, S., Ishikawa, H. O., Ito, M., Kitagawa, M., Harigaya, K., Spana, E., Bilder, D., Perrimon, N. and Matsuno, K. (2003) “neurotic, a novel maternal neurogenic gene, encodes an O-fucosyltransferase that is essential for Notch-Delta interactions.,” *Development*, 130(20): 4785–95.

Savignac, M., Simon, M., Edir, A., Guibbal, L. and Hovnanian, A. (2014) “SERCA2 dysfunction in Darier disease causes endoplasmic reticulum stress and impaired cell-to-cell adhesion strength: rescue by Miglustat.,” *The Journal of investigative dermatology*. 134(7): 1961–70.

Saxena, M. T., Schroeter, E. H., Mumm, J. S. and Kopan, R. (2001) “Murine notch homologs (N1-4) undergo presenilin-dependent proteolysis.,” *The Journal of biological chemistry*, 276(43): 40268–73.

Sayer, R. a, Lancaster, J. M., Pittman, J., Gray, J., Whitaker, R., Marks, J. R. and Berchuck, A. (2005) “High insulin-like growth factor-2 (IGF-2) gene expression is an independent predictor of poor survival for patients with advanced stage serous epithelial ovarian cancer.,” *Gynecologic oncology*, 96(2): 355–61.

Schäfer, S., Stumpp, S. and Franke, W. W. (1996) “Immunological identification and characterization of the desmosomal cadherin Dsg2 in coupled and uncoupled epithelial cells and in human tissues.,” *Differentiation; research in biological diversity*. International Society of Differentiation, 60(2): 99–108.

Scheller, J., Chalaris, A., Garbers, C. and Rose-John, S. (2011) “ADAM17: a molecular switch to control inflammation and tissue regeneration.,” *Trends in immunology*, 32(8): 380–7.

Schlondorff, J., Becherer, J. and Blobel, C. (2000) “Intracellular maturation and localization of the tumour necrosis factor α convertase (TACE),” *Biochem. J*, 138: 131–138.

Schmidt, A., Langbein, L., Rode, M., Pratzel, S., Zimbelmann, R. and Franke, W. W. (1997) “Plakophilins 1a and 1b: widespread nuclear proteins recruited in specific epithelial cells as desmosomal plaque components,” *Cell and tissue research*, 290: 481–499.

Schmidt, M. H. H., Bicker, F., Nikolic, I., Meister, J., Babuke, T., Picuric, S., Müller-Esterl, W., Plate, K. H. and Dikic, I. (2009) “Epidermal growth factor-like domain 7 (EGFL7) modulates Notch signalling and affects neural stem cell renewal.,” *Nature cell biology*, 11(7), 873–80.

Schneeberger, E. E. and Lynch, R. D. (2004) “The tight junction: a multifunctional complex.,” *American journal of physiology, Cell physiology*, 286(6), pp. C1213–28.

Schneider, M. R. and Wolf, E. (2008) “The epidermal growth factor receptor and its ligands in female reproduction: insights from rodent models.,” *Cytokine & growth factor reviews*, 19(2): 173–81.

Schneider, M. R. and Wolf, E. (2009) “The epidermal growth factor receptor ligands at a glance.,” *Journal of cellular physiology*, 218(3): 460–6.

Schulze, K., Galichet, A., Sayar, B. S., Scothern, A., Howald, D., Zymann, H., Siffert, M., Zenhäusern, D., Bolli, R., Koch, P. J., Garrod, D., Suter, M. M. and Müller, E. J. (2012) “An adult passive transfer mouse model to study desmoglein 3 signaling in pemphigus vulgaris.,” *The Journal of investigative dermatology*, 132(2): 346–55.

Scott, A. J., O’Dea, K. P., O’Callaghan, D., Williams, L., Dokpesi, J. O., Tatton, L., Handy, J. M., Hogg, P. J. and Takata, M. (2011) “Reactive oxygen species and p38 mitogen-activated protein kinase mediate tumor necrosis factor α-converting enzyme (TACE/ADAM-17) activation in primary human monocytes.,” *The Journal of biological chemistry*, 286(41): 35466–76.

Scott, C. A., Rajpopat, S. and Di, W.-L. (2013) “Harlequin ichthyosis: ABCA12 mutations underlie defective lipid transport, reduced protease regulation and skin-barrier dysfunction.,” *Cell and tissue research*, 351(2), pp. 281–8.

Scott, C. A., Tattersall, D., O’Toole, E. A. and Kelsell, D. P. (2012) “Connexins in epidermal homeostasis and skin disease.,” *Biochimica et biophysica acta*. 1818(8): 1952–61.

Scott, J. A., Shewan, A. M., den Elzen, N. R., Loureiro, J. J., Gertler, F. B. and Yap, A. S. (2006) “Ena/VASP proteins can regulate distinct modes of actin organization at cadherin-adhesive contacts.,” *Molecular biology of the cell*, 17(3): 1085–95.

Scott, J. A. and Yap, A. S. (2006) “Cinderella no longer: alpha-catenin steps out of cadherin’s shadow.,” *Journal of cell science*, 119(Pt 22): 4599–605.

Senet, P., Peyri, N., Berard, M., Dubertret, L. and Boffa, M. (1997) “Thrombomodulin, a functional surface protein on human keratinocytes, is regulated by retinoic acid,” *Archives of Dermatological Research*, 289(3): 151–157.

Sengupta, S., Peterson, T. and Sabatini, D. (2010) “Regulation of the mTOR complex 1 pathway by nutrients, growth factors, and stress,” *Molecular cell*, 40(2): 310–322.

Serre, G., Mils, V., Haftek, M., Vincent, C., Croute, F., Réano, A., Ouhayoun, J. P., Bettinger, S. and Soleilhavoup, J. P. (1991) “Identification of late differentiation antigens of human cornified epithelia, expressed in re-organized desmosomes and bound to cross-linked envelope.,” *The Journal of investigative dermatology*, 97(6): 1061–72.

Sestan, N., Artavanis-Tsakonas, S. and Rakic, P. (1999) “Contact-Dependent Inhibition of Cortical Neurite Growth Mediated by Notch Signaling,” *Science*, 286(5440): 741-746.

Shao, J., Lee, S. B., Guo, H., Evers, B. M. and Sheng, H. (2003) “Prostaglandin E 2 Stimulates the Growth of Colon Cancer Cells via Induction of Amphiregulin Prostaglandin E 2 Stimulates the Growth of Colon Cancer Cells via Induction of Amphiregulin,” *Cancer research*, 63: 5218–5223.

Shi, C.-S., Shi, G.-Y., Chang, Y.-S., Han, H.-S., Kuo, C.-H., Liu, C., Huang, H.-C., Chang, Y.-J., Chen, P.-S. and Wu, H.-L. (2005) “Evidence of human thrombomodulin domain as a novel angiogenic factor.,” *Circulation*, 111(13): 1627–36.

Shi, S. and Stanley, P. (2003) “Protein O-fucosyltransferase 1 is an essential component of Notch signaling pathways.,” *Proceedings of the National Academy of Sciences of the United States of America*, 100(9): 5234–9.

Shiina, H., Breault, J. E., Basset, W. W., Enokida, H. and Urakami, S. (2005) “Functional Loss of the γ -Catenin Gene through Epigenetic and Genetic Pathways in Human Prostate Cancer Functional Loss of the g -Catenin Gene through Epigenetic and Genetic Pathways in Human Prostate Cancer,” *Cancer research*, 65: 2130–2138.

Shimada, Y., Imamura, M., Wagata, T., Yamaguchi, N. and Tobe, T. (1992) “Characterization of 21 newly established esophageal cancer cell lines.,” *Cancer*, 69(2): 277–84.

Shimizu, A., Ishiko, A., Ota, T., Tsunoda, K., Amagai, M. and Nishikawa, T. (2004) “IgG binds to desmoglein 3 in desmosomes and causes a desmosomal split without keratin retraction in a pemphigus mouse model.,” *The Journal of investigative dermatology*, 122(5): 1145–53.

Shimizu, M., Fukunaga, Y., Ikenouchi, J. and Nagafuchi, A. (2008) “Defining the roles of beta-catenin and plakoglobin in LEF/T-cell factor-dependent transcription using beta-catenin/plakoglobin-null F9 cells.,” *Molecular and cellular biology*, 28(2): 825–35.

Shin, H. M., Minter, L. M., Cho, O. H., Gottipati, S., Fauq, A. H., Golde, T. E., Sonenshein, G. E. and Osborne, B. a (2006) “Notch1 augments NF-kappaB activity by facilitating its nuclear retention.,” *The EMBO journal*, 25(1), pp. 129–38.

Shirakata, Y., Amagai, M., Hanakawa, Y., Nishikawa, T. and Hashimoto, K. (1998) “Lack of mucosal involvement in pemphigus foliaceus may be due to low expression of desmoglein 1.,” *The Journal of investigative dermatology*, 110(1): 76–8.

Shoyab, M., Plowman, G., McDonald, V., Bradley, J. and Todaro, G. (1989) “Structure and Function of Human Amphiregulin: A Member of the Epidermal Hrowth Factor Family,” *Science*, 243: 78–80..

Simon, M., Haftek, M., Sebbag, M., Montezin, M., Girbal-Neuhauser, E., Schmidtt, D. and Serre, G. (1996) “Evidence that filaggrin is a component of cornified cell envelopes in human plantar epidermis.,” *Biochem. J*, 317: 173–177.

Simon, M., Jonca, N., Guerrin, M., Haftek, M., Bernard, D., Caubet, C., Egelrud, T., Schmidt, R. and Serre, G. (2001) “Refined characterization of corneodesmosin proteolysis during terminal differentiation of human epidermis and its relationship to desquamation.,” *The Journal of biological chemistry*, 276(23): 20292–9.

Singh, B. and Coffey, R. J. (2014) “From wavy hair to naked proteins: the role of transforming growth factor alpha in health and disease.,” *Seminars in cell & developmental biology*. 28: 12–21.

Sinnathamby, G., Zerfass, J., Hafner, J., Block, P., Nickens, Z., Hobeika, a, Secord, a a, Lyerly, H. K., Morse, M. a and Philip, R. (2011) “ADAM metallopeptidase domain 17 (ADAM17) is naturally processed through major histocompatibility complex (MHC) class I molecules and is a potential immunotherapeutic target in breast, ovarian and prostate cancers.,” *Clinical and experimental immunology*, 163(3): 324–32.

Song, Y., Li, L., Ou, Y., Gao, Z., Li, E., Li, X., Zhang, W., Wang, J., Xu, L., Zhou, Y., Ma, X., Liu, L., Zhao, Z., Huang, X., Fan, J., Dong, L., Chen, G., Ma, L., Yang, J., Chen, L., He, M., Li, M., Zhuang, X., Huang, K., Qiu, K., Yin, G., Guo, G., Feng, Q., Chen, P., Wu, Z., Wu, J., Ma, L., Zhao, J., Luo, L., Fu, M., Xu, B., Chen, B., Li, Y., Tong, T., Wang, M., Liu, Z., Lin, D., Zhang, X., Yang, H., Wang, J. and Zhan, Q. (2014) “Identification of genomic alterations in oesophageal squamous cell cancer.,” *Nature*. 509(7498): 91–5.

Sotillos, S., Roch, F. and Campuzano, S. (1997) “The metalloprotease-disintegrin Kuzbanian participates in Notch activation during growth and patterning of Drosophila imaginal discs.,” *Development (Cambridge, England)*, 124(23): 4769–79.

South, A. P. (2012) “The double-edged sword of Notch signalling in Cancer,” *Semin Cell Dev Viol*, 23(4): 458–464.

South, A. P., Purdie, K. J., Watt, S. a, Haldenby, S., den Breems, N. Y., Dimon, M., Arron, S. T., Kluk, M. J., Aster, J. C., McHugh, A., Xue, D. J., Dayal, J. H. S., Robinson, K. S., Rizvi, S. M. H., Proby, C. M., Harwood, C. a and Leigh, I. M. (2014) “NOTCH1 Mutations Occur Early during Cutaneous Squamous Cell Carcinogenesis.,” *The Journal of investigative dermatology*. 134(10): 2630-8.

Spindler, V., Endlich, A., Hartlieb, E., Vielmuth, F., Schmidt, E. and Waschke, J. (2014) “The Extent of Desmoglein 3 Depletion in Pemphigus Vulgaris Is Dependent on Ca2+-Induced Differentiation,” *The American Journal of Pathology*. 179(4): 1905–1916.

Sportoletti, P., Baldoni, S., Cavalli, L., Del Papa, B., Bonifacio, E., Ciurnelli, R., Bell, A., Tommaso, A., Rosati, E., Crescenzi, E., Mecucci, C., Screpanti, I., Marconi, P., Martelli, M., Di Ianni, M. and Falzetti, F. (2010) “NOTCH1 PEST domain mutation is an adverse prognostic factor in B-CLL,” *British journal of haematology*, 151(4): 404–6.

Ståhl, S., Branca, R. M., Efazat, G., Ruzzene, M., Zhivotovsky, B., Lewensohn, R., Viktorsson, K. and Lehtiö, J. (2011) "Phosphoproteomic profiling of NSCLC cells reveals that ephrin B3 regulates pro-survival signaling through Akt1-mediated phosphorylation of the EphA2 receptor.," *Journal of proteome research*, 10(5):2566-78

Ståhl, S., Kaminskyy, V. O., Efazat, G., Hyrslova Vaculova, a, Rodriguez-Nieto, S., Moshfegh, a, Lewensohn, R., Viktorsson, K. and Zhivotovsky, B. (2013) "Inhibition of Ephrin B3-mediated survival signaling contributes to increased cell death response of non-small cell lung carcinoma cells after combined treatment with ionizing radiation and PKC 412.," *Cell death & disease*, 4: e454.

Stanley, J. R., Koulu, L., Klaus-Kovtun, V. and Steinberg, M. S. (1986) "A monoclonal antibody to the desmosomal glycoprotein desmoglein I binds the same polypeptide as human autoantibodies in pemphigus foliaceus.," *The Journal of Immunology* , 136 (4): 1227–1230.

Stappenbeck, T., Lamb, J., Corcoran, C. M. and Green, K. (1994) "Phosphorylation of the desmoplakin COOH terminus negatively regulates its interaction with keratin intermediate filament networks.," *Journal of Biological Chemistry*, 269(47): 29351–29354.

Steinert, P. M. (1998) "Biochemical Evidence That Small Proline-rich Proteins and Trichohyalin Function in Epithelia by Modulation of the Biomechanical Properties of Their Cornified Cell Envelopes," *Journal of Biological Chemistry*, 273(19): 11758–11769.

Sternlicht, M. and Sunnarborg, S. (2005) "Mammary ductal morphogenesis requires paracrine activation of stromal EGFR via ADAM17-dependent shedding of epithelial amphiregulin," *Development*, 132(17): 3923–3933.

Stevens, H. P., Kelsell, D. P., Bryant, S. P., Bishop, D. T., Spurr, N. K., Weissenbach, J., Marger, D., Marger, R. S. and Leigh, I. M. (1996) "Linkage of an American pedigree with palmoplantar keratoderma and malignancy (palmoplantar ectodermal dysplasia type III) to 17q24. Literature survey and proposed updated classification of the keratodermas.," *Archives of dermatology*, 132(6): 640–51.

Stokes, A., Joutsa, J., Ala-Aho, R., Pitchers, M., Pennington, C. J., Martin, C., Premachandra, D. J., Okada, Y., Peltonen, J., Grénman, R., James, H. a, Edwards, D. R. and Kähäri, V.-M. (2010) "Expression profiles and clinical correlations of degradome components in the tumor microenvironment of head and neck squamous cell carcinoma.," *Clinical cancer research : an official journal of the American Association for Cancer Research*, 16(7): 2022–35.

Stransky, N., Egloff, A., Tward, A., Kostic, A., Cibulskis, K., Sivachenko, A., Kryukov, G., Lawrence, M., Sougnez, C., McKenna, A., Schefler, E., Roamos, A., Stojanov, P., Carter, S., Voet, D., Cortes, M., Auclair, D., Berger, M., Saksena, G., Guiducci, C., Onofrio, R., Parkin, M., Romkes, M., Weissfeld, J., Seethala, R., Wang, L., Rangel-Escareno, C., Fernandez-Lopez, J., Hidalgo-Miranda, A., Melendez-Zajgla, J., Winckler, W., Ardlie, K., Gabriel, S., Meyerson, M., Lander, E., Getz, G., Golub, T., Garraway, L. and Grandis, J. (2011) "The mutational landscape of head and neck squamous cell carcinoma," *Science*, 333(6046): 1157–1160.

Su, A. I., Wiltshire, T., Batalov, S., Lapp, H., Ching, K. a, Block, D., Zhang, J., Soden, R., Hayakawa, M., Kreiman, G., Cooke, M. P., Walker, J. R. and Hogenesch, J. B. (2004) "A gene atlas of the mouse and human protein-encoding transcriptomes.," *Proceedings of the National Academy of Sciences of the United States of America*, 101(16): 6062–7.

Sudo, T., Mimori, K., Nagahara, H., Utsunomiya, T., Fujita, H., Tanaka, Y., Shirouzu, K., Inoue, H. and Mori, M. (2007) "Identification of EGFR mutations in esophageal cancer.," *European journal of surgical oncology : the journal of the European Society of Surgical Oncology and the British Association of Surgical Oncology*, 33(1): 44–8.

Suh, P.-G., Park, J.-I., Manzoli, L., Cocco, L., Peak, J. C., Katan, M., Fukami, K., Kataoka, T., Yun, S. and Ryu, S. H. (2008) "Multiple roles of phosphoinositide-specific phospholipase C isozymes.," *BMB reports*, 41(6): 415–34..

Swiatek, P. J., Lindsell, C. E., del Amo, F. F., Weinmaster, G. and Gridley, T. (1994) “Notch1 is essential for postimplantation development in mice.,” *Genes & Development*, 8(6): 707–719.

Szalad, A., Katakowski, M., Zheng, X., Jiang, F. and Chopp, M. (2009) “Transcription factor Sp1 induces ADAM17 and contributes to tumor cell invasiveness under hypoxia.,” *Journal of experimental & clinical cancer research* 28:129.

Tachibana, K., Nakanishi, H., Mandai, K., Ozaki, K., Ikeda, W., Yamamoto, Y., Nagafuchi, a, Tsukita, S. and Takai, Y. (2000) “Two cell adhesion molecules, nectin and cadherin, interact through their cytoplasmic domain-associated proteins.,” *The Journal of cell biology*, 150(5): 1161–76.

Talmadge, J. E., Donkor, M. and Scholar, E. (2007) “Inflammatory cell infiltration of tumors: Jekyll or Hyde.,” *Cancer metastasis reviews*, 26(3-4): 373–400.

Tattersall, D., Scott, C. a, Gray, C., Zicha, D. and Kelsell, D. P. (2009) “EKV mutant connexin 31 associated cell death is mediated by ER stress.,” *Human molecular genetics*, 18(24): 4734–45.

Teh, M.-T., Parkinson, E. K., Thurlow, J. K., Liu, F., Fortune, F. and Wan, H. (2011) “A molecular study of desmosomes identifies a desmoglein isoform switch in head and neck squamous cell carcinoma.,” *Journal of oral pathology & medicine : official publication of the International Association of Oral Pathologists and the American Academy of Oral Pathology*, 40(1): 67–76.

Terrinoni, A., Leta, A., Pedicelli, C., Candi, E., Ranalli, M., Puddu, P., Paradis, M., Angelo, C., Bagetta, G., Melino, G. and Baggetta, G. (2004) “A novel recessive connexin 31 (GJB3) mutation in a case of erythrokeratodermia variabilis.,” *The Journal of investigative dermatology*, 122(3): 837–9.

Van Tetering, G., van Diest, P., Verlaan, I., van der Wall, E., Kopan, R. and Vooijs, M. (2009) “Metalloprotease ADAM10 is required for Notch1 site 2 cleavage.,” *The Journal of biological chemistry*, 284(45): 31018–27.

Thastrup, O., Dawson, A., Scharff, O., Foder, B. and Cullen, P. (1994) “Thapsigargin, a novel molecular probe for studying intracellular calcium release and storage,” *Agents Actions*, 43(3-4): 187–193.

Thomas, A. C., Cullup, T., Norgett, E. E., Hill, T., Barton, S., Dale, B. a, Sprecher, E., Sheridan, E., Taylor, A. E., Wilroy, R. S., DeLozier, C., Burrows, N., Goodyear, H., Fleckman, P., Stephens, K. G., Mehta, L., Watson, R. M., Graham, R., Wolf, R., Slavotinek, A., Martin, M., Bourn, D., Mein, C. a, O’Toole, E. a and Kelsell, D. P. (2006) “ABCA12 is the major harlequin ichthyosis gene.,” *The Journal of investigative dermatology*, 126(11): 2408–13.

Thomason, H. a, Scothern, A., McHarg, S. and Garrod, D. R. (2010) “Desmosomes: adhesive strength and signalling in health and disease.,” *The Biochemical journal*, 429(3): 419–33.

Troyanovsky, R. B., Klingelhöfer, J. and Troyanovsky, S. (1999) “Removal of calcium ions triggers a novel type of intercadherin interaction.,” *Journal of cell science*, 112 (Pt 2, pp. 4379–87.

Tsai, W.-C., Hsu, P. W.-C., Lai, T.-C., Chau, G.-Y., Lin, C.-W., Chen, C.-M., Lin, C.-D., Liao, Y.-L., Wang, J.-L., Chau, Y.-P., Hsu, M.-T., Hsiao, M., Huang, H.-D. and Tsou, A.-P. (2009) “MicroRNA-122, a tumor suppressor microRNA that regulates intrahepatic metastasis of hepatocellular carcinoma.,” *Hepatology (Baltimore, Md.)*, 49(5): 1571–82.

Tschachler, E. (2007) “Psoriasis: the epidermal component.,” *Clinics in dermatology*, 25(6): 589–95.

Tselepis, C., Chidgey, M., North, a and Garrod, D. (1998) “Desmosomal adhesion inhibits invasive behavior.,” *Proceedings of the National Academy of Sciences of the United States of America*, 95(14): 8064–9.

Tsunematsu, R., Nakayama, K., Oike, Y., Nishiyama, M., Ishida, N., Hatakeyama, S., Bessho, Y., Kageyama, R., Suda, T. and Nakayama, K. I. (2004) “Mouse Fbw7/Sel-10/Cdc4 is required for notch degradation during vascular development.,” *The Journal of biological chemistry*, 279(10): 9417–23.

Tzahar, E., Waterman, H., Chen, X., Levkowitz, G., Karunagaran, D., Lavi, S., Ratzkin, B. J. and Yarden, Y. (1996) “A hierarchical network of interreceptor interactions determines signal transduction by Neu differentiation factor/neuregulin and epidermal growth factor.,” *Molecular and cellular biology*, 16(10): 5276–87.

Urban, S. and Freeman, M. (2003) “Substrate specificity of rhomboid intramembrane proteases is governed by helix-breaking residues in the substrate transmembrane domain.,” *Molecular cell*, 11(6): 1425–34.

Urban, S., Lee, J. R. and Freeman, M. (2001) “Drosophila rhomboid-1 defines a family of putative intramembrane serine proteases.,” *Cell*, 107(2): 173–82.

Valenta, T., Hausmann, G. and Basler, K. (2012) “The many faces and functions of β-catenin.,” *The EMBO journal*, 31(12): 2714–36.

Vasioukhin, V., Bauer, C., Yin, M. and Fuchs, E. (2000) “Directed actin polymerization is the driving force for epithelial cell-cell adhesion.,” *Cell*, 100(2): 209–19.

Vassar, R. and Fuchs, E. (1991) “Transgenic mice provide new insights into the role of TGF-alpha during epidermal development and differentiation.,” *Genes & Development*, 5(5): 714–727.

Vauclair, S., Nicolas, M., Barrandon, Y. and Radtke, F. (2005) “Notch1 is essential for postnatal hair follicle development and homeostasis.,” *Developmental biology*, 284(1): 184–93.

Vembar, S. and Brodsky, J. (2008) “One step at a time: endoplasmic reticulum-associated degradation,” *Nature Reviews Molecular Cell Biology*, 9(12): 944–957.

Venturi, G., Tu, L., Kadono, T., Khan, A., Fujimoto, Y., Oshel, P., Bock, C., Miller, A., Albrecht, R., Kubes, P., Steeber, D. and Tedder, T. (2003) “Leukocyte migration is regulated by L-selectin endoproteolytic release,” *Immunity*, 19: 713–724.

Wallis, S., Lloyd, S., Wise, I., Ireland, G., Fleming, T. P. and Garrod, D. (2000) “The alpha isoform of protein kinase C is involved in signaling the response of desmosomes to wounding in cultured epithelial cells.,” *Molecular biology of the cell*, 11(3): 1077–92.

Wang, G. L., Jiang, B. H., Rue, E. a and Semenza, G. L. (1995) “Hypoxia-inducible factor 1 is a basic-helix-loop-helix-PAS heterodimer regulated by cellular O2 tension.,” *Proceedings of the National Academy of Sciences of the United States of America*, 92(12): 5510–4.

Wang, G. and Semenza, G. (1995) “Purification and characterization of hypoxia-inducible factor 1,” *Journal of Biological Chemistry*, 270(3): 1230–1237.

Wang, G.-Q., Abnet, C. C., Shen, Q., Lewin, K. J., Sun, X.-D., Roth, M. J., Qiao, Y.-L., Mark, S. D., Dong, Z.-W., Taylor, P. R. and Dawsey, S. M. (2005) “Histological precursors of oesophageal squamous cell carcinoma: results from a 13 year prospective follow up study in a high risk population.,” *Gut*, 54(2), pp. 187–92.

Wang, J., Wang, N., Xie, J., Walton, S. C., McKown, R. L., Raab, R. W., Ma, P., Beck, S. L., Coffman, G. L., Hussaini, I. M. and Laurie, G. W. (2006) “Restricted epithelial proliferation by lacritin via PKCalpha-dependent NFAT and mTOR pathways.,” *The Journal of cell biology*, 174(5), pp. 689–700.

Wang, M. (2011) “Notch signaling and Notch signaling modifiers,” *The international journal of biochemistry & cell biology*, 43(11): 1550–1562.

Wang, X., Pasolli, H. A., Williams, T. and Fuchs, E. (2008) “AP-2 factors act in concert with Notch to orchestrate terminal differentiation in skin epidermis.,” *The Journal of cell biology*, 183(1): 37–48.

Wang, X.-J., Feng, C.-W. and Li, M. (2013) “ADAM17 mediates hypoxia-induced drug resistance in hepatocellular carcinoma cells through activation of EGFR/PI3K/Akt pathway.,” *Molecular and cellular biochemistry*, 380(1-2): 57–66

Wang, Y., Zhang, Y. and Ha, Y. (2006) “Crystal structure of a rhomboid family intramembrane protease.,” *Nature*, 444(7116): 179–80.

Wang, Y., Zheng, Z. and Hu, D. (2013) “Inhibition of EphA4 expression promotes Schwann cell migration and peripheral nerve regeneration.,” *Neuroscience letters*. Elsevier Ireland Ltd, 548: 201–5.

Warneke, V. S., Behrens, H.-M., Haag, J., Krüger, S., Simon, E., Mathiak, M., Ebert, M. P. a and Röcken, C. (2013) “Members of the EpCAM signalling pathway are expressed in gastric cancer tissue and are correlated with patient prognosis.,” *British journal of cancer*, 109(8): 2217–27.

Waschke, J., Spindler, V., Bruggeman, P., Zillikens, D., Schmidt, G. and Drenckhahn, D. (2006) “Inhibition of Rho A activity causes pemphigus skin blistering.,” *The Journal of cell biology*, 175(5): 721–7.

Wasserman, J. D., Urban, S. and Freeman, M. (2000) “A family of rhomboid-like genes: Drosophila rhomboid-1 and roughoid/rhomboid-3 cooperate to activate EGF receptor signaling.,” *Genes & development*, 14(13): 1651–63.

Watt, F. M. (1984) “Selective migration of terminally differentiating cells from the basal layer of cultured human epidermis.,” *The Journal of cell biology*, 98(1): 16–21.

Weaver, J. M. J., Ross-Innes, C. S., Shannon, N., Lynch, A. G., Forshew, T., Barbera, M., Murtaza, M., Ong, C.-A. J., Lao-Sirieix, P., Dunning, M. J., Smith, L., Smith, M. L., Anderson, C. L., Carvalho, B., O’Donovan, M., Underwood, T. J., May, A. P., Grehan, N., Hardwick, R., Davies, J., Oloumi, A., Aparicio, S., Caldas, C., Eldridge, M. D., Edwards, P. a W., Rosenfeld, N., Tavaré, S. and Fitzgerald, R. C. (2014) “Ordering of mutations in preinvasive disease stages of esophageal carcinogenesis.,” *Nature genetics*. Nature Publishing Group, 46(8): 837–843.

Weber, S., Niessen, M. T., Prox, J., Lüllmann-Rauch, R., Schmitz, A., Schwanbeck, R., Blobel, C. P., Jorissen, E., de Strooper, B., Niessen, C. M. and Saftig, P. (2011) “The disintegrin/metalloproteinase Adam10 is essential for epidermal integrity and Notch-mediated signaling.,” *Development*, 138(3): 495–505.

Weiler, H. and Isermann, B. H. (2003) “Thrombomodulin.,” *Journal of thrombosis and haemostasis :* 1(7): 1515–24.

Weinmaster, G., Roberts, V. J. and Lemke, G. (1991) “A homolog of Drosophila Notch expressed during mammalian development.,” *Development (Cambridge, England)*, 113(1): 199–205.

Weinmaster, G., Roberts, V. J. and Lemke, G. (1992) “Notch2: a second mammalian Notch gene.,” *Development*, 116(4): 931–41.

Weng, A. P., Ferrando, A. a, Lee, W., Morris, J. P., Silverman, L. B., Sanchez-Irizarry, C., Blacklow, S. C., Look, a T. and Aster, J. C. (2004) “Activating mutations of NOTCH1 in human T cell acute lymphoblastic leukemia.,” *Science*, 306(5694): 269–71.

Werner, H. (2012) “Tumor suppressors govern insulin-like growth factor signaling pathways: implications in metabolism and cancer.,” *Oncogene*. 31(22): 2703–14.

Wertheimer, E., Trebicz, M., Eldar, T., Gartsbein, M., Nofeh-Moses, S. and Tennenbaum, T. (2000) “Differential roles of insulin receptor and insulin-like growth factor-1 receptor in differentiation of murine skin keratinocytes.,” *The Journal of investigative dermatology*, 115(1): 24–9.

Wickline, E. D., Du, Y., Stolz, D. B., Kahn, M. and Monga, S. P. S. (2013) “γ-Catenin at adherens junctions: mechanism and biologic implications in hepatocellular cancer after β-catenin knockdown.,” *Neoplasia*, 15(4): 421–34.

Wilgoss, A., Leigh, I. M., Barnes, M. R., Dopping-Hepenstal, P., Eady, R. A., Walter, J. M., Kennedy, C. T. and Kelsell, D. P. (1999) “Identification of a novel mutation R42P in the gap junction protein beta-3 associated with autosomal dominant erythrokeratoderma variabilis.,” *The Journal of investigative dermatology*, 113(6): 1119–22.

Wilkin, M. B., Carbery, A.-M., Fostier, M., Aslam, H., Mazaleyrat, S. L., Higgs, J., Myat, A., Evans, D. a P., Cornell, M. and Baron, M. (2004) “Regulation of notch endosomal sorting and signaling by Drosophila Nedd4 family proteins.,” *Current biology,* 14(24): 2237–44.

Willmarth, N. E. and Ethier, S. P. (2006) “Autocrine and juxtacrine effects of amphiregulin on the proliferative, invasive, and migratory properties of normal and neoplastic human mammary epithelial cells.,” *The Journal of biological chemistry*, 281(49): 37728–37.

Wilson, K., Mill, C., Lambert, S., Buchman, J., Wilson, T., Hernandez-Gordillo, V., Gallo, R., Ades, L., Settleman, J. and Reise II, D. (2012) “EGFR ligands exhibit functional differences in models of paracrine and autocrine signaling,” *Growth Factors*, 30(2): 107–116.

Wiszniewski, L., Limat, A., Saurat, J., Meda, P. and Salomon, D. (2000) “Differential expression of connexins during stratification of human keratinocytes,” *Journal of investigative dermatology*, 115: 278–285.

Witters, L., Scherle, P., Friedman, S., Fridman, J., Caulder, E., Newton, R. and Lipton, A. (2008) “Synergistic inhibition with a dual epidermal growth factor receptor/HER-2/neu tyrosine kinase inhibitor and a disintegrin and metalloprotease inhibitor.,” *Cancer research*, 68(17): 7083–9.

Wu, G., Lyapina, S., Das, I., Li, J., Gurney, M., Pauley, a, Chui, I., Deshaies, R. J. and Kitajewski, J. (2001) “SEL-10 is an inhibitor of notch signaling that targets notch for ubiquitin-mediated protein degradation.,” *Molecular and cellular biology*, 21(21): 7403–15.

Wu, Q., Suo, Z., Risberg, B., Karlsson, M. G., Villman, K. and Nesland, J. M. (2004) “Expression of Ephb2 and Ephb4 in breast carcinoma.,” *Pathology oncology research : POR*, 10(1): 26–33.

Wu, Y., Huang, A., Li, T., Su, X., Ding, H., Li, H., Qin, X., Hou, L., Zhao, Q., Ge, X., Fang, T., Wang, R., Gao, C., Li, J. and Shao, N. (2014) “MiR-152 reduces human umbilical vein endothelial cell proliferation and migration by targeting ADAM17.,” *FEBS letters*. Federation of European Biochemical Societies, 588(12): 2063–9.

Wybenga-Groot, L. E., Baskin, B., Ong, S. H., Tong, J., Pawson, T. and Sicheri, F. (2001) “Structural basis for autoinhibition of the Ephb2 receptor tyrosine kinase by the unphosphorylated juxtamembrane region.,” *Cell*, 106(6): 745–57.

Xia, G., Kumar, S. R., Masood, R., Krasnoperov, V., Quinn, D. I., Henshall, S. M., Sutherland, R. L., Pinski, J. K., Daneshmand, S., Buscarini, M., Stein, J. P., Zhong, C., Broek, D., Roy-burman, P. and Gill, P. S. (2005) “EphB4 Expression and Biological Significance in Prostate Cancer EphB4 Expression and Biological Significance in Prostate Cancer,” *Cancer research*, 65: 4623–4632.

Xia, G., Kumar, S. R., Stein, J. P., Singh, J., Krasnoperov, V., Zhu, S., Hassanieh, L., Smith, D. L., Buscarini, M., Broek, D., Quinn, D. I., Weaver, F. a and Gill, P. S. (2006) “EphB4 receptor tyrosine kinase is expressed in bladder cancer and provides signals for cell survival.,” *Oncogene*, 25(5): 769–80.

Xiao, K., Oas, R. G., Chiasson, C. M. and Kowalczyk, A. P. (2007) “Role of p120-catenin in cadherin trafficking.,” *Biochimica et biophysica acta*, 1773(1): 8–16.

Yamada, A., Fujita, N., Sato, T., Okamoto, R., Ooshio, T., Hirota, T., Morimoto, K., Irie, K. and Takai, Y. (2006) “Requirement of nectin, but not cadherin, for formation of claudin-based tight junctions in annexin II-knockdown MDCK cells.,” *Oncogene*, 25(37): 5085–102.

Yamada, Y., Midorikawa, T., Oura, H., Yoshino, T., Ohdera, M., Kubo, Y. and Arase, S. (2008) “Ephrin-A3 not only increases the density of hair follicles but also accelerates anagen development in neonatal mice.,” *Journal of dermatological science*, 52(3): 178–85.

Yamamoto, N., Tanigaki, K., Han, H., Hiai, H. and Honjo, T. (2003) “Notch/RBP-J signaling regulates epidermis/hair fate determination of hair follicular stem cells.,” *Current biology : CB*, 13(4): 333–8.

Yamamoto, Y., Aoyama, Y., Shu, E., Tsunoda, K., Amagai, M. and Kitajima, Y. (2007) “Anti-desmoglein 3 (Dsg3) monoclonal antibodies deplete desmosomes of Dsg3 and differ in their Dsg3-depleting activities related to pathogenicity.,” *The Journal of biological chemistry*, 282(24): 17866–76.

Yamane, S., Ishida, S., Hanamoto, Y., Kumagai, K.-I., Masuda, R., Tanaka, K., Shiobara, N., Yamane, N., Mori, T., Juji, T., Fukui, N., Itoh, T., Ochi, T. and Suzuki, R. (2008) “Proinflammatory role of amphiregulin, an epidermal growth factor family member whose expression is augmented in rheumatoid arthritis patients.,” *Journal of inflammation*, 5:5

Yan, Y., Luo, Y.-C., Wan, H.-Y., Wang, J., Zhang, P.-P., Liu, M., Li, X., Li, S. and Tang, H. (2013) “MicroRNA-10a is involved in the metastatic process by regulating Eph tyrosine kinase receptor A4-mediated epithelial-mesenchymal transition and adhesion in hepatoma cells.,” *Hepatology (Baltimore, Md.)*, 57(2): 667–77.

Yan, Z., Zou, H., Tian, F., Grandis, J. R., Mixson, A. J., Lu, P. Y. and Li, L.-Y. (2008) “Human rhomboid family-1 gene silencing causes apoptosis or autophagy to epithelial cancer cells and inhibits xenograft tumor growth.,” *Molecular cancer therapeutics*, 7(6): 1355–64.

Yang, L., Chen, Y., Cui, T., Knösel, T., Zhang, Q., Albring, K. F., Huber, O. and Petersen, I. (2012) “Desmoplakin acts as a tumor suppressor by inhibition of the Wnt/β-catenin signaling pathway in human lung cancer.,” *Carcinogenesis*, 33(10): 1863–70.

Yang, N.-Y., Fernandez, C., Richter, M., Xiao, Z., Valencia, F., Tice, D. a and Pasquale, E. B. (2011) “Crosstalk of the EphA2 receptor with a serine/threonine phosphatase suppresses the Akt-mTORC1 pathway in cancer cells.,” *Cellular signalling*. Elsevier Inc., 23(1): 201–12.

Yassin, T. M. and Toner, P. G. (1976) “Langerhans cells in the human oesophagus.,” *Journal of anatomy*, 122(Pt 2): 435–45.

Yin, T. and Green, K. (2004) “Regulation of desmosome assembly and adhesion,” *Seminars in cell & developmental biology*, 15: 665–677.

Yin, T. and Green, K. J. (2004) “Regulation of desmosome assembly and adhesion.,” *Seminars in cell & developmental biology*, 15(6): 665–77.

Yoda, M., Kimura, T., Tohmonda, T., Morioka, H., Matsumoto, M., Okada, Y., Toyama, Y. and Horiuchi, K. (2013) “Systemic overexpression of TNFα-converting enzyme does not lead to enhanced shedding activity in vivo.,” *PloS one*, 8(1): e54412.

Yokoyama, a, Muramatsu, T., Ohmori, T., Higuchi, S., Hayashida, M. and Ishii, H. (1996) “Esophageal cancer and aldehyde dehydrogenase-2 genotypes in Japanese males.,” *Cancer epidemiology, biomarkers & prevention*, 5(2): 99–102.

Yoshida, H. (2007) “ER stress and diseases,” *Febs Journal*, 274: 630–658.

Yu, A. S. L., McCarthy, K. M., Francis, S. a, McCormack, J. M., Lai, J., Rogers, R. a, Lynch, R. D. and Schneeberger, E. E. (2005) “Knockdown of occludin expression leads to diverse phenotypic alterations in epithelial cells.,” *American journal of physiology. Cell physiology*, 288(6): C1231–41.

Yu, C.-C., Tsai, L.-L., Wang, M.-L., Yu, C.-H., Lo, W.-L., Chang, Y.-C., Chiou, G.-Y., Chou, M.-Y. and Chiou, S.-H. (2013) “miR145 targets the SOX9/ADAM17 axis to inhibit tumor-initiating cells and IL-6-mediated paracrine effects in head and neck cancer.,” *Cancer research*, 73(11): 3425–40.

Zaiss, D. M., Yang, L., Shah, P. R., Kobie, J. J., Urban, J. F. and Mosmann, T. R. (2006) “Amphiregulin, a TH2 cytokine enhancing resistance to nematodes.,” *Science (New York, N.Y.)*, 314(5806): 1746.

Zelinski, D., Zantek, N., Stewart, J., Irizarry, A. and Kinch, M. (2001) “EphA2 overexpression causes tumorigenesis of mammary epithelial cells,” *Cancer research*, 61: 2301–2306.

Zettl, M., Adrain, C., Strisovsky, K., Lastun, V. and Freeman, M. (2011) “Rhomboid Family Pseudoproteases Use the ER Quality Control Machinery to Regulate Intercellular Signaling.,” *Cell*. Elsevier Inc., 145(1): 79–91.

Zhang, C., Tian, L., Chi, C., Wu, X., Yang, X., Han, M., Xu, T., Zhuang, Y. and Deng, K. (2010) “Adam10 is essential for early embryonic cardiovascular development.,” *Developmental dynamics : an official publication of the American Association of Anatomists*, 239(10): 2594–602.

Zhang, L., Bhattacharya, S., Leid, M., Ganguli-Indra, G. and Indra, A. K. (2012) “Ctip2 is a dynamic regulator of epidermal proliferation and differentiation by integrating EGFR and Notch signaling.,” *Journal of cell science*, 125(Pt 23): 5733–44.

Zhang, X., Gureasko, J., Shen, K., Cole, P. a and Kuriyan, J. (2006) “An allosteric mechanism for activation of the kinase domain of epidermal growth factor receptor.,” *Cell*, 125(6): 1137–49.

Zhou, B.-B. S., Peyton, M., He, B., Liu, C., Girard, L., Caudler, E., Lo, Y., Baribaud, F., Mikami, I., Reguart, N., Yang, G., Li, Y., Yao, W., Vaddi, K., Gazdar, A. F., Friedman, S. M., Jablons, D. M., Newton, R. C., Fridman, J. S., Minna, J. D. and Scherle, P. a (2006) “Targeting ADAM-mediated ligand cleavage to inhibit HER3 and EGFR pathways in non-small cell lung cancer.,” *Cancer cell*, 10(1): 39–50.

Zhou, Z., Liu, F., Zhang, Z.-S., Shu, F., Zheng, Y., Fu, L. and Li, L.-Y. (2014) “Human rhomboid family-1 suppresses oxygen-independent degradation of hypoxia-inducible factor-1α in breast cancer.,” *Cancer research*, 74(10): 2719–30.

Zhuang, G., Brantley-Sieders, D. M., Vaught, D., Yu, J., Xie, L., Wells, S., Jackson, D., Muraoka-Cook, R., Arteaga, C. and Chen, J. (2010) “Elevation of receptor tyrosine kinase EphA2 mediates resistance to trastuzumab therapy.,” *Cancer research*, 70(1): 299–308.

Ziegler, S. F. and Artis, D. (2010) “Sensing the outside world: TSLP regulates barrier immunity.,” *Nature immunology*, 11(4): 289–93.

Zou, H., Thomas, S. M., Yan, Z.-W., Grandis, J. R., Vogt, A. and Li, L.-Y. (2009) “Human rhomboid family-1 gene RHBDF1 participates in GPCR-mediated transactivation of EGFR growth signals in head and neck squamous cancer cells.,” *The FASEB journal :* 23(2): 425–32.

Appendix A:
Control experiments and supporting results for Chapter 3

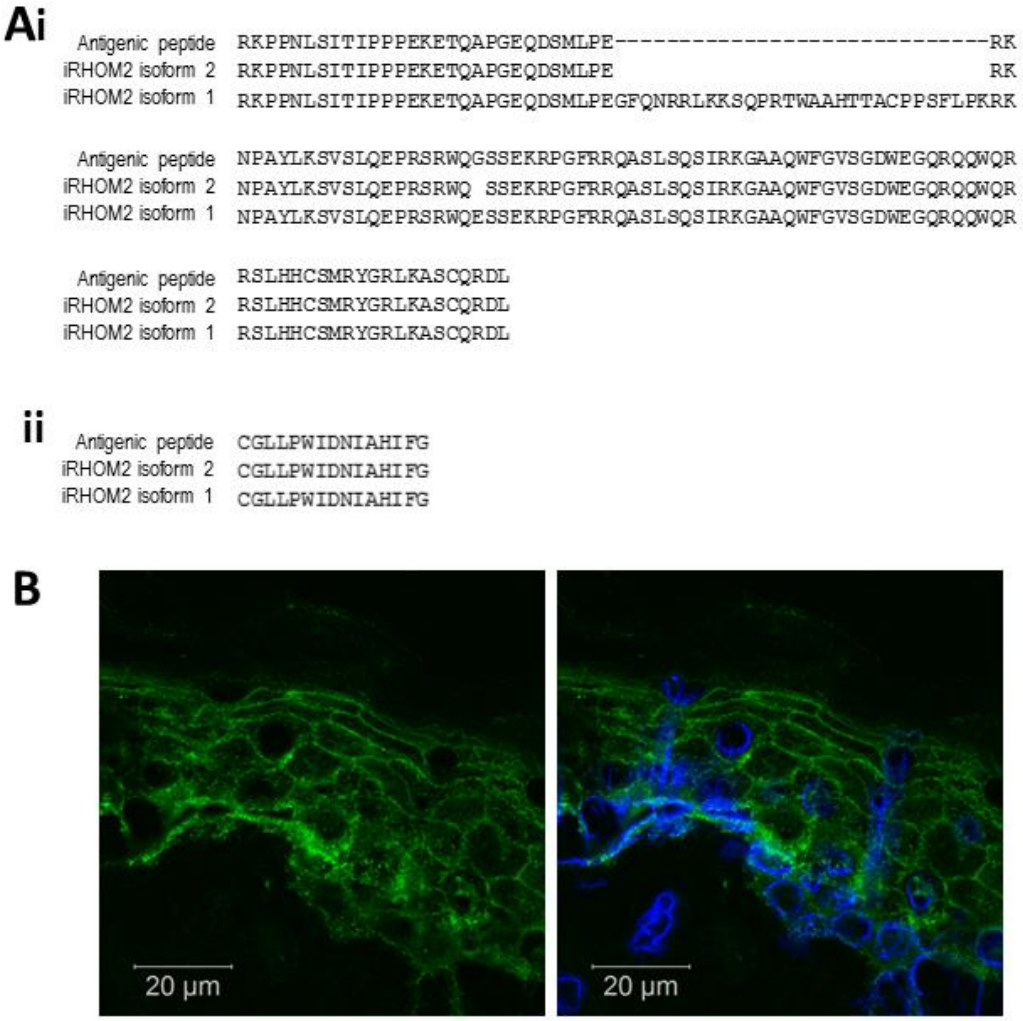

Appendix A1 Anti-RHBDF2 antibody epitopes and confirmation of cell-surface iRHOM2 localisation in the skin. A: Alignments of the protein sequences of iRHOM2 isoforms 1 and 2 with the antibody epitopes for (i) the anti-RHBDF2 antibody used throughout the thesis (from Sigma-Aldrich), and (ii) the custom-made antibody shown in part B. B: Cell-surface staining of iRHOM2 in the epidermis with an additional antibody: custom made anti-RHBDF2 antibody R2437. Images were taken on the Zeiss Meta 510 confocal microscope. iRHOM2 staining is shown in green, and DAPI nuclear staining shown in blue.

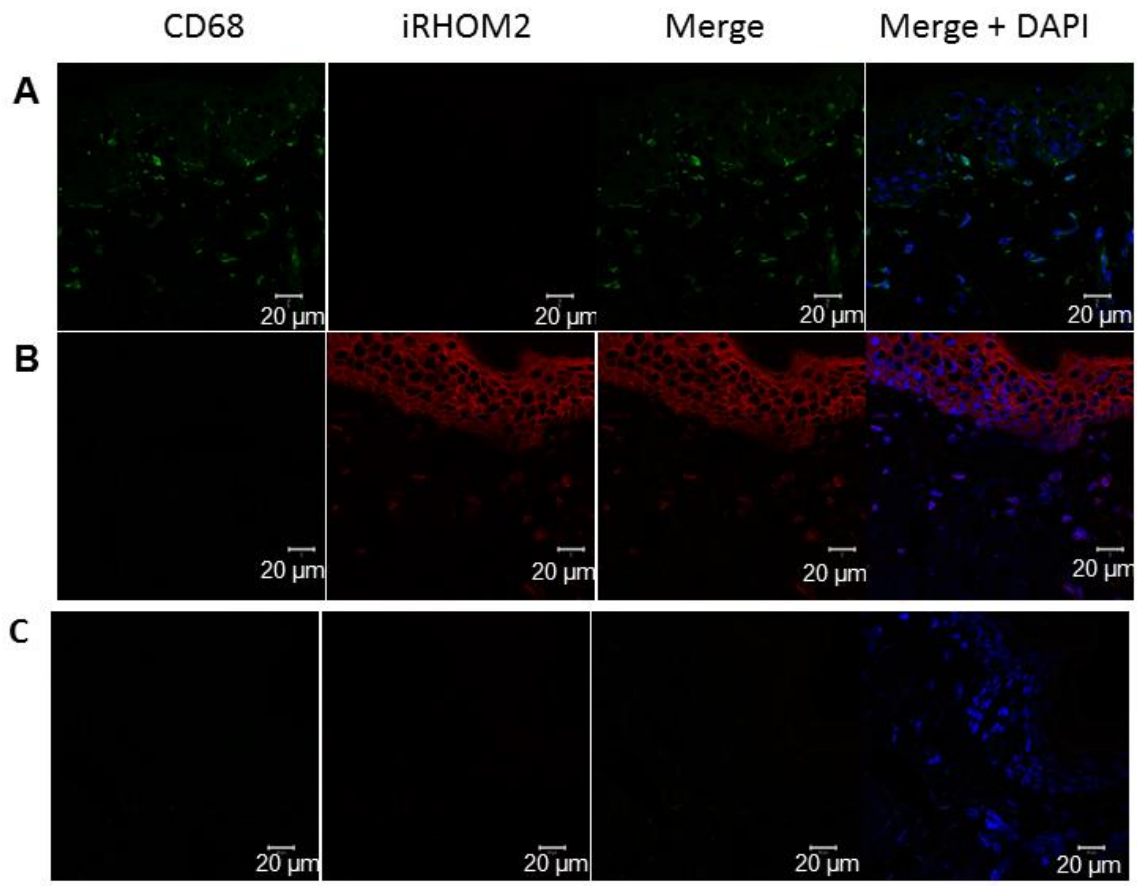

Appendix A2 Controls for co-localisation between iRHOM2 and CD68 in frozen skin sections. **A:** CD68 staining with rabbit and mouse secondary antibodies **B:** iRHOM2 staining with rabbit and mouse secondary antibodies. **C:** Negative controls

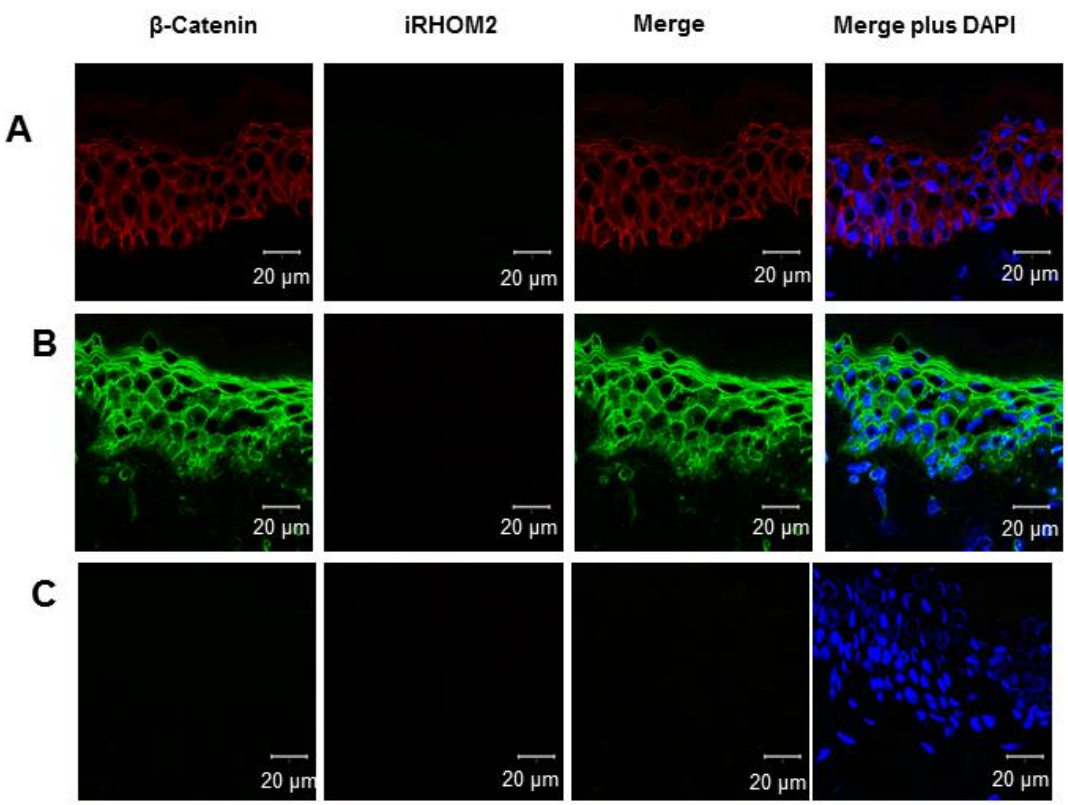

Appendix A3 Control staining from β-catenin-iRHOM2 co-localisation in TOC skin sections shown in figure 3.2.7. **A:** β-catenin plus Rb and Mo secondary antibodies, **B:** iRHOM2 plus Rb and Mo secondary antibodies, **C:** negative control staining.

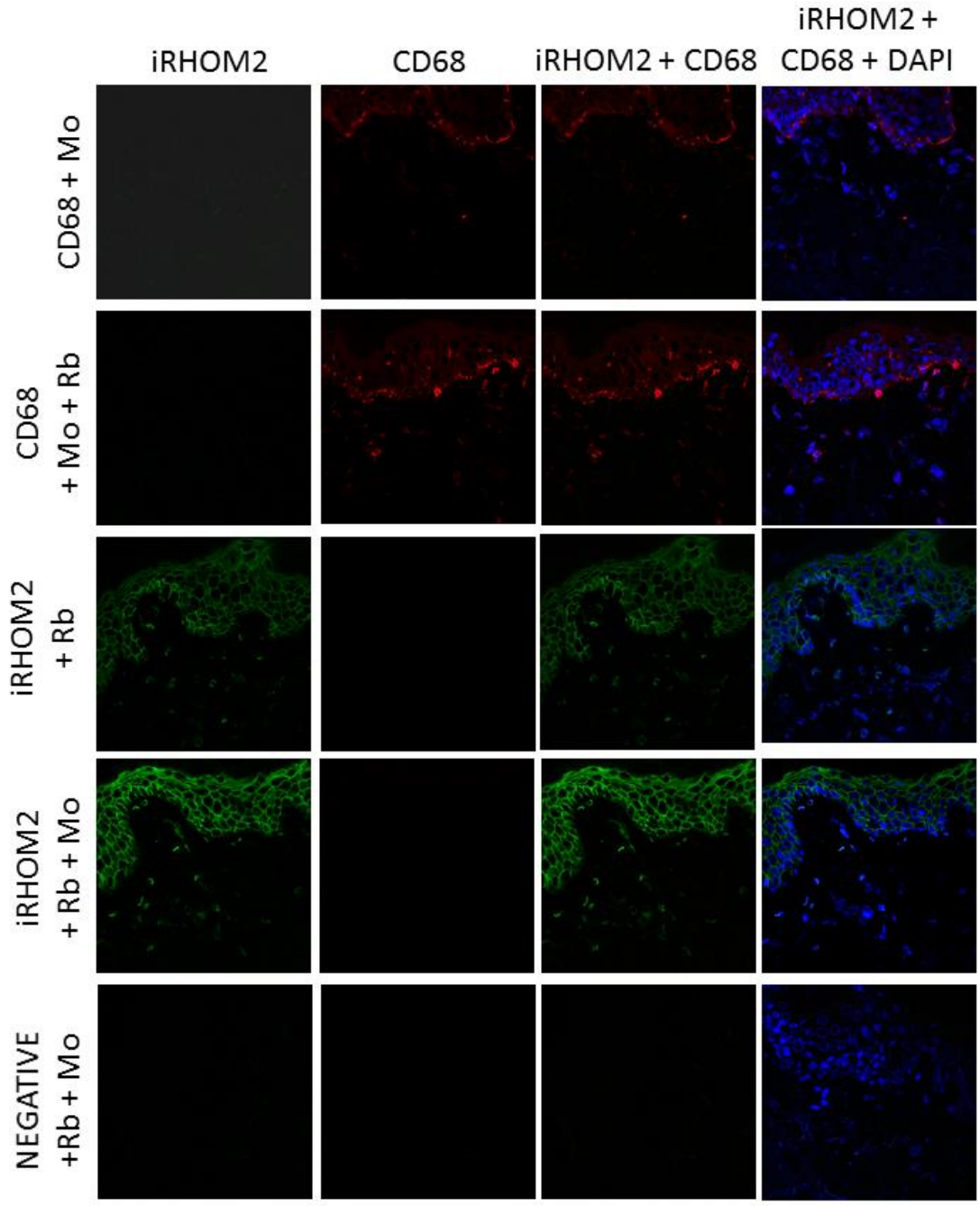

Appendix A4 Control staining for iRHOM2-CD68 co-localisation shown in Chapter 3. Control staining was carried out in normal breast skin. Brightness and contrast are increased by 20 %, as in figure 3.2.8 in Chapter 3. Rb and Mo refers to the species of the secondary antibody used (anti-Rabbit or anti-Mouse)

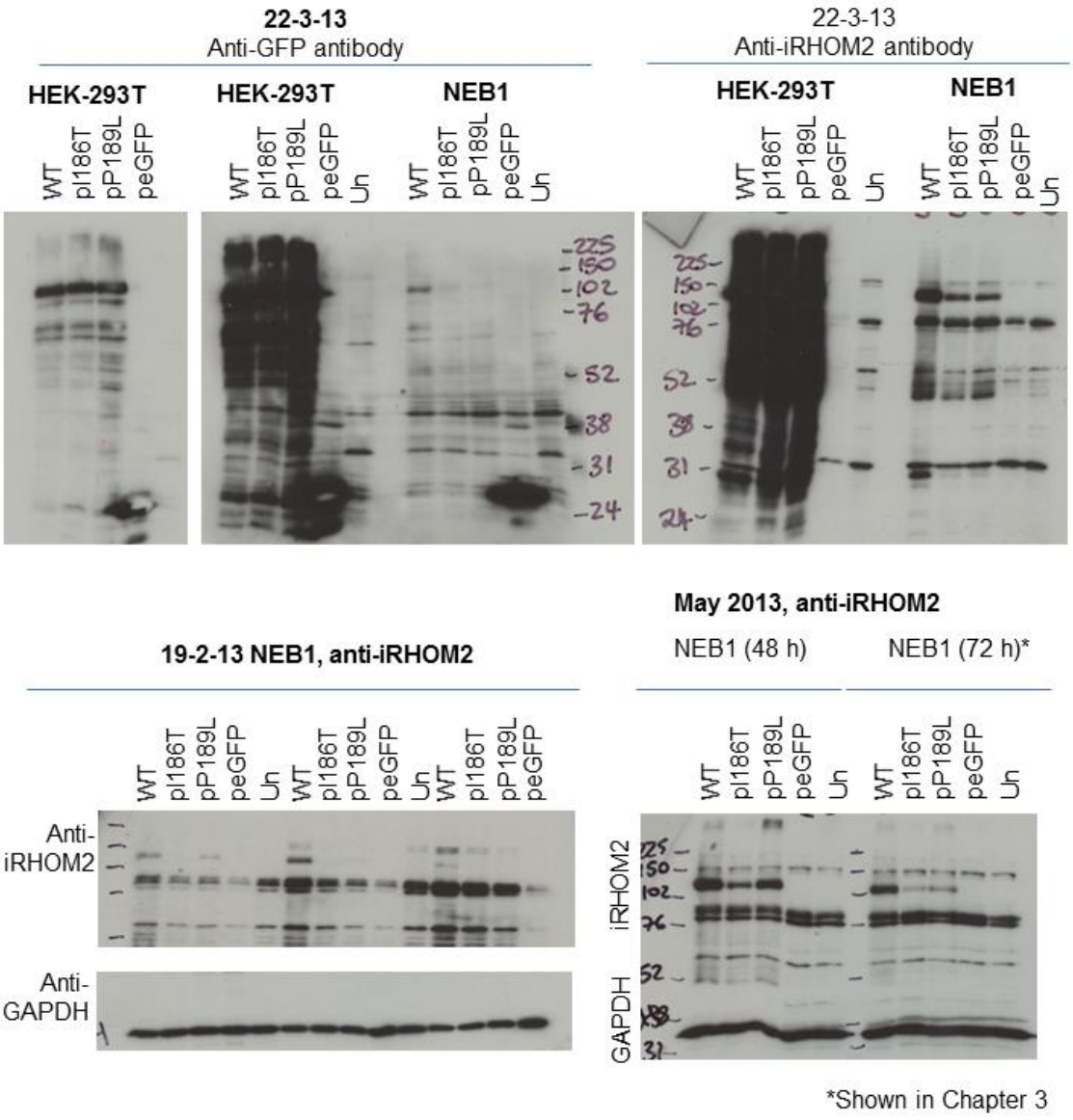

Appendix A5 Repeats of the iRHOM2-GFP overexpression studies shown in figure 3.2.10. Western blots were carried out with cell lysates from NEB1 or HEK293T cells overexpressing WT or mutant iRHOM2-GFP as indicated, and were performed with either anti-iRHOM2 or anti-GFP antibodies, also as indicated.

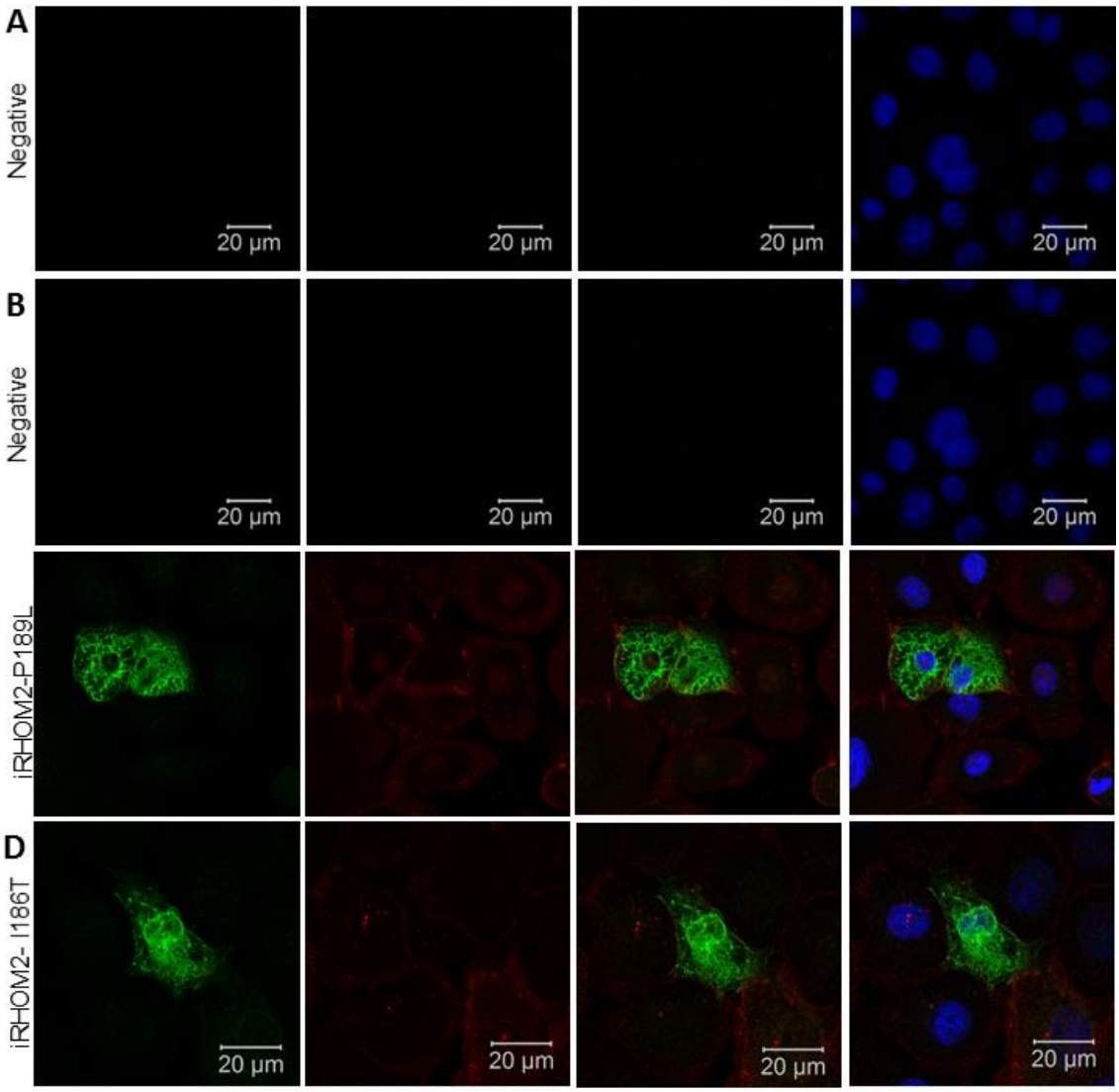

Appendix A6 Controls and additional images for figure 3.2.12. **A** and **B**: Negative controls for E-Cadherin (**A**), and PG (**B**) co-localisation with iRHOM2-GFP-WT. **C:** Co-localisation of overexpressed iRHOM2-GFP-P189L with E-Cadherin. **D:** co-localisation of iRHOM2-GFP-I186T with β-catenin. iRHOM2-GFP is shown in green, E-cadherin and β-catenin shown in red, and DAPI nuclear stain in blue. Images were taken on the Zeiss Meta 710 Confocal microscope.

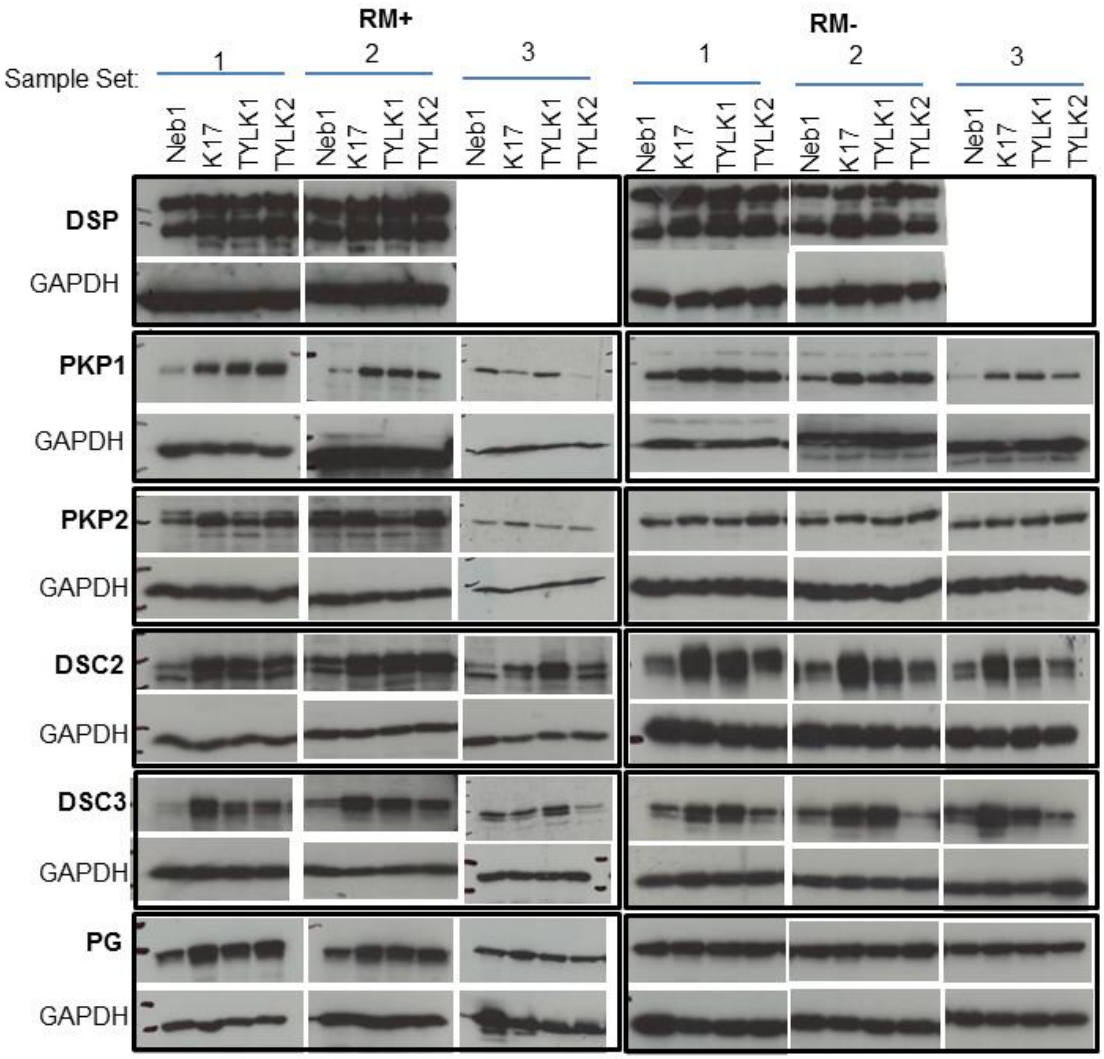

Appendix A7 Individual repeats of the desmosome western blots in chapter 3

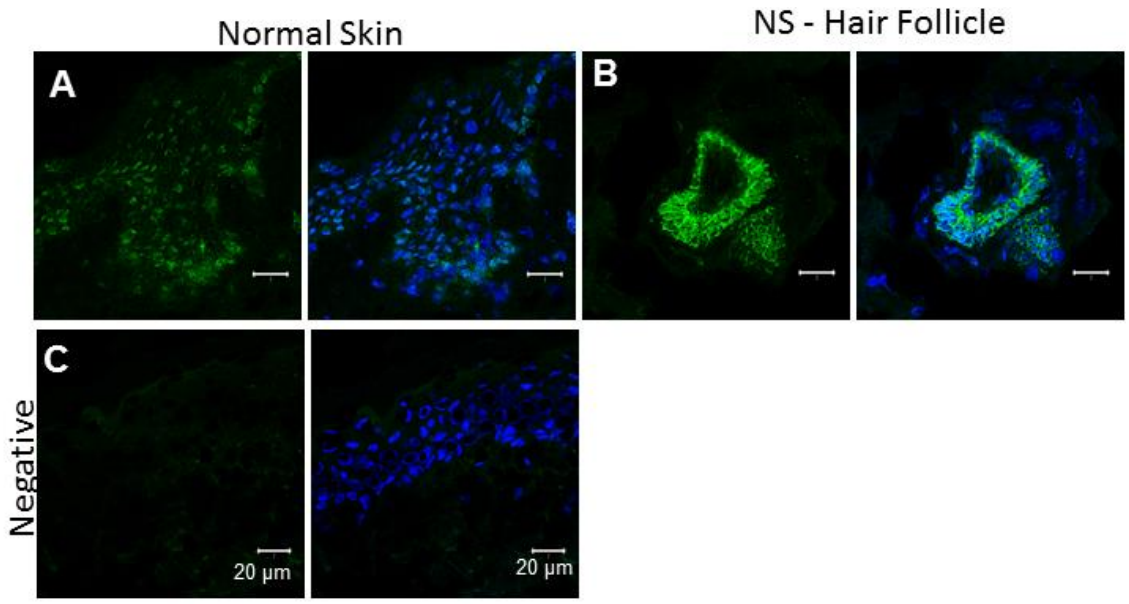

Appendix A8 DSG2 in normal Epidermis: IHC of DSG2 was performed in normal frozen epidermis sections with antibody 10D2. **A**: Normal skin epidermis from breast tissue, **B:** Sweat glandd in the same normal skin section, **C**: negative control. Brightness and contrast were increased by 10 % for each image. DSG2 is shown in green, DAPI nuclear stain shown in blue. Images were taken on the Zeiss Meta 710 Confocal microscope.

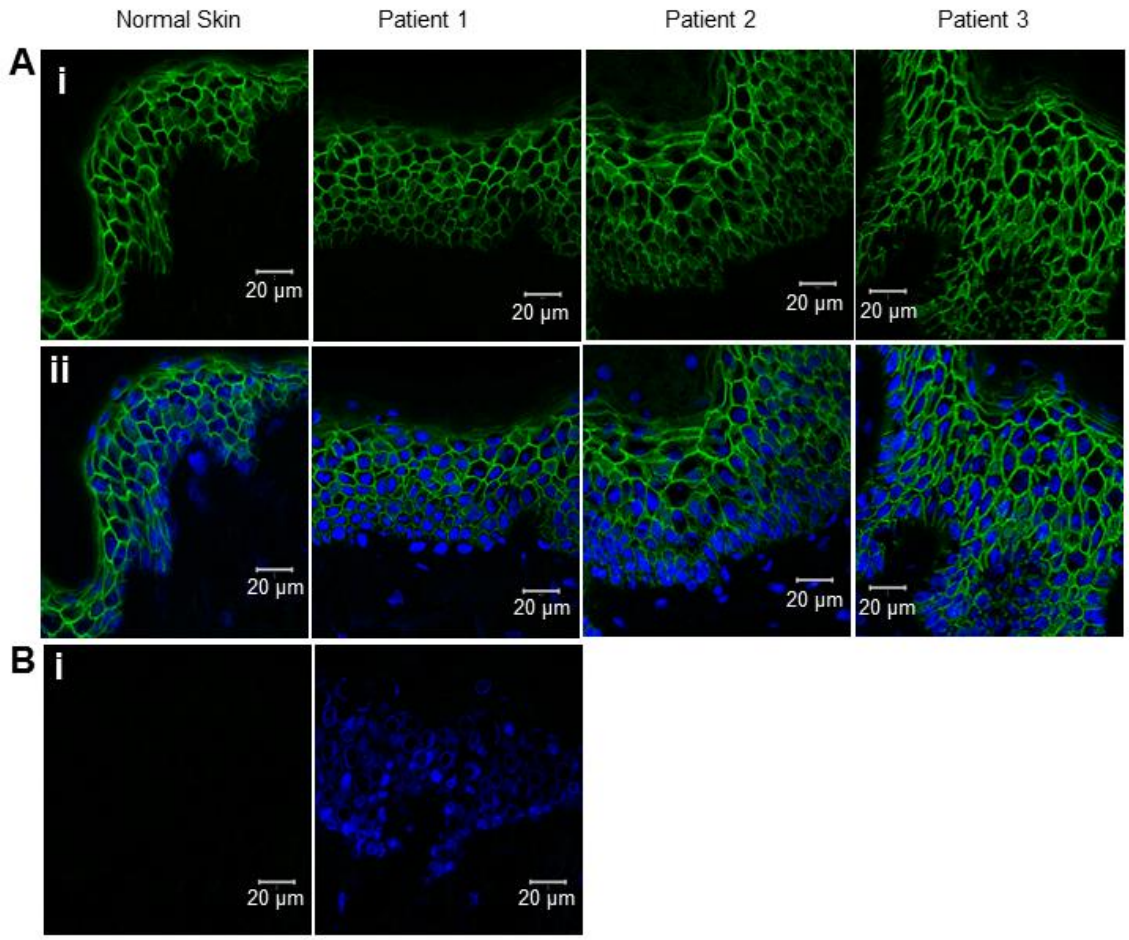

Appendix A9 DSG1 staining in control and TOC epidermis. A: IHC was performed with an antibody against DSG1 in normal skin from breast tissue, and TOC Patient 1, Patient 2 and Patient 3. **B:** Negative control staining. DSG1 is shown in green and DAPI nuclear stain in blue. Images were taken on the Zeiss Meta 710 Confocal microscope.

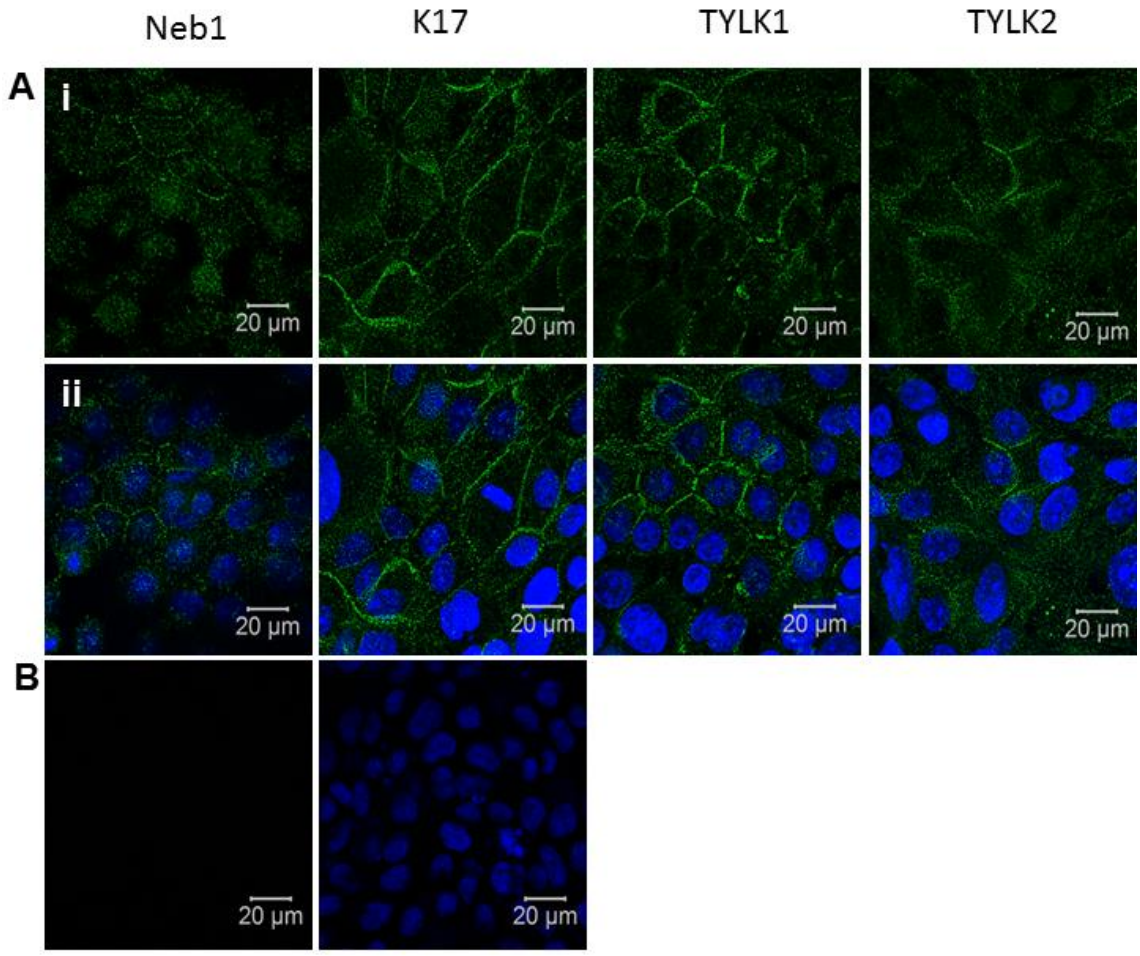

Appendix A10 DSG1 ICC in control and TOC keratinocytes. ICC was performed in MeAc fixed cells. **A:** DSG1-stained cells are shown in the presence (i) and absence (ii) of DAPI nuclear stain. **B:** Negative control staining. DSG1 is shown in green, and DAPI nuclear staining shown in blue. Images were taken with the Zeiss Meta 710 Confocal microscope.

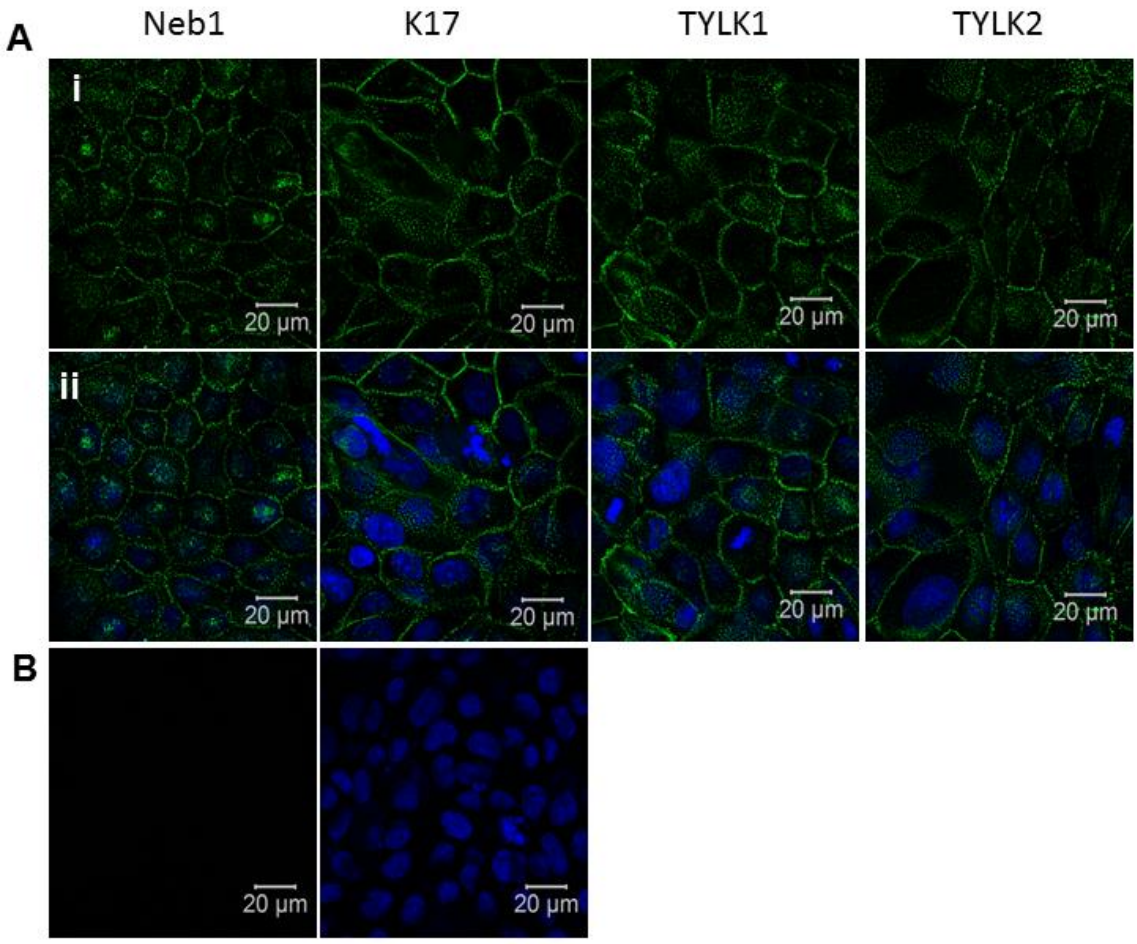

Appendix A11 DSG2 localisation in control and TOC cells. ICC was performed with the DSG2 10D2 antibody in MeAc-fixed cells after culture in the presence of EGF **(A). B:** shows negative control staining. DSG2 is shown in green, and DAPI nuclear stain is shown in blue. Images were taken on the Zeiss Meta 710 Confocal microscope.

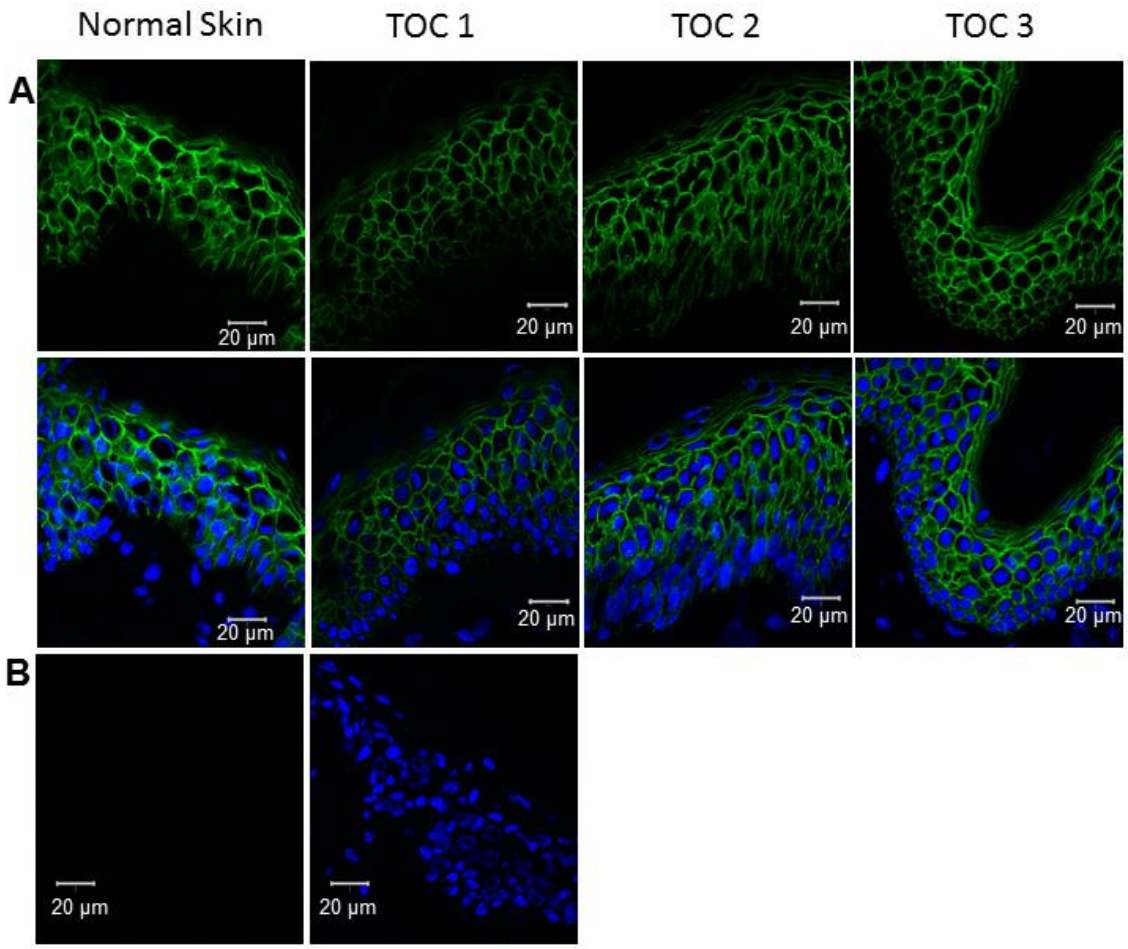

Appendix A12 Staining of desmogleins 1 and 2 in control and TOC epidermis. IHC was performed on frozen skin sections with antibody DSG3.10 which recognises DSG1 and 2 **(A)**. DSG1 and 2 are shown in green, in the presence or absence of DAPI nuclear stain which is shown in blue. Negative control staining is shown in **B.** Images were taken in the Zeiss Meta 710 confocal microscope.

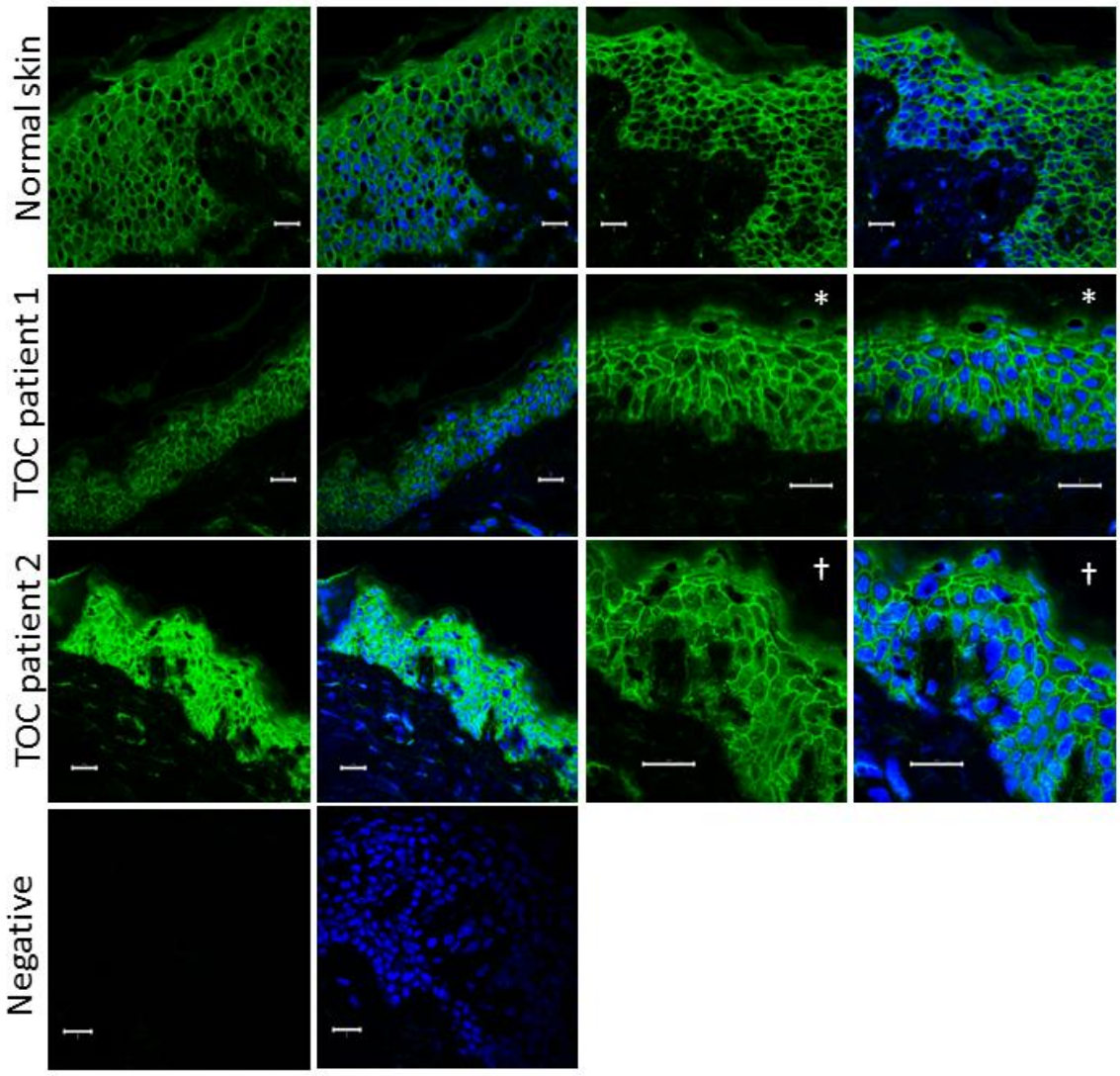

Appendix A13 DSC2 staining in control and TOC epidermis. IHC showing DSC2 staining in normal skin from breast, and TOC patients 1 and 2, as well as negative control staining, as indicated. The images marked with * are from patient 1, with the same brightness but increased zoom compared to the images on the left. The images marked with † are from patient 2, with reduced brightness and increased zoom compared with the images on the left. DSC2 is shown in green and DAPI nuclear stain shown in blue. Images were taken on the Zeiss Meta 710 confocal microscope.

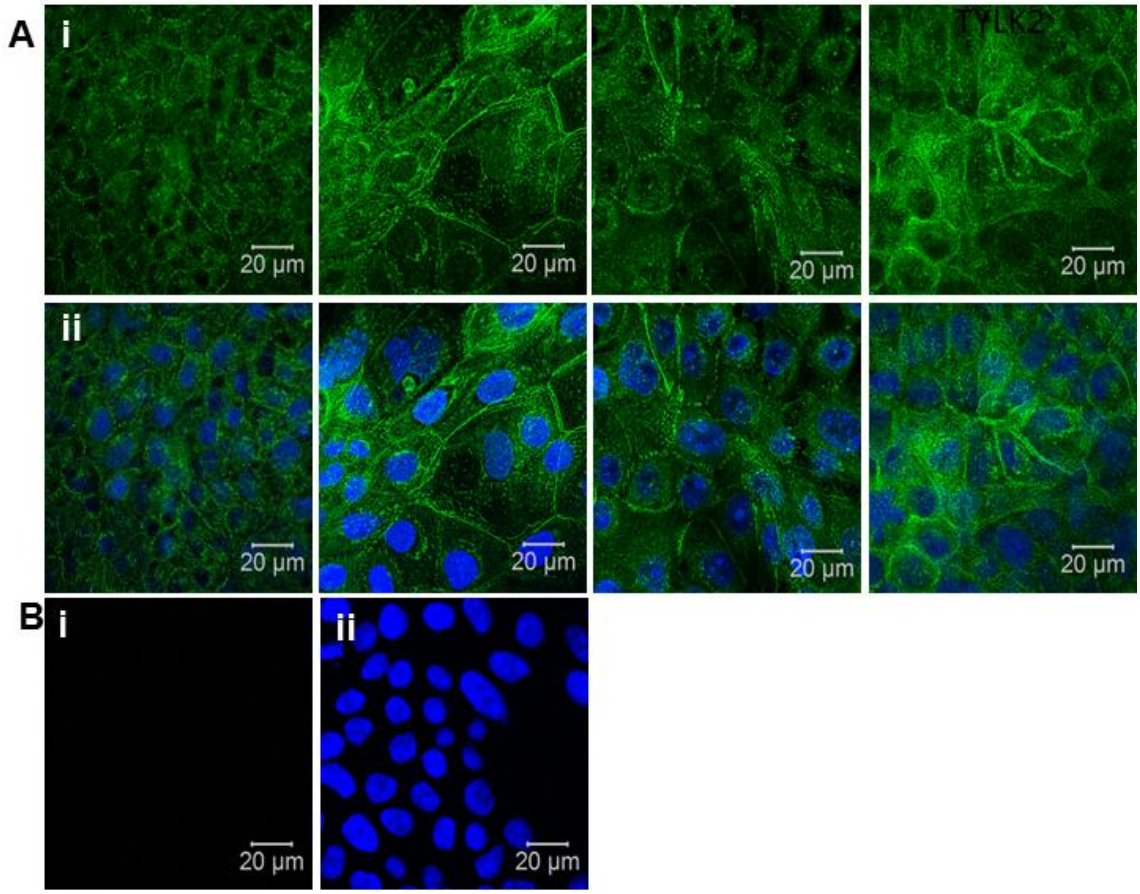

Appendix A14 DSC2 localisation in control and TOC keratinocytes. ICC of DSC2 in control and TOC keratinocytes **(A)** shown in the presence and absence of DAPI nuclear stain, which is shown in blue. DSC2 is shown in green. Negative control staining is shown in **B.** Images were taken on the Zeiss Meta 710 confocal microscope.

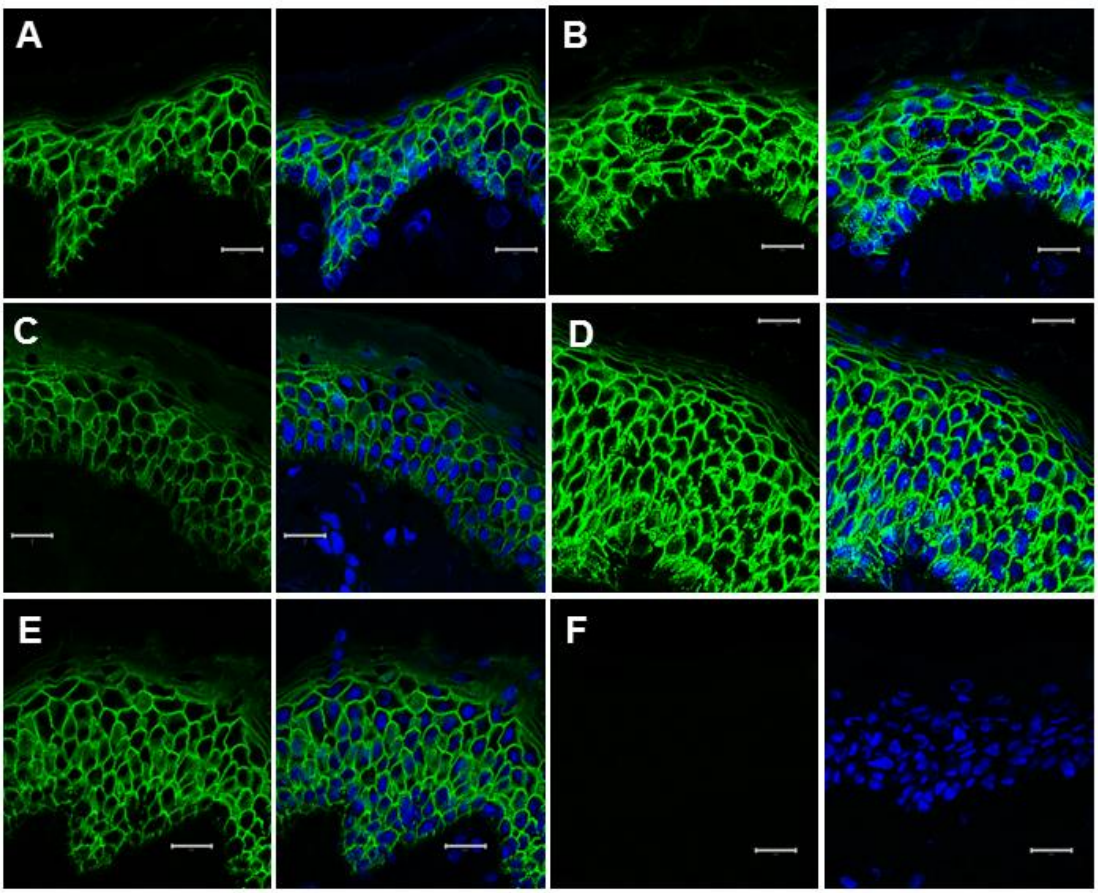

Appendix A15 DSC3 in normal and TOC skin. **A:** Normal skin from breast, **B:** Normal Facelift skin**, C:** TOC patient 1, **D:** TOC patient 2, **E:** TOC patient 3, **F:** Negative control. All shown in the presence and absence of DAPI nuclear stain, in blue. DSC3 staining in shown in green. Images were taken on the Zeiss Meta 710 Confocal microscope.

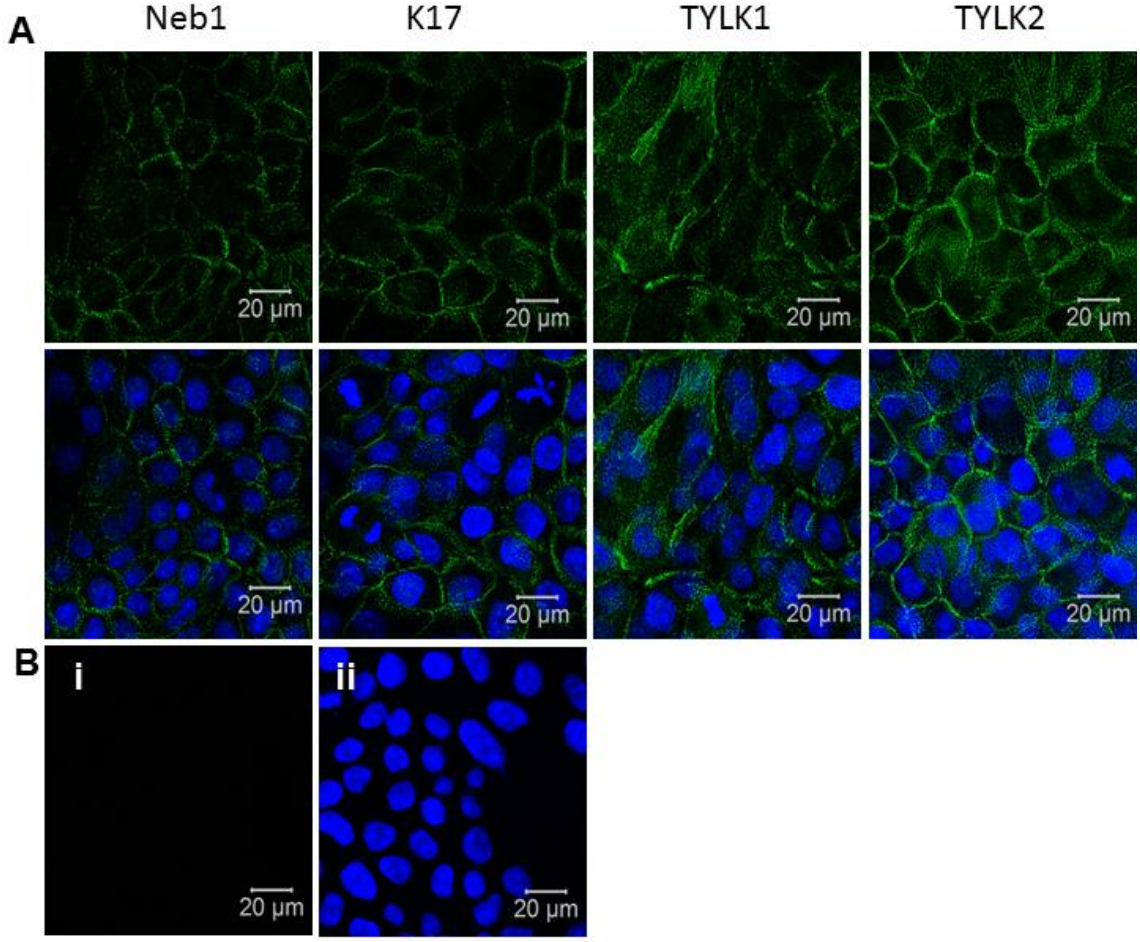

Appendix A16 DSC3 localisation in control and TOC keratinocytes. ICC was performed against DSC3, in MeAc-fixed cells, shown in **A**, with negative control staining in **B.** DSC3 is shown in green, and DAPI nuclear stain in blue. Images were taken on the Zeiss meta 710 confocal microscope.

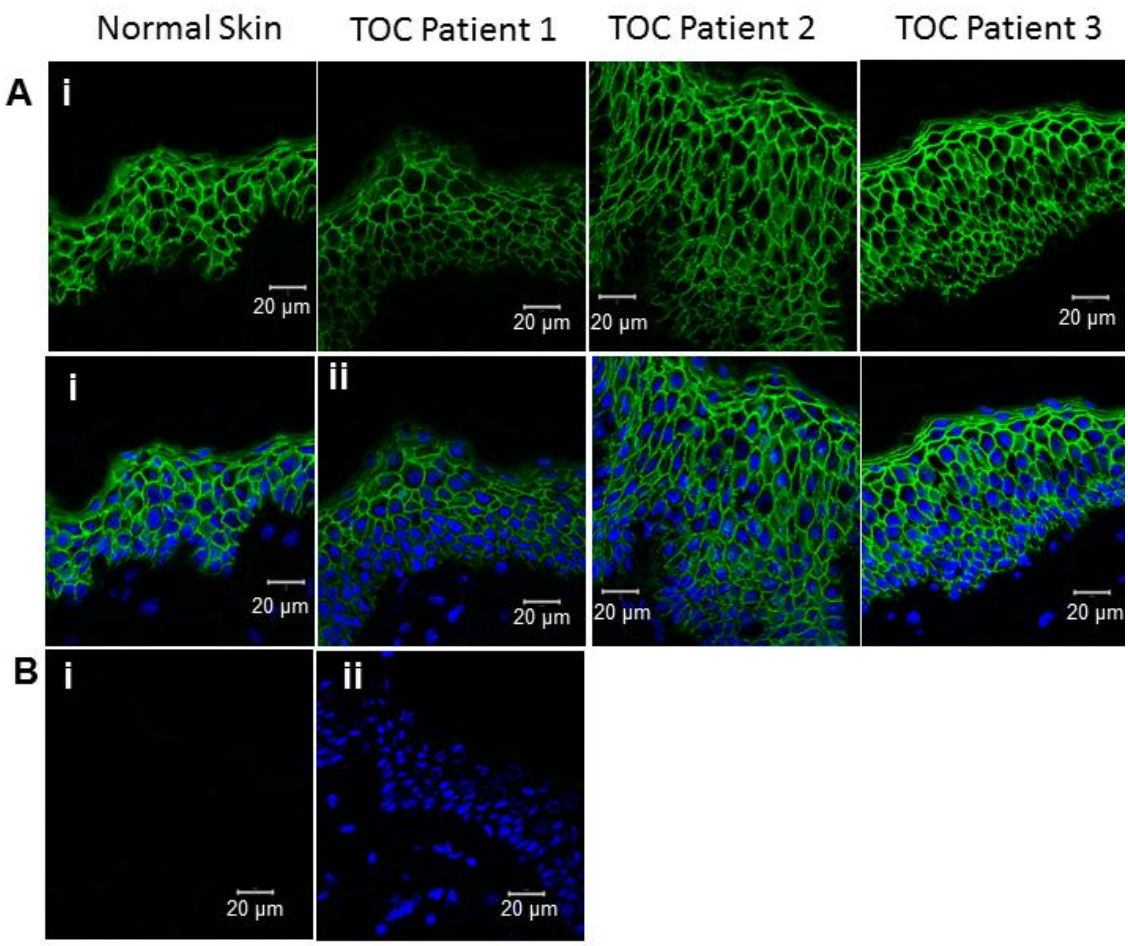

Appendix A17 PG localisation in control and TOC epidermis. IHC was performed in normal frozen skin from breast, and TOC interfollicular epidermis. **A:** PG staining, **B:** negative control staining. PG is shown in green, DAPI nuclear staining in blue. Images were taken on the Zeiss Meta 710 LSM confocal microscope.

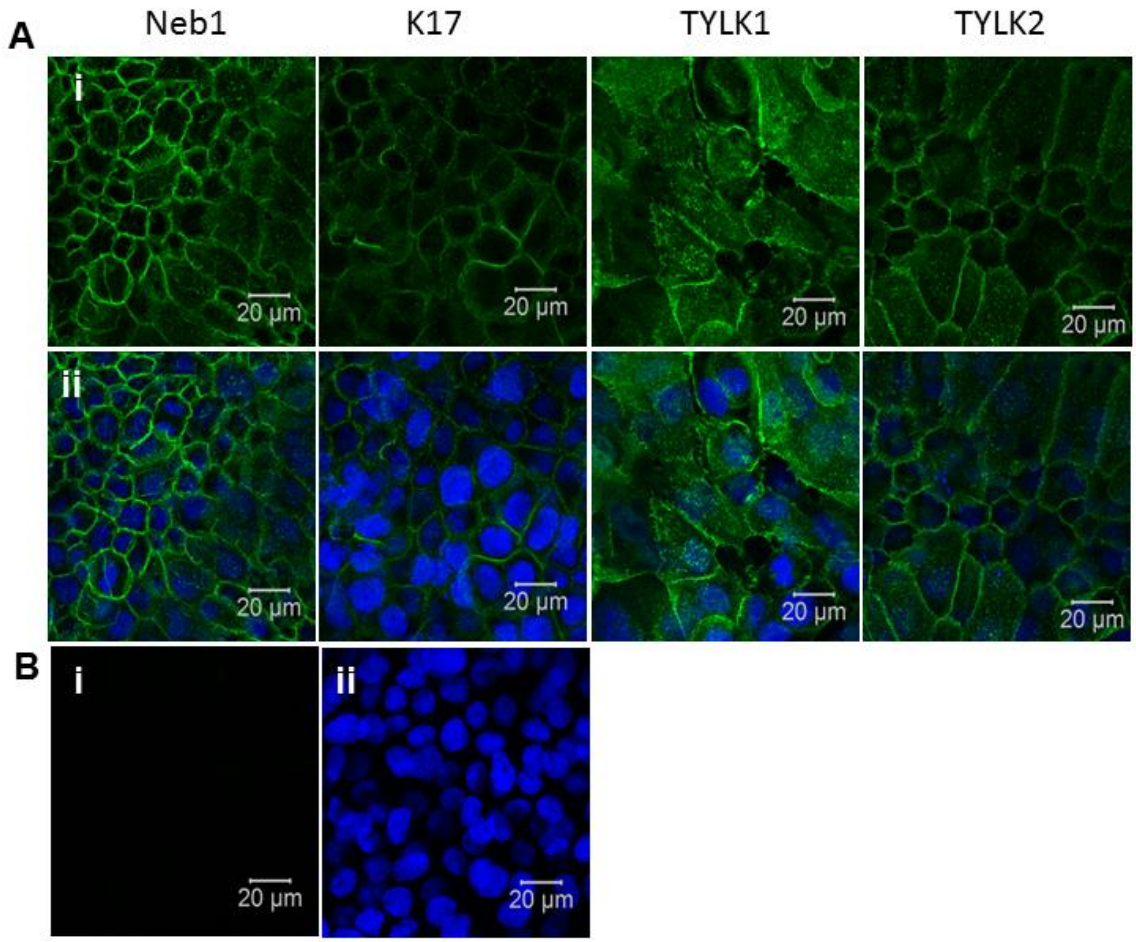

Appendix A18 PG localisation in control and TOC keratinocytes. ICC with an antibody against PG in MeAc fixed cells **(A),** with negative controls shown in **B.** PG is shown in green and DAPI nuclear stain in blue. Images were taken on the Zeiss Meta 710 confocal microscope.

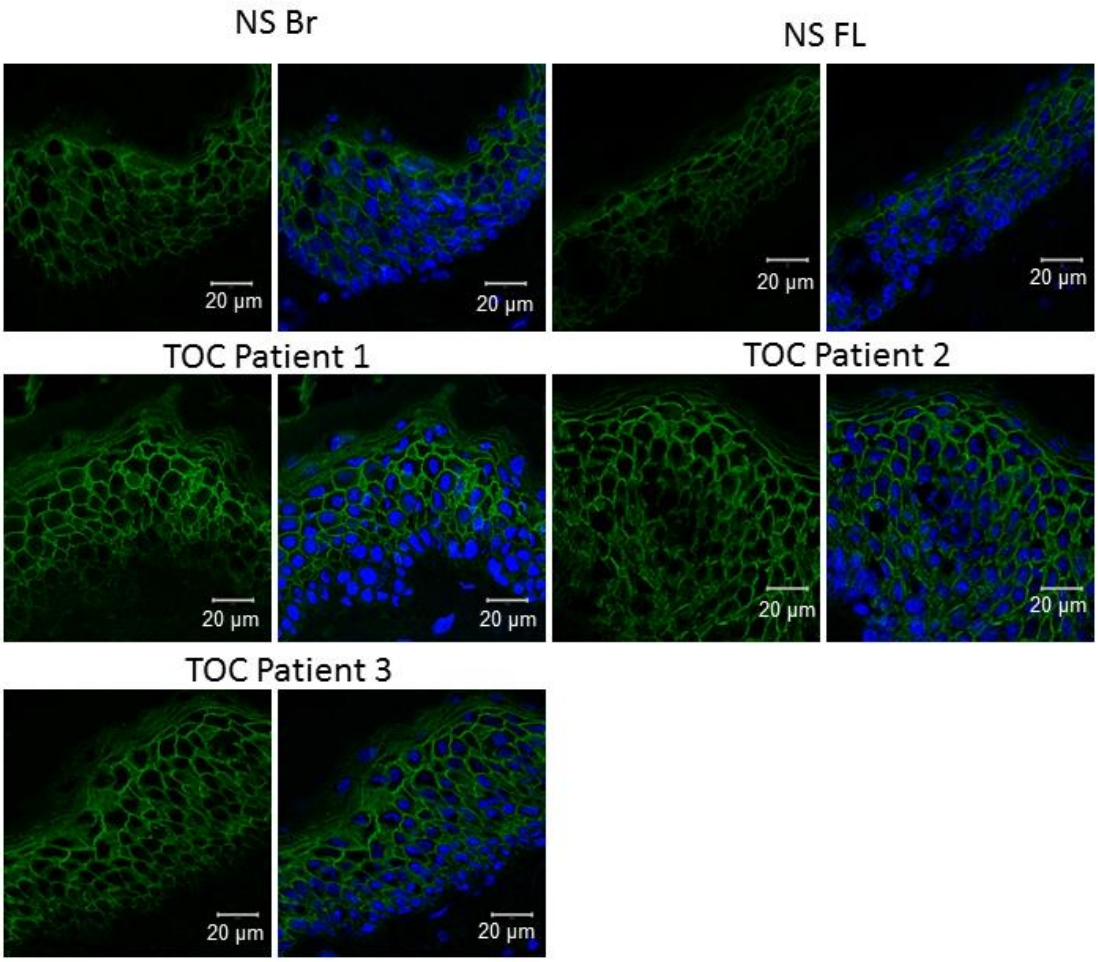

Appendix A19 PKP1 IHC in frozen sections from control and TOC epidermis. IHC against PKP1 was performed in normal skin (NS) from breast (Br) and facelift (FL), and in the interfollicular frozen skin sections from TOC patients 1, 2 and 3 as indicated. PKP1 is shown in green, DAPI nuclear stain in blue. Images were taken with the Zeiss Meta 710 confocal microscope.

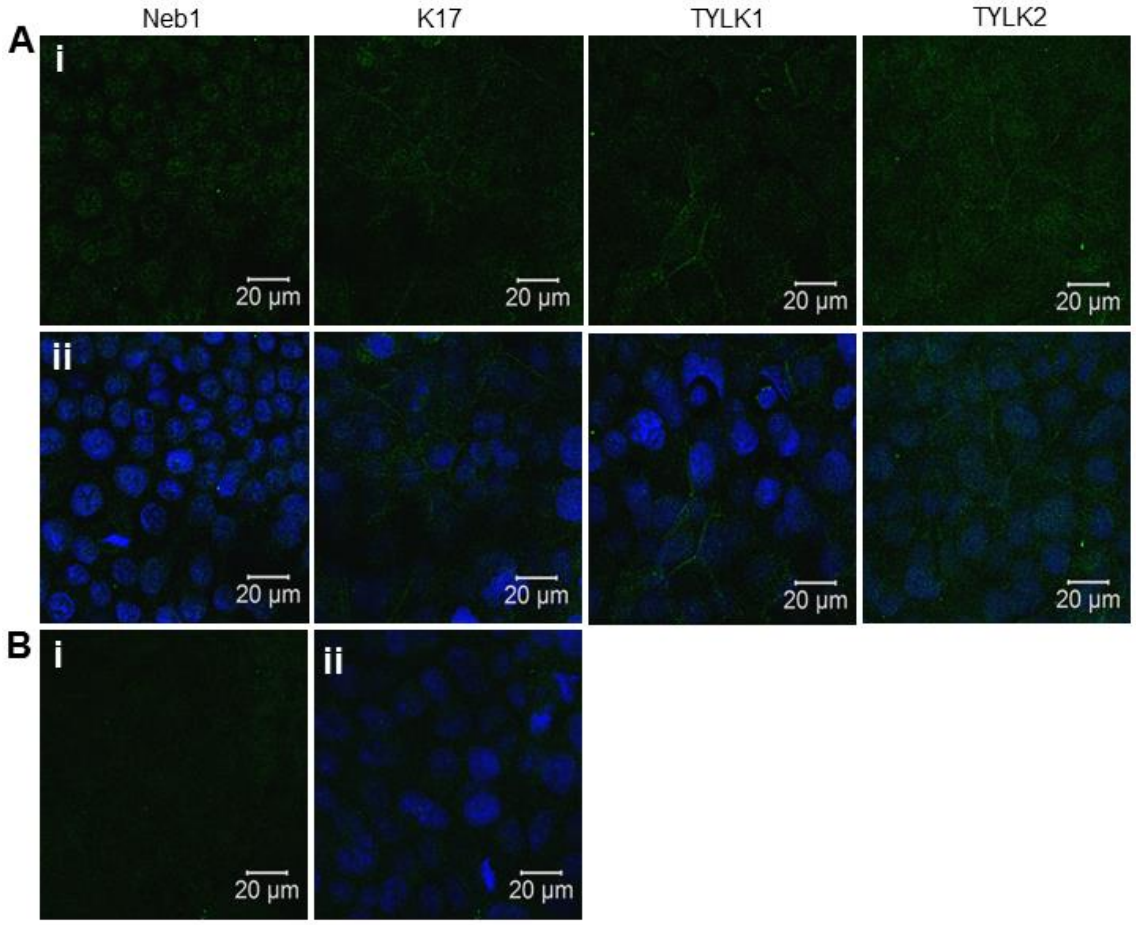

Appendix A20 PKP1 localisation in control and TOC keratinocytes ICC with an antibody against PKP1 in MeAc fixed cells **(A),** with negative controls shown in **B.** PKP1 is shown in green and DAPI nuclear stain in blue. Images were taken on the Zeiss Meta 710 confocal microscope.

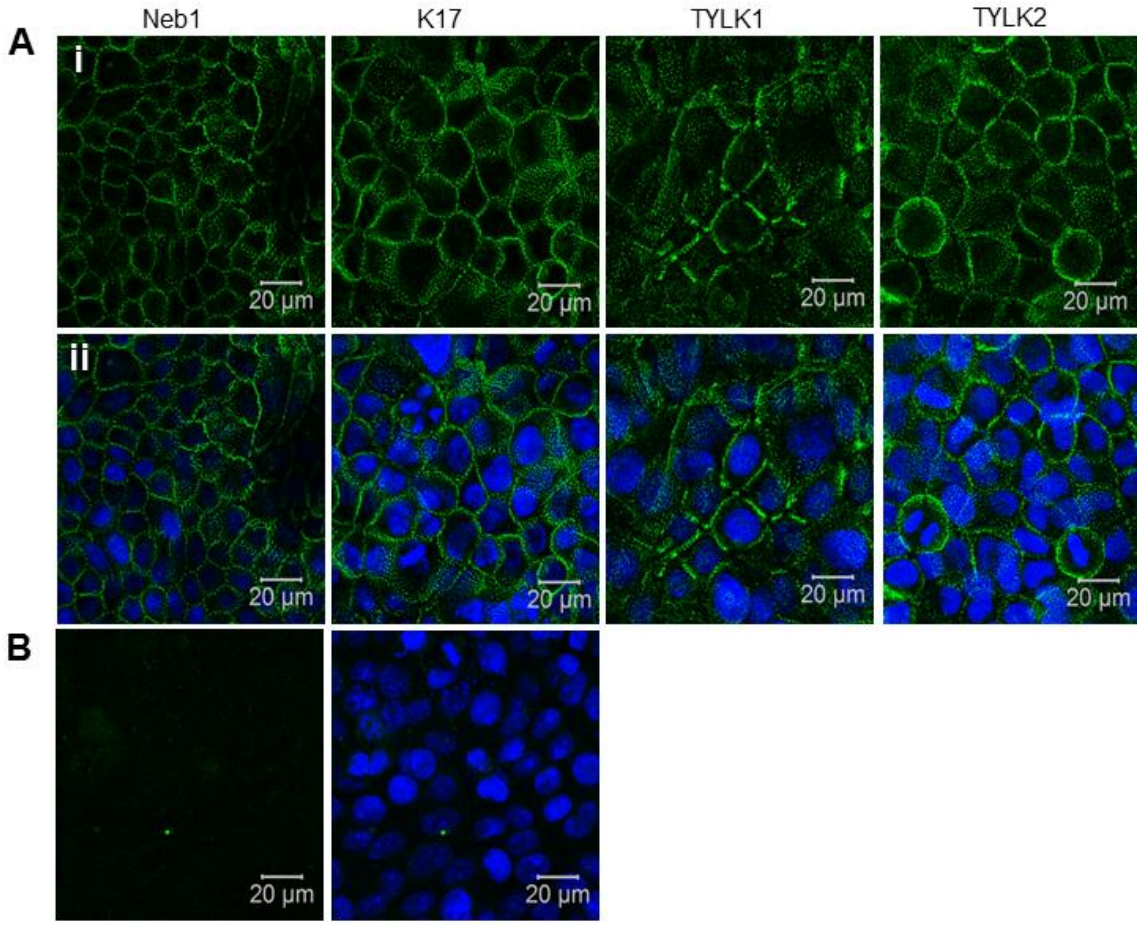

Appendix A21 PKP2 localisation in control and TOC keratinocytes ICC with an antibody against PKP2 in MeAc fixed cells **(A),** with negative controls shown in **B.** PKP2 is shown in green and DAPI nuclear stain in blue. Images were taken on the Zeiss Meta 710 confocal microscope.

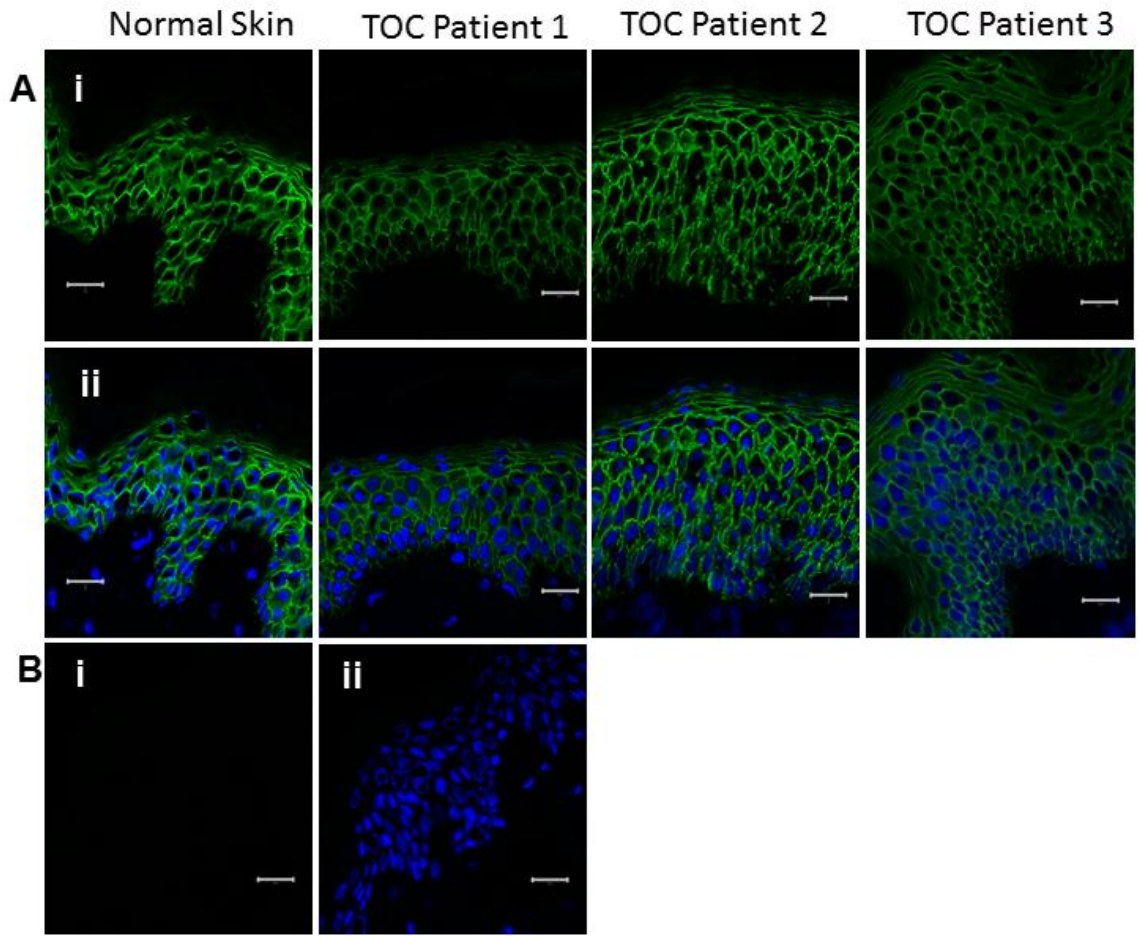

Appendix A22 DSP localisation in control and TOC epidermis. IHC with the DSP 11-5F antibody in MeAc fixed sections **(A),** with negative controls shown in **B.** DSP is shown in green and DAPI nuclear stain in blue. Images were taken on the Zeiss Meta 710 confocal microscope.

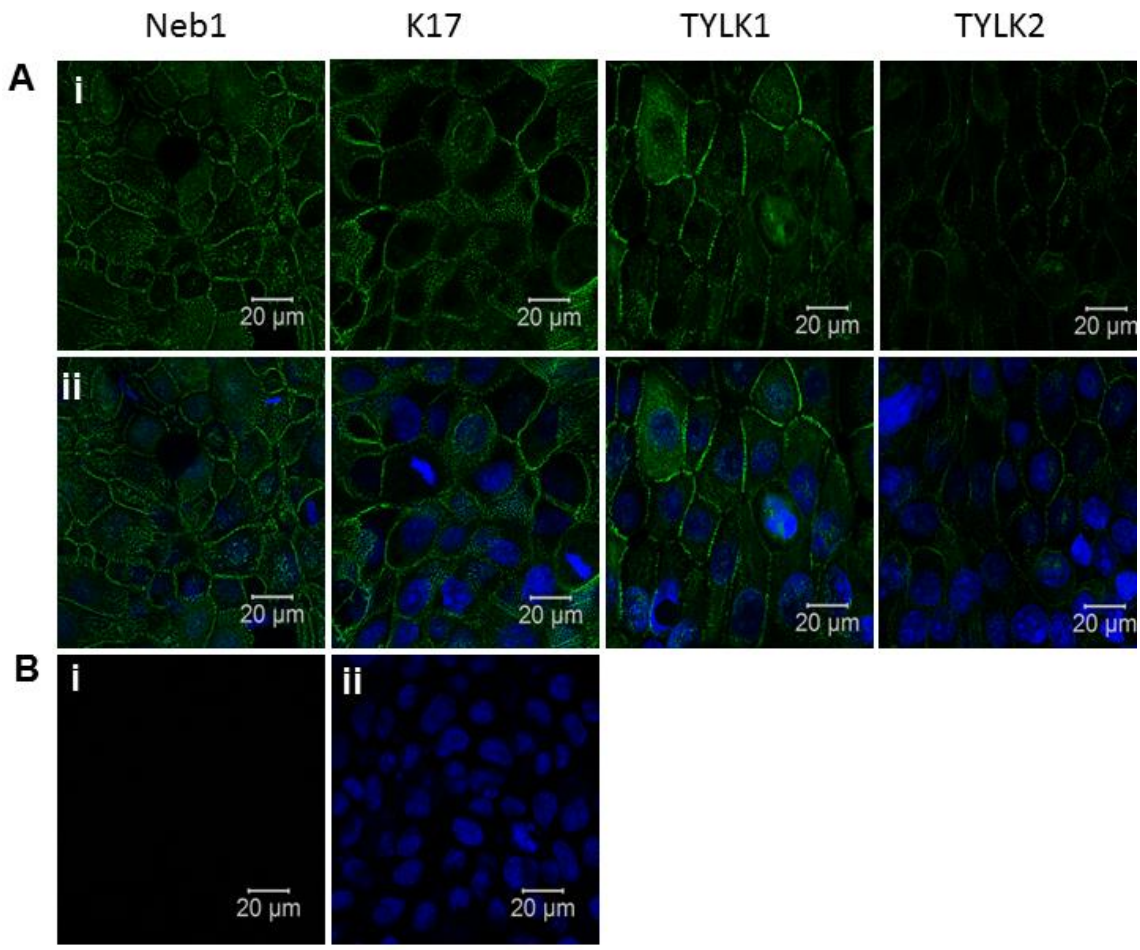

Appendix A23 DSP localisation in control and TOC keratinocytes ICC with the DSP 11-5F antibody in MeAc fixed cells **(A),** with negative controls shown in **B.** DSP is shown in green and DAPI nuclear stain in blue. Images were taken on the Zeiss Meta 710 confocal microscope.

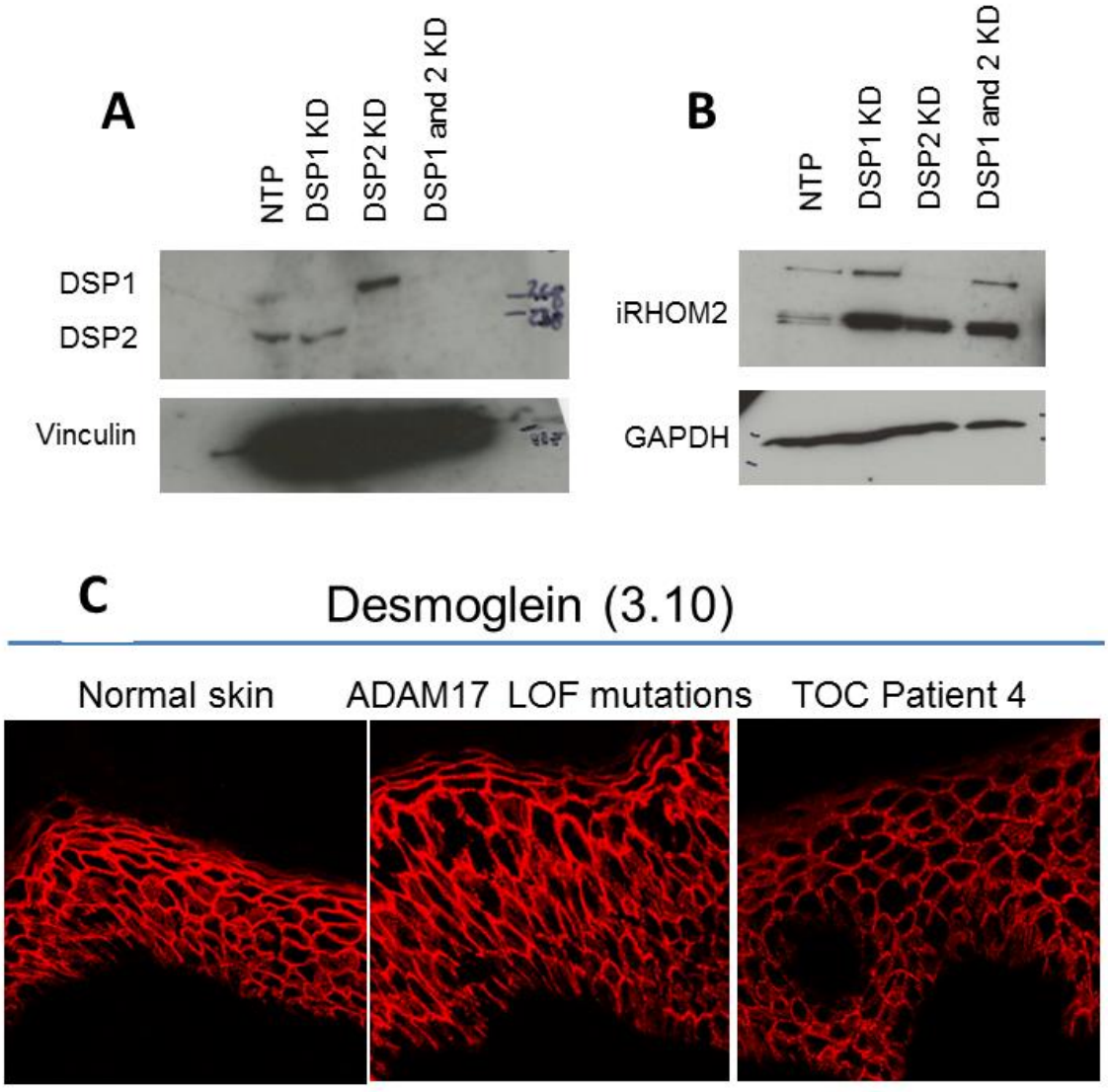

Appendix A24 iRHOM2 is up-regulated in HaCaT keratinocytes following DSP knock-down in one experiment. Western blots showing **A:** DSP isoforms 1 and 2 with vinculin loading control, and **B:** iRHOM2 with GAPDH loading control. These findings were not reproducible. **C:** IHC with antibody DSG3.10, which recognises both DSG1 and 2 in normal epidermis, epidermis with ADAM17 LOF mutations, and in TOC patient 4.

Appendix B:
Control Experiments and Supporting results for Chapter 4 - iRHOM2 signalling pathways in the skin

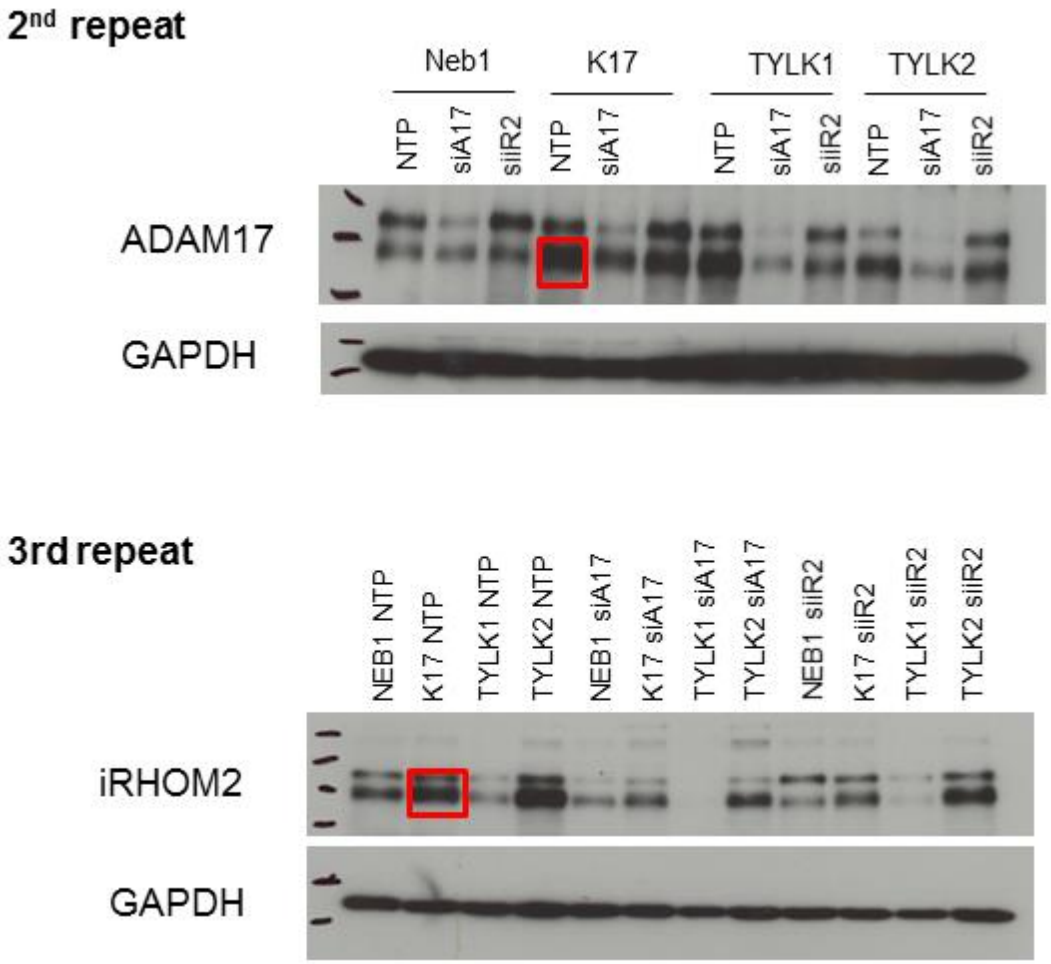

Appendix B1 Repeats of the ADAM17 and iRHOM2 siRNA knock-down experiments shown in chapter 4.

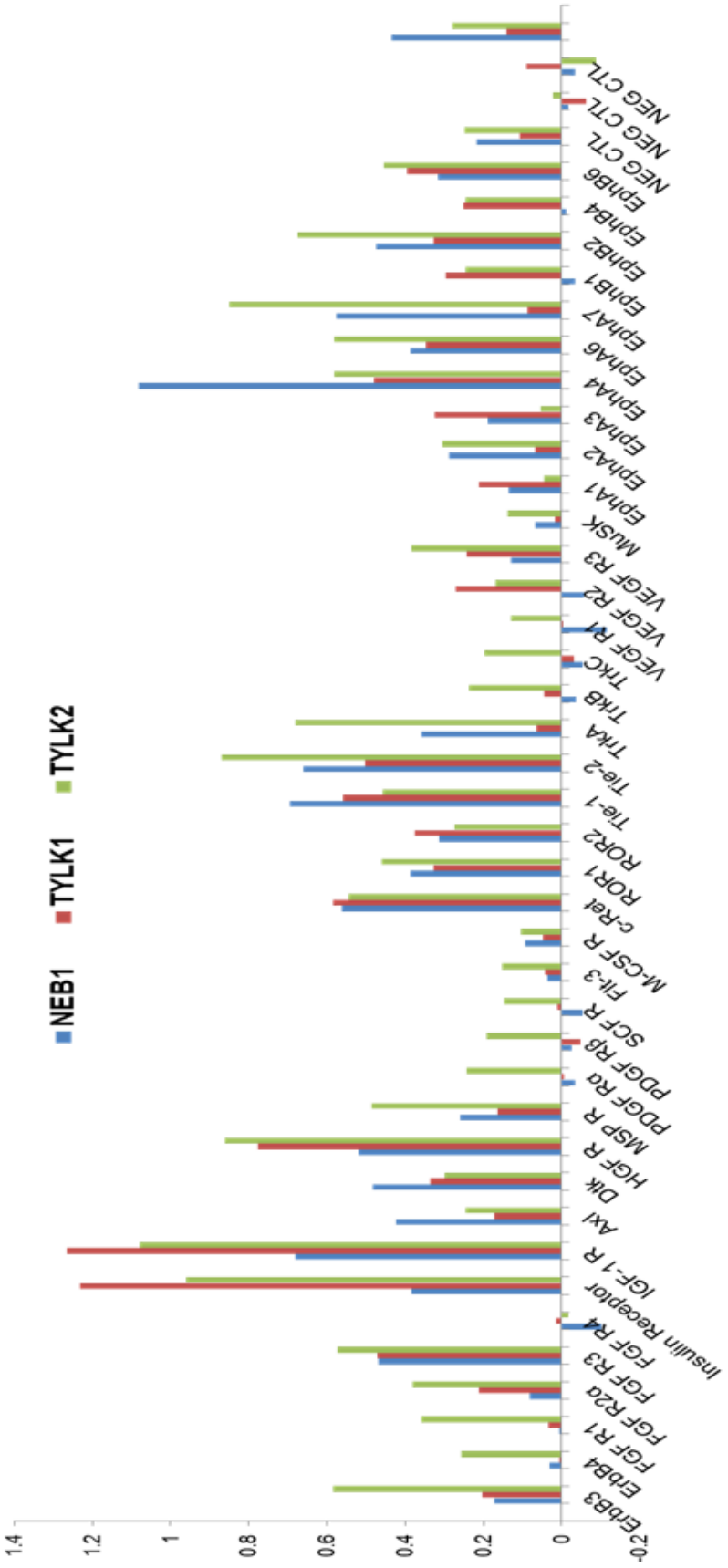

Appendix C2 Densitometry analysis of each protein on the phospho-RTK array shown in chapter 4.

Densitometry was performed using Image J software, on the array. A 5 min exposure of the array to ECL plus was used for the densitometry analysis.

Appendix B2 Densitometry analysis of phospho-RTK arrays shown in chapter 4

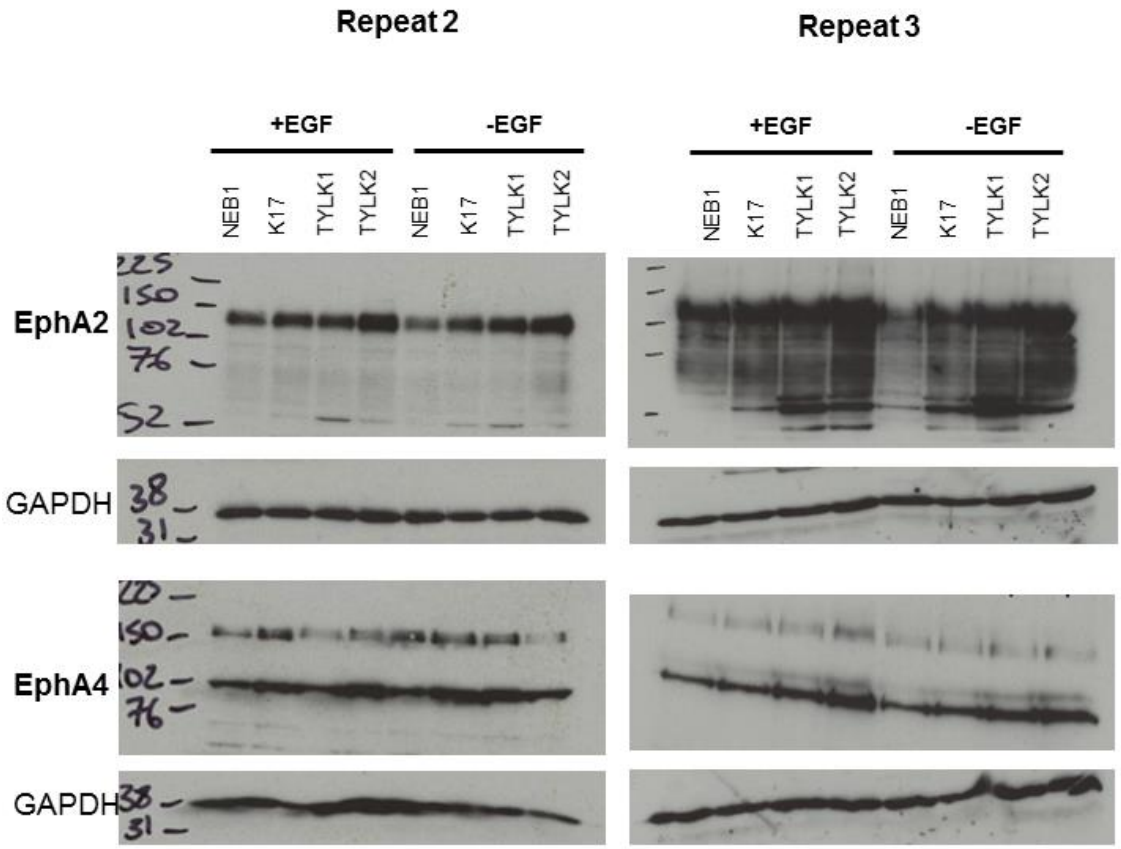

Appendix B3 Repeats of EphA2 and EphA4 western blots in keratinocytes following culture in the presence or absence of EGF (RM+ or RM-)

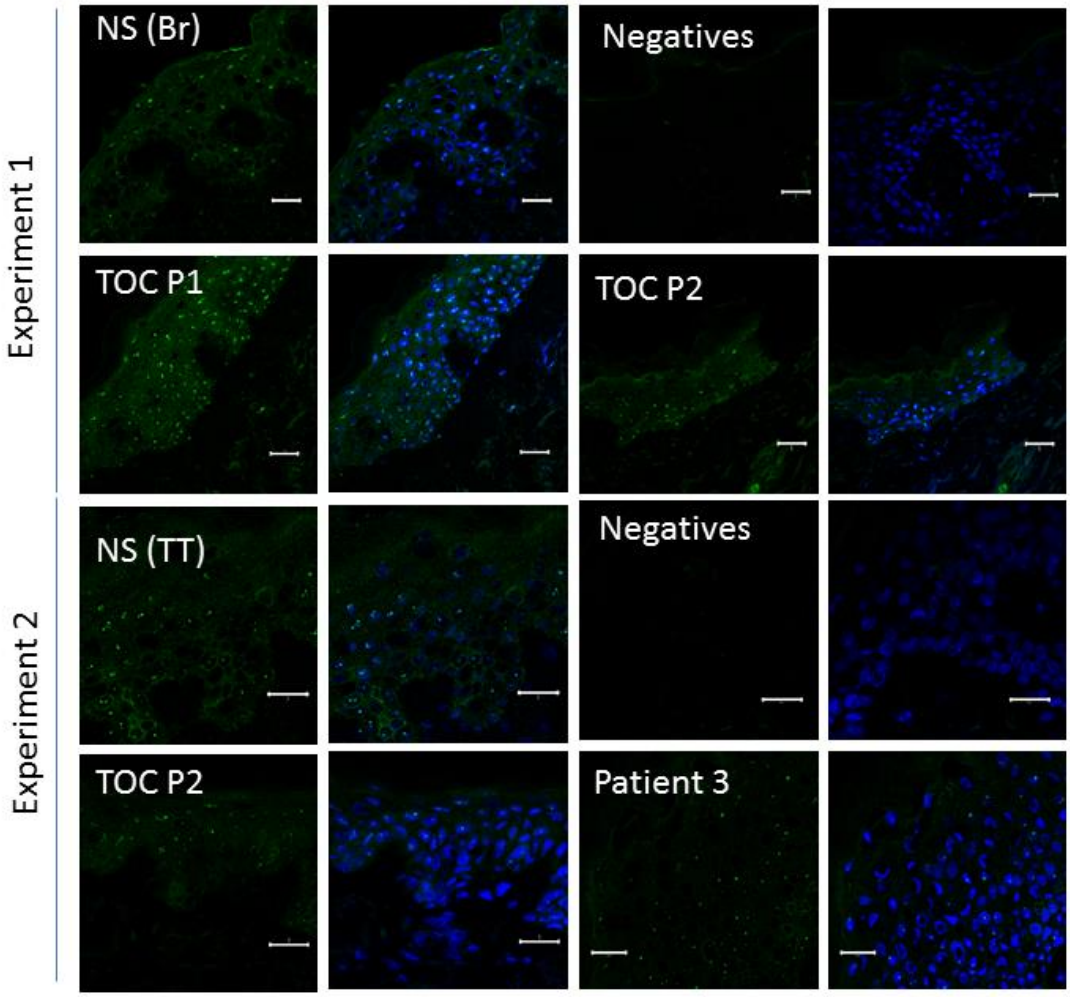

Appendix B4 NOTCH1 S1, S2 and NICD localisation in control and TOC epidermis with AbCam ChIP grade antibody. Images from two experiments are shown as indicated. NOTCH1 is shown in green, DAPI nuclear staining in blue. Scale bars represent 20 μm. Images were taken on the Zeiss Meta 710 confocal microscope. NS, normal skin; Br, breast; P1-3, patients 1-3; TT, tummy tuck.

Appendix C:
Control Experiments and Supporting results for Chapter 5 – iRHOM2 localisation and expression in cancer

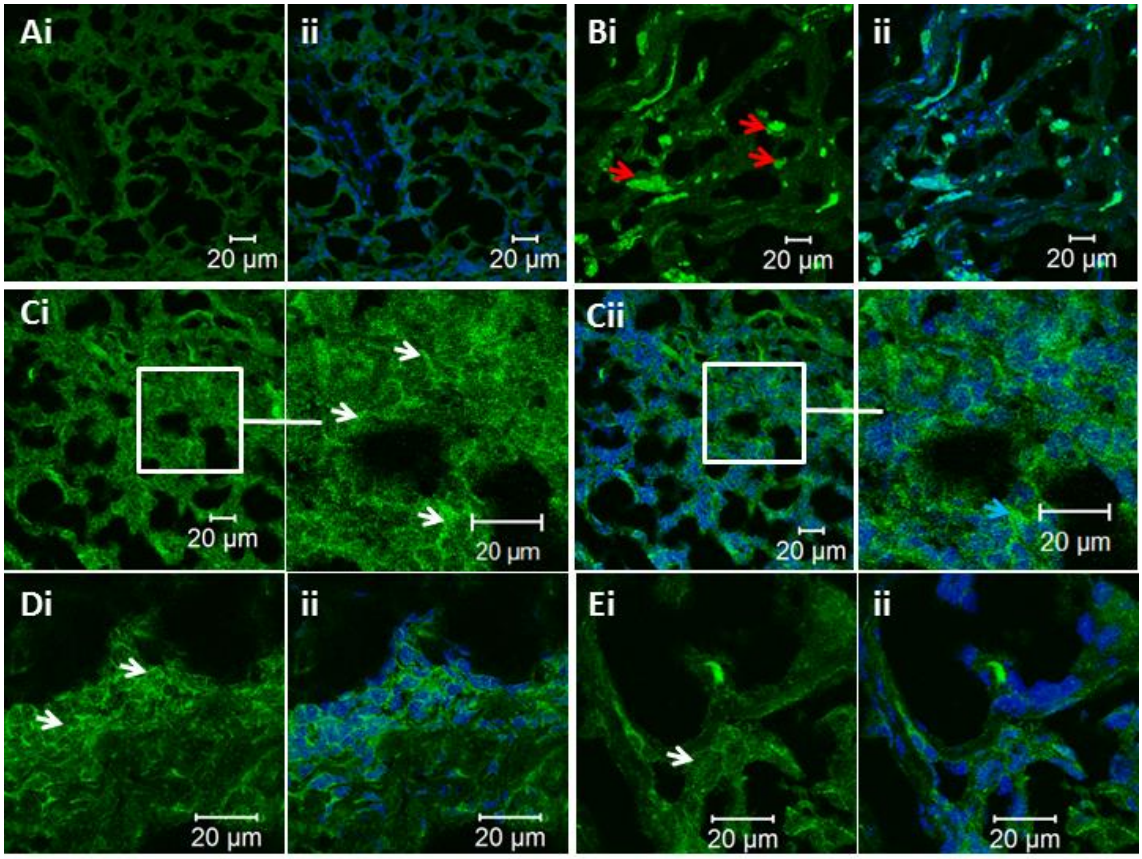

Appendix C1 Variable localisation of iRHOM2 within tissue sections in a biopsy from a frozen Breast Carcinoma. Images represent different regions of the same biopsy at magnifications of 40X (**A, B, C**) and 100X (**D, E**) in the presence (ii) and absence (i) of nuclear marker DAPI, shown in blue. iRHOM2 staining is shown in green. Image **C** is shown with and without DAPI, with the right hand images a close-up of the region indicated by the white box. Images were taken with the LSM 510 Confocal Microscope. Microscope settings were varied to achieve the best picture of the localisation. Red arrows indicate small, brighter areas of tissue staining, perhaps indicating infiltrating immune cells. White arrows show examples of plasma membrane staining.

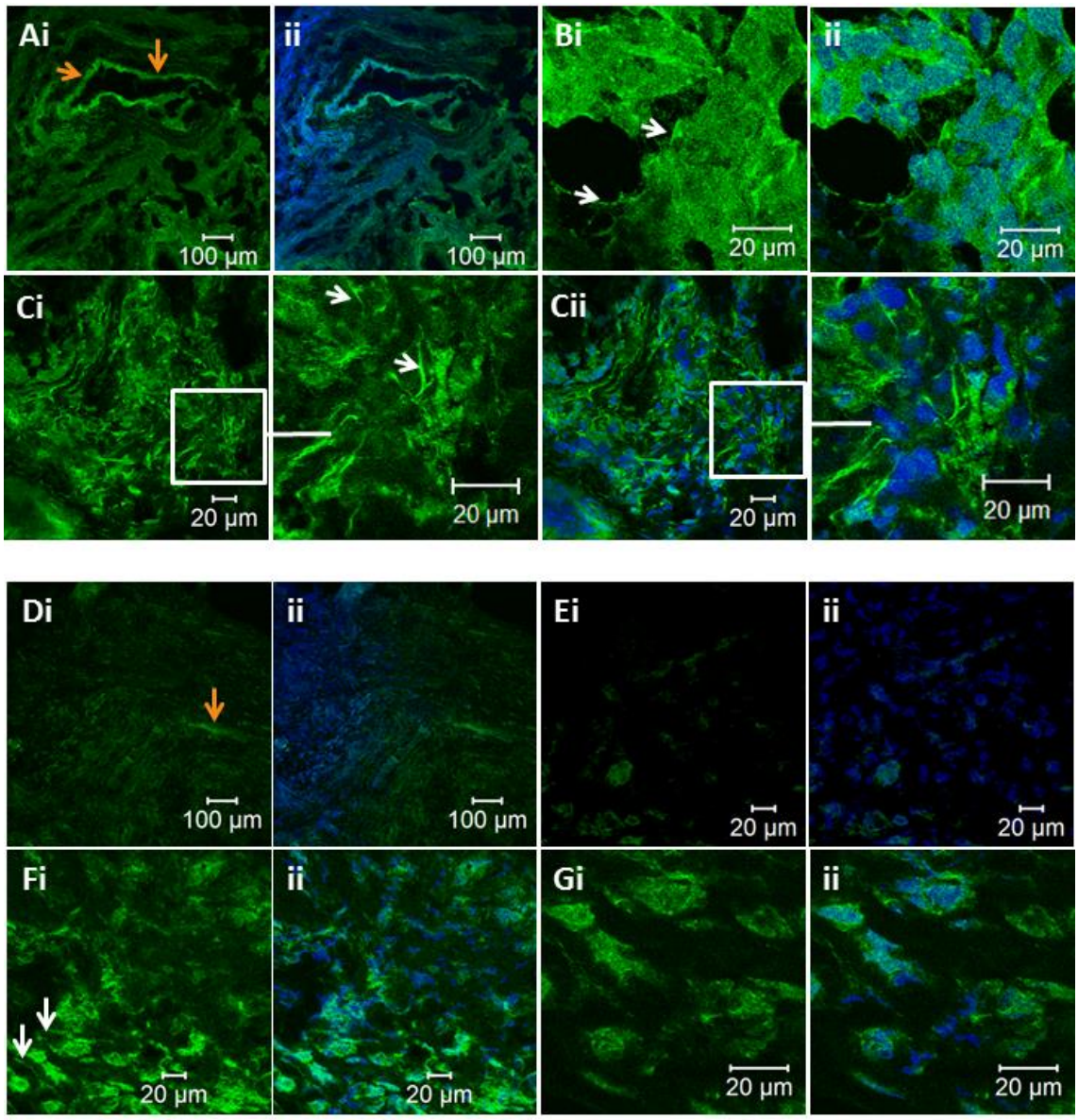

Appendix C2 iRHOM2 localisation in Breast Ductal Carcinoma and Breast Lobular Carcinoma. Frozen sections were stained and images are taken from regions of the samples. Breast Ductal Carcinoma is shown in **A-C**, and breast lobular carcinoma shown in **D-G**. Images were taken at magnifications of 10X (**A, D**), 40X (**C, E, F**) 100X (**B, G**) with (i) and without (ii) DAPI nuclear stain, shown in blue. The images on the right in Ci and Cii are a close-up view of the region indicated by the white box on the left hand picture. Images were taken on the Zeiss LSM 510 Confocal microscope and the settings adjusted for each image to visualise iRHOM2 localisation. White arrows indicate possible plasma membrane staining, and orange arrows indicate regions and the edge of the tissue that appear to have brighter iRHOM2 staining. Red arrows show individual cells with particularly bright iRHOM2 staining, potentially infiltrating macrophages.

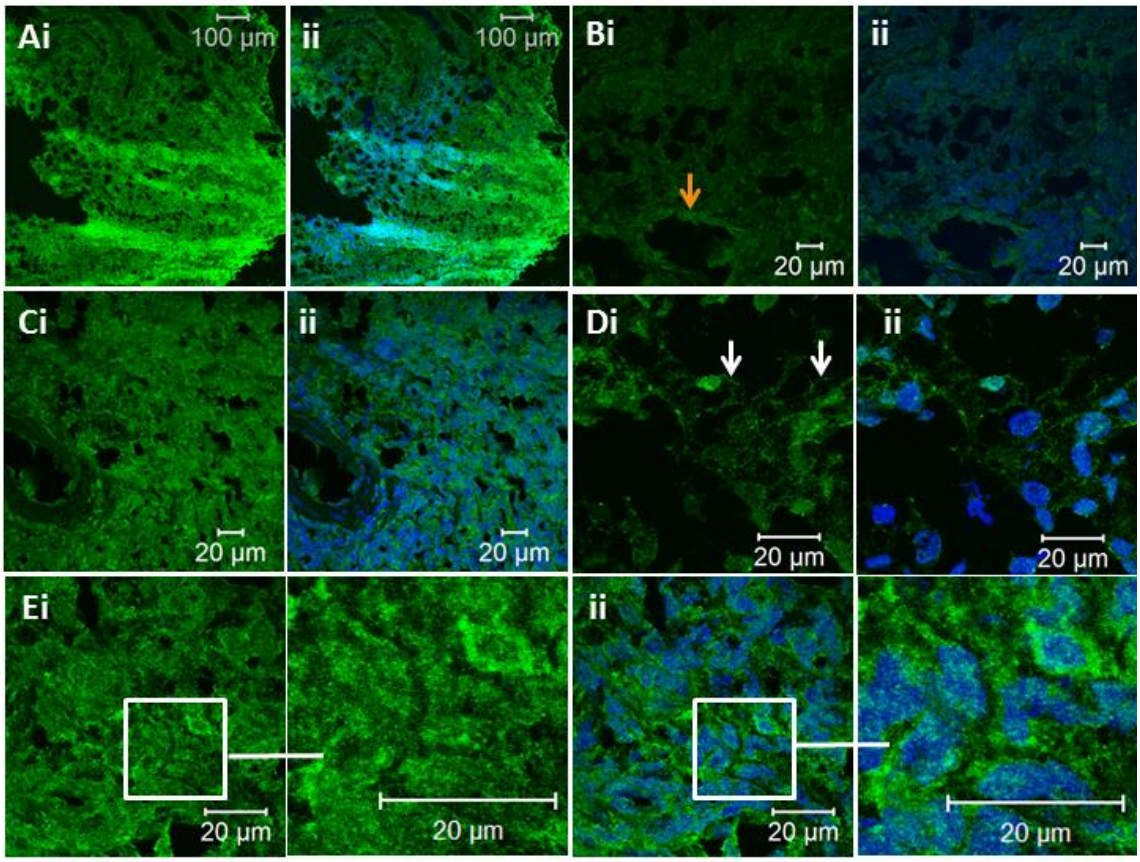

Appendix C3 iRHOM2 localisation in Neuroblastoma. Immunohistochemistry of iRHOM2 in a frozen Neuroblastoma section. Images were taken at 10X (**A**), 40X (**B,C**) and 100X (**D and E**). Orange arrows represent brighter staining at a tissue edge, white arrows represent possible plasma membranous staining. Images were taken on the LSM 510 confocal microscope. Microscope settings were adjusted for each picture. Image **Ei** and ii, the right hand images are zoomed in images of the region of the left hand images indicated by the white box.

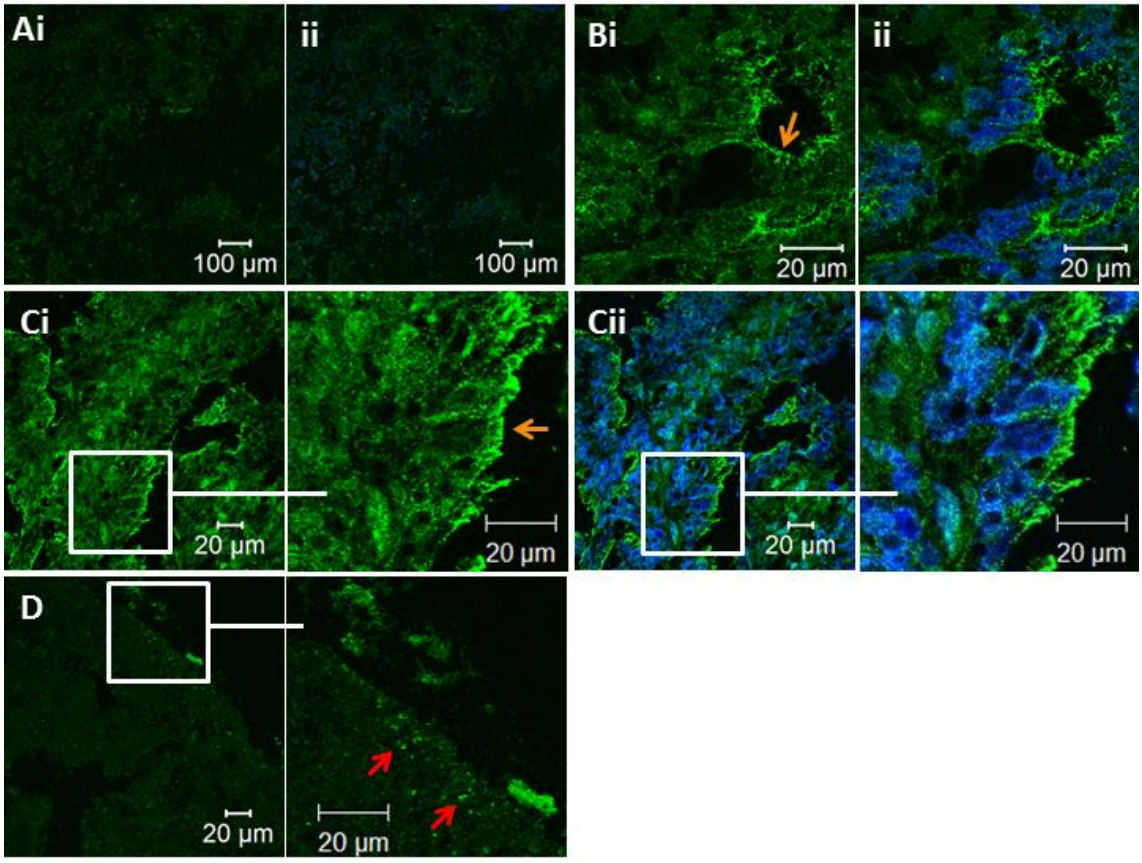

Appendix C4 iRHOM2 localisation in Endometrial adenocarcinoma. Immunohistochemistry of iRHOM2 in a frozen section from an adenocarcinoma. Images were taken using the LSM 510 Confocal microscope at a magnification of 10X (**A**) or 40X (**B-D**). Microscope settings were adjusted for each region of the section. Orange arrows indicate brighter iRHOM2 staining at the tissue edge, and red arrows indicate brighter iRHOM2 staining in individual cells, possibly infiltrating immune cells although these cells are smaller than those seen in other tissue sections.

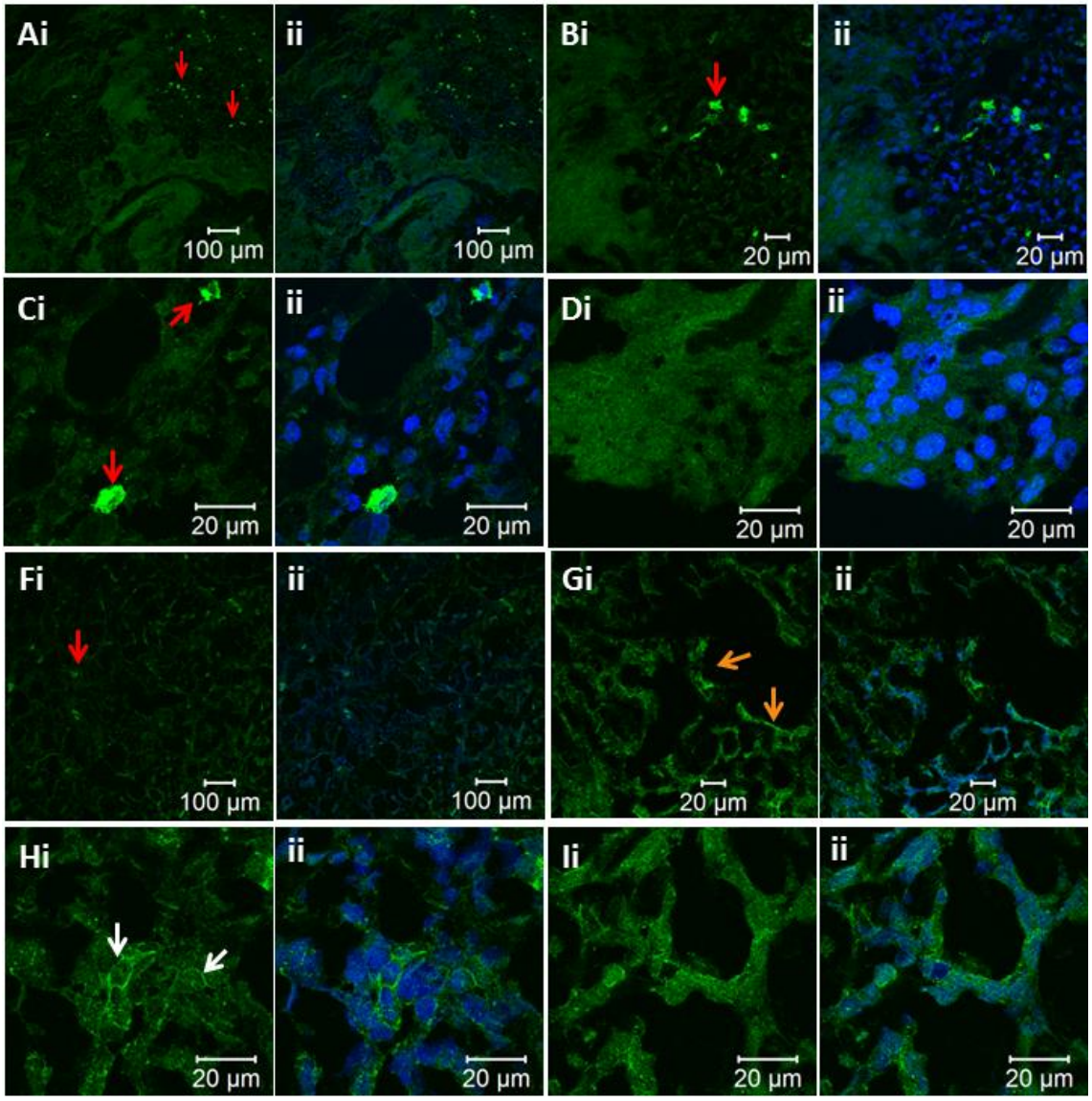

Appendix C5 iRHOM2 localisation in Cervical Squamous Cell Carcinoma and Lung Carcinoma. Images were taken at magnifications of10X (**A, F**), 40X (**B, G**) and 100X (**C, D, H, I**). Red arrows represent individual cells staining brightly for iRHOM2 (likely infiltrating macrophages), and white arrows indicate plasma membranous staining. Images were taken on the LSM 510 Confocal microscope. Microscope settings were adjusted for each individual image.

Position	CDS Mutatic	AA Mutation	Mutation	Count	Type	Tissue	1000 Gen?	EVS?	Protein coding and not on EVS
5	c.13C>G	p.R5G	213736	1	Substitution - Missense	Breast	No		
18	c.54C>T	p.P18P	238096	1	Substitution - coding silent	Prostate	No		
54	c.162C>T	p.A54A	1264135	1	Substitution - coding silent	Oesophagus	No	Yes	
75	c.224C>T	p.T75M	177899	1	Substitution - Missense	Large intestine	No		
103	c.308G>A	p.R103H	1301620	1	Substitution - Missense	Urinary tract	No		
107	c.319C>T	p.R107C	305416	1	Substitution - Missense	Soft tissue	No		
107	c.320G>A	p.R107H	1223686	1	Substitution - Missense	Large intestine	No		
115	c.345G>A	p.K115K	966987	1	Substitution - coding silent	Endometrium	No		
150	c.448C>G	p.L150V	1264137	1	Substitution - Missense	Oesophagus	No		
158	c.472C>T	p.P158S	1293549	1	Substitution - Missense	Cervix	No		
210	c.630G>T	p.S210S	1518191	1	Substitution - coding silent	Lung	No		
228	c.682G>A	p.V228I	1223683	1	Substitution - Missense	Large intestine	No		
256	c.766G>A	p.D256N	1223684	1	Substitution - Missense	Large intestine	No		
267	c.799G>T	p.G267C	1287615	1	Substitution - Missense	Autonomic ganglia	No		
339	c.1015C>T	p.R339W	1223687	1	Substitution - Missense	Large intestine	No		
348	c.1042G>A	p.A348T	356800	1	Substitution - Missense	Lung	No		
354	c.1060C>T	p.Q354*	1223685	1	Substitution - Nonsense	Large intestine	No		
367	c.1101G>A	p.E367E	1518201	1	Substitution - coding silent	Lung	No		
370	c.1110G>T	p.P370P	701998	1	Substitution - coding silent	Lung	No		
392	c.1174G>A	p.V392I	966970	1	Substitution - Missense	Endometrium	No		
412	c.1236C>T	p.F412F	121743	1	Substitution - coding silent	Upper aerodigestiv	No		
428	c.1284G>T	p.A428A	701999	1	Substitution - coding silent	Lung	No		
429	c.1287C>T	p.P429P	1518202	1	Substitution - coding silent	Lung	No		
478	c.1433G>A	p.C478Y	1378305	1	Substitution - Missense	Large intestine	No		
483	c.1449G>A	p.P483P	1378304	1	Substitution - coding silent	Large intestine	No		
485	c.1453G>A	p.V485M	1378303	1	Substitution - Missense	Large intestine	No		
579	c.1736delA	p.N579fs*40	1378259	1	Deletion - Frameshift	Large intestine	No		
580	c.1739G>A	p.S580N	1478491	1	Substitution - Missense	Breast	No		
580	c.1740C>T	p.S580S	84315	1	Substitution - coding silent	Pancreas	No		
635	c.1903A>C	p.M635L	556765	1	Substitution - Missense	Lung	No		
654	c.1962C>T	p.Y654Y	81658	1	Substitution - coding silent	Ovary	No		
732	c.2194G>A	p.V732M	270035	1	Substitution - Missense	Large intestine	No		
754	c.2261T>G	p.V754G	1493536	1	Substitution - Missense	Kidney	No		
828	c.2482C>T	p.R828C	1264136	1	Substitution - Missense	Oesophagus	No		
834	c.2502C>G	p.F834L	396691	1	Substitution - Missense	Lung	No		
842	c.2524G>A	p.D842N	1518215	1	Substitution - Missense	Lung	No		
848	c.2544C>T	p.Y848Y	1378137	1	Substitution - coding silent	Large intestine	No		
851	c.2553C>T	p.D851D	1378136	1	Substitution - coding silent	Large intestine	No	Yes	
	c.953+1G>T	p.?	247035	1	Unknown	Prostate	No		

Comfirmed somatic
Unknown origin
(None previously reported)

Appendix C6 iRHOM1 (*RHBDF1*) mutations from the COSMIC database

AA Mutation	Mutation	Count	Type			Tissue	1000 Genomes?	EVS?	Protein coding and not on EVS
p.P41S	349448	1	Substitution - Missense			Lung	No		
p.A67V	195609	1	Substitution - Missense			Large Intestine	No		
p.P178S	233264	1	Substitution - Missense			Skin	No		
p.P208L	437441	1	Substitution - Missense			Breast	No	Yes	
p.T213T	349447	1	Substitution - coding silent			Lung	No		
p.P214P	371342	1	Substitution - coding silent			Lung	No	Yes	
p.G215R	1563631	1	Substitution - Missense			Large Intestine	No	Yes	
p.S230Y	1480044	1	Substitution - Missense			Breast	No		
p.R234H	1223690	1	Substitution - Missense			Large Intestine	No		
p.R255C	1223689	1	Substitution - Missense			Large Intestine	No		
p.V332V	1522246	1	Substitution - coding silent			Lung	No		
p.G340G	1130155	1	Substitution - coding silent			Prostate	No		
p.R352R	247037	1	Substitution - coding silent			Prostate	No		
p.V357V	383916	1	Substitution - coding silent			Lung	No		
p.R364W	1480043	1	Substitution - Missense			Breast	No		
p.S381I	1522247	1	Substitution - Missense			Lung	No		
p.R392Q	332722	1	Substitution - Missense			Lung	No		
p.R401W	1223688	1	Substitution - Missense			Large intestine	No		
p.T416M	195608	1	Substitution - Missense			Large Intestine	No		
p.A471fs*208	1386231	1	Deletion - Frameshift			Large Intestine	No		
p.S506S	238097	1	Substitution - coding silent			Prostate	No		
p.G531V	314789	1	Substitution - Missense			Lung	No		
p.M534V	1480042	1	Substitution - Missense			Breast	No		
p.V548V	1287616	1	Substitution - coding silent			Autonomic ganglia	No		
p.E558*	1480041	1	Substitution - Nonsense			Breast	No		
p.K573R	247036	1	Substitution - Missense			Prostate	No		
p.C577Y	1195190	1	Substitution - Missense			Lung	No		
p.M619I	984721	1	Substitution - Missense			Endometrium	No		
p.G621C	1386230	1	Substitution - Missense			Large Intestine	No		
p.V650fs*29	111586	1	Deletion - Frameshift			Ovary	No		
p.L684L	1324830	1	Substitution - coding silent			Ovary	No		
p.F697F	374260	1	Substitution - coding silent			Lung	No		
p.L728P	1386229	1	Substitution - Missense			Large Intestine	No		
p.V756E	473411	1	Substitution - Missense			Kidney	No		
p.L757I	195607	1	Substitution - Missense			Large Intestine	No		
p.L783L	1386228	1	Substitution - coding silent			Large Intestine	No		
p.A786T	294761	1	Substitution - Missense			Large Intestine	No		
p.Y799H	195606	1	Substitution - Missense			Large Intestine	No		
p.F839F	1318447	1	Substitution - coding silent			Haematopoetic and	No		

Comfirmed somatic
Unknown origin
(None previously reported)

Appendix C7 iRHOM2 (*RHBDF2*) mutations from the COSMIC database